AD NUMBER

AD846086

NEW LIMITATION CHANGE

TO

Approved for public release, distribution unlimited

FROM

Distribution authorized to U.S. Gov't. agencies and their contractors; Administrative/Operational Use; NOV 1968. Other requests shall be referred to US Air Force Flight Dynamics Laboratory, Attn: FDTE, Wright-Patterson AFB, OH 45433. Export Control.

AUTHORITY

AFFDL ltr, 31 May 1973
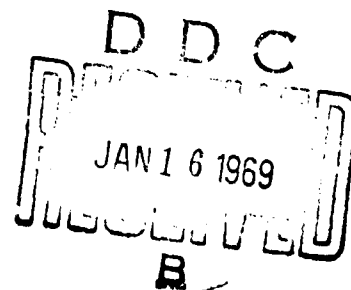
AFFDL-TR-68-127
VOLUME 1

AD846086

PROJECT HICAT
HIGH ALTITUDE CLEAR AIR TURBULENCE
MEASUREMENTS AND METEOROLOGICAL CORRELATIONS

WALTER M. CROOKS, FREDERIC M. HOBLIT, FINIS A. MITCHELL, et al

Lockheed-California Company

D D C

JAN 1 6 1969

B

AIR FORCE FLIGHT DYNAMICS LABORATORY
AIR FORCE SYSTEMS COMMAND
WRIGHT-PATTERSON AIR FORCE BASE, OHIO

ACCESSION for		
CFSTI	WHITE SECTION	☐
DDC	BUFF SECTION	☑
UNANNOUNCED		☐
JUSTIFICATION		
BY		
DISTRIBUTION/AVAILABILITY CODES		
DIST.	AVAIL. and/or SPECIAL	

PROJECT HICAT
HIGH ALTITUDE CLEAR AIR TURBULENCE
MEASUREMENTS AND METEOROLOGICAL CORRELATIONS

WALTER M. CROOKS, FREDERIC M. HOBLIT, FINIS A. MITCHELL, et al

Lockheed-California Company

VOLUME I

PAGES_____
ARE
MISSING
IN
ORIGINAL
DOCUMENT

FOREWORD

This report was prepared by the Lockheed-California Company, Burbank, California, for the Air Force Flight Dynamics Laboratory, Wright-Patterson Air Force Base, Ohio, under Contract F33615-67-C-1461, "High Altitude Critical Atmospheric Turbulence (HICAT)", ADP 682E. the Lockheed-California Company report number is LR 21718, dated July 29, 1968. The manuscript was released by the authors on September 27, 1968 for publication.

Air Force Flight Dynamics Laboratory management responsibility was under the ALLCAT Program Director, Mr. E. Brazier with Mr. J. P. Boone as the Air Force Project Engineer. The Lockheed-California Company Program Manager was Mr. C. B. Fabian with Mr. W. M. Crooks as the Technical Leader.
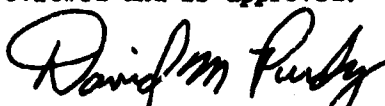
All HICAT aircraft operations and field team logistics support were under the direction of Lt. Col. J. .T. King, USAF, Air Force Flight Test Center, Directorate of Systems Test, V/STOL Operations Branch, Edwards Air Force Base, California.

Special Acknowledgments are due to the following personnel who actively participated in developing high altitude meteorological forecasts during field operations: Mr. L. C. Brown, Meteorological Office, Royal Aircraft Establishment, Bedford, England; 1st Lt. J. A. Calcoate, Det. 19, 26th Weather Sq., Barksdale Air Force Base, Louisiana; Lt. R. E. Introne, Jr., Det. 4, 8th Weather Sq., Loring Air Force Base, Maine; Capt. K. W. Craw, Jr., Det. 5, 5th Weather Wing, Howard Air Force Base, Canal Zone; CWO B. H. Nunes, Det. 11, 6th Weather Wing, Patrick Air Force Base, Florida; Capt. D. W. Shong, Det. 21, 6th Weather Wing, Edwards Air Force Base, California. The assistance and advice of Major G. R. Hammond, ALLCAT Staff Meteorologist and Dr. J. A. Dutton of Pennsylvania State University are also gratefully acknowledged.

Acknowledgement is made for the valuable assistance of the following Lockheed-California Company personnel: Mr. R. V. Jensen and Miss Joanne McPheeters, data analysis; Mr. D. W. Thompson, field team operation; Messrs R. H. Cook and R. C. Quist, instrumentation; Messrs. R. D. Baker, E. A. Goulette, P. J. Tersigni, and J. M. Rapp, data processing; Messrs. E. V. Ashburn, D. T. Prophet, and D. E. Waco, meteorology; and Mr. R. P. Boal, editor.

This report consists of two volumes. Volume I contains the main body of the report plus Appendix I, Detailed Analysis, and Appendix II, Data Processing. Volume II contains Appendix III, HICAT Flight Test Log, Appendix IV, Time Histories, Appendix V, Gust Velocity Power Spectra, and Appendix VI, Meteorological Summaries of Tests.

This technical report has been reviewed and is approved.

DAVID M. PURDY, 1st Lt., USAF
Chief, Experimental Mechanics Branch
Structures Division

ii

ABSTRACT

This report describes the high altitude clear air turbulence (HICAT)
measurements and meteorological correlations derived from Air Force U-2 flights
with emphasis upon the results achieved since 13 March 1967, the program
extension date. The program effort required the measurement of CAT velocity
components at altitudes of 45,000 to 70,000 feet in 6 geographic areas.
Instrumentation carried aboard the U-2 consisted of a PCM System, an inertial
navigation system, aerodynamic and aircraft response sensors including a fixed
vane gust probe, oscillograph recorder, and a digital magnetic tape recorder.
Instrumentation capabilities permitted CAT measurements in the wavelength
range from about 100 to 50,000 feet. The program objective was to determine
the statistical characteristics of high altitude CAT so as to improve struc-
tural design criteria. In addition, meteorological forecasts and analyses
were to be correlated with the CAT measurements to improve CAT forecast pro-
cedures. In the Extended Program, 18.3 hours of high altitude CAT were located
and recorded in flights covering over 156,000 miles from bases in England,
Louisiana, Maine, Panama, Florida, and California. Actual vertical, lateral,
and longitudinal gust velocity time histories and power spectra were deter-
mined and analyzed. Peak counts of true vertical gust velocity and derived
equivalent gust velocity were obtained. A practical procedure for forecasting
high altitude CAT was developed. The pilot's log, gust velocity time histories
and power spectra, as well as flight tracks and meteorological descriptions of
all the tests appear in Volume II of this report.

Distribution of this Abstract is unlimited.

TABLE OF CONTENTS

VOLUME I

TABLE OF CONTENTS (Continued)

Page

TABLE OF CONTENTS (Continued)

LIST OF ILLUSTRATIONS

LIST OF ILLUSTRATIONS (Continued)

LIST OF ILLUSTRATIONS (Continued)

x

LIST OF ILLUSTRATIONS (Continued)

LIST OF ILLUSTRATIONS (Continued)

LIST OF ILLUSTRATIONS (Continued)

LIST OF ILLUSTRATIONS (Continued)

LIST OF ILLUSTRATIONS (Continued)

LIST OF ILLUSTRATIONS (Continued)

LIST OF ILLUSTRATIONS (Concluded)

LIST OF TABLES

SYMBOLS

a_i — Induced cg normal acceleration.

a_F — Longitudinal acceleration in aircraft axes (ft/sec^2); positive forward.

a_L — Lateral acceleration in aircraft axes (ft/sec^2); positive to the right.

a_N — Normal acceleration in aircraft axes (ft/sec^2); positive upward.

a_Z — Vertical acceleration in earth reference axes (ft/sec^2); positive upward.

c — Mean aerodynamic chord.

$C(\ )$ — Cospectrum function.

C_h — Cospectral estimates

C_{L_α} — Wing lift curve slope (1/rad).

C_{N_α} — Alpha-vane rate-of-change of normal force coefficient with angle-of-attack (1/rad).

C_{N_β} — Beta-vane rate-of-change of normal force coefficient with side-slip angle (1/rad).

f — Cyclic frequency (cycles/sec).

f_c — Numerical filtering cutoff frequency (cycles/sec).

f_r — Rolloff frequency.

f_s — Sampling frequency = $1/\Delta t$ (samples/sec).

f_t — Numerical filtering termination frequency (cycles/sec).

$F(\ )$ — Probability distribution function.

$F_{N_{M\alpha}}$ — Measured alpha-vane normal force (lb); positive up.

$F_{N_{M\beta}}$ — Measured beta-vane normal force (lb); positive to the left.

g	Acceleration of gravity (ft/sec^2)
$g(\ )$	Statistical frequency of occurrence.
$G(\ )$	Statistical frequency of exceedance.
$h(t)$	Time domain weighting function of numerical filter $(1/sec)$.
$H(f)$	Transfer function designed for numerical filter.
$H*(f)$	Transfer function of numerical filtering weights.
H_{pc}	Corrected pressure altitude (ft).
H_{pn}	Indicated pressure altitude (ft).
$\left|H_c(\ )\right|$	Amplitude of frequency response function determined by cross spectrum method.
$\left|H_s(\ )\right|$	Amplitude of frequency response function determined by power spectrum method.
k	Degrees of freedom.
k_b	Fuselage flexibility factor $(rad/ft/sec^2)$.
K_g	Gust alleviation factor $= .88\,\mu_g/(5.3 + \mu_g)$.
L	Scale of turbulence (ft).
L_h	Raw power spectral estimates.
L_x	Moment arm from gust probe to accelerometer location (ft).
m	Number of spectral estimates, or slope of the power spectral density high frequency asymptote on a log-log plot, or mass of gust sensing vane $(lb\text{-}sec^2/ft)$.
M_i	Indicated Mach number.
M_T	True Mach number.
$N(\ )$	Frequency of exceedance of parenthetical quantity.
N,n	Number, or total number.

xx

SYMBOLS (Continued)

N_o — Characteristic frequency (cps).

N_w — Number of numerical filtering weights.

P_a — Ambient pressure (lb/ft^2).

P_s — Static pressure (lb/ft^2).

q_c — Differential pressure (lb/ft^2).

$q(\ )$ — Quadrature spectrum function.

q_h — Quadrature spectral estimates.

$r(t)$ — Time domain transfer function of unit elevator impulse.

$R(\tau)$ — Autocorrelation function.

R_p — Estimates of autocorrelation function.

$R_{xy}(\ )$ — Cross correlation function.

R_{xy_p} — Estimates of cross correlation function.

S — Wing area (ft^2).

S_V — Vane area (ft^2).

t,T — Time (sec).

t_a — Ambient temperature (deg C).

t_t — Total temperature (deg C).

T_n — Elapsed time of a data run (sec).

U_{AG_X}, U_F — Longitudinal gust component in earth reference axes measured in the horizontal plane parallel to the average grid heading of the aircraft over the duration of a run (fps); positive aft.

U_{AG_Y}, U_L — Lateral gust component in earth reference axes measured in the horizontal plane and perpendicular to the average grid heading of the aircraft over the duration of the run (fps); positive to the left.

U_{AG_Z}, U_V	Vertical gust component in earth reference axes measured perpendicular to the horizontal plane (fps); positive upward.
U_{de}	Derived equivalent gust velocity (fps); positive upward.
V_e	Equivalent airspeed (fps).
V_{in}	Indicated airspeed (fps).
V_T	True airspeed (fps).
$V_{X'}$	Aircraft grid-X-velocity in earth reference axes (fps); positive to the east.
$V_{Y'}$	Aircraft grid-Y-velocity in earth reference axes (fps); positive to the north.
w_c	Central smoothing weight.
w_n	Numerical filtering weights.
W	Aircraft weight (lb).
$W_I(f)$	Transfer function of ideal integration = $1/2\pi f$.
$W_s(f)$	Transfer function of Simpson's one-third rule integration.
$W_T(f)$	Transfer function of trapezoidal rule integration.
$x(\ )$	Random function.
x_q	Discrete function.
y	Load, stress, or other quantity varying with time.
y_q	Discrete function.
α	Angle-of-attack (rad); positive for relative wind upward.
β	Sideslip angle (rad); positive for relative wind from the right.
Γ	Gamma function
γ	Inclination with respect to the horizontal of the instantaneous relative wind (rad).

xxii

δ_E Elevator angle (deg).

δH_p Altitude static position error correction (ft).

δM Mach number static position error correction.

Δ Incremental value. When used for time series data, increments are with respect to mean or linear trend of data.

Δt Sampling interval (sec).

ϵ_U Velocity discrepancy (ft/sec).

η Wind direction angle (deg); clockwise from north to the direction the wind is blowing.

θ Aircraft pitch angle (rad); positive nose up.

θ_M Aircraft pitch angle measured by inertial platform (rad); positive nose up.

$\dot{\theta}$ Aircraft pitch rate (rad/sec).

λ Turbulence wavelength (ft).

Λ Aircraft heading angle (rad); clockwise from north.

μ_g Aircraft mass ratio - $2W/\rho g\, C_{L_\alpha} c\, S$.

ρ Air density (lb-sec^2/ft^4).

ρ_o Air density at sea level (lb-sec^2/ft^4).

σ Air density ratio, ρ/ρ_o, RMS value of time history.

σ_s Standard root-mean-square deviation.

σ_w Standard deviation of any gust velocity component, w. (ft/sec).

σ_y Standard deviation of y.

τ Time lag (sec).

ϕ Aircraft roll angle (rad); positive right wing down.

ϕ_M Aircraft roll angle measured by inertial platform (rad); positive right wing down.

SYMBOLS (Continued)

$\dot{\phi}$ — Aircraft roll rate (rad/sec).

$\Phi(\ )$ — Power spectral density function.

Φ_n — Power spectral density estimates.

$\Phi_{xy}(\ )$ — Cross spectrum function.

Φ_{xy_h} — Cross-spectral estimates.

ψ — Aircraft yaw angle (rad); positive nose right.

$\dot{\psi}$ — Aircraft yaw rate (rad/sec).

ω — Angular frequency (rad/sec).

Ω — Reduced frequency $= 2\pi/\lambda$ (rad/ft).

NOTE: — A bar over a symbol indicates a mean value.

A caret over a symbol indicates that a filtering transformation has been performed.

METEOROLOGICAL SYMBOLS USED:

T — Thunderstorm

RW — Rainshowers

R — Rain

⬭ — Line of radar echoes.

☁ — Area of radar echoes.

+	Increasing	
+/-	Increasing slowly	
+/+	Increasing rapidly	
-	Decreasing	Intensity of radar echo.
-/-	Decreasing slowly	
-/+	Decreasing rapidly	
NC	No change	

NE — No radar echo.

NA — Observation not available.

xxiv

SYMBOLS (Concluded)

NO — Equipment not operating.

☐ — Area of severe weather forecast.

$\underline{hhh}$ — Height of radar echo tops.

$\overline{hhh}$ — Height of radar echo bases.

→xx — Cell movement with speed xx (knots).

ΔN — Distance (nautical miles)

ΔT — Temperature change (°Kelvin).

ΔZ — Height change (meters).

ΔP — Pressure change (millibars).

GLOSSARY OF RADIOSONDE OBSERVATION STATIONS

UNITED STATES

Station No.	Code	Name
(UJ-30)*		
402	WAL	Wallops Island, Virginia
403	DIA	Dulles Airport, Virginia
425	HTS	Huntington, West Virginia
503	TEB	Teterboro, New Jersey
506	ACK	Nantucket, Massachusetts
518	ALB	Albany, New York
520	PIT	Pittsburgh, Pennsylvania
528	BUF	Buffalo, New York
606	PWM	Portland, Maine
712	CAR	Caribou, Maine
(UJ-31)		
201	NQX	Key West, Florida
202	MIA	Miami, Florida
206	JAX	Jacksonville, Florida
208	CHS	Charleston, South Carolina
211	TPA	Tampa, Florida
221	VPS	Valpariso, Florida
222	PNS	Pensacola, Florida
226	MGM	Montgomery, Mississippi
232	BVE	Boothville, Louisiana
235	JAN	Jackson, Mississippi
304	HAT	Hatteras, North Carolina
311	AHN	Athens, Georgia
317	GSO	Greensboro, North Carolina
327	BNA	Nashville, Tennessee
334	MEM	Memphis, Tennessee
(UJ-32)		
240	LCH	Lake Charles, Louisiana
248	SHV	Shreveport, Louisiana
250	BRO	Brownsville, Texas
251	CRP	Corpus Christi, Texas
255	VCT	Victoria, Texas
259	GSW	Fort Worth, Texas
261	DRT	Del Rio, Texas
265	MAF	Midland, Texas
266	ABI	Abilene, Texas
340	LIT	Little Rock, Arkansas
344	FSM	Fort Smith, Arkansas
353	OKC	Oklahoma City, Oklahoma
363	AMA	Amarillo, Texas
445	CBI	Columbia, Missouri
451	DDC	Dodge City, Kansas
456	TOP	Topeka, Kansas
465	GLD	Goodland, Kansas
469	DEN	Denver, Colorado
532	PIA	Peoria, Illinois
(UJ-33)		
429	DAY	Dayton, Ohio
553	OMA	Omaha, Nebraska
562	LBF	North Platte, Nebraska
637	FNT	Flint, Michigan
645	GRB	Green Bay, Wisconsin
694	HON	Huron, South Dakota
695	STC	St. Cloud, Minnesota
747	INL	International Falls, Minnesota
(UJ-34)		
576	LND	Lander, Wyoming
597	MFR	Medford, Oregon
681	BOI	Boise, Idaho
694	SLE	Salem, Oregon
764	BIS	Bismarck, North Dakota
768	GGW	Glasgow, Montana
773	GTF	Great Falls, Montana
762	GEG	Spokane, Washington
797	UIL	Quillayute, Washington

UNITED STATES (Cont)

Station No.	Code	Name
(UJ-35)		
270	ELP	El Paso, Texas
274	TUS	Tucson, Arizona
280	YUM	Yuma, Arizona
290	MYF	Montgomery Field, San Diego, Calif.
291	NSI	San Nicolas Island, California
295	LAX	Los Angeles, California
365	ABQ	Albuquerque, New Mexico
374	INW	Winslow, Arizona
385	UCC	Yucca Flat, Nevada
386	LAS	Las Vegas, Nevada
393	VBG	Vandenburg Air Force Base, California
476	GJT	Grand Junction, Colorado
486	ELY	Ely, Nevada
493	OAK	Oakland, California
572	SLC	Salt Lake City, Utah
583	WMC	Winnemucca, Nevada
	EDW	Edwards Air Force Base, California

CANADA

Station No.	Code	Name
600	SA	Sable Island, Nova Scotia
722	MW	Maniwaki, Quebec
807	AR	Argentia, Newfoundland
811	ZV	Seven Islands, Quebec
815	JT	Stephenville, Newfoundland
816	YR	Goose Bay, Newfoundland
826	NI	Nitchiquon, Quebec
836	MO	Moosonee, Ontario

CARIBBEAN

Station No.	Code	Name
394	MTY	Monterrey, Mexico
644	MID	Merida, Mexico
692	VER	Veracruz, Mexico
001	MCSP	San Andres Island, Colombia
016	MKKF	Kindly Field, Bermuda
063	MYGM	Great Abaco, Bahamas
076	ZQBL	Harbour Isle, Bahamas
118	ZQJT	Turks Isle, Bahamas
355	MUCM	Camaguey, Cuba
367	MUGM	Guantanamo, Cuba
384	MKCG	Georgetown, Grand Cayman Island
397	MKJP	Kingston, Jamaica
486	MDSD	Santo Domingo, Dominican Republic
501	KSWA	Swan Island, U.S.A.
526	MJSJ	San Juan, Puerto Rico
806	MHHO	Howard AFB, Canal Zone
866	MACM	Juliana Airport, St. Martin
897	MFFR	Raizet Airdrome, Guadelupe
954	MKPB	Seawell Airport, Barbados
988	MACC	Dr. Plesman Airport, Curacao
967	CGU	Chaguaramas Bay, Trinidad
222	MCBO	Bogata, Colombia

EUROPE

Station No.		Name
415		Stavanger, Norway
084		Goteborg, Sweden
005		Lerwick, Shetland Isles
026		Stornoway, Scotland
170		Shanwell, Scotland
322		Aughton, England
496		Hemsby, England
774		Crawley, England
808		Camborne, England
980		Longbush, England
953		Valentia, Ireland
260		DeBilt, Netherlands
447		Uccle, Belgium
110		Brest/Guipavas, France
145		Trappes, France
180		Nancy, France
513		Köln, Germany

Ocean Weather Ship "I" (99°N, 19°W)

SECTION I

INTRODUCTION

BACKGROUND

The establishment of design criteria for the faster, higher flying aircraft of the future requires a detailed knowledge of the intended operating environment. Sometime before 1962 the Air Force Flight Dynamics Laboratory recognized the need for better definition of the atmospheric turbulence environment, particularly for altitudes above 50,000 feet (Reference 1). Turbulence data available then was derived almost entirely from NASA VGH[1] recordings acquired during U-2 operations totaling 192 flights in five world areas (Reference 2). These flights were generally made for purposes not directly related to atmospheric turbulence. About half of the data from these flights, or approximately 5-1/2 hours, were for turbulence above 50,000 feet.

The Air Force realized the danger of relying solely on the acceleration response of the U-2 aircraft as a measure of turbulence at high altitudes. A supersonic or hypersonic vehicle of possibly radical configuration, flying four to ten (or more) times the speed of the U-2, will obviously have a somewhat different response to turbulence than the U-2. An aircraft flying at these high speeds would be affected much more by longer turbulence wavelengths and less by the shorter wavelengths than the relatively slow flying U-2. For these reasons, the Air Force initiated a program to measure high altitude clear air turbulence (HICAT[2]) at altitudes above 50,000 feet in several areas of the world. The principal objective of the program was to statistically define the characteristics of high altitude CAT so as to improve structural design criteria. To accomplish this result, an Air Force U-2 was instrumented so that true gust velocity components encountered along the aircraft flight path could be determined.

Lockheed-California Company was directed to install and maintain the turbulence measuring instrumentation in the U-2 as well as to process and analyze the data. In this joint effort, the Air Force was to supply the instrumentation, maintain and fly the HICAT aircraft, and provide overall direction of the program. Under a separate contract (Reference 3), Lockheed was directed to utilize the data gathered in the flight program to develop an analytical model of high altitude CAT. Such a model could then provide meteorologists with an overall basis for the prediction of the occurrence and intensity of atmospheric regions of turbulent air. An adequate model would permit the assessment of CAT for almost any high altitude route based upon weather data records

---

[1] Aircraft velocity, center-of-gravity acceleration, and altitude

[2] For broader applicability, the program title was changed by the Air Force to High Altitude Critical Atmospheric Turbulence in 1967.

1

of prior years. Such an analysis could provide pseudo-operational statistical data of considerable value to the aircraft designer particularly in the evaluation of aircraft structural fatigue due to CAT.

PROGRAM HISTORY

Most of the aircraft instrumentation for the first phase of the program was provided off-the-shelf from Air Force inventory. In many instances standard instruments were supplied which were not particularly intended for turbulence research. This first HICAT instrumentation system was designed so that the analog signals from the sensors modulated the output of strain controlled oscillators to produce frequency modulated signals. The FM signals were then recorded onboard the aircraft with a magnetic tape recorder.

In the case of the gust probe, the government-furnished differential pressure instrument was designed for low altitude measurements and not adaptable to very high altitudes. Consequently, at the request of the Air Force, Lockheed designed and built a high altitude gust sensor. The sensor design was based upon the fixed-vane principle which had been utilized successfully in a prior investigation of tail buffeting turbulence on the U.S. Navy P-3A patrol bomber. Fortunately, it was possible to adapt the fixed-vane gust sensors to the nose boom previously fabricated for the differential pressure probe.

The first HICAT checkout flight occurred on 20 February 1964 and the first HICAT search on 3 April 1964. In the period ending 15 July 1964, 18 HICAT search flights were completed, 5 from Edwards Air Force Base, California, 4 from Patrick Air Force Base, Florida, and 9 from Ramey Air Force Base, Puerto Rico. In this initial phase of the program, the HICAT aircraft had to be shared on a day-to-day basis with other higher priority Air Force programs. For this reason, the flights only occasionally coincided with optimum turbulence forecasts. Nevertheless, about 6 hours of high altitude CAT of predominantly light-to-moderate intensity were encountered on these flights. Turbulence in the wavelength range from 60 to 2500 feet was located and recorded approximately 14 percent of the time at altitudes above 50,000 feet. The program successfully demonstrated the feasibility of locating and measuring significant amounts of high altitude CAT. Complete documentation of this phase of the HICAT program is presented in Reference 4.

Recognizing the need for better instrumentation to obtain longer wavelength measurements, the Air Force redirected and extended the HICAT program on 15 February 1965. The redirection required installation of a new digital instrumentation system capable of measuring turbulence waves up to at least 12,000 feet and possibly up to 60,000 feet in length. First flight with the new instrumentation occurred 8 October 1965 at Edwards Air Force Base. After several check flights, high altitude CAT search flights were resumed on 16 November 1965, and continued under the redirected contract until 17 February 1967. During this period, 114 high CAT search flights were performed along with 32 incidental flights. Over 29 hours of CAT were recorded in the operations conducted from bases in Hawaii, New Zealand, Australia, Puerto Rico, Alaska, California, and Massachusetts. This phase of the HICAT program is described in detail in Reference 5.

On 13 March 1967, the HICAT program was again extended, this time under a new
Air Force contract (Reference 6). In this extension the HICAT search flights
were to be conducted from bases in Great Britain, Louisiana, Maine, Panama,
Florida, and California. In addition, the extended program was improved in
two important aspects. The first improvement required the addition of a full
time meteorologist to the HICAT field team. In this way high altitude CAT
forecasts and search techniques could be improved, meteorological coordina-
tion and air weather data acquisition assured, and meteorological data
analysis considerably enhanced. The second improvement provided for a more
extensive and detailed analysis of the flight measurements than was possible
under the original contract. For completeness this analysis was to consider
the data gathered under the original contract and presented in Reference 5 as
well as the new CAT data.

PROGRAM PHILOSOPHY

It is important to distinguish HICAT flights from those U-2 flights made for
other purposes and identified by the term "operational". Operational flights
are frequently used to obtain VGH statistical data with respect to the
incidence of high altitude CAT encountered randomly. HICAT tests on the other
hand involve deliberate flights into regions of turbulence or suspected
turbulence. The emphasis is entirely upon measuring the turbulence so as to
define its intensity as a function of spatial frequency or wavelength. An
equally important objective of the HICAT flights is to sample in so far as
possible the entire known variety of atmospheric phenomena associated with
high altitude CAT. In this way considerable meteorological insight can be
gained and high altitude forecasting techniques significantly improved.

SECTION II

INSTRUMENTATION SYSTEM

The primary airborne data acquisition system is a digital pulse code modulation (PCM) system. The system accepts both analog and digital data signals from various remote sources in the test aircraft (Figure 1) and processes them into a digital format at 25 samples per second. The system block diagram is shown in Figure 2. Data from this system is recorded on 1-inch magnetic tape in a parallel format comprised of 10 data bits, one parity bit, and one synchronizing clock bit. The analog data signals are also recorded concurrently in analog form on an oscillograph for purposes of quick-look analysis and data sensor performance evaluation after each flight. These data signals are supplied to the oscillograph following the low-pass presample filtering that takes place within the PCM system. The effect of the analog filtering is illustrated by the PCM frequency response data shown in Figure 3. The major components of the instrumentation system are housed in the aircraft Q-bay just behind the pilot. The basic HICAT instrumentation list including sensor characteristics is shown in Table I.

Analog data signals are routed to the PCM system from a variety of sensors located throughout the test aircraft. A fixed-vane gust probe mounted on a nose-boom provides measurements of vertical and lateral gust forces. An inertial navigation system provides information on aircraft attitude, vertical acceleration, horizontal velocity, and horizontal displacement. Additional acceleration, temperature, angular rate, altitude, and control surface position information is supplied from other sensors appropriately located throughout the aircraft.

Each analog signal is conditioned to a 0- to +5-volt level prior to entry into the PCM system. Signal conditioning equipment includes attenuation networks, dc amplifiers, and phase sensitive demodulators. The PCM system also accommodates five channels of external digital information which is entered directly into the system through switch closures on the pilot's control panel and other remote locations.

The digital magnetic tape generated in the airborne system is subsequently processed through a PCM ground station. This equipment decommutates the time-multiplexed data and makes it available to a buffer-formatter which assembles the data into a preprogrammed computer-compatible format. Under control of the formatter, an output tape deck generates a gapped-format magnetic tape which is then processed through digital computing equipment. The ground station also provides for limited visual display and digital-to-analog conversion of selected data channels. The airborne oscillograms are used primarily as editing aids preparatory to ground station processing.

Details of the airborne instrumentation, the ground station and field checkout equipment are presented in Appendix II of Reference 5.

Figure 1   Aircraft Instrumentation Location Diagram

Figure 2   HICAT Digital Instrumentation System Block Diagram
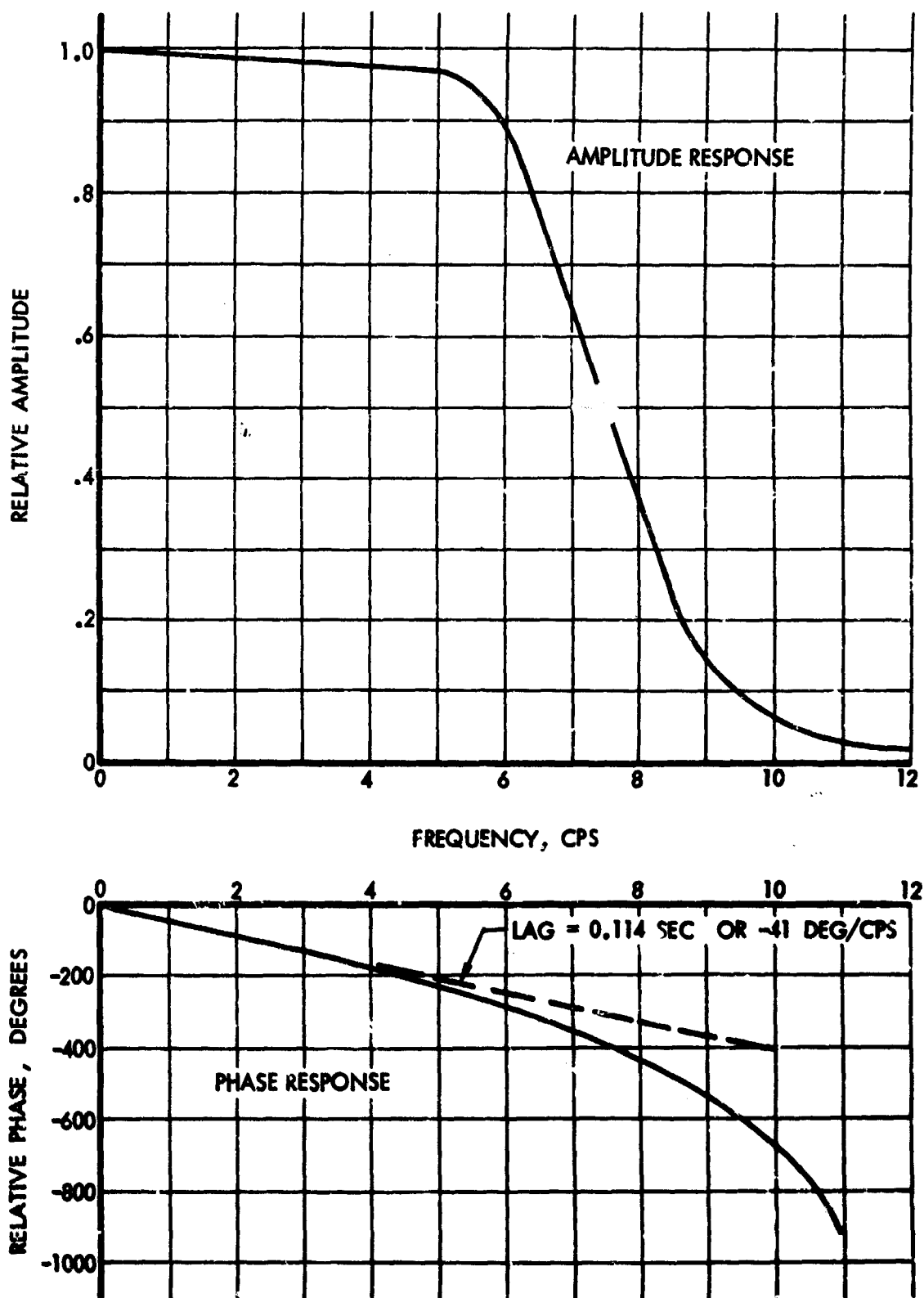
Figure 3   HICAT PCM Frequency Response With Passive Low-Pass Filters

TABLE I
HICAT INSTRUMENTATION LIST AND SENSOR CHARACTERISTICS

Measurement	Inst Type	Ship Location	Mfr and Model No.	Inst Range	Meas Range	System Resolution	Accuracy[1] (% RMS)
α-Vane Force[2]	Vane	Probe FS 56	Lockheed FT 3809	±12 lb	±2 lb	.004 lb[3]	±1.3[4]
β-Vane Force[2]	Vane	"	" "	±12 lb	±2 lb	.004 lb[3]	±1.3[4]
Probe Norm Acc[5]	Acc	"	United Controls PAL-5655	1.0 ±3.0g	1.0 ±3.0g	.006g	±0.9
Probe Lat Acc[5]	Acc	"	" "	±3g	±3g	.006g	±0.9
CG Norm Acc[5]	Acc	FS 408	" "	1.0 ±1.5g	1.0 ±1.5g	.003g	±0.6
CG Lat Acc[5]	Acc	"	" "	±.5g	±.5g	.001g	±0.8
CG Long Acc[5]	Acc	"	" "	±.5g	±.5g	.001g	±0.8
L Wing Nod Acc[5]	Acc	WS 175	" "	1.0 ±1.5g	1.0 ±1.5g	.003g	±0.9
R Wing Nod Acc[5]	Acc	"	" "	1.0 ±1.5g	1.0 ±1.5g	.003g	±0.9
Ind Airspeed[6]	Δ Press.	Probe	Rosemount 831V4	0-1 psid	0-200 Kn	.20 kn[7]	±1.0
Coarse Alt	Press.	A/C Nose	" P 96D	0-15 psi	0-75 kft	28-620 ft	±2.2[4]
Fine Alt[8]	Press.	"	" 830 G1	0-2 psi	46-75 kft	20-83 ft	±0.8
Vernier Alt[8]	Δ Press.	"	" 830 G1 & 521A	.125 psi	Incr 46-75 kft	1.2-5.2 ft	±0.8
Total Temp	Temp	"	" 102	0,-80°C	0,-80°C	.08°C	±0.2
Pitch Rate[9]	Gyro	"	R.C. Allen F2880-045	±10°/Sec	±10°/Sec	.02°/Sec	±0.8
Roll Rate[9]	Gyro	"	" "	±10°/Sec	±10°/Sec	.02°/Sec	±0.8
Yaw Rate[9]	Gyro	"	" "	±10°/Sec	±10°/Sec	.02°/Sec	±0.8
L Aileron Pos	Pot	L Wing	Giannini 851725-93	360°	±15°	.06°	±2.2[4]
Elevator Pos	Pot	Tail	" "	360°	-15° +30°	.05°	±2.2[4]
Rudder Pos	Pot	"	" "	360°	±10°	.04°	±2.2[4]
Fuel Counter[10]	Ctr	Fus	SODECO –	Full Load	Full Load	.5 Gal	
Pitch Angle	Stable Platform	Q-Bay FS 288	Litton LN-3-2A	±90°	±15°	.03°	±0.51
Roll Angle	"	"	" "	±90°	±15°	.03°	±0.51
Heading Sine	"	"	" "	±1.0	±.707	.11°-.16°	±0.52
Heading Cosine	"	"	" "	±1.0	±.707	.11°-.15°	±0.52
Vert Accel	"	"	" "	1 ±8g	1.0 ±1.0g	.002g	±0.7[4]
X-Velocity	"	"	" "	±2000 fps	±1000 fps	2 fps	±1.1[4]
Y-Velocity	"	"	" "	fps	±1000 fps	2 fps	±1.1[4]
X-Distance	"	"	" "	Pole-to-Pole	±500 nmi	1.0 nmi	±1.7
Y-Distance	"	"	" "	±1500 nmi	±500 nmi	1.0 nmi	±1.7

NOTES:
(1) Accuracy determined by using equation (8), Section 5, and includes such factors as linearity, hysteresis, zero stability, etc., of the basic instruments

(2) Natural frequency 155 cps, damping ratio 0.4% critical

(3) Approximately equal to 0.02 degrees

(4) Includes effects of some signal conditioners

(5) Natural frequency 300 cps, damping ratio 70% critical

(6) Natural frequency 3000 cps, damping ratio <1% critical

(7) At 120 knots

(8) Stability is 0.1% FS per 6 months.

(9) Natural frequency 15 cps, damping ratio 70% critical

(10) Driven from ship's fuel consumption instrumentation

SECTION III

DATA ACQUISITION

HICAT BASES OF OPERATION

The data acquisition phase of the HICAT program was designed to obtain CAT search flights in various areas of the world over all types of terrain. Whenever possible the optimum season for high altitude CAT in a particular region was selected on the basis of the best available meteorological opinion. The actual selection of a particular base of operation was made by the Air Force, consistent with the requirements for U-2 operations. In the current (i.e., extended) program HICAT searches were conducted from the following bases:

- Royal Aircraft Establishment (RAE), Bedford, England, U.K.

- Barksdale Air Force Base, Shreveport, Louisiana, U.S.A.

- Loring Air Force Base, Limestone, Maine, U.S.A.

- Albrook Air Force Base, Balboa, Canal Zone (Panama)

- Patrick Air Force Base, Cocoa, Florida, U.S.A.

- Edwards Air Force Base, Edwards, California, U.S.A.

The schedule of HICAT operations is shown in Figure 4. Approximately one month of search flight operations was performed at each base.

HICAT PILOTS

The U-2 HICAT flights were performed by Edwards Air Force Flight Test Center V/STOL Operations Branch pilots under the command of Lt. Col. James J. King. Pilots flying HICAT missions in addition to Lt. Col. King were the following: Lt. Col. J. H. Ludwig, Majors T. H. Smith, A. P. Johnson, J. G. Basquez, K. J. Mason, and Captain R. E. Palmer.

HICAT FLIGHT SCHEDULING

When the program began, it was thought that HICAT flights would be made at optimum times during the day as determined by the field meteorologist. The realities of remote flight test operations and the limitations of meteorological forecasts resulted in some practical compromises. Aircraft, instrumentation, and weather permitting, flights were scheduled Monday through Friday as long as two or more pilots were available. (When only one pilot was available, as occurred part of the time in Maine and Panama, only three flights a week were planned.) Normally, HICAT flights were scheduled during daytime hours with

9

the takeoff at about 10:00 AM local time. For the few night flights that were made, takeoff was scheduled between 4:30 PM and 8:00 PM local time.

HICAT FLIGHT PROCEDURES

On the day of a flight, a flight plan was prepared, based upon a CAT forecast derived from the most recent weather observations. The pilot was then briefed on the high altitude CAT conditions predicted en route and any special flight tests to be performed.

If the flight was to be over water and more than 200 miles from land, an additional aircraft was required to patrol the search area to provide navigational aid and air rescue support. A C-97 Air Rescue transport was used for this purpose in England and Panama.

The flights usually began about midmorning, as mentioned above, and were of three to six hours duration. The instrumentation was operated continuously throughout the flight. The aircraft normally began the CAT searches at an altitude of about 50,000 feet. If no turbulence was encountered, the aircraft alternately climbed and descended at altitudes above 50,000 feet while en route. If significant CAT was encountered, fairly level straight runs were made through the turbulence. During these runs, the autopilot was turned off and control activity minimized. In order to define the CAT area an X-pattern was frequently flown.

Flight procedures differed somewhat in those HICAT tests coordinated with the meteorological investigations conducted by other organizations. Four tests were flown from Barksdale Air Force Base in conjunction with the National Severe Storms Laboratory (NSSL) of the Institutes for Environmental Research at Norman, Oklahoma. In these tests the HICAT aircraft was vectored by the NSSL radio back and forth over thunderstorm areas on the basis of ground radar observations.

Five tests were flown from Edwards Air Force Base in cooperation with the investigation of mountain waves conducted by the National Center for Atmospheric Research at Boulder, Colorado. The procedure followed for these tests required the aircraft to fly roughly east and west over the Front Range Mountains just west of Boulder or over the Sangre de Cristo Range west of Pueblo, Colorado. Successive runs of about 100 nautical miles length were performed while increasing the altitude in 3000-foot increments for each run above 50,000 feet.

CAT intensity was usually evaluated subjectively by the pilot as well as from a mechanical cockpit accelerometer. Pertinent weather observations (i.e., winds, clouds, etc.) were noted along with necessary flight and navigational information. On most flights the pilot also took 35mm color photographs of the clouds (if any) in the vicinity of the CAT area.

During many of the flights when the air was especially smooth, control pulses and smooth symmetric pitch maneuvers (roller coasters) were performed. This was done in order to check the polarity and behavior of the instrumentation as well as to check the efficacy of the gust velocity determination.

At the end of a HICAT flight, the pilot was debriefed by the Lockheed field
meteorologist and the Lockheed field engineer. These meetings were tape
recorded for later evaluation in conjunction with the meteorological analysis.
Also, immediately after the flight, the quick-look oscillograph record was
processed and examined. Turbulence penetrations were evaluated as well as the
performance of the instrumentation. Peak turbulence accelerations were deter-
mined at this time in order to classify the intensity of the CAT encounter and
for comparison with the pilot's notes.

HICAT SEARCH STATISTICS

As the Flight Test Log appearing in Appendix III shows, 106 HICAT test flights
were made totaling 477.6 flight hours. Of these flights, 92 were planned
searches for high altitude CAT, with 66 resulting in CAT encounters ranging in
intensity from light to severe. In addition, high altitude CAT was encountered
in 6 of the 14 incidental flight tests. The incidental flight tests or non-
search tests included aircraft check flights, instrumentation check flights, and
ferry flights. Overall, 18.3 hours of high altitude CAT were recorded, 17.8
hours resulting from planned searches based upon CAT forecasts. Figure 5
summarizes the relative success of HICAT searches at each of the bases of
operation. The figure indicates that on a percentage basis the Louisiana
flights encountered the largest amounts of CAT and the Maine flights the least
amount of CAT.

The following tabulation summarizes all the HICAT flight experience including
that from the Initial and Redirected HICAT programs:

HICAT Program	Test Period	Tests	Tests Encountering HICAT	Flight Hours	HICAT Hours
Initial	Feb 64 - Oct 64	33	17	94.5	7.4
Redirected	Oct 65 - Feb 67	146	84	649.5	29.2
Extended	Mar 67 - Feb 68	106	72	477.6	18.3
All	Feb 64 - Feb 68	285	173	1221.6	54.9

Track maps of the HICAT search flights in the current (Extended) program are
presented in Appendix VI along with a meteorological description of the condi-
tions at the time of each flight and pertinent pilot comments. Track maps for
the Initial program appear in Reference 4 and those for the Redirected program
are presented in Reference 5, Volume III.
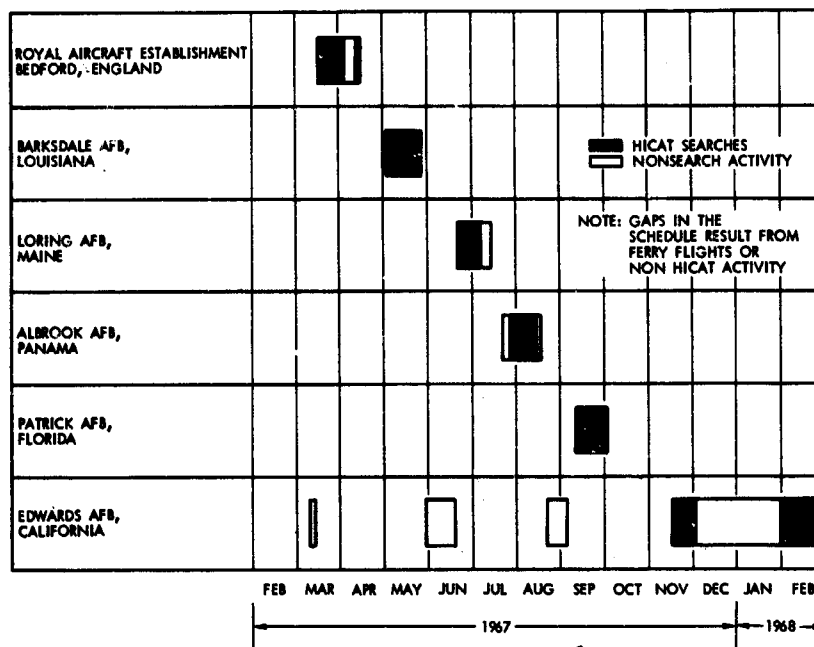
Figure 4   Schedule of HICAT Operations
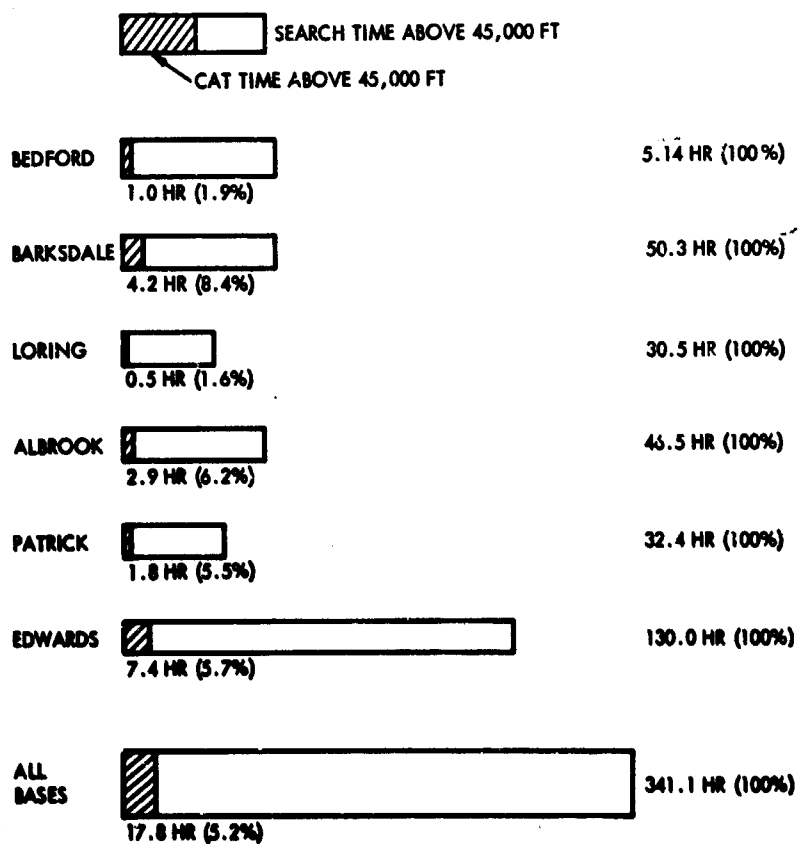
Figure 5   CAT Percentage in Search Flights by Base

SECTION IV

DATA PROCESSING

GENERAL

The purpose of the data processing phase of the HICAT program was to retrieve edited raw turbulence data recorded digitally on an airborne PCM magnetic tape, convert the data to a computer-compatible format on the HICAT PCM Ground Station, and then process it through a series of computer programs designed to provide data for a statistical analysis of high altitude clear air turbulence.

Automatic data handling techniques were essential in processing the large volume of data required for the HICAT program. The total amount of data processed was equivalent to about 18 hours of turbulence. This required the processing of approximately 70 million data points and the preparation of several thousand plots of gust velocity time histories and power spectra. An IBM System/360 Model 50/75 computer was used to process the data and to perform the statistical computations. A CALCOMP automatic plotter with magnetic tape input was used for the graphical presentation of the data.

DATA ACQUISITION

Flight test data were recorded simultaneously on both a PCM magnetic tape and an oscillogram. The PCM magnetic tape was used as the primary recording medium and the oscillogram was used for a quick-look evaluation of the test data and the instrumentation system by the field team.

After the postflight evaluation, all of the test data including the quick-look oscillogram, PCM magnetic tape, instrumentation and flight data sheets, track maps, meterological data, pilot's flight log and pilot's photos were transmitted to the HICAT project office at the Lockheed-California Company in Burbank, California, for distribution and processing. Figure 6 diagrams the data acquisition activities at the field site.

DATA OPERATIONS

In order to verify the quality of the PCM magnetic tape and check for possible malfunctions of the airborne PCM data acquisition system, the airborne PCM magnetic tape was played back through the PCM ground station as soon as it was received. The time recorded on the tape was checked by means of a translated visual display in terms of days, hours, minutes, and seconds. Each of the data channels was given a rudimentary check by means of a visual decimal display. Fourteen digital-to-analog converters on the ground station coupled to a direct-write oscillograph recorder could be used for further checking and

13
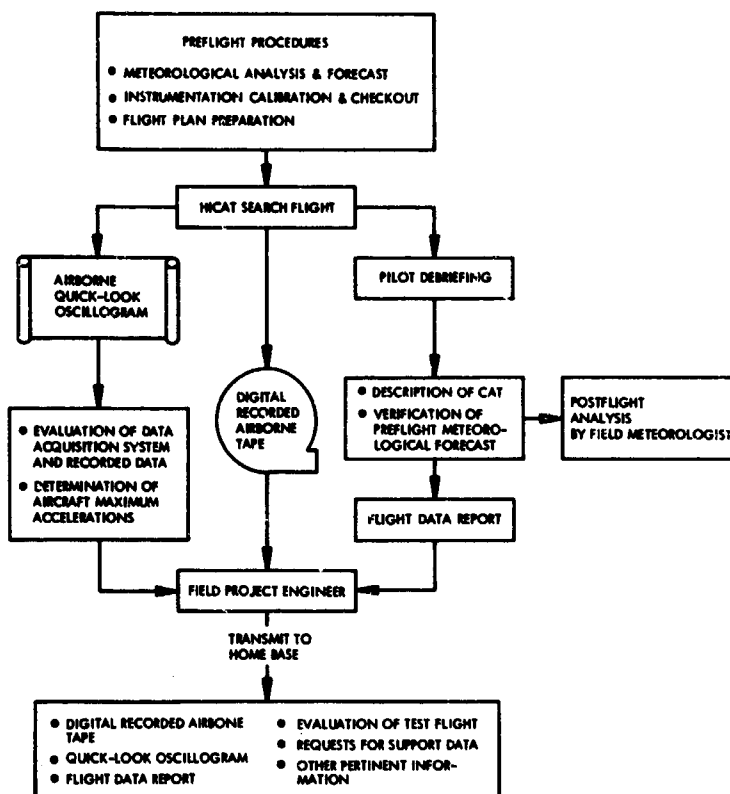
Figure 6 Data Acquisition Activities at the Field Site

troubleshooting. Notice of any instrumentation system malfunctions discovered in this checkout was immediately transmitted to the field team.

Instrumentation and flight data records received from the field team after each flight were appraised to obtain the current status of the instrumentation calibrations and configuration prior to the processing of any data.

DATA EDITING

The airborne oscillograph record was utilized to select data samples for computer processing. When the airborne oscillogram was unsatisfactory or missing, an oscillograph record was generated on the PCM ground station from the airborne magnetic tape. The editing process consisted of the following basic steps:

- Evaluation of instrumentation performance

- Selection of turbulence samples to be processed and determination of their start and stop times

- Determination of turbulence intensity and character

- Determination of aircraft attitude and control motions during CAT penetrations.

Details of the editing process from the analysis point of view are presented in Section V.

PCM DATA PROCESSING GROUND STATION

The editing results defined the tape sections to be processed by the PCM ground station. The ground station then performed the following functions: retrieval of data from the airborne magnetic tape, decommutation, digital-to-analog conversion with analog display, conversion of the data to computer-compatible format, and the recording of reformatted data onto computer magnetic tape. The flight data, originally recorded on tape at 1-7/8 inches per second, was played into the ground station at 30 inches per second, or 16 times the real-time recording speed.

A more detailed description of the ground station is provided in Appendix II of Reference 5.

COMPUTER SYSTEMS OPERATIONS

Six computer programs were designed to process and analyze the turbulence data recorded on the ground station output tapes:

1. Basic data program

2. Gust velocity program

3. Statistical analysis program

4. Spectral analysis program

5. Elevator response program

6. Numerical filtering program.

A detailed description of these programs appears in Appendix II.

Routine reduction of the turbulence data recorded on each ground station magnetic tape culminated in the production of two additional tapes corresponding respectively to the first two programs above: (1) an intermediate tape containing the reduced basic measurement samples in engineering units; and (2) a final output tape recording the variables, the derived equivalent gust velocity, and the 3-axis gust velocity components. The analysis programs (the third and fourth programs above) were designed to accept either of the two computer-generated tapes as their data source. The last two programs were used in a special investigation of selected turbulence samples. The elevator response program accepts the intermediate basic data output tape as its data source. The program generates a tape formatted identically to the intermediate basic

data tape except that it contains additional elevator response data. The numerical filtering program accepts the final gust velocity output tape as its data source. Its function is to numerically high-pass filter selected quantities from the final gust velocity output tape and generate an output tape containing these filtered parameters. This output tape is again formatted identically to the final output tape.

Figure 7 diagrams the operations required to convert the airborne tape to an edited and calibrated computer tape. Figure 8 indicates the sequential operations involved in the implementation of the various HICAT computer programs. The heavy lines indicate routine processing. The dashed lines indicate optional programs used for special investigations.

BASIC DATA PROGRAM

The basic data program utilizes the tape generated by the ground station to perform certain reduction functions for each measurement. In this process the program reads, disassembles, and translates the packed PCM data into a standardized computing format. The frame times were monitored to ensure that the correct time interval was maintained. The measurement samples were then calibrated into engineering units and error checked to detect and correct spurious data points. Finally, the calibrated measurement samples were low-pass filtered by applying selected sets of Martin-Graham numerical filtering
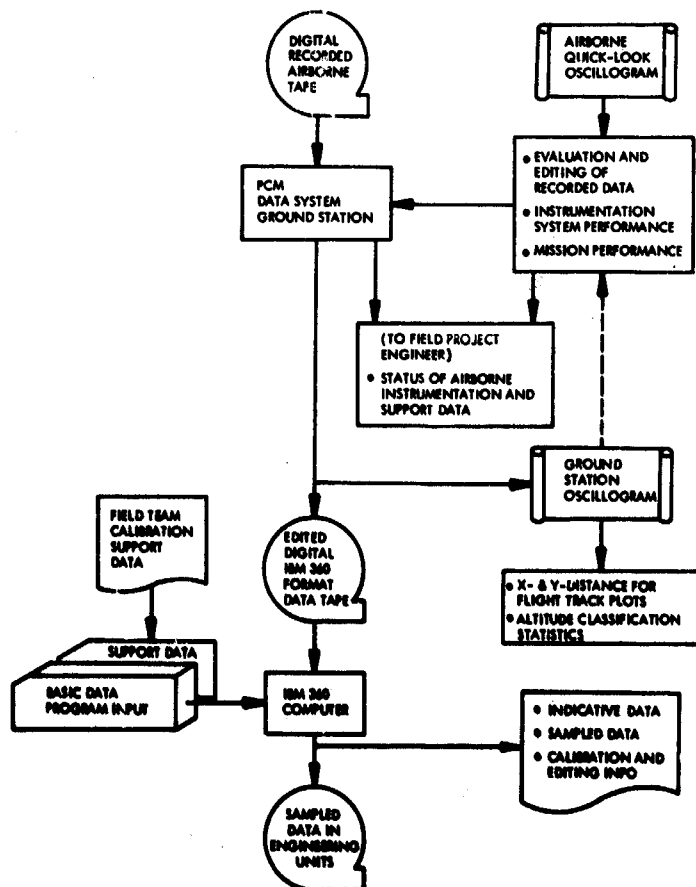
Figure 7 Airborne Tape Conversion Flow Chart
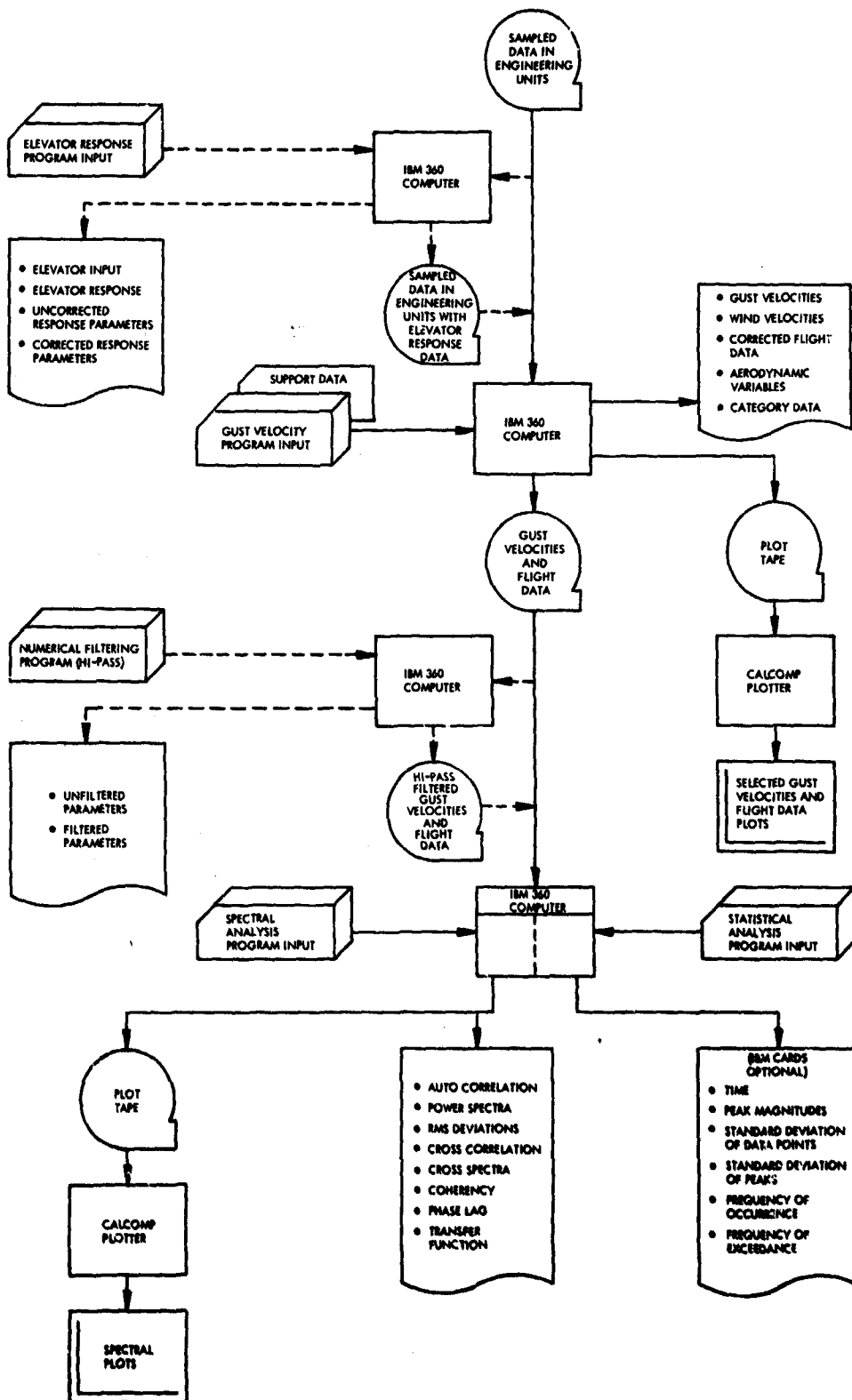
Figure 8 Data Processing Flow Chart

weights designed to pass only the useful frequency response range of each measurement. A description of the derivation and application of the numerical filters designed for HICAT data is given in Appendix II.

Upon completion of data reduction, the basic data were recorded on magnetic tape and also tabulated in a time series. When necessary, fully annotated time history plots of the basic data could be generated.

GUST VELOCITY PROGRAM

The gust velocity program used the tape generated by the basic data program to compute and output on tape the following parameters for the CAT data:

- Aerodynamic variables such as V_T, H_{pc}, t_a, M_T, etc.

- Derived equivalent gust velocity

- Gust velocity component terms

- Gust velocity vertical, lateral, and longitudinal components

- Wind velocity and heading.

The methods employed to determine these parameters are presented in Appendix II.

The gust velocity program was designed to compute the gust velocity components by several alternate methods utilizing various combinations of measurements. These options were made available so that some gust velocity components could still be obtained despite an instrument malfunction.

Time history plots of gust velocities and other parameters recorded on the final data tape may be generated as required.

STATISTICAL ANALYSIS PROGRAM

The runs found to be acceptable after reviewing the basic data were processed in the statistical analysis program. This program utilizes two statistical counting methods to determine the frequency of occurrence of "peaks" in the data. The two methods are described in considerable detail in Section V, as well as in Appendix II. Time series standard deviations (i.e., RMS values) were also computed in both counting methods. This information was computed routinely for cg normal acceleration and derived equivalent gust velocity in order to evaluate the turbulence intensity level.

SPECTRAL ANALYSIS PROGRAM

To define the statistical characteristics of the turbulence data in the frequency domain, the gust velocity components and other selected parameters recorded on the computer-generated tapes were processed through the spectral

analysis program. This program employed techniques developed by Tukey (Reference 7) to compute power spectral estimates. It is completely described in Appendix II. Tabular listings of the spectral data and spectral plots were automatically generated by this program.

ELEVATOR RESPONSE PROGRAM

Unit impulse time responses are used in this program to remove the effects of elevator motion from cg normal acceleration and derived equivalent gust velocity time histories. The data generated by the program is compatible with the other analysis programs. The program is described in Appendix II.

NUMERICAL FILTERING PROGRAM

This program was designed to apply a number of high-pass digital filters to the data contained on the final gust velocity tape. A discussion of the program is presented in Appendix II. The filtering program generates an output tape containing the desired filtered quantities in a format compatible with any of the HICAT analysis programs.

SECTION V

ANALYSIS AND DISCUSSION OF RESULTS

GENERAL

The HICAT program results are based upon flight measurements of aircraft cg acceleration response and the true or absolute gust velocity components together with measurements of the related aerodynamic and meterological variables. These measurements are compiled for analysis in statistical tabulations, time histories, peak counts, and gust velocity power spectra. A comprehensive presentation of all the HICAT measurements available for analysis is provided by the HICAT Test Summary, discussed briefly below and presented in Appendix I.

It is the purpose of this section to describe and analyze these results with emphasis upon the point of view of the aircraft structural designer. The main features of this presentation are the following:

- A description of the CAT data editing procedures and the equation used to compute gust velocities from the flight measurements.

- An examination, by geographical region, of CAT relative frequency of occurrence and intensity per flight mile within various altitude bands. This analysis is based mainly upon U_{de} peak counts determined from time histories of the aircraft cg acceleration response. The effect of elevator input upon U_{de} determination is described. True gust velocity peak counts are also analyzed.

- An evaluation of the true gust velocity power spectra utilizing two different averaging methods to obtain spectra for aircraft design. The representation of gust velocity spectra by various mathematically defined curves is also discussed.

- An examination of certain special statistical relationships of CAT to determine probability distributions of rms velocities for the three gust components, to determine the isotropy of the turbulence, and to evaluate the stationarity of the vertical gust velocity.

HICAT TEST SUMMARY

The HICAT test summary table, Appendix I, provides a brief tabular description of all high altitude CAT encounters in order by test and run number. Test conditions are summarized by tabulations of time, location, altitude, airspeed, temperature, heading and wind. The turbulence is classified by intensity and terrain, as well as by values of cg acceleration, derived equivalent gust velocity and true gust velocity. The table is intended to convey the scope of the results while at the same time characterizing each CAT run with sufficient detail to permit an independent assessment of the measured data.

Section V

DATA EDITING

The selection of CAT samples for data processing and analysis was based upon
an edit of the flight measurements recorded on the quick-look oscillogram.
Turbulence samples were selected primarily from an evaluation of the cg nor-
mal acceleration response of the aircraft. The acceleration sensitivity of
the oscillograph trace was approximately 0.9g per inch, which provided a
reading resolution of 0.01g. If continuous rapid cg acceleration disturbances
were observed in excess of ±0.05g, turbulence was considered to be present.
Small, high-frequency oscillations in the gust probe measurements normally
provided further evidence of the presence of CAT. Usually, the pilot would
confirm the presence of CAT by activating his oscillograph event marker.

A turbulent region as defined above was considered to be significant (i.e.,
worth processing) if frequent cg acceleration peaks of ±0.10g or more were
observed. In this event, sample[3] start and stop times were noted to the
nearest 5 seconds. An attempt was made to note all significant samples.
However, those turbulence patches of less than 10 seconds duration, corre-
sponding to about one mile in physical length, were usually ignored. CAT
encountered in turns, particularly unsteady turns, was usually excluded also.

Generally speaking, no special attempt was made to edit recordings that did
not contain the relatively rapid oscillations normally associated with the
confused mixing of turbulence (nearly always noted by the pilot). It was,
of course, recognized that some long wave phenomena (e.g., gravity waves or
undulance) might exist apart from those regions commonly identified as
turbulent. However, no such perturbations were observed except for those
rare oscillations caused by the pilot or by a malfunctioning autopilot.

Each edited sample was characterized by a subjective description of the CAT
in words as well as in terms of the estimated level of the cg acceleration
peaks. In general, the following classification, derived originally from
HICAT pilots' comments, was observed.

Frequently occurring peak g increment	CAT description
±0.05 to ±0.10	Very light (VL)
±0.10 to ±0.25	Light (L)
±0.25 to ±0.50	Moderate (M)
±0.50 to ±0.75	Severe (S)
±0.75 or greater	Extreme (X)

---

[3]After processing in the ground station, CAT samples are usually called runs
and referred to by a run number.

22

Figure 9 illustrates the relationship between the data editor's subjective evaluation of CAT intensity and the various measures of turbulence intensity, i.e., cg acceleration, derived equivalent gust velocity, and true (absolute) gust velocity. The measurements are rms values computed from time series data or, in the case of the vertical gust velocity, power spectral data.

As an aid to later analysis, the aircraft attitude during the turbulence penetration was noted, i.e., level, climbing, descending or turning. In this connection, average rates of climb or descent less than about 400 feet per minute were considered to be level.

Frequent or excessive use of the controls as evidenced by changes in control surface positions or fuel flow rate were also noted. Relatively slow, large-amplitude motions of the elevator were suspect if the turbulence was very light and occasionally resulted in a CAT sample being passed over.

DISTRIBUTION OF TURBULENCE BY ALTITUDE

The amount of turbulence encountered in a given altitude band obviously depends upon the amount of turbulence which naturally occurs in the particular band as well as the time or distance searched within the band. Figure 10 graphically depicts the number of miles flown in 5000-foot altitude bands above 45,000 feet for each base of operations and for all bases and for all bases including data from the Redirected program. Figure 11 shows the number of miles of turbulence encountered in the same altitude bands in similar fashion.

These two figures considered together appear to indicate a possible increase in the occurrence of turbulence in the 50,000 to 55,000-foot band when all bases are considered.

GUST VELOCITY TIME HISTORIES

The gust velocity time histories are presented in Appendix IV, Volume II. A gust velocity time history is shown corresponding to each run for which gust velocity power spectra are presented in Appendix V.

A typical gust velocity time history appears in Figures 12 and 13. The first figure presents time histories of the three gust velocity components along with derived equivalent gust velocity, corrected pressure altitude and ambient air temperature. The second figure shows the associated time histories of true airspeed, roll angle, aircraft heading, elevator position, cg longitudinal acceleration, and cg normal acceleration.

Determination of Absolute Gust Velocity Components

The determination of the absolute gust velocity components of atmospheric turbulence from an aircraft requires the measurement of (1) the motion of the air disturbances with respect to the aircraft and (2) the motion of the aircraft with respect to the ground. In the HICAT instrumentation system the air disturbances relative to the aircraft are measured with a gust probe; the aircraft motion relative to the ground is determined by an inertial platform.

23
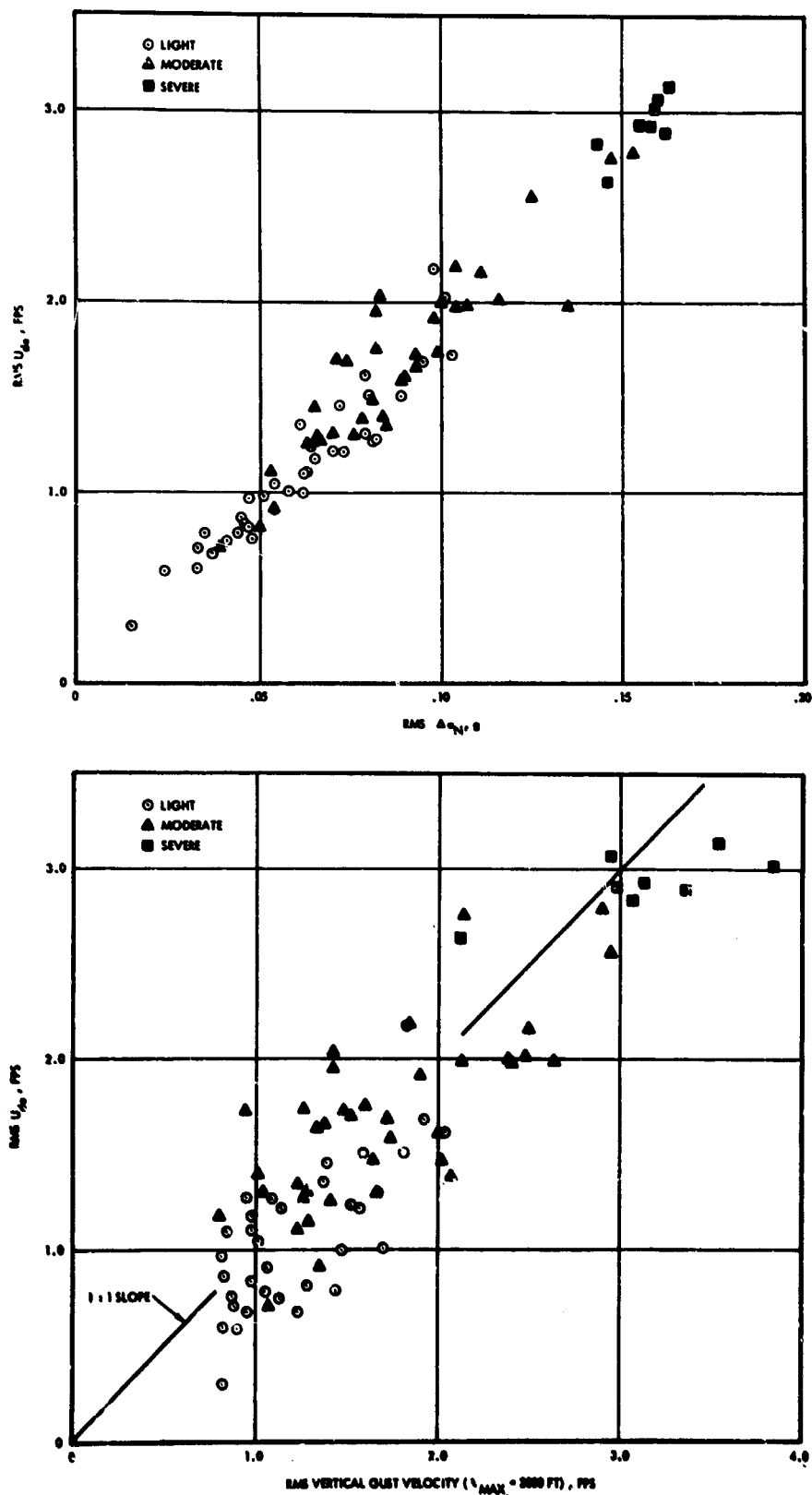
Figure 9   Subjective CAT Intensity Evaluations Compared with
Measured RMS Gust Velocity Parameters
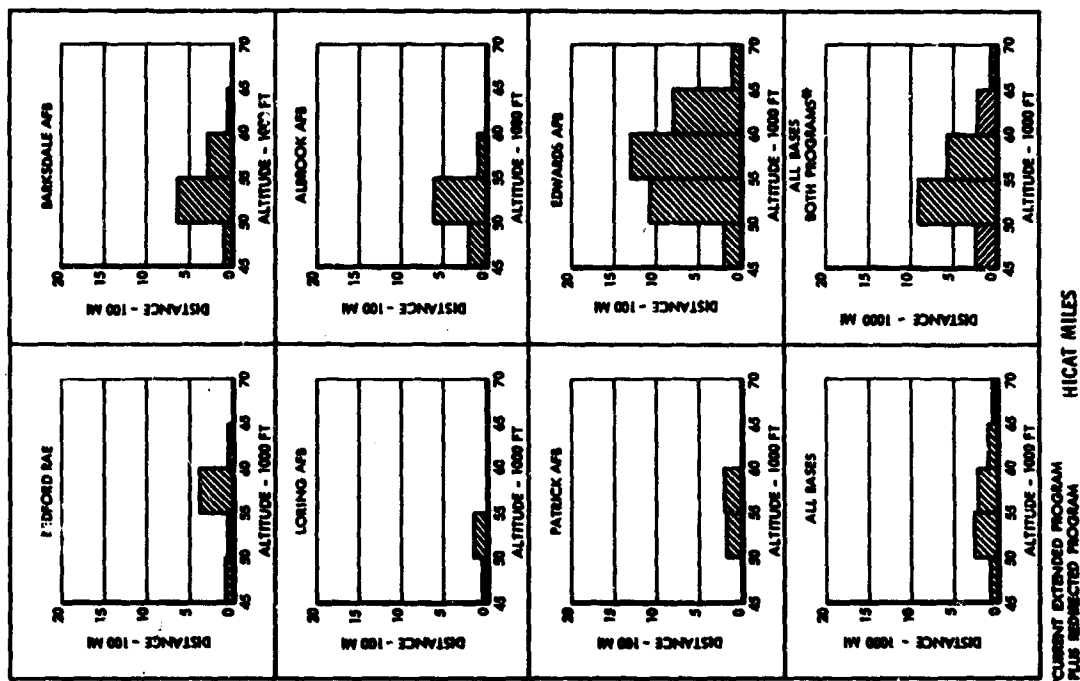
Figure 11 Distribution of CAT Miles by Altitude Band for Each Base
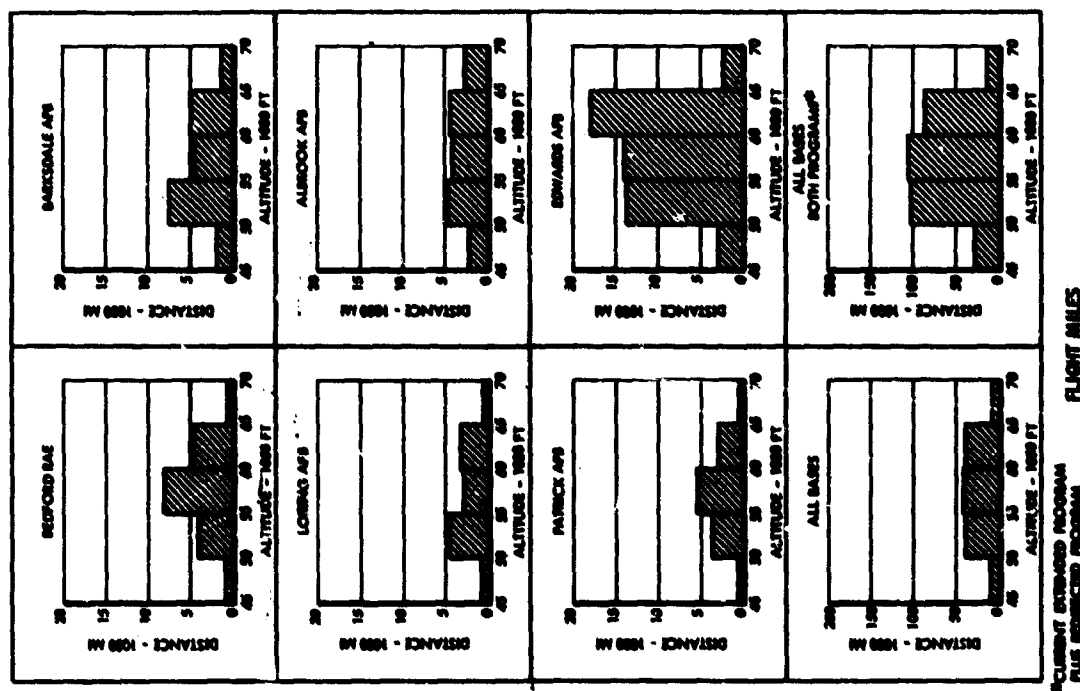
Figure 10 Distribution of Flight Miles by Altitude Band for Each Base
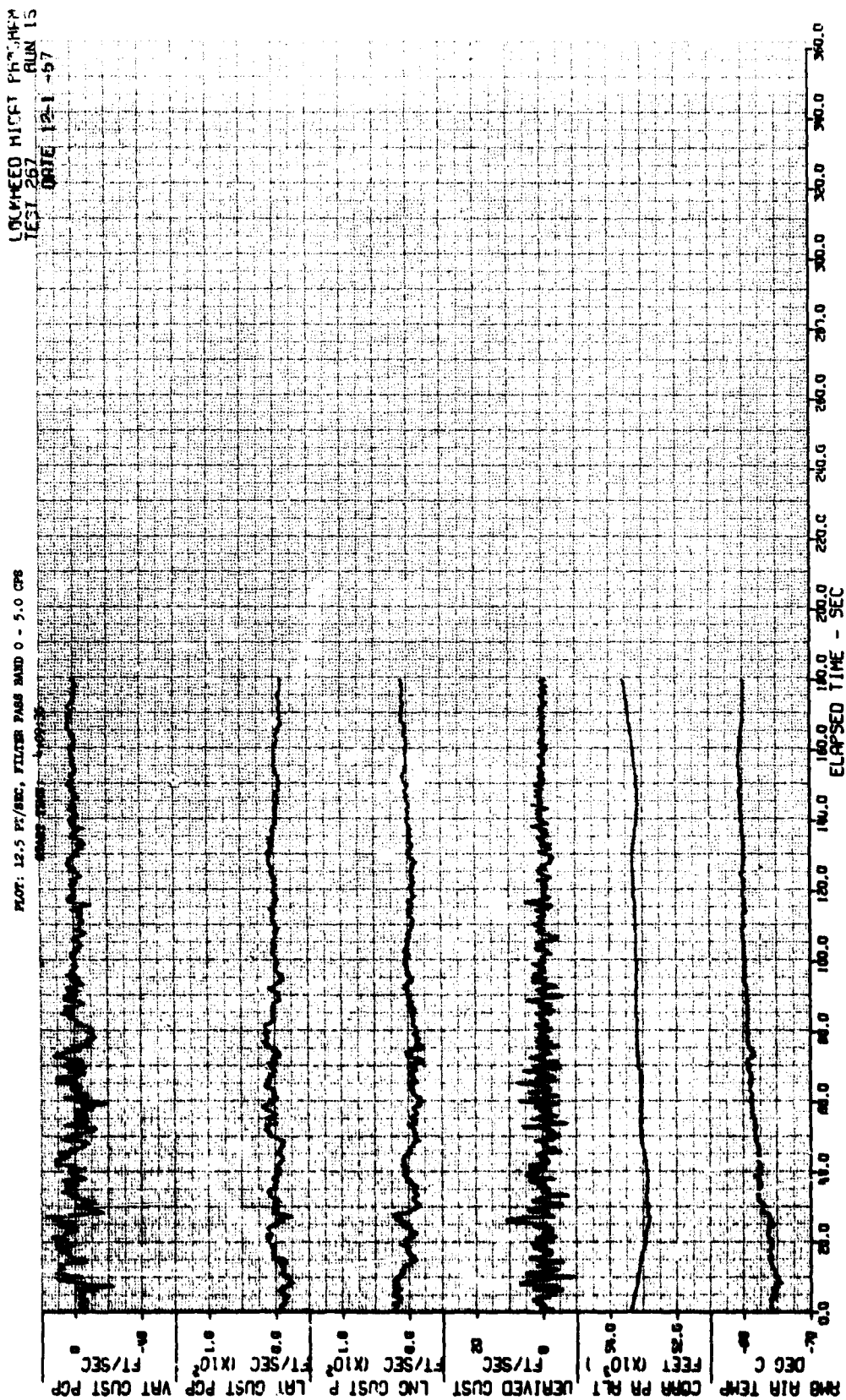
Figure 12 Typical Time History of Gust Velocities
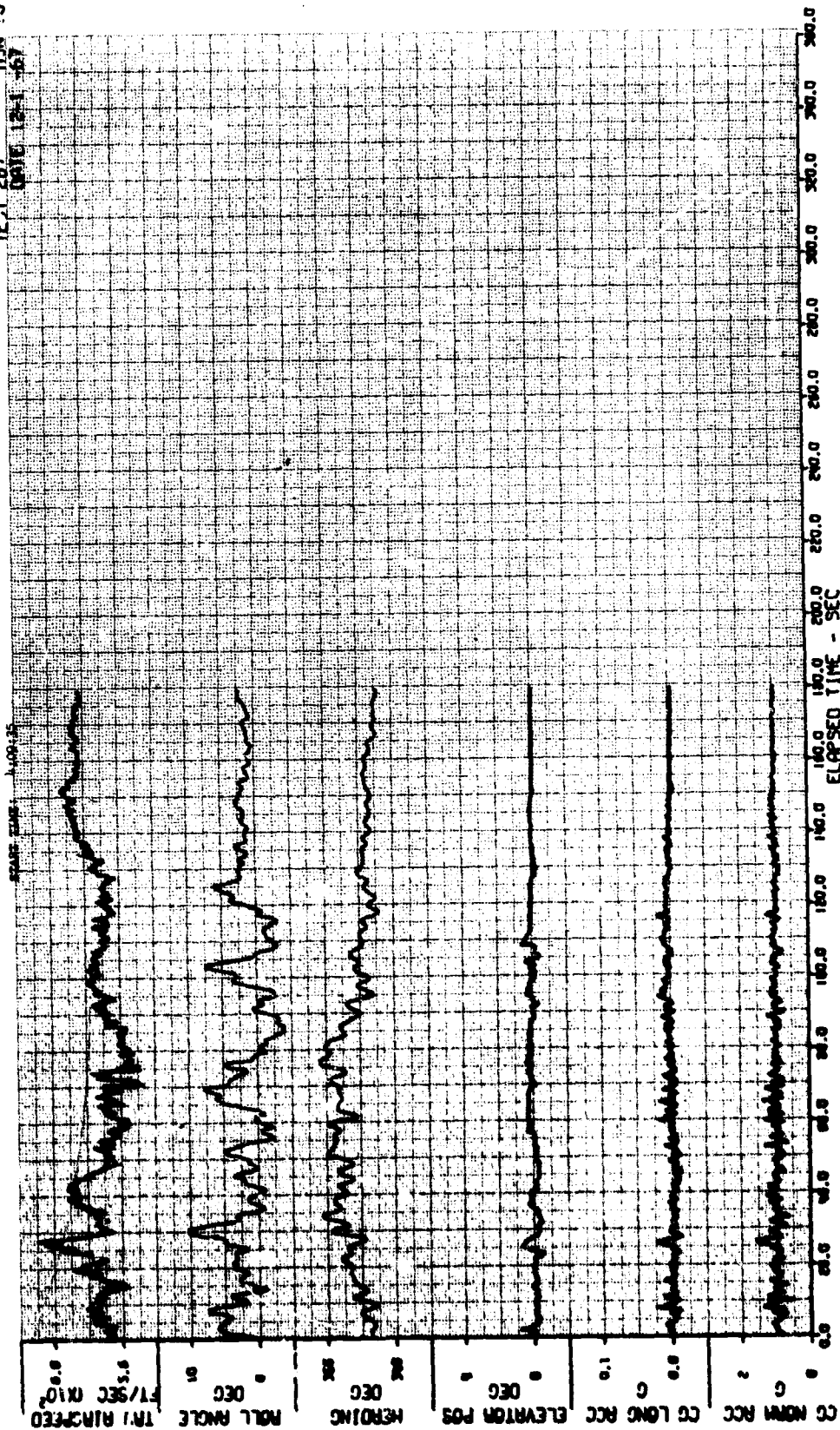
Figure 13 Typical Time History of Flight Parameters

The basic equations used to determine the vertical, lateral, and longitudinal gust velocity components from the HICAT measurements are given below:

$$U_V = V_T \Delta\alpha + V_T \Delta\beta\Delta\phi - V_T \Delta\theta + \int \Delta a_Z dt + L_X \Delta\dot\theta$$

$$U_L = V_T \Delta\beta - V_T \Delta\alpha\Delta\phi + V_T \Delta\psi - \Delta V_{X'} \cos\overline\Lambda + \Delta V_{Y'} \sin\overline\Lambda + L_X \dot\psi$$

$$U_F = \Delta V_T - \Delta V_{X'} \sin\overline\Lambda - \Delta V_{Y'} \cos\overline\Lambda$$

The Δ's indicate zero-mean quantities. Linear trends are removed from the gust components after all the terms are summed. When inertial platform measurements were defective, independent acceleration and rate gyro measurements were used to compute the gust velocities as described in Appendix II. The derivation of all of the gust velocity equations is given in Appendix IV of Reference 5.

Determination of Derived Equivalent Gust Velocity, U_{de}

The derived equivalent gust velocity is a fictitious gust velocity inferred from measured airplane cg normal accelerations. The concept has been used for many years to determine airplane structural design loads and accelerations for gust conditions. It is based on a simple theory in which the following major assumptions are made:

- The airplane is rigid.

- The airplane is free to rise but not pitch.

- The airplane is in steady level flight prior to entry into the gust.

- The gust velocity profile is a one-minus-cosine shape with a length of 25 wing chords.

Under these assumptions, the maximum airplane acceleration, in g's, is given by

$$\Delta a_{N_{max}} = \left[\frac{C_{L_\alpha} \rho_0 S V_e K_g}{2W} \right] U_{de} \tag{1}$$

or, conversely,

$$U_{de} = \left[\frac{2W}{C_{L_\alpha} \rho_0 S V_e K_g} \right] \Delta a_{N_{max}} \tag{2}$$

where

$$K_g = \frac{.88\mu_g}{5.3 + \mu_g} \qquad\qquad (3)$$

$$\mu_g = \frac{2W}{C_{L_\alpha} \rho c g S} \qquad\qquad (4)$$

In equation (2), U_{de} is the maximum gust velocity in the one-minus-cosine profile. The subscript "d" in U_{de} stands for derived and the "e" for equivalent.[4] It emphasizes the fact that when U_{de} is obtained from flight-measured cg normal accelerations using equation (2), it is not an actual gust velocity but a derived equivalent quantity. U_{de} can be interpreted as the gust velocity that would produce the measured value of $\Delta a_{N_{max}}$ if the restrictions contained in the basic assumptions were met. One assumption that is not even closely met is that pertaining to gust shape; the simple one-minus-cosine shape of fixed length bears little resemblance to the actual complex gust velocity profiles measured in the atmosphere. Nevertheless, it has been found that this highly simplified theory gives a very good indication of the relative acce erations experienced in turbulence by various airplanes. As a result, it has been a very useful design tool. If statistical data on cg accelerations of existing airplanes are converted to U_{de} form by means of equation (2), then the acceleration experience of a new airplane can be predicted by means of equation (1). This approach has been used for many years both in establishing design loads and in defining repeated loads spectra for fatigue analysis; only recently has it been supplemented by newer theories that are more precise both in their description of the gust pattern and their treatment of the airplane dynamics.

It is clear, however, that the derived equivalent gust velocities inferred from cg accelerations are, in fact, fictitious gust velocities that bear little relation to actual gust velocities that might be measured directly. It is also clear from the above derivation that U_{de} should be regarded as applying only to peak values, obtained from the measured peak values of Δa_N. As a matter of convenience, however, it has become common practice to apply the bracketed term on the right-hand side of equation (2) to the entire Δa_N time history and to designate the resulting variable U_{de}. Thus, when peak values are read from the time history, no further conversion is necessary. Also, this term can be regarded as a normalizing factor which places not only peak values of acceleration, but acceleration time histories as well, on a common basis largely independent of the characteristics of any individual airplane. In the HICAT program a time history of U_{de} is computed for each run from the measured time history of cg normal acceleration. Average values are used during a run for all quantities in the expression for U_{de} except Δa_N.

---

[4] $U_{de} = U_d (\rho/\rho_o)^{1/2}$, so that at sea level U_{de} is equal in magnitude to the derived gust, U_d.

29
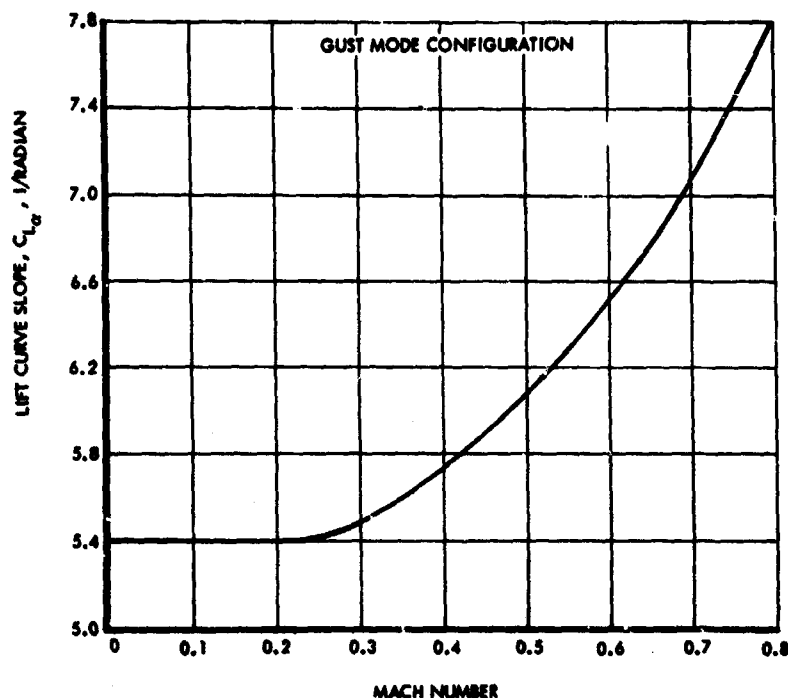
Figure 14 HICAT Aircraft Lift Curve Slope Versus Mach Number

The variations during any single run of these other quantities are generally small enough to have a negligible effect on the values of U_{de}. Values of S, c, and C_{L_α} used in calculating U_{de} were as follows:

$S = 600 \text{ ft}^2$,

$c = 8.4 \text{ ft}$,

C_{L_α} as shown in Figure 14.

PEAK COUNT AND EXCEEDANCE DATA

Objectives

The gust velocity peak count analysis has two objectives:

- Determination of the level of turbulence encountered and correlation with existing published data, particularly the VGH data presented for the U-2 in References 2 and 8.

- Determination of the stationarity of turbulence (as traversed by the airplane) by comparing HICAT cumulative peak count distributions with peak count distributions given by theory for a stationary Gaussian process (Rice's equation).

In support of the first objective, primary emphasis was placed upon peak counts of the derived equivalent gust velocity, U_{de}. Relatively complete U_{de} peak counts were obtained. Peak counts of absolute gust velocities were also obtained. However the number of such peak counts was limited for the following reasons:

(1) The very long wavelength components of the turbulence corresponding to frequencies of 0.015 cps or less can contribute substantially to the peak count data, yet are of uncertain validity because of instrumentation resolution limitations.

(2) With high pass filtering performed to remove the very long wavelength components from the data, the resulting peak counts depend upon the filter used. The proper interpretation and use of such peak counts is not evident at this time. It is not clear how such peak counts might be used directly in developing design criteria, and inasmuch as the filter characteristic is quite arbitrary, valid comparisons with peak count data obtained in other programs would depend upon agreement as to the filter to be used.

(3) To date, gust velocity peak counts have been of value chiefly in establishing gust intensity statistics from VGH data for normal operations. In the HICAT programs, there has been no attempt to obtain either a random sample of the atmosphere or one that would simulate normal aircraft operations. Consequently, in this program, extensive peak counting has been considered to be of secondary importance, and the measure of relative turbulence intensities given by the HICAT U_{de} peak counts is considered adequate.

As a result, peak counting of absolute gust velocities was confined to a few of the more severe turbulence encounters.

In support of the second objective, determination of CAT stationarity, peak counts were obtained of both U_{de} and the vertical component of absolute gust velocity for a number of representative runs.

Procedures

Two different procedures, described below, were used in peak counting the HICAT data.

Mean Crossing Count - In the first procedure, peaks were defined as maxima occurring between adjacent zero crossings, based on the time history after removal of linear trends. This definition is a very simple one that has been used quite generally. In obtaining the peak count, the peaks were classified by absolute magnitude within various intervals - that is, both positive and negative peaks were included and combined. The numbers of peaks falling in the various intervals were then accumulated, starting with the highest interval. Thus the resulting peak count curves give the number of peaks in excess of any given value of the parameter counted.

Positive Slope Level Crossing Count - In the second peak counting procedure, the number of positive slope crossings of positive levels defines the number of peaks in excess of that level. Similarly, negative slope crossings of negative levels define negative peaks[5]. This peak counting technique is inherently cumulative, so that a cumulative sum is obtained by simply combining the counts of positive and negative peaks. This technique gives the kind of peak count that is predicted theoretically for a stationary Gaussian process by Rice's equation, as discussed in this section under Stationarity. Comparison of peak count curves obtained in this manner with the corresponding theoretical curves given by Rice's equation for the same runs provides information that can be extremely important when measured gust velocity rms values are used in establishing a model of the atmosphere for design use.

Classification Intervals - The classification intervals for both peak counting techniques were 0.05g for Δa_N and 1.0 foot per second for U_{de} and absolute gust velocity. In order to eliminate the counting of many insignificant peaks in the mean crossing method, a threshold was established about the mean equal in magnitude to ±10% of the basic counting interval. However, since the emphasis in the positive slope level crossing count is upon the frequency of occurrence of peaks of all sizes at all levels, no threshold was used.

Comparison of Results Using Mean Crossing and Positive Level Slope Crossing Procedures - The peak counting procedure that is most preferred for relating actual peak counts to available theory, as noted above, is the positive slope crossing procedure. On the other hand, frequency of exceedance data are often available only on a mean crossing basis. In fact, peak counting of the vast body of VGH data would probably be quite difficult on any other basis. Consequently, it is of interest to compare the results of the two types of count.

---

[5]Both positive and negative crossings of the zero or reference level are counted.

Such comparisons are shown, for a representative collection of runs, in Figures 15 and 16. The particular runs chosen are those used in the investigation of stationarity later in this section.

Figure 15 shows the effect of the peak counting procedure on U_{de} peak counts. The curves given by the two methods will usually coincide at both ends. The number of positive-slope zero crossings is equal or within one count of the total number of individual positive peaks, and usually the one highest peak will define the same point on both curves.[6] In between, the "positive-slope level crossing" curve is always higher than the "mean crossing" curve. This relation must hold because wherever the time history reaches a maximum, decreases through a level (but not to zero), and then increases through the level to another maximum, there will be only one mean crossing peak but two positive slope level crossings.

The closeness of the curves given by the two procedures is somewhat variable, but generally the agreement is very good. The maximum difference between the two curves on the frequency-of-exceedance scale ranges from a factor of 1.10 for case 107-14 to 1.40 for cases 102-2, 266-12, and 266-17.

Inasmuch as the U_{de} peak counts are frequently distorted by pilot inputs to the elevator, it is of interest to compare the peak counting procedures also on the basis of high-pass-filtered time histories of the absolute gust velocity. Such comparisons are shown in Figure 16. The time histories used were of the vertical component of the gust velocity and were high-pass filtered using the 7000-ft filter described under "Peak Counts of Absolute Gust Velocity" later in this section. The filtered time history of absolute gust velocity is a quantity that should be roughly comparable to U_{de}. Ideally, U_{de} also results from high-pass filtering of the absolute vertical gust velocities, where, in this case, the filter is the airplane. The difference between the peak count methods is a little greater in Figure 16 than in Figure 15, whereas one might have expected it to be less because of the absence of any effect of pilot action. In Figure 16, the maximum difference between the two curves on the frequency-of-exceedance scale ranges from a factor of 1.20 for case 147-4 to 1.9 for case 220-10.

The smaller difference between methods for the U_{de} data than for the U_v data may be related to the band width of the data. A very narrow band random time history will consist of successive cycles at almost constant frequency, which vary only gradually in amplitude. For such a time history, almost any conceivable peak counting procedure will give the same result. It is only where the time history contains a wide band of frequencies that rules are needed to define what is meant by a peak. The U_v time history has a band width extending from roughly 0.1 cps (the termination frequency of the high-pass filter) to 5 cps (the cutoff frequency of the low-pass filter). On the other hand, the U_{de} time history is confined to a considerably narrower band width. The termination frequency of the airplane as a high-pass filter is about 0.5 cps (as indicated by the frequency-response functions shown under the discussion of $\bar{A}$ Values for Use in Determining σ_w Distributions later in this section);

---

[6] Under certain conditions it is possible to have several crossings of the highest level with only one maxima.
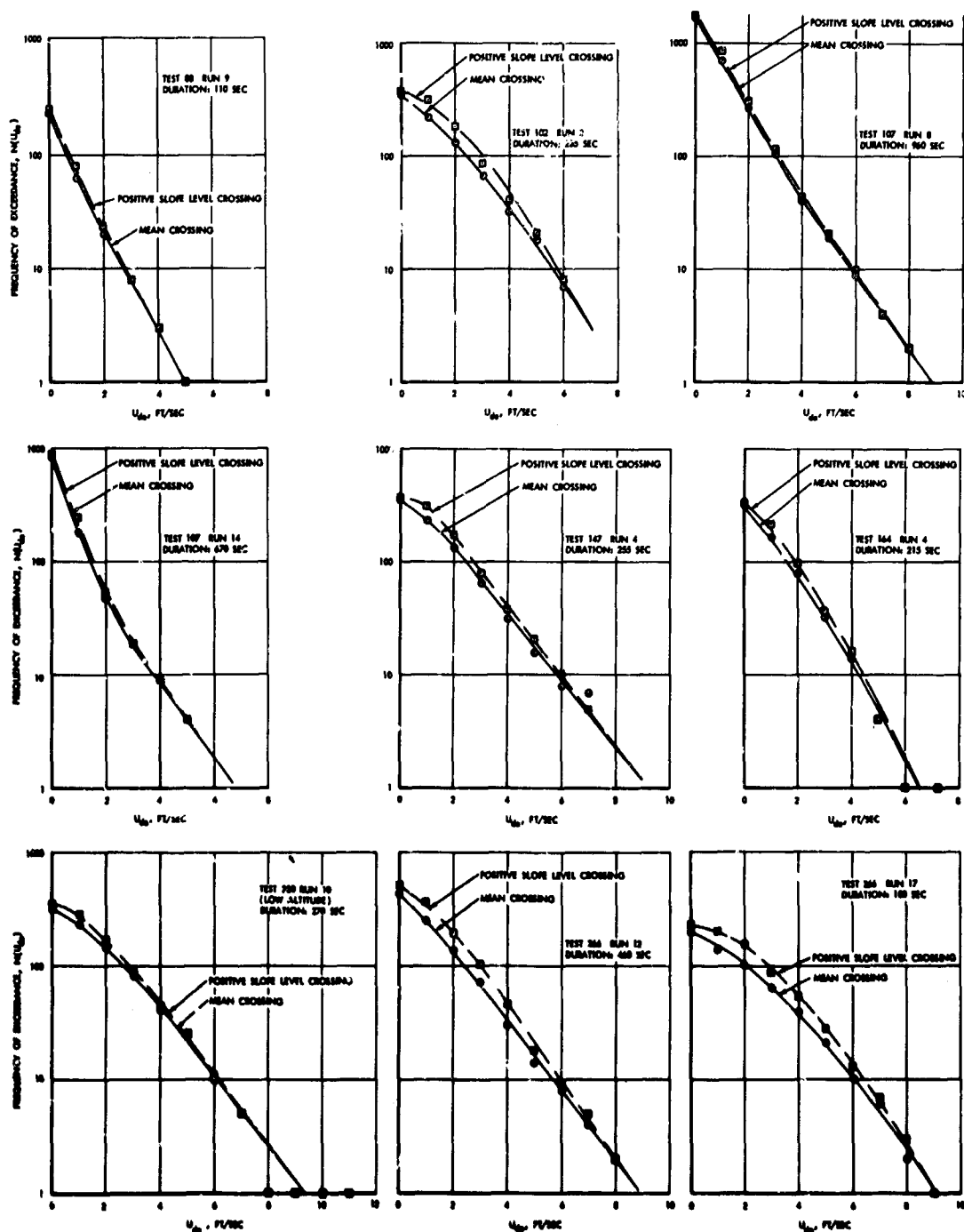
Figure 15   Comparison of Frequency of Exceedance of U_{de} Based on Positive Slope Level Crossing and Mean Crossing Counts
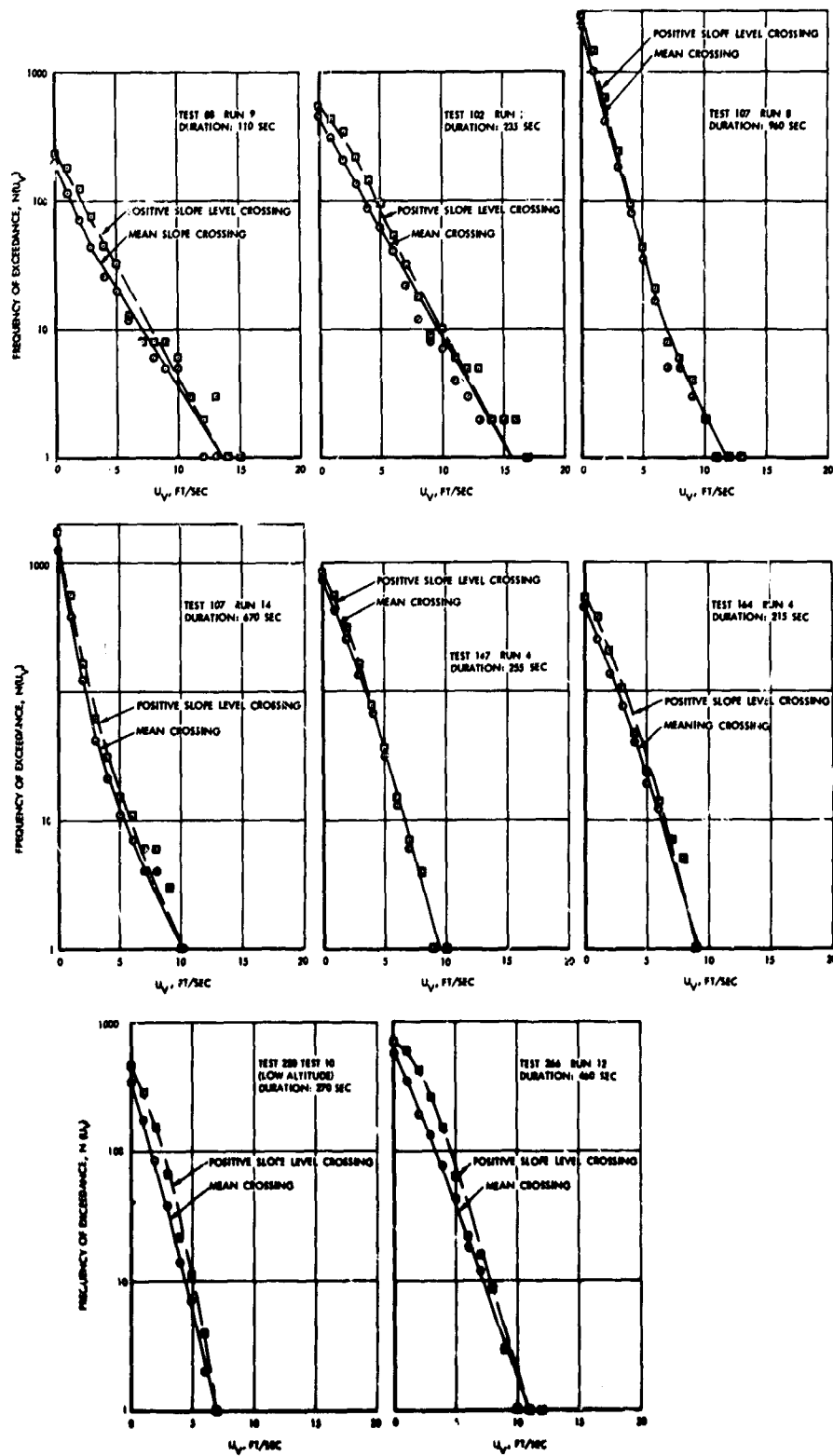
Figure 16 Comparison of Frequency of Exceedance of U_V (7000-ft
High-Pass Filtered) Based on Positive Slope Level
Crossing and Mean Crossing Counts

35

and the low-pass filter cutoff frequency used in obtaining cg normal acceleration and U_{de} is 3 cps. Thus there is some reason to expect a smaller difference between methods for the U_{de} peak counts than for the absolute gust velocity peak counts.

U_{de} Peak Counts

The U_{de} peak count data presented herein represent virtually all of the turbulence encountered during the 1965-1967 and 1967-1968 HICAT programs. A limited amount of turbulence data, however, was not included for a variety of reasons. Peak counts were obtained only for the portions of the flight records identified as runs, as explained under Data Editing.

Difficulties with the airborne instrumentation precluded obtaining peak counts from some runs. Peak counts were not obtained for runs in which maneuvering was conspicuous and led to load factors that could be misinterpreted as significant gust response. As noted earlier, the oscillograph records were edited so as to provide runs containing reasonably continuous turbulence. Accordingly, some very short bursts of rough air were not classified as runs so peak counts were not made of these data. Finally, some runs contained measurement anomalies, caused by radio transmission interference or other electrical noise, which prevented their being processed. The data that were lost or discarded for these reasons amount to only a very small percentage of the total in the peak count summary and, hence, do not affect the conclusions regarding the peak count data.

HICAT peak count data were obtained during flights specifically directed toward locating and measuring turbulence. As a result, the HICAT data would be expected to reflect a more severe exposure than VGH data obtained in routine operations. The latter data would reflect a more random sampling of the atmosphere, or perhaps actually a bias toward less frequent and less severe turbulence. Such a bias could result from the use of turbulence avoidance procedures or from the possibility that operational missions would be less frequently carried out under the type of weather conditions likely to occur in conjunction with turbulence. Another factor that might augment the severity of HICAT encounters is that, in a number of instances, once a turbulent region was found, repeated passes were made through the same region in different directions. On the other hand, there were two or three occasions when the pilot maneuvered the aircraft out of the turbulence because of its severity.[7] As a result, for these cases some of the higher gust velocities may have been missed.

The miles flown in high altitude CAT are considered to be those "runs" defined under Data Editing. Generally, the criterion used as a guide in breaking the flight records into runs was that the cg acceleration trace be continuously disturbed (±0.05g) and exhibit frequent peaks in excess of ±0.10g,

---

[7]Severe turbulence in the sense that airframe fatigue load damage was possible although actual cg accelerations were well below limit values.

corresponding to an average U_{de} of about 1.7 fps. This criterion is, of course, arbitrary and quite subjective in its application. In fact, some of the very long runs needed to establish power spectral densities at the longest wavelengths included scattered regions in which no ±0.10g peaks occurred.

The U_{de} peak counts presented in this section were obtained by the mean-crossing method for consistency with the peak count data available from VGH recorders for operational flights. Flight miles are statute miles and were obtained from flight time by multiplying by an average airspeed of 700 fps.

Summary of Data by Location - The peak count data obtained from the 1965-1967 HICAT flights are summarized in Figure 17 taken from Reference 5. Figure 17 presents frequency of occurrence of derived equivalent gust velocity, U_{de}, per flight mile from each of seven bases of operation, together with the summation per total flight mile (statute).

The peak count data obtained from the 1967-1968 HICAT program are summarized in Figure 18. Figure 18 presents frequency of occurrence of derived equivalent gust velocity, U_{de}, per mile from each of six bases of operation, together with the summation per total flight-mile. It can be seen that the most severe turbulence in either program was encountered during the 1967-68 flights from Edwards AFB, California. The maximum measured incremental value of cg acceleration, 1.1g, resulted in a maximum value of U_{de} of 22 fps.[8]

Envelopes of the 1965-1967 HICAT and 1967-1968 HICAT date presented in Figures 17 and 18 are compared in Figure 19. Figure 19 clearly shows that on a flight-mile basis the 1967-1968 HICAT data contain much higher and lower levels of turbulence than the 1965-1967 HICAT data. The combined total for both programs is also shown.

Most Severe Individual Runs - The frequency of excecdance curves of U_{de} per flight mile for two of the HICAT runs in which the highest U_{de} and cg normal acceleration peaks were recorded are shown in Figure 20. Run 18 of Test 266 contains the highest peak, a cg acceleration increment of 1.1 and a U_{de} of 22 fps, recorded in the HICAT program. Run 14 of Test 266 does not include as high a single peak, but otherwise its exceedance curve is considerably more severe than that for Run 18.

These curves, particularly that for Run 14 of Test 266, exhibit a much shallower slope than shown in Figure 18 for either the average for Edwards AFB or the average for the entire 1967-68 HICAT program. This shallower slope indicates that the turbulence encountered in these two runs is much more severe than the average for all runs. The U_{de} peaks encountered in Run 14 of Test 266, for example, at a given frequency of exceedance per mile in turbulence, range from 2 to nearly 4 times as great as those shown by the curve representing the average of all of the Edwards AFB runs.

To obtain an indication of the cg acceleration peaks experienced in these runs, the U_{de} values can be divided by 20 to approximate the acceleration in g.

---

[8]This value occurred without significant elevator input and was associated with a true gust velocity increment of about + 40 ft/sec.
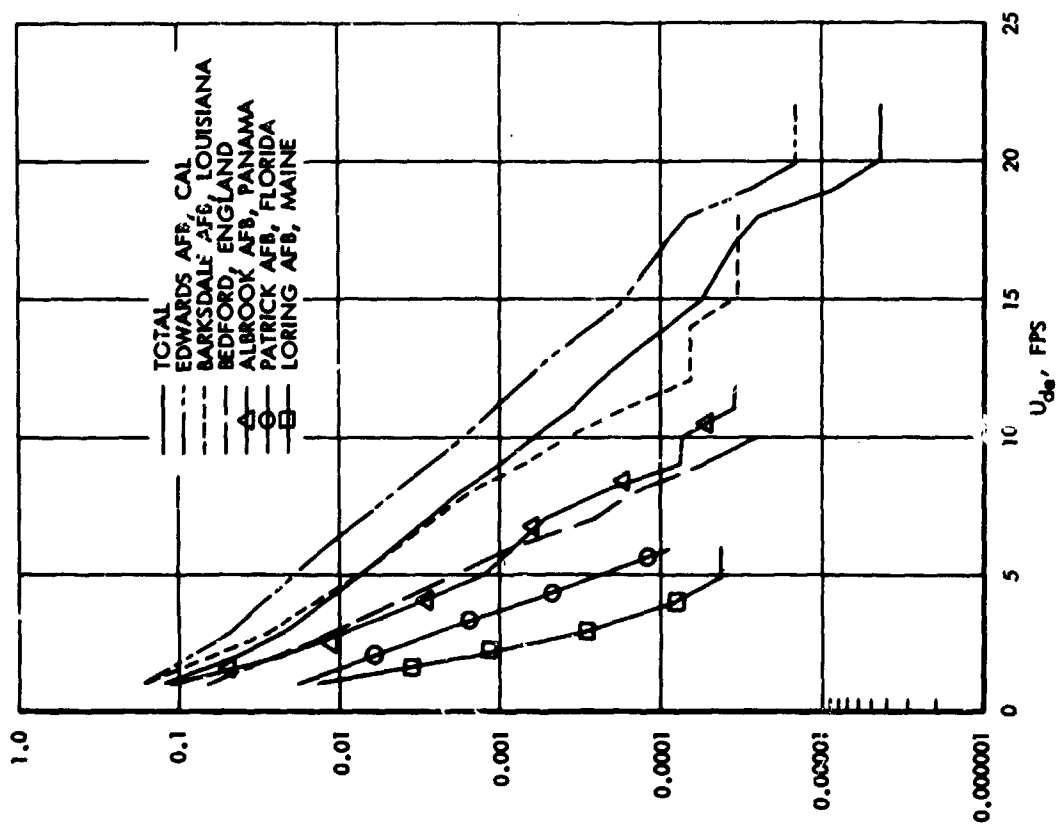
Figure 18   Frequency of Exceedance of U_{de} per Flight Mile, Various Locations, 1967-1968 HICAT
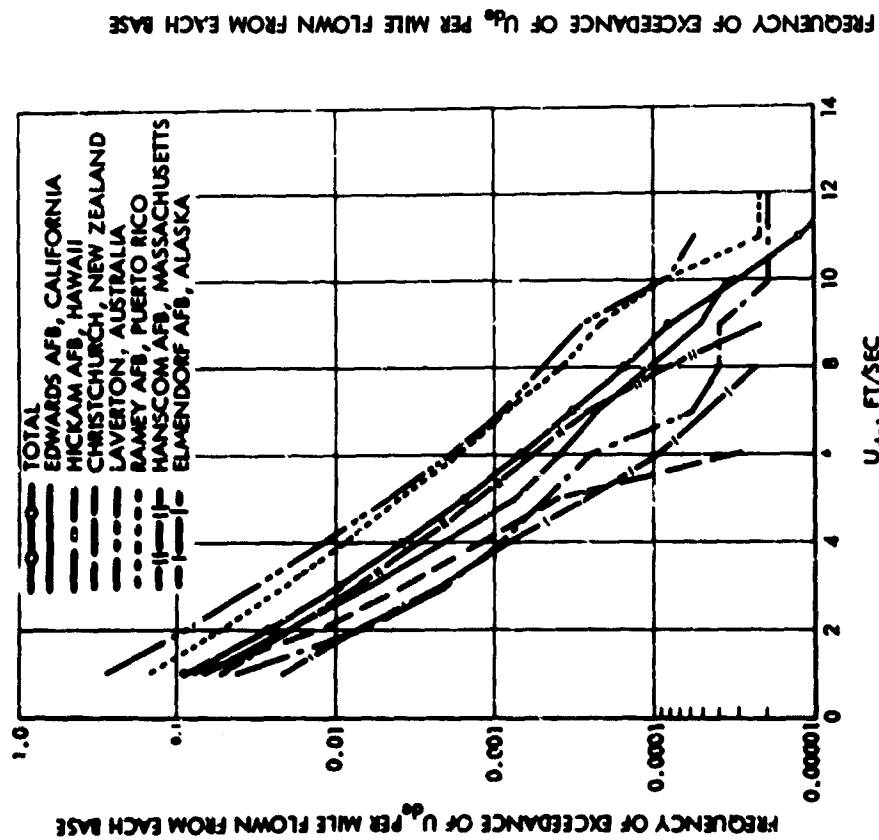
Figure 17   Frequency of Exceedance of U_{de} per Flight Mile, Various Locations, 1965-1967 HICAT

Figure 20 Frequency of Exceedance of U_{de} per Flight
Mile

Figure 19 Frequency of Exceedance of U_{de} per Flight
Mile, Various Locations - Comparison of
1965-1967 and 1967-1968 HICAT Envelopes

Effect of Altitude - A breakdown of frequency of exceedance of U_{de} by altitude bands is shown in Figure 21. All available data from both the 1965-1967 and 1967-1968 HICAT programs are included. The 50,000-55,000 foot band shows the highest turbulence levels. The turbulence level decreases as the altitude increases, with the exception of the lowest altitude band of 45,000 to 50,000 feet. The lower gust severity in the 45,000-50,000 foot band may reflect a real trend, or may be the result of an inadequate sample for this band.

Comparison with U-2 Operational VGH Data - Figure 22 presents a comparison by altitude band of the exceedance data obtained in both the redirected and extended HICAT programs with similar data obtained with VGH recorder during operational U-2 flights. The operational data were obtained in a continuing program, the first significant results of which were presented in Reference 2. The results shown herein were taken from Reference 8; they represent roughly three times as many miles of flight as the earlier reference. The flight miles represented by the HICAT data and by the operational data, in the pertinent altitude range of 50,000 to 70,000 feet, compare as follows:

Altitude Band, Ft	Flight Miles, HICAT	Flight Miles, Operational VGH
50,000-60,000	217,000	142,000
60,000-70,000	116,000	577,000
Total in these bands	333,000	719,000

As noted in Reference 2, the data sample available at that time reflecting operations over Japan showed turbulence of much greater severity than samples from other geographic areas. It was found, moreover, that the high gust frequencies shown for the Japanese operations resulted primarily from just two turbulence encounters, both at about 52,000 feet, over a total distance of 350 miles. The U_{de} frequencies of exceedance were therefore shown, in both References 2 and 8, separately with and without inclusion of the Japanese data, and are shown similarly in Figure 22.

Regardless of whether or not the Japanese data are included, both the HICAT data and the operational data indicate the turbulence exposure to be more severe for the 50,000-60,000 foot band than for the 60,000-70,000 foot band.

In the 60,000-70,000 foot band, and in the 50,000-60,000 foot band with the Japanese data excluded, the operational gust velocities are seen to be only about half as high as the HICAT gust velocities, at a given frequency of exceedance.

In the 50,000-60,000 foot band, even with the Japanese data included, the HICAT exposure is somewhat more severe than the operational exposure. The nearly constant vertical distance between the HICAT line and the operational VGH line (the two highest solid lines) suggests a different percent of time in turbulence. The indication is that the percent of time in turbulence was about three times as high in the HICAT flights as in the operational flights. Both the higher percent of time in turbulence in the HICAT program and the greater average severity of the turbulence encountered (as indicated by the shallower slopes) are consistent with the deliberate efforts in the HICAT program to find turbulence.

40
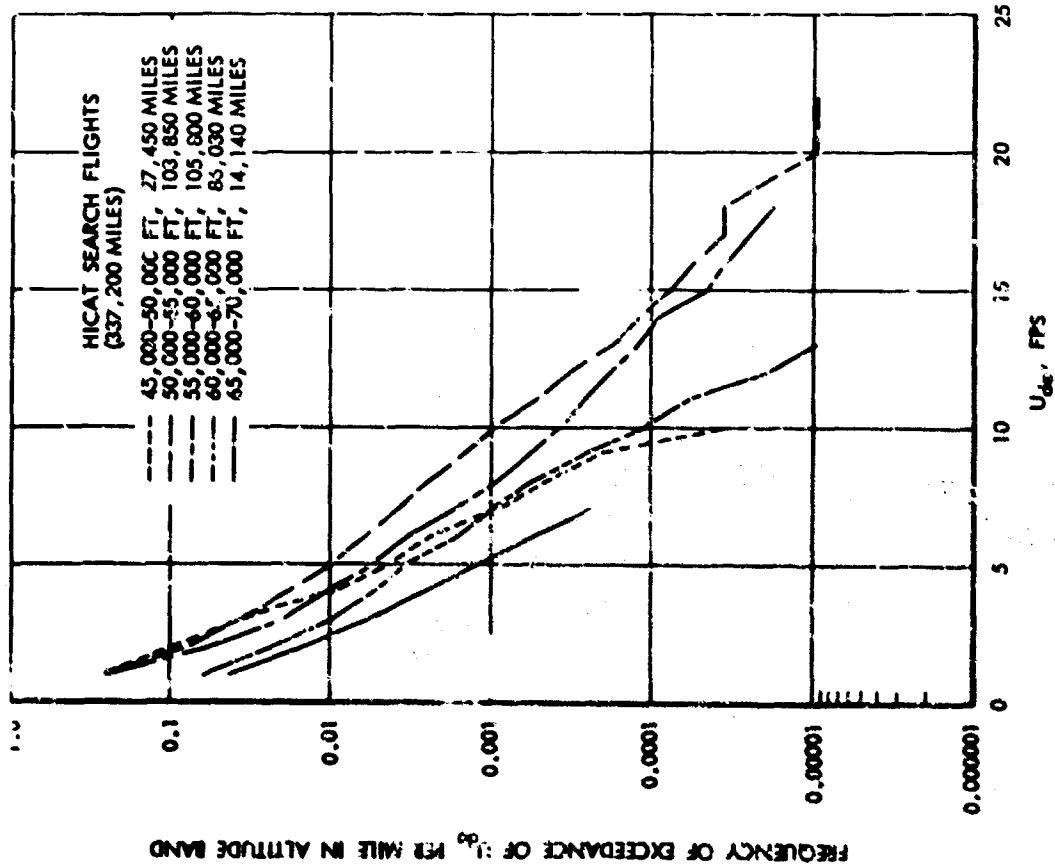
Figure 22 Frequency of Exceedance of U_{de} per Flight Mile for Two Altitude Bands, Comparison of HICAT With Operational VGH Data

Figure 21 Frequency of Exceedance of U_{de} per Flight Mile in Various Altitude Bands

Section V

Comparison with Current Design Requirements - Figure 23 presents the variation of U_{de} with altitude presently used in design of military aircraft (Reference 9). Superimposed on this figure are the maximum values of U_{de} obtained in the HICAT program to date, including the data from Test 33 reported in the HICAT interim report (Reference 4), as well as the data from the 1965-1967 and 1967-1968 HICAT programs. Approximately 436,000 miles have been flown in HICAT flights to date (including flights made before the program redirection), and the design values of U_{de} between 45,000 and 70,000 feet have not been exc ded. A signficant margin exists between the highest recorded value of U_{de} and the design value at the corresponding altitude.
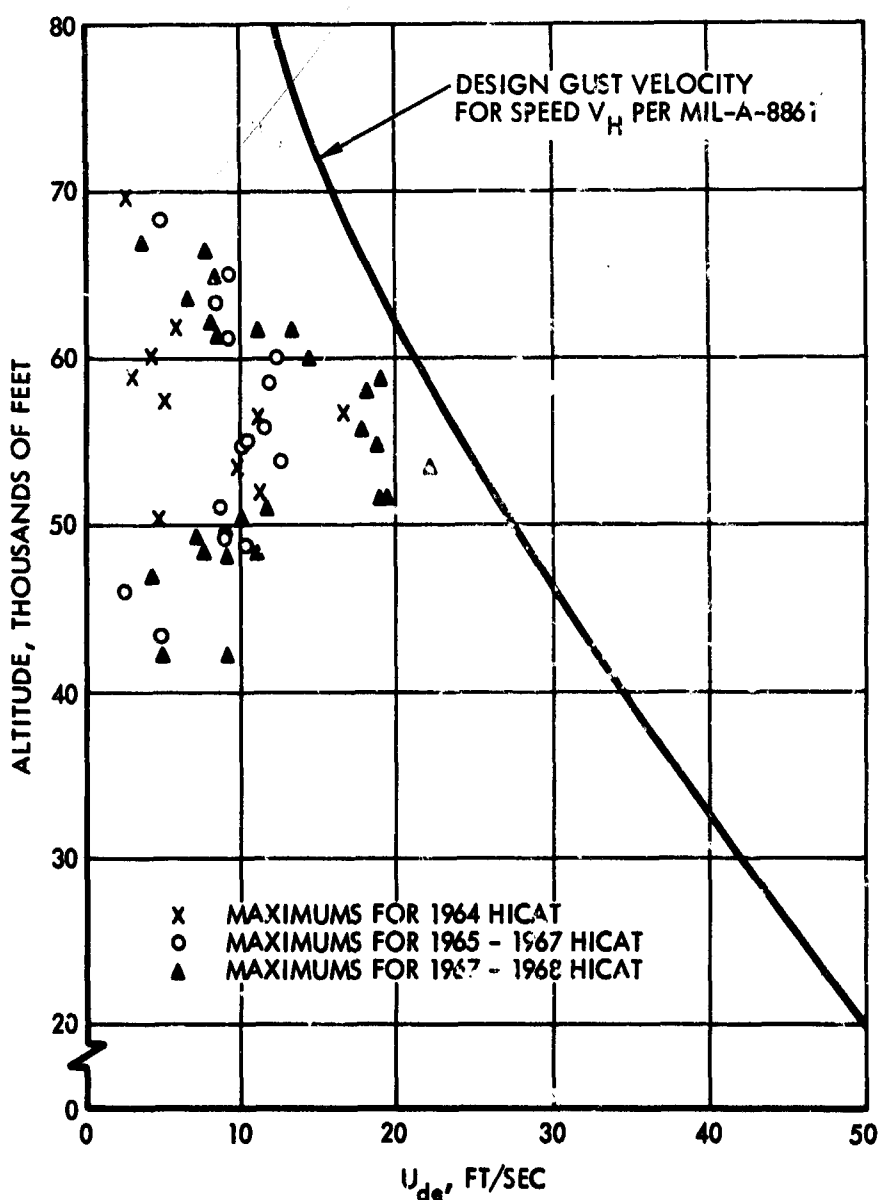
Figure 23 Comparison of Highest Measured U_{de} Values With Design Requirements

42

Effect of Elevator Motion on U_{de} Data

A striking feature of some of the U_{de} time histories obtained in the HICAT program is the occasional presence of "gusts" of unusual duration - 10 seconds or more - and substantial magnitude, as illustrated by the following sketch (a portion of Test 266 Run 12):

ELAPSED TIME, SEC
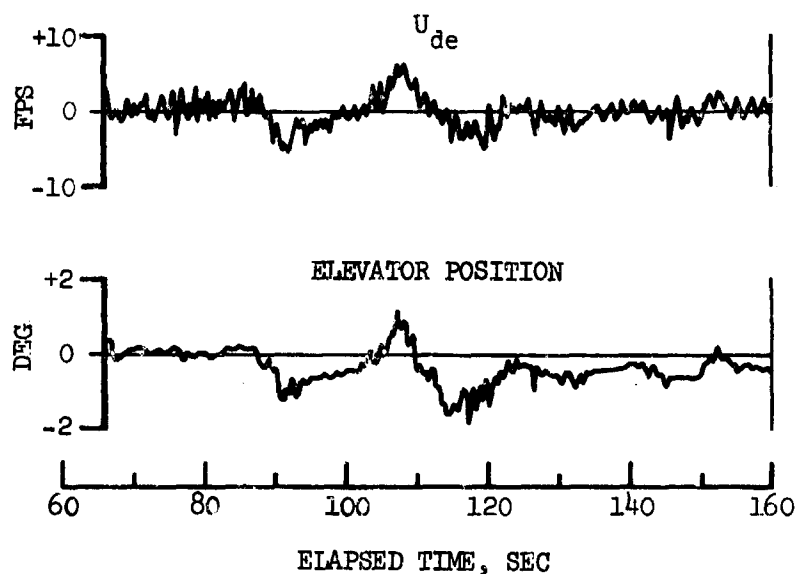
Three such "gusts" appear in this time history - alternately negative, positive, and negative - from time 90 to 120 seconds.

Gusts of this duration would be of little note in an absolute gust velocity trace. But U_{de} - the derived equivalent gust velocity - is simply the airplane cg normal acceleration multiplied by a constant. And the airplane response characteristics are such that, no matter what the duration of the gust, a significant acceleration in one direction ordinarily would not persist for longer than two or three seconds. Thus it is not surprising that the elevator position time history shown above apparently confirms that the U_{de} excursions result from a maneuver produced by the pilot.

If what is observed in this very short sample of one run characterizes the major part of the HICAT data, then the removal of the effect of the maneuver from the U_{de} time histories would have a significant effect on the U_{de} peak counts. Clearly, the highest peaks would be substantially reduced, and many more low peaks would be counted.

A quantitative evaluation of the effect on the peak counts of removing the maneuver contribution would be of considerable interest. In determination of U_{de} or cg acceleration peak counts from VGH or other data, and in calculating σ_w distributions from the peak counts, it is easy to forget that the acceleration time histories may not represent purely the effects of turbulence and that, in fact, it may be quite difficult to separate the effects of turbulence from the effects of maneuvers. The maneuvering found to occur in some HICAT flights may or may not be representative of that occurring in operational flights from which VGH records are obtained. Nevertheless, an attempt to evaluate the magnitude of the maneuver effect in a limited number of HICAT runs appeared to be worthwhile.

For this purpose, analysis was performed on four runs. For convenience, the analysis utilized the cg acceleration time histories; manifestly, exactly the same results would have been obtained using the U_{de} time histories instead.

It might be mentioned that not all elevator motion should necessarily be regarded as due to maneuvering. If the pilot is flying essentially "stick-free," the elevator may tend to float in direct response to the turbulence itself and in response to the airplane motions induced by the turbulence. Similarly, the pilot may attempt to alleviate specific gusts by control motion and may thus become part of the airplane dynamic system. In the work described in the following paragraphs, it is the total effect of the elevator motion that is evaluated.

Method of Removing Effect of Elevator from U_{de} Time Histories - The method used to remove the effect of elevator motion from the cg normal acceleration time histories is identical to that described in References 10 and 11. First, a test is conducted during flight in smooth air and at the selected altitude and airspeed, an elevator pulse is introduced. This consists of displacing the elevator substantially and then returning it to the trim position, all in a period of about a second. From the recorded time histories of the elevator motion and the resulting cg acceleration, it is possible to calculate the cg acceleration time history that would result from a unit elevator displacement impulse - i.e., an elevator pulse of infinitely short duration. The elevator time history measured in an actual run through turbulence is then divided into many very short elements, each of which is treated as an impulse. Superposition of the cg acceleration time histories produced by each of these impulses then gives the cg acceleration time history produced by the elevator motion over the entire run. The specific application of this procedure to the HICAT data is described in Appendix I.

For HICAT, two elevator pulse tests were conducted, one in which the elevator pulse was positive and one negative. The resulting unit-impulse responses were averaged. Inasmuch as the flight conditions were nearly identical, the two unit-impulse responses should have agreed. Unfortunately, the differences were sufficient to cast some doubt on the accuracy with which the effects of elevator motion could be removed. Also, the unit-impulse response used applies exactly only for the particular speed, altitude, airplane weight, and cg position at which obtained, whereas the various HICAT runs all differ somewhat in flight condition. It should be emphasized, therefore, that in the work that follows, the effect of the elevator motion is never completely removed. At best, only some substantial part will be removed, perhaps on the order of two thirds to three quarters of the total effect.

Selection of Runs for Analysis - A total of four runs was chosen for evaluating the effect of elevator motion on the cg normal acceleration. They are:

Test	Run	Duration, seconds	Altitude, feet	EAS, Knots
262	11	400	59,000	130
265	17	165	60,000	125
266	12	450	56,000	129
266	7	65	54,500	138

Test 266-7 is not included in the list of runs used for power spectral analysis (Table II) because of its short duration, but is included here because of the large amount of elevator motion and the accompanying cg normal acceleration peaks it contains.

In selecting the above runs it was necessary that they be for flight conditions close to that for which the unit-impulse response was calculated (55,000 ft, 139 KEAS), as the response of the airplane varies considerably with both equivalent airspeed and air density. It was also required that the runs contain a substantial amount of elevator motion.

Discussion of Time Histories - The time histories of the four runs analyzed are shown in Figures 24 through 27. For tests 262-11, 265-17, and 266-12 five time histories are shown. The first (at the bottom of each figure) is the adjusted elevator position. This is simply the actual elevator position with the mean value for the entire run subtracted out. The second time history (moving up the page) is the cg normal acceleration. This is shown as measured, with the acceleration due to gravity included. It is also shown after high-pass filtering (4th from the bottom) for comparison with corrected cg normal acceleration. The 3rd time history is the induced cg normal acceleration. This is the increment of cg normal acceleration which is calculated as due to the elevator motion. It is obtained by approximating the adjusted elevator position by a series of impulses, and applying the time response due to a unit elevator impulse to each of these impulses. The responses due to these impulses are then summed at each instant of time to give the induced cg normal acceleration time history. The corrected incremental cg normal acceleration (5th from the bottom) is obtained by subtracting both the mean acceleration and the induced cg normal acceleration from the cg normal acceleration time history. This is the cg normal acceleration that theoretically should have resulted from the turbulence had no elevator motion been present during each run. It has been high-pass filtered to remove long term trends produced by trim changes and inaccuracies in the correction process.

Examining these four time histories, it is evident, first, that there is a strong tendency for cg normal acceleration peaks to correspond with elevator position peaks. In Figure 24, in fact, the two time histories are remarkably similar in shape. Next, the induced cg acceleration time history is seen to reproduce, fairly closely in some cases, the shape of the cg normal acceleration trace; the most conspicuous difference between these two time histories is in the frequency components of wavelength shorter than one or two seconds, which are largely suppressed in the induced acceleration time history. The corrected incremental cg normal acceleration trace reflects the close

45

Figure 24 Elevator Effect Removal Time History - Test 262, Run 11

Figure 25 Elevator Effect Removal Time History - Test 265, Run 17

Figure 26 Elevator Effect Removal Time History - Test 266, Run 12

48

LOCKHEED HICAT PROGRAM
TEST 266   RUN 7
DATE 12-1-67

PLOT: 12.5 PT/SEC, FILTER PASS BAND 0 - 5.0 CPS EXCEPT AS NOTED
START TIME: 23:74:??
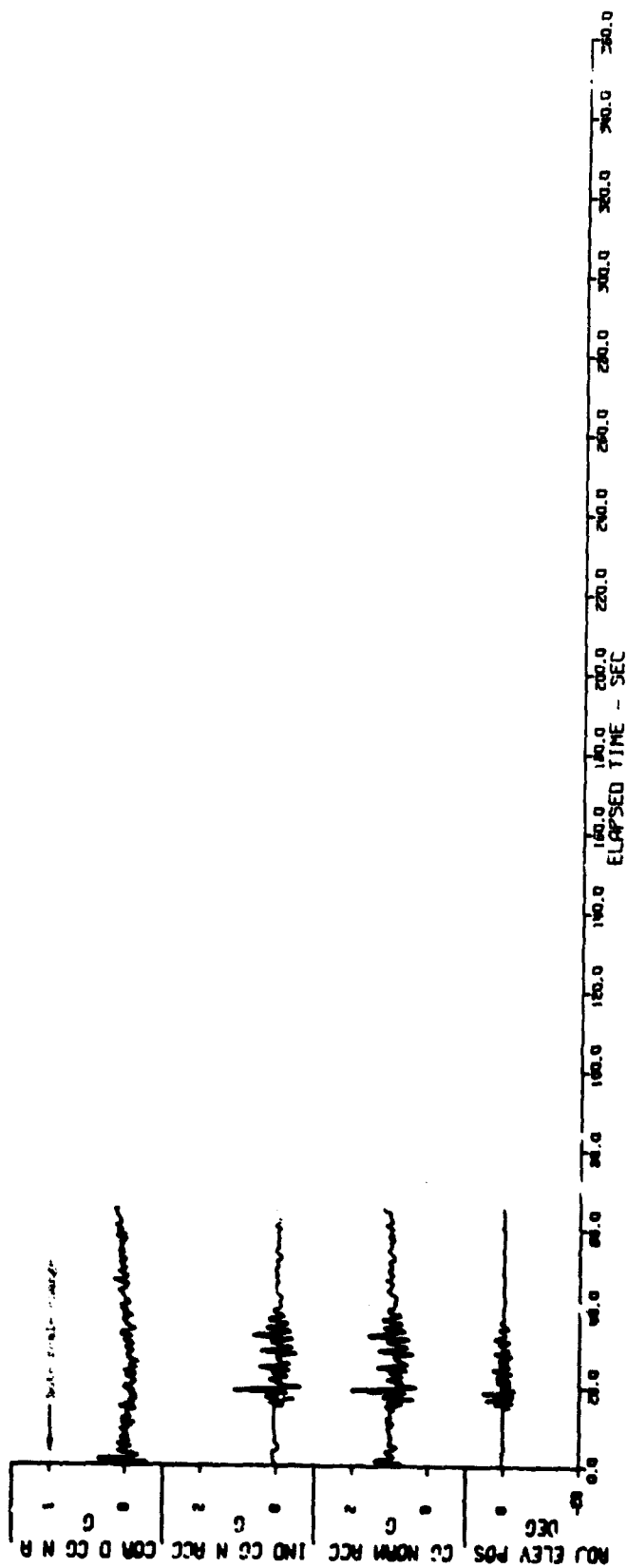
Figure 27 Elevator Effect Removal Time History - Test 266, Run 7

similarity of the cg acceleration and induced cg acceleration traces. In
Figure 24, for example, nearly all evidence has been lost of the numerous high
peaks of several seconds duration, and the highest peaks are decreased by
approximately a factor of 2. Thus it is quite clear that in this run nearly
all of the large peaks of several seconds or more duration are primarily the
result of elevator motion.

A somewhat different characteristic is shown for Run 266-7, in Figure 27.
Here there is no visual evidence of actual maneuvers, as the longest wave-
lengths evident are no longer than about 2 seconds. Nevertheless, removal of
the elevator effect reduces the cg acceleration excursions by a factor of
three or four. In this case, it appears that the pilot may have been attempting
to control the response of the airplane to turbulence and was actually
accentuating it. Note that the shortness of the run made high-pass filtering
unnecessary and consequently the filtered uncorrected cg acceleration time
history was omitted.

Discussion of Peak Counts - Peak counts of cg normal acceleration were com-
puted for the three runs for which filtered time histories are shown. A
comparison of the peak counts before and after the effect of elevator motion
is removed, on the basis of both the filtered and unfiltered time histories,
is shown in Figure 28. The "mean crossing" peak count procedure was used.

The significant curves in each figure are those representing the filtered data
(dash lines). Although the change in the peak count curve due to removing
the elevator effect differs in magnitude from run to run, the qualitative
features are the same. The highest peaks are reduced significantly, whereas
the total number of peaks increases. The effect of the high-pass filtering
is seen to be significant only for Run 266-12; this is the run for which it
was clear from the time histories that a filter was needed.

Discussion of Coherencies - Various coherency functions of interest were
computed for the three runs investigated and are shown in Figure 29. Probably
the most illuminating figures are the first one for each run. These show the
coherency between the cg acceleration, both uncorrected and corrected, and
the absolute gust velocity. At frequencies above about one cps, the two
coherencies are nearly the same and fairly close to unity. At lower fre-
quencies, the coherency drops off and is especially low between the uncorrected
acceleration and the gust velocity. It follows that in this frequency range
there must be some input other than the gust velocity that is producing the
cg acceleration response. This evidently is the pilot input to the elevator.
The lack of coherency indicates an independent (or perhaps nonlinear) pilot
maneuver input rather than an input in which the pilot responds linearly to
the turbulence as part of the airplane dynamic system.

The solid line curves at the bottom of Figure 29 are also of interest. The
consistently low coherency over the frequency range, between gust velocity
and elevator position, indicates that there is no strong tendency for the
elevator to respond to the gust input, either directly or through the action
of the pilot.
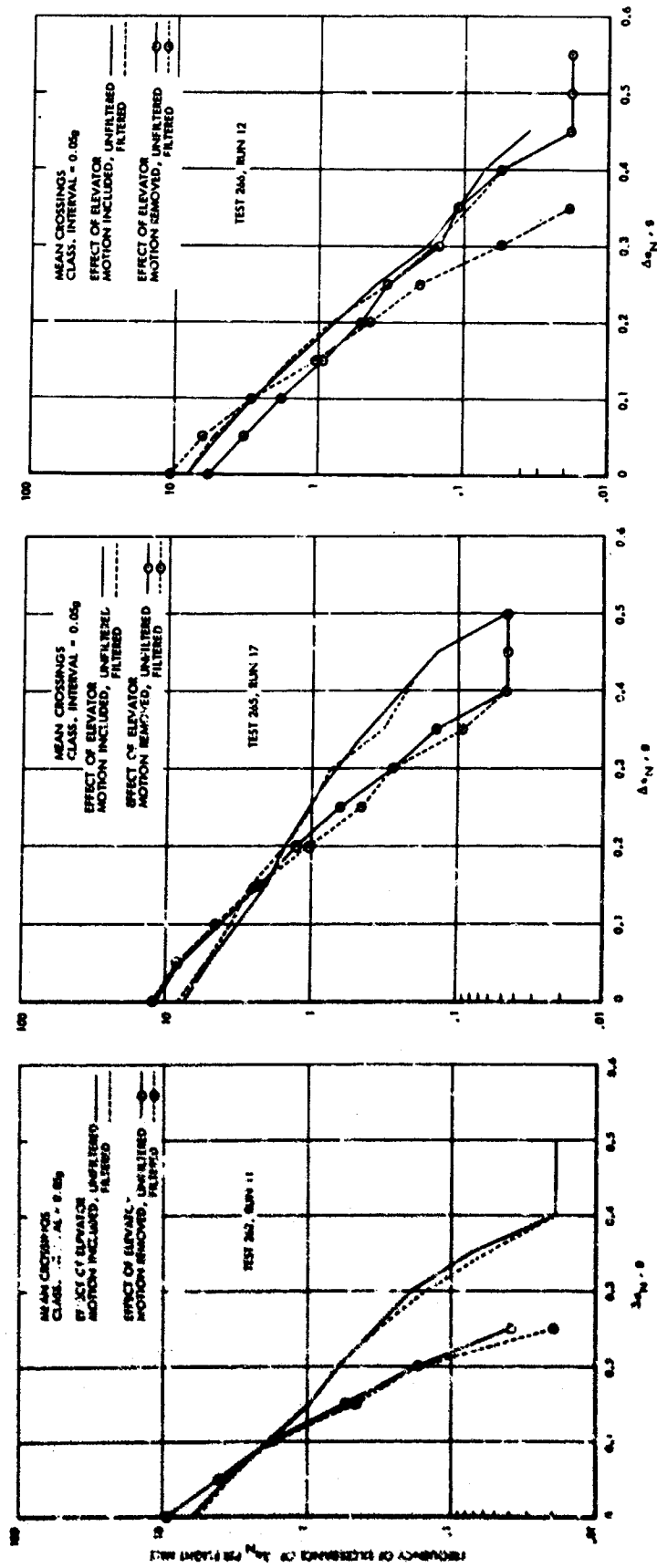
Figure 28 Frequency of Exceedance of CG Normal Acceleration per Flight Mile
With and Without Effect of Elevator Motion

51
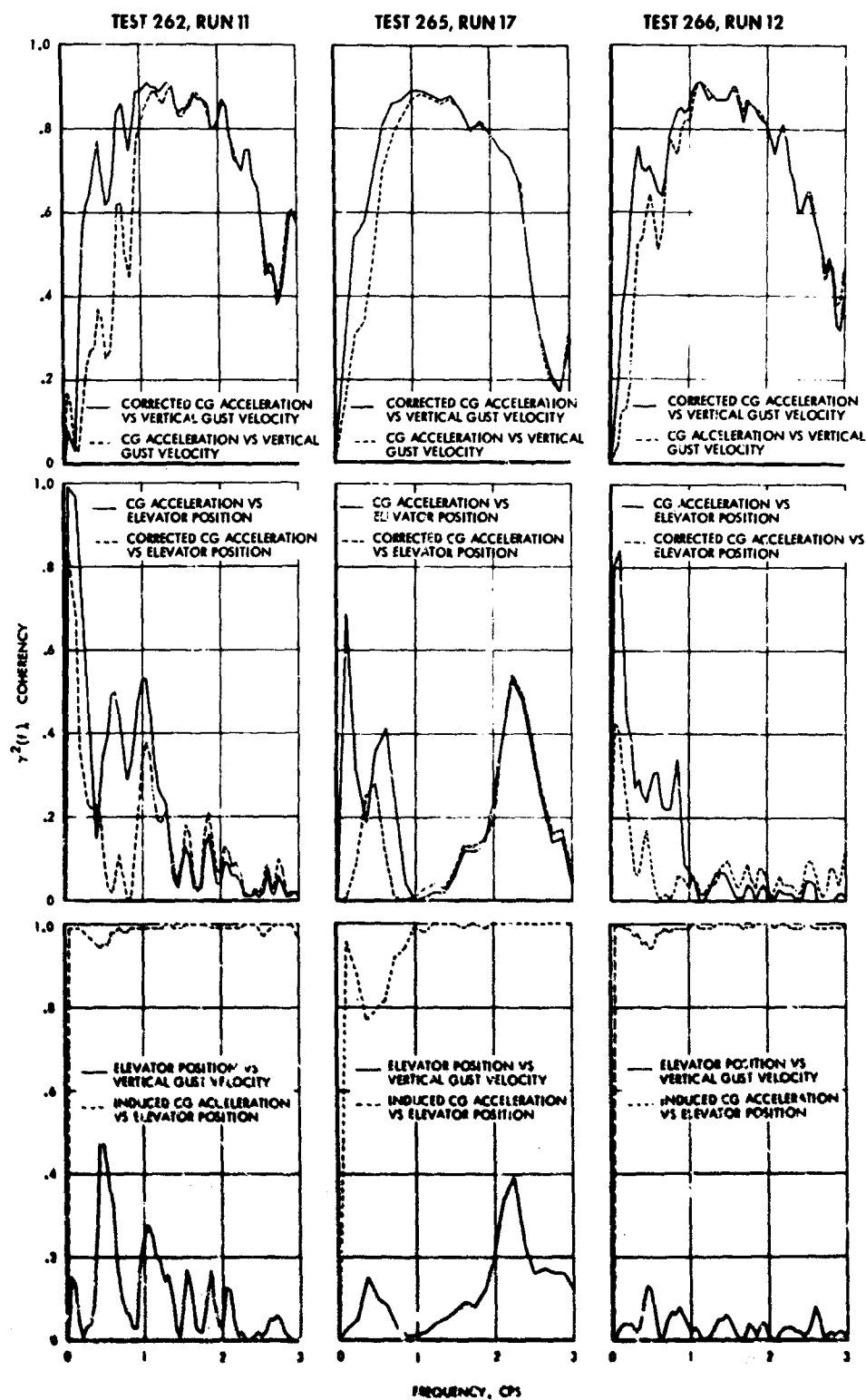
Figure 29   Coherency Functions - Elevator Input Effect Evaluation

Concluding Remarks - From the various time histories and peak count curves shown, it is evident that pilot inputs to the elevator increased the larger acceleration and U_{de} values in some of the HICAT runs by factors ranging from around 0.2 to as much as 4.0. The runs analyzed are not typical of all the HICAT data, however, since the basis for their selection was the appearance of significant motion in the elevator time histories. Therefore, it would appear that for the HICAT data as a whole the effect of pilot input would average considerably less.

$\overline{A}$ Values for Use in Determining σ_w Distributions from VGH Data

Background - In establishing probability distributions of rms gust velocity for use in airplane design, there has been great dependence upon the vast store of VGH data obtained under operational conditions.

To derive σ_w distributions from the cg acceleration peak counts available from the VGH data, two quantities, $\overline{A}$ and N_0, must be known. Both quantities depend upon the airplane, the flight condition, and the assumed shape of the gust power spectral density function. $\overline{A}$ is the ratio of the rms cg acceleration to the rms gust velocity, i.e., $\overline{A} = \sigma_{a_N}/\sigma_w$; it is analogous to the ratio a_N/U_{de} used in obtaining U_{de} peak counts from cg acceleration data. N_0 is the characteristic frequency of the cg acceleration response.

In design, $\overline{A}$ and N_0 are determined analytically. A frequency-response function is first obtained by dynamic analysis. At each frequency, the gust power spectral density is then multiplied by the square of the amplitude of the frequency-response function to give the power spectral density of the cg acceleration. The rms values of the cg acceleration and the gust velocity are obtained as the square roots of the areas under the respective power spectral density curves, and $\overline{A}$ is given by their ratio. N_0 is the radius of gyration of the cg acceleration power spectral density about zero frequency.

For use in determining σ_w distributions from flight data, $\overline{A}$ is usually obtained by means of simple theory in which the airplane is considered to be rigid and to be free to plunge (vertically) but not pitch. The shape of the gust power spectral density function used in obtaining $\overline{A}$ must be the same as will be used when applying the resulting σ_w distributions to design. N_0 need not be known exactly; an estimate is made based on any source that may be available.

The simple theory for obtaining $\overline{A}$ has been found to give good results when applied to the piston engine generation of transport aircraft. Analysis shows that the pitch freedom has little effect on the response; and the analysis provides a factor (close to unity) that can be applied to account for the effect of flexibility and elastic mode dynamic response. For other airplanes, however, flying at different altitudes, it is likely that the simple theory is inadequate. The presence of gust-measuring instrumentation on a U-2 airplane in the HICAT program offered an excellent opportunity to determine frequency-response functions in flight, compare the resulting $\overline{A}$ values with those given by the simple theory, and establish realistic values of N_0.

Determination of Frequency Response Functions and $\bar{A}$ Values - Two methods are available for determination of frequency-response functions from flight data. Both methods are described, and their relative merits discussed, in Reference 12.

The first is called the spectrum method. It follows directly from the familiar relationship between the power spectrum of a random disturbance (the input) and the power spectrum of the response (the output) of a linear system to this disturbance:

$$\Phi_z(f) = |H(f)|^2 \Phi_x(f)$$

In this discussion the input or disturbance is the gust velocity and the output or response is the aircraft cg acceleration. Thus, with power spectra of absolute gust velocity and airplane cg acceleration available from the flight records, the amplitude squared of the frequency-response function is given simply by

$$|H(f)|^2 = \frac{\Phi_z(f)}{\Phi_x(f)}$$

The second method is called the cross spectrum method. It follows from the less familiar relationship, for linear systems, between the power spectrum $(\Phi_x(f))$ of a random input disturbance and the cross spectrum $(\Phi_{xz}(f))$ between the input and the system response. From this relationship, the frequency-response function is given by the expression

$$H(f) = \frac{\Phi_{xz}(f)}{\Phi_x(f)}$$

Both $\Phi_{xz}(f)$ and $H(f)$ are, in general, complex quantities. Thus, the frequency-response function obtained by this method defines phase angle as well as amplitude. Inasmuch as $\Phi_{xz}(f)$ is complex it can be written

$$\Phi_{xz}(f) = c(f) - i\, q(f)$$

where c, the real part, is called the co-spectrum and q, the imaginary part, is called the quadrature spectrum. The amplitude squared of the frequency-response function, which is the quantity used in calculating $\bar{A}$ and N_o, is then given by

$$| H(f)|^2 \; = \; \frac{[c(f)]^2 + [q(f)]^2}{\left[\Phi_x(f)\right]^2}$$

The frequency-response values given by both methods are, of course, averages over the same bandwidths as the power spectral density curves from which they are derived.

An adv ntage of the cross spectrum method that is sometimes important is that it provides information on phase angle as well as amplitude. Where experimentally determined frequency-response functions are to be used only for determination of $\bar{A}$ and N_o values, however, this advantage is not pertinent.

A more important advantage of the cross spectrum method is that the frequency-response estimates are less subject to systematic errors or distortions arising from a variety of noise errors. Thus, use of the cross spectrum method would tend, in the present application, to eliminate the effect of extraneous pilot inputs to the elevator; although any elevator motions that followed linearly from the turbulence itself, either directly or through the pilot as a part of the dynamic system, would be accounted for.

Frequency-response functions were obtained by both the spectrum and cross spectrum methods from the records of five representative HICAT runs. These runs were selected to include at least several runs for which the turbulence intensity was substantial, several runs with fairly good stationarity, and runs having various amounts of elevator input relative to the turbulence intensity. The following tabulation identifies the runs and pertinent characteristics.

Power spectra of airplane cg acceleration were then computed from these frequency-response functions, on the assumption of two different shapes of gust power spectrum; that given by the Von Karman formula with L = 2500 feet (now generally in favor) and that given by the Dryden formula with L = 1000 feet (much used in the past, for example in Reference 13). The formulas for these two shapes are given under Mathematically Defined Gust Velocity Power Spectral Density Curves in Appendix I. The frequency-response functions and cg acceleration spectra obtained for these five runs are shown in Appendix I.

Test and Run No.	Run Duration (sec)	RMS 2** of U_y (fps)	Stationarity Evaluation	Elevator Motion Relative to Gust Intensity
220-10*	225	1.42	Fair	Medium
264-18	240	2.26	Fair	Small
266-10	455	2.98	Poor	Medium
266-12	450	1.26	Good	Large
266-18	185	3.13	Good	Small

*Low altitude
**RMS value between shortest wavelength and a wavelength cutoff of 2000 ft (see Gust Velocity Spectral Plots, Section V).

A closer examination of the results for one representative run, however, will be illuminating. For this purpose, the various plots for Run 12 of Test 266 are grouped together in Figure 30. The amplitude squared of the frequency-response function is shown first, in Figure 30(a). The spectrum method is seen to give considerably higher values than the cross spectrum method, especially at the lower frequencies. The ratio of the amplitudes given by the two methods is as low as 1.15 in the frequency range between 1 and 2 cps, but increases to nearly 2.0 at 0.6 cps and is on the order of 50 at 0.1 cps or less. Both methods show peaks at about 0.6 cps and about 2.2 cps. The first clearly reflects the longitudinal short-period mode response. The second is believed to reflect the response in the wing first bending mode.

The effect on the frequency-response functions of removing the effect of elevator motion on the cg acceleration, by the method described earlier in this section, is shown in Figure 30(b). Above about 1 cps, the effect of removing the elevator motion is negligible. At the 0.6 cps peak, the value given by the cross spectrum method is reduced slightly, while the value given by the spectrum method is reduced substantially; the agreement between the two methods is thus improved. In the very low frequency range, 0 to 0.2 cps, removing the effect of elevator motion improves the agreement tremendously. Thus it is concluded that much of the disagreement between the two methods is due to elevator inputs not linearly related, or perhaps not directly related in any fashion, to the gust velocity.
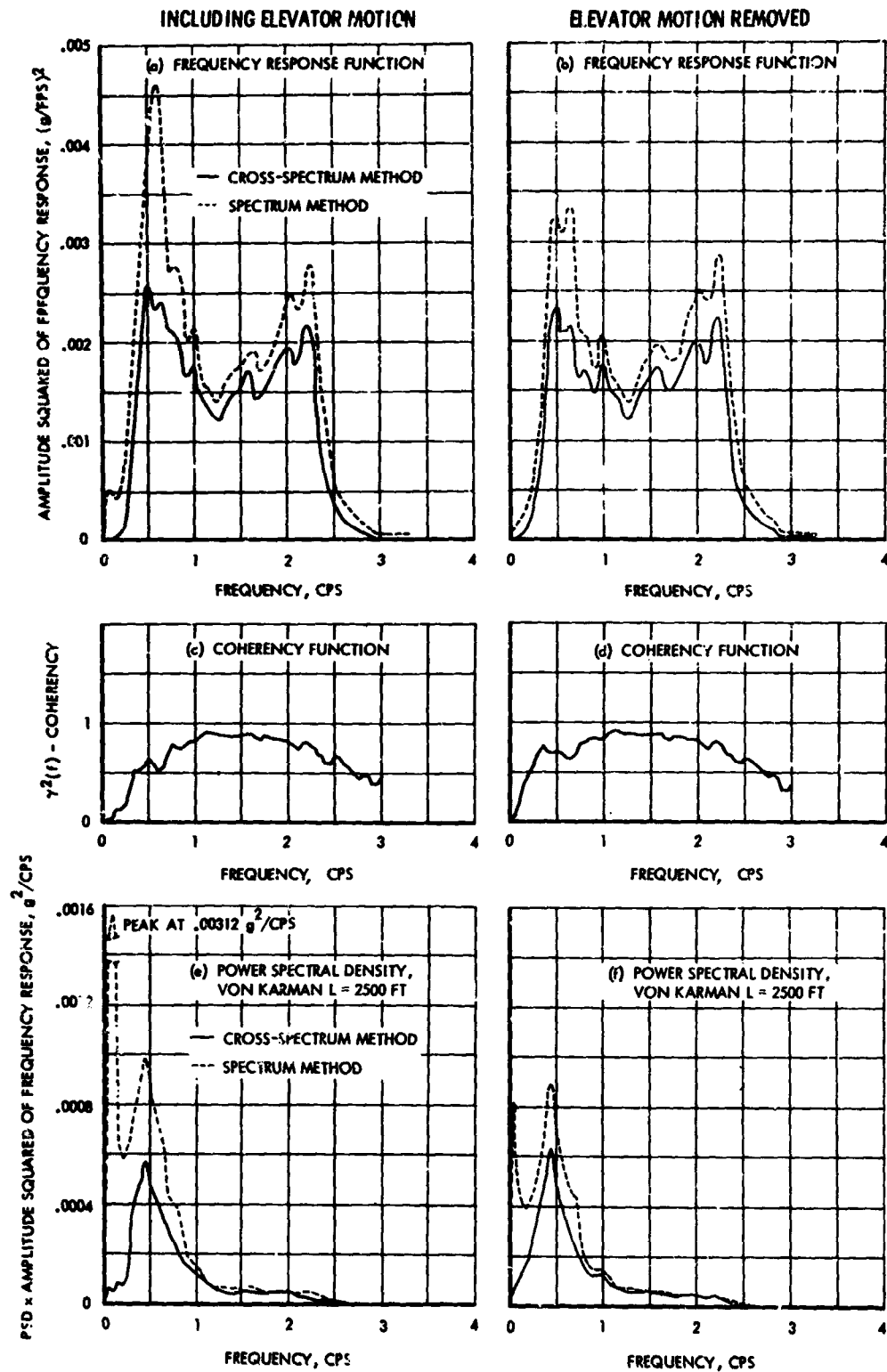
Figure 30 Frequency Response Functions, Coherencies, and Power Spectra
of Test 266 Run 12, Before and After Effect of Elevator
Motion is Removed

Section V

The disagreement between the frequency-response functions given by the two methods bears an interesting relation to the coherency functions, shown in Figures 30(c) and (d). Comparing first Figures 30(a) and (c), it is seen that in the frequency range from 1 to 2 cps, where the agreement in frequency-response functions is good, the coherency is excellent, lying in the range .85 to .90. At the 0.6 cps peak, where the frequency-response functions begin to disagree more markedly, the coherency has dropped to as low as 0.50. In the frequency-range of 0 to 0.2 cps, where the agreement is extremely poor, the coherency is less than 0.15. Comparing Figures 30 (b) and (d), the same relation is seen in the 1 to 2 cps range. But at the 0.6 cps peak, where the disagreement in frequency-response functions is less, the coherency has increased from 0.50 to 0.65. At frequencies below 0.2 cps, the coherency has increased markedly - at 0.15 cps, for example, from 0.13 to 0.40.

The influence of the frequency-response function on the computed $\bar{A}$ values depends upon the area under the cg acceleration psd curve. Psd curves obtained from the frequency-response curves of Figures 30(a) and (b) are shown in Figures 30(e) and (f). Figure 30(e) emphasizes the great importance of the frequency-response function at the very low frequencies. In Figure 30(a), the discrepancy between the two methods in the 0 to 0.2 cps range is quite inconspicuous. But when the frequency response is multiplied by the gust spectrum, to give the power spectra shown in Figure 30(e), the importance of this region becomes evident. Even with the effect of the elevator nominally removed, the spectrum method results in a much greater area under the curve in the 0 to 0.2 cps range than given by the cross spectrum method.

Results and Discussion - $\bar{A}$ values obtained for the five HICAT runs analyzed are shown in the following tabulation:

| Test and Run Number | $\bar{A}$ [g/(ft/sec)] | | | | | |
| | Von Karman Gust Spectrum, L = 2500 ft | | | Dryden Gust Spectrum, L = 1000 ft | | |
	Cross Spectrum	Spectrum	Theory	Cross Spectrum	Spectrum	Theory
220-10*	0.0246	0.0278	0.0187	0.0278	0.0324	0.0238
264-18	0.0157	0.0302	0.0114	0.0185	0.0347	0.0140
266-10	0.0148	0.0268	0.0140	0.0183	0.0286	0.0175
266-12	0.0184	0.0287	0.0134	0.0221	0.0321	0.0166
266-12**	0.0186	0.0244	0.0134	0.0225	0.0275	0.0166
266-18	0.0163	0.0232	0.0139	0.0198	0.0280	0.0171

*Low Altitude
**Elevator Motion Removed

Values are shown based on both cross spectrum and spectrum methods of determining the experimental frequency-response functions and also as given by simple theory. The theoretical values are based on theory developed originally by Fung (Reference 14), in which the airplane is considered rigid and free to plunge but not pitch; the values shown in the table were obtained from Figure 5-2 of Reference 15 for the Von Karman spectral shape and from similar curves, unpublished, for the Dryden spectral shape.

To better show the comparison between experimental and theoretical values, ratios of experimental to theoretical $\bar{A}$ are shown in the following table:

Test and Run Number	$\bar{A}_{EXP.}/\bar{A}_{THEORY}$			
	Von Karman Gust Spectrum, L = 2500 ft		Dryden Gust Spectrum, L = 1000 ft	
	Cross Spectrum	Spectrum	Cross Spectrum	Spectrum
220-10[*]	1.31	1.48	1.17	1.36
264-18	1.38	2.65	1.32	2.48
266-10	1.06	1.91	1.04	1.64
266-12	1.37	2.14	1.33	1.93
266-12[**]	1.39	1.82	1.36	1.66
266-18	1.17	1.67	1.16	1.63
Average (excluding 266-12[**])	1.26	1.97	1.20	1.81
*Low Altitude **Elevator Motion Removed				

N_o values obtained for the five HICAT runs are shown in the following table:

Test and Run Number	$N_o \sim$ Characteristic Frequency $\sim$ CPS			
	Von Karman Gust Spectrum, L = 2500 ft		Dryden Gust Spectrum, L = 1000 ft	
	Cross Spectrum	Spectrum	Cross Spectrum	Spectrum
220-10[*]	0.77	0.79	0.67	0.66
264-18	0.81	0.50	0.75	0.46
266-10	1.08	0.66	0.97	0.65
266-12	0.73	0.55	0.76	0.67
266-12[**]	0.72	0.62	0.73	0.68
266-18	0.90	0.72	0.87	0.66
Average (excluding 266-12[**])	0.86	0.64	0.80	0.62
*Low Altitude **Elevator Motion Removed				

$\bar{A}$ values obtained experimentally using the cross spectrum method are seen to average about 20 to 25 percent higher than those given by the Fung theory. $\bar{A}$ values given by the spectrum method are seen to be nearly twice the theoretical values. N_O values are seen to average about 0.80 to 0.85 by the cross spectrum method and 0.60 by the spectrum method.

Whether the spectrum method or the cross spectrum method is more appropriate is not immediately evident. As noted on page 55, (4th paragraph) and as discussed at length in Reference 12, the cross spectrum method gives frequency-response (transfer function) estimates that are less subject to a variety of noise errors than does the spectrum method. The cross spectrum method, therefore, would appear to give a truer relation between gust velocity time history and the acceleration time history resulting directly therefrom. Also, the transfer function that it defines is the one that probably will be matched more closely by the best available theory (at the present state of the art). Nevertheless, it is important that the entire design procedure, including the collection and processing of VGH data, lead to airplane loads that reflect the total accelerations that occur in turbulence, including the "noise" that is not linearly related to the turbulence. It is pertinent, therefore, to examine which method of transfer function determination is most likely to accomplish this result.

Suppose that the cross spectrum method is used. The resulting transfer function will be used to infer gust velocities from VGH acceleration data. These gust velocities will be overestimated, because a "correct" transfer function is applied to the entire acceleration - that part which is noise as well as the part actually due to the gust velocity. In design, a "correct" transfer is again used (the only kind available). The resulting acceleration, being derived from overestimated gust velocities, will also be overestimated, and this overestimation will provide for the noise likely to be present in flight of the new airplane through turbulence.

On the other hand, suppose that the spectrum method is used. Gust velocities will be correctly inferred. In design, the "correct" transfer function, used with the "correct" gust velocities, will lead to a "correct" evaluation of the accelerations due directly to the turbulence. But the increment in acceleration due to noise - which will actually occur - will not be accounted for. Thus it would appear that $\bar{A}$'s and N_o's based on transfer functions given by the cross spectrum method are the appropriate ones to use for design application although those given by the spectrum method may give a truer picture of the actual turbulence.

If the ratios of experimental to theoretical $\bar{A}$ found here are considered valid, σ_w distributions obtained from U-2 VGH data, utilizing the simple theory described earlier, would appear to be too severe for design use by a factor of roughly 1.2 to 1.25.

Peak Counts of Absolute Gust Velocity

High-Pass Filtering of Absolute Gust Velocity Time Histories - Peak counts of airplane acceleration (and, in turn, U_{de}) have been obtained from VGH records for many years and utilized in the design of aircraft as well as in the study of atmospheric turbulence. The simple physical significance of the peak count presentation makes it appear desirable for application also to absolute gust velocity measurements.

Peak counts of absolute gust velocity, however, must be performed and interpreted with some care because of the uncertainties which accrue at very low frequencies (long wavelengths) due to instrument errors and lack of measurement resolution. These effects may manifest themselves as noise and yet still appear almost indistinguishable from true turbulence. In the discussion that follows, it is shown that high-pass filtering is necessary to minimize this uncertainty, but that some of the turbulence is unavoidably removed along with the noise.

Theoretical Effect of Low Frequency Components on Peak Counts - An indication of how much the presence of noise may influence the peak counts can be obtained by consideration of the power spectral density (psd) of the measured turbulence. The many gust velocity psd's shown in Appendix V generally continue to rise more or less according to the $-5/3$ power of frequency down to the lowest frequencies shown. Whether the lowest frequency components of the turbulence as measured are primarily turbulence or primarily noise will affect the conclusions drawn as to the magnitudes of the gust peaks actually present in the atmosphere. The difference in magnitudes can be evaluated by means of Rice's equation[9].

$$N(w) = N_o \, e^{-1/2(w/\sigma_w)^2}$$

where:

w = any given component of the gust velocity.

σ_w = rms value of w, equal to the square root of the area under the psd curve.

$N(w)$ = average number of crossings per unit time or distance, with positive slope, of the value w (in effect, the number of peaks in excess of w).

N_o = characteristic frequency, equal to the radius of gyration of the power-spectral density function of w about zero frequency.

It is seen that $N(w)$ depends upon N_o and σ_w, both of which can be evaluated from the power spectral density.

To show the effect of the low frequency components on the magnitudes of the peaks, frequency of exceedance curves were calculated based on the two simplified psd curves shown in Figure 31. The two curves designated A and B are truncated vertically at the low frequency end at points a and b, respectively, and at the high frequency end at c. The three values of $1/\lambda$ can be regarded

---

[9]This equation applies theoretically only to a stationary Gaussian random process. It is known that high altitude clear air turbulence does not fully satisfy this requirement; but the trends deduced from the equation should be valid.

as arbitrary. Actually, however, point c was taken as the upper limit of integration for the HICAT psd's (5 cps) for a typical flight speed of 700 fps. Point b was taken as the effective cutoff frequency of the 7000 ft filter defined in Appendix I; this frequency is such that, in Figure 92, the area under the truncated psd curve is the same as under the filtered psd curve. Point a is at one-fourth the frequency of point b. The vertical position of the psd curve in Figure 31 is such that RMS 2 (as defined under Gust Velocity Spectra Plots) is 1 fps.
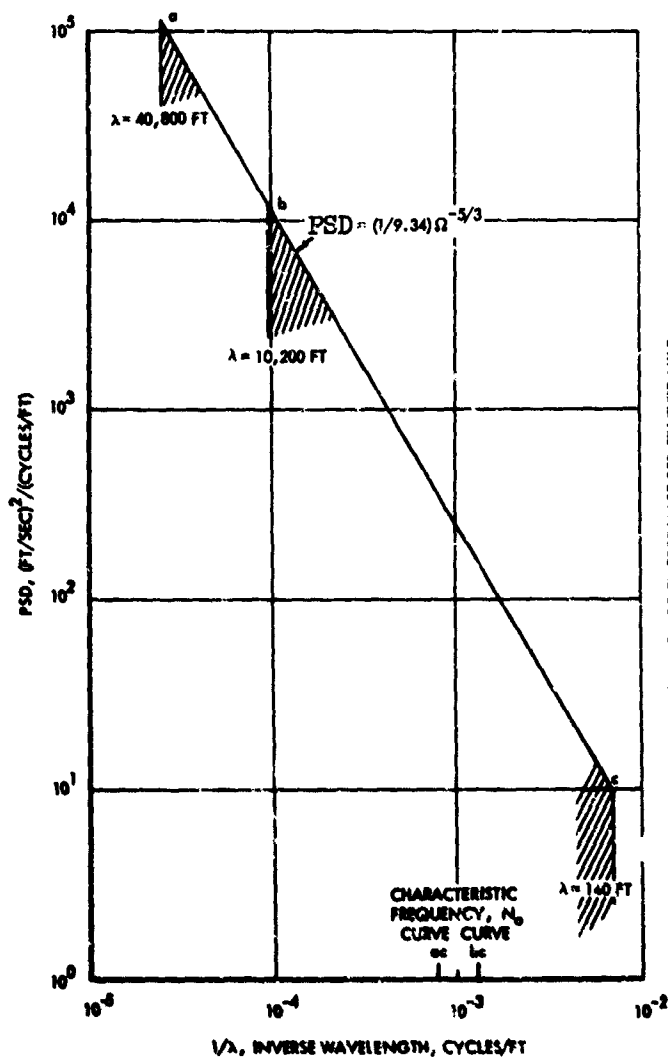
Figure 31 Idealized Power Spectral Density Curves
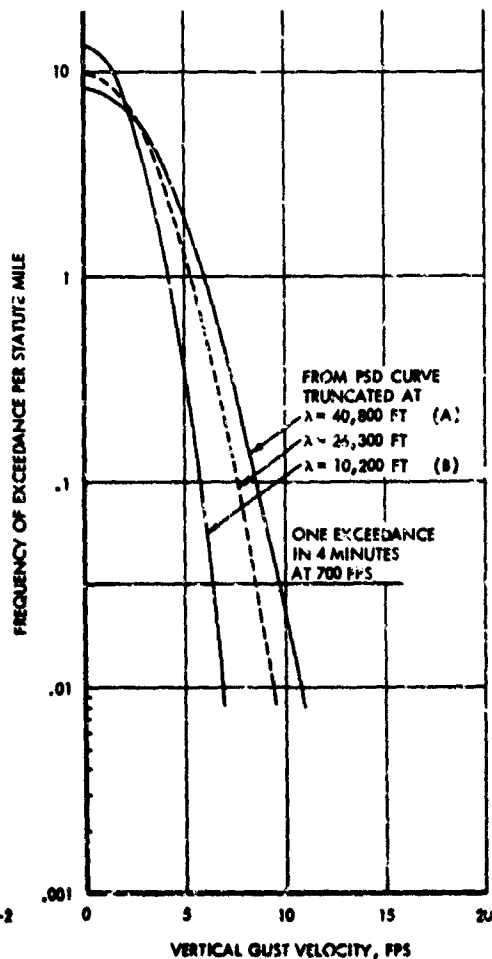
Figure 32 Exceedance Curves Corresponding to Various Truncations of a Single Power Spectral Density Curve

Values of σ and N_O for the two psd's were evaluated analytically. The following results were obtained:

	Curve A	Curve B	Ratio, A/B
σ, fps	2.96	1.82	1.63
N_O, cps	0.000773	0.00125	0.62

The resulting exceedance curves, as given by Rice's equation, are shown by the two solid lines in Figure 32. The highest peak expected in a 4-minute run at 700 fps is indicated at a frequency of exceedance of $5280/(700)(4)(60) = .0317$ per mile. For each curve, the intercept at $w = 0$ is equal to $2N_O$. (The factor of 2 appears because crossings of both positive and negative levels are combined.) The abscissas, at any given value of $N(w)/N_O$, are proportional to σ_w. It is seen that, as the longer wavelength components are added, as in going from curve B to curve A, the exceedance curve shifts slightly down but expands substantially to the right. For the particular case shown, a reduction by a factor of 4 in the low frequency cutoff results in a factor of 1.55 increase in the expected magnitude of the largest peak. Similar results are obtained when the psd's are truncated horizontally at points a and b instead of vertically.

High-Pass Filtering as a Means of Removing Noise - From the above results, it is clear that the presence of the low frequency components will have a major effect on the resulting peak counts no matter whether the components are considered to be turbulence, or instead are considered to be noise and in some way removed from the time histories. If noise is indeed present at the lower frequencies, a high pass digital filter can be applied to the measured time histories to eliminate the frequency components involved. In the use of such a filter, however, a decision must be made as to the frequencies to be eliminated.

In terms of power spectral densities, it would be most fortunate if a frequency could be found such that everything above this frequency were clearly turbulence and everything below, noise. This would be easy if the psd were found to have a shape such as:
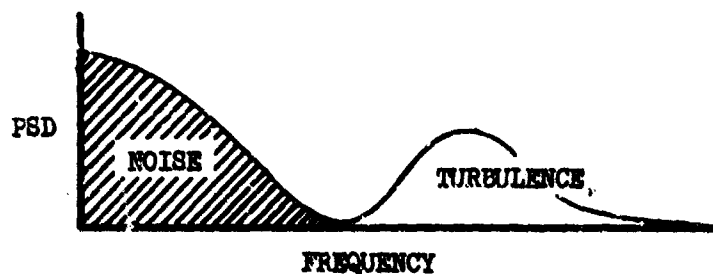
A filter would simply be chosen that eliminated the frequency components in the noise range and retained those in the turbulence range.

Section V

Unfortunately, such shapes do not seem to occur. Instead, as noted earlier
the measured psd's almost invariably show a trend in which the psd continues
to increase with decreasing frequency. Thus there is undoubtedly an overlap
of turbulence and noise:
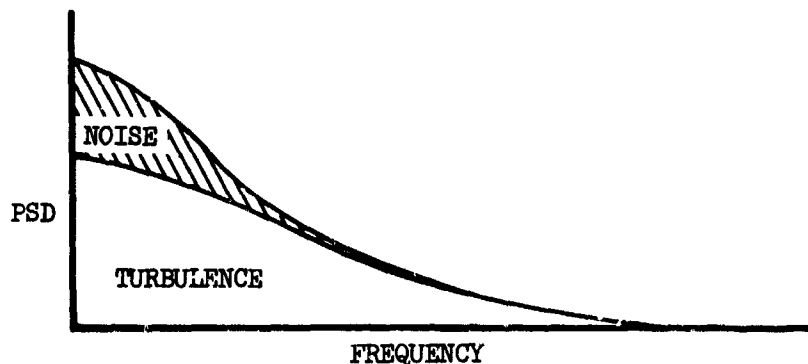
The filter, of course, has no way of distinguishing between turbulence and
noise; it acts upon the total of noise and turbulence, attenuating only as a
function of frequency. Consequently, if the noise is to be removed, a sub-
stantial part of the turbulence may have to be removed also. In addition,
there is some uncertainty regarding the frequency below which the noise
becomes significant. To be sure that very little noise is retained, the
filter cutoff frequency must be chosen relatively high, i.e., toward the
shorter wavelengths.

The quantitative effect on the peak count curves of removing substantial con-
tributions to the time history in the low frequency range was discussed above;
representative results were shown in Figure 32. This earlier discussion
regarded the components being removed as noise; the results are equally
indicative, however, of the effect of removing the low frequency components
of the actual turbulence.

How much of the turbulence is left in after filtering is clearly rather
arbitrary, depending upon the filter characteristics selected. For the
filtered time history and the peak counts derived therefrom to have the most
meaning, it would be desirable for the filter characteristics to be

  (1) simply defined

  (2) the same from program to program.

The simplest filter for analysis purposes would be a sharp one. This filter
would pass without reduction all components above a given frequency and remove
completely all those below this frequency. Such a filter is impractical to
realize, however, and some compromise is necessary. Some degree of standardi-
za ion of filter characteristics from program to program, on the other hand,
should be practical. Comparison of peak counts would then be meaningful and
useful, even th ugh it might not be practical to make direct application on
an absolute basis.

64

In summary, for absolute gust velocity peak count to be meaningful, it is clearly necessary to high-pass filter the time histories to remove any noise that may be present; such filtering, however, will certainly remove some unknown amount of the turbulence along with the noise.

Selection of Filter Characteristics - The definition of two digital filters for use in high-pass filtering the HICAT absolute gust velocity data is discussed in Appendix I. The two filters selected are of the Martin-Graham type.

The first is virtually identical, on a spatial frequency basis, to that used in the LO-LOCAT program. It passes all wavelengths up to 7000 feet and virtually eliminates all wavelengths longer than 17,000 feet. The second retains considerably longer wavelength components. It passes all wavelengths up to 20,000 feet, and virtually eliminates all wavelengths longer than 40,000 feet. These two filters are designated herein as the 7000-foot filter and the 20,000-foot filter, respectively.

HICAT Peak Count Data - Peak counts of the vertical component of absolute gust velocity are shown for selected HICAT runs in Figure 33. Three peak count exceedance curves are presented for each run. They are derived respectively from the gust velocity time series obtained without high pass filtering as well as with 20,000 ft and 7000 ft high-pass filtering. The peak counts shown were obtained by the positive slope crossing method.

In all of the figures, the three curves tend to plot in the same relation to each other as predicted by theory (Figure 32). In particular, the effect of filtering is to increase the intercept at $U_V = 0$ and more importantly to reduce the U_V values at low exceedance levels. However, the separation of the curves is much less than the theory predicts. For a factor of 4 difference in cutoff frequency, the theory was seen to predict a factor of 1.55 in gust velocity at a frequency of exceedance level of one in 4 minutes. For the 7000- and 20,000-foot filters actually used, the effective cutoff frequencies correspond to wavelengths of 10,200 and 26,300 ft respectively. (These frequencies are such that, in Figure 96, the areas are the same under the truncated and the filtered psd curves.) For these filters, differing in cutoff frequency by a factor of 2.6, the theory predicts a 1.35 factor in gust velocity (Figure 32). In contrast, the curves obtained by applying the 7000- and 20,000-ft filters to the measured data differ by factors ranging from roughly 1.02 to 1.26 at comparable exceedance levels (0.03 to 0.10 peaks per mile). At roughly this same frequency of exceedance level, the gust velocity of the unfiltered time history ranges from about 1.00 to 1.22 times that associated with the 20,000-ft filter.

The quantitative discrepancy between theory and test is apparently explained, at least in part, by a smaller contribution of long wavelength gusts to the original unfiltered time history than assumed in the theoretical calculations. The power-spectral densities that have been calculated for these runs are not conclusive in this respect, as they generally are not defined through the very-low-frequency range of interest. The slopes of the psd curves, however, at the lowest frequencies at which the curves are defined, are much shallower than the -1.67 slope assumed in the theory. In four of the five cases, these
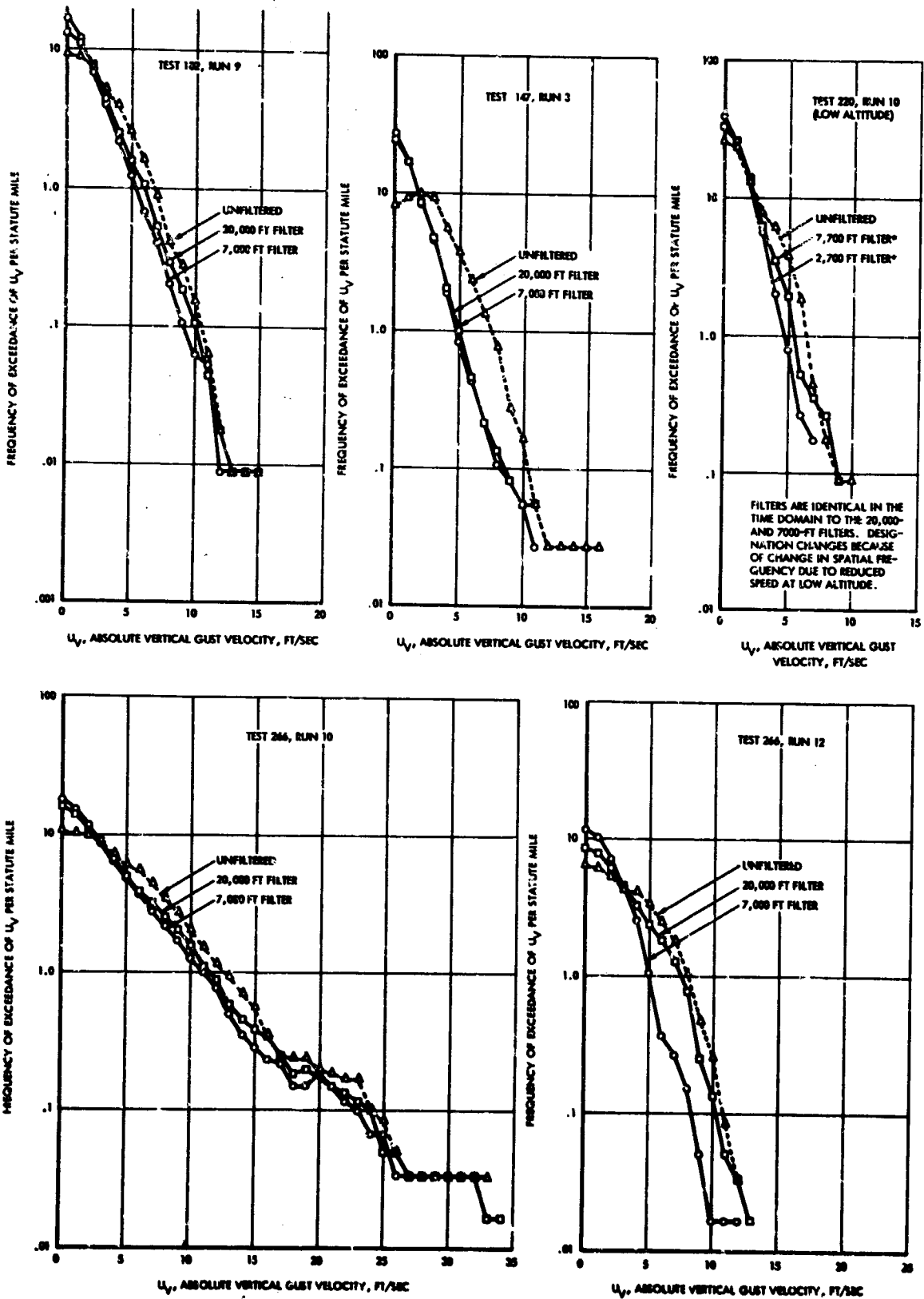
Figure 33 Frequency of Exceedance of U_V per Mile Using Positive Slope Level Crossing Count

slopes lie in the range -0.7 to -1.3. In the fifth case (Run 266-12), the slope has a relatively constant value of -1.6 up to 12,000 ft, the longest wavelength resolved and for this case the difference between the peak count curves for the 7000- and 20,000-ft filters was one of the largest, i.e., in closest agreement with theory.

In general it appears that the effect on the peak count curves of high pass filtering, or of the filter cutoff chosen, is considerably less than would have been inferred from the theoretical treatment of an idealized case in the previous section. This result provides evidence that the very low frequency "noise" in the HICAT data is relatively insignificant.

In comparing the measured peak counts with the theoretical curves of Figure 32, much of the measured data are seen to plot approximately as straight lines, in contrast to the parabolic shapes obtained theoretically. This difference is probably due primarily to lack of stationarity, as discussed later in this section.

It will be noted that one of the runs shown, Run 220-10, is a low altitude run at a much lower true airspeed. Use of the available digital filters at this reduced speed resulted in filter termination frequencies corresponding to wavelengths of 7700 and 2700 ft instead of 20,000 and 7000 ft, respectively. The results for this case are quite comparable to those for the high altitude cases.

Peak count data for a number of runs are totaled and plotted in Figure 34(a) and (b). These were obtained by the level crossing procedure. U_{de} peak counts for the same runs are also shown for comparison. In Figure 34(a) eight runs are included; the 7000-ft filter was used. In Figure 34(b) curves are shown for a smaller number of runs but based on both the 7000-ft and 20,000-ft filters. U_{de} values are seen to be roughly 2/3 of the U_V values at the same frequency of exceedance, in both figures. However on a derived basis, U_d, is seen to be about 40 to 80 percent larger than the corresponding U_V values indicating that the true gust velocities are overestimated by the derived gust equation for the U-2.

A comparison of peak counts for the three components of 20,000-foot filtered absolute gust velocity for a typical run are shown in Figure 35. The relative intensities in the three directions indicated by the peak count curves are roughly the same for the lower values of absolute gust velocity.

GUST VELOCITY POWER SPECTRAL ANALYSIS

General

The power spectrum or power spectral density of a function (e.g., a gust velocity time history) describes the manner in which the total average power of the function (velocity amplitude squared/cycles per second) is distributed over the frequency range. In essence it provides a statistical measure of the mean square amplitude of a measurement for each of a number of narrow but discrete frequency bands. The square root of the sum of all these values over the frequency range of the spectrum gives the rms value of the spectrum data.
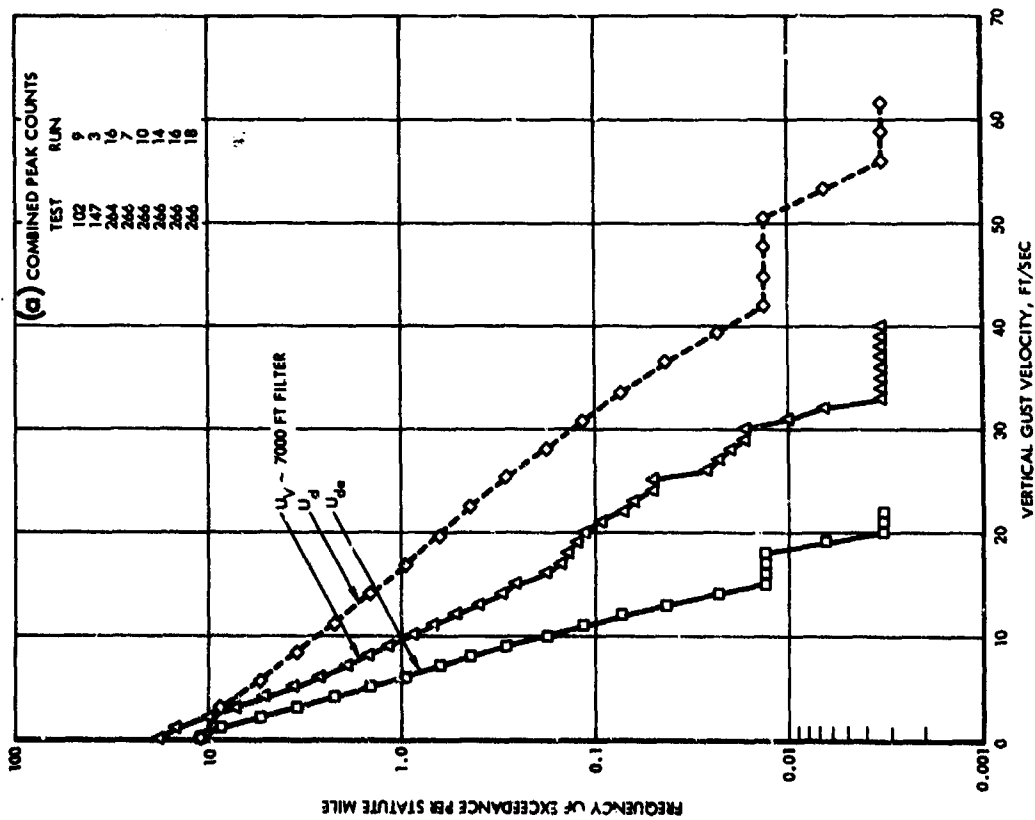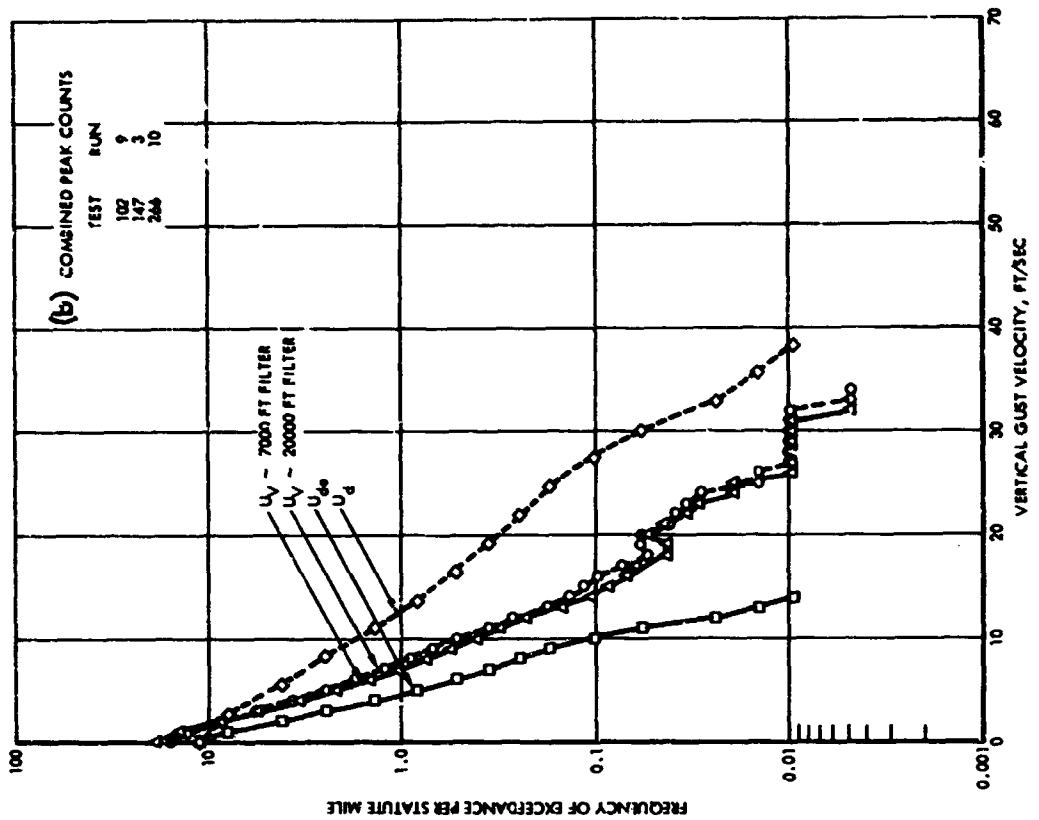
Figure 34 Frequency of Exceedance of Vertical Gust Velocity per Mile Using Level Crossing Count
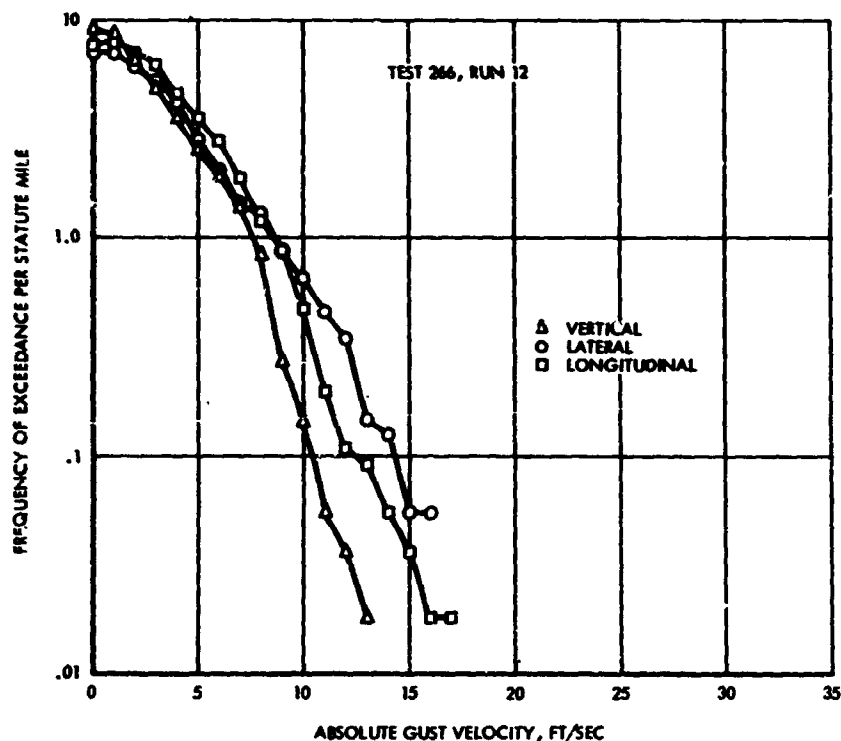
Figure 35 Frequency of Exceedance of 20,000 Ft Filtered Absolute Gust
Velocities for All Three Components Using Level Crossing
Count - Test 266, Run 12

Normally, power spectra from uniform time series data are computed and plotted
as a function of frequency in cycles per second or radians per second. How-
ever, for atmospheric turbulence, it is desirable to interpret the frequency
in terms of wavelength in feet per cycle or inverse wavelength in cycles per
foot. Thus, to obtain the ordinates of the spectra in cycles per foot, the
ordinate and abscissa values are respectively multiplied and divided by the
aircraft speed in feet per second.[10]

The methods used for computing power spectra and associated statistical func-
tions are described in detail in Appendix II.

HICAT Power Spectral Considerations

One of the most important objectives of the HICAT program is to determine gust
velocity spectra for turbulence waves ranging from about 100 feet to as much
as 50,000 feet in length. Spectral determinations of uniform statistical
reliability require that turbulence sample lengths increase in proportion to
the largest wavelength of interest in the spectrum. Since turbulent patches
and hence turbulent recordings vary considerably in length some patches will
be too short for a reliable long wave spectrum analysis but quite adequate for
a medium or short wave analysis.

---

[10]The average true airspeed of the aircraft for each turbulence run was the
value used for the HICAT spectra.

69

Section V

In the HICAT program, spectra are always computed so as to provide a selected minimum level of statistical reliability equivalent to 20 sample lengths of the longest wave or 80 statistical degrees of freedom. This is done by varying the wavelength resolution of the spectrum in several discrete steps to suit the turbulence sample length (see Reference 5, Section V). In effect, this means that some spectra will extend to much lower frequencies and longer wavelengths than others. The rms values (called RMS Spectra on the plots, e.g., see Figure 36) characterizing individual spectra are thus not comparable unless the spectra cover the same wavelength range.

To enable spectra with different low frequency limits to be compared, additional rms values were computed using the following standard long wavelength cutoffs: 1000, 2000, 4000, 10,000, 20,000, and 40,000 feet. The high frequency or short wavelength limit was established for convenience at the wavelength corresponding to 5.0 cps and thus varied slightly with aircraft speed, e.g., at 700 feet per second, 5 cps corresponds to a wavelength of 700/5 or 140 feet.

Gust Velocity Spectra Plots

The plots of the power spectra of the vertical, lateral, and longitudinal gust velocity components are presented in Appendix V. Figure 36 of this section shows typical examples of vertical, lateral, and longitudinal spectra.[11]

Note that the rms gust velocity characterizing the entire spectrum as well as the rms values for various intermediate wavelength cutoffs are tabulated on the plots. The intermediate wavelength cutoffs are abbreviated by dropping the thousands, (i.e., 1 = 1000 ft, 2 = 2000 ft, etc.).

Figure 37 compares the envelope of all the HICAT spectra with similar data obtained from the Douglas NB-66B High Altitude Gust survey (Reference 16) and the Australian TOPCAT program (Reference 17). The HICAT spectra overlay the TOPCAT spectra which were also clear air but fall slightly below the upper limit of the B-66 thunderstorm data, as might be expected. To provide a low-altitude yardstick for comparison, a spectral envelope of moderate intensity turbulence for HICAT landing approaches is shown. Note the characteristic -5/3 slope.

Mathematically Defined Gust Power Spectral Density Curves

For use in aircraft design, as well as for comparison of measured data with various proposed theories, it is often desirable to represent atmospheric turbulence power spectral density curves by means of mathematical expressions.

To assist in finding simple, mathematically defined curves that best fit the measured shapes, several families of curves are developed and presented in Appendix I. Four basic families are included. For each basic family, curves are provided for high-frequency exponents, m, of -1, -7/6, -4/3, -3/2, -5/3, -11/6, and -2, respectively. For each value of m, curves are shown for scales of turbulence, L, of 500, 1000, 2000, 4000, and 8000 ft, and ∞.

---

[11]The gust velocity time history from which these HICAT spectra were obtained appears in Figures 12 and 13.

TEST 28715 EC 53574
DATE 01 DEC 67
START TIME0 -4 -35
DURATION   3 -0
NO. LAGS   50
TIME INCR   0.080
NO. POINTS 2258
DEG FREEDOM 90
WIND: 172°/ 9 KN

VERTICAL ————————
  RMS Spectra   3.8324
  RMS 4   3.2936
  RMS 2   2.5711
  RMS 1   1.9042

LATERAL ————————
  RMS Spectra   4.0800
  RMS 4   3.3006
  RMS 2   2.3682
  RMS 1   1.8292

LONGITUDINAL ————————
  RMS Spectra   3.8688
  RMS 4   3.1808
  RMS 2   2.3567
  RMS 1   1.7852

POWER SPECTRAL DENSITY- (FT/SEC)²/CYCLES/FT

INVERSE WAVELENGTH-CYCLES/FT
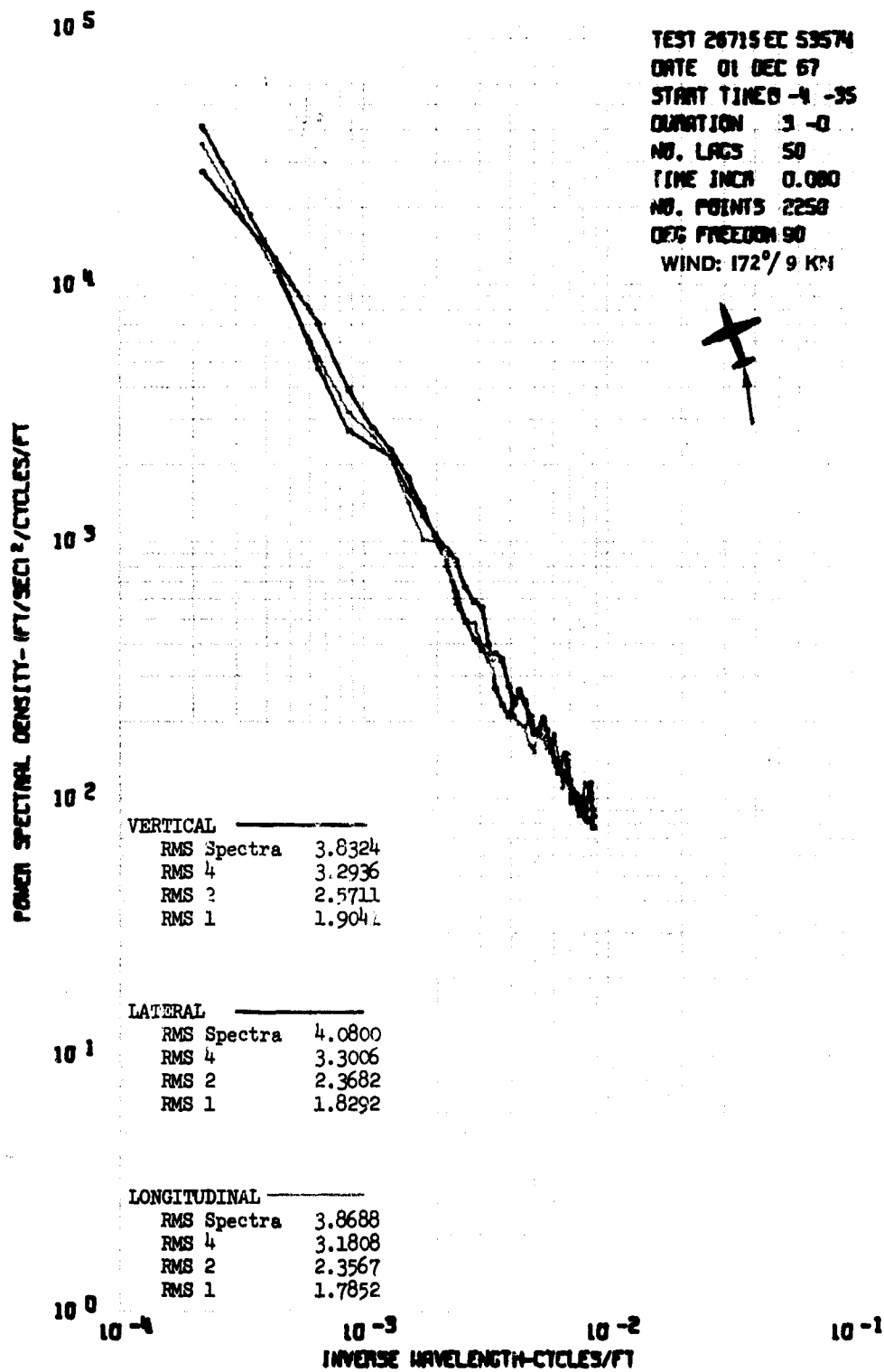
Figure 36 Typical Power Spectra of Vertical, Lateral, and Longitudinal
           Gust Velocity Components

71
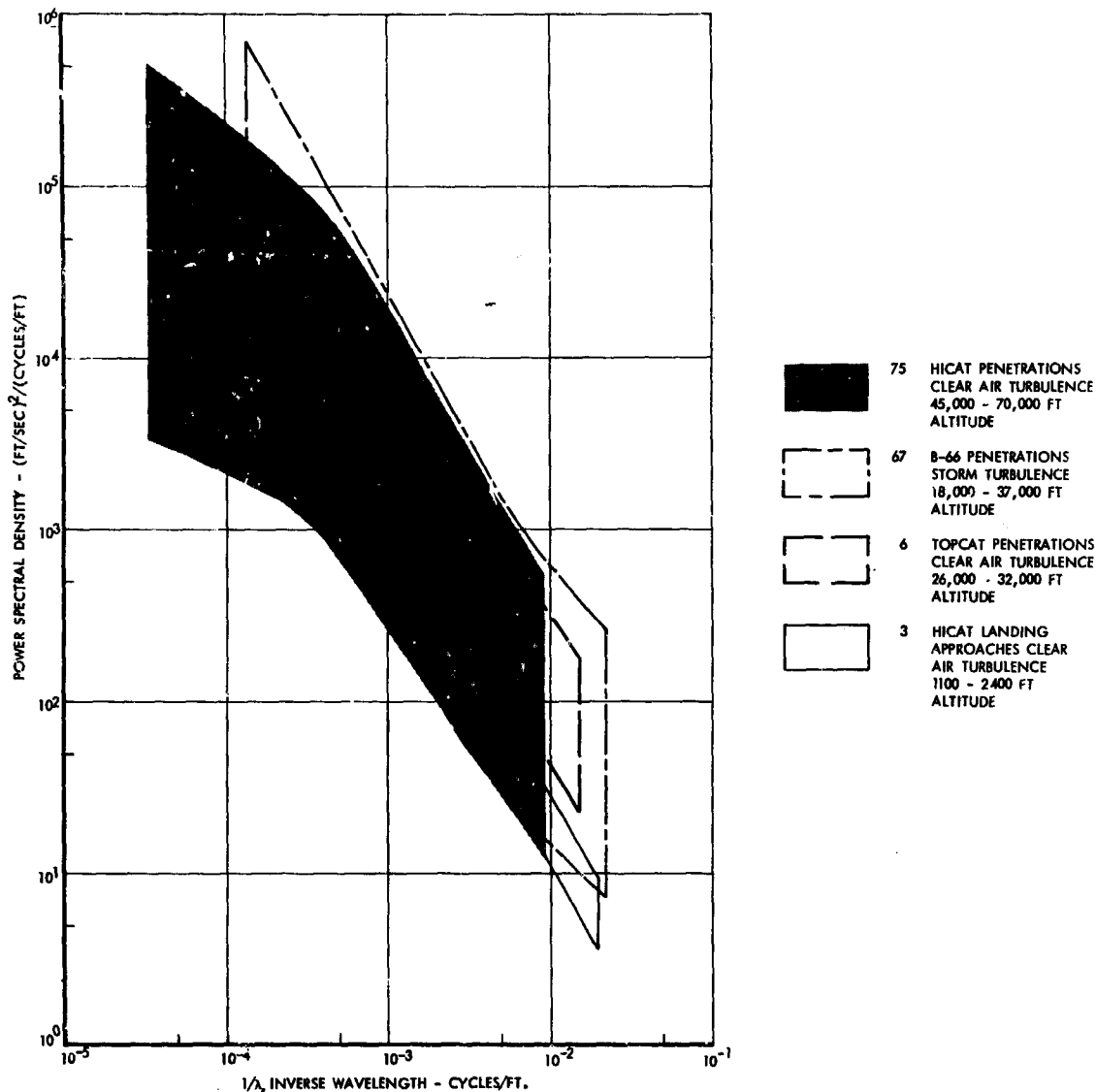
Figure 37 Comparison of Gust Velocity Power Spectral Envelopes

Figure 38 compares the four families for an m of -5/3 and an L of 1000 ft and ∞ . It should be noted that all curves shown are arbitrarily positioned vertically to be asymptotic to the same m = -1.667 straight line. To indicate the correct relative levels of the Taylor-Bullen Longitudinal and Taylor-Bullen Transverse spectra, for completely isotropic turbulence, the longitudinal spectrum shown should be lowered in the ratio 0.75.

Average Spectral Shape

It can be observed that the shapes of the gust velocity power spectra shown in Appendix V display considerable variability. As a result, some sort of averaging of the many curves is desirable to obtain a shape useful for aircraft design. Various ways of obtaining such an average are possible. One
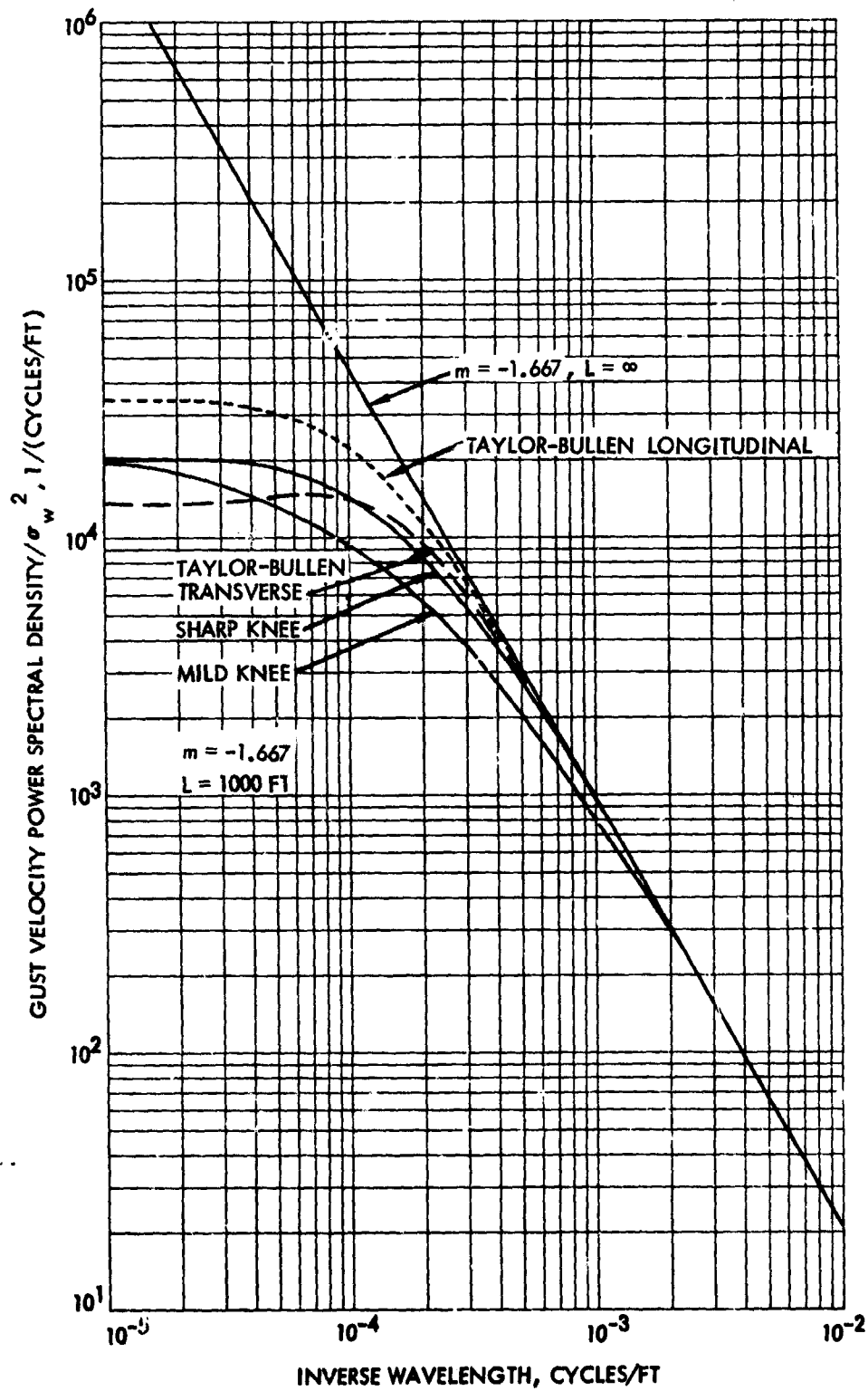
Figure 38 Comparison of Four Mathematically Defined Gust Power Spectral
Density Curves, m = 1.667, L = 1000 Ft and ∞

possibility would be to normalize all the curves by dividing by $\sigma_{\bar{w}}^2$ and take a simple average. This approach was, in fact, used for a number of the HICAT runs. A somewhat different approach, however, which appears to offer several distinct advantages, is used herein for the major part of the analysis.

Cumulative Probability Approach - This latter approach can best be understood by following the detailed description of its application to the HICAT data as given below. A brief summary at this point, however, is pertinent. From the many power spectral density (psd) curves that are to be averaged, a cumulative probability curve is prepared of the psd values read at a given frequency (inverse wavelength). This process is repeated for various frequencies covering the range of interest. A probability level is then selected, and the psd value corresponding to this probability is read from each curve. Each of the psd values read corresponds to a different frequency, and a plot versus frequency gives the desired average psd curve.

The advantages of this approach are the following:

● Under the normalizing and averaging approach, turbulence of all intensities contributes equally to the averages. But very mild turbulence is of negligible importance to airplane design and is much more subject to inaccuracy of measurement. It is therefore desirable to look separately at turbulence at various intensity levels. This is accomplished under the cumulative probability approach simply by reading power spectral densities from the probability curves at more than one probability level.

● In normalizing the power spectral densities in preparation for averaging, the vertical, lateral, and longitudinal gust power spectral densities would ordinarily each be normalized by dividing by their individual σ_w^2 value. A direct comparison of intensities in the three directions is thus lost.

● Because of uncertainty in measuring the very long wavelength components of the turbulence, the true overall rms gust velocity is quite uncertain. The appropriate rms to be used for normalizing, therefore, is an arbitrary one obtained by integration of the psd between appropriate limits. The value obtained will differ materially, depending upon the limits selected. For example, the σ_w value obtained by integration with a lower limit at $\lambda = 40,000$ ft may be 2 to 3 times that obtained using a lower limit of 2000 ft. This vast difference in the rms value that may be used to describe the same patch of turbulence has led to much confusion in the past. To minimize such confusion, great care is required in the use of rms values, and wherever their use can be avoided, it would appear desirable to do so.

● The procedure in which average psd curves are obtained from cumulative probabilities is believed to be particularly appropriate for arriving at a spectral shape for design use. For example, consider two airplanes. Airplane A feels predominantly gust frequencies over a narrow band in the vicinity of $\lambda = 400$ ft, and

airplane B over a narrow band in the vicinity of $\lambda = 20,000$ ft.
The design loads obtained for these two airplanes will depend
upon the design gust power spectral densities at their respective
frequencies. If design power spectral density curves utilize
average shapes obtained as described above, the design power spectral
density values will be exceeded with the same probability for both
airplanes, regardless of what turbulence intensity may be selected as
a design level. Clearly, the two airplanes will be of consistent
strength, as desired; the possible variation of spectral shape
from one patch of turbulence to another is quite unimportant.
While real airplanes generally respond over broader frequency bands
than assumed in this illustration, the general line of reasoning
still applies and the same conclusions hold.

The HICAT gust velocity spectra chosen for analysis are listed in Table II.
Only spectra were selected of intensity such that RMS 2 values were 1 fps or
greater. Spectra indicative of instrument malfunctions or those from time
histories containing obvious instrumentation malfunctions or other irregulari-
ties were excluded. All spectra from both the Redirected and the Extended
programs meeting these requirements were utilized.

First, all of the power spectra were faired to eliminate obvious irregularities
such as the closely spaced oscillations at the high frequency end. For the
most part, at the low frequency end the curves were left unfaired from the
lowest frequency to a frequency four or five times this value, with the fairing
becoming progressively heavier as the frequency increased beyond this point.
A typical example of how the curves were faired is shown in Figure 39.

The faired curves were then read at frequencies corresponding to wavelengths
of 200, 400, 1000, 2000, 4000, 10,000, 20,000, and 40,000 feet. It can be
observed that all of the measured spectra provide data at wavelengths of 200,
400, 1000, and 2000 feet, while progressively fewer curves extend to wave-
lengths of 4000, 10,000, 20,000, and 40,000 feet.

At each of these frequencies, cumulative probability curves of power spectral
density (psd) were prepared. In obtaining each probability distribution, the
psd values read were grouped into an adequate number of equal bands to facili-
tate plotting. Inasmuch as the longer runs actually represented larger
samples of data, the various runs were weighted by length in accordance with
the following table:

Actual duration of run in minutes	Assumed duration of run in minutes	Resulting number of times counted
1.33 - 3	2	1
3 - 5	4	2
5 - 7	6	3
7 - 9	8	4
9 - 11	10	5
11 - 13	12	6
13 - 16	14	7

75

Section V

Test Run	Test Run	Test Run	Test Run	Test Run	Test Run
54-3	164-4	257-13	265-17	267-15	280-1.
88-9	180-2	262-8	265-31	267-16	280-12
90-9(F)	180-4	262-10	265-38	267-22	280-13
90-12(F)	190-3	262-11	266-10	267-25	280-16
102-2	197-7	264-6	266-12	267-26	281-2(L)
102-3	198-3	264-13	266-14	267-28	282-2
102-5(L)	198-9	264-14	266-16	269-4(L)	282-3
102-6	198-12	264-16	266-18(L)	273-2	282-4
102-8	198-13(L)	264-18	266-22	279-2(L)	283-2(L)
102-9(L)	202-8 (F)	265-2	267-8	279-3	
102-12(L)	233-3	265-12	267-9	280-3(F)	
102-16	247-4(L)	265-14	267-11	280-6	
107-8	257-11	265-15	267-14(L)	280-10	

Note: (F) = Longitudinal component excluded
       (L) = Lateral component excluded
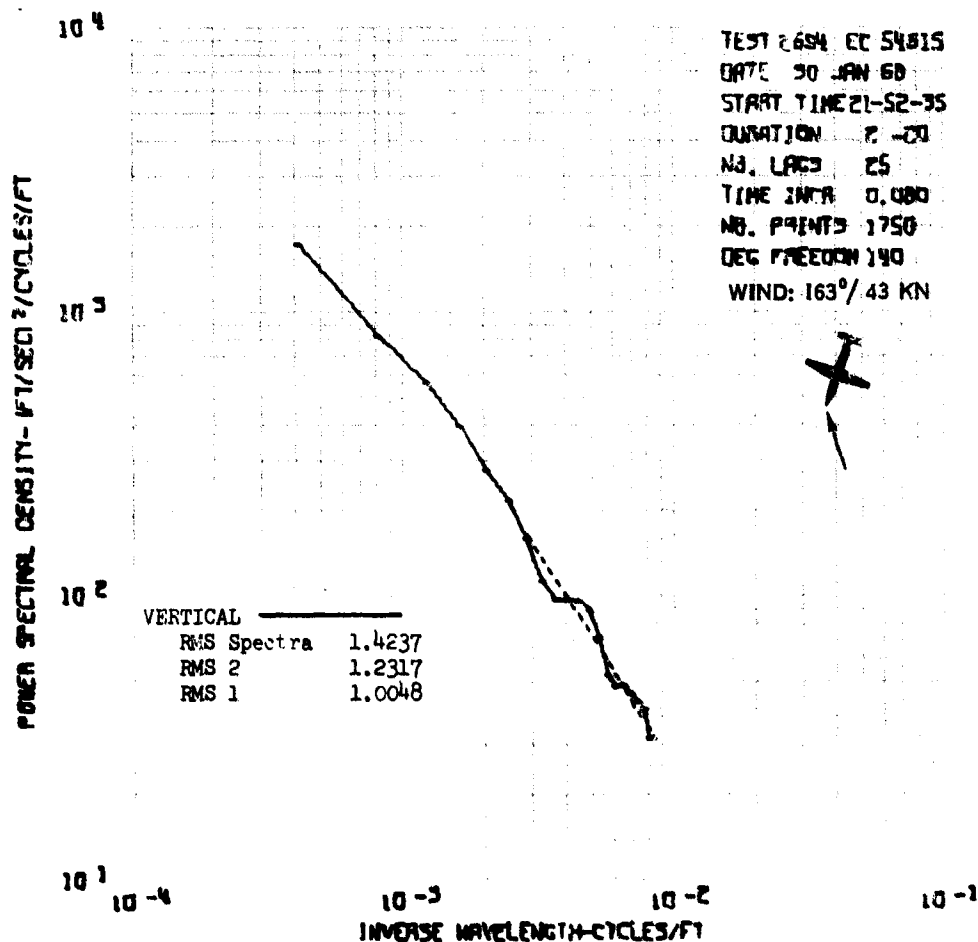
Figure 39 Example of Fairing of Gust Velocity Power Spectral Density Curves

The resulting curves are shown in Figures 40, 41, and 42. Curves for frequencies corresponding to λ = 20,000 ft and λ = 40,000 feet are not shown because there were too few runs in CAT of sufficient duration (13 minutes or more) to resolve these long wavelengths.

The curves in Figure 40 include only wavelengths (λ) from 200 through 2000 feet and utilize data from all the runs listed in Table II. The curves in Figure 41 extend to a wavelength of 4000 ft; in preparing these curves only those runs were included for which psd values were available at λ = 4000 feet. Similarly, the data in Figure 42 extend to a wavelength of 10,000 ft, and only those runs were included for which psd values were available at λ = 10,000 feet.

In Figure 40, each of the cumulative probability curves was faired by means of a straight line, as shown. Psd values were read as indicated by the plus symbols, at probabilities of .01, .1, and .5. The values at a probability of .01 were read from the straight line; at probabilities of .1 and .5, however, where each point represented a large sample, the value was read either from the actual straight line segment through the plotted points, or at a more representative average location if the actual curve was somewhat irregular.

At each of the three probability levels, the psd values thus read were then plotted versus inverse wavelengths to give Figure 43. An average psd curve was thus obtained at each of three probability levels. The curves corresponding to the lower probability levels are most pertinent for direct practical application, as they reflect the more severe turbulence. The curves corresponding to the higher probability levels, however, are based on much more data and are statistically more reliable.

The cumulative gust probability curves of Figures 41 and 42 were treated in the same way as the corresponding curves of Figure 40, except that in Figure 42 only two of the three probability levels could be read. Also, the cumulative probabilities shown in Figure 42 are considerably more irregular than those appearing in the preceding figures, so that somewhat more judgment was necessary in reading values at the two probability levels. The same basic rules followed for the λ = 2000 ft and λ = 4000 ft groups of curves were applied here with slightly more leeway. The resulting power spectral densities are shown in Figures 44 and 45.

Average Normalized Spectrum Approach - The number of HICAT runs for which psd's might be obtained with reasonable confidence at wavelengths of 20,000 or 40,000 ft is quite limited, totaling only about 6 for the combined 1965-67 and 1967-68 programs. As a result, the cumulative probability method for obtaining an average spectral shape was found not to be usable for these runs. In order to obtain average spectral shapes that would extend to the 20,000 to 40,000 ft wavelength range, a more direct approach was used. This involved normalizing the individual faired spectra by dividing the density estimates by the square of a suitably defined rms value and taking a simple average at each frequency. For comparison, the same procedure is also applied to the spectra defined to λ = 10,000 ft for runs comprising the ten special HICAT tests described in Appendix I. The normalized spectra used for this purpose are presented in Figures 101 and 102, Appendix I.
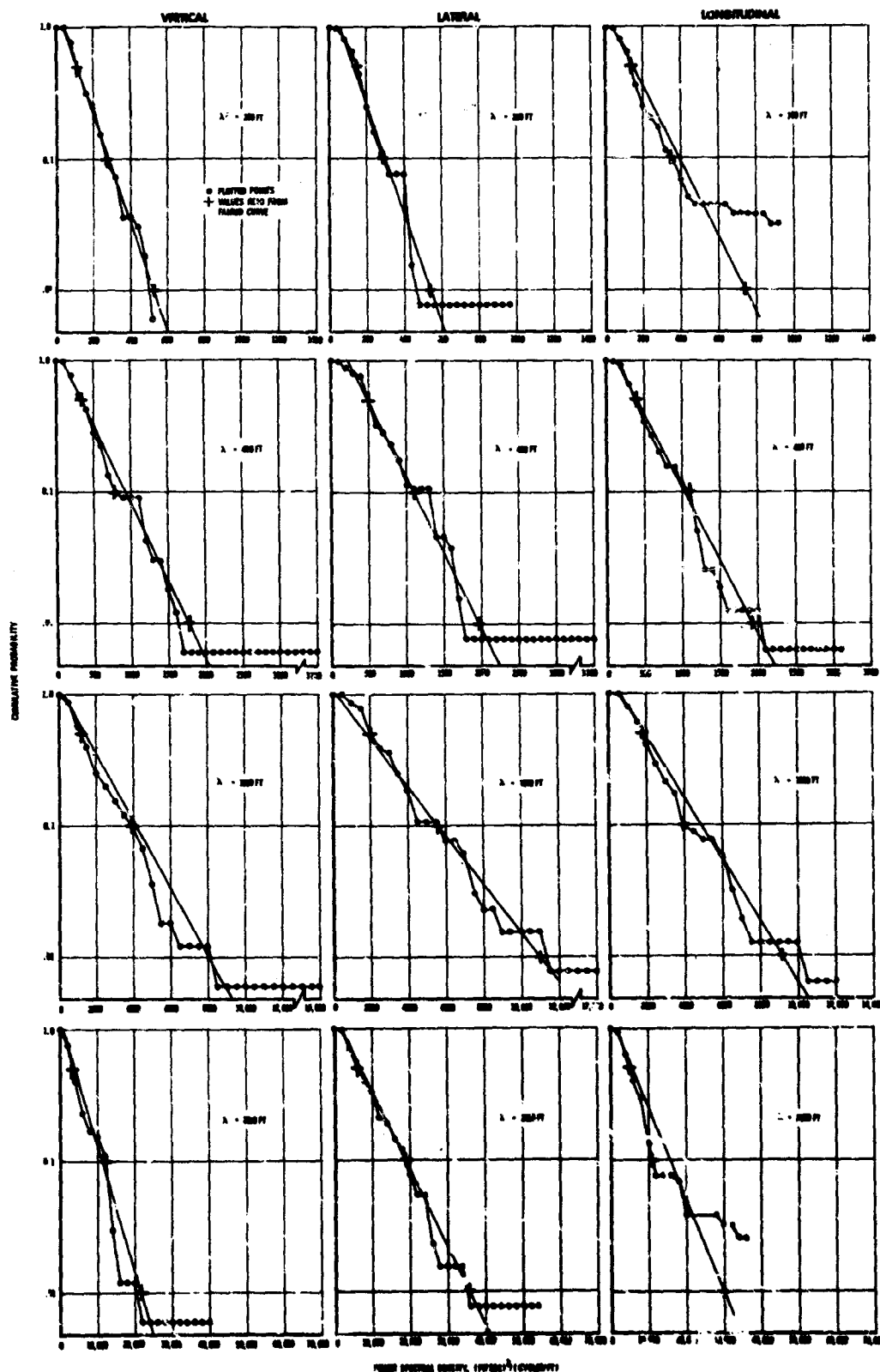
Figure 40   Cumulative Probability of Power Spectral Density for
            Various λ - Vertical, Lateral, and Longitudinal Gust,
            Maximum λ = 2000 ft
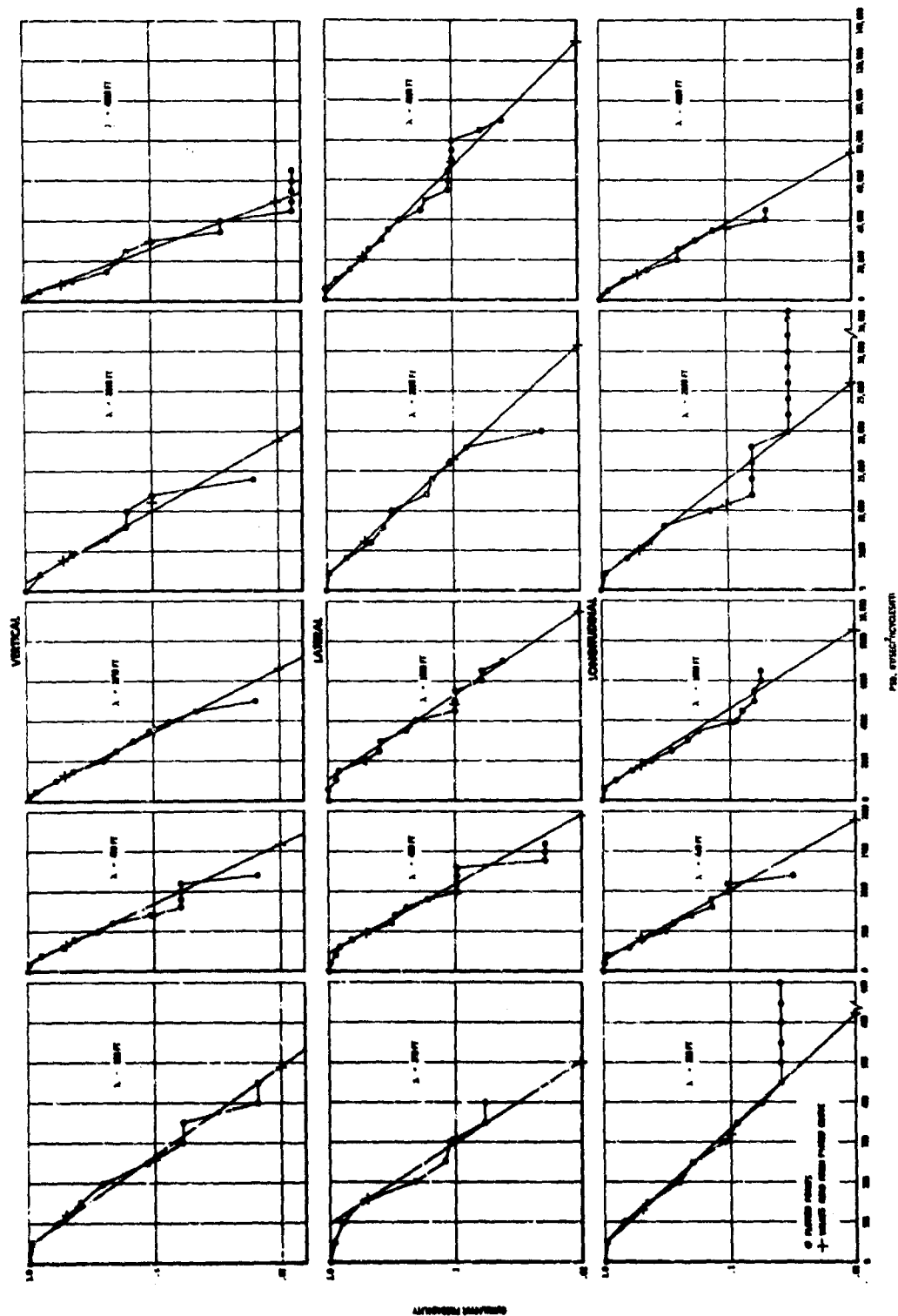
Figure 41 Cumulative Probability of Power Spectral Density for Various λ – Vertical, Lateral, and Longitudinal Gusts, Maximum λ = 4000 ft
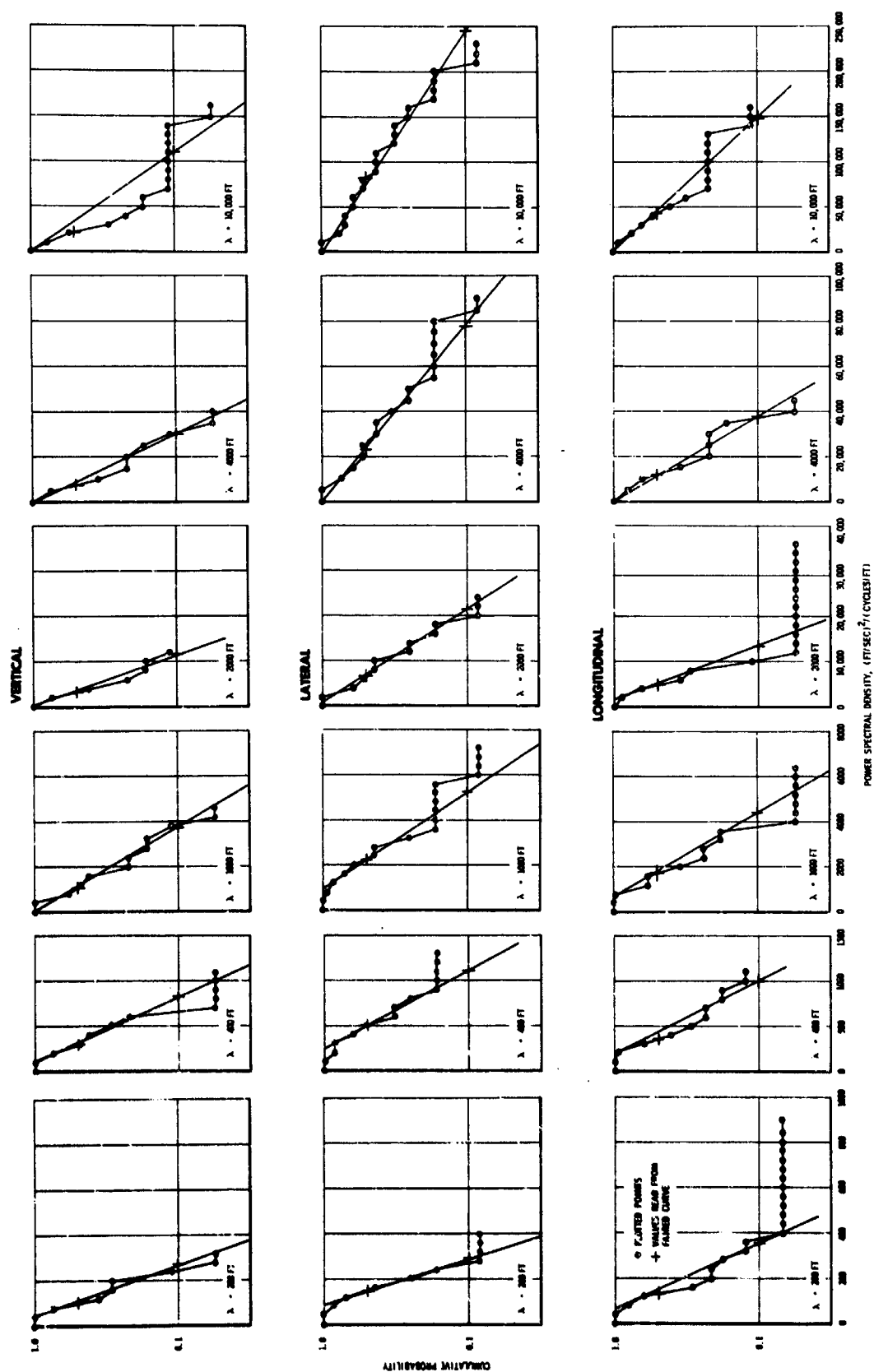
Figure 42   Cumulative Probability of Power Spectral Density for Various λ – Vertical, Lateral, and Longitudinal Gusts, Maximum λ = 10,000 ft
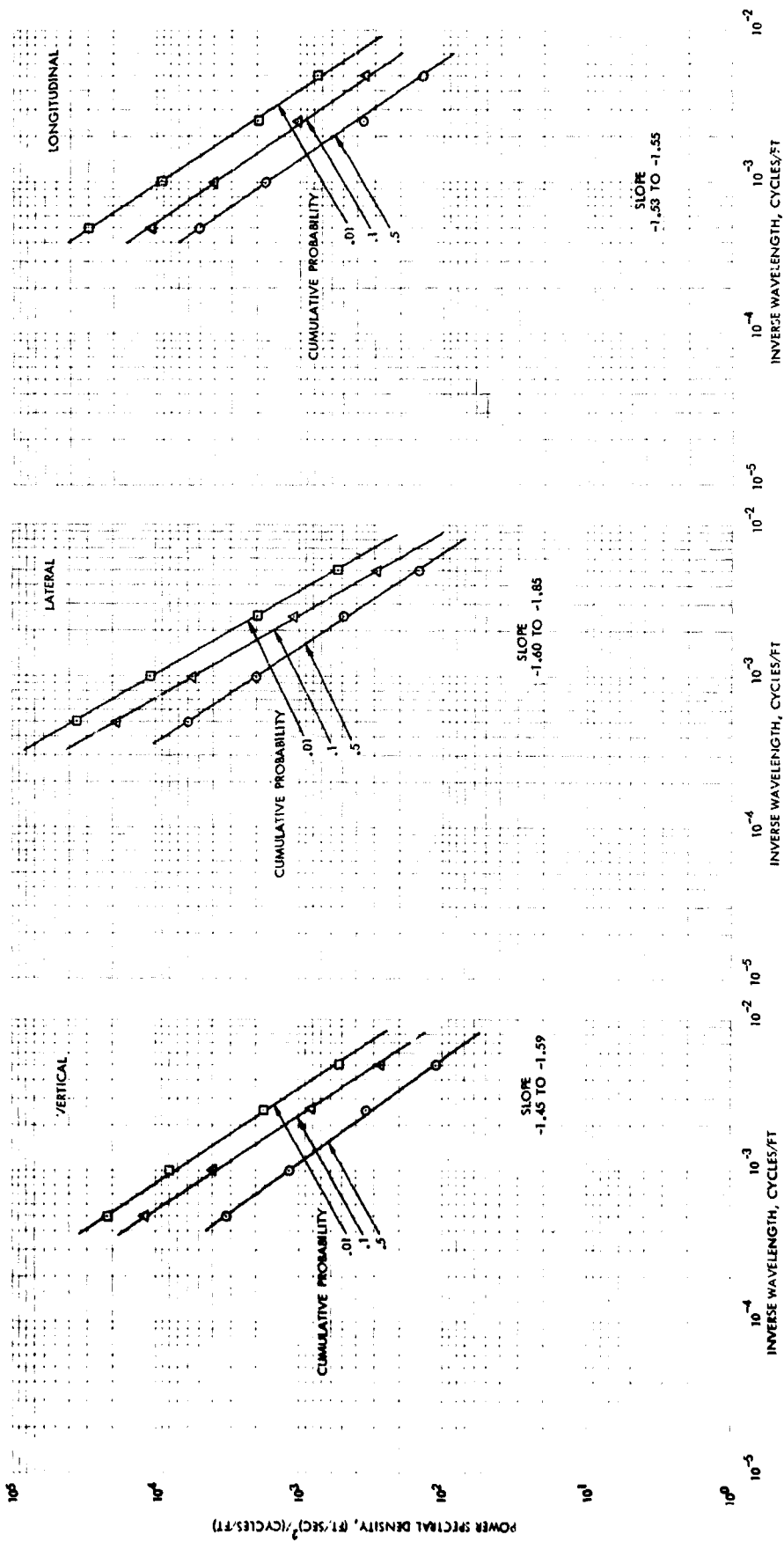
Figure 43 Average Power Spectral Density Based on Cumulative Probability, Maximum λ = 2000 ft
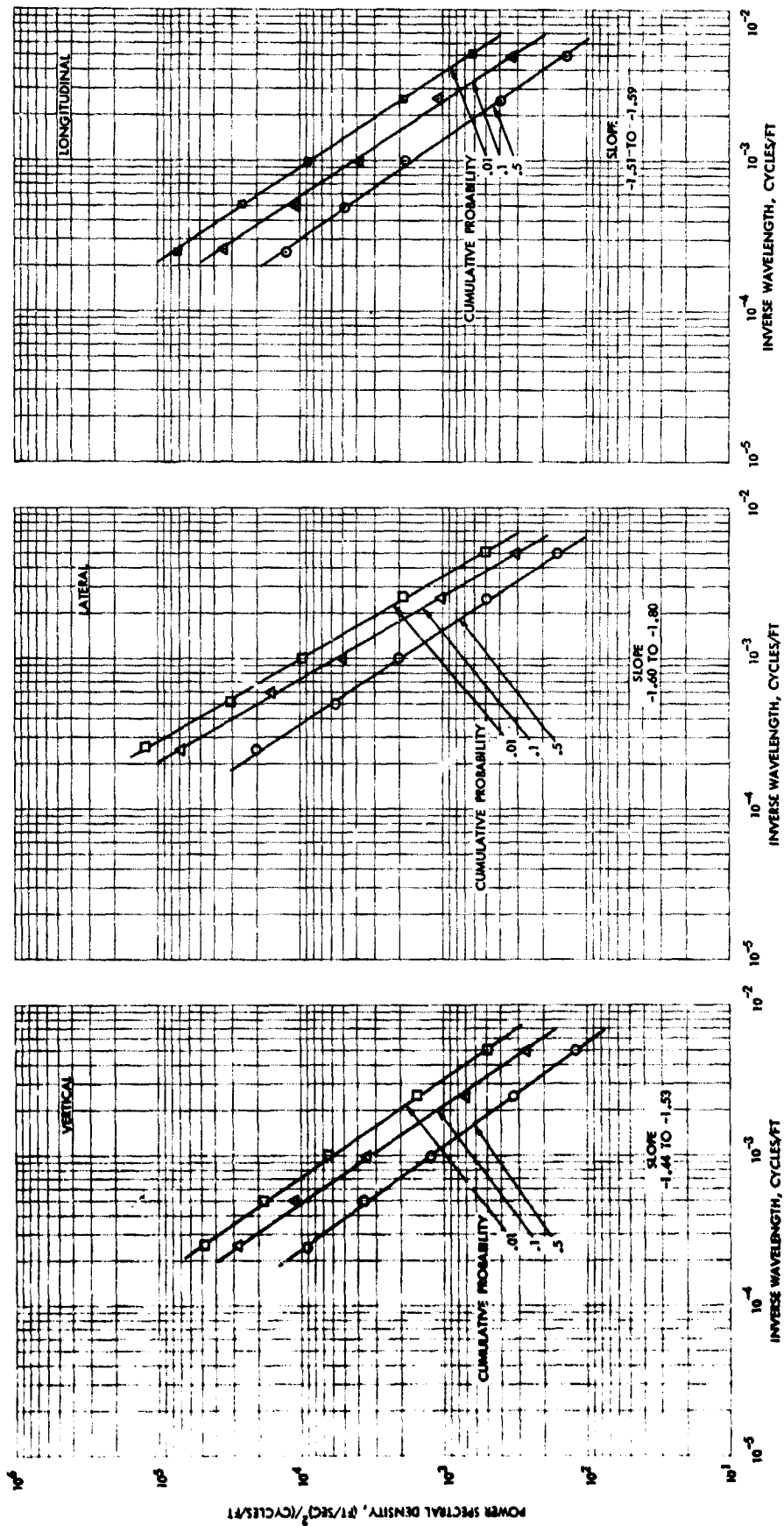
Figure 44 Average Power Spectral Density Based on Cumulative Probability, Maximum λ = 4000 ft
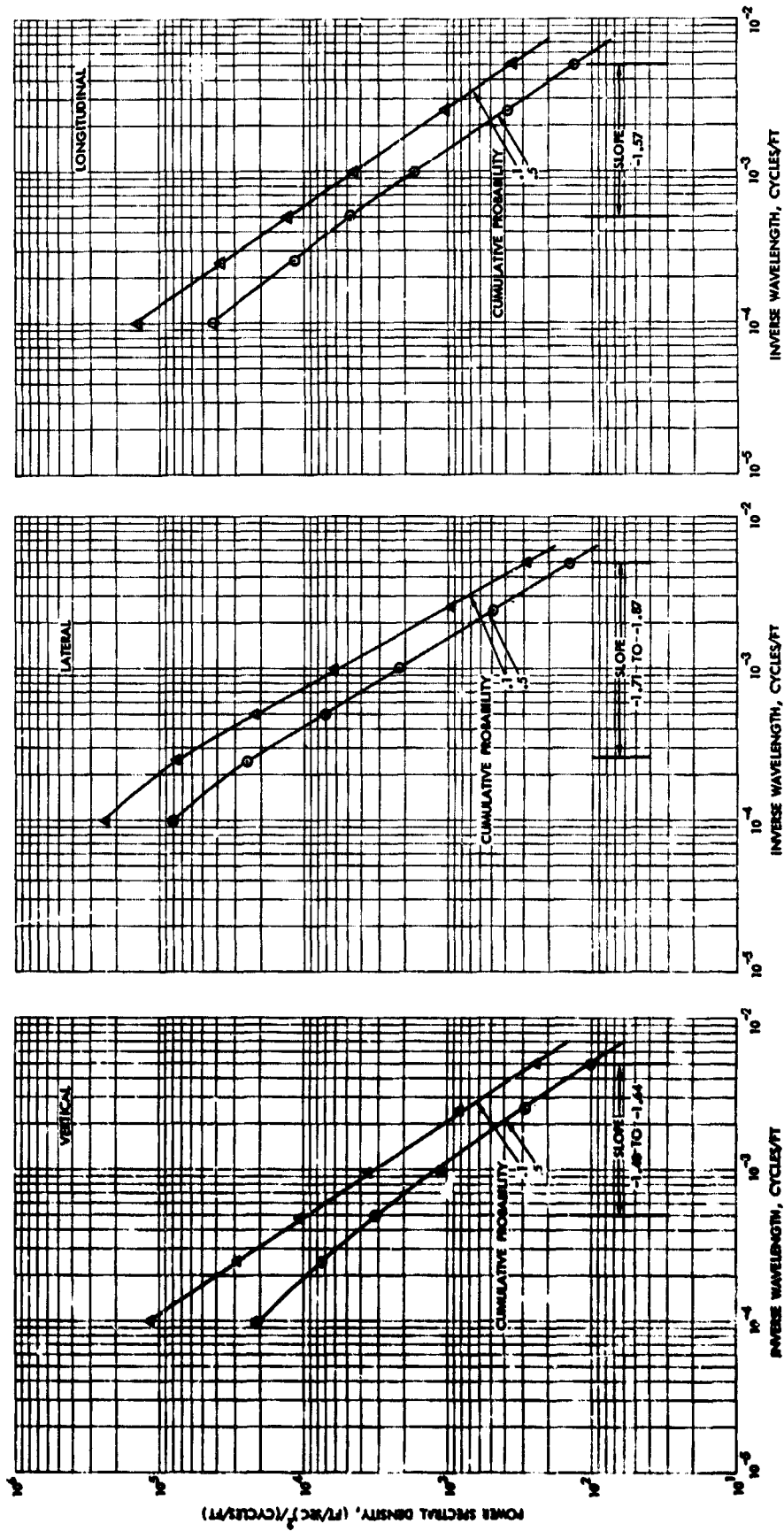
Figure 45 Average Power Spectral Density Based on Cumulative Probability; Maximum λ = 10,000 ft

Section V

Normalization of the spectral components was based on the RMS 2 value of the component gust velocity. Use of an individual normalizing factor for each of the three components permits a direct comparison of spectral shape in the three directions, at any desired frequency. Selection of RMS 2 as a basis for normalizing is somewhat arbitrary. As noted earlier in pointing out the advantages of the cumulative probability approach, the true rms is quite uncertain because of the inherent difficulty in accurately measuring the long wavelength components of the turbulence. Therefore, a spectral rms, with the integration confined to a frequency range for which there is no doubt as to the validity of the measurements, provides a much more concrete basis for normalizing than an rms computed directly from the time history. The quantities RMS 2, RMS 4, and RMS 10 would all be acceptable as a result of this consideration. However, since RMS 2 is available for all runs for which psd's were determined, it was used.

Averages were obtained for each group of normalized spectra and are shown in Figures 47 and 48. These spectra are discussed on the next page.

Results and Discussion - Cumulative Probability Approach - Average spectral shapes obtained by the cumulative probability approach described above are shown in Figures 43, 44, and 45.

For all three gust velocity components in Figure 43 (maximum λ = 2000 ft), the psd curves plot as straight lines. The vertical and lateral gust velocity components for the .1 and .01 probability levels are parallel. At the .5 probability level, the psd's have a shallower slope than the psd's at the low probability levels. The slopes of the psd's for the longitudinal gust component are equal for the .5 and .1 probability level; the slope is slightly steeper at the .01 probability level. The slopes for the vertical and longitudinal gust components are somewhat shallower, at all wavelengths and at all three probability levels, than the -1.67 and -2.00 values currently used in design and analysis. The lateral component curves for the .1 and .01 probability levels have a slope which is comparable to that currently being used for design and analysis, but the curve for the .5 probability level is more shallow. The absence of any bending in the psd curves, within the frequency range shown, makes it impossible to infer a scale of turbulence by visually comparing the psd's with the mathematically defined psd's shown in Appendix I.

The results obtained for maximum λ = 4000 ft, shown in Figure 44, are similar to the results for maximum λ = 2000 ft and the slopes are very nearly identical. Again the absence of any bend in the curves over the range of frequencies shown makes it impossible to infer a specific scale of turbulence from the mathematically defined psd's although one may infer that the scale of turbulence cannot be less than some particular value.

The curves of average spectral shape obtained for wavelengths up 10,000 ft are shown in Figure 45. Despite the leeway in reading values from the cumulative probability curves (Figure 42), the scatter of the points on the psd plots is not great. At the longer wavelengths included in these figures, some slight bending of the curves is evident. Scales of turbulence at which the mathematically defined curves of Appendix I fit these experimental curves are roughly as follows:
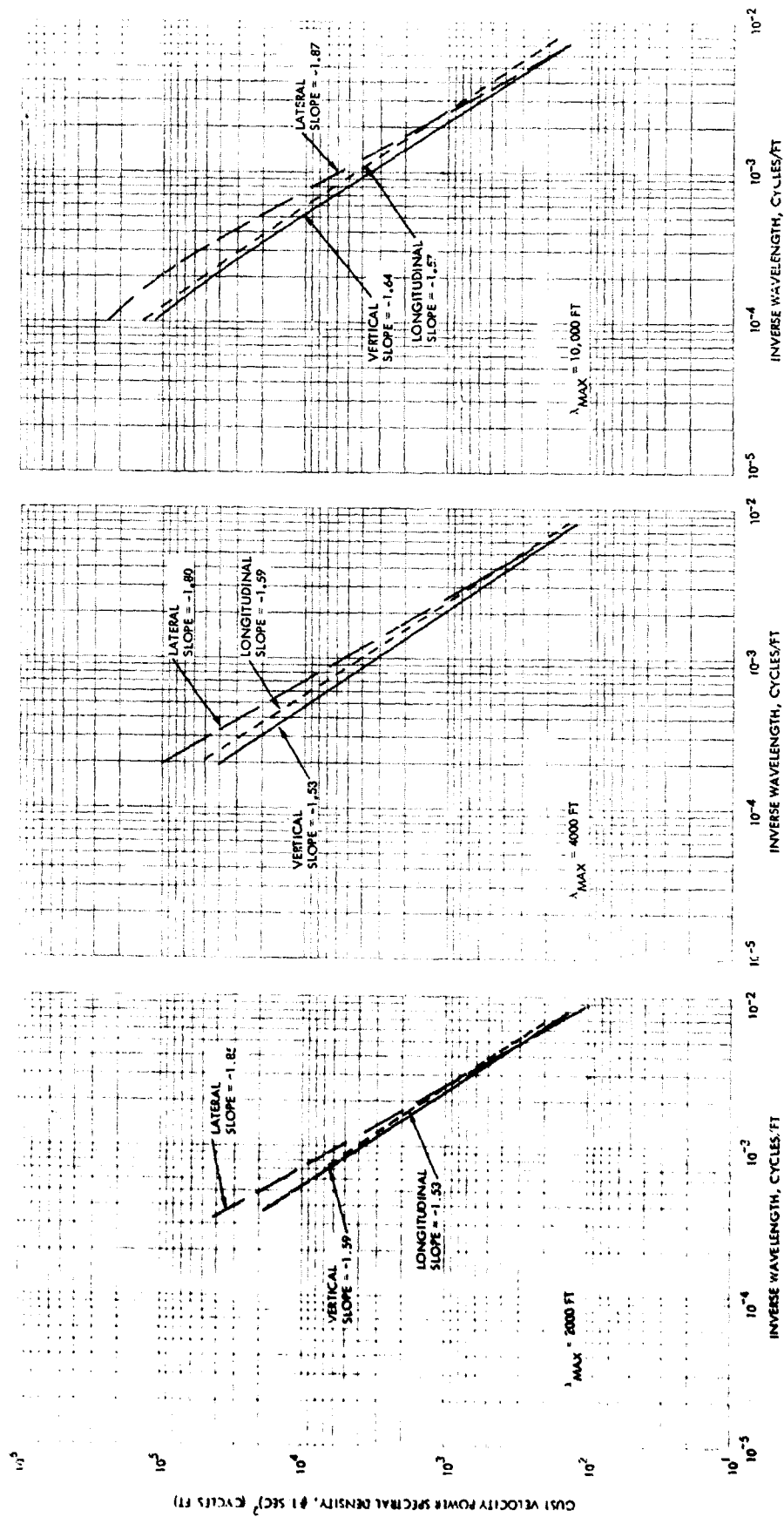
Figure 46 Comparison of Power Spectral Densities for 3 Components, Cumulative Probability of .1, Maximum λ = 2000, 4000, 10,000 Ft.

Section V

Scale of Turbulence, L, ft

Family	Vertical Prob.=.1	Vertical Prob.=.5	Lateral Prob.=.1	Lateral Prob.=.5	Longitudinal Prob.=.1	Longitudinal Prob.=.5
Taylor-Bullen	2000	2000	2000	1800	4000	4000
Sharp Knee	2000	2000	1500	1900	2000	2000
Mild Knee	4000	4000	3500	3500	4000	4000

It should be emphasized, however, that for these spectra the curvature is so slight, especially when considered relative to the scatter of the plotted points, that a scale of turbulence is not reliably defined. Consequently the tabulated scales should be regarded as minimum values.

Comparisons between the psd's for the vertical, lateral, and longitudinal components of turbulence, all at the 0.1 probability level, are shown in Figure 46. All three curves show the psd for the vertical component of turbulence to have a somewhat shallower slope than that for the lateral component. The longitudinal component for maximum $\lambda = 2000$ ft and 10,000 ft has a shallower slope than either the vertical or lateral components; for maximum $\lambda = 4000$ ft, the longitudinal component is intermediate between the slopes for vertical and lateral.

Results and Discussion - Average Normalized Spectrum Approach - The spectral shapes obtained by averaging the normalized spectra are shown in Figures 47 and 48. Figure 47 covers the full range of wavelengths from 200 to 40,000 ft. Figure 48 shows the average spectrum for each component of gust velocity for runs covering the range of wavelengths from 200 to 10,000 ft that were used for detailed meteorological analysis in Appendix I.

In Figure 47, all three curves are very nearly straight lines over the entire frequency range, although the vertical spectra might be viewed as starting to bend down at the lowest frequencies, and the lateral spectra changes slope at roughly the midpoint of the frequency range. Inferred scales of turbulence are:

Scale of Turbulence, L, ft

Family	Vertical	Lateral	Longitudinal
Taylor-Bullen	3300	4000	6000
Sharp Knee	8000	>8000	4000
Mild Knee	16000	>4000	>8000

86

Figure 48 Direct-Average of Normalized Power Spectral Density, 3 Components Maximum λ = 10,000 Ft.

Figure 47 Direct-Average of Normalized Power Spectral Density, 3 Components Maximum λ = 40,000 Ft.

Section V

Slopes of the three curves in Figure 47 are as follows:

Component	Average Slope - Wavelength Range < 1000 ft
Vertical	-1.34
Lateral	-1.65
Longitudinal	-1.50

In Figure 48, all three curves are also very nearly straight lines over the entire frequency range. Inferred scales of turbulence are:

Family	Scale of Turbulence, L, ft		
	Vertical	Lateral	Longitudinal
Taylor-Bullen	> 2000	> 3000	2000
Sharp Knee	> 4000	> 3000	3000
Mild Knee	> 8000	> 8000	3000

The three curves in Figure 48 all have a slope of about -1.71. A comparison of the average slopes obtained from Figures 47 and 48 with the slopes obtained using the cumulative probability approach shows that, over the high frequency range alone, the slopes for the lateral and longitudinal gust components are in good agreement. The slopes of the psd's for the vertical component, however, show more variation. The value of -1.34 obtained from Figure 47 is considerably lower than the value of -1.71 obtained from Figure 48, whereas the values from the cumulative probability approach fall between these values, with a tendency towards the higher value.

Average slopes over the full range of wavelength in Figure 47 are somewhat lower than the slopes over the high frequency range alone, whereas, in Figure 48, the average slopes are more nearly constant throughout the frequency range. This is probably due to the tendency of the psd's to bend down at longer wavelengths, and it would be expected that more bending would have occurred in psd's extending to $\lambda = 40,000$ ft than in psd's extending to $\lambda = 10,000$ ft.

Although the average psd's are generally fairly straight lines over the entire frequency range, individual spectra are often much less regular. This irregularity is clearly shown in the plots of normalized spectra in Appendix I. In Figure 101, for example, a number of the curves break away from a fairly steep high-frequency slope at wavelengths between 2000 and 10,000 ft and then resume the original slope at somewhat longer wavelengths. Upon averaging, the result is a nearly straight line of considerably shallower slope than might be thought characteristic of the individual spectra. It is believed likely in some cases that the initial breaking away from the high-frequency slope is a real property of the turbulence, whereas the resumption of the steep slope at longer wavelengths represents the presence of noise.

Concluding Remarks - In assessing the spectra shown in Figures 43 through 48, it is felt that the data up to wavelengths of 10,000 ft (and possible extrapolated to 12,000 or 15,000 feet, if a larger sample size were available) provide valid representations of the atmosphere. At wavelengths of 20,000 ft and above, the situation is less clear because the data sample is much smaller, the gust intensity level is generally considerably less, and the possibility of some extraneous influence is correspondingly greater. However, even these latter spectra are believed to be conservative from a design standpoint.

In evaluating the scale of turbulence, it should be remembered that the range of values shown here apply to average power spectra. Individual power spectra making up the average may have somewhat larger or smaller scales though only a few spectra actually bend over and become flat within the range of the HICAT measurements. However, based upon the apparent bending of the average spectra, a scale of turbulence in the range 2000 to 4000 feet would appear to fit most of the analyzed data.

SPECIAL STATISTICS

Probability Distributions of RMS Gust Velocity

Probability distributions of rms values of the three components of absolute gust velocity, for the runs for which all three components are available as identified in Table II, are shown in Figure 49. The rms gust velocities upon which the curves in this figure are based are the RMS 2 values; these were obtained by integrating the power spectral densities over the frequency range from .0005 cycles per foot (λ = 2000 ft) to the highest frequency at which the power spectral densities were defined, corresponding to 5.00 cps and averaging about .007 cycles per foot. The low frequency limit of integration was selected for this figure as the lowest frequency common to all the power spectral densities obtained.

Cumulative probability distributions rather than probability densities are shown because this form of presentation is more amenable to drawing quantitative conclusions. For any given rms gust velocity, the cumulative probability read from the appropriate curve is the probability that the given rms gust velocity is exceeded.

Also of interest are similar probability distributions of rms values based upon inclusion of longer wavelengths. For this reason, probability distributions of RMS 10 are also presented, in Figure 49. These latter probability distributions are based upon a somewhat smaller data sample, however, since RMS 10 values were obtained only for runs of at least 6.7 minutes duration. The rms gust velocities upon which the curves in Figure 49 are based are the values obtained by integrating the power spectral densities over the frequency range from .0001 cycle per foot (λ = 10,000 ft) to about .007 cycle per foot.

It is also felt that probability distributions of rms values emphasizing considerably shorter wavelengths than RMS 2 would be of value, particularly for comparing the three components of gust velocity. All runs include wavelengths down to approximately 100 to 150 feet; however, the low frequency limit of integration for which rms values are available is 1000 feet. Consequently the desired probability distributions must be of some other quantity which can be related to the rms values. A suitable quantity for this purpose is

the square root of the faired psd at some appropriate single frequency. Such a quantity is proportional to the rms value, as intensity varies, for a given shape of power-spectral density curve and; therefore provides a measure of relative gust intensities at shorter wavelengths. A frequency corresponding to $\lambda = 200$ ft was selected to define this quantity which is then designated $\sqrt{\Phi_{200}}$. The resulting probability distributions are shown in Figure 50. The square root of the faired psd values upon which the curves in this figure are based can be interpreted as being a constant times the rms values that would be obtained by integrating the power spectral densities over a very small frequency range at .005 cycles per foot.

To convert the rms and $\sqrt{\Phi}$ values plotted herein to rms values that would be obtained if various shapes of power spectral density function were fitted to the data and the integration carried out from zero to infinite frequency, the rms (or square root of psd) values would be multiplied by approximately the following factors:

Spectral Shape		RMS 10	RMS 2	$\sqrt{\Phi_{200}}$
Von Karman,	L = 2500 ft	1.42	2.48	.42
Dryden,	L = 1000 ft	1.15	1.97	.41
Dryden,	L = 2000 ft	1.55	2.72	.57

The factors for RMS 2 and RMS 10 were obtained from the theoretical curves noted by evaluating the ratios

$$\frac{\sqrt{\int_{0}^{\infty} \Phi\left(\frac{1}{\lambda}\right) d\left(\frac{1}{\lambda}\right)}}{\sqrt{\int_{.0005}^{.007} \Phi\left(\frac{1}{\lambda}\right) d\left(\frac{1}{\lambda}\right)}} \quad \text{and} \quad \frac{\sqrt{\int_{0}^{\infty} \Phi\left(\frac{1}{\lambda}\right) d\left(\frac{1}{\lambda}\right)}}{\sqrt{\int_{.0001}^{.007} \Phi\left(\frac{1}{\lambda}\right) d\left(\frac{1}{\lambda}\right)}}$$

respectively for RMS 2 and RMS 10. The factors for $\sqrt{\Phi_{200}}$ were obtained by calculating Φ, from the equation defining the spectral shape, at a frequency $1/\lambda = .005$ cycles per foot, and from this obtaining $\sigma/\sqrt{\Phi}$, the desired factor.

In obtaining the probability distributions shown in Figures 49 and 50, variation in length of runs was accounted for approximately by weighting the various runs, as discussed previously under Average Spectral Shape.

The probability distributions shown apply to the flight time included in "runs" as defined under Data Editing in Section IV, of 80 seconds or more duration. To convert to a basis of total flight time, all of the curves would be shifted down in roughly the ratio .033, which is the ratio of time in runs of 80 seconds or more duration to the total flight time for which data are available.
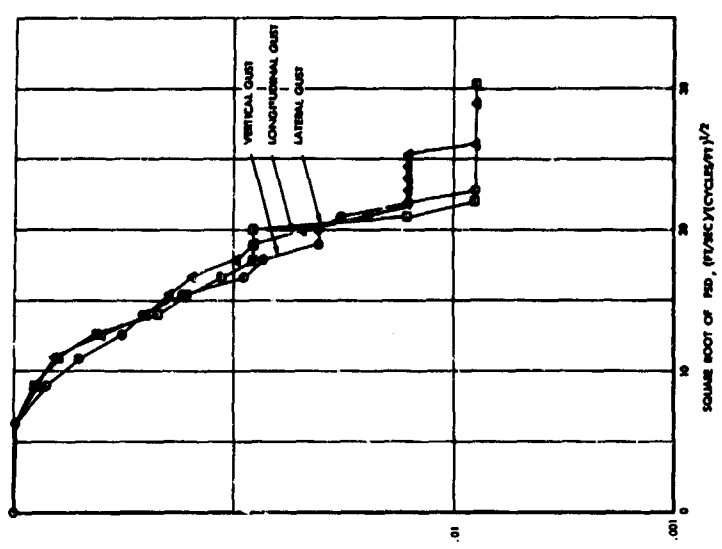
Figure 50 Cumulative Probability Distribution of $\sqrt{\Phi}$ at λ = 200 Ft.
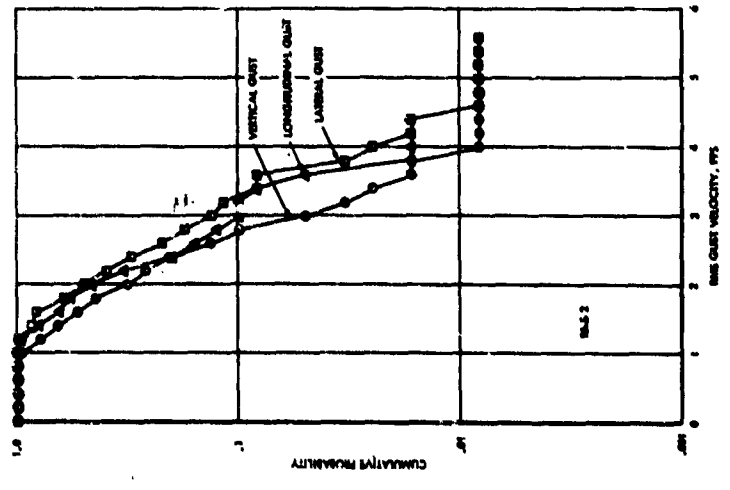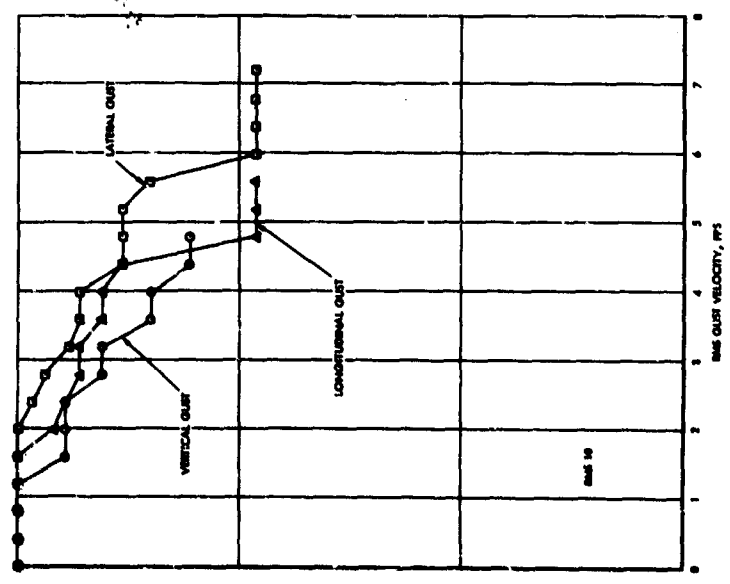
Figure 49 Cumulative Probability Distributions of RMS 2 and RMS 10 Gust Velocities

The flatness of all the curves for rms gust velocities below 1.0 fps, or $\sqrt{\Phi}$ below about 5 fps/$\sqrt{\text{cpf}}$, is due to excluding data in mild turbulence - that is, turbulence of RMS-2 intensity less than 1 ft/sec.

It should be emphasized that each rms value utilized in preparing these figures was an overall value for a given run, and that in many of the runs the rms gust velocities varied significantly during the run. If this variation were to be taken into account, the probability distributions would show much higher rms values at the low probability levels. This phenomenon is discussed in detail under Stationarity.

Isotropy

Knowledge of the probable isotropy of turbulence is important chiefly to provide answers to the following questions:

- First, should the turbulence intensities used for design be the same for the three components of turbulence, vertical, lateral, and longitudinal? This question is important because design levels are ordinarily based primarily upon measurement of airplane center-of-gravity normal acceleration during a great many hours of routine operational flight. Thus, the design intensity of the vertical component of gust velocity is established fairly directly. The determination of realistic design intensities of the lateral and longitudinal components must depend upon more complete data from a much smaller sample, such as provided by the HICAT program.

- Second, should the airplane be considered to be subjected to the design intensity of all three components of turbulence simultaneously, or when one component is at its maximum is it probable that the intensities of the other two will be significantly lower?

The isotropy of the turbulence measured in the HICAT program is indicated in this report in three ways. Each is discussed separately in the following paragraphs.

Isotropy as Indicated by Gust Velocity PSD's - First, in order to determine whether the isotropy picture is the same at all frequencies (inverse wavelengths), the comparative psd plots shown in Figures 46 through 48 are examined. The results differ somewhat from figure to figure. However, it appears reasonable to give the greatest weight to Figure 46, which represents the largest samples. On this basis, the figures collectively indicate that all three components have about the same intensity (as measured by psd) at the shortest wavelength at which measurements were made (100 to 150 ft). They also show the vertical component to decrease in intensity, relative to the lateral as the wavelength increases. Thus, at the longer wavelengths, the vertical component of turbulence appears to be somewhat less severe than the lateral. The longitudinal component tends to fall between the vertical and the lateral.

For isotropic turbulence, psd's of the vertical and lateral components should agree. Theory indicates, however, that ratios of the longitudinal component to the lateral or vertical component in the constant exponent region of the psd depend upon the exponent and have the following values:

Exponent	Φ_F/Φ_L Ratio of longitudinal to lateral psd	σ_F/σ_L Ratio of longitudinal to lateral spectral rms velocities
-2	2/3	.817
-5/3	3/4	.866
-3/2	4/5	.895
-4/3	6/7	.926
-1	1	1.000

In the HICAT program, the direction of flight through the turbulence presumably is random. Hence the turbulence should appear isotropic in the horizontal plane, and the tabulated ratios between longitudinal and lateral psd values should hold. In comparing the vertical component with the lateral or longitudinal, however, isotropy does not appear to be so necessary, as the mechanism generating the turbulence might be inherently directional.

For an exponent of -3/2 to -5/3, characteristic of the HICAT psd's, the theoretical ratio of longitudinal to lateral psd's is seen from the table to be about .75 to .80. The general impression given by Figures 46 and 47 is that the actual ratio is closer to unity, especially at the shorter wavelengths. However, the differences are perhaps so small as to be buried in the scatter of the data.

The comparison of vertical and lateral components does seem to indicate the turbulence to be isotropic at the shorter wavelengths but to be clearly less severe in the vertical direction than the lateral as the wavelengths increase.

Isotropy as Indicated by Probability Distributions of RMS Gust Velocity - In the second approach to evaluation of isotropy, the rms values and, similarly, the $\sqrt{\Phi_{200}}$ values of the three components of gust velocity are read from the cumulative probability curves of Figures 49 and 50 at a given probability level, and the pertinent ratios are calculated. This approach is considered to be somewhat more reliable than the first because the vertical, lateral, and longitudinal intensities were all obtained from the same group of runs.

It is seen first that the ratio of longitudinal to lateral gust velocity is roughly 1.00 for $\sqrt{\Phi_{200}}$, 0.90 for RMS 2, and 0.82 for RMS 10 throughout the probability range. The corresponding theoretical value, as indicated by the table in the preceding section, is in the range 0.86 to 0.90. The values based upon RMS 2 and RMS 10 are in reasonable agreement with the theory; the value based upon $\sqrt{\Phi_{200}}$ cannot be considered in agreement with the theory, but does reflect a continuation of the trend defined by the RMS 2 and RMS 10 ratios. The general trend with wavelength is qualitatively the same as indicated by the psd curves of Figure 46.

Ratios of lateral to vertical gust velocity are as indicated in the following table:

Region of Curve	$\dfrac{(\sqrt{\Phi_{200}})_{LAT}}{(\sqrt{\Phi_{200}})_{VERT.}}$	$\dfrac{(RMS\ 2)_{LAT}}{(RMS\ 2)_{VERT.}}$	$\dfrac{(RMS\ 10)_{LAT}}{(RMS\ 10)_{VERT.}}$
Low intensity, high probability	1.15	1.25	1.45
High intensity, low probability	1.00	1.20	1.25

The ratio tends to decrease with increasing turbulence intensity, with the high-intensity values being probably the more significant. The trend with wavelength is qualitatively the same as indicated by the psd plots; the vertical and lateral components are approximately equal in intensity at the short wavelengths, whereas the lateral component becomes significantly more severe at the longer wavelengths.

Isotropy as Indicated by Probability-Paper Plots of Ratios of RMS Gust Velocity - The above approaches give information pertinent to answering the first question posed, i.e., What relative intensities of vertical and lateral gust are appropriate for design? They do not, however, shed any light on the isotropy of individual patches of turbulence.

For this latter purpose, as well as to obtain an independent indication of the average ratios amongst the three components, a third approach was followed. Ratios of longitudinal to lateral, lateral to vertical, and longitudinal to vertical spectral rms gust velocities were obtained for all the available runs listed in Table II. These ratios were also calculated based on the square root of the psd's at $\lambda = 200$ feet. Probability distributions of the ratios were then obtained, weighted according to duration of run as described previously in the paragraph entitled Probability Distributions of RMS Gust Velocity. Plots of these probability distributions on probability paper are shown in Figures 51, 52, and 53. The probability indicated by the curves is the probability that the ratio is less than the indicated value.

A Gaussian, or normal, probability is indicated by a straight line on such a plot. The value of the variable at a probability of 50 percent is the mean. The difference between the mean and the value read at a probability of 15.9 or 84.1 percent is the standard deviation.

A summary of the pertinent values as obtained from the curves follows:

Ratio	$\sqrt{\Phi}_{200}$			RMS 2			RMS 1C		
	Mean	Std Dev	70% Probability Band	Mean	Std Dev	70% Probability Band	Mean	Std Dev	70% Probability Band
Long./Lat	1.00	.11	0.89-1.11	0.93	.14	0.79-1.07	0.79	.10	0.69-0.89
Lat/Vert	1.06	.11	0.95-1.17	1.24	.21	1.03-1.45	1.57	.37	1.20-1.94
Long./Vert	1.06	.09	0.97-1.15	1.16	.16	1.00-1.32	1.24	.16	1.08-1.40

The distributions for the ratio of longitudinal to lateral $\sqrt{\Phi_{200}}$, RMS 2, and RMS 1C, shown in Figures 51, 52, and 53, respectively, are almost straight lines. The respective mean values of 1.00, 0.93, and 0.79 are in excellent agreement with the ratios of 1.00, 0.90, and 0.82 indicated in the section entitled Isotropy as Indicated by Probability Distributions of RMS Gust Velocity. In 70 percent of turbulence encounters, it would be expected that the ratio of longitudinal to lateral intensities would lie between the two values listed in the above summary table under the headings "70% Probability Band."

Examination of the distributions for the ratio of lateral to vertical $\sqrt{\Phi_{200}}$, RMS 2, and RMS 10 shown in Figures 51, 52, and 53, respectively, indicates a fairly good straight line fit. Indicated means are shown in the summary table above. The mean values agree quite well with ratios obtained at a probability of about 0.5 from Figures 49 and 50 and listed after "Low intensity, high probability" in the table on the preceding page. The variation of the ratio with turbulence intensity noted on the basis of Figures 49 and 50, is quite possibly a real effect, as the presentation of the gust intensity ratios versus probability is inherently dominated by the lower intensities, of less interest.

The above discussion of the ratios of lateral to vertical applies generally to the longitudinal-to-vertical curves in Figures 51, 52, and 53. The values of the mean are consistent with means of 1.00 or less on the longitudinal-to-lateral curves.

Summary - Each of the three approaches used above to investigate isotropy, in general, shows the same relationship amongst the three components of gust velocity, the lateral component tends to be the most severe, and the vertical component tends to be the least severe. All three components tend to be about equal in severity (say within 15 percent rms) at the highest measured frequencies (roughly 0.007 cycles per foot); however, the lateral component tends to become somewhat more severe at the lower frequencies. For example, at a wavelength of 10,000 feet the ratio of lateral to vertical rms ranges from 1.25 to 1.45. The observed percentage differences amongst the three components,
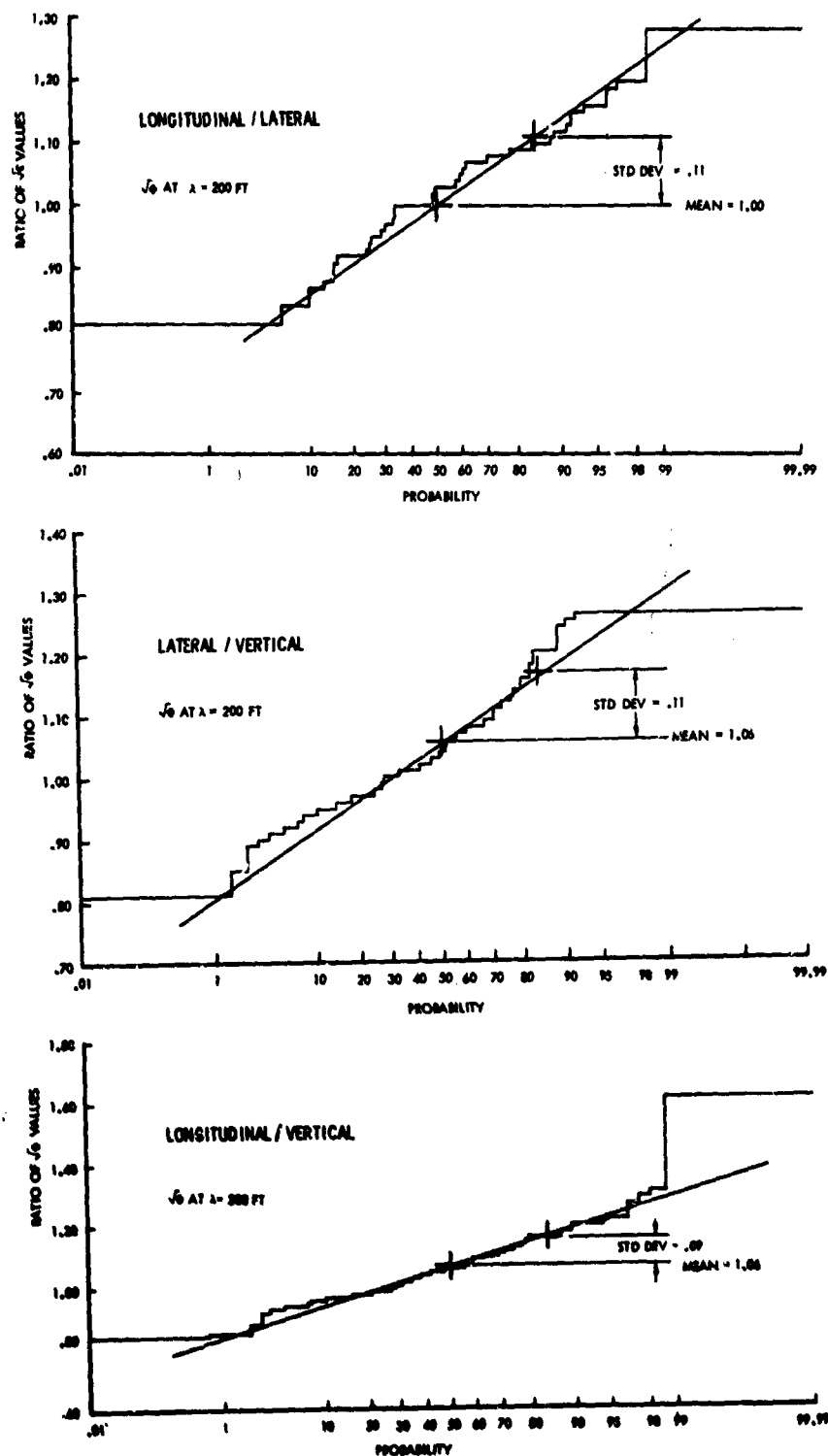
Figure 51 Probability Distribution of $\sqrt{\Phi}$ Ratios at $\lambda = 200$ Ft
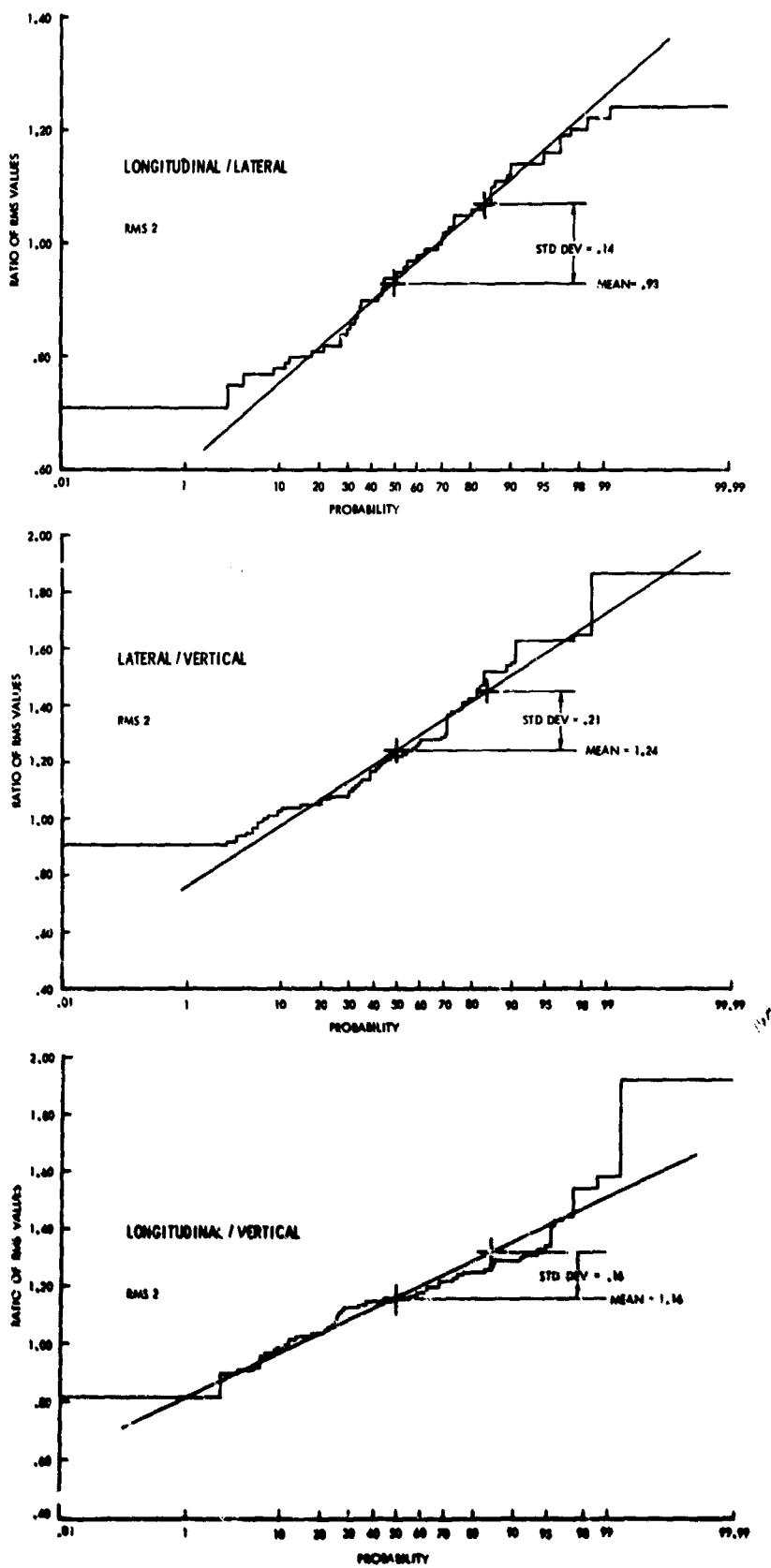
Figure 52 Probability Distribution of Gust Velocity Component Ratios, RMS 2

Section V
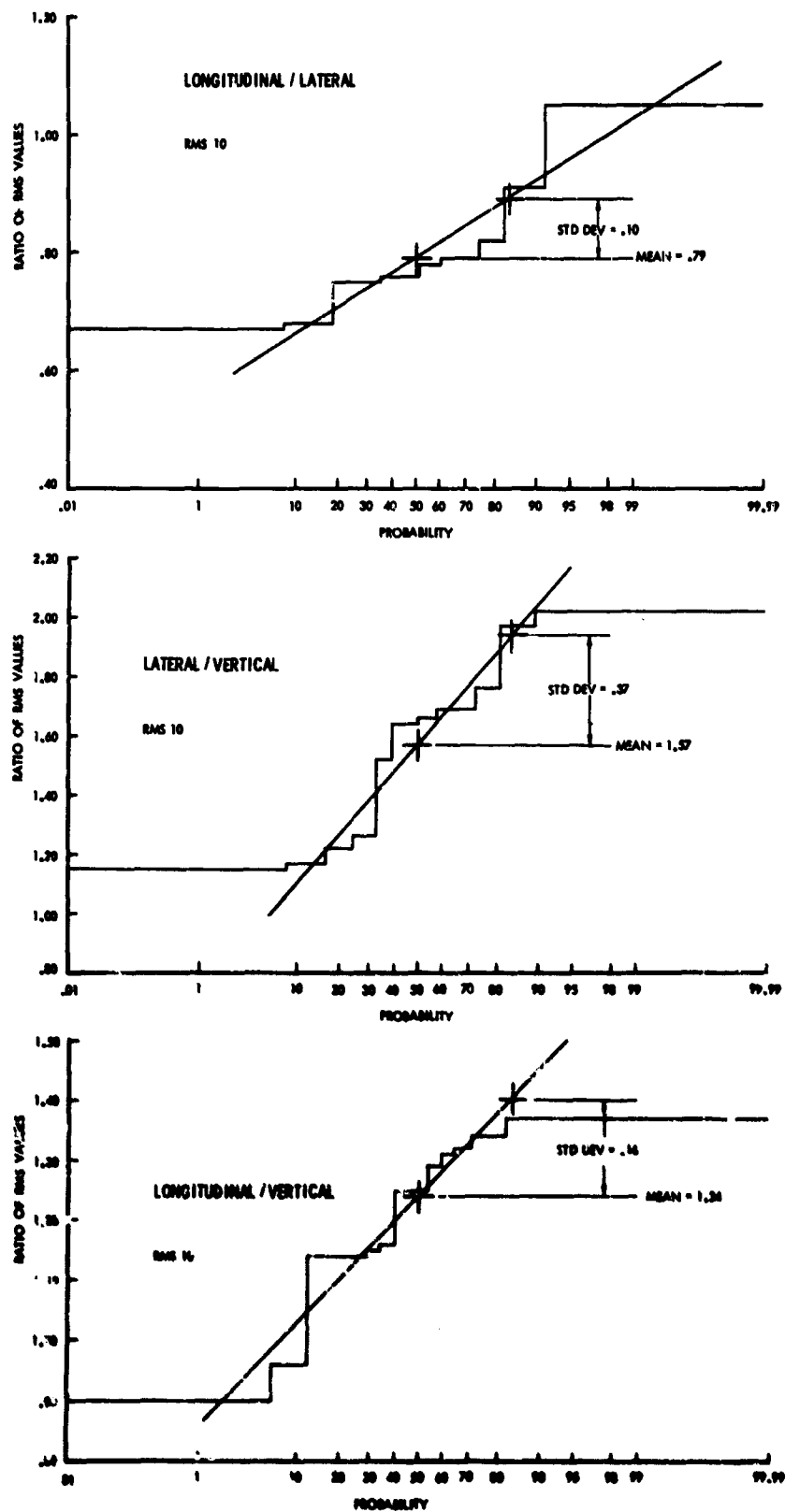
Figure 53 Probability Distribution of Gust Velocity Component Ratios, RMS 10

98

however, are not considered large enough, in view of the samples sizes available, to justify a conclusion that high altitude clear air turbulence, on the average, is anisotropic. On the other hand, individual runs show considerably more variation amongst the three components than do the averages. The standard deviations obtained from the probability paper plots of ratios of rms gust velocity, which range from 0.09 to 0.37, show that fairly large variations in isotrophy exist from run to run.

Stationarity

Definition - By "stationarity", as the term is used in this report, is meant the property of a time history whereby the statistical parameters of the time history, such as its mean, its root-mean-square value, its power spectral density, and so on, do not change with time.[12]

Importance of Stationarity - In any application of measured rms gust velocity values to problems of structural design or, perhaps to a lesser degree, ride comfort, stationarity of the sample is of major importance. Stationarity is important because of its effect on the relationship of peak values of load or acceleration to rms values. For determining the strength needed to withstand one-time loading, on either a "limit" or an "ultimate" basis, the peak value expected once in some very long time, such as the life of the airplane, is needed. For evaluating resistance to structural fatigue, the expected frequency of occurrence of peaks over a wide range of load levels is required. Rms values are a necessary measure of turbulence intensity, but are of actual use only as a means of determining expected peak values.

In the application of the continuous turbulence concept to problems of structural design and ride comfort, the atmosphere is first idealized as consisting of finite patches of turbulence, each of which, as traversed by an airplane, is stationary and Gaussian. This finite patch model is then usually replaced by one in which the intensity varies continuously, but so slowly with time that the theoretical input-output relations still hold.

---

[12]This definition should not be confused with a different one sometimes used in atmospheric turbulence studies. A time history of gust velocity or of airplane response results from the passage of an airplane through a pattern of gust velocities that ordinarily is assumed "frozen" in space. The stationarity of the time history is then a reflection of the homogeneity of the frozen pattern. If the terminology were to be chosen with emphasis on the turbulence itself instead of passage of the airplane through it, what is called "stationarity" in this report would then be called "homogeneity." The term "stationarity" would then be used to denote the property whereby the statistical parameters representative of a given homogeneous region in space remain constant with time. This usage is employed in reports of the Low-Level Critical Air Turbulence Program conducted under USAF contract No. AF 33(615)-3724. However, when turbulence is measured by an airplane passing through the turbulence, all that is directly measured is a time history, not an instantaneous pattern in space. Also, any application of the results of the turbulence measurements will be to the prediction of statistical characteristics of a time history of an airplane flying through turbulence. Consequently, in this report, the term "homogeneity" will not be used, and "stationarity" will refer to the properties of the measured time histories rather than to the pattern of the turbulence.

Section V

The prediction of load (or acceleration) peaks due to turbulence is invariably based on Rice's equation, which relates frequency of exceedance to load level:

$$N(y) = N_c \, e^{-\frac{1}{2}(y/\sigma_y)^2}$$

This equation can be derived theoretically, under the assumption that the time history is stationary and Gaussian.[13] The quantity $N(y)$, although its formal definition is not in terms of "peaks", provides a good approximation to the number of peaks per unit time in excess of given values of y, for any reasonable definition of a "peak." The approximation is especially good for values of y/σ greater than 2 or for time histories characterized by a narrow-band power spectral density.

For flight through many patches of turbulence of various intensities, as would be experienced over the entire life of any given airplane, Rice's equation is applied, in effect, to each patch separately. The exceedances contributed by all the various patches are then added together to give a total.

Rice's equation, which relates peak values to rms intensities, is clearly of great practical importance. Its validity, however, depends upon the gust time histories being both stationary and Gaussian. The degree to which these two conditions are met, therefore, would appear to be among the more important properties of atmospheric turbulence to measure. In past programs directed toward the measurement of absolute gust velocity time histories, however, little if any attention has been given, quantitatively, to these properties - either separately or in terms of their overall effect on the closeness with which Rice's equation applies.

Whether any given sample of turbulence is Gaussian may be rather difficult to determine, and no attempt has been made in connection with the HICAT data. Not only must the gust velocity itself be Gaussian, but the joint probability distribution between the gust velocity and its first derivative must also be Gaussian. Furthermore, until it is established that the function is stationary, it is not at all clear how one could tell whether it is Gaussian, since, as will be evident later, a time history made up of two segments of different intensities, each of which is stationary and Gaussian, will not have a Gaussian distribution overall.

---

[13]It should be noted that the Gaussian nature of the time history does not result in a Gaussian distribution of the peaks. A Gaussian time history is characterized by a Gaussian - or normal - distribution of values read from the time history, either at random or at an arbitrary uniform time interval. Rice's equation, which, as noted above, approximates the probability distribution of the peaks, has the same mathematical form as the equation for the Gaussian probability density. But Rice's equation inherently represents a cumulative distribution. When it is differentiated to give the probability density, it no longer has the Gaussian form.

But it is quite evident from even a casual glance at the HICAT time histories, shown in Appendix IV of this report or Appendix VI of Reference 5, that a turbulence penetration of several minutes duration is usually far from stationary. Typically, patches of relatively severe turbulence are interspersed with regions of comparable duration where the turbulence is clearly less severe, or even quite mild.

How important this lack of stationarity may be to structural design depends upon how the model of atmospheric turbulence to be used for structural design is developed. A necessary element of all such models is a probability distribution (or a set of such distributions) of σ_w. These distributions have been determined in two ways.

The earliest power spectral models, developed in NACA TR 1272 and TN 4332 (References 13 and 18), utilized peak counts of airplane cg normal acceleration obtained by VGH recorder to deduce probability distributions of σ_w. With this approach, stationarity was no particular problem. The only requirement was that the turbulence intensity vary gradually enough so that the input-output relationship for a stationary Gaussian process would apply. If the turbulence intensity stayed sensibly constant for periods as short as 15 or 20 seconds, this requirement would be met. In fact, even if the turbulence were not Gaussian, the effects would tend to be the same in deriving the model and in applying it to new designs so that approximately correct loads for the new designs would result.

More recently, major programs have been instituted in which large bodies of turbulence data are collected in a time history form suitable for processing to give power spectral densities of absolute gust velocity. The first of these was the B-66 low level gust program (Reference 19) in which power spectra were obtained for some 385 four-minute samples of turbulence. With such data available, the former indirect method of obtaining σ_w distributions could be bypassed; a σ_w value was available for each four-minute run, and the probability distributions could be obtained directly.

However, examination of the B-66 data indicated an anomaly. In comparing the B-66 σ_w probability distribution with that proposed in NACA TN 4332, the B-66 distribution was seen to be much milder. Yet the U_{de} peak counts obtained in the B-66 program were more severe than those from which the TN 4332 σ_w distributions were derived.

In attempting to account for this discrepancy, it was found that a major source was the failure of Rice's equation to predict the peak-to-rms ratio. And there was rather convincing evidence, discussed below, that this failure was due to lack of stationarity. Thus it can be concluded that when σ_w distributions are obtained by the second approach, the stationarity of the turbulence samples will have a major effect on the σ_w distributions obtained.

Theoretical Effect on Peak Count Curves of Lack of Stationarity - In other programs in which airplane load time histories had been recorded during flight through turbulence (in particular, the Electra flight test program conducted in mid-1960), examination of the records indicated a distinct likelihood that

runs of four-minute duration would include some fractions that were sensibly non-stationary. Furthermore, for test runs of two to five minutes' duration, Rice's equation ordinarily predicts ratios of peak-to-rms load of about 3 to 3.5; yet values of this ratio as high as 5 or 6 had occasionally been noted in the flight records. It was felt that it would be illuminating, therefore, to examine theoretically the effect of nonstationarity (with respect to turbulence intensity) on the peak-to-rms relationship. A Gaussian process would be assumed.

For this purpose, it is convenient to plot exceedance curves on coordinates of log $N(y)$ vs y^2. On these coordinates, Rice's equation plots as a straight line, as shown in Figure 54(a). In this figure, y has been replaced by a specific quantity, U_{de}. As noted earlier, y can be any quantity that varies in response to a varying gust velocity as an input. The cg normal acceleration is such a quantity, and U_{de} is simply this times a constant. In Figure 54(a) the units of $N(U_{de})$ are number of positive slope crossings per duration of run. Thus, a value of $N(U_{de}) = 1$ denotes the one highest peak in the run.

It is to be emphasized that the derived equivalent gust velocity is not of interest as such, but only as an indicator of characteristics of the turbulence itself. Peak counts of absolute gust velocity, especially if the time histories are first appropriately filtered, can be used just as well for this purpose. In fact, if pilot input effects are small, the U_{de} time history can be regarded as a time history of absolute vertical gust velocity to which a particular filter, the airplane transfer function, has been applied.

For a sample of turbulence that is stationary and Gaussian, a plot of log $N(U_{de})$ vs U_{de}^2 will be a straight line, since Rice's equation will apply. Figure 54(a) represents such a case.

Suppose now, that an actual patch of turbulence consists of two portions, both stationary but of different rms levels. For example, consider a patch of which the first 90 percent yields an rms of 1.75 fps and the last 10 percent an rms of 3.50 fps. The overall rms will be

$$\sqrt{0.90 \times 1.75^2 + 0.10 \times 3.50^2} = 2.00 \text{ fps}$$

The expected exceedance curve for such a patch can be obtained by adding together the contributions of the two parts, taking account of the relative time in each as shown in Figure 54(b).

The significant result shown in this figure is that the expected highest peak for the actual nonstationary patch is 40 percent higher than that obtained by application of Rice's equation to the patch as a whole. It is clear that if the only rms gust velocity considered were that for the patch as a whole, calculated airplane load peaks would be low by some 30 percent. Similarly, if rms values for many runs were obtained in the same way and a probability distribution obtained, the highest load peaks would again be substantially underpredicted.
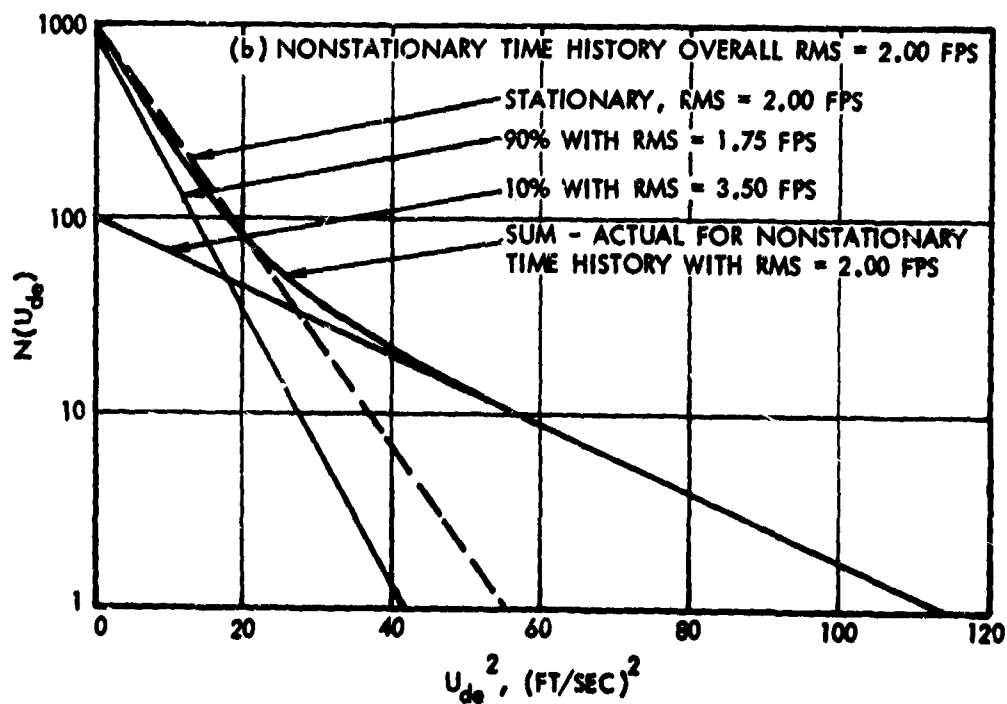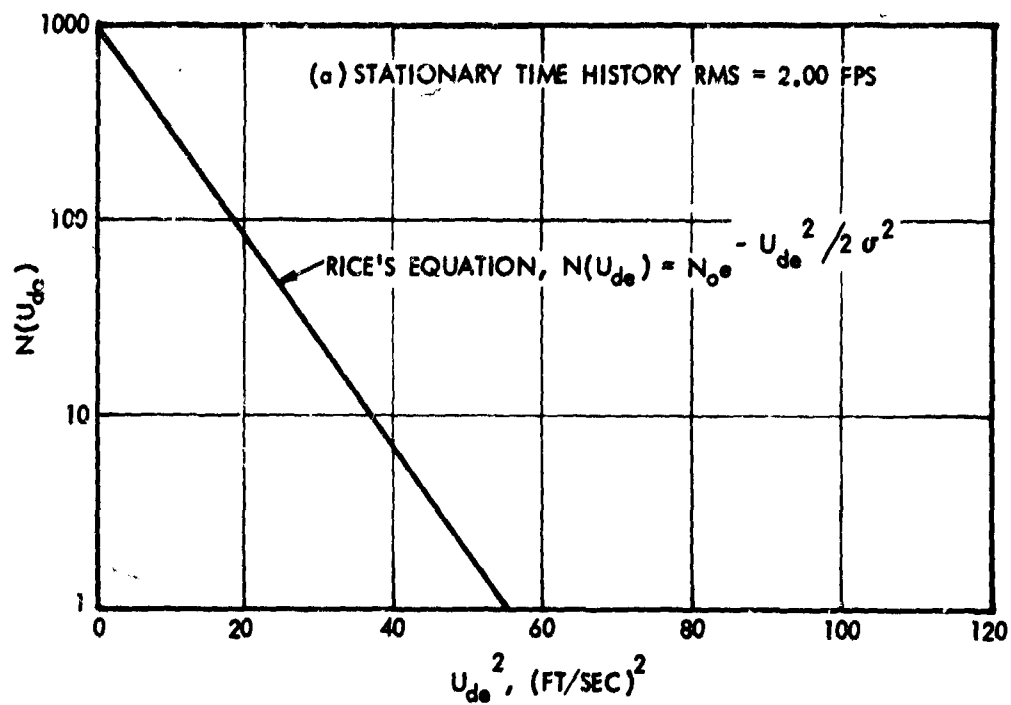
Figure 54 Theoretical Effect of Nonstationarity on U_{de} Exceedance Curves

It might be remarked that, in the example shown in Figure 54(b), the
10 percent of the time at the high rms value need not be at either the
beginning or the end of the run, but might have occurred in the middle; or it
might have occurred in still smaller portions, distributed at intervals
throughout the run. In all cases, the exceedance curve would have been the
same. The only requirement is that the individual stationary portions be
long enough, or the rms level vary gradually enough, so that the theoretical
input-output relations for a stationary random process apply.

The same principle would apply if more than two rms levels were present. Here,
the sum curve in Figure 54(b) would have been made up of the sum of three or
more straight lines. It is interesting to note that even with a continuous
variation in σ_w over the run, it is likely that the actual exceedance curve
can be approximated quite closely by adding as few as two or three straight
lines, representing a correspondingly small number of discrete σ_w values.

Comparison with B-66 Test Data - To see whether actual turbulence samples
would display a shape of exceedance curve similar to that of Figure 54(b),
exceedance curves were prepared from the published U_{de} peak count data for the
B-66 tests. The resemblance was indeed striking. Moreover, the ratio of
measured peak value to peak value predicted by Rice's equation was found to
average about 1.3, which together with other factors, was sufficient to
account for the anomaly in the comparisons with the TN 4332 data. (Reference 13).

Thus it became very clear that if σ_w probability distributions are based on
σ_w values obtained as averages over runs of roughly four minutes or longer
duration, the results will be dangerously misleading for use in predicting
airplane load or acceleration peaks.

Stationarity of HICAT Test Data - A comparable examination of the HICAT data
was therefore considered to be in order. Several examples of plots of $N(U_{de})$
versus $(U_{de})^2$ and of $N(U_V)$ versus $(U_V)^2$ are shown in Figures 55 and 56. The
U_V time histories used in obtaining these plots were high-pass filtered using
the 7000 ft filter described under Peak Counts of Absolute Gust Velocity.
These plots represent the following runs:

Test and Run	Base Location	Duration (sec)	RMS U_{de}
88-9	New Zealand	110	0.87
102-2	Australia	235	1.78
107-8	Australia	960	1.14
107-14	Australia	670	0.74
147-4	Puerto Rico	255	1.90
164-4	Alaska	215	1.42
220-10	Maine (low alt.)	270	1.95
266-12	California	460	1.74
266-17	California	180	2.35

Cases (test and run) 88-9, 107-8, 107-14, and 147-4 were selected more or less
at random, covering a range of durations, locations, and rms levels. These

were later found not to include the runs that appeared most stationary from their time histories. As a result, cases 102-2 and 164-4 from the 1965-1967 HICAT program and cases 266-12 and 266-17 from the 1967-1968 program were added. Case 220-10 was added as a single sample of low-altitude turbulence, obtained during a landing approach.

In all cases the experimental curve has the characteristic concave-upward shape indicated theoretically in Figure 54(b). Also, in all cases, a very close fit to the test points is obtained by adding only two straight-line components, to give the curve labeled "sum." This closeness of fit is rather remarkable when one notes the many different intensities displayed in several of the time histories (Appendix IV).

In Figures 55 and 56, the lines representing Rice's equation are plotted using the U_{de} and U_V rms values obtained from the time histories, and N_O values equal to the total number of peaks counted using the mean crossing procedure.

Ratios of the U_{de} and U_V values read from the faired test-data curve to those read from the curve of Rice's equation at $N(U_{de})$ or $N(U_V) = 1$ are as follows:

Case	U_{de}^2 Test	U_{de}^2 Rice	U_{de}^2 Ratio	U_{de} Ratio	U_V^2 Test	U_V^2 Rice	U_V^2 Ratio	U_V Ratio
88-9	25	7.9	3.16	1.78	214	65	3.30	1.82
102-2	54	37	1.46	1.21	289	105	2.75	1.66
107-8	76	19	4.00	2.00	151	29	5.21	2.29
107-14	36.5	6.2	5.79	2.41	100	15	6.66	2.58
147-4	70	41	1.70	1.31	92	44	2.08	1.44
164-4	42.8	23	1.86	1.37	81	37	2.19	1.48
220-10*	94	42	2.24	1.50	49	30	1.63	1.28
266-12	78.5	37	2.12	1.46	120	64	1.87	1.37
266-17	81	60	1.35	1.16	---	---	---	---

*low altitude run

(Reliable U_V data were not available for case 266-17 because a large roll angle occurred which exceeded the range of the instrumentation (±15°) during most of the run.) For even the four cases for which the time histories had the appearance of rather good stationarity (102-2, 164-4, 266-12, and 266-17), the U_{de} and U_V ratios tend to be substantially greater than unity. (For only one of these, 266-17, was the ratio of 1.16 fairly close to unity.) And values of these ratios in the vicinity of 2.0 or more are seen to occur for two runs that appeared least stationary.
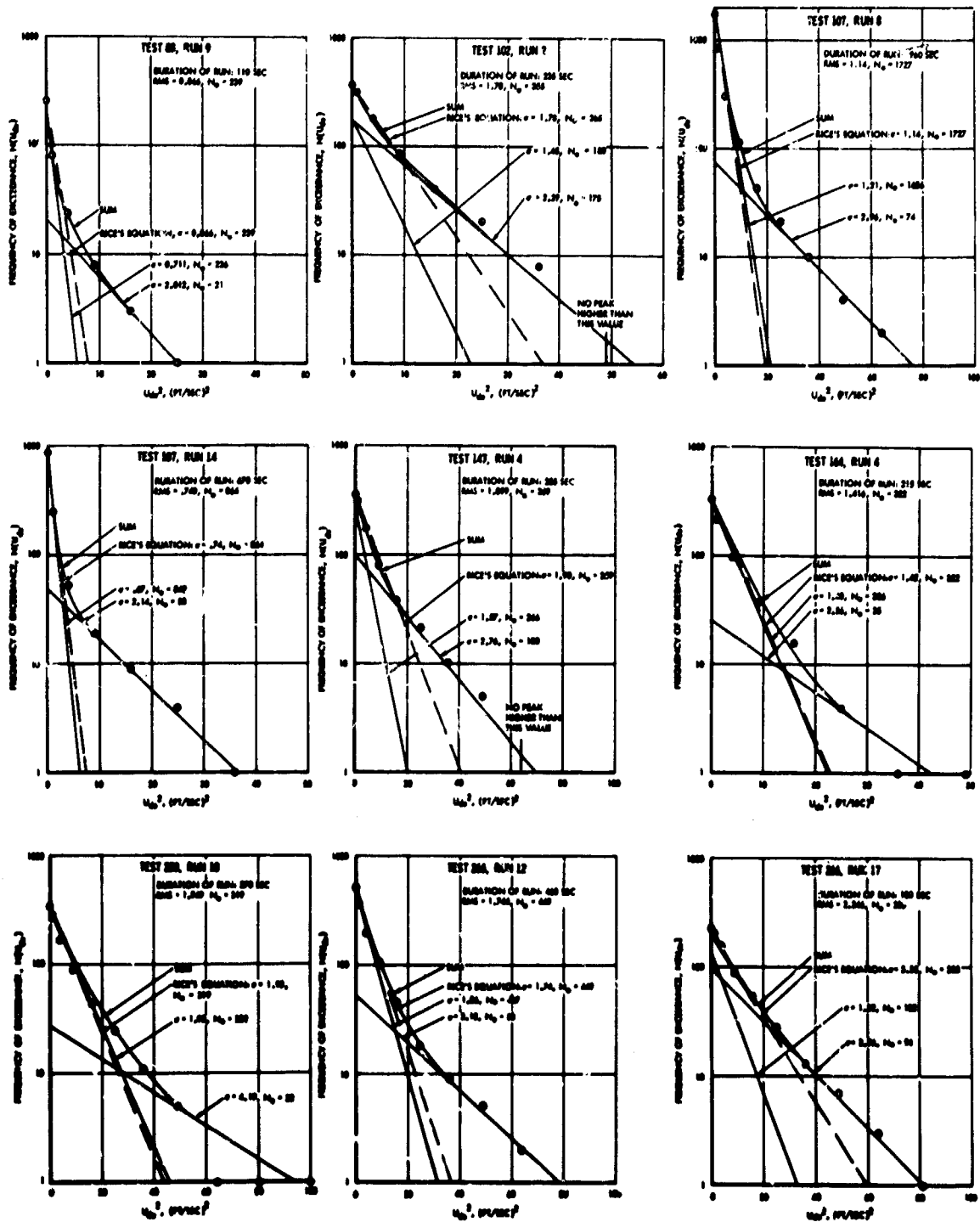
Figure 55 Frequency of Exceedance of U_{de} Based on Positive Slope Level
Crossing Count and Comparison with Rice's Equation
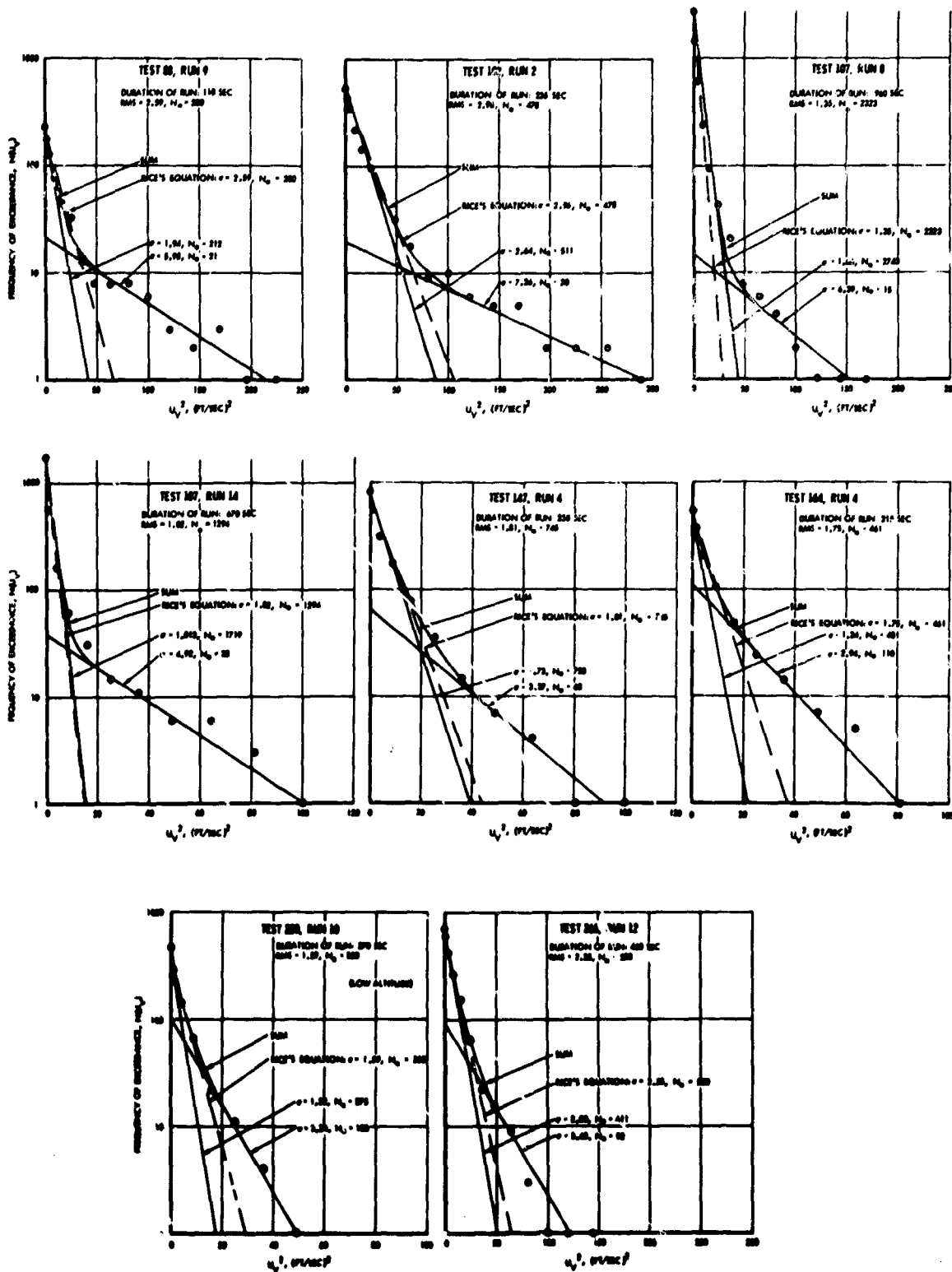
Figure 56 Frequency of Exceedance of U_V Based on Positive Slope Level
Crossing Count and Comparison with Rice's Equation

In comparison, application of the same technique to the 27 four-minute runs from the B-66 low level gust study (Reference 19) for which U_{de} peak counts were available gave ratios fairly well scattered over the range 1.05 to 1.57. The range for the B-66 data is seen to be lower than for the HICAT data.[14] This difference is consistent with the impression, gained from visual examination of records of earlier low-altitude flights of the contractor's airplanes, that low-altitude turbulence tends to be more nearly stationary than high altitude turbulence.

Applicability of Rice's Equation to the HICAT Data - The qualitative agreement in shape between Figure 54(b) and the curves shown in Figures 55 and 56, together with the conspicuous lack of stationarity in many of the time histories, makes it quite plausible that lack of stationarity is the predominant reason for the disagreement between the measured exceedance curves and the theoretical curves given by Rice's equation. The fact that the ratios obtained in the B-66 analysis include some close to unity further suggests that no other cause is necessary.

The possibility is certainly not ruled out, of course, that some of the discrepancy between measured peak counts and Rice's equation is due to the time history not being Gaussian. Indeed, if the constant-rms portions into which the run is considered to be divided are vanishingly short, it might be more valid to regard the time history simply as non-Gaussian. The distinction is believed to be of secondary importance, however. What is important is that, for whatever reason, the peak-to-rms ratio is not in agreement with Rice's equation, and the degree of disagreement is an important property of the turbulence. Nevertheless, it does appear that the disagreement between Rice's equation and test is due primarily to lack of stationarity and that the magnitude of this disagreement can be regarded as a useful measure of stationarity.

Concluding Discussion - The significant conclusions with respect to stationarity of the HICAT data are:

1. Examination of the gust velocity time histories indicates significant variations in intensity throughout the run, in nearly all runs. This variation appears to be more pronounced than that for low-altitude turbulence.

2. Apparently as a result of this lack of stationarity, the ratios of peak value to rms value for any given run, of any airplane response quantity, are in excess of the ratios predicted by Rice's equation by factors ranging from 1.16 to 2.58.

3. Any probability distribution derived from average-over-the-run σ_w values will lead to a gross underprediction of the higher load peaks when applied in airplane design.

---

[14] Note that the HICAT low altitude case (220-10) yields ratios within the range established for the B-66 data.

A systematic evaluation of stationarity for all the HICAT runs is beyond the scope of the present program. In fact, such an evaluation is not necessary because no attempt was made to obtain a random sample of turbulence intensities from which a probability distribution could be obtained that would be useful for design. In other programs, however, overall probability distributions of rms gust velocity may well be an important output. If so, it is extremely important that the effect of nonstationarity be properly accounted for. A technique for accomplishing this might involve breaking down each run into two or more rms levels in accordance with the concept illustrated in Figures 55 and 56.

DATA QUALITY EVALUATION

Frequency Response

PCM Frequency Response - The pulse code modulation (PCM) system low-pass filters and digitizes all the HICAT measurements. To check the input/output relationships of this vital system, an end-to-end frequency response test was performed. The results as obtained from the magnetic tape recording are shown in Figure 3 in Section II. Figure 3 indicates the PCM system amplitude response to be flat within about 3% from 0 to 5 cps, and attenuated to a value of 2% at 12 cps. Also, Figure 3 shows the average phase lag per channel in the frequency range from 0 to 4 cps is 41 degrees/cps corresponding to a constant time lag of 0.114 second. This response is due almost entirely to the analog filters.

Transducer Frequency Response - In general, all of the primary gust maneuvering instrumentation (i.e., gust sensing vanes, airspeed, total temperature, and accelerometers) have frequency responses flat to within 1% over the frequency range of interest (up to 5 cps), with the exception of the gyro and vertical platform measurements. These have flat responses up to the numerical filter cutoff frequencies shown for individual measurements in Table IX, Appendix II.

Noise and Drift Effects

Instrument Noise - Undesired signals of whatever origin are usually referred to as noise. High frequency noise associated with the transducer measurements was removed or at least greatly attenuated by the passive low-pass filters of the PCM as indicated by Figure 3 of Section II. To further reduce the noise and thereby improve the quality of the computed gust velocities, numerical low-pass filters were used. The characteristics of these filters are illustrated in Figure 162, Appendix II. The measurements and their respective filters are listed in Table IX, Appendix II. The filter cutoffs were selected to correspond approximately with the upper end of the useful response range of the individual measurements.

System Noise and Drift - The noise and long term drift behavior of the gust measuring system were examined by evaluating several "zero-input" ground test records as if they were high altitude gust penetrations. This was accomplished by computing gust velocities in the usual way[15] after setting the mean values of total temperature, pressure altitude, and indicated airspeed to give a calculated true airspeed of about 700 feet per second. The resulting drift

---

[15]Except that linear trends were not removed.
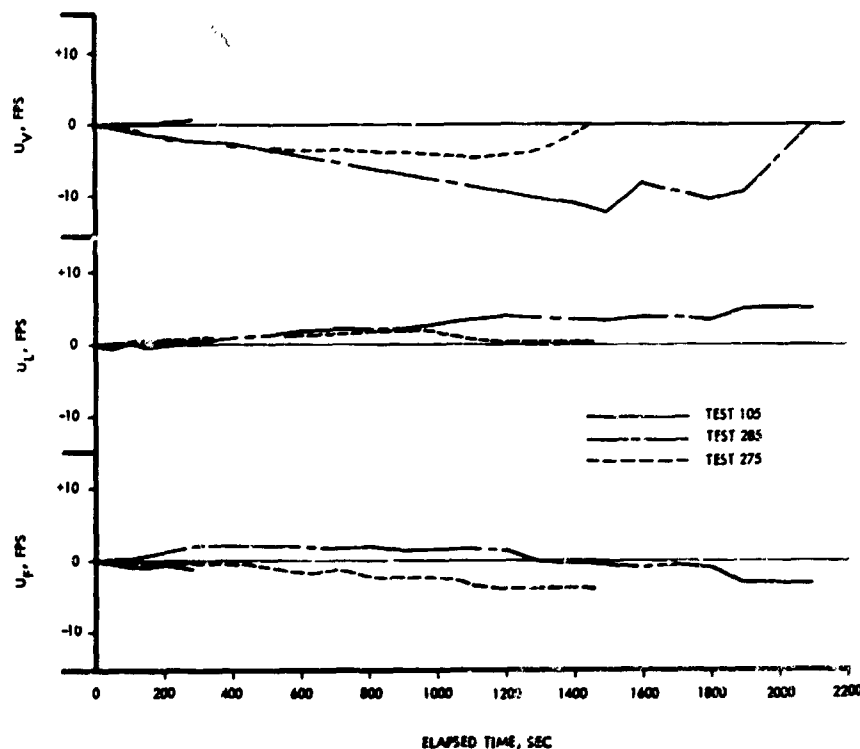
Figure 57 Drift Time Histories

time histories are shown for each gust velocity component and for each test in Figure 57. The vertical gust velocity is near zero at the end of the run because the platform vertical acceleration (the main source of vertical gust drift) was integrated with respect to the mean value of acceleration. In the case of the lateral and longitudinal gust velocities, the platform performs the integration internally and provides a velocity signal which contains the main drift error.

Since linear drift effects will normally be removed in the determination of the gust velocities, the deviations of most interest are the nonlinear ones.

The drifts illustrated (possibly, though not necessarily, typical of high altitude tests) do not appear to have significant deviations at periods of interest (< 30 seconds) to HICAT.

Examination of the gust velocity spectra in Figure 58, which was computed for the longest of the drift runs, confirms this observation. The power spectral density of any of the gust velocity drift components at a wavelength of 20,000 feet is very small compared to any of the long wave turbulence spectra shown in Appendix V.

To make the comparison easier and more meaningful a minimum level HICAT spectrum was established and is shown in Figure 58. This spectrum roughly approximates the lower border of the HICAT gust PSD envelope in Figure 37 while providing an RMS-2 gust intensity of 1.0 ft/sec. By dividing the power spectral density of this spectrum by similar values from the drift spectra,

110
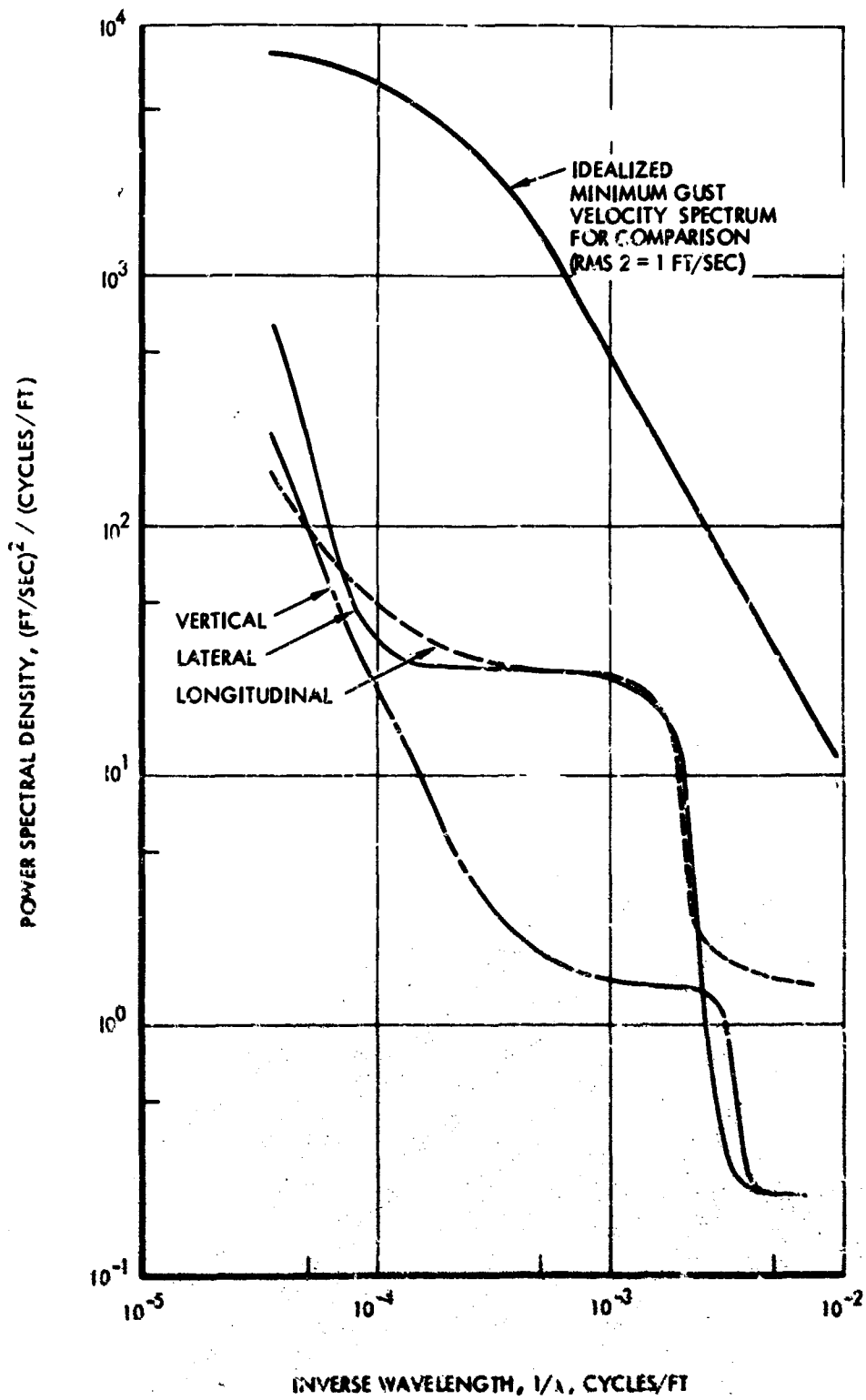
Figure 58 Gust Velocity Noise Spectra
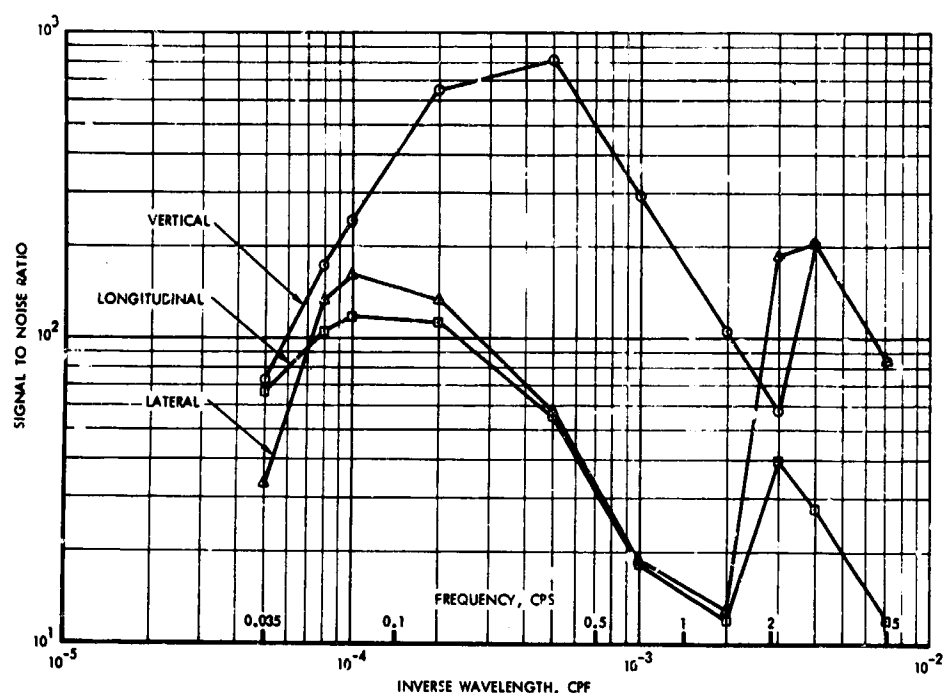
Figure 59   Gust Velocity Signal to Noise Ratio
(Power Spectral Density Basis)

an estimate[16] of the instrumentation system signal-to-noise ratio is obtained
for each gust component. Figure 59 shows the result and indicates the rela-
tive quality of the component velocity measurements on the basis of signal-
to-noise ratio. The vertical component is clearly the best, while the lateral
and longitudinal are generally of lower quality[17] However, all components
have minimum level signal-to-noise ratios of about ten or better on a power
basis.

Gust Velocity Measurement Accuracy

Component Accuracy - The measurement accuracy of each HICAT transducer appears
in the final column of Table I, Section II. These are percentage rms values
of the transducer measurements before they are filtered and digitized in the
PCM system. The table indicates all the measurements which are used in the
gust velocity equations have basic accuracies of ±1.3 percent rms or better.
Limitations of calibration equipment and procedures will contribute another
0.3 to 1.0 percent to this figure.

---

[16] It must be emphasized that this is only an estimate since the noise in
actual flight can be increased by pilot inputs, vibration, elastic mode
response, etc., and will vary from test to test. At the same time the sig-
nal will normally be larger than the minimum level shown.

[17] In Reference 5 it was shown that the resolution of the vertical gust instru-
mentation was about a factor of two better than that for the other two gust
measurements.

The analog filters attenuate the measurement signals slightly, depending upon the frequency. This effect varies from filter to filter, but can be as much as two or three percent at 5 cps. At frequencies less than 1 cps, the average attenuation amounts to less than 0.5 percent of the input amplitude.

The PCM digitizing process introduces another very small error. This error is ±0.5 percent ±1/2 of the least significant bit, which is equivalent to an accuracy capability of 0.1 percent.

Gust Velocity Errors - A rough estimate of the error in the gust velocity determination may be established from examination of the basic gust velocity equations and consideration of the error in the various individual measurements. For this purpose the gust velocity equations are reproduced below in somewhat simplified form, ignoring second order terms.

$$U_V = V_T \Delta \alpha - V_T \Delta \theta + \Delta U_{PG_Z} \tag{5}$$

$$U_L = V_T \Delta \beta + V_T \Delta \psi - \Delta U_{PG_Y} \tag{6}$$

$$U_F = \Delta V_T - \Delta U_{PG_X} \tag{7}$$

By applying the following relationships from Reference 20, the error may be estimated for each gust velocity component.

$$y = F(x_1, x_2 \dots x_n)$$

$$\sigma_y^2 = \sum_{i=1}^{n} \left(\frac{\partial F}{\partial x_i} \right)^2 \sigma_i^2 \tag{8}$$

where

σ_y^2 = variance of y

x_i = ith-numbered x term contributing an error

σ_i^2 = variance of the ith term.

Section V

The resulting equations for the one-sigma error are as follows:

$$\sigma_{U_V} = \left[\left(V_T \sigma_\alpha\right)^2 + \left(\Delta\alpha \sigma_{V_T}\right)^2 + \left(V_T \sigma_\theta\right)^2 + \left(\Delta\theta \sigma_{V_T}\right)^2 + \sigma_{U_Z}^2\right]^{1/2} \qquad (9)$$

$$\sigma_{U_L} = \left[\left(V_T \sigma_\beta\right)^2 + \left(\Delta\beta \sigma_{V_T}\right)^2 + \left(V_T \sigma_\psi\right)^2 + \left(\Delta\psi \sigma_{V_T}\right)^2 + \sigma_{U_Y}^2\right]^{1/2} \qquad (10)$$

$$\sigma_{U_F} = \left[\sigma_{V_T}^2 + \sigma_{U_X}^2\right]^{1/2} \qquad (11)$$

The rms error (neglecting linear drift) was estimated for each measurement as follows:

$$\sigma_\alpha = \pm 0.20° \qquad \sigma_\theta = \pm 0.12° \qquad \sigma_{V_T} = \pm 2.8 \text{ fps} \qquad \sigma_{U_Y} = 1.4 \text{ fps}$$

$$\sigma_\beta = \pm 0.20° \qquad \sigma_\psi = \pm 0.20° \qquad \sigma_{U_Z} = \pm 1.4 \text{ fps} \qquad \sigma_{U_X} = 1.4 \text{ fps}.$$

An average airspeed of 700 fps was used for V_T with the other constant values, selected to be representative of fairly severe high altitude CAT, as follows:

$$\Delta\alpha = \pm 2.5° \qquad \Delta\theta = \pm 6.5°$$

$$\Delta\beta = \pm 2.5° \qquad \Delta\psi = \pm 5.0°$$

By making the appropriate substitutions in equations (9), (10), and (11), the following gust velocity error estimates were obtained:

One-Sigma Gust Velocity Error

Gust Component	σ Error
Vertical	±3.1 fps
Lateral	±3.7 fps
Longitudinal	±3.1 fps

114

From a theoretical standpoint, gust velocity errors other than systematic errors should be less than the values indicated about 70 percent of the time. Since the assumed randomness of errors is always questionable, it may be more significant to consider the relative magnitude of the errors. On this basis, the lateral component appears to have a significantly larger error than the other two components because of combined heading and airspeed measurement errors.

Gust Velocity Errors in Roller Coaster Maneuvers

Several times during the course of the HICAT program, smooth symmetric pitch maneuvers or roller coasters were performed in calm air to verify the performance of the instrumentation and check the gust velocity equations. If the air is perfectly calm and the instruments are calibrated accurately and working properly, the result of the gust velocity determination should be very nearly zero, i.e., in agreement with the test conditions.

The implications of this statement can be best understood by examining a somewhat simplified vertical gust velocity equation, as it applies to a roller coaster,

$$U_V = V_T \left(\Delta \alpha - \Delta \theta \right) + \int \Delta a_Z dt$$

For U_V to be exactly zero at all times during the maneuver requires that the difference in the first term precisely cancel the second term. This, of course, will not happen unless the measurements are perfect in amplitude as well as phase[18]. Normally, this is not the case and a small discrepancy will result. This discrepancy can result from small errors in all the components as well as from a large error in just one.

Figure 60 illustrates the behavior of the individual measurement terms and the resulting velocity discrepancy for an actual roller coaster maneuver. The angle of attack and acceleration are seen to have almost exactly the same phase, with the result that the maximum value of the integral (i.e., the plunge velocity) occurs when $V_T \Delta \alpha$ is zero and $V_T \Delta \theta$ is at or near its peak. The resulting velocity discrepancy in this case is ±4.5 feet per second.

It is important to realize at this point that the elevator input in the roller coaster maneuver is not the same as a pure gust input. In a roller coaster the cg acceleration associated with the vertical (plunge) velocity is produced by pitching the aircraft nose in the direction of the plunge, whereas in turbulence (without elevator motion) the aircraft will ordinarily respond oppositely from stability considerations but can also pitch or plunge independently, i.e., randomly. Thus the velocity discrepancy associated with a roller coaster is evidence of an imperfection in one or more of the measurements in the system, but it is not necessarily a measure of actual gust velocity error in turbulence. This latter error can only be established by identifying the error contributing components and then determining the contribution of each component to the overall gust velocity measurement on an rms basis.

---

[18]Compensating errors are possible but exactly compensating errors are very unlikely.
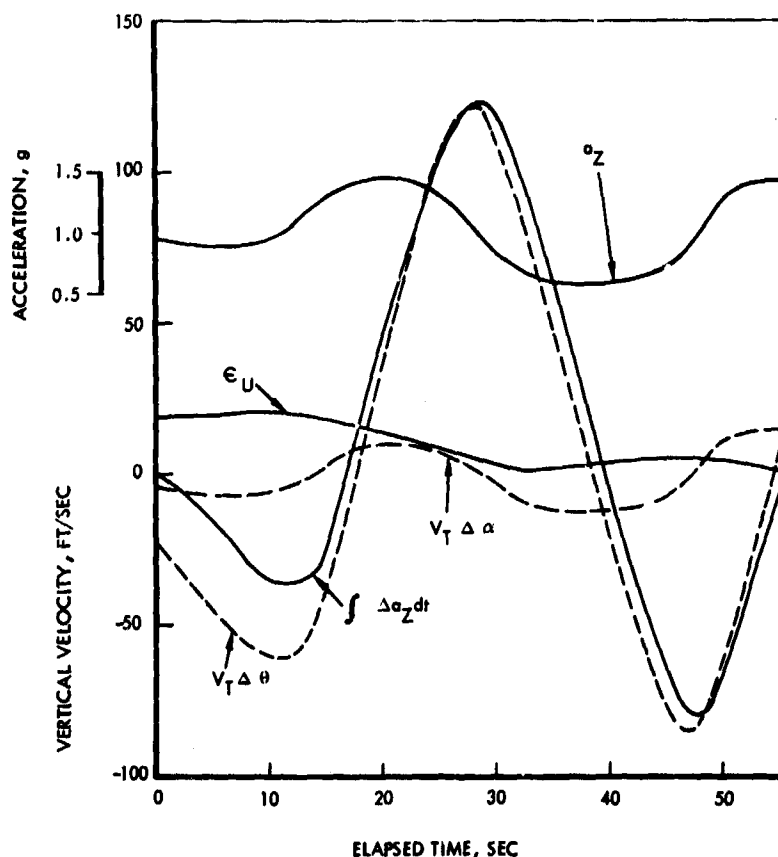
Figure 60   Roller Coaster Maneuver Gust Parameter Time History

It should also be recognized that pilot inputs in turbulence are analogous to performing roller coasters in turbulence and thus produce similar errors. If pilot inputs are small or absent, then the error from this source will be small or absent. The system errors will remain, of course, but without augmentation by the pilot.

In previous HICAT work (Reference 5) an apparently significant velocity discrepancy[19] was shown to occur in roller coaster maneuvers. The amplitude of the error appeared to increase with the period and amplitude of the control input. In order to better evaluate this effect a series of roller coaster maneuvers of differing oscillatory periods were performed. Figure 61 shows an example of the gust velocity time histories obtained from one of these maneuvers. The vertical gust component shown has a 15-second oscillation of roughly ±3 ft/sec amplitude obviously resulting from the pilot's elevator motion. However, the 15-second oscillation is very small or absent entirely

---

[19]Although the individual source(s) producing the discrepancy were never clearly identified, considerable effort was made to improve the quality of the measurements and thereby reduce the discrepancy. These efforts consisted of improving calibration procedures, increasing vertical acceleration resolution by reducing the range and installing a new airspeed transducer.
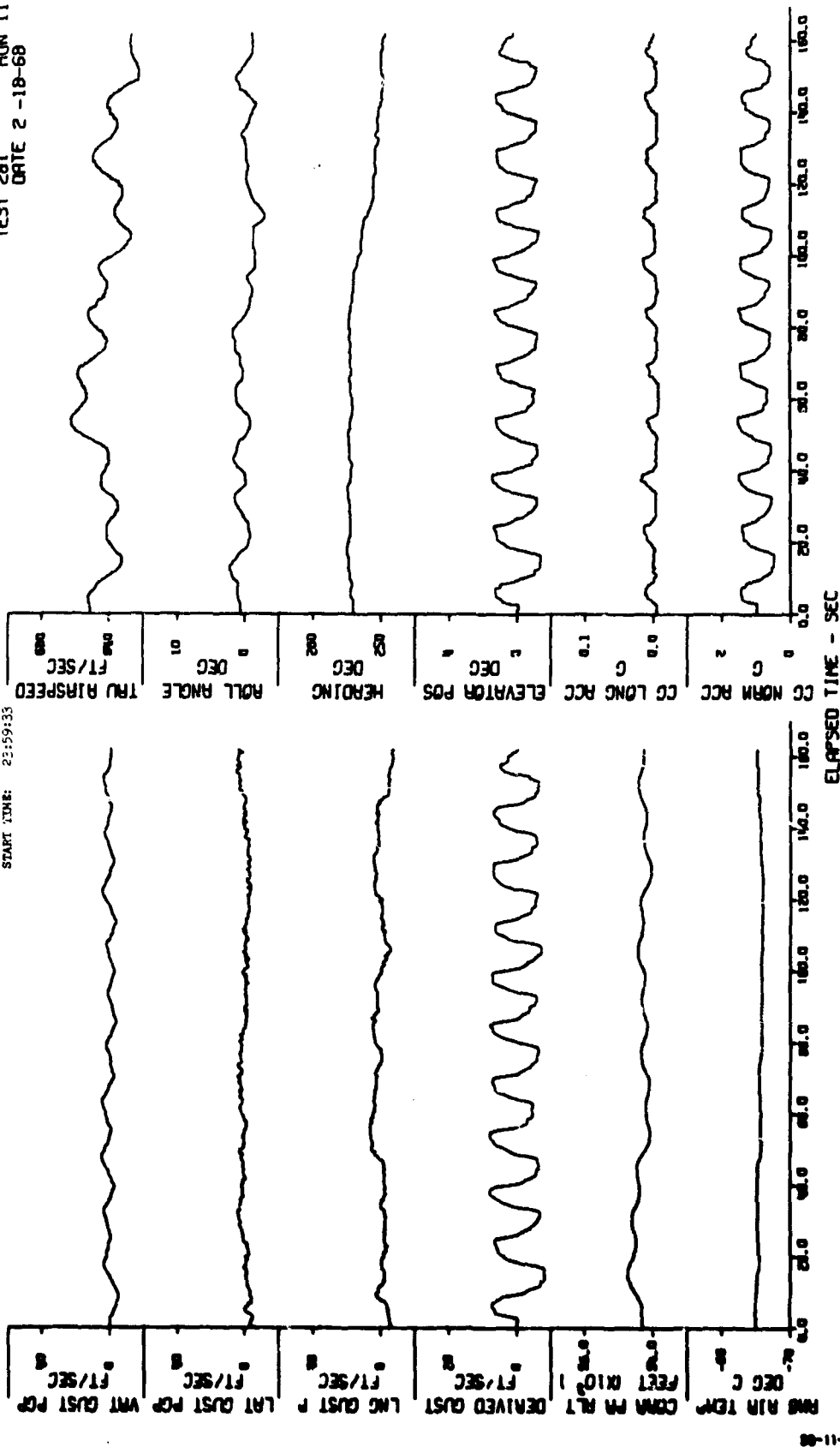
Figure 61 Roller Coaster Maneuver Time History

from the lateral and longitudinal gust velocity time histories. The nonzero lateral and longitudinal components appear to result from longer period secondary effects (i.e., changes in heading, speed, altitude) rather than directly from pitch control input.

On the basis of data from this maneuver and others like it, the vertical gust velocity error per degree of elevator deflection was determined and plotted in Figure 62. It indicates clearly that the error per degree increases with the period of the maneuver, as noted earlier.

The actual magnitude of the gust velocity discrepancy is shown in Figure 63 as a function of the peak vertical velocity of the aircraft measured in the various roller coaster maneuvers. The figure indicates errors of about the size estimated earlier (i.e., in the Gust Velocity Error section) which increase linearly with overall vertical velocity input.

The percentage velocity discrepancy[20] as a function of roller coaster maneuver period is presented in Figure 64. The percentage decreases from 10 to 4.7 over the range of maneuver periods from 4 to 35 seconds corresponding to gust wavelength of about 2800 to 24,000 feet. As Figure 64 shows, the 10 percent discrepancy values are actually only 1 to 2 ft/sec in magnitude and come from low amplitude maneuvers where the measurement resolution was poorest.

At much lower periods than those shown (i.e., $T < 1.0$ sec), the gust velocities are measured almost entirely in terms of $V_T \Delta \alpha$ since gross aircraft responses are negligible. Accuracy of this term is of the order of ± 2 ft/sec; however, velocity differences as small as 0.2 ft/sec are resolved.

Alternate Gust Velocity Calculation

In case of a malfunction or failure of one or more of the gust measuring instruments, and in particular the inertial platform, some backup instruments were provided. These consisted mainly of normal, lateral, and longitudinal accelerometers near the aircraft center of gravity and angular rate gyros in the nose. Figure 65 and Figure 66 show a comparison by component of gust velocity spectra computed using platform measurements with similar spectra computed using integrated cg accelerations and angular rates, i.e., the "alternate" measurements. Some relatively small discrepancies are noted in the vertical and lateral spectra at the longer wavelengths. In general, however, the agreement between the two kinds of spectra appears to be very good.

Low Altitude Gust Velocity Spectra

In order to provide additional confidence in the high altitude gust velocity spectral determinations, it is desirable to compare them with similar measurements made by other investigators with different instruments. If the characteristics of measured spectra agree, the presumption is usually that both sets

---

[20]The discrepancy between two quantities both of which are believed in error is usually divided by two in determining the percentage; however, this was not done in this case.
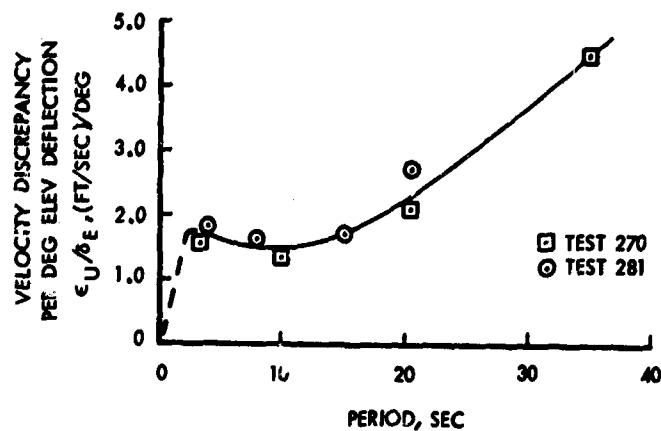
Figure 62   Velocity Discrepancy per Degree Elevator Deflection
versus Roller Coaster   Period
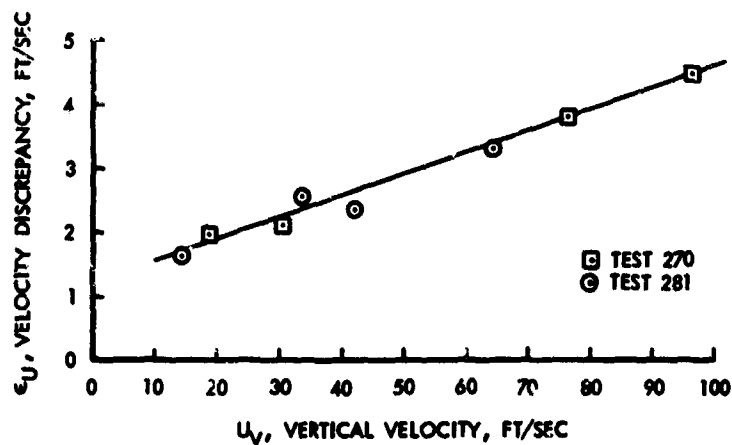
Figure 63   Velocity Discrepancy versus Aircraft Vertical
Velocity in Roller Coaster Maneuvers
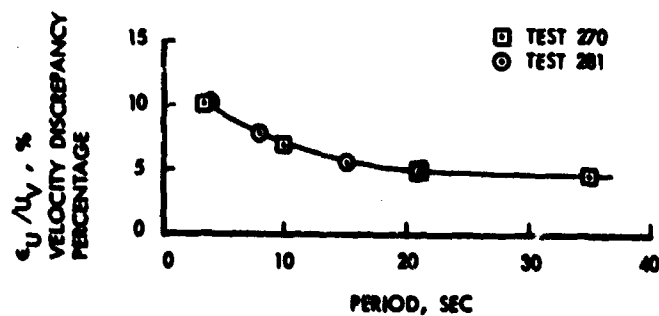
Figure 64   Velocity Discrepancy versus Roller Coaster Period

119
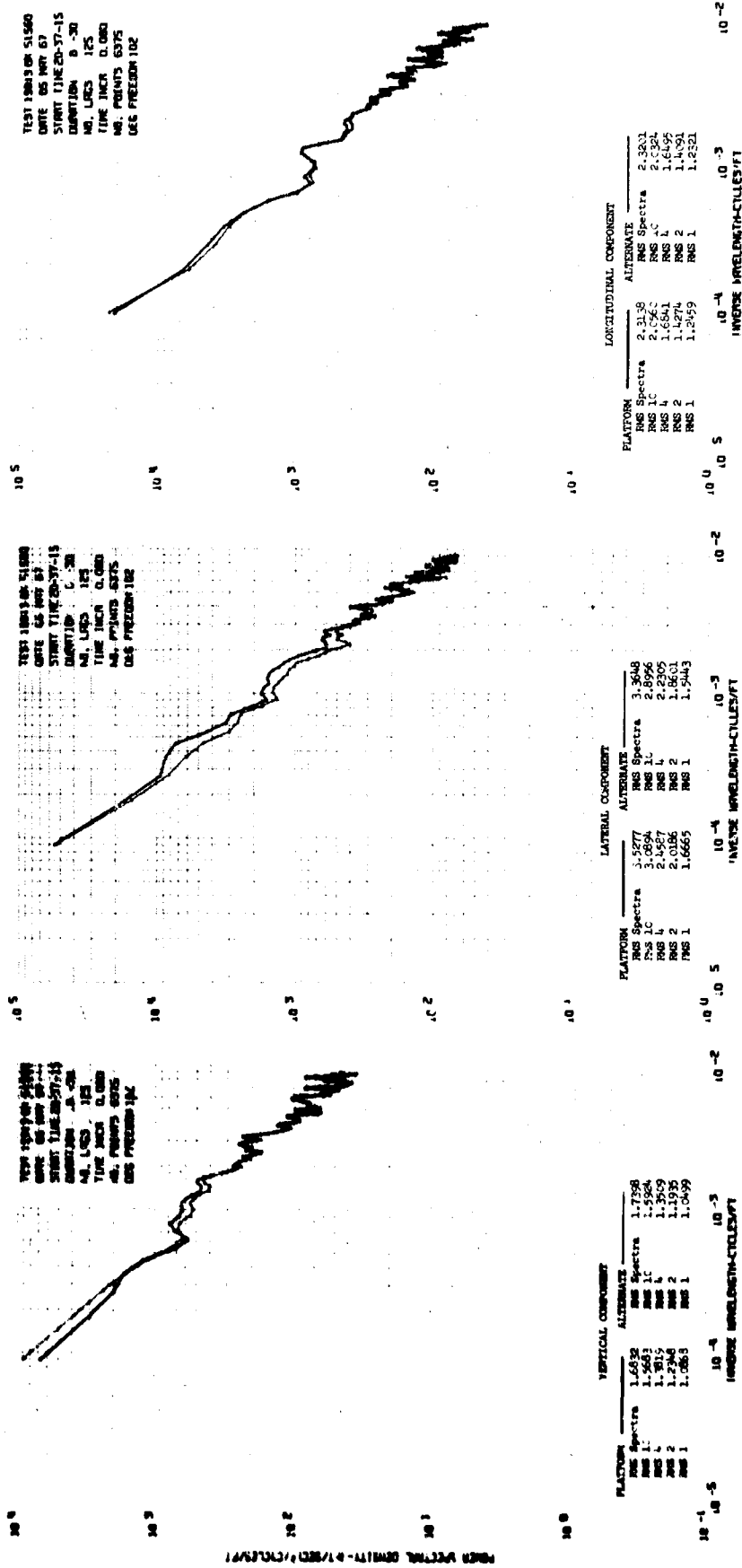
Figure 65 Power Spectral Comparison of Gust Velocity Measurement Methods-Test 198
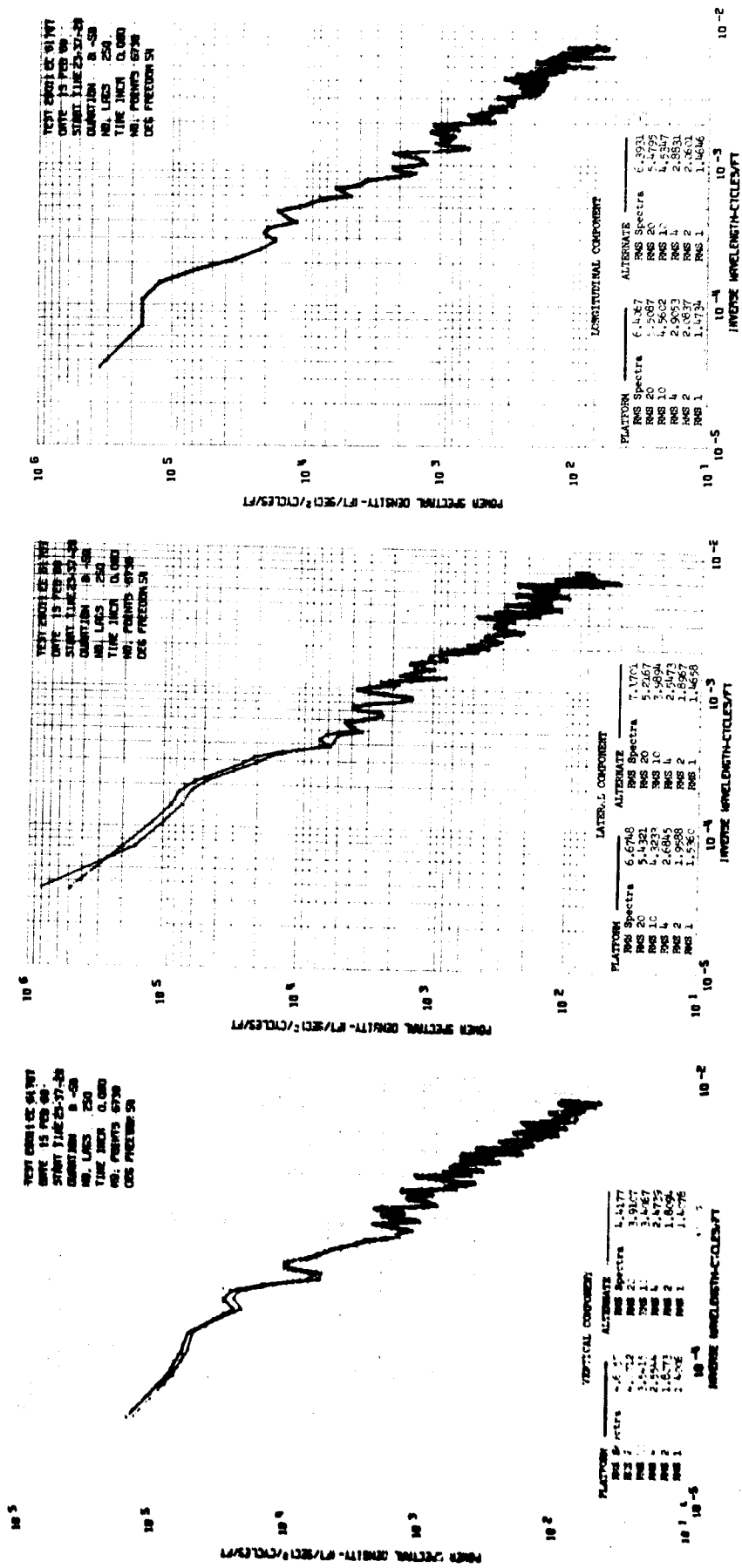
Figure 66 Power Spectral Comparison of Gust Velocity Measurement Methods-Test 280
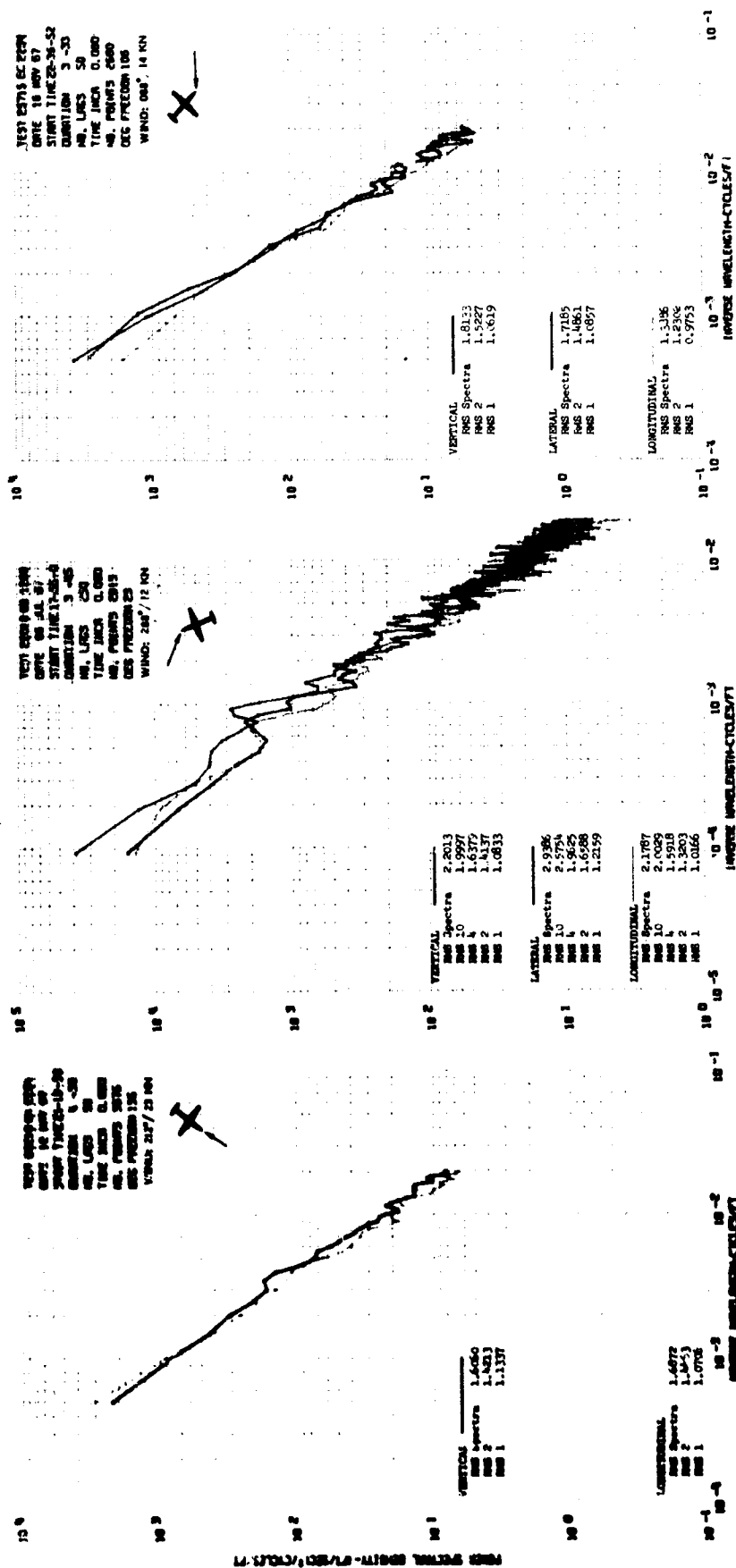
Figure 67. Low Altitude Gust Velocity Spectra

of measurements are correct. Unfortunately, this particular kind of check is not possible with the HICAT data because similar high altitude measurements have not been made as yet.[21] However, this difficulty may be partially circumvented by using the HICAT system to obtain low altitude gust velocity spectra for which an abundance of comparison data exist, most notably the Boeing LO-LOCAT data (Reference 21).

Low altitude spectra were obtained from the landing approach portion of three HICAT tests. The spectra appear in Figure 67. Note that all the gust velocity component spectra appear to have well defined -5/3 slopes and to be reasonably isotropic. This agrees with other low altitude gust velocity data and in particular the extensive LO-LOCAT data. Time histories for these tests are included with the high altitude CAT data in Appendix IV, Volume II.

----

[21] It is expected that some gust velocity data will eventually be obtained from XB-70 tests.

SECTION VI

METEOROLOGICAL ASPECTS

A major goal of the HICAT program was the collection and analysis of meteorological data pertinent to the study and determination of the physical conditions associated with clear air turbulence.

This section of the report lists the sites selected for sampling and tells why they were selected, describes the forecast procedures used at the various sites, discusses some data collection problems, and comments concerning accuracy of upper level observations. Methods of predicting CAT are also discussed. A discussion of the relation between meteorological analyses and observed turbulence and an evaluation of HICAT forecast methods are presented. Finally, the HICAT procedure for the prediction of turbulence in the 40,000 to 70,000 foot range is submitted.

In order to substantiate the analysis methods described herein a detailed analysis of ten HICAT tests is provided in Appendix IG. Meteorological summaries are compiled for all the HICAT search flights in Appendix VI, Volume II. The summaries include flight track maps, RAOB charts of temperature versus pressure, and 70 (or 100) mb charts of temperature and wind. Detailed information about individual CAT encounters (i.e., runs) is provided in the HICAT Test Summary Table in Appendix IA.

SITE SELECTION AND FIELD FORECAST METHODS

Site Selection and Discussion of Operations

Six sites were selected from which to base the U-2 flights for the HICAT program. These sites were selected to provide a variety of meteorological and geographical conditions for the study of high altitude clear air turbulence and, in addition, to complement the data obtained during the previous HICAT flight program. The six bases of operation were as follows:

(1) Bedford, England: March-April, 1967

A British base of operations was selected to provide an opportunity to fly over the British Isles during periods of intense tropospheric storms and their associated jetstreams. An additional objective was to fly the U-2 in conjunction with an instrumented Canberra aircraft operated by the Royal Aircraft Establishment (RAE). The Canberra sampled altitudes in the 20,000 to 40,000-foot range along the same route flown by the U-2.

(2) Barksdale Air Force Base, Louisiana: May 1967

The primary purpose of operations from this base in the central
United States was to fly over areas of convective activity, i.e.,
thunderstorms, squall lines, and fronts. Missions were planned and
daily liaison was maintained with the National Severe Storms Labora-
tory (NSSL) at Norman, Oklahoma. NSSL predicted when and where con-
vective activity could be expected. If the area of interest was
within the range of the laboratory's radar network, HICAT flights
were scheduled to coordinate with the NSSL Rough Rider flights. If
the probability of storm activity was low, then HICAT missions were
planned to investigate areas of turbulence predicted by Global
Weather Central (GWC) or the HICAT meteorologist.

(3) Loring Air Force Base, Maine: June-July, 1967

New England, Nova Scotia, and Newfoundland frequently have low pres-
sure systems that move southwest to northeast across this region.
Aloft, jetstreams frequently converge and intensify. These condi-
tions are favorable for the production of abundant turbulence.
Another reason for selecting the site was its proximity to future
supersonic transport routes.

(4) Albrook Air Force _ se, Canal Zone (Panama): July-August, 1967

The primary objective for conducting HICAT tests from Panama was to
investigate turbulence over the Intertropical Convergence Zone
(ITZ).[22] The months of July and August are favorable for ITZ activ-
ity. A secondary objective was to measure turbulence intensity over
well-developed isolated thunderstorms.

Numerous missions were completed above well developed thunderstorms
and three flights were conducted over the ITZ, viz., tests 227, 228,
and 231.

(5) Patrick Air Force Base, Florida: September-October, 1967

Florida was selected as the base from which to investigate clear air
turbulence over a tropical storm or hurricane. September is con-
sidered the month most favorable for hurricane development.

Two hurricanes formed and moved within range during this period.
Flights were made over hurricane Doria on 11 September (Test 241)
and Beulah on 20 September (Test 247).

(6) Edwards Air Force Base, California: Nov-Dec 1967, Jan-Feb 1968

When originally planning the HICAT winter activity, it was expected
that HICAT flights would be conducted from Okinawa and a base in the
Mediterranean area. However, for a number of reasons, this period
of the project was completed at Ed ds AFB, California.

----

[22] The axis, or a portion of the axis, of the broad tradewind current of the
tropics. This axis is the dividing line between the northeast trade winds
in the northern hemisphere and the southeast trade winds in the southern
hemisphere.

In retrospect, this was a fortunate turn of events, since more turbulence, in terms of intensity and duration, was encountered in flights from Edwards AFB than at any of the five previous locations.

Joint tests were conducted with the National Center for Atmospheric Research to investigate turbulence associated with mountain waves (Tests 279, 280, 281, 282, and 283).

Forecasting Methods

During the initial HICAT program and the redirected HICAT program, local meteorological facilities personnel were utilized for forecasting. In most cases, these personnel had little or no experience in forecasting CAT at levels above 40,000 ft. Consequently the Global Weather Central (GWC) forecasts were used to some extent at all the bases. These forecasts comprise the only strictly comparable methods used at more than one base until the advent of the extended HICAT program and the employment of a field meteorologist for the HICAT Project.

England - CAT forecasting at Bedford, England, was a joint effort by British and HICAT meteorologists. The forecasts utilized Global Weather Central (GWC) data together with analyses of the 100, 70, and 50 mb constant pressure surface, tropopause height, RAOBs, and in some cases Richardson numbers. Jetstreams were routinely observed that crossed over the Scottish mountains. Whenever possible, an attempt was made to fly in the Global Weather Central (GWC) forecast area as well as in the most favorable area selected by the HICAT and British meteorologists.

Louisiana - HICAT forecasts at Barksdale AFB (near Shreveport) were made with the assistance of base forecast personnel. The forecast method required analysis of the 70 mb pressure surface and horizontal temperature gradient. Also at this time, analyses were begun of the 70 mb Δz (12 hour height change in meters of the 70 mb surface). RAOBs were analyzed and inspected for vertical temperature gradients. Particular attention was paid to the presence of inversions as related to the Haymond technique for forecasting turbulance (Reference 22).

Maine - At Loring AFB the forecast procedure was essentially the same as that at Barksdale AFB, Louisiana. Basic weather maps analyzed were the 100 and 70 mb constant pressure surfaces with horizontal temperature gradients overlayed, Δz (70 mb height change chart), RAOB analyses, and chart of the thickness variation between the 70 mb and the 50 mb levels. By analysis of the thickness variation, determinations concerning temperature advection were made.

The overall forecast was a cooperative effort between the HICAT meteorologist and Loring AFB forecasters. The Global Weather Central (GWC) forecast was received and evaluated each operational day. The GWC and HICAT forecasts agreed about one-fourth of the time. When the forecasts did not correspond, an attempt was made to fly the HICAT aircraft in both areas.

Panama - At Albrook AFB, data analyzed were the 70 mb constant pressure chart with isotherms, the Δz chart, the 70 mb-50 mb thickness and RAOBs. The locally analyzed surface map was used to determine the degree of activity in the Intertropical Convergence Zone. Pilot and radar reports were also used to augment these data. Howard Air Force Base, Canal Zone, weather personnel cooperated with the HICAT meteorologist in the turbulence forecast effort.

Operations from Panama clearly indicated the difficulty of operating over regions where there are few weather stations. An average of eight RAOBs were received each reporting period for an area of 3,600,000 square miles - approximately one-tenth the number received for a similar area in the United States. Unfortunately, GWC forecasts, because of higher priority transmissions, were frequently received too late to be useful.

Florida - Weather personnel at Patrick AFB assisted the HICAT meteorologist in making high altitude forecasts for operations over the southeastern states region. Forecasting procedures, except those for hurricanes, were initially quite similar to methods used at the previous three locations. A few synoptic events occurred, however, which indicated that a distinctive relationship between horizontal temperature gradient and streamlines of the wind flow pattern might be used as a parameter for forecasting the location of turbulent areas. Subsequent analyses for these characteristics proved favorable.

California - At Edwards AFB the 100, 70, and 50 mb analyses of constant pressure surface, isallohypse,[23] thickness patterns, and RAOBs were utilized when appropriate. Additionally, and as was done during the final phases of operations from Patrick AFB, a detailed analysis was made of the horizontal and vertical temperature gradients and the horizontal two-dimensional wind vector field.

The first upper level pattern, based on the thermal trough and wind flow method that indicated turbulence, was observed on 17 November, 1967. The pilot encountered moderate to severe CAT in the forecast area. This method of forecasting was used on subsequent missions.

AVAILABILITY AND LIMITATIONS OF METEOROLOGICAL DATA

At the beginning of the Extended HICAT Program (March 1967), a comprehensive literature survey was conducted to determine what meteorological information was available relative to analysis and forecasting of turbulence in the upper troposphere-lower stratosphere.

As indicated in the preceding forecast methods discussion, there was little need for high altitude forecasts in the past, except for the operation of a few special purpose Air Force aircraft. There were some theoretical studies concerning turbulence in general that had some relevance, but at that time they had not been tested. It was necessary therefore to develop analysis

---

[23]A line of equal change in height of a constant pressure surface over a specified prior interval of time.

techniques from which high altitude turbulence forecasts could be made. A prerequisite was that the forecasts be based upon data available on the national weather reporting network.

DATA ACCURACY

During the HICAT program a continuing effort has been made to reduce the errors normally associated with the analysis and evaluation of meteorological data. It is believed that the errors are at a minimum even though in some instances it was necessary to make choices between two or more data sources (e.g., aircraft observation, teletype reports, national weather records center data), when obviously only one could be correct. When these problems occurred, personal judgment regarding the proper selection of data was the only recourse. Some aspects of weather data errors are discussed below.

Radiosonde Data

Since nearly all correlations of turbulence with meteorological factors involve the use of radiosonde and rawinsonde data, mention should be made of the accuracy of this data. It is probable, however, that discrepancies resulting from the spatial distribution of radiosonde stations (approximately 250 nm between stations in the U.S.A.) and from time differences between soundings (usually 12 hours and up to 24 hours in some foreign countries) have more effect on the results than the accuracy of the instruments themselves.

Hodge (Reference 23) has deduced that resolution of ground equipment and evaluators plus interpolation errors cause a scatter band of around 1°C in the sounding profile. The scatter increases with height, probably due to the longer time interval between reference points in the upper levels resulting in a larger number of temperature interpolations. An error of 1°C in a 2000-foot layer would result in a 7-foot height error (Reference 24). Scatter resulting from the plotting of soundings of one radiosonde observation recorded on two sets of ground equipment imply that the major portion of the scatter does not result from the radiosonde itself (Ref. 20). Factory flight simulation tests have shown that errors greater than 1°C occur in using the U.S. Weather Bureau radiosonde only 11 percent of the time. The rawinsonde balloon system can be affected appreciably by precipitation and ice formation. In addition, the drag coefficient increases as the balloon changes shape from approximately a teardrop near the surface to a sphere at higher levels (Reference 24).

Other factors influencing the reliability of wind data include lack of coherence between significant levels used in determining the temperature sounding and the levels of reported winds, rounding off of direction (to the nearest 10° in some countries), and the decreasing reliability of both recorded speeds and directions as the angle of the balloon approaches the horizon. In Australia, where wind speeds in the winter may exceed 100 knots over large height intervals, it is not uncommon for a balloon to travel 100 miles or more from the station by the time it reaches 60,000 feet. This, in turn adds to the difficulty of coordinating the spatial distribution of turbulence reports with radiosonde data.

Section VI

Comparison of U-2 and RAOB Data

During the climbout portion of HICAT Test 102, temperature measurements were obtained based upon two-second averages of the sampled data. These values are plotted in Figure 68 and compared with radiosonde observations from Laverton (the flight's point of origin) and Wagga (about 230 miles northeast of Laverton) as well as with the U.S. Standard Atmosphere.

A close agreement exists between the flight measurements and the radiosonde data from Laverton, despite a time discrepancy of over one hour. Agreement with Wagga data is not as good because of the distance from Wagga to the climbout flight path. Since the wind direction at Laverton deviated very little with height, the distance the balloon travelled can be approximated by knowing its ascent rate and the average wind speed over the layer from surface to 56,000 feet. Thus, the distance is approximately 55 miles. Average wind directions over this layer for Laverton and Wagga were 215° and 225° respectively. The aircraft's heading from takeoff to the leveling out point, 90 miles northeast of Laverton, was 30°; only 5° away from the direction the balloon was traveling. Hence, it can be concluded that the flight measurements and Laverton's radiosonde data were sampled along paths in close approximation with each other.

Accuracy of Wind Data

Three principal techniques are used to measure winds at the HICAT flight altitudes. The most commonly used technique is referred to as RAWIN. The RAWIN system consists of a radar giving azimuth and elevation angle of a conventional, balloon-borne radiosonde. When GMD-2 radar or equivalent is available, the slant range distance is also obtained. The other two principal systems consist of higher precision radar and either a Rose balloon or a Jimsphere balloon. These balloons are fixed diameter, super-pressure balloons that are especially designed to follow the wind more nearly than the conventional balloons. The Rose balloon is a smooth sphere, and the Jimsphere balloon has irregularly space protuberances upon a 2-meter diameter sphere.

None of these systems directly indicates the wind at a given altitude. The wind velocity is computed using the horizontal positions at two distinct times. During this time interval the balloon has risen through a finite altitude interval. Hence, the computed wind for the midpoint of the altitude interval is based upon the horizontal distances of two points at different altitudes. The difference between the true wind and the computed wind is a function of the accuracy to which the time interval and the positions of the two points are known compared to the magnitude of the altitude interval. For the present purpose it is not necessary to discuss the relative merits of the Rose and the Jimsphere balloons. It is sufficient to state that detailed studies and experiments with the Rose and Jimsphere balloons and their radar tracking systems have definitely established that there are many features of the wind that are not detectable by the widely used RAWIN system. In the RAWIN system the points used to compute the wind are approximately 600 meters different in altitude. In the Rose and Jimsphere systems the difference in altitude is approximately 50 meters. Also, the higher precision radar used in the Rose and Jimsphere systems determines the balloon positions more accurately by

130
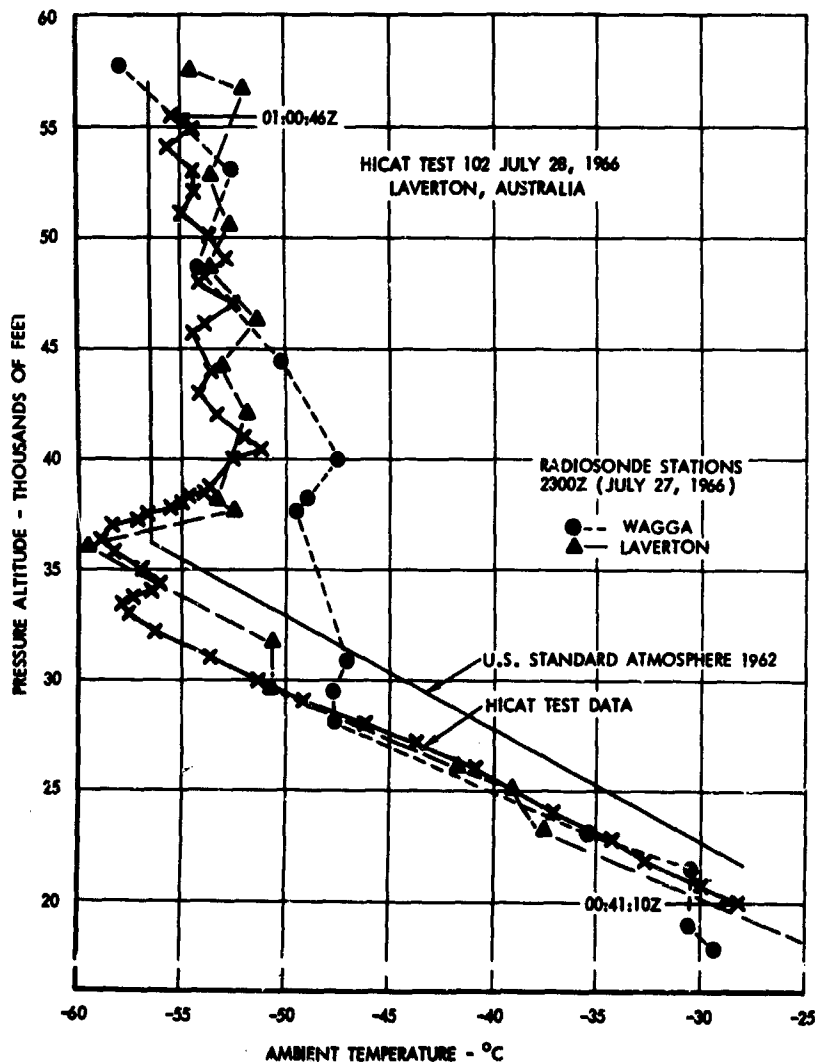
Figure 68   Comparison of HICAT Temperature Data with Radiosonde Data

approximately an order of magnitude. The results obtained by the Jimsphere and the Rose balloon systems indicate wind profiles significantly different from the profiles obtained by the RAWIN system. For example, the Jimsphere system gives the winds at 25-meter intervals of altitude and these profiles show many fluctuations of the wind with altitude that the RAWIN system does not distinguish.

Unfortunately, the Rose and Jimsphere wind sensor systems are relatively new; they are used at only a few selected locations and for special purposes while the older RAWIN system is the only system used routinely and extensively. Further limitations are placed upon the practical use of the wind data by the methods used to transmit and store the RAWIN data. The winds are reported

for significant pressure surface altitudes (e.g., 70 mb surface level) and for 5000-foot altitude intervals above 20,000 feet. Directions are reported only to the nearest 10°. These widely spaced altitudes combined with the inaccuracy of the wind determination for any given altitude make it impossible to compute small scale vertical wind shears.

For these reasons the wind observations available to the aviation meteorologist lack the resolution desired for accurate calculation of wind shears at the HICAT levels and are considered inadequate for use in the prediction of high altitude clear air turbulence.

ANALYSES

Prior to the beginning of HICAT operations on 16 November, 1967, from Edwards Air Force Base, California, a number of meteorological analysis techniques had been tested with varying degrees of success. Analyses of tropopause slopes, horizontal and vertical wind shear, Richardson numbers, isobaric surfaces, pressure height changes, and thickness patterns did not provide any outstanding indications that these parameters could be developed into objective forecast techniques. It should be recalled that any forecast technique developed must be based on the use of routinely available teletype and facsimile data.

A discussion of the problems and results of various analyses during the extended phase of the HICAT program follows.

Temperature Gradients

Horizontal Gradients - That a relation exists between horizontal temperature gradients and clear air turbulence in the troposphere has been recognized for some time. Kadlec (Reference 25) in his analysis of 963 airline flights wrote, "a refinement in the theory that atmospheric temperature changes may indicate clear air turbulence indicates that a rate of temperature change of 1°C per minute with a total change of 2°C is the most effective combination for detecting impending significant turbulence."

The flights studied by Kadlec were generally at altitudes below 40,000 feet, so it was not established whether his hypothesis would apply to the lower stratosphere. It is significant that Corwin (Reference 26) observed a horizontal temperature gradient of 5°C/120 nm to be associated with CAT in the tropospheric range of 15,000 to 40,000 feet.

Vertical Gradients - The association between CAT and large vertical temperature gradients has also been recognized for some time. S. M. Serebreny (Reference 27) stated in 1954, "Turbulence is a result of an abrupt increase or decrease of wind velocity in the thermal gradient. The stronger the vertical shear the more stable the lapse rate." This comment concerned turbulence observed in the troposphere but was considered probably applicable to turbulent conditions in the HICAT range.

Frederick B. Haymond, CWO, USAF (Reference 22) in evaluating 953 forecasts for 100 U-2 flights out of Davis-Monthan Air Force Base, Arizona, observed that excellent forecast verification was achieved by predicting stratospheric CAT to occur in areas and near levels of large inversions as follows:

<1.5°C/1000 ft	No CAT
1.5° to 2.5°C/1000 ft	Light CAT
2.5° to 4.0°C/1000 ft	Moderate CAT
>4°C/1000 ft	Severe CAT

D. T. Prophet (Reference 28) has postulated that these vertical temperature gradients are manifestations of the character of the turbulence producing wave. He has calculated wave dimensions and the approximate rms vertical accelerations that an aircraft might experience in the area of a vertical sounding.

Temperature Gradients in HICAT Tests - From the foregoing it appeared that horizontal and vertical temperature gradients would be useful indicators of high altitude clear air turbulence. The unknown factor, of course, was whether the relation between horizontal and vertical temperature gradients and CAT in the stratosphere would be similar to the relation between horizontal and vertical temperature gradients and CAT in the troposphere. Ultimately it was determined that when correlation between space and time[24] and observed CAT was good, temperature gradients were considered to be better indicators of turbulence in the 50,000 to 70,000 foot range than any other routinely available meteorological data. In this context the temperature gradients include large lapse rates as well as large inversion rates obtained from RAOB reports.

A suggested relation between temperature gradients and CAT is indicated in Table III. This relation is based on studies of high altitude CAT histories of measured turbulence encounters between 45,000 and 70,000 feet and the associated meteorological analyses. The section on HICAT Forecast Procedures refers to specific examples.

TABLE III TEMPERATURE GRADIENTS AND HIGH ALTITUDE CAT

Temp Gradient	Horizontal (°C/25 nm)	Vertical (°C/1000 ft)	Turbulence
Small	<1.0	<1-1/2	None to very light
Medium	1 to 2	1-1/2 to 2-1/2	Light to moderate
Large	>2.0	>2-1/2	Moderate to severe

[24]Space: altitude ±1000 feet and radius of 100 nautical miles of RAOB station, Time: 12 hours or less.

The horizontal temperature gradients referred to in Table III are those
measured from analysis of the appropriate pressure surface. Accurate deter-
mination of the horizontal temperature gradient for an interval less than
the spacing between RAOB stations is a somewhat subjective procedure. This
factor must be considered when using the table as a forecast guide.

Associated with the horizontal and vertical temperature gradients are wave
patterns that appear in temperature analyses along the 70 mb surface. These
waves, as defined by horizontal temperature analysis, are about 300 to
1000 nm long. As the wavelength decreases and the ratio of wave height to
wavelength increases, the following relations between turbulence and wave
patterns have been observed:

- Large waves have been found to be associated with moderate or
  greater CAT, medium waves with light to moderate CAT, and small
  waves with light or less CAT.

- In terms of the ratio of wave height to half wavelength, large
  waves have a ratio of approximately 4/3 or greater, medium waves
  have a ratio of about 4/3 to 3/4, and small waves a ratio of about
  3/4 or less.

An example of a medium wave and the determination of the ratio is shown in
Figure 69. Examples of medium to large waves appear in Figures 129, 146, and
152. Small wave examples appear in Volume II, Appendix VI, Tests 214, 217,
and 263. Waves tend to be large in areas of pronounced cyclonic curvature of
the maximum velocity wind flow. In areas of straight line or weak anticyclonic
wind flow, waves tend to be small. Compare this with the large wave over the
ABQ, DEN, AMA area in Figure 77.

Constant Pressure Surfaces

The mandatory reporting levels corresponding closely to the operating alti-
tudes for project HICAT were at 100 mb, 70 mb, and 50 mb. The 70 mb chart
was adopted as being most representative of the level of interest. Analysis
of the constant pressure surface and horizontal temperature field, which are
usually overlayed on one chart, were drawn separately in order to reduce
personal bias. One particularly notable feature apparent from the analysis
of the 70 mb constant pressure surfaces and associated winds was the manner
in which the observed winds seem to vary from the gradient winds. The wind
flow is often across the height contours (ageostropic) and when such is the
case the result is rising and subsiding air.

Examination of the 70 mb constant pressure surface charts (Figures 70 through
73) illustrate the short wave (300-800 mi) appearance of the 70 mb pressure
surface as compared with the usually uniform long sine wave (1000 to 3000
miles) characteristic of the 500 mb, 300 mb or 200 mb surface. Note also
that in comparing the 70 mb winds, for example, with the 70 mb constant
pressure surface (Figures 73 and 77), the winds vary considerably from
geostropic flow.

WAVE HEIGHT/HALF WAVELENGTH = 525 NM/445 NM = 1.18
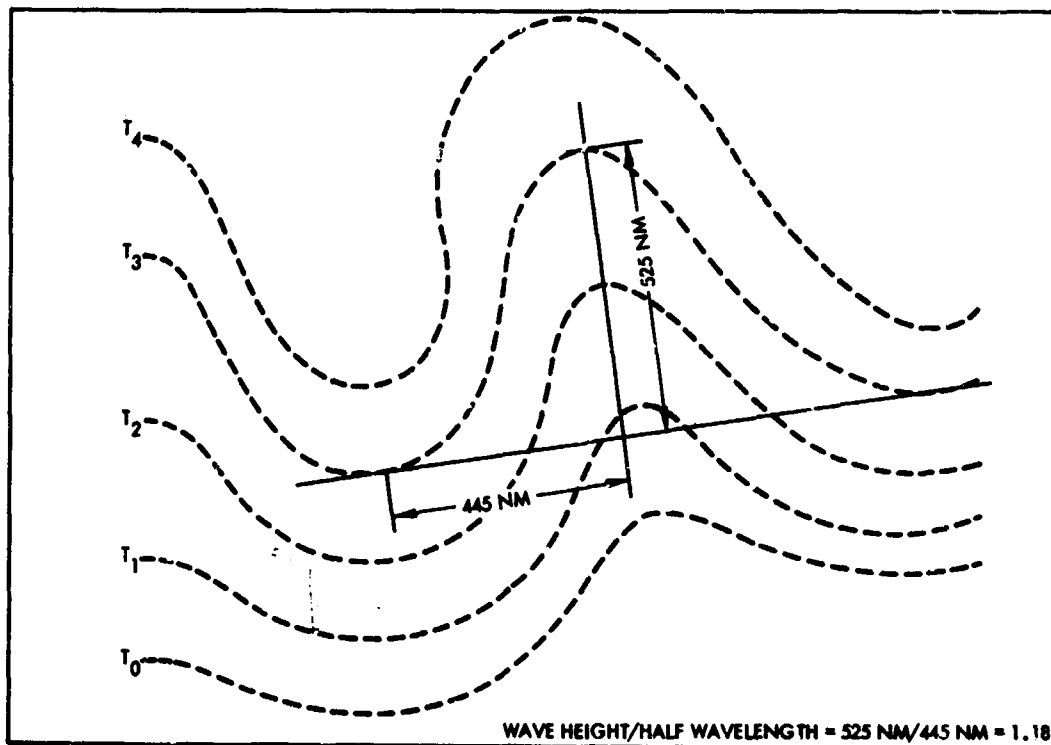
Figure 69   Medium Height Horizontal Isothermal Wave Pattern

Pressure Height Changes

Analyses of the change in height, in meters, of the 70 mb constant pressure surface were completed on approximately 40 tests. It was thought that if turbulence was in fact directly associated with vertical motion, then changes in heights (Δz) of the constant pressure surface would be a good indicator of the possible existence of turbulent areas. No conclusions were reached concerning this method for locating turbulence; however, it is believed the procedure warrants further study.

Thickness Variation Between Constant Pressure Surfaces

One reason for thickness analysis is to determine if thermal change is occurring in a layer. The thermal change may be a result of advection, radiation, or some other process. If thermal change is occurring, there should be packing or spreading of the isotherms. Since certain horizontal temperature gradients are known to be associated with CAT, it is logical to assume that thickness patterns may be an indicator of turbulent areas. This procedure was not tested during this phase of project HICAT because of manpower considerations but is considered a technique worthy of further study.
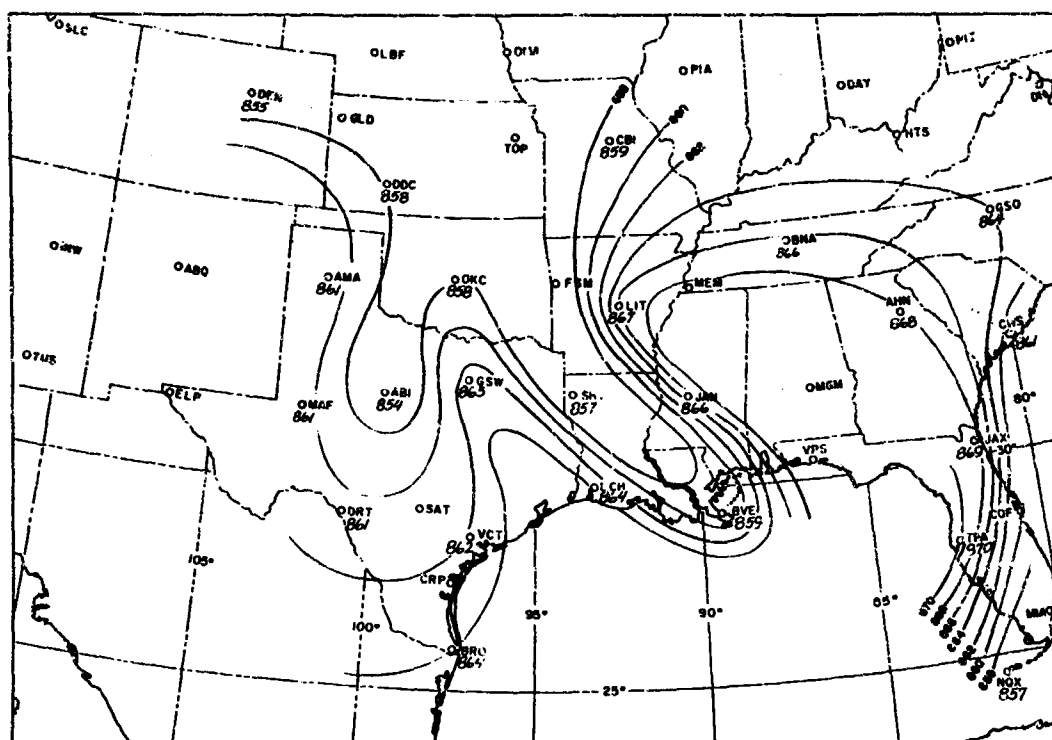
Figure 70   70 MB Constant Pressure Chart - Test 202
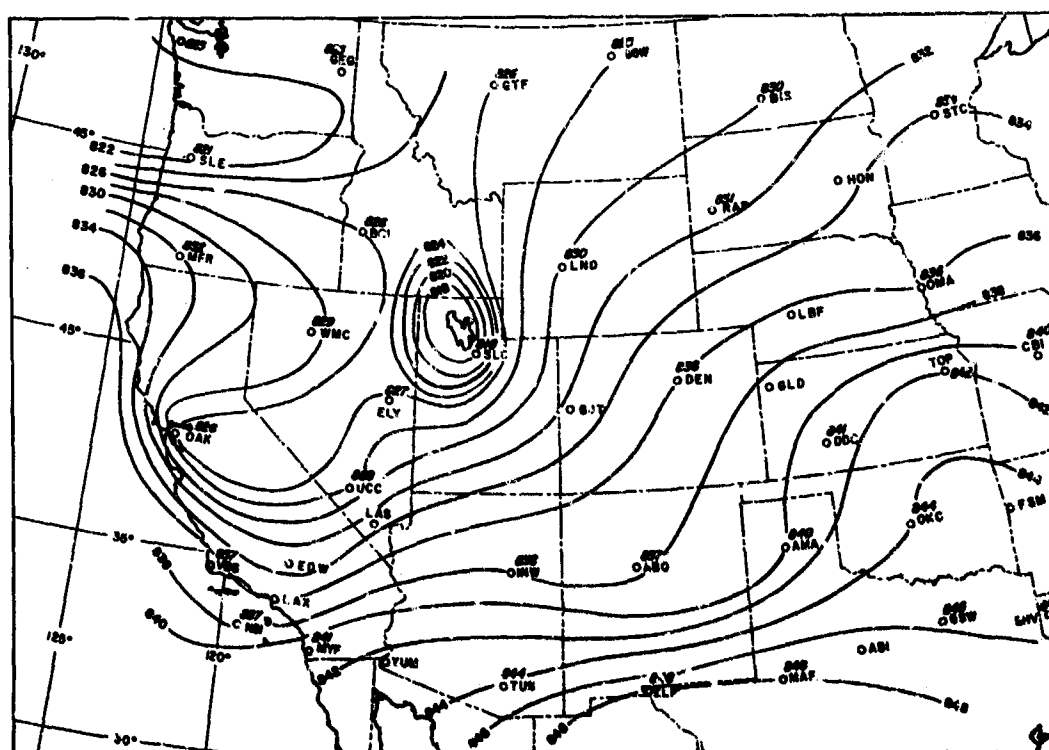
Figure 71   70 MB Constant Pressure Chart - Test 264
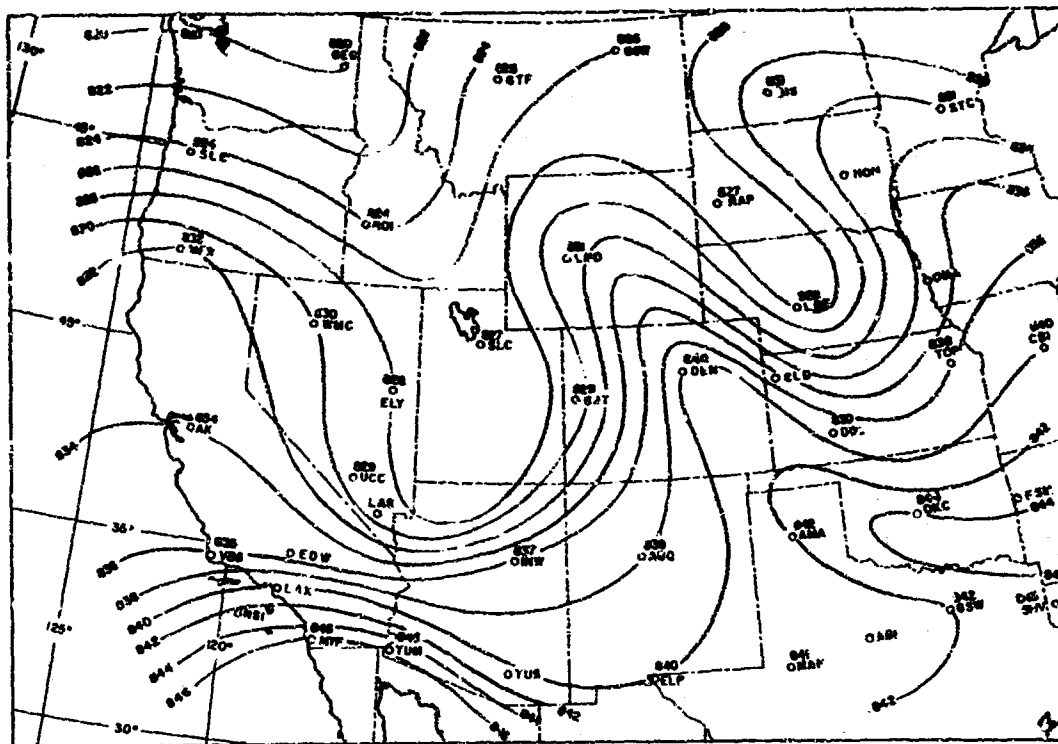
Figure 72   70 MB Constant Pressure Chart - Test 265
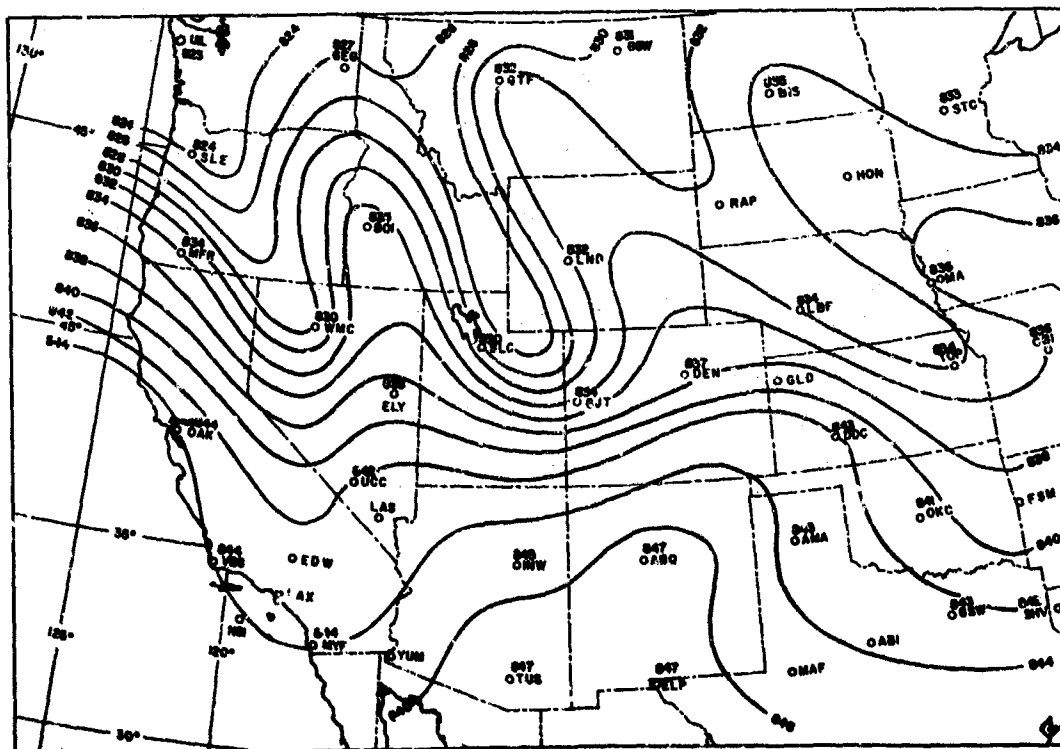
Figure 73   70 MB Constant Pressure Chart - Test 266
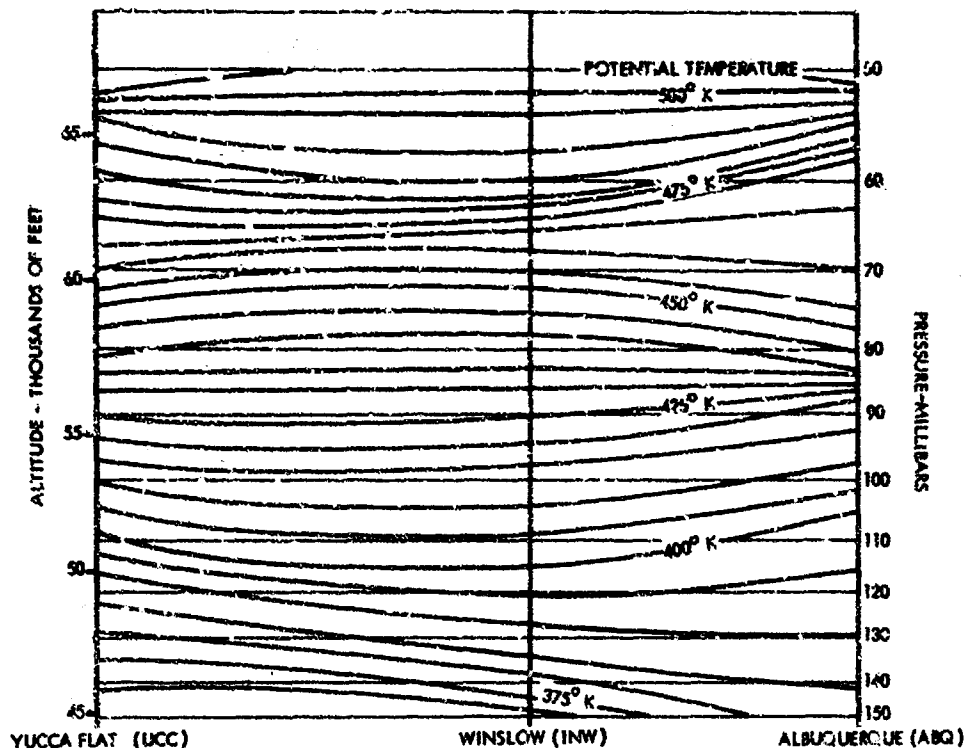
Figure 74   Isentropic Chart - Test 266

Isentropic Surfaces

Isentropic surfaces (surfaces of constant potential temperature in respect
to time and space) were analyzed for a number of special cases.

In their paper, "The Nature of Clear Air Turbulence," Reiter and Hayman
(Reference 29) stated, "It became evident, however, that all cases of
moderate and severe CAT were located in, or very close to, the axis of a
downward drop in the isentropic surfaces - the isentropic trough." These
were observations of turbulence located in the troposphere. It seemed
logical to assume, however, that the processes involved would apply to tur-
bulence in the HICAT range, and analyses were completed in order to corre-
late with observed turbulence (Appendix IG, Tests 202, 204, 218, 220, 264,
265, and 266).

Figure 74 is an isentropic cross section through Yucca Flat, Nevada, Winslow,
Arizona, and Albuquerque, New Mexico at 0000Z, 2 December 1967.

The Baroclinic zone[25] is quite pronounced over Albuquerque, New Mexico. As
stated above by Reiter and Hayman, the turbulence was encountered near the
axis of an isentropic trough. It should be noted, however, that the turbu-
lence has decreased to very light at 57,500 feet which was at the low point

---

[25]The state of stratification in a fluid in which surfaces of constant
pressure (isobaric) intersect surfaces of constant density (isosteric).

138

in the isentropic trough. The severe CAT was observed to be at about 54,000 feet which was slightly below the level of the inversion. Although the turbulence was in fact along the axis of the isentropic trough, the severe turbulence was in an isentropic hump. It is perhaps more significant that the turbulence occurred near the vertical axis of a zone in which there was considerable packing and spreading of the isentropes.

Cloud Photographs

In order to obtain information concerning cloud structure over which turbulence was sampled, U-2 pilots sometimes took pictures with a hand-held 35 mm camera.

Approximately 1000 color shots were made during the period of this report. Although the pictures cannot be included as a part of this report, one interesting example is shown in Figure 75. Below the photograph is a diagram of the hurricane cloud formation. The unshaded area represents approximately the area shown in the photo. This picture was taken as the pilot was flying in the Southwest quadrant of hurricane Doria which at that time was about 300 nautical miles east of Norfolk, Virginia, and near 37°N, 71°W.

Terrain

Table IV provides a comparison of observed CAT intensity over three categories of terrain for all HICAT test runs. The percent of the total flight time over each terrain category is shown in parenthesis. Turbulence runs were classified light, moderate, or severe and then assigned to the appropriate terrain classification. The percentage of each intensity in a given category and the percentage of runs per category are also presented.

TABLE IV CAT INTENSITY VERSUS TERRAIN

Total Flt Time (%) / CAT Intensity	Terrain Category						
	(27%) Water		(37%) Flat Lands Relief Diff < 2500 ft		(36%) Mountains Relief Diff > 2500 ft		All Categories
	No. of Runs		No. of Runs		No. of Runs		No. of Runs
Light	40	80%	118	67%	101	49%	259	60%
Moderate	10	20%	55	31%	79	38%	144	33%
Severe	0	0%	3	2%	27	13%	30	7%
Total	50	11%	176	41%	207	48%	433	100%
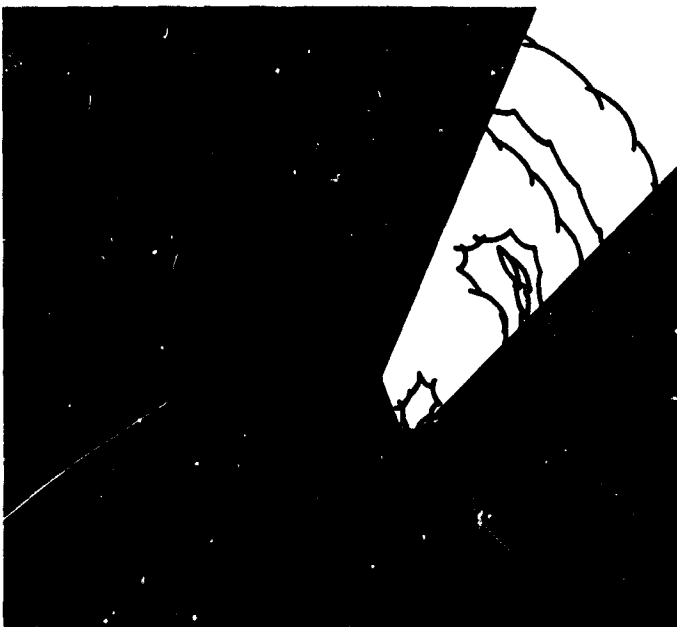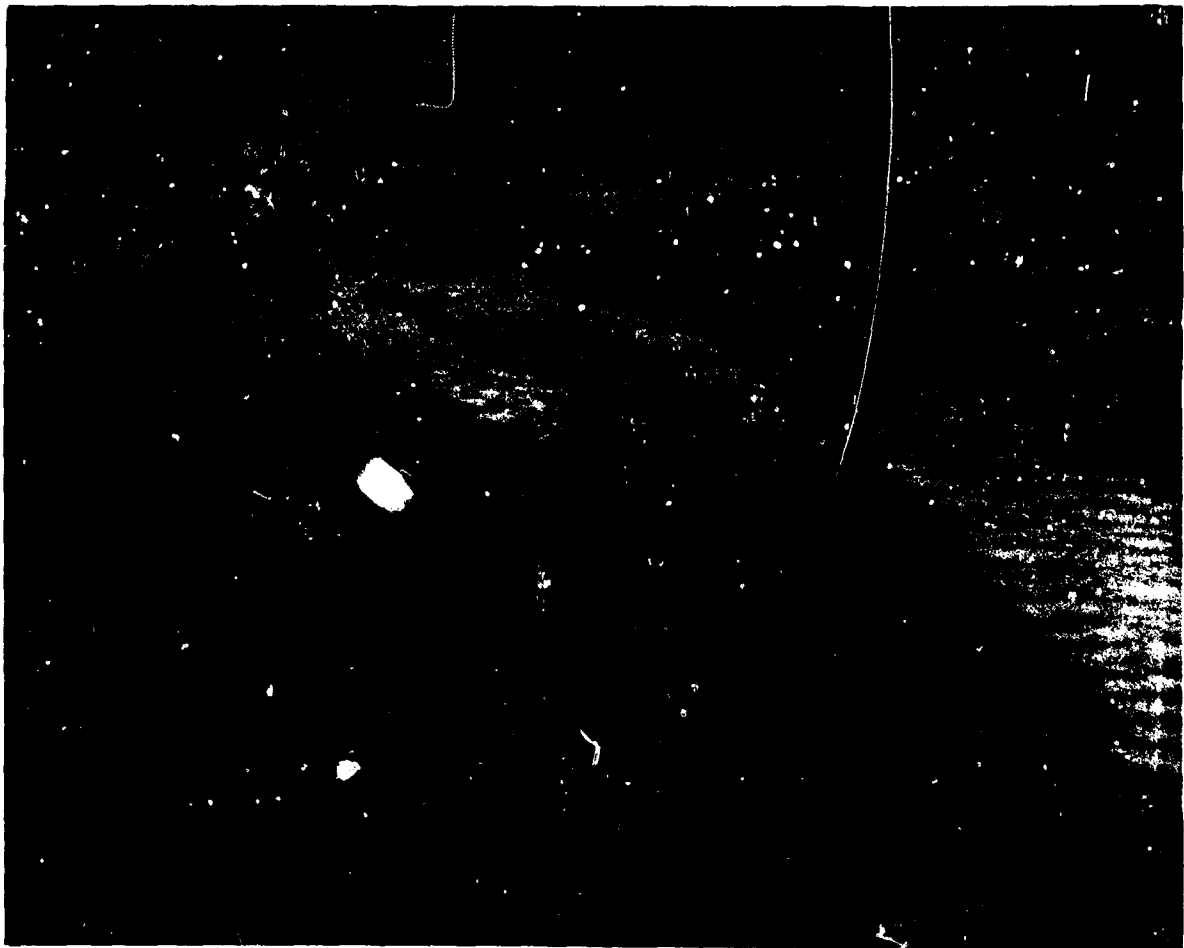
THE UNSHADED AREA OF
THE DIAGRAM CORRE-
SPONDS TO THE VIEW OF
HURRICANE DORIA
VISIBLE IN THE PHOTO-
GRAPH

Figure 75   Cloud Structure of Hurricane Doria

The distribution of the turbulence by severity indicates the more intense CAT is associated with an increase in relief difference. There is some evidence of an increase in the amount of turbulence encountered over mountains and flat lands as opposed to water. This appears to be true because roughly equal time was flown over each category and yet a much smaller number of encounters of turbulence occurred over water.

FORECAST EVALUATION

Verification of weather forecasts has been a controversial subject for more than sixty years and has affected nearly the entire field of meteorology. Brier and Allen (Reference 30) have given a comprehensive review of the methods as well as the problems of forecast verification. Some of the methods reviewed by them have been applied to the forecasts made by the HICAT meteorologist.

Before any satisfactory verification scheme is adopted it is necessary to determine the primary purpose to be served by the verification and the forecasts. The observations must be given in explicit terms; either categorical or numerical terms must be used. In this report, the verification data presented will be used as a basis from which to compare future work. The expression of the forecast and the observations in explicit terms is not a simple matter although it may appear so. The terms very light turbulence, light turbulence, moderate turbulence, and severe turbulence were used throughout this program. These subjective terms can be given objective interpretation as described in Data Editing, Section V.

In the following paragraphs, the intensity classification of turbulence runs given by the editor of the oscillograph records were used. It is important to note, however, that in many instances the pilot reports differed significantly in both the degree and location of the turbulence. Most of these differences arise from subjective reactions of the pilot in registering the CAT while some are due to the subjective evaluation of the editor in selecting and categorizing CAT samples. Samples which were very light or very short were normally ignored, as described in Section V. A few samples went unedited if they coincided with instrument malfunctions or large amplitude aircraft maneuvers.

To satisfy the requirement of objectivity with respect to the forecasts, it is also necessary to set specific limits on the time, location, and altitude in addition to the degree of turbulence. For the first forecast verification the limits were that portion of the entire flight above 45,000 ft. Table V is a contingency table for 89 HICAT search flights in the Extended program.

From this table it is seen (on the diagonal) that 46 (52%) of the forecasts were correct and 80 (90%) were within one intensity category of being correct. Table VI indicates the percent of time each observed category was correctly forecast.

TABLE V   CONTINGENCY TABLE FOR HICAT FORECASTS
BY FLIGHT FOR ALL FLIGHTS FORECAST

CAT Intensity Observed (Edited)	CAT Intensity Forecast					
	None	Very Light	Light	Moderate	Severe*	Total
None	4	0	5	2	0	11
Very light	1	7.	16	2	0	26
Light	0	3	17	3	0	23
Moderate	0	0	8	18	0	26
Severe	0	0	0	3	0	3
Total	5	10	46	27	0	89

*A special problem arises with forecasts of regions of severe turbulence
 because the Air Force prohibits flights to such regions. Consequently,
 some slight downward bias in forecast intensity level is introduced.

Another commonly used measure of forecast skill is the skill score defined by

$$S = \frac{R - E}{T - E}$$

where

R is the number of correct forecasts

T is the total number of forecasts

E is the expected value based on some standard such as chance,
   persistence, or climatology.

TABLE VI   PERCENT OF TIME OBSERVED CAT INTENSITY
CATEGORY WAS CORRECTLY FORECAST

	CAT Intensity Forecast				
	None	Very Light	Light	Moderate	Severe
Percent correct	80	27	74	69	0

When E is based on chance, it is defined by

$$E = \Sigma \frac{R_i C_i}{T}$$

where

R_i is the total of the ith row of a contingency table

C_i is the total of the ith column of a contingency table

Under such a verification system, perfect forecasts give a score of 1.0, and for forecasts no better than chance the score is 0.0. For the forecasts in Table V the skill score is .35. The computation of the pure chance score from the values given in Table V makes no allowance for skill in designating the flight path.

From Table V, if a weight 0 is assigned to a correct forecast, weight 1 to a forecast one category off, weight 2 to a forecast two categories off, etc., the standard deviation will be one category.

The contingency table for HICAT forecasts by legs for 30 flights is shown in Table VII. A leg is defined as the flight route between primary navigational check points. The legs averaged about 300 miles. An example of the HICAT forecast and verification form used is shown in Figure 76 for Test 256. From this table it is seen that 41 (44%) of the forecasts were correct and 62 (67%) were within one category. The skill score is 0.23.

An analysis of the forecasts by altitude and by legs gave the following results: of those forecasts that were correct by category, 28 specified the observed altitude within ±1000 feet, 2 specified the observed altitude within ±2500 feet, and 3 specified the observed altitude within ±5000 feet.

TABLE VII CONTINGENCY TABLE FOR HICAT FORECAST
BY LEGS FOR 30 FLIGHTS

Observed Turbulence	CAT Intensity Forecast					
	None	Very Light	Light	Moderate	Severe	Total
None	19	6	25	0	0	50
Very Light	1	1	5	0	0	7
Light	3	0	16	1	0	20
Moderate	0	0	7	5	0	12
Severe	0	0	2	2	0	4
Total	23	7	55	8	0	93

HICAT FORECAST · VERIFICATION FORM

Flight #: __256__ Date: __16 NOV 1967__ Pilot: __MAJ JOHNSON__ Base: __EDWARDS AFB, CAL.__

TOT: __~1820 Z__   LAT: __22:55 Z__

Flight Route by Legs

Fcst: |EDW| ⌐ VL -530' ⌐ |OAK|

Ver: | ⌐ VL 470 ⌐ |

Fcst: |OAK| ⌐ LT, 500-550' ⌐ |38 N/118 W|

Ver: |LT 590'   LT 570' ⌐ |

Fcst: |38 N/118 W ⌐ LT 500-550' ⌐   ⌐ VL 530' ⌐ |LAS|

Ver: | ⌐LT 510 ⌐   LT 550' |

Fcst: |LAS| |EDW|

Ver: | |

Fcst: | |

Ver: | |

Fcst: | |

Ver: | |

VL: ± .05 - .1g   Lt: ± .1 - .25g   Mod: ± .25 - 5g   Svr: ± .5 - .75   Ext: >.75g

Figure 76   HICAT Forecast and Verification Form

A different evaluation by flights shows that for 89 flights:

CAT forecast	CAT observed	Observed/forecast
84 Flights	77 Flights	82%

For five flights out of 89, the forecast was for no CAT. Four flights observed no CAT, one flight observed light CAT. Evaluation of 93 forecasts for flight route legs shows that CAT was forecast 70 times and observed 43 times for a score of 62%.

Thus, while comparisons among these scores are interesting and indicate by their variability the difficulties of scoring forecast verifications, the actual scores themselves are not statistically significant. They do not differentiate factors associated with location, season, meteorological situation, or the forecaster's learning curve. However, some of the forecast verification scores[26] may have some value for future comparisons.

---

[26]Most notably those for the "30 flights" at Edwards AFB where only one forecasting method was used.

HICAT FORECAST PROCEDURE

From experience gained through the use of analysis and forecast procedures
described and discussed previously, a method is presented for the prediction
of CAT in the lower stratosphere which is considered objective enough in
scope to be an effective forecast tool. The method works best with current
meteorological data. Data more than twelve hours old should not be used.

The procedure is as follows:

STEP I: SELECT LEVEL OF INTEREST AND ANALYZE THE MOST APPROPRIATE MANDATORY
LEVELS FOR HORIZONTAL ISOTHERMS AND WIND FLOW

To select the proper level to be analyzed, determine the altitude to be flown
and analyze the mandatory reporting surface nearest the level of interest.
For example, if the altitude to be flown is 63,500 feet, or close to that
altitude, the 70 mb chart would be most appropriate, and one level would
probably suffice. If the altitude to be flown is 57,000 feet, it would be
desirable to analyze the 100 mb and 70 mb levels.

The upper level analyses must then be inspected for well defined thermal
troughs and ridges. In the stratosphere, a thermal trough is said to exist
where the warm air (isotherms) dips southward, and a thermal ridge is said
to exist where the cold air (isotherms) projects northward. Utilize Table III
and the subsequent horizontal isothermal wave analysis as a CAT forecast guide.

Figure 77 is a good example of a thermal pattern that was associated with
severe turbulence. Note that the thermal pattern defines a wave with a ratio
of height to half wavelength of 330 mi/240 nm of 1.37. This is considered
a large wave. Waves of this dimension are associated with turbulent condi-
tions and one can assume turbulence will be abundant in the regions where
they are located. Also, note the 10°C horizontal temperature gradient between
Albuquerque (ABQ) and El Paso (ELP).

An example of the type of horizontal thermal pattern where turbulence will be
light or nonexistent is shown in Figure 78. The isotherms are widely spaced
(2°C/600 nm) and are near zonal (i.e., east-west) in the area that was
sampled. No turbulence was encountered (i.e., in agreement with the hori-
zontal criteria of Table III).

STEP II: PLOT ALL RAOBS ADJACENT TO FLIGHT ROUTE TO INCLUDE DATA 10,000 FEET
ABOVE AND BELOW THE FLIGHT ALTITUDE

Inspect the RAOBS for vertical temperature gradients, utilizing Table III as
a forecast guide. Note that in the RAOB analyses presented in tests 182
through 285 (Appendix IG and VI), observations for the 150 - 50 mb layers
were plotted. The range was from 45,000 to 67,500 feet, which adequately
covered the altitudes of interest in Project HICAT.

An example of a large vertical temperature gradient is that shown for ABQ in
Figure 79. For the layer 51,500 to 56,500 feet, a vertical gradient of
3°C/1000 feet was observed. Severe turbulence was present in this layer.
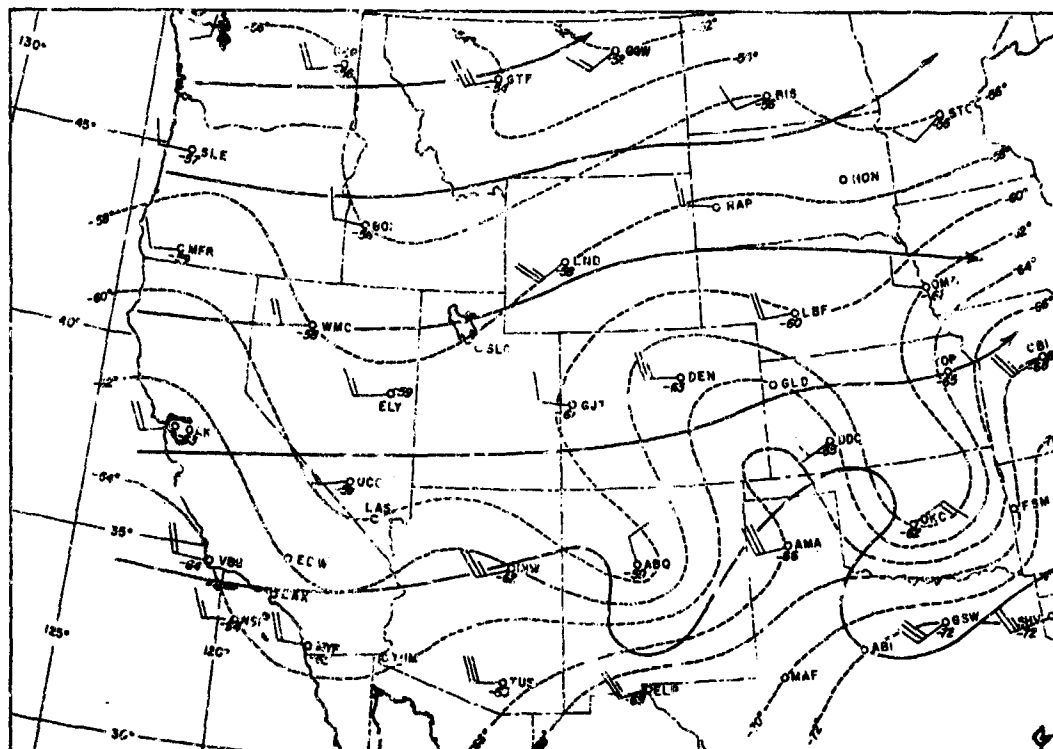
Figure 77   70 MB Temperatures and Winds Chart - Test 266
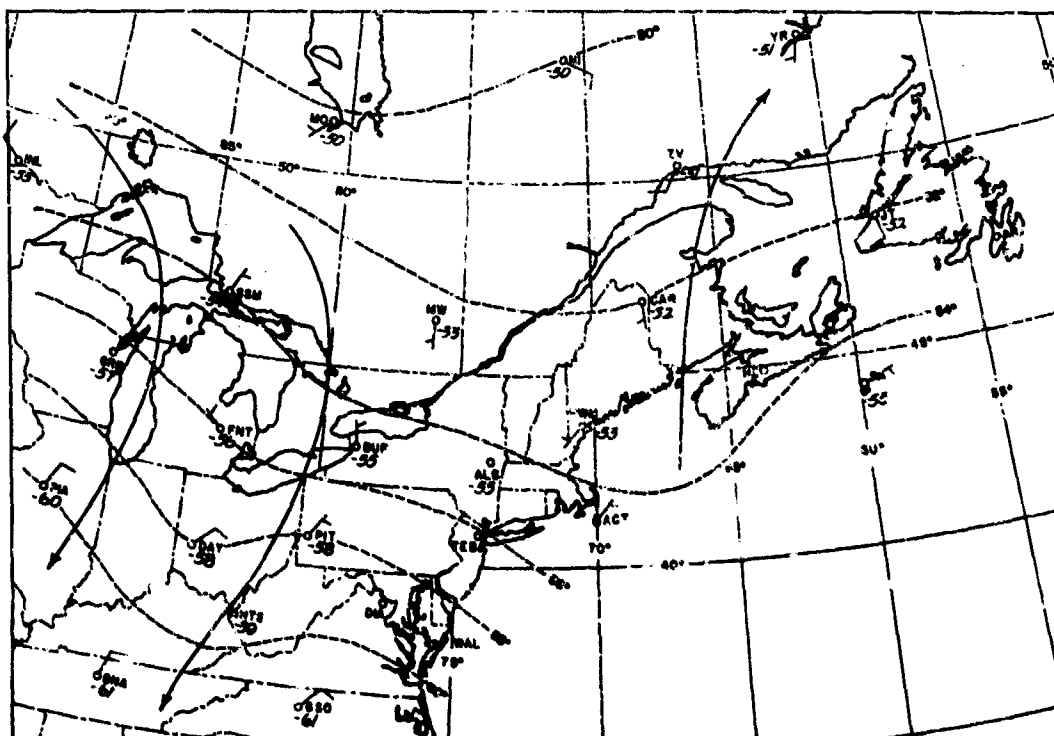
Figure 78   70 MB Temperatures and Winds Chart - Test 218
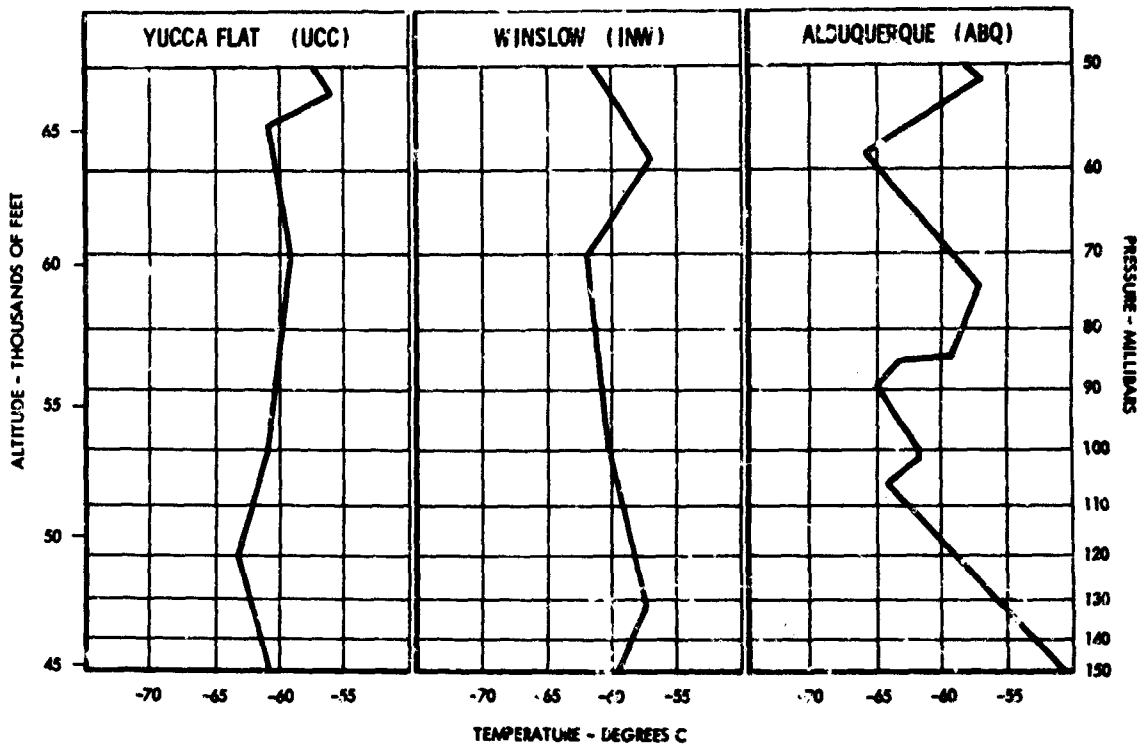
Figure 79   RAOB Charts - Test 266

An example of a small vertical temperature gradient is that shown for Caribou in Figure 80. The gradient is 0.17°C/1000 feet. No CAT was found in this case.

An important point in this procedure is the proper selection of the layer to be considered. To illustrate, consider the soundings for Dodge City (DDC) and Oklahoma City (OKC) in Figure 81. To examine the vertical temperature gradient for DDC, the level selected should be from 61 mb to 50 mb. For OKC it would be desirable to inspect the entire sounding from 150 mb to 50 mb.

STEP III: FORECASTING CHANGES IN TURBULENT CONDITIONS

Some general observations concerning the prediction of movement and changes in intensity of turbulence in the 45,000 - 70,000 feet range are as follows:

   (a)   Turbulent conditions usually move at the speed of major systems apparent at the 500-200 mb levels (mountain waves excepted).

   (b)   HICAT tests indicate that turbulence is abundant above regions of pronounced cyclonic curvature of a strong jetstream and moves near the speed of the axis of the jetstream trough.[27]

---

[27]This type of turbulence would probably continue in one location as long as an active trough remained in the area.
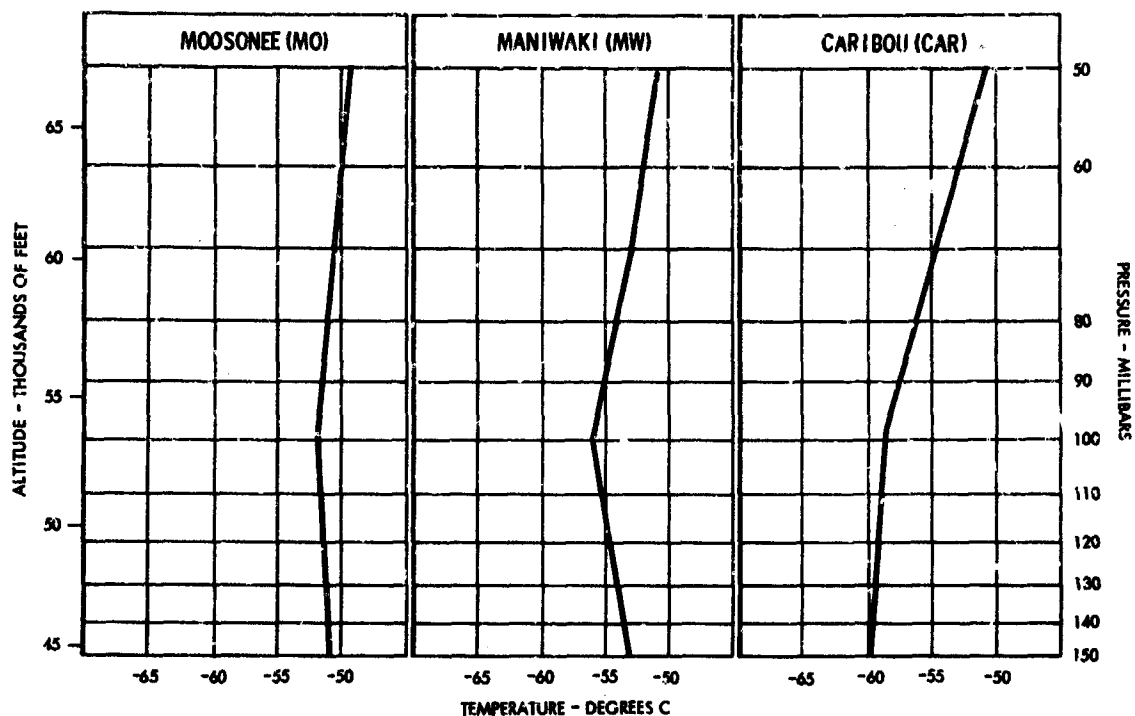
Figure 80   RAOB Charts - Test 218
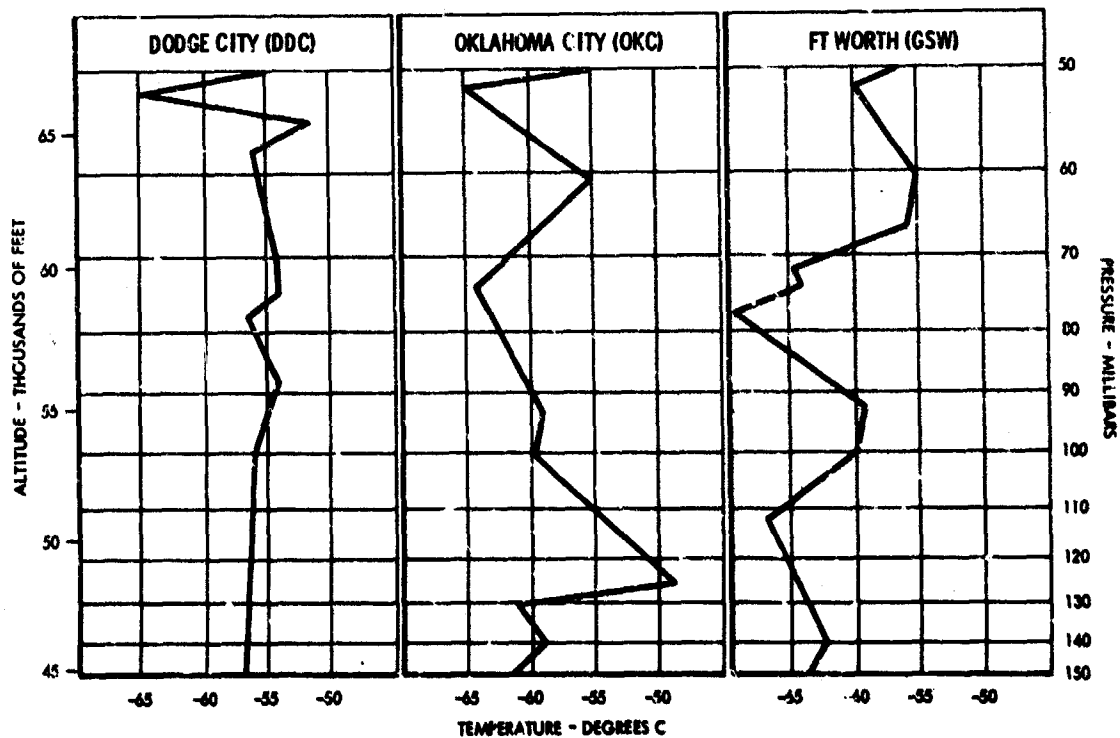
Figure 81   RAOB Charts - Test 197

(c) Turbulence is usually light or nonexistent in areas where the general circulation (wind flow) is near straight line or slightly anti-cyclonic (mountain waves excepted).

(d) Turbulence may be expected to increase over areas of active squall line development.

(e) Turbulence (based on radiosonde and aircraft observations) has been observed to last from a few minutes to over 72 hours at one location.

The procedure described above can be used by any forecaster having access to first and second transmissions of rawinsonde or radiosonde data and is a relatively rapid practical procedure for routine use.

RECAPITULATION

In reviewing the various types of analyses and forecast procedures that have been used in connection with the meteorological support of the HICAT program, the following aspects appear to be most significant:

- Detailed analyses of the ten special HICAT tests show convincingly that certain features apparent from isentropic analyses are related to the occurrence of CAT. For example, in all cases where isentropic analysis was accomplished and significant turbulence was encountered near in time and space to the analysis area, the turbulence was found to occur along the vertical axis of a pronounced baroclinic zone. In areas of little baroclinicity or small slopes in the isentropic surfaces, turbulence was very light or absent.

- The ageostropic concept, or that of wind flowing across the height contours, is not conclusively substantiated in this report. However, comparing the 70 mb pressure analyses in Figures 70, 71, 72, and 73 with the corresponding wind analysis in Figures 105, 140, 146, and 152, one can see evidence that strongly supports the idea of ageostropic flow. In these cases turbulence could be attributed to vertical motion created by flow across the pressure height contours.

- The relationship between CAT and the horizontal and vertical temperature gradients and horizontal isothermal wave patterns appears to be substantiated by the HICAT data. The horizontal and vertical gradients found to be associated with high altitude CAT in the lower stratosphere are similar to those previously found to be associated with CAT at lower altitudes, i.e., in the upper troposphere.

SECTION VII

CONCLUSIONS

The HICAT measurements were obtained in U-2 test flights covering approximately 412,000 statute miles in twelve geographical areas[28]. The following conclusions are based upon an analysis of the clear air turbulence measured in these flights in the altitude band from 45,000 to 70,000 feet:

1. A comparison of the turbulence measured in the HICAT program with that measured by VGH recorders in U-2 operational flights (Reference 8) on the basis of frequency of exceedance of derived equivalent gust velocity indicates the following:

- In both programs, the turbulence in the 60,000 to 70,000 foot altitude band was less severe than in the 50,000 to 60,000 foot band.

- In both altitude bands, the intensities encountered in the HICAT program were significantly more severe than reflected in the operational data, and yet the maximum U_{de} was 12 percent below the value ordinarily specified for structural design.

2. The HICAT gust velocity power spectral densities are characterized, on the average, by slopes on the log-log plots of -1.44 to -1.71 for the vertical and longitudinal components of turbulence. On the same basis the lateral component was found to have slopes of -1.60 to -1.87[29]. Where comparable data are available, the longitudinal slopes are about the same as reported previously for the Redirected HICAT program in Reference 5. However, the vertical and lateral slopes range about 7 percent steeper than those of Reference 5, possibly because of the increased gust intensity of the newer data.

3. The HICAT gust velocity power spectral density curves, on the average, remain straight or nearly straight on the log-log plots to wavelenths approaching 10,000 feet. The corresponding average scale of turbulence, defined as the constant L in the Von Karman equation or similar equations, is at least 2000 feet.

4. The turbulence encountered in the HICAT flights appeared to be distinctly nonstationary, i.e., the statistical properties of the gust velocity time series data were found to vary significantly within the turbulence samples. As a result at least in part of this lack of stationarity, the ratio of peak airplane acceleration to rms acceleration measured during a CAT traverse was found to to range from 1.16 to 2.58 times the ratio predicted by theory (Rice's equation) for a stationary Gaussian time history.

---

[28] Includes both the Extended and the Redirected programs.

[29] The higher range of values in this component is attributed to instrument noise.

5. A comparison of the gust velocity component power spectral densities indicates all three components to be about equal in severity at the highest measured frequencies (roughly 0.007 cycles per foot); it shows the lateral components however, to become somewhat more severe at the lower frequencies. RMS gust velocities obtained by integrating the power spectral densities over the frequency range from 0.0005 to 0.007 cycles per foot (2000 ft to 100 ft wavelengths) indicate that the lateral component is more severe than the longitudinal by 10 percent and more severe than the vertical by 20 percent. At the longer wavelengths, there is some indication that these percentages increase. However, in view of the somewhat lower quality of the lateral gust velocity measurements, the observed percentage differences amongst the three components are not considered large enough to justify a conclusion that high altitude clear air turbulence, on the average, is anisotropic.

6. Pilot elevator control motions were found to augment the effects of the turbulence, i.e., to produce higher cg accelerations and thus higher U_{de} values. In four turbulence runs where elevator motion was extensive, the highest U_{de} peaks were increased by factors of 3 to 4 in one run and by factors of 1.25 to 2.00 in the others. However, the effect in the HICAT data on the average is judged to be considerably less than the lowest factor above.

7. Values of $\bar{A}$ (ratio of rms cg normal acceleration to rms gust velocity) used for obtaining probability distributions of rms gust velocity from operational VGH data are about 25 percent higher for the U-2, when based on measured frequency-response functions determined by the cross spectrum method, than when obtained by the simple theory ordinarily used for this purpose. As a result, the rms gust velocity distributions obtained using the simple theory are about 25 percent more severe than would be obtained using the measured frequency-response functions determined by the cross spectrum method. The N_0 value for the U-2 is about 0.85 cps. A considerably greater effect on $\bar{A}$ and a smaller value of N_0 are found when the spectrum method is used. These results are applicable when the rms gust velocity is related to the rms cg acceleration by means of a Von Karman spectral shape with L = 2500 feet.

8. Use of a high-pass numerical filter that passed without attenuation all wavelengths shorter than 7000 feet, and virtually eliminated all wavelengths longer than 17,000 feet, was found to reduce the highest gust velocities by from 7 to 23 percent as determined from the peak counts of absolute gust velocities.

9. From a meteorological standpoint the following conclusions are significant:

- In the HICAT altitude range above the tropopause, observed CAT intensity was found to vary in proportion to the magnitude of the horizontal and vertical temperature gradients.

- Isotherms along the 70 mb constant pressure surface were found to display wave-like patterns. The wave steepness, as defined by horizontal temperature analysis, was found to be proportional to CAT intensity.

- In the HICAT altitude range of the lower stratosphere, and above regions of pronounced cyclonic curvature of the maximum winds in the troposphere, waves as indicated by isotherms along a constant pressure surface tend to be steep and therefore are associated with CAT of moderate to severe intensity.

- In the HICAT altitude range of the lower stratosphere and above regions of straight or slightly anti-cyclonic light winds in the upper troposphere, waves as indicated by isotherms along a constant pressure surface, tend to be shallow and therefore are associated with CAT of light or less intensity.

- Turbulence in HICAT range of the lower stratosphere is frequently encountered above the region of the major tropospheric trough and moves near the speed of the axis of the trough (mountain waves excepted).

- The foregoing factors were used to develop a practical procedure for forecasting CAT in the lower stratosphere. The procedure was substantiated with HICAT aircraft test measurements.

APPENDIX I

DETAILED ANALYSIS

This appendix contains certain details of the analysis and results required to substantiate the discussion of Sections V and VI. It consists of the following subsections:

Appendix IA

A. HICAT TEST SUMMARY TABLE

This appendix consists of the HICAT Test Summary Table. Most of the entries
are self-explanatory; however, some amplification is presented in the follow-
ing paragraphs.

An "f" under the test number indicates a ferry flight respectively. The sym-
bols following the run numbers[30], L (level), T (turn), C (climb), and D (descent)
are indicative of the aircraft flight path during the turbulence penetration.
X and Y distances from the base are obtained from the inertial platform.
Average altitude is obtained when possible from the high-altitude pressure
sensor and has been corrected for position error. The aircraft heading angle
is obtained from the inertial platform and can differ from the ground track
angle depending upon atmospheric winds. The heading angle is measured from
true north to the direction the aircraft is pointed. The average wind direc-
tion, following meteorological convention, is measured from true north to the
direction from which the wind is blowing.

The intensity of the turbulence in each run is indicated in several ways. It
is classified subjectively in accordance with the oscillogram editing notes as
VL (very light), L (light), etc. It is described by the maximum and minimum
incremental cg acceleration, the maximum and minimum derived equivalent gust
velocity, the root mean square (rms) cg acceleration, and rms derived equiva-
lent gust velocity. In addition, where true gust velocity components were
computed, the CAT intensity is also indicated by truncated spectral rms values
at 2000-foot wavelength and at the maximum standard wavelength, i.e., one of
the following: 4000, 10,000, 20,000 or 40,000 feet. For some runs a consider-
able reduction in statistical reliability was accepted in order to obtain rms
data up to the 40,000-foot wavelength. These cases are indicated by an aster-
isk. Also shown for some cases are the rms deviations obtained directly from
the gust velocity component time histories.

Gaps in the table occur when the cg acceleration or U_{de} peak count data indi-
cate the turbulence was of insufficient intensity or duration to warrant further
processing to determine gust velocity time histories and power spectra. Gaps
also result from instrument or equipment malfunctions.

---

[30] Test 280-7 is not a separate run as indicated; it is actually the result of
combining two shorter adjacent runs (i.e., runs 5 and 6) to obtain better
resolution of long waves.

FLIGHT	DATE	IDENT	RUN	START TIME (GMT)	RUN NUMBER	LOCATION (Start x,y)(End x,y) n.mi.	ALTITUDE (Avg) feet	AIRSPEED (Avg True) knots	HEADING (Avg True) degrees	WIND (Avg) deg/kn	TEMP (Avg) °C	TERRAIN CLASS.	TURB CLASS.	Δu_g (max)	u_DE (max) fps	RMS Δu_g	RMS u_DE fps	RMS @ λ=2000 ft u_f	u_L	u_y	RMS @ λ=λmax u_f	u_L	u_y	λmax ft	RMS TIME HISTORY u_y	u_L	u_y
Alberta	3-13-67	180 (r)	21	19:03:45	90	+331+34 / +336+17	61,300	403	081	229/43	-59.5	M	M	+0.24/-0.34	+5.2/-7.6	.065	1.45	2.02	2.38	2.14	2.02	2.38	2.14	2	2.95	5.41	8.21
			31	19:05:15	40	+342+36 / +347+36	61,000	408			-59.1	M	M	-0.26/-0.18	+5.6/-3.9	.061	1.35										
			41	19:06:30	110	+350+36 / +363+13	61,300	405	105	254/32	-58.5	M	L-M	+0.21/-0.38	+4.6/-8.5	.061	1.36	1.37	1.90	1.55	1.37	1.90	1.55	2	2.40	6.64	4.36
			51	19:09:40	125	+373+30 / +87+32	61,300	409	083	249/28	-58.8	M	M-S	+0.25/-0.24	+5.5/-5.1	.061	1.32										
			61	19:16:10	50	+419+41 / +124+43	61,000	403			-57.7	M	M	+0.26/-0.18	+5.9/-4.0	.051	1.15										
			71	19:33:45	145	+560+70 / +576+76	60,900	411	072	254/23	-59.8	M	L-M	+0.24/-0.1	+5.1/-2.9	.037	0.77										
			81	19:39:38	27		60,200	408			-59.6	M	L-M	+0.25/-0.38	+5.2/-8.1	.076	1.61										
			91	19:44:10	130		60,800	406	095	256/44	-58.1	M	L	+0.18/-0.15	+3.9/-3.3	.033	0.71	0.88									
			101	20:34:40	45	+979+119 / +987+119	61,000	403			-59.5	F	M	+0.15/-0.16	+3.1/-3.3	.032	0.81										
			111	21:01:00	90	+1175+157 / +1181+159	60,780	412			-61.1	F	M-L	+0.21/-0.24	+4.0/-2.7	.043	0.34										
			121	21:28:35	25	+1296+183 / +1300+186						F	L													
			131	22:24:30	75	+1764+349 / +1770+355	60,800	412			-57.1	F	L	+0.10/-0.11	+1.9/-2.1	.024	0.44										
Hanover	3-16-67	181(r)	21	06:43:30	80	+209-12 / +219-12	61,600	392			-58.5	M	L	+0.49/-0.28	+11.1/-6.3												
Bedford	3-17-67	182	C3	21:12:45	140		48,200	356			-52.0	F	L-M	+0.27/-0.25	+5.6/-5.2	.079	1.80	1.39	1.49	1.77	1.75	1.99	2.35	4	7.20	11.69	17.47
			31	21:49:00	305		55,600	401			-54.5	M	L-M	+0.32/-0.21	+6.4/-5.1	.054	1.12										
			41	21:54:05	165		55,500	404			-52.5	M	L-M	+0.16/-0.06	+3.2/-1.2	.072	1.46										
			51	21:59:55	40		55,700	403			-52.0	M	L	+0.06/-0.45	+1.5/-9.3	.061	1.25										
			61	22:51:45	210		55,100	400			-55.8	M	VL-L	+0.45/-0.13	+9.3/-8.8	.015	0.30	0.82									
			71	23:57:30	90		48,000	338	350	276/32	-51.1	W	M-S			.125	2.56	2.95	3.78	2.68	2.95	3.78	2.68	2	5.16	21.18	13.99
Bedford	3-21-67	184	21	09:44:25	150	+12+68 / +11+84	55,000	388	350	276/32	-55.7	F	L	+0.17/-0.21	+3.4/-3.1	.058	1.16										
			30	13:06:40	210	-124+47 / -111-24	57,800	384	036	257/10	-58.0	F	VL	+0.13/-0.40	+2.2/-1.8	.028	0.50										
Bedford	3-22-67	185	21	09:56:15	60	-76+125 / -77-112	61,600	400			-50.5	F	M	+0.16/-0.16	+3.5/-3.5	.050	1.08										

*RMS value from data with less than 80 degrees of freedom

M - Mountains (relief difference >2500 ft)
F - Flat lands (relief difference <2500 ft)
W - Water

VL - Very Light
L - Light
M - Moderate
S - Severe

Flight Path
L - Level
D - Descent

C - Climb
D - Descent

Legend / notes (margin):

RMS value from data with less than 50 degrees of freedom

VL : Very Light
L : Light
M : Moderate
S : Severe

M : Mountains (relief difference > 2500 ft)
F : Flat Lands (relief difference < 2500 ft)
W : Water

Flight Data
L : Low
I : High   C : Climb
            D : Descent

Appendix IA

Legend notes (right margin):
- M = Mountains (relief difference > 2500 ft)
- F = Flat lands (relief difference < 2500 ft)
- W = Water

- VL = Very Light
- L = Light
- M = Moderate
- S = Severe

- S = Climb
- D = Descent

- *RMS value from data with less than 60 degrees of freedom

TL - Very Light
L - Light
M - Moderate
S - Severe

R = Mountains (relief difference >2500 ft)
F = Flat Lands (relief difference <2500 ft)
T = Timber

1 = Good
2 = Poor

BASE	DATE	TEST	RUN	START TIME (GMT)	RUN LENGTH	LOCATION (Start x,y) (End x,y)	ALTITUDE (Avg)	AIRSPEED (Avg True)	HEADING (Avg True)	WIND (Avg)	TEMP (Avg)	TERRAIN CLASS.	TURB CLASS.	Δa_z (max)	U_{DE} (max)	RMS Δa_z	RMS U_{DE}	RMS @ λ = 5000 ft			RMS @ λ = λ_{max}				RMS TIME HISTORY		
																		U_V	U_L	U_T	U_V	U_L	U_T	λ_{max}	U_V	U_L	U_T
				hr:min:sec	sec	nmi	feet	knots	degrees	deg/kt	°C			g	fps	g	fps	fps	fps	fps	fps	fps	fps	k ft	fps	fps	fps
Barksdale	5-16-67	205	2L	17:43:25	20	+ 483 +455 + 483 +456						M	L	+0.16 -0.12	+ 2.8 - 2.1	.042	0.71										
			3L	17:59:55	90	+ 483 +448 + 486 +438						M	M	+0.29 -0.23	+ 4.8 - 3.8	.059	0.99										
			4L	18:01:50	310	+ 486 +435 + 486 +404	51,800	378	180	232 / 35	-59.0	M	L-M	+0.27 -0.17	+ 4.5 - 2.8	.050	0.84										
			5L	18:11:30	40	+ 488 +408 + 487 +412	51,400					M	L	+0.17 -0.23	+ 3.1 - 4.3	.055	1.02										
			6L	18:13:	365	+ 488 +420 + 490 +450	51,800	356	000	223 / 43	-58.0	M	L-M	+0.22 -0.25	+ 4.1 - 4.6	.037	0.68	0.95									
			7L	18:23	70	+ 491 +497 + 484 +451	52,300					M	L-M	+0.23 -0.18	+ 4.4 - 3.3	.050	0.93										
			8L	18:25:00	60	+ 484 +442 + 484 +442	52,100					M	L-M	+0.12 -0.10	+ 2.2 - 1.9	.034	0.63										
			9L	18:27:00	240	+ 484 +436 + 484 +414	51,700	352	185	239 / 28	-60.2	M	L	+0.20 -0.18	+ 3.7 - 3.3	.029	0.53										
			10L	18:43:45	960	+ 507 +437 + 471 +445	51,800	352	273	206 / 26	-58.4	M	M	+0.24 -0.32	+ 4.4 - 5.9	.039	0.71	1.07	1.74	1.34	1.26	2.56	1.74	10	1.56	4.90	3.61
			11T	18:53:05	90	+ 471 +445 + 464 +448	51,300					M	L-M	+0.24 -0.41	+ 4.4 - 7.3	.095	1.70										
			12T	18:55:05	95	+ 462 +446 + 467 +430	52,700					M	L	+0.16 -0.37	+ 2.8 - 6.7	.099	1.80										
			13L	18:56:40	370	+ 468 +439 + 492 +436	51,900	365	098	223 / 35	-59.5	M	L	+0.13 -0.13	+ 2.1 - 2.3	.023	0.39										
			19L	20:14:40	100							F	L														
			20L	20:18:55	150							F	L-M														
Barksdale	5-17-67	206	2L	17:32:20	45		55,900					F	VL	+0.05 -0.04	+ 0.9 - 0.7	.018	0.36										
			3L	19:04:40	105		58,000					F	L-M	+0.27 -0.37	+ 4.7 - 6.5	.074	1.31										
Barksdale	5-20-67	207	6L	21:00:15	65							F	L-M														
			7L	21:08:20	145							F	VL-L														
			8L	21:11:00	80							F	M														
			9L	21:24:55	50							F	L														
			10L	21:27:10	25							F	L-M														
			11L	21:30:05	90							F	L														
			12T	21:32:15	80							F	L														

Flight Pat.:
L - Level
C - Climb
T - Turn
D - Descent

M - Mountains (relief difference > 2500 ft)
F - Flat Lands (relief difference < 2500 ft)
W - Water

VL - Very Light
L - Light
M - Moderate
S - Severe

*RMS value from data with less than 80 degrees of freedom

VL - Very Light
L - Light
M - Moderate
S - Severe

*MKS value from data with less than 50 degrees of freedom

M : Mountains (relief difference >2500 ft)
F : Flat Lands (relief difference <2500 ft)
W : Water

Appendix IA

VL - Very Light.
L - Light.
M - Moderate
S - Severe

H - Mountains (relief difference > 1500 ft)
F - Flat Lands (relief difference < 1500 ft)
W - Water

VL - Very Light
L - Light
M - Moderate
S - Severe

H - Mountains (relief difference > 500 ft.)
F - Flat Lands (relief difference < 500 ft.)
W - Water

VL = Very Light
L = Light
M = Moderate
H = Severe

S = Mountains (relief difference > 500 ft)
F = Flat Lands (relief difference < 500 ft)
W = Water

This value from data with less than 30 degrees of freedom

Slope Code
L = Level
S = Sea

C = Clear
P = Partly Cloudy

Appendix IA

RUN NO	START TIME (GMT) hr:min:sec	RUN LENGTH sec	LOCATION (West x,y) (Dkm x,y) nmi	ALTITUDE (Avg) feet	AIRSPEED (Avg True) knots	HEADING (Avg True) degrees	WIND (Avg) deg/kn	TEMP (Avg) °C	TERRAIN CLASS	TURB CLASS	Δaₙ (max) g	u_Δn (max) fps	RMS Δaₙ g	RMS u_Δn fps	u_γ	u_L	u_p	u_γ	u_L	u_p	λmax ft	u_γ	u_L	u_p
6L	03:26:45	50		53,100	364	186	266 / 77	-60.0	F	L	+0.14 / -0.12	+2.4 / -2.0	.034	0.60	3.36	4.18	3.62							
8L	03:28:20	125		51,600	165	167	270 / 32	-57.4	M	S	+0.78 / -0.68	+14.0 / -12.1	.162	2.09									
9T	03:33:55	125		51,500	358	349	269 / 54	-57.8	M	M-S	+0.41 / -0.39	+7.5 / -7.2	.081	1.47	1.64	2.31	1.99							
10T	03:43:50	85		51,500					M	L	+0.26 / -0.25	+5.1 / -4.8	.064	1.25									
11L	03:47:20	80		52,700	335	254	219 / 20	-58.5	M	L	+0.24 / -0.26	+4.9 / -5.2	.079	1.62	2.04	2.20	2.34							
12L	03:48:40	65		52,500					M	L	+0.15 / -0.14	+3.2 / -3.0	.058	1.22									
13L	03:51:30	60		52,500	366	186	238 / 35	-56.2	M	L-M	+0.22 / -0.19	+3.9 / -3.3	.067	1.20									
14L	03:54:20	455		52,700	371	171	211 / 29	-59.5	M	M					1.33	1.46	1.45	2.54	3.57	2.77	10			
15L	04:09:35	180		53,200	340	343	172 / 9	-61.1	M	M					2.57	2.37	2.36	3.29	3.30	3.18	4			
16L	04:12:55	115		53,900	352	344	239 / 27	-62.0	M	M	+0.30 / -0.23	+5.6 / -4.9	.070	1.31	1.28	1.45	1.48	1.28	1.45	1.48	2	2.31	8.59	8.54
17L	04:19:15	50		54,700	365	175	148 / 29	-62.9	M	L-M	+0.27 / -0.20	+3.5 / -4.1	.053	0.95									
18L	04:20:35	55		54,600					M	L	+0.23 / -0.23	+4.0 / -3.2	.068	1.21									
19L	04:23:50	55		51,600					M	L	+0.18 / -0.16	+2.9 / -2.6	.056	1.04									
20L	04:25:05	70		51,000					M	L	+0.16 / -0.16	+2.6 / -2.1	.041	0.66									
21T	04:29:00	50		51,600	358	284	341 / 64	-59.3	M	S	+0.84 / -0.51	+14.0 / -9.3	.139	2.42	2.00	2.45	2.23	2.30	3.19	2.81	4	3.26	7.67	8.76
22L	04:29:50	170		51,600	352	258	235 / 33	-57.1	M	M	+0.48 / -0.19	+8.6 / -3.6	.090	1.61									
23L	04:34:25	40		51,600	344	255	252 / 38	-56.7	M	L-M	+0.51 / -0.51	+8.4 / -8.6	.091	1.69									
24T	04:37:40	85		52,100	330	053	210 / 16	-58.9	M	S	+0.79 / -0.44	+15.6 / -8.6	.144	2.82									
25L	04:39:05	100		52,100	335	081	273 / 46	-60.8	M	L	+0.33 / -0.18	+6.2 / -3.5	.051	0.98	1.18	1.26	1.39	1.18	1.26	1.39	2	3.64	4.43	3.88
26C	04:49:35	180		55,200	397	266	218 / 26	-61.0	M	L-M	+0.29 / -0.27	+4.5 / -4.2	.081	1.27	1.09	1.38	1.39	1.32	1.77	1.87	4	2.60	3.56	5.56
27T	04:52:35	70		56,200	406	259	213 / 42	-62.5	M	M	+0.34 / -0.47	+5.2 / -7.1	.098	1.51									
28L	04:53:45	160		55,600	413	246	201 / 30	-61.5	M	M	+0.69 / -0.67	+10.1 / -9.9	.135	1.98	2.13	2.36	2.30	2.66	3.54	3.15	4	3.19	7.37	8.10
29T	04:56:25	60		55,500	416	251	238 / 25	-59.7	M	M	+0.29 / -0.31	+4.2 / -4.9	.086	1.25									
30L	05:45:40	165		66,200	429	271	342 / 9	-64.4	F	VL	+0.09 / -0.13	+1.4 / -2.1	.021	0.36									
2L	18:12:15	35		>6,500					M	VL	+0.08 / -0.11	+1.4 / -1.9	.035	0.39									
3L	18:15:55	15		57,300					M	VL	+0.06 / -0.06	+1.0 / -1.0	.019	0.31									
5L	19:28:25	44		53,500					F	L	+0.02 / -0.02	+0.2 / -0.2												

Flight Path
L - Level C - Climb
T - Turn   D - Descent

M - Mountains (relief difference >2500 ft)
F - Flat lands (relief difference <2500 ft)
W - Water

VL - Very Light
L - Light
M - Moderate
S - Severe

*RMS value from data with less than 80 degrees of freedom

DATE	TEST	RUN	START TIME (GMT) hr:min:sec	RUN LENGTH sec	LOCATION (Start x,y)(End x,y) nmi	ALTITUDE (Avg) feet	AIRSPEED (Avg True) knots	HEADING (Avg True) degrees	WIND (Avg) deg/kn	TEMP (Avg) °C	TERRAIN CLASS	TURB CLASS	Δa_n (max) g	U_{DE} (max) fps	RMS Δa_n g	RMS U_{DE} fps	RMS @ λ - 2000 ft U_y fps	U_L fps	U_P fps	RMS @ λ - λ_{max} U_y fps	U_L fps	U_P fps	λ_{max} kft	RMS TIME HISTORY U_y fps	U_L fps	U_P fps
12-02-67	268	6L	19:36:20	67	+760 +157 / +758 +157	54,700					F	L														
		7L	19:59:25	64	+653 + 91 / +646 + 90	52,400					M	VL														
		8L	20:09:00	180	+593 + 81 / +574 + 81	47,800	411	254	332 / 38	-66.4	M	L	+0.32 +4.1	-0.42 -5.4	.068	0.89										
		9L	20:41:35	70	+405 + 40 / +198 + 38	51,900					M	L	+0.22 +3.2	-0.24 -3.5	.061	0.89										
1-30-68	269	2L	20:29:20	50	-65 +294 / -52 +298	63,000					M	L	+0.5 +5.2	-0.28 -5.6	.059	1.18										
		3L	20:45:20	75	-40 +311 / -44 +313	62,800					M	L	-0.50 +3.6	-0.21 -3.8	.058	1.06										
		4L	21:58:35	140	+44 +349 / +10 +337	53,900	364	200	163 / 43	-56.4	M	L	+0.16 +3.0	-0.14 -2.6	.037	0.68	1.23			1.23			2	1.87		
		5L	22:07:20	30	+28 +258 / +28 +254	60,300					M	L	+0.16 +2.7	-0.14 -2.4	.051	0.86										
1-31-68	270	2L	21:15:40	11	+99 + 24 / +99 + 25	54,200					M	VL	+0.12 +2.1	-0.12 -2.2	.045	0.79										
		3L	21:21:50	180	+129 + 54 / +148 + 67	54,400	407	053	279 / 35	-59.1	M	VL	+0.35 +6.2	-0.28 -4.9	.062	1.11	0.98			0.98						
		4L	21:50:40	55	+325 + 34 / +132 + 32	62,700					M	VL	+0.14 +2.6	-0.13 -2.6	.048	0.94										
2-02-68	273	2L	22:12:15	95	+ 46 +377 / +44 +368	55,000	378	194	229 / 25	-66.2	M	L	+0.30 +5.0	-0.24 -4.0	.079	1.31	1.67	2.76	2.35	1.67	2.76	2.35	2	2.30	11.10	7.00
2-09-68	277	2L	20:15:15	205	-13 - 71 / -28 - 52	50,200	401	373	333 / 44	-64.1	F	?	+0.35 +5.6	-0.33 -5.0	.055	0.88										
		3L	20:20:50	165	-41 - 52 / -52 - 43	50,400	416	300	325 / 42	-63.7	F	L	+0.26 +4.0	-0.28 -4.2	.048	0.73										
2-14-68	279	2L	21:20:15	110	+612 +120 / +623 +124	55,400	399	073	316 / 42	-62.2	M	L	+0.17 +2.8	-0.16 -2.7	.054	0.91	1.06			1.06		1.25	2	3.65		4.91
		3L	22:38:55	100	+551 + 3 / +546 + 8	58,400	413	205	314 / 6	-64.1	M	L	+0.28 +4.4	-0.28 -4.5	.062	1.00	1.47	2.16	1.85	1.47	2.16	1.85	2	2.69	8.24	3.76
2-15-68	280	3L	22:04:15	155	+608 +237 / +625 +235	54,000	384	098	282 / 28	-60.7	M	M-L	+0.70 -12.8	-0.69 -12.5	.153	2.79	2.90	2.86	2.94	2.90	2.86	2.94	2	9.02	10.98	14.15
		5L	22:34:25	350	+609 +243 / +653 +240	55,500	404	266	267 / 48	-64.8	M	VL	+0.10 +1.6	-0.12 -2.1	.086	0.43	2.64	2.40	2.16	5.07	5.82	4.57	10	8.14	11.77	21.15
		6L	22:40:15	530	+653 +239 / +630 +240	55,590	375	271	278 / 30	-63.1	M	M	+0.93 +17.4	-0.95 -17.8	.107	1.99	2.00	1.88	1.68	4.94 5.75	5.29 5.97	4.87 6.94	20 10°			
		7L	22:34:25	890	+630 +240 / +601 +240	55,500	387	269	271 / 37	-63.7	M	VL-M														
		10L	23:03:25	475	+558 +239 / +551 +234	58,500	375	093	301 / 38	-63.2	M	W(S-L)	+0.97 +19.0	-0.73 -14.3	.111	2.16	2.50	2.61	2.58	4.86	5.69	4.68	10	9.45	16.77	2.95
		11L	23:37:20	539	+674 +235 / +581 +238	61,500	419	273	276 / 17	-60.8	M	L-M	+0.61 +10.5	-0.60 -10.3	.069	1.51	1.81	1.96	2.08	1.07 1.21	5.43 5.22	5.51 5.48	26 10°	4.57	12.19	10.86
		12L	00:03:15	255	+608 +240 / +592 +236	64,700	420	094	337 / 26	-64.2	M	M-L	+0.47 +8.3	-0.42 -7.4	.095	1.69	1.92	2.11	2.21	2.57	3.17	3.25	4	5.80	7.32	14.78

Light Path: L - Level, T - Turn; C - Climb, D - Descent

M - Mountains (relief difference >2000 ft); F - Flat lands (relief difference <2000 ft); W - Water

VL - Very Light; L - Light; M - Moderate; S - Severe

*RMS value from data with less than 80 degrees of freedom

BASE	DATE	TEST	RUN	START TIME (GMT) hr:min:sec	RUN LENGTH sec	LOCATION (Start x,y)(End x,y) n.mi	ALTITUDE (Avg) feet	AIRSPEED (Avg True) knots	HEADING (Avg True) degrees	WIND (Avg) deg/kn	TEMP (Avg) °C	TERRAIN CLASS.	TURB CLASS.	$\Delta\sigma_w$ (max) g	U_{DE} (max) fps	RMS A_w g	RMS U_{DE} fps	RMS @ λ=2000 ft U_w fps	U_L fps	U_F fps	RMS @ λ-λ_{max} U_w fps	U_L fps	U_F fps	λ_{max} x ft	RMS TIME HISTORY U_w fps	U_L fps	U_F fps
Edwards	2-15-68	280	13L	00:11:30	320	-639 +248 / -607 -237	66,400	403	257	307 / 22	-65.8	M	L	+0.10 / -0.35	+7.8 / -6.8	.064	1.24	1.52	1.60	1.51	2.03	2.23	1.98	4	4.21	8.34	8.69
			14L	00:16:50	120	-607 -237 / -593 -236	66,900	414	265	318 / 36	-62.3	M	VL	+0.19 / -0.14	+3.6 / -2.6	.046	0.88										
			15L	00:28:25	130	-608 -237 / -620 -236	59,900					M	M	+0.82 / -0.57	+14.5 / -10.0	.176	3.12										
			16L	00:36:55	140	-612 -217 / -596 -215	60,200	392	265	325 / 34	-65.4	M	M	+0.13 / -0.50	+7.5 / -8.6	.116	2.02	2.48	2.48	2.25	2.48	2.48	2.25	2	5.38	7.30	6.16
Edwards	2-18-68	281	2L	22:17:30	210	-624 +227 / -604 -234	55,600	387	289	301 / 25	-66.1	M	L	+0.24 / -0.31	+4.0 / -5.3	.073	1.22	1.14	-	1.41	1.53	-	1.89	4			
			1L	23:07:15	150							M	M														
Edwards	2-19-68	282	2L	22:12:45	345	-649 +237 / -614 -250	61,500	414	292	307 / 25	-62.3	M	M	+0.41 / -0.65	+6.9 / -11.2	.076	1.30	1.66	1.80	2.00	2.36	2.57	2.63	4	4.74	10.22	9.24
			3L	22:27:20	155	-575 -250 / -558 -243	63,600	408	251	323 / 21	-64.1	M	L	+0.15 / -0.25	+2.8 / -4.5	.044	0.79	1.44	1.81	1.67	1.44	1.81	1.67	2	2.51	5.58	6.71
			4L	22:31:55	80	-546 -237 / -538 -235	63,800	416	251	316 / 30	-63.1	K	L	+0.26 / -0.22	+4.5 / -3.9	.058	1.01	1.70	2.61	2.19	1.70	2.61	2.19	2	2.46	10.37	5.40
Edwards	2-26-68	283	2L	22:02:35	95	-687 + 74 / -676 + 75	61,300	407	279	301 / 25	-62.3	M	L	+0.17 / -0.24	+3.0 / -1.2	.047	0.82	1.28	-	1.84	1.28	-	1.84	2	2.05	-	4.97
Edwards	2-29-68	285	7L	21:25:15	170	-343 +215 / -354 +227	42,000	350	343		-48.5	M	L	+0.32 / -0.31	+5.0 / -4.8	.082	1.28	0.95	1.23	1.49	1.05	1.50	1.70	4			
			8L	21:29:10	135	-358 +231 / -367 +238	42,000	350	053		-51.3		VL	+0.21 / -0.23	+3.2 / -3.6	.064	0.99										

RMS value from data with less than 80 degrees of freedom

M - Mountains (relief difference >2500 ft)
F - Flat Lands (relief difference <2500 ft)
W - Water

VL - Very Light
L - Light
M - Moderate
S - Severe

Flight Path:
L - Level   C - Climb
T - Turn   D - Descent

B. METHOD OF REMOVING EFFECT OF ELEVATOR FROM U_{de} TIME HISTORIES

The method used to remove the effect of elevator motion from the cg normal acceleration time histories was obtained from References 10 and 11.

In order to use the method, flight test data was required. This was obtained from several elevator pulse maneuvers in which measurements of elevator motion and the resulting cg normal acceleration were made. The flight condition for the pulses was based upon an approximate average of all the runs listed in Appendix I of Reference 5, i.e., altitude of 55,000 feet, Mach number of 0.70, and equivalent airspeed of 139 knots. In addition to the elevator pulses, roller coaster maneuvers were also performed. All maneuvers were performed in smooth air.

Two elevator pulses were chosen for this analysis. The time histories of adjusted elevator position and incremental cg normal acceleration for these pulses are shown in Figures 82 through 85. One set of time histories is for a positive elevator pulse and the other for a negative elevator pulse.

The first step in determining the time response of cg normal acceleration due to a unit elevator impulse is to evaluate the Fourier transforms of each of the elevator pulses and responses. This is accomplished by using the numerical procedure and tables presented in References 10 and 11. A requirement for using this method is that both the initial value (at zero time) and the steady state value, after the pulse and response have decayed, be zero. The time histories as measured are shown as dotted lines.

It can be seen that the steady state value of elevator position and cg normal acceleration are not at zero for any of the four time histories. This required that an increment of elevator angle or cg normal acceleration be added to each of the curves so that a final value of zero would be achieved. These increments are shown as dashed lines. This was done in a manner which is believed not to have a significant effect on the final results. For each set of time histories, the increment that was added maintains a constant ratio of cg normal acceleration to elevator angle at each instant of time. The increments were added gradually over a relatively long period of time to avoid introducing any bias at the higher frequencies. The time histories as used in this analysis are shown as solid lines.

The computation of the Fourier transforms requires the time histories to be approximated by a series of steps of uniform width. The amplitude of each step is then used in the computation in conjunction with the appropriate set of tables in References 10 and 11. The accuracy of the computation is a function of the number of steps used and also the number of frequencies at which the computation is performed. The steps which were used to approximate the time histories are superimposed on the time histories in Figures 82 through 8..

From the Fourier transforms, the amplitude ratio and corresponding phase angle of the frequency-response function of the dynamic system is calculated for each run. The amplitude ratio is obtained by dividing the amplitude of the output (cg normal acceleration) by the amplitude of the input (elevator

177
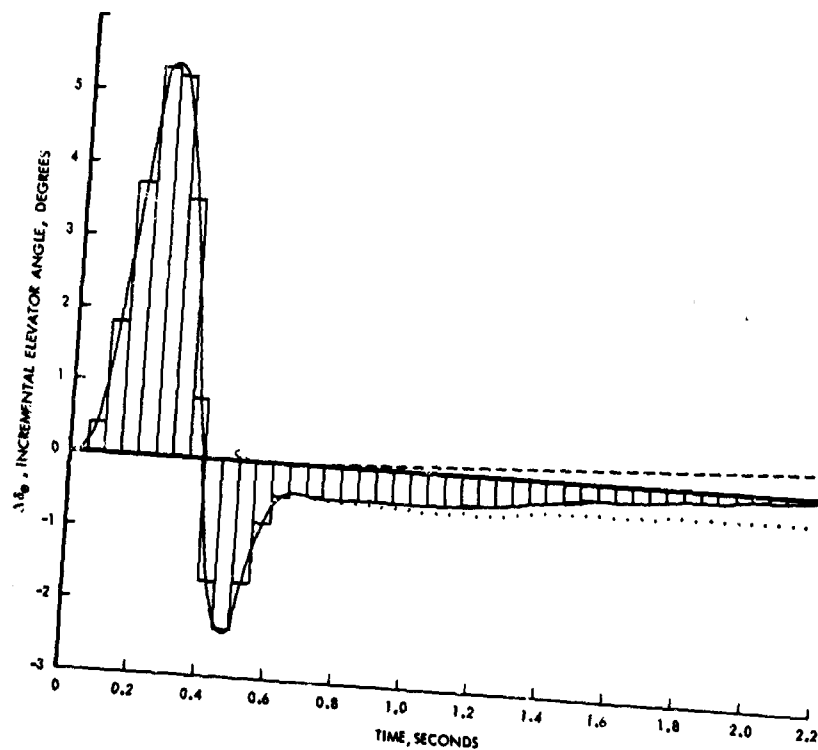
Figure 82   Incremental Elevator Angle Time History
(Positive Elevator Pulse)
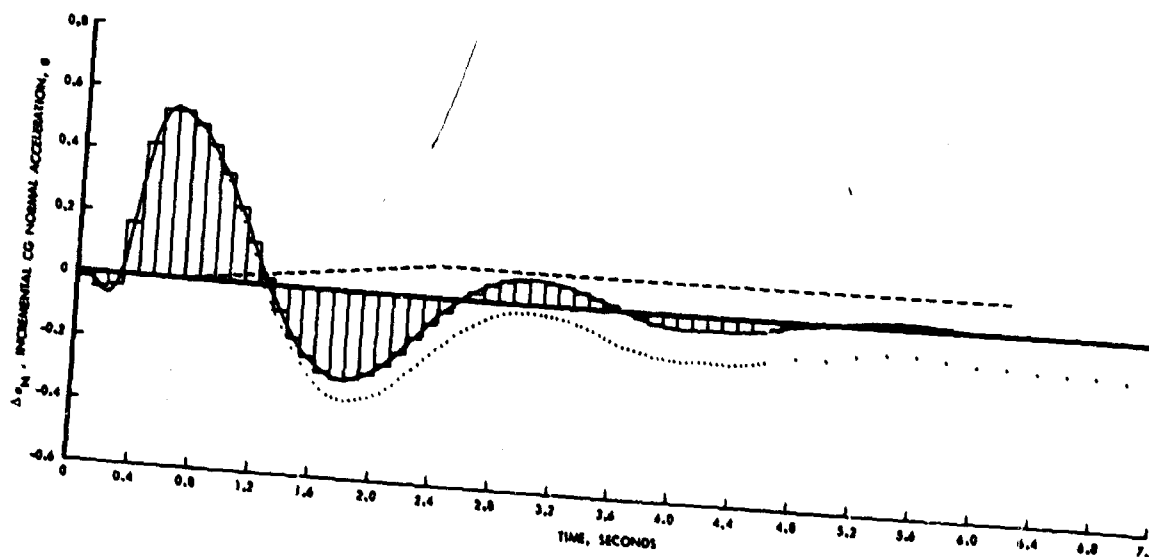
Figure 83   Incremental CG Normal Acceleration Time History,
Due to Positive Elevator Impulse
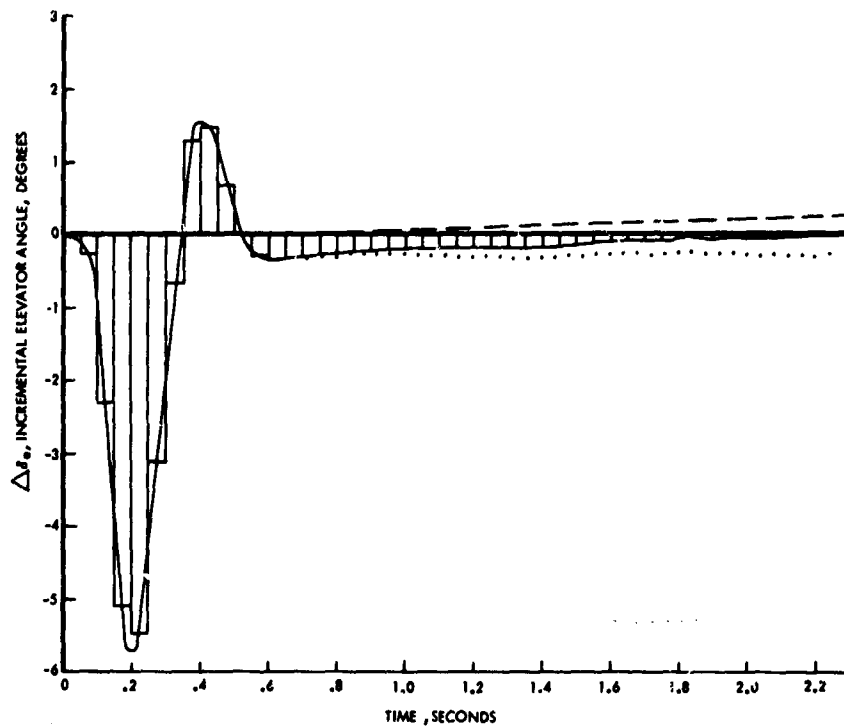
Figure 84   Incremental Elevator Angle Time History
(Negative Elevator Pulse)
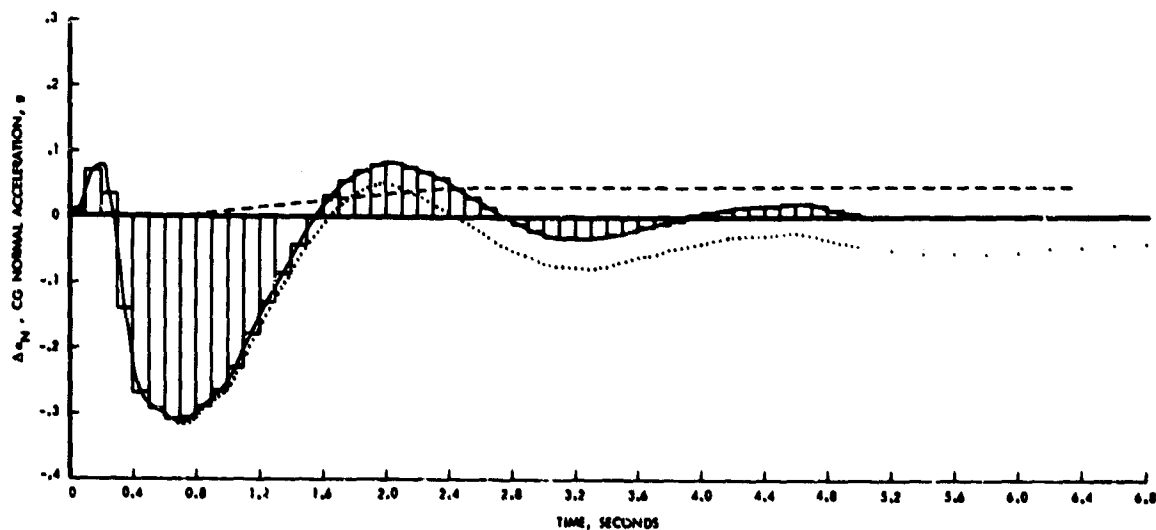
Figure 85   Incremental CG Normal Acceleration Time History,
Due to Negative Elevator Impulse

position) at each of the frequencies for which values of the Fourier transform were calculated. The phase angle of the frequency response is obtained by subtracting the elevator position phase angle from the cg normal acceleration phase angle at each of the frequencies for which values of the Fourier transform were calculated.

It is now possible to obtain the time history of cg normal acceleration due to a unit elevator impulse. This is done in a manner very similar to that above where the Fourier transforms were calculated. The real part of the frequency-response functions is calculated. Then these are approximated by steps in a manner similar to that used to approximate the time histories. The method and tables of References 10 and 11 are then used to compute the time responses. The calculated time responses of cg normal acceleration due to a unit elevator impulse are shown as solid curves in Figure 86.

It can be seen that the two time responses are in only fair agreement with each other. This discrepancy could be caused by the adjustments made initially to the time histories or to lack of resolution in the elevator position instrumentation. Also, if the time histories and the real parts of the frequency-response functions had been approximated by a larger number of narrower steps, unit-impulse response time histories might have been in somewhat better agreement.

For the purpose of removing the effect of elevator motion from the cg normal acceleration time histories, a single time response function is desired. Therefore, an average of the two time histories was computed for use in this analysis. This is shown as a dashed curve in Figure 86.

To obtain a better physical picture of how the airplane responds to an elevator input, the average unit-impulse response shown in Figure 86 was converted to the unit step, or "indicial", response shown in Figure 87.

To check the validity of the average unit-impulse response function, it was applied to five roller coaster maneuvers, each of different frequency varying from 0.05 to 0.625 cps. The roller coaster input and response data are presented in Figure 88. (For an explanation of the plot format see Section V, Effect of Elevator Motion on U_{de} Data.) The time history at the top of each figure is the derived equivalent gust velocity based on incremental cg normal acceleration correction for elevator input. Since all the roller coaster maneuvers were performed in smooth air, both of these quantities should be zero. Deviations reflect errors or inadequacies in the method. Comparison of the corrected incremental cg normal acceleration with the cg normal acceleration in the five roller coasters indicates that approximaterly 75 to 90 percent of the effect of elevator motion has been removed.
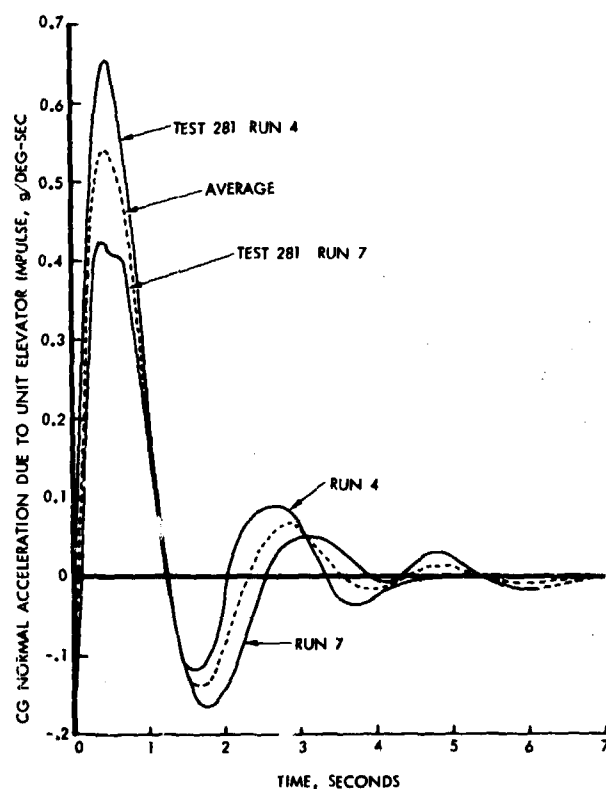
Figure 86   Time Response of CG Normal Acceleration Due to Elevator Impulse
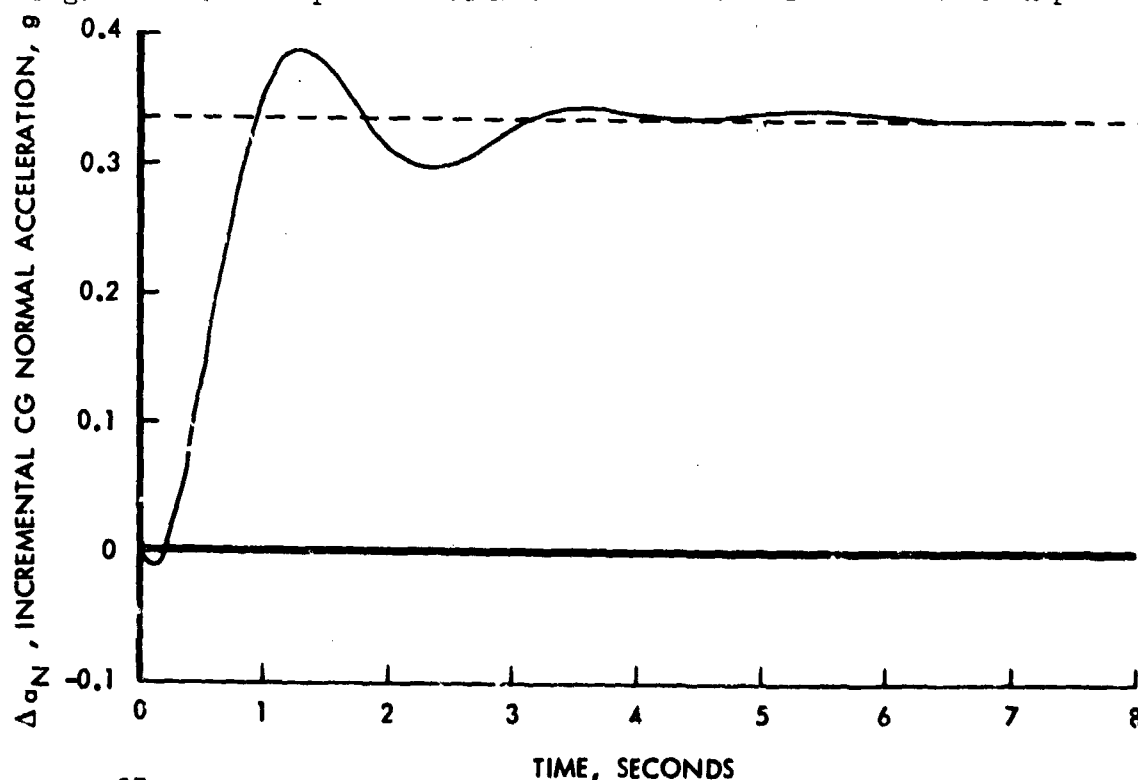
Figure 87   Incremental CG Normal Acceleration Time History Due to Unit Step
Based on Average Time Response Function
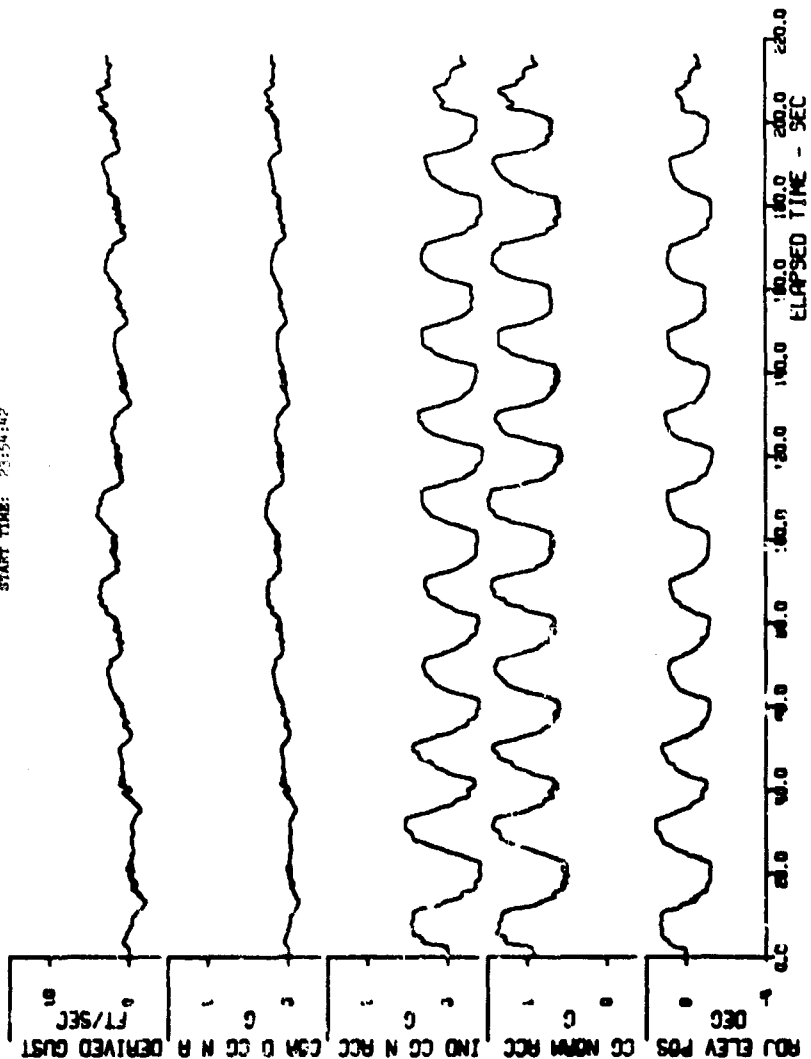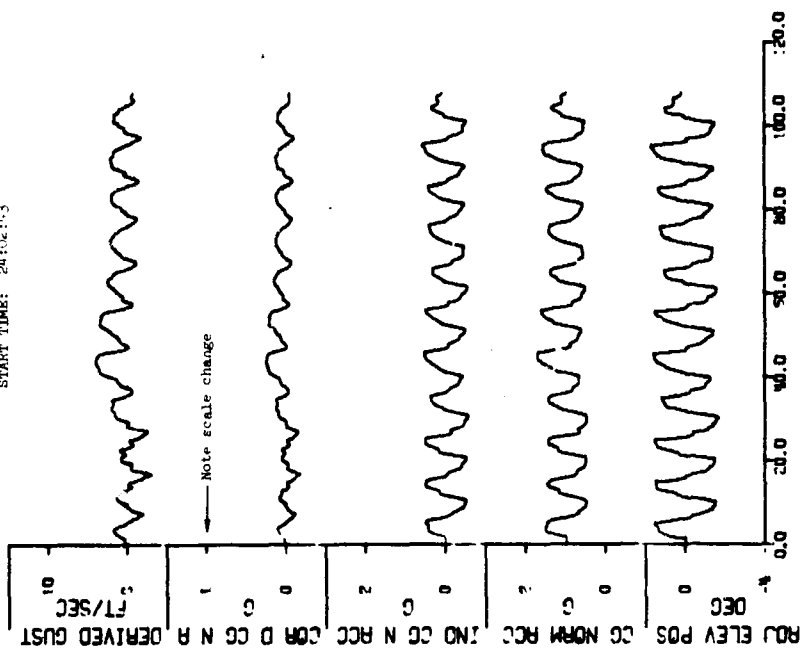
Figure 88 Roller Coaster Input and Response Data
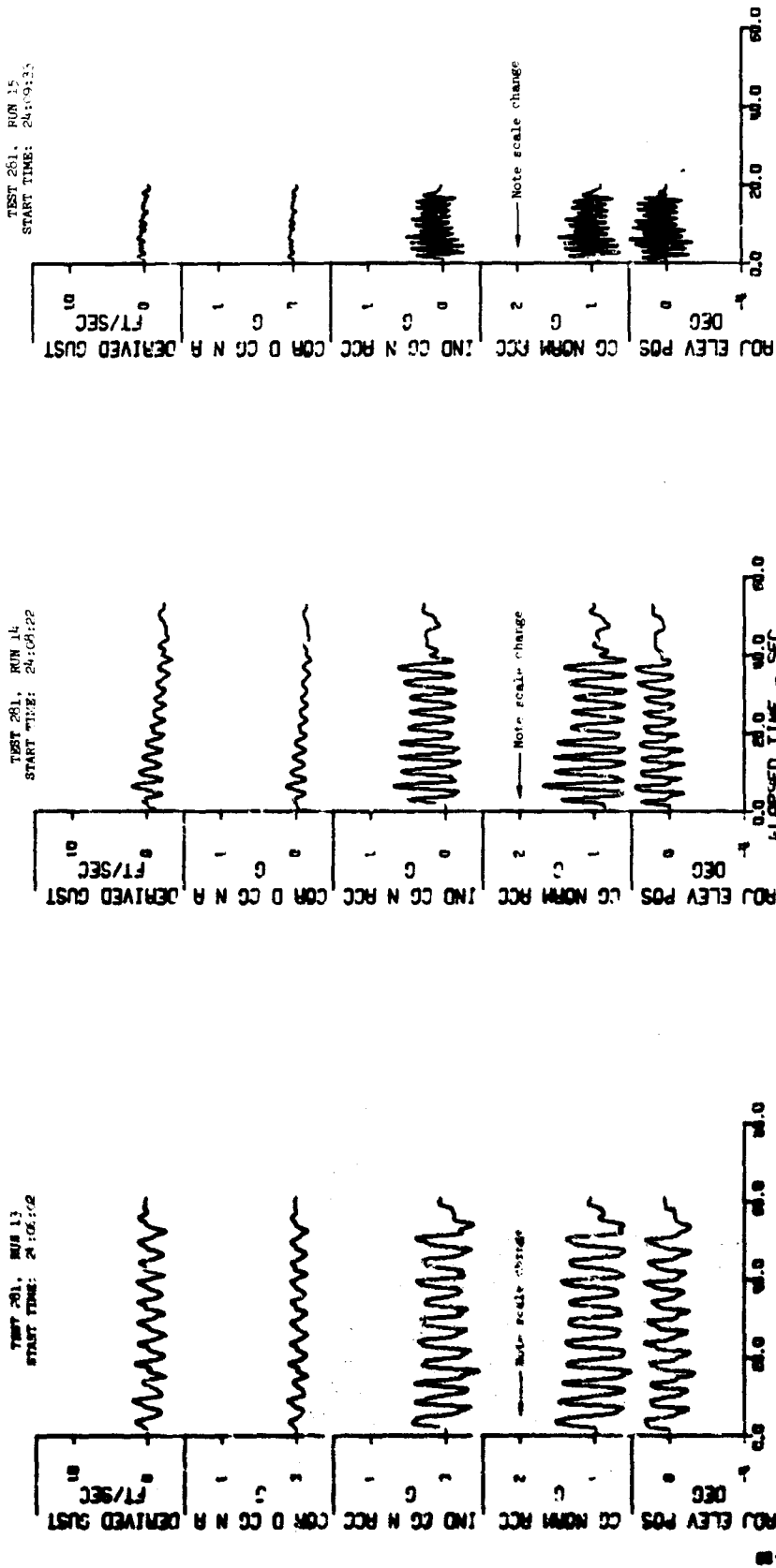
Figure 88 Roller Coaster Input and Response Data (Concluded)

C.   FREQUENCY RESPONSE FUNCTIONS AND DERIVED CG ACCELERATION SPECTRA

Frequency response functions and the cg acceleration spectra derived
therefrom, for five cases, are shown in Figure 89. Note that
for Test 266 Run 12 data are also shown for cg acceleration time histories
from which the effect of elevator motion has been removed. Cg acceleration
spectra are shown based on two shapes of gust spectra - Von Karman,
$L = 2500$ ft, and Dryden, $L = 1000$ ft. These curves are discussed in more
detail in Section V.
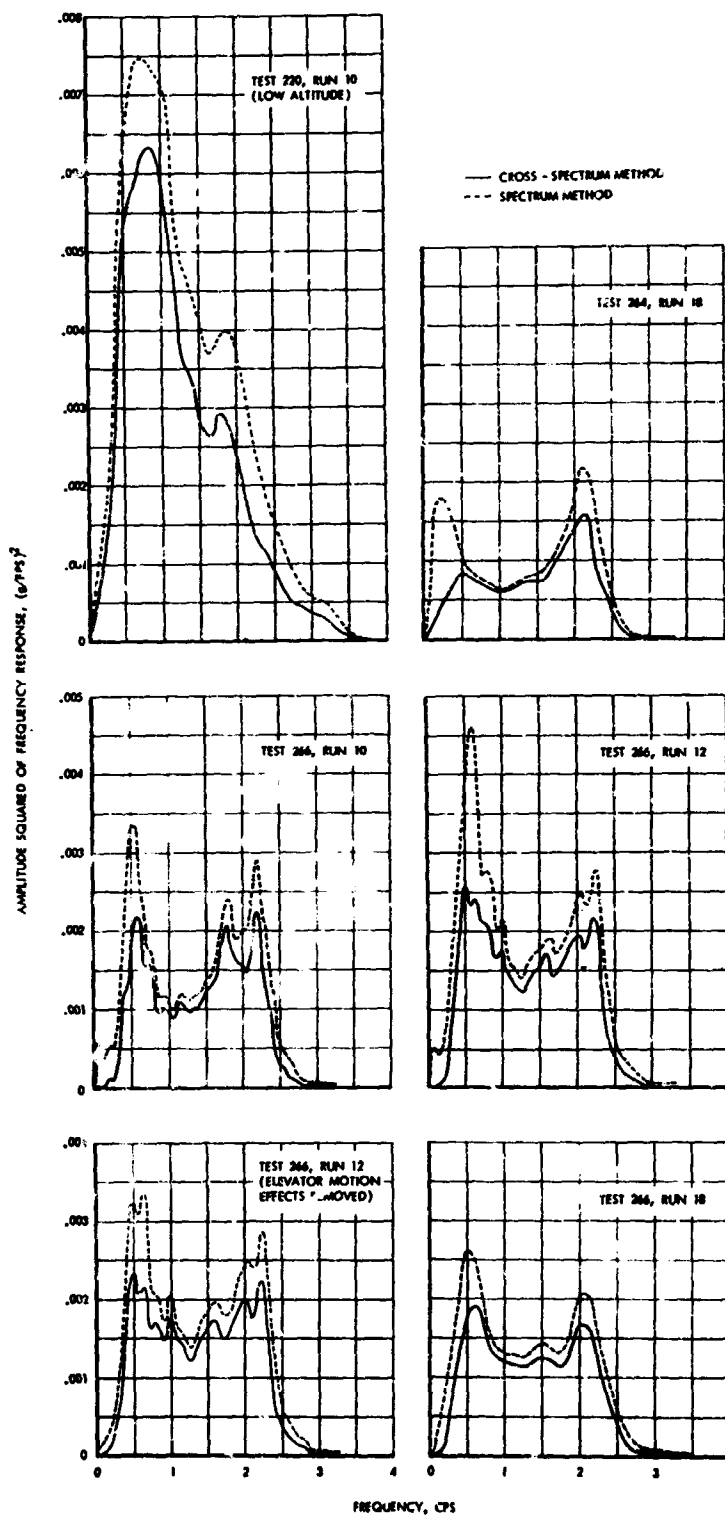
Figure 89 Frequency Response Functions and Derived CG Acceleration Power
Spectral Densities
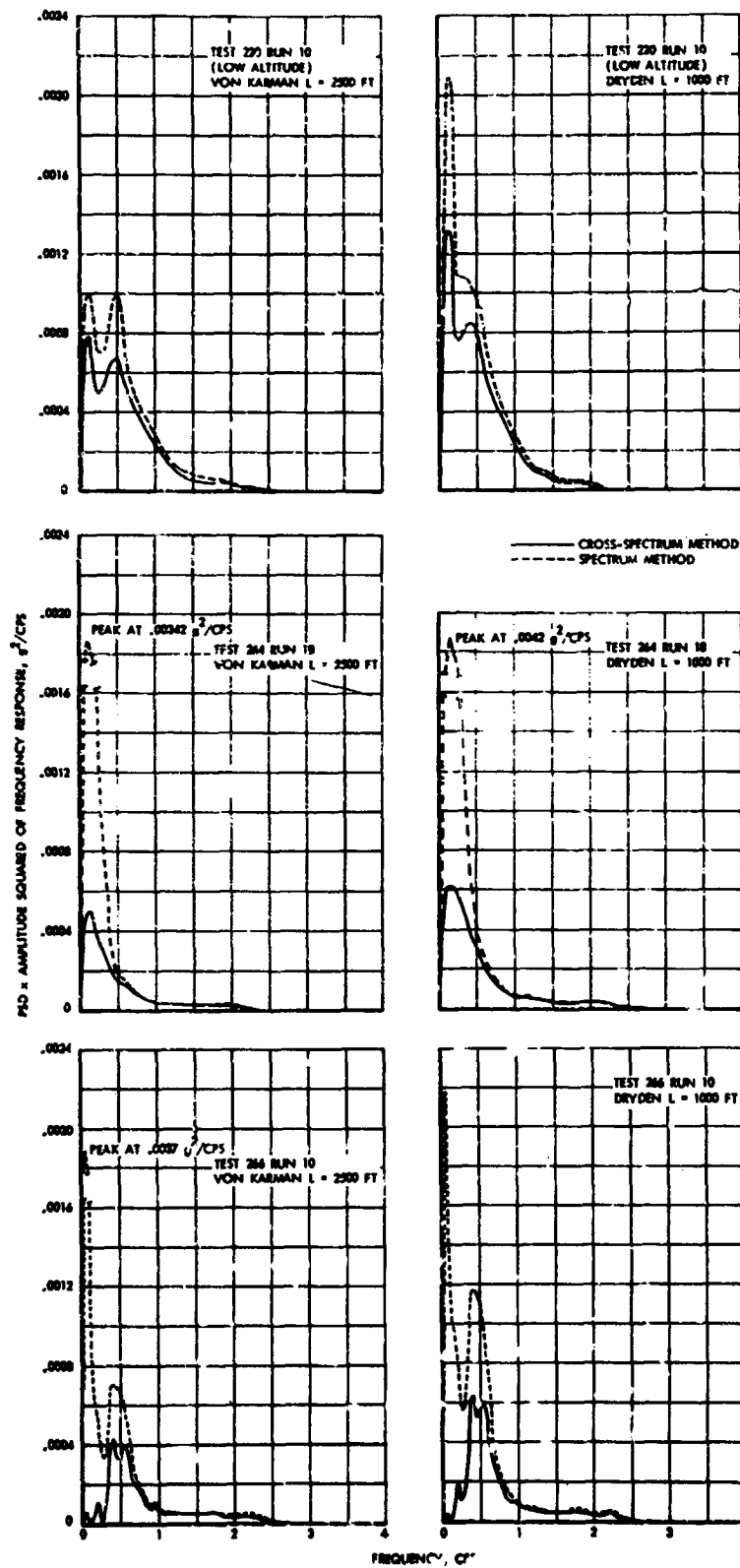
Figure 89   Frequency Response Functions and Derived CG Acceleration Power
Spectral Densities (Continued)
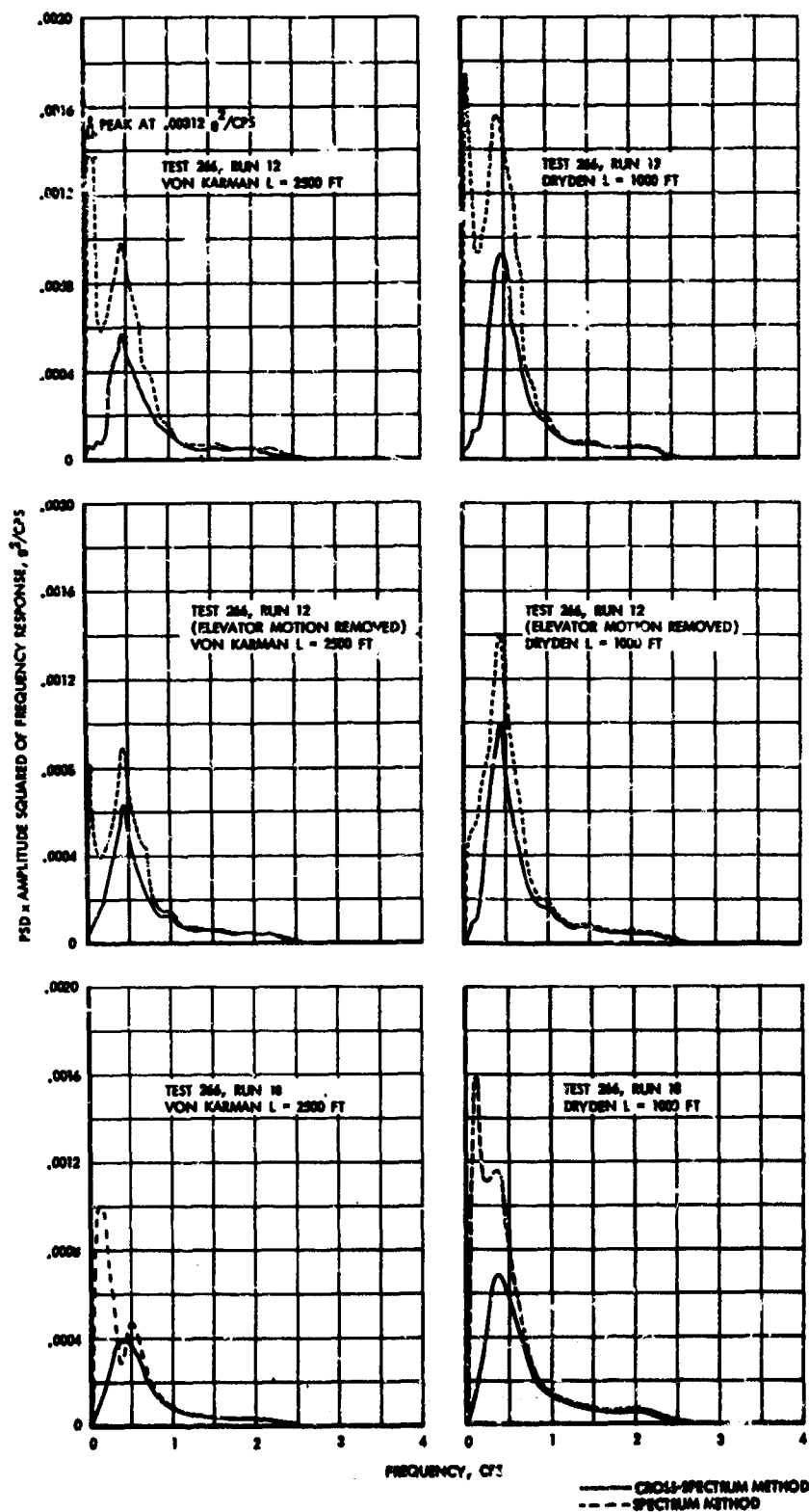
Figure 89 Frequency Response Functions and Derived CG Acceleration Power
Spectral Densities (Concluded)

D. SELECTION OF FILTER CHARACTERISTICS FOR HIGH-PASS FILTERING OF ABSOLUTE
    GUST VELOCITY

Selection Criteria

In selecting the characteristics of the high-pass filter to be used
preparatory to peak counting the HICAT absolute gust velocities, the follow-
ing criteria are pertinent:

   (1) The cutoff should be as sharp as practicable.

   (2) The number of filter weights should be a minimum to avoid excessive
       computer time and to minimize the additional record needed at the
       beginning and end of each run.

   (3) The filter should remove only those frequency components which may
       contain significant amounts of noise.

   (4) The filter characteristics should, on the other hand, be equivalent
       to those used in other major turbulence investigation programs, as
       far as practical, to permit direct comparison of the peak counts
       of the filtered time histories.

Characteristics of the Martin-Graham Filter

The Martin-Graham form of digital filter, used for extensive low-pass filter-
ing of the HICAT basic measurements as described in Appendix II, was also
selected for high-pass filtering the absolute gust velocities. This filter
is characterized by the theoretical gain function shown in the following
sketch:

f_c = CUTOFF FREQUENCY

f_t = TERMINATION FREQUENCY

Δf_r = ROLLOFF FREQUENCY BAND
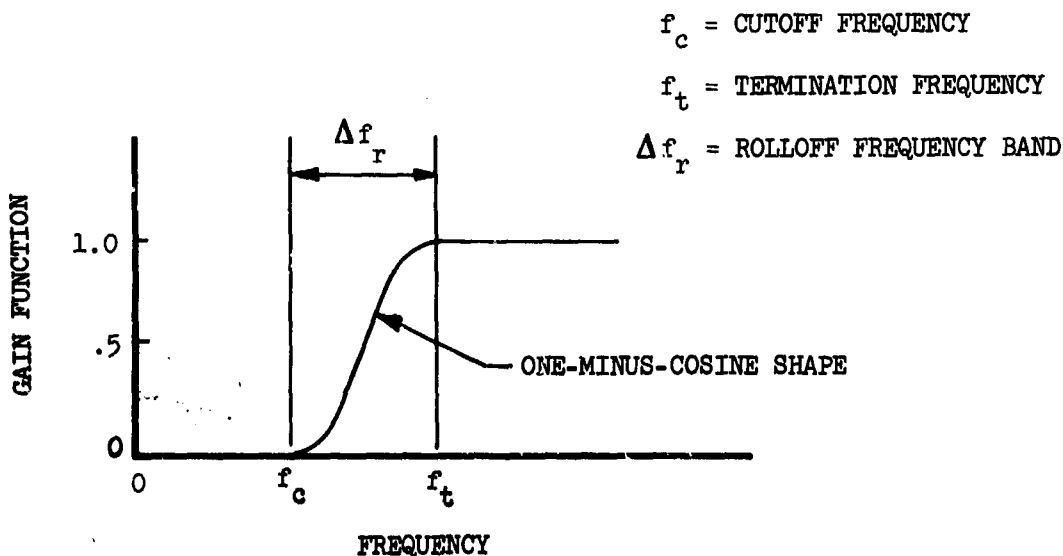
The accuracy with which the actual gain function matches the theoretical depends upon the number of filter weights, N_w. To limit the error to nominally 1%, the number of filter weights must be at least

$$\overline{N}_w = \frac{4f_s}{\Delta f_r} + 1$$

where f_s is the sample rate. For the HICAT time histories, $f_s = 12.5$ cps, so that

$$\overline{N}_w = \frac{50}{\Delta f_r} + 1$$

The required additional length of run at each end is given by

$$\frac{1}{2}(N_w - 1)\frac{1}{f_s}$$

or, for the HICAT data,

$$0.04(N_w - 1)$$

It is seen that the sharper the filter, as defined by a small value of Δf_r, the greater the required number of filter weights. Thus, to satisfy criterion (1), above, tends to require many filter weights; whereas, criterion (2) calls for the smallest possible number.

Family of Filters

In order to obtain the best compromise between the preceding criteria (1) and (2), the filter gain function has been computed for the family of filters listed in Table VIII. This family of filters covers a range of the two pertinent dimensionless parameters, f_c/f_t and $N_w/\overline{N}_w$. Examination of the resulting gain functions provides a basis for selecting values of the dimensionless parameters; consideration is then given later to choice of specific values of f_t and f_c.

TABLE VIII HIGH-PASS FILTERS INVESTIGATED

Case	f_c	f_t	f_c/f_t	N_w	$\overline{N}_w$	$N_w/\overline{N}_w$
a	0.0217	0.100	0.217	639	639	1.00
b	0.0217	0.100	0.217	383	639	0.60
c	0.0217	0.100	0.217	319	639	0.50
d	0.0217	0.100	0.217	255	639	0.40
e	0.030	0.100	0.300	715	715	1.00
f	0.030	0.100	0.300	429	715	0.60
g	0.030	0.100	0.300	357	715	0.50
h	0.030	0.100	0.300	287	715	0.40
i	0.040	0.100	0.400	833	833	1.00
j	0.040	0.100	0.400	501	833	0.60
k	0.040	0.100	0.400	417	833	0.50
l	0.040	0.100	0.400	333	833	0.40
m	0.050	0.100	0.500	1001	1001	1.00
n	0.050	0.100	0.500	601	1001	0.60
o	0.050	0.100	0.500	501	1001	0.50
p	0.050	0.100	0.500	401	1001	0.40
q	0.060	0.100	0.600	1251	1251	1.00
r	0.060	0.100	0.600	751	1251	0.60
s	0.060	0.100	0.600	627	1251	0.50
t	0.060	0.100	0.600	501	1251	0.40

The resulting gain functions are shown in Figure 90[31]. One of the significant differences among the various cases is in the size of the ripples in the vicinity of f_c and f_t; values of this ripple error are summarized in Figure 91[32]. The errors indicated in this figure are the maximum departure (plus or minus) of the gain function from unit above f_t, and from zero below f_c, respectively.

Examination of either the gain functions themselves or the ripple errors plotted in Figure 91 suggests that N_w can be taken considerably less than $\overline{N}_w$ without excessive error. They also indicate that the maximum errors in the vicinity of f_c and f_t are not equal and that their relation is very sensitive to small variations in both $N_w/\overline{N}_w$ and f_c/f_t.

LO-LOCAT Filter

The one major turbulence-measurement program to date in which a given high-pass filter has been used preparatory to peak counting is the LO-LOCAT program.

---

[31]The frequency scale of the figures is shown in dimensional form, but can easily be read on the dimensionless basis, f/f_t, simply by dividing the numbers shown by 10.

[32]Values for $f_c/f_t = 0$ were obtained from gain functions for filters not included in the family of Table VIII.
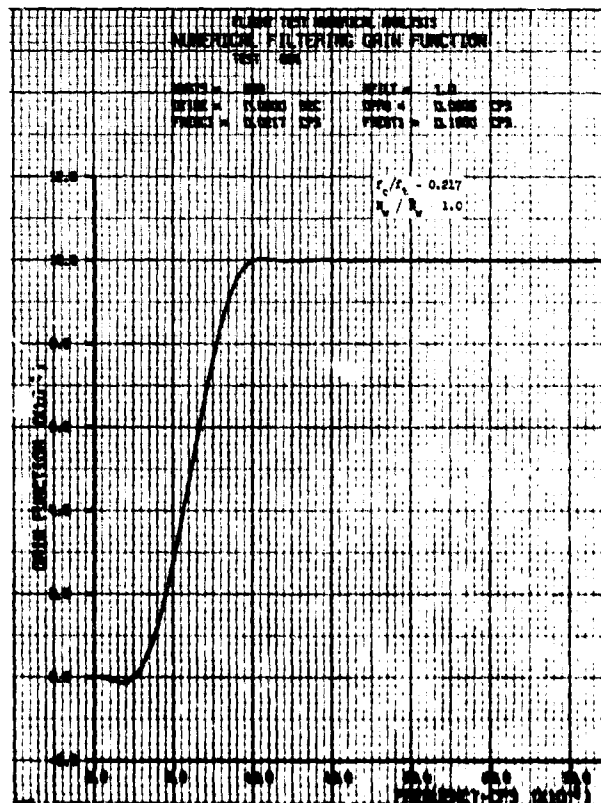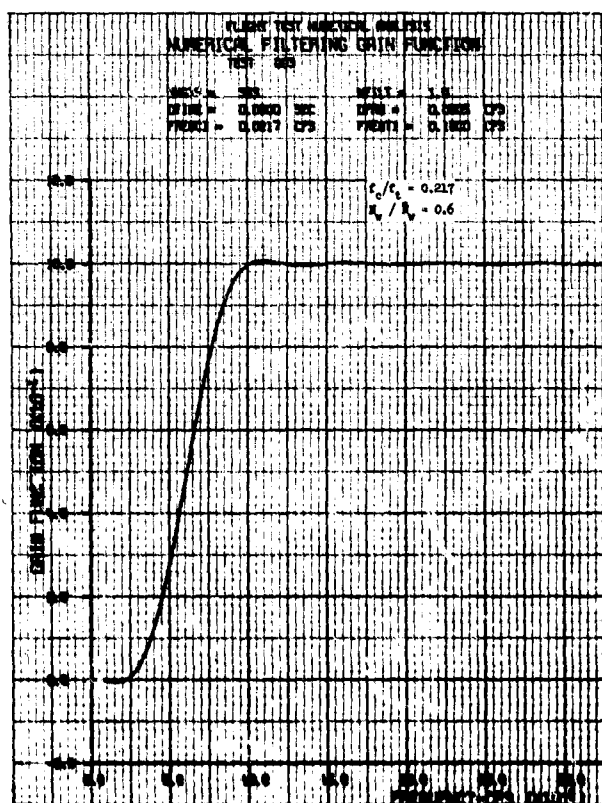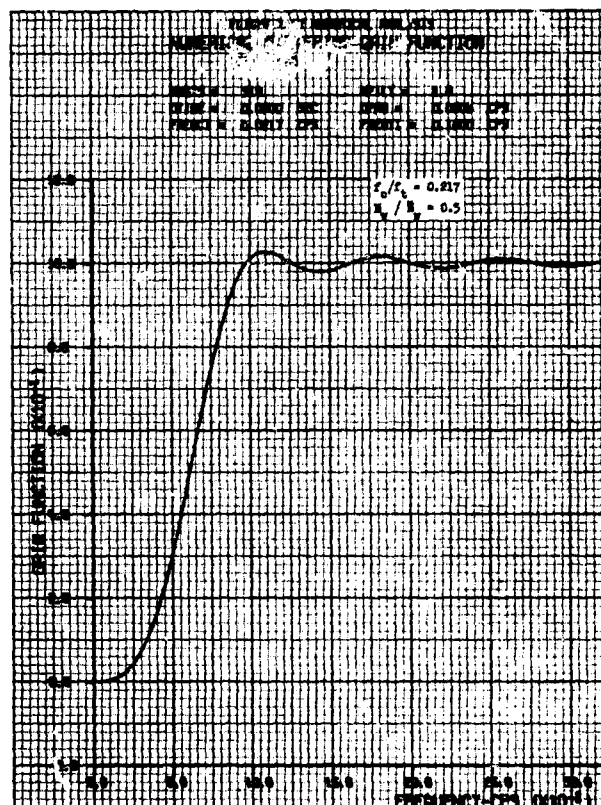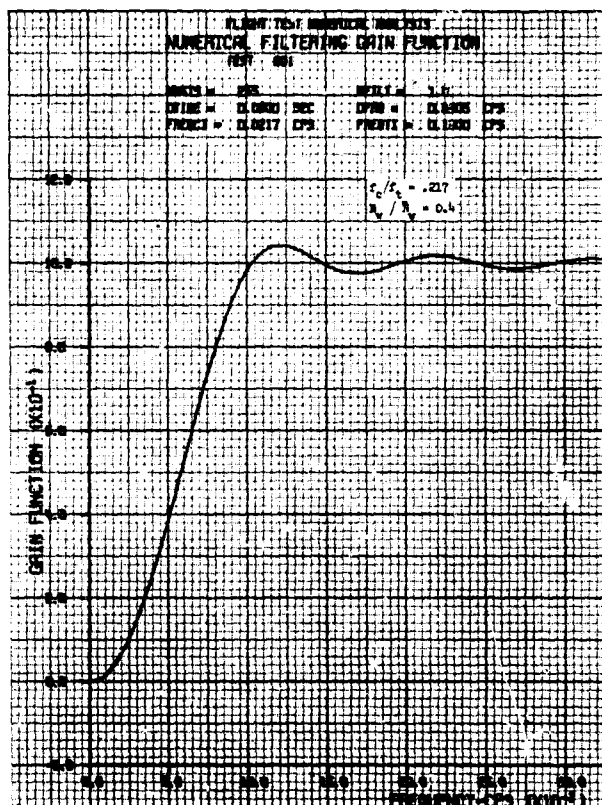
Figure 90   Numerical Filtering Gain Functions
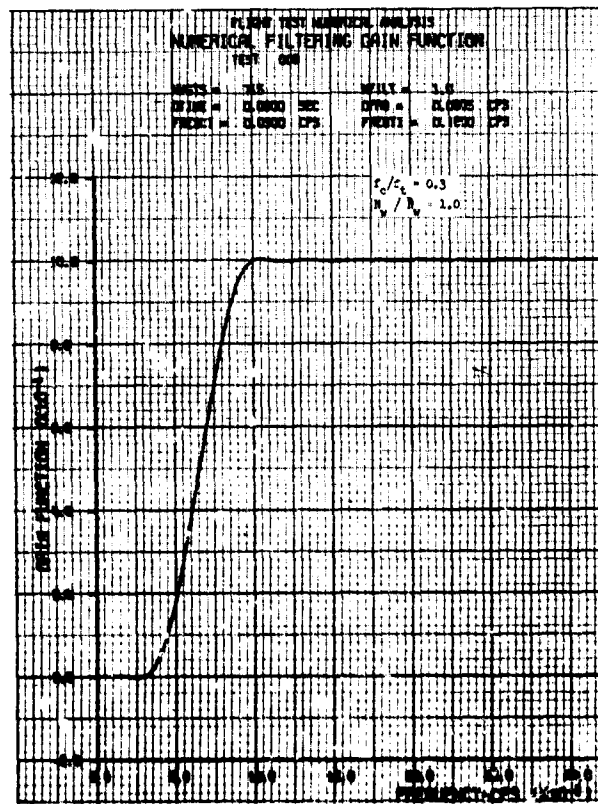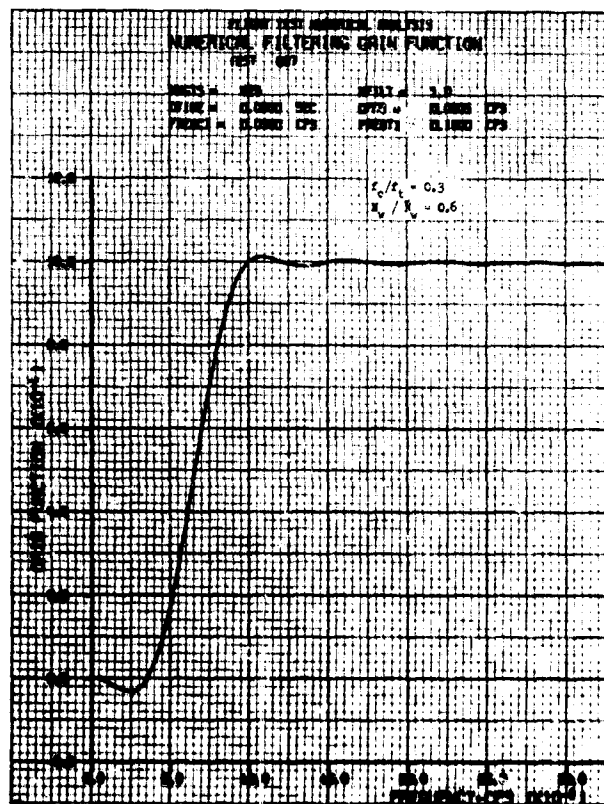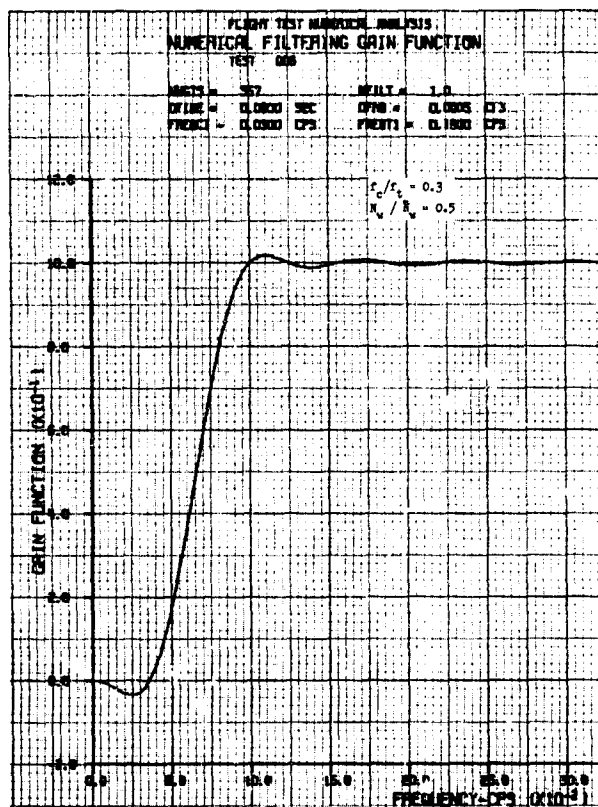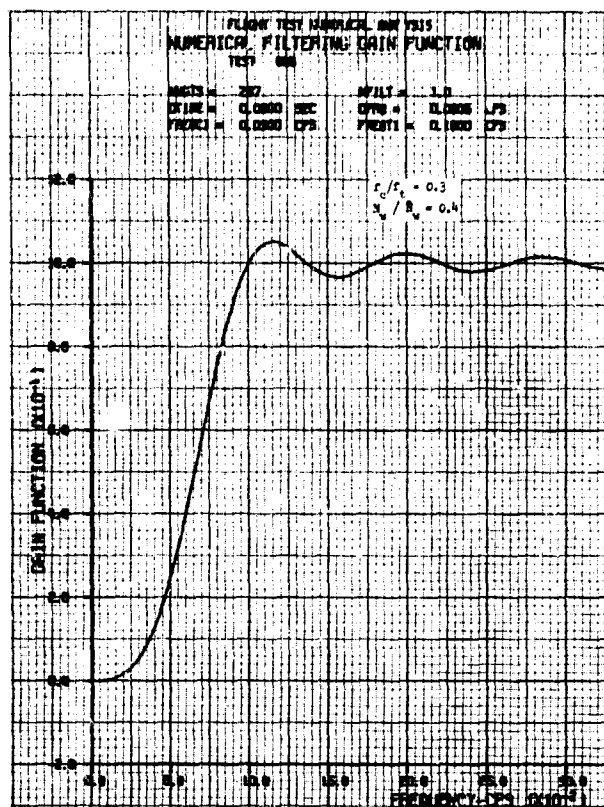
Figure 90 Numerical Filtering Gain Functions (Continued)
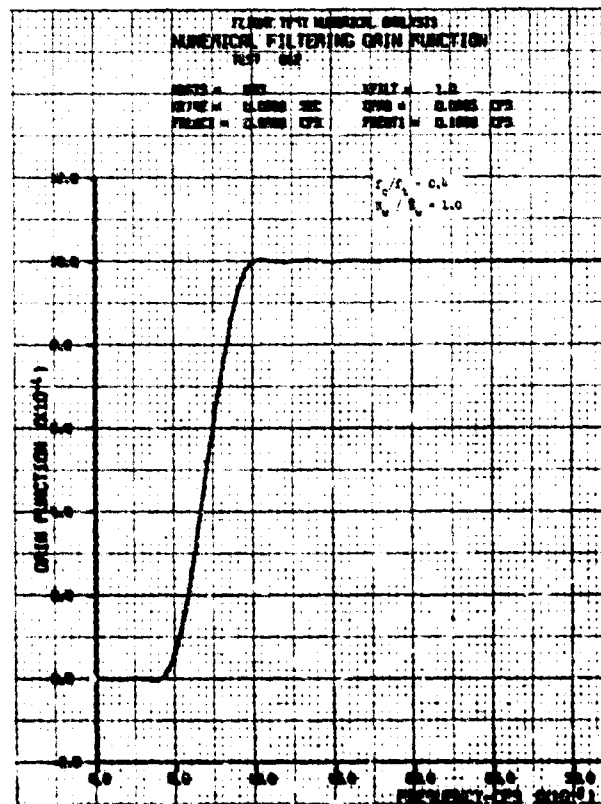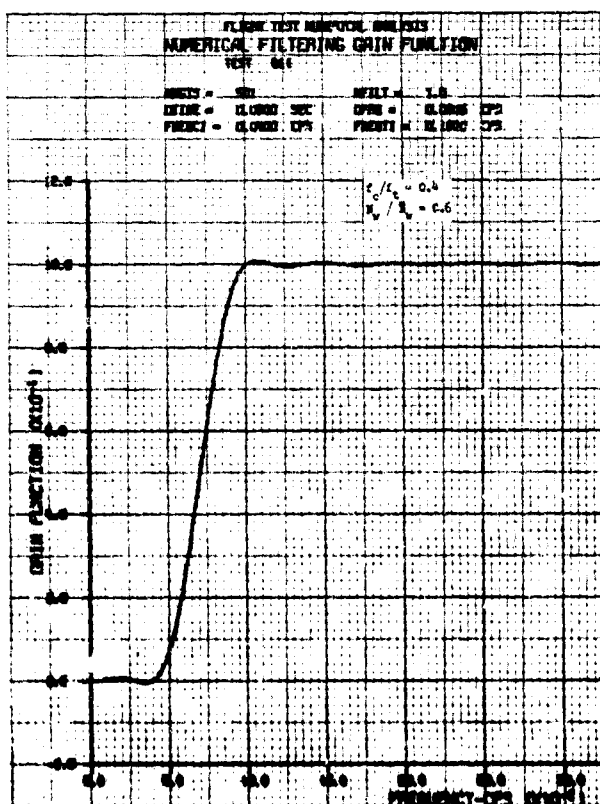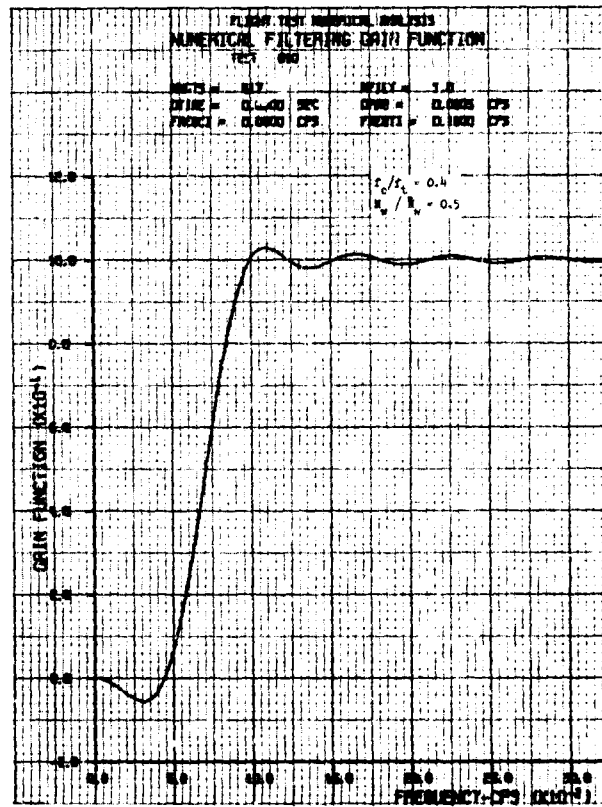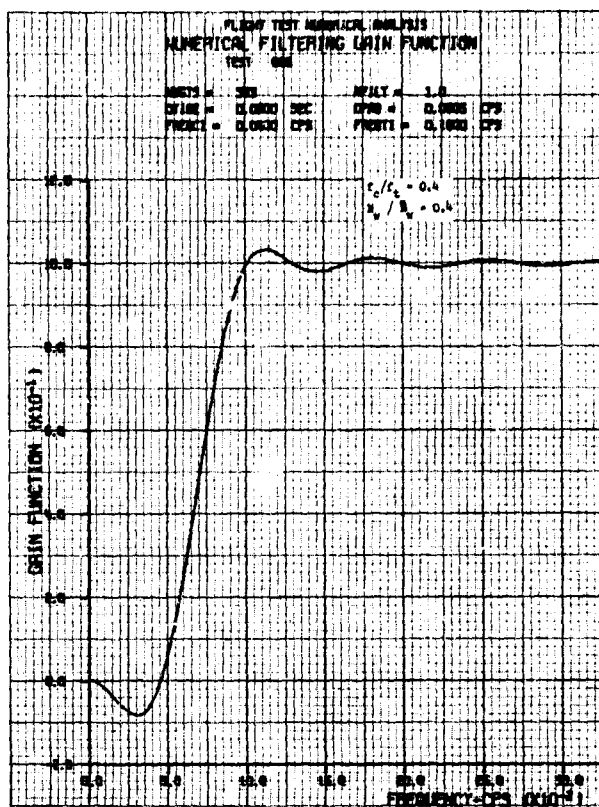
Figure 90   Numerical Filtering Gain Functions (Continued)
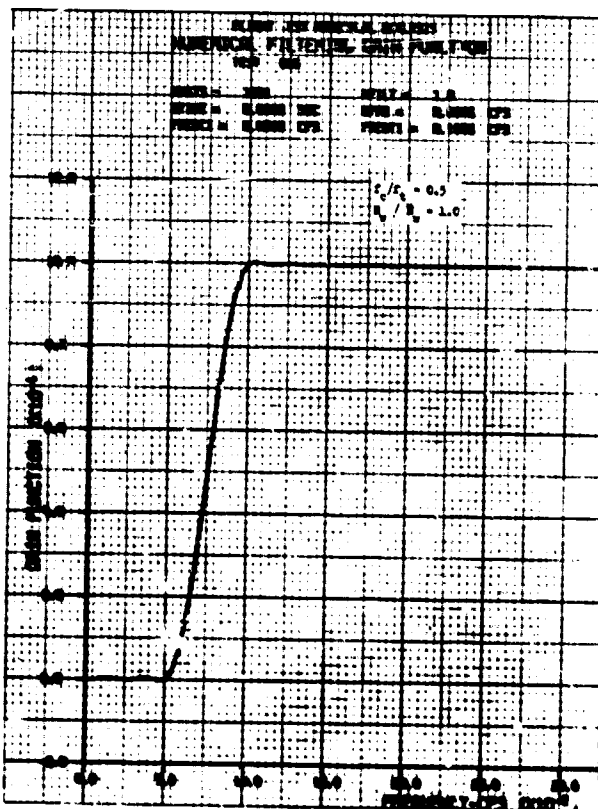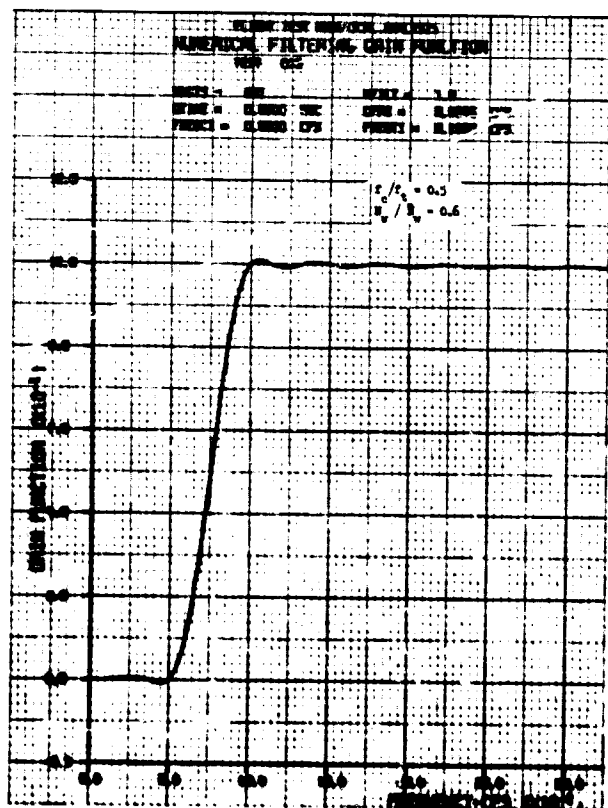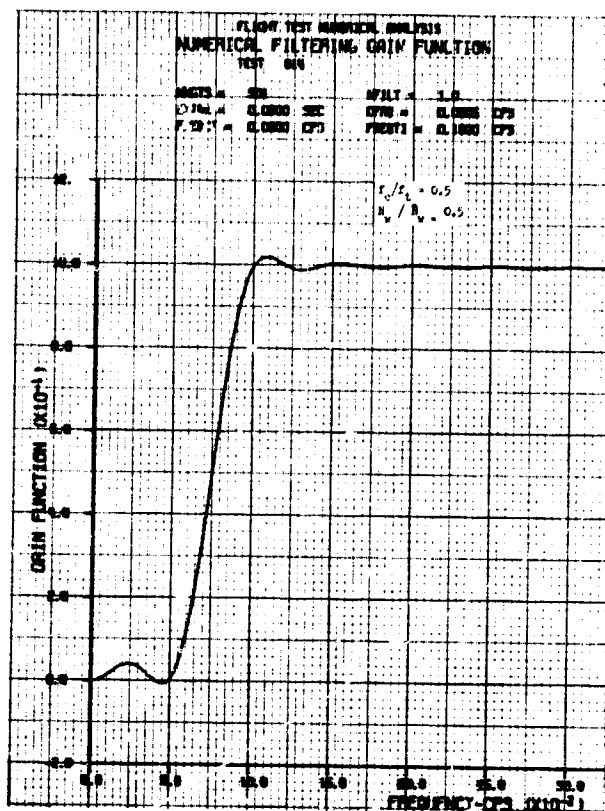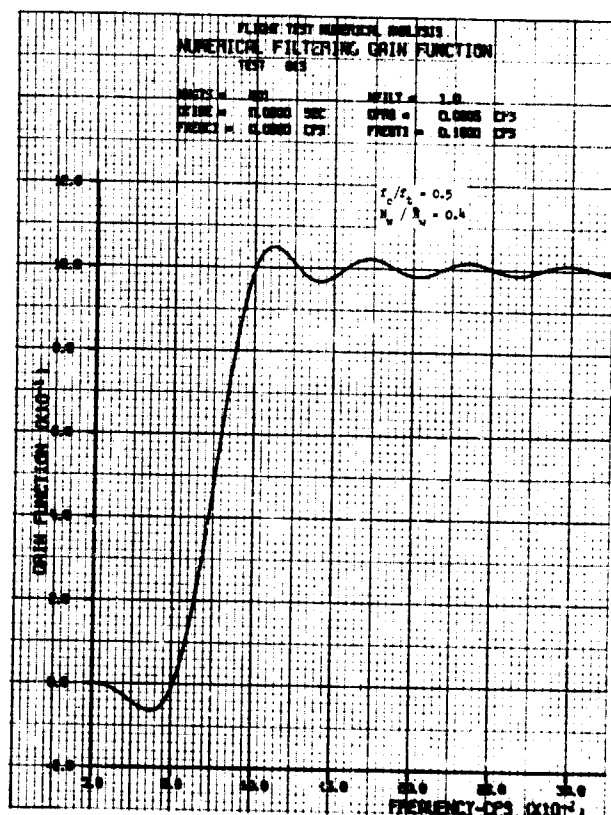
Figure 90 Numerical Filtering Gain Functions (Continued)
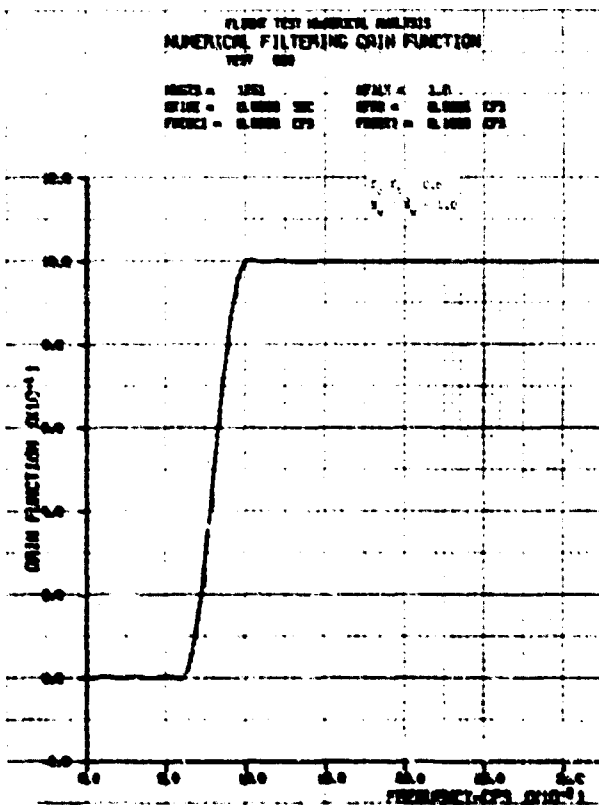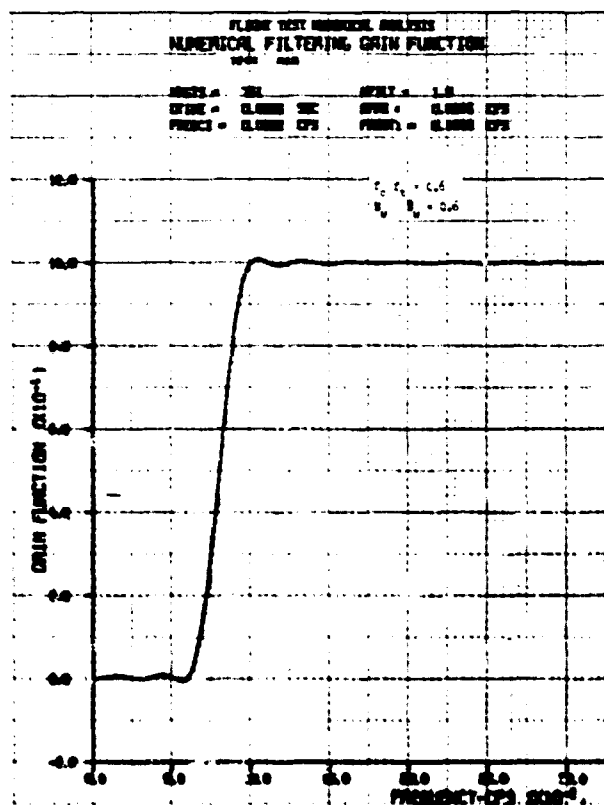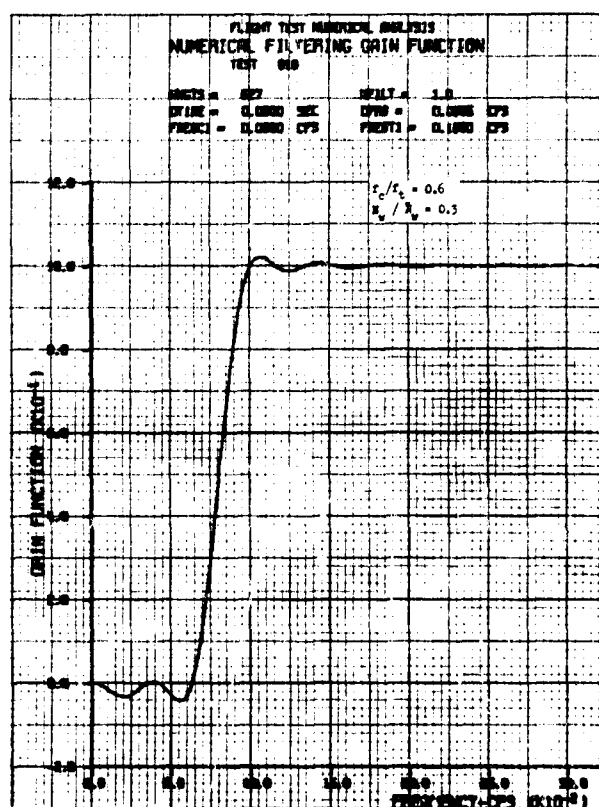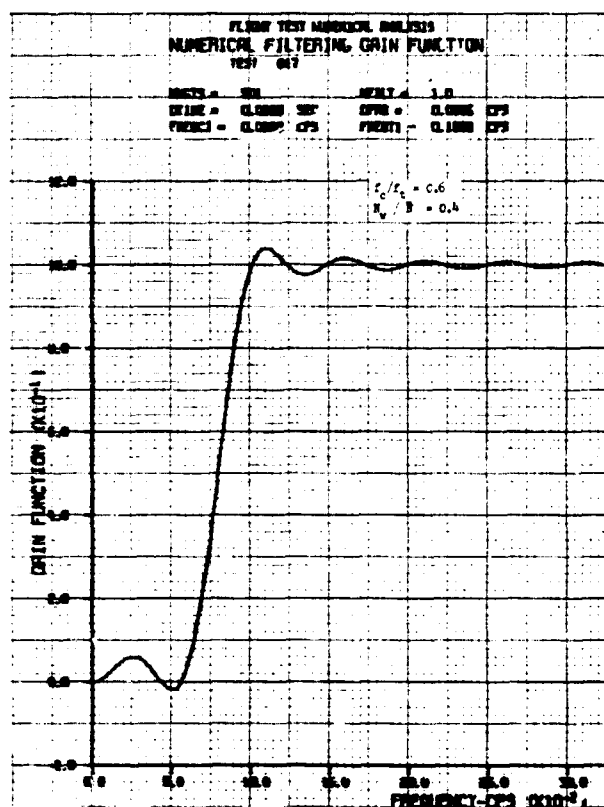
Figure 90   Numerical Filtering Gain Functions (Concluded)
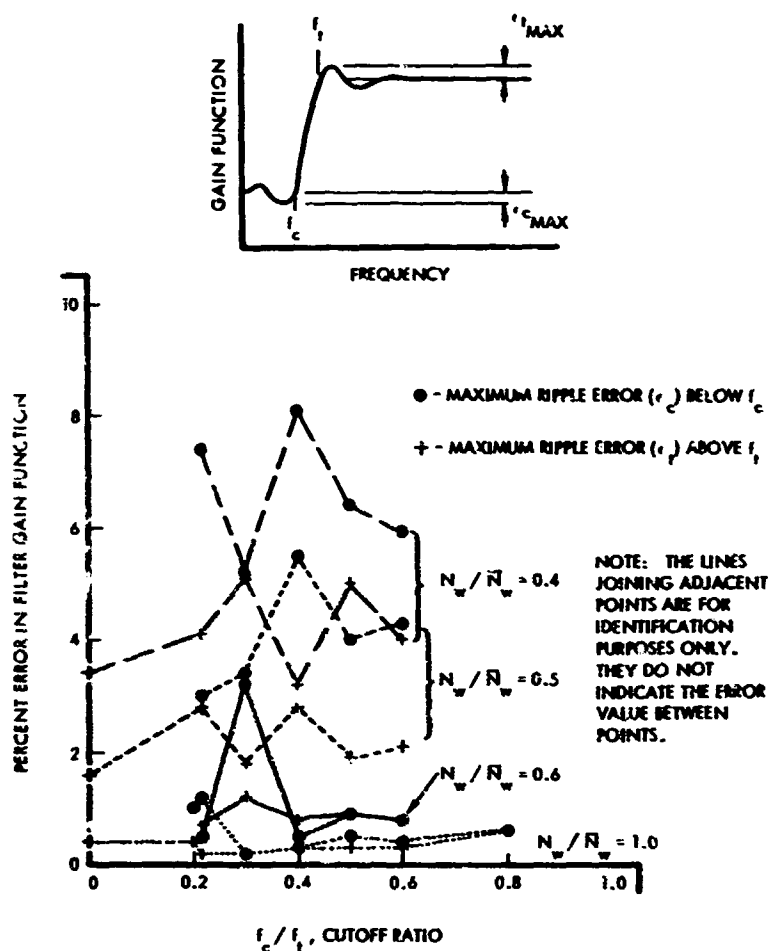
Figure 91 Effect of Cutoff Ratio (f_c/f_t) and Filter Weight Ratio $(N_w/\bar{N}_w)$ on Numerical Filter Ripple Errors

The LO-LOCAT filter is characterized by values of f_c and f_t, respectively, of 0.010 and 0.046. The resulting value of f_c/f_t is 0.217. The number of filter weights used is 141 and the sampling frequency is 2.0 cps; the resulting value of $N_w/\bar{N}_w$ is 0.63.

It can be seen from Figures 90 and 91 that the LO-LOCAT filter provides a particularly good fit to the theoretical filter gain function, at a minimum cost in number of filter weights. For example, Figure 91 indicates that, for a value of $N_w/\bar{N}_w$ of 0.60, the actual errors are much less at $f_c/f_t = 0.217$ than at 0.300. At $f_c/f_t = 0.217$, the improvement in going from $N_w/\bar{N}_w = 0.50$ to 0.60 is considerable; whereas, further increasing $N_w/\bar{N}_w$ to 1.00 produces no additional improvement.

Selection of f_c/f_t and $N_v/\bar{N}_w$ Values

For the HICAT program a much sharper cutoff than provided by the LO-LOCAT filter appeared to be desirable at this point. Moreover a considerably greater ripple error could be tolerated. In particular, it appeared that f_c/f_t might be increased to 0.500 and $N_w/\bar{N}_w$ reduced to perhaps 0.40.

Before adopting particular filter values, however, it was considered desirable to examine the filter characteristics on the basis of their effects on the power spectral density (psd) of the filtered time history. The psd is a useful tool in the selection of the filter characteristics because of the information it can provide about the effect of the filter on the frequency of exceedance curves that will be obtained from the filtered time histories.

As indicated in the section, High-Pass Filtering of Absolute Gust Velocity Time Histories, the frequency of exceedance depends primarily upon the rms (root-mean-square) value of the time history, σ, and secondarily upon its characteristic frequency, N_0. Both of these quantities follow directly from the power spectrum, σ as the square root of the area under the curve and N_0 as the radius of gyration of this area about zero frequency.

For the purpose of studying the effect of various filters on the power spectral density of the filtered time history, the input, or unfiltered time history, was considered to have a power spectral density varying as the -5/3 power of the frequency.

The four solid-line output curves show the effect of the theoretical filter for values of f_c/f_t of 0.217, 0.300, 0.400, and 0.500, respectively. The significant fact brought out by all of these curves is that the effective f_c, for all practical purposes, is appreciably higher than the nominal, or actual, f_c. Considering, for example, the first curve, for which $f_c/f_t = 0.217$, it is seen that frequencies up to $f/f_t = 0.400$, or even higher, contribute negligibly to the area under the curve. For example, the area under the curve up to a frequency of even $f/f_t = 0.500$ is only about 2% of the total. The even smaller percentage effect of this increment in area on the rms value, σ, is evident from the relation

$$\frac{\sigma_2}{\sigma_1} = \sqrt{\frac{A + \Delta A}{A}} \cong 1 + \frac{1}{2}\frac{\Delta A}{A}$$

which gives the effect on the rms value of a small increment, ΔA, in the area under the power spectral density curve. The reason for the very small values of the output at frequencies substantially above f_c is that, in determining the output power spectral density, the input is multiplied by the square of the filter gain function rather than the first power. This effect overshadows the influence of the increasing input at the lower frequencies. Thus it is seen that the need for a sharper filter than defined by $f_c/f_t = 0.217$ (the LO-LOCAT filter) is much less pressing than would be inferred from the gain function plots of Figure 90.
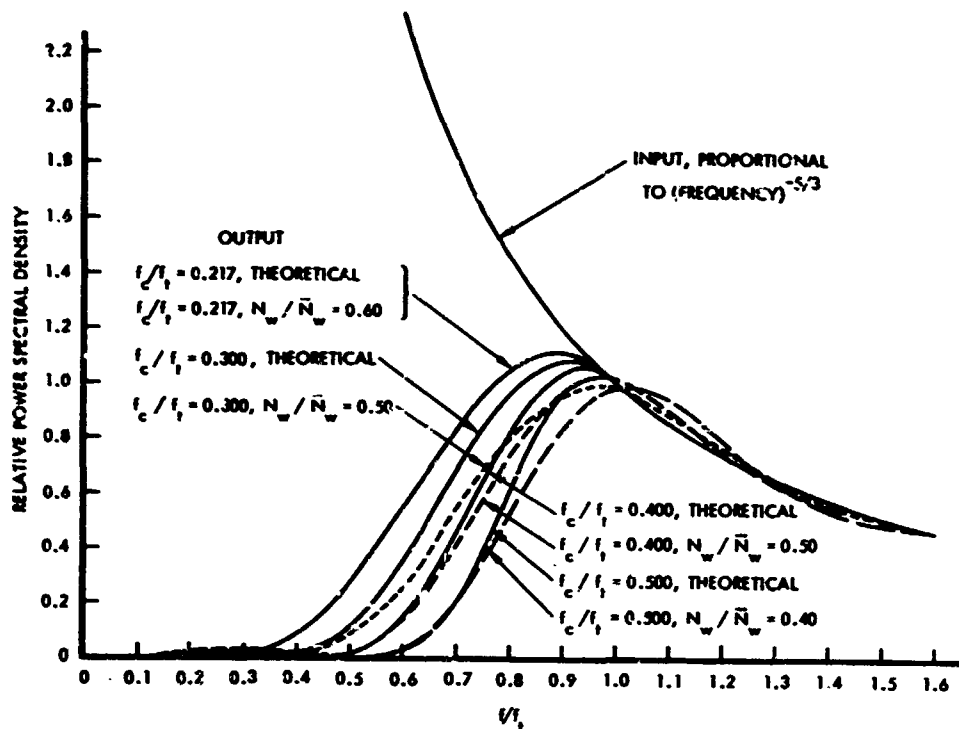
Figure 92 Effect of Various High-Pass Filters on Output Power
Spectral Density

The various dash lines in Figure 92 indicate the effect of a finite number of filter weights. The long-dash line shows the effect of $N_w/\bar{N}_w = 0.40$ with $f_c/f_t = 0.500$. The significant fact emphasized by this curve is the much larger effect, on area under the curve, of the gain function ripple at f_t than the ripple at f_c, even though the gain function ripple is somewhat larger at f_c than f_t (Figure 91). Because the output is equal to the input multiplied by the square of the filter gain function, the 5% ripple in the gain function just above f_t leads to a 10% error in the power spectral density. At f_c, however, the square of the 6.7% error is extremely small (0.45%) so that despite the much larger input at the lower frequency, the resulting ripple in the output is negligible. On the basis of this curve, the ripple associated with $N_w/\bar{N}_w = 0.40$ at $f_c/f_t = 0.500$ appears excessive. On the other hand, the errors associated with $N_w/\bar{N}_w = 0.50$ for either $f_c/f_t = 0.400$ or $f_c/f_t = 0.300$ in Figure 92 would be considered acceptable. For these cases, the maximum error in the power spectrum at any frequency above f_t is 6% for $f_c/f_t = 0.400$ and 4% for $f_c/f_t = 0.300$; the effects on the rms value and on the characteristic frequency are very small.

On the basis of the foregoing discussion, it appears desirable to retain, for at least one HICAT filter, the f_c/f_t and N_w/N_e values of the LO-LOCAT filter. The effective f_c for this filter is close to 0.500, a value considered acceptable, and the agreement of theoretical with actual filter gain functions is excellent.

Selection of f_t Values

To select logically a particular value of f_t, it is necessary to express the filter characteristics in terms of spatial frequency (cycles per foot) instead of a time-based frequency (cycles per second). To make this conversion, the true airspeed must be known. In order to relate the HICAT filter to the LO-LOCAT filter, airspeeds for both programs are necessary. A sampling of LO-LOCAT airspeeds is shown in Figure 93 and of HICAT airspeeds in Figure 94. The LO-LOCAT cases are those for which the necessary data were available in the monthly progress reports. The HICAT cases include all runs listed in Appendix I of Reference 5 for which the necessary data were provided.

From Figure 93, the average LO-LOCAT speed appears to be about 328 fps. However, the addition of more Griffiss Air Force Base points (only three were available) would be expected to lower the average. Also, the LO-LOCAT filter has been described as having a 7000 foot cutoff wavelength; this in conjunction with the f_t value of 0.046 cps infers a speed of 322 fps. Therefore, 322 fps is taken as the characteristic speed of the LO-LOCAT runs. Figure 93 shows the vast majority of the runs to lie within ±10% of this speed.

The effect of an error in selecting an average speed will result in an equal percentage error in cutoff frequency. For a power spectral density function that varies as the -5/3 power of frequency, it can be shown that the rms value of the time history varies inversely as the 1/3 power of the cutoff frequency. Thus even an error as great as 10% in the assumed or average speed would have but a 3% effect on the rms value of the filtered time history.

Based on the selected speed of 322 fps, the characteristic wavelengths of the LO-LOCAT filter are:

$$\lambda_t = \frac{V}{f_t} = \frac{322 \text{ fps}}{0.046 \text{ cps}} = 7000 \text{ ft}$$

$$\lambda_c = \frac{V}{f_c} = \frac{322 \text{ fps}}{0.010 \text{ cps}} = 32,200 \text{ ft}$$
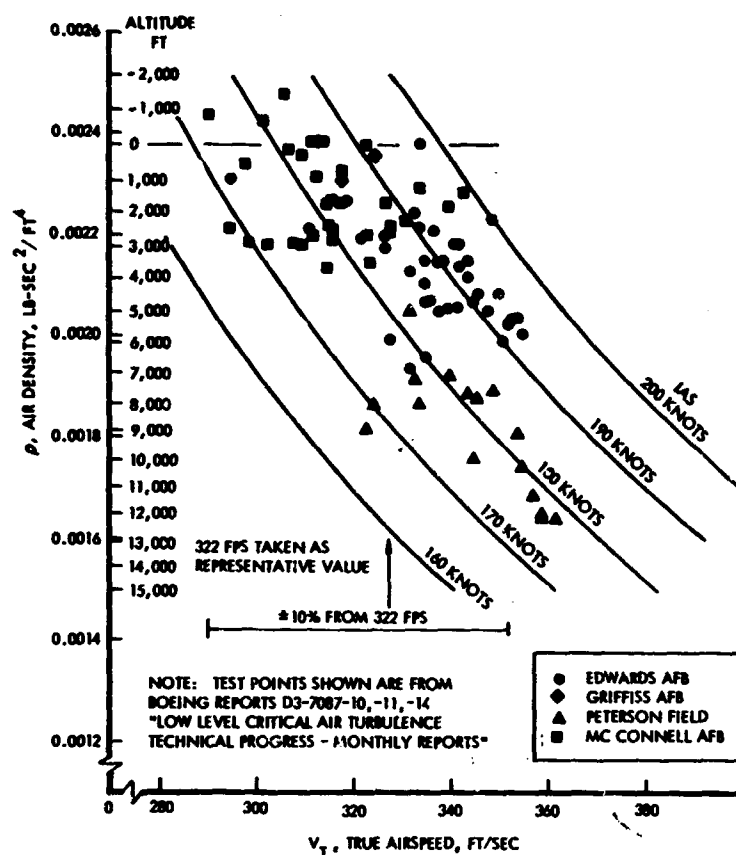
Figure 93 True Airspeed versus Air Density for LO-LOCAT Test Data
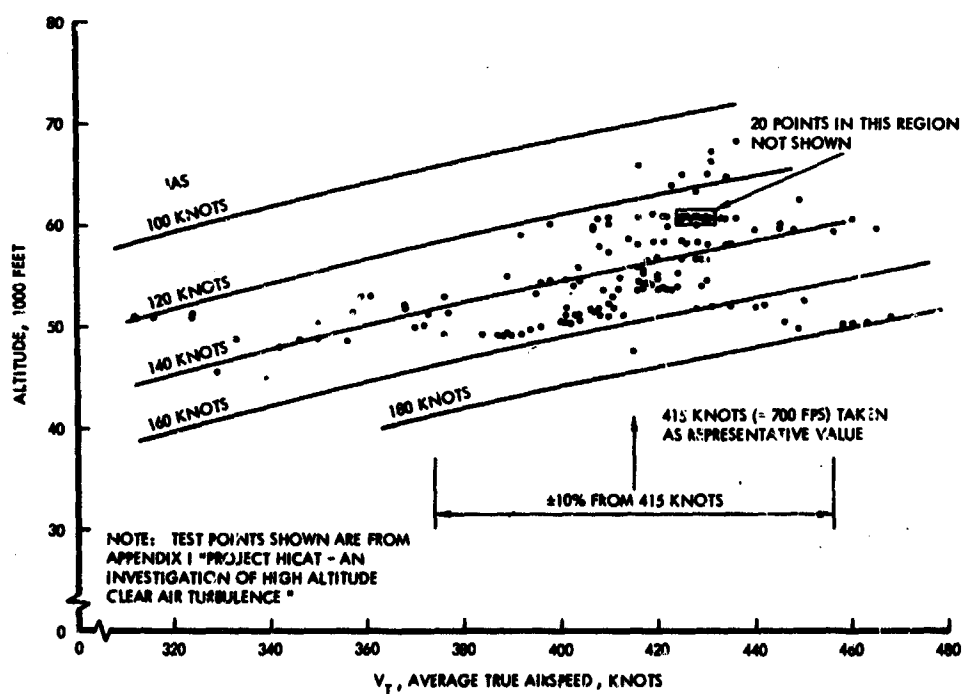
Figure 94 Average True Airspeed versus Altitude for HICAT Test Data

where

V = velocity

λ_t = wavelength corresponding to termination frequency

λ_c = wavelength corresponding to cutoff frequency.

From Figure 94 an appropriate average HICAT speed is seen to be about 415 knots, or 700 fps. Again, the vast majority of runs lies within ±10% of this speed; and of the runs falling significantly outside this band (at the low speed end), the majority occurred on a single flight.

Ideally, it would be desirable to establish for the HICAT program a high-pass filter having given characteristics on a spatial frequency basis and to retain these filter characteristics for all runs. Inasmuch as the actual filtering must be accomplished using data sampled at a constant interval in seconds (rather than feet), a different filter would be required for each run, depending upon the airspeed. Actually, because of the relatively small scatter of the HICAT airspeeds, this complication is unnecessary. Therefore, the desired filter will be defined first on a spatial frequency basis and converted to a cps basis by using the average true airspeed of 700 fps. As pointed out in connection with the LO-LOCAT speed variation, the effect on the rms value of the filtered time histories and hence the frequency of exceedance will be negligible.

HICAT High-Pass Filters

It is desired that the first of the HICAT high-pass filters be equivalent spatially, i.e., in terms of wavelength, to the LO-LOCAT filter. Frequency of exceedance data obtained with such a filter may be directly compared with similar LO-LOCAT data to investigate the effect of altitude on gust intensity. Inasmuch as the LO-LOCAT values of f_c/f_t and $N_w/\overline{N}_w$ have already been determined to be suitable for the HICAT filter, it remains only to set λ_t the same for both filters. Accordingly, for the HICAT filter,

$$f_t = V/\lambda_t = 700 \text{ fps}/7000 \text{ ft} = 0.10 \text{ cps.}$$

The characteristic wavelengths of this filter are the same as those of the LO-LOCAT filter described above.

Inasmuch as the HICAT time histories contain valid data at wavelengths longer than the 7000 ft values characteristic of the filter selected above, it is desirable to define a second high-pass filter that retains considerably longer wavelengths. For this purpose, an f_t of 0.035 cps, corresponding to a wavelength of 20,000 feet is selected. For this filter, there would seem to be a somewhat greater need for a sharp cutoff, but no requirement to match the filter characteristics of other turbulence-measuring programs. Accordingly, f_c/f_t is increased to 0.300 and $N_w/\overline{N}_w$ is decreased to 0.50.
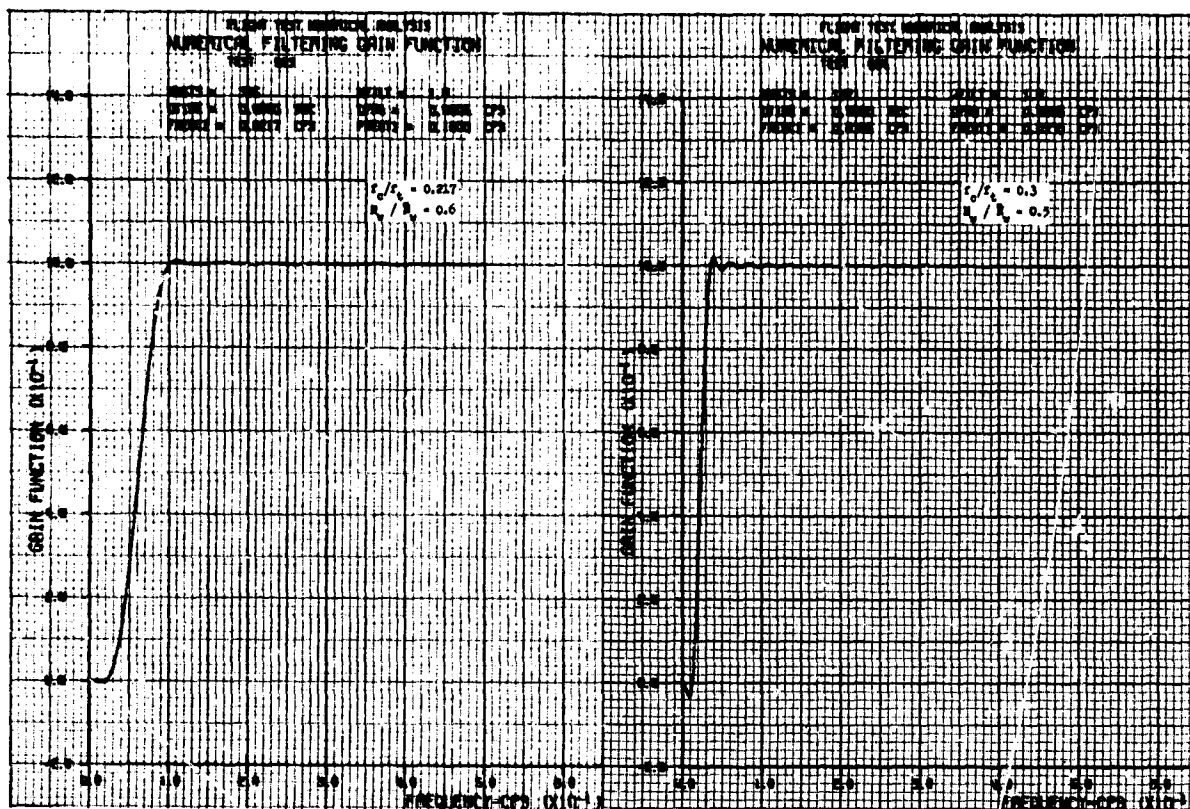
Figure 95   Numerical Filtering Gain Functions (High-Pass Filters)

Pertinent characteristics of these two filters are summarized in the following tabulation:

HICAT High Pass Filter Characteristics

f_t (cps)	λ_t (ft)	f_c (cps)	λ_c (ft)	$\lambda_{c_{eff}}$ (ft)	Δf_r (cps)	N_w	ΔT (sec)	T_n (sec)	f_c/f_t	$N_w/\overline{N}_w$
0.1000	7000	0.0217	33200	17500	0.0783	385	15.4	200	0.217	0.60
0.0350	20000	0.0105	66700	40000	0.0245	1021	41.0	572	0.300	0.50

In the preceding tabulation, ΔT is the additional length of run at each end needed to accommodate the filter; and T_n is the minimum length of run necessary to achieve the desired statistical reliability in spectral calculations for a maximum wavelength λ_t. The minimum run length is given by $20/f_t$.

For convenience, these two filters are designated herein by their termination wavelengths as the 7000 ft filter and 20,000 ft filter, respectively. The gain functions of these two filters are shown in Figure 95. Output power spectral density functions, on the assumption of an input varying as the -5/3 power of frequency, are shown in Figure 96.

202
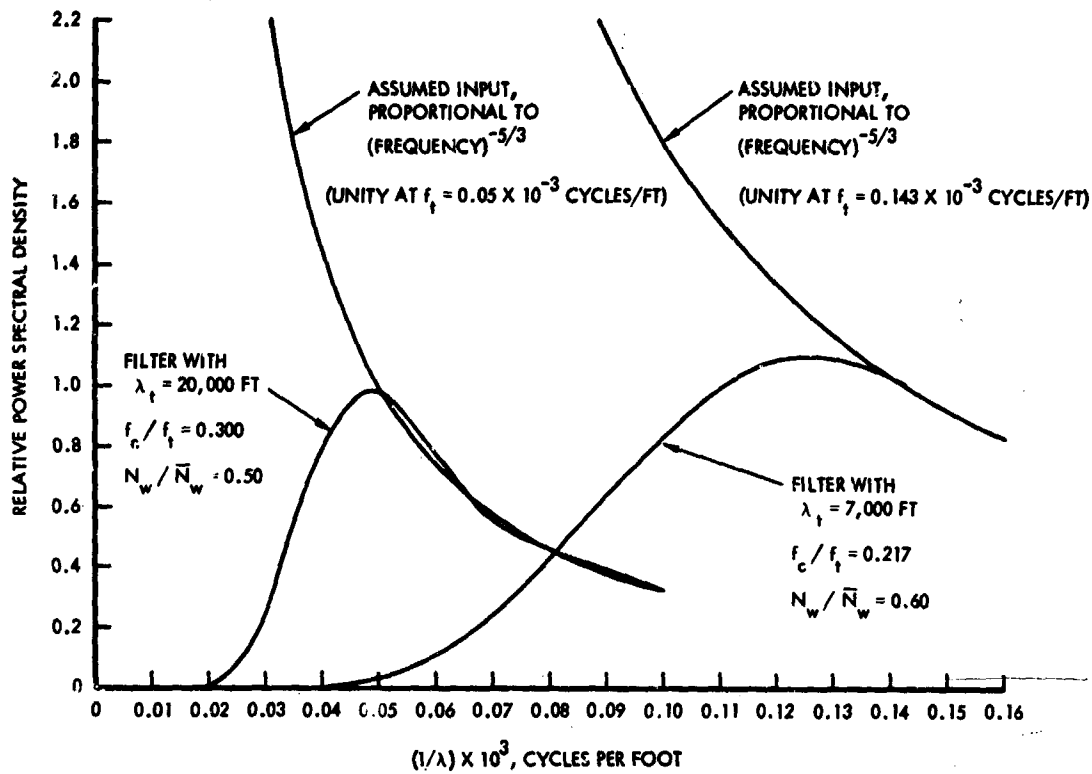
Figure 96 Effect of HICAT High-Pass Filters on Output Power Spectral Density

E. MATHEMATICALLY DEFINED GUST VELOCITY POWER SPECTRAL DENSITY CURVES

For use in aircraft design, as well as for comparison of measured data with various proposed theories, it is often desirable to represent atmospheric turbulence power spectral density curves by means of mathematical expressions.

Current theories indicate that, over a frequency range comparable to that studied in the HICAT program, the gust velocity power spectra are likely to be characterized by the following:

- At very low frequencies, a power spectral density that does not vary with frequency.

- At high frequencies, a power spectral density that varies inversely as some constant power of frequency.

- A transition between these two regions.

The mathematical expressions that are most frequently proposed to represent gust velocity power spectral densities are generally in a form such that the high-frequency exponent and the nature of the transition are defined. These expressions, however, generally contain two parameters to which any desired values may be assigned. One of these parameters, the rms value of the gust velocity (σ_w), measures the intensity of the turbulence, and the other (usually designated by the symbol L and called the scale of turbulence) is a shape parameter that defines the frequency at which the transition occurs between the horizontal and sloping regions of the curve on the usual log plot.

To assist in finding simple, mathematically-defined curves that best fit the measured shapes, several families of curves are shown in this Appendix. All are arbitrarily shown at a level such that the high-frequency asymptote passes through a power spectral density (psd) value of 10^3 (fps)^2/cpf at a frequency of 10^{-3} cpf.

Four basic families are included. For each basic family, curves are provided for high-frequency exponents, m, of -1, -7/6, -4/3, -3/2, -5/3, -11/6, and -2, respectively. For each value of m, curves are shown for scales of turbulence, L, of 500, 1000, 2000, 4000, and 8000 ft, and ∞. Figure 38 compares the four families for an m of -5/3 and an I of 1000 ft and ∞.

The first family includes both the Von Karman spectrum (exponent = -5/3) and the Dryden spectrum (exponent = -2) as special cases. The basic equations for this family are given by Taylor in Reference 31; he credits N. I. Bullen with suggesting their use. Accordingly, this family is designated herein the Taylor-Bullen family. The general form of the equation for this family is

$$\Phi(\Omega) = \frac{\sigma^2 L}{\pi} \frac{\left[1 + 2(n+1) b^2 (\Omega L)^2\right]}{\left[1 + b^2(\Omega L)^2\right]^{n+3/2}} \qquad (12)$$

where n is related to the slope of the high frequency asymptote on the log-log plot, m, as follows:

$$n = \frac{1}{2}(-m - 1)$$

or conversely,

$$m = -1 - 2n$$

and b is defined by

$$b = \frac{\Gamma(n)}{\sqrt{\pi}\,\Gamma(n + \frac{1}{2})}$$

and is equal to 1/L times the constant, a, used by Taylor. Values of n, b, and b^2 for the curves shown herein are as follows:

m	n	b	b^2
-1	0	∞	∞
-7/6	1/12	4.10	16.81
-4/3	1/6	2.318	5.373
-3/2	1/4	1.671	2.792
-5/3	1/3	1.339	1.793
-11/6	5/12	1.139	1.297
-2	1/2	1.000	1.000

The resulting equations are:

$$m = -1: \qquad \Phi(\Omega) = (\text{Constant}) \frac{1}{\Omega}$$

$$m = -\frac{7}{6}: \qquad \Phi(\Omega) = \frac{\sigma^2 L}{\pi} \frac{[1 + 36.42(\Omega L)^2]}{[1 + 16.81(\Omega L)^2]^{19/12}}$$

$$m = -\frac{4}{3}: \qquad \Phi(\Omega) = \frac{\sigma^2 L}{\pi} \frac{[1 + 12.57(\Omega L)^2]}{[1 + 5.37(\Omega L)^2]^{5/3}}$$

$$m = -\frac{3}{2}: \qquad \Phi(\Omega) = \frac{\sigma^2 L}{\pi} \frac{[1 + 7.00(\Omega L)^2]}{[1 + 2.80(\Omega L)^2]^{7/4}}$$

$$m = -\frac{5}{3}: \qquad \Phi(\Omega) = \frac{\sigma^2 L}{\pi} \frac{[1 + 4.78(\Omega L)^2]}{[1 + 1.79(\Omega L)^2]^{11/6}}$$

$$m = -\frac{11}{6}: \qquad \Phi(\Omega) = \frac{\sigma^2 L}{\pi} \frac{[1 + 3.69(\Omega L)^2]}{[1 + 1.30(\Omega L)^2]^{23/12}}$$

$$m = -2: \qquad \Phi(\Omega) = \frac{\sigma^2 L}{\pi} \frac{[1 + 3.00(\Omega L)^2]}{[1 + (\Omega L)^2]^2} \quad .$$

This family of equations, as proposed by Bullen and Taylor, applies to the component of turbulence perpendicular to the direction of traverse, i.e., to vertical and lateral gusts as measured in the HICAT program.

The second family is that defined by Taylor and Bullen for the component of turbulence in the direction of traverse, designated the longitudinal component in the HICAT program. This family is designated herein the Taylor-Bullen Family Longitudinal Gust, or simply, the Taylor-Bullen Longitudinal Family. Where necessary to distinguish these two families, the first may be designated the Taylor-Bullen Transverse Family. The general equation for the Taylor-Bullen Longitudinal Family is

$$\Phi(\Omega) = \frac{2\sigma^2 L}{\pi} \frac{1}{[1 + b^2(\Omega L)^2]^{n+1/2}} \quad . \tag{13}$$

Appendix IE

The values of n and b corresponding to various value of m are the same as for the first Taylor-Bullen family. The resulting equations are:

$$m = -1: \qquad \Phi(\Omega) = (\text{Constant})\frac{1}{\Omega}$$

$$m = -\frac{7}{6}: \qquad \Phi(\Omega) = \frac{2\sigma^2 L}{\pi}\frac{1}{[1 + 16.81(\Omega L)^2]^{7/12}}$$

$$m = -\frac{4}{3}: \qquad \Phi(\Omega) = \frac{2\sigma^2 L}{\pi}\frac{1}{[1 + 5.37(\Omega L)^2]^{2/3}}$$

$$m = -\frac{3}{2}: \qquad \Phi(\Omega) = \frac{2\sigma^2 L}{\pi}\frac{1}{[1 + 2.80(\Omega L)^2]^{3/4}}$$

$$m = -\frac{5}{3}: \qquad \Phi(\Omega) = \frac{2\sigma^2 L}{\pi}\frac{1}{[1 + 1.79(\Omega L)^2]^{5/6}}$$

$$m = -\frac{11}{6}: \qquad \Phi(\Omega) = \frac{2\sigma^2 L}{\pi}\frac{1}{[1 + 1.30(\Omega L)^2]^{11/12}}$$

$$m = -2: \qquad \Phi(\Omega) = \frac{2\sigma^2 L}{\pi}\frac{1}{[1 + (\Omega L)^2]}$$

This family differs most conspicuously from the first Taylor-Bullen family in that the small hump to the left of the knee is eliminated.

The third family is designated the sharp-knee family. This shape also differs from the Taylor-Bullen shape in that the small hump to the left of the knee is eliminated. In addition, the frequency at which the knee occurs remains about the same for all values of m from -1 to -2; in contrast, the knee in the Taylor-Bullen family shifts to much lower frequencies as m approach -1. The equation is simply

$$\Phi(\Omega) = \frac{\text{Constant}}{1 + (\Omega L)^{-m}} \qquad (14)$$

where $(-m) = 1$, $7/6$, $4/3$, $3/2$, $5/3$, $11/6$, and 2. For the special case of $m = -2$, this equation is identical to equation (2).

The fourth family is designated the mild-knee family. The equation is

$$\Phi(\Omega) = \frac{\text{Constant}}{(1 + \Omega L)^{-m}} \qquad \cdot \qquad (15)$$

For the special case of $m = -2$, this family yields the equation proposed by Lappe in Reference 32. The presence of a first-degree term in the denominator (with $m = -2$) results in a much milder knee. The sharp-knee and mild-knee families become more alike as $(-m)$ decreases, and they are identical when $m = -1$. At the frequency defined by the intersection of the low frequency (horizontal) and high frequency asymptotes, ratios of actual psd to the value defined by the intersection are as follows:

	$m = -2$	$m = -4/3$	$m = -1$
Sharp-knee family	0.50	0.50	0.50
Mild-knee family	0.25	0.40	0.50

The four families of power spectral density curves are shown in the following figures:

- Taylor-Bullen   Transverse   Figure 97
- Taylor-Bullen   Longitudinal   Figure 98
- Sharp Knee   Figure 99
- Mild Knee   Figure 100
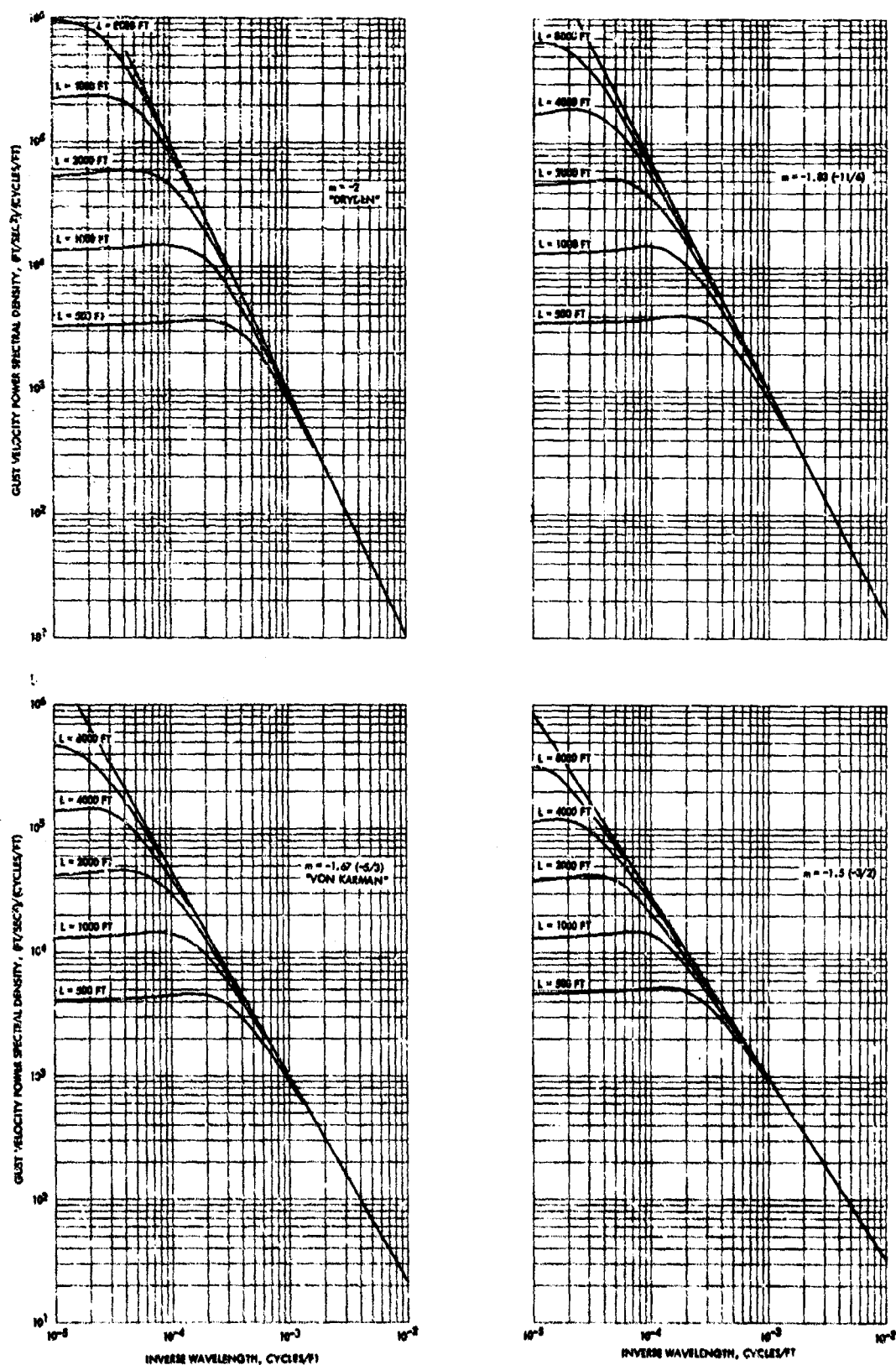
Figure 97   Mathematically Defined Gust Power Spectral Density Curves,
Taylor-Bullen Family - Transverse Gust
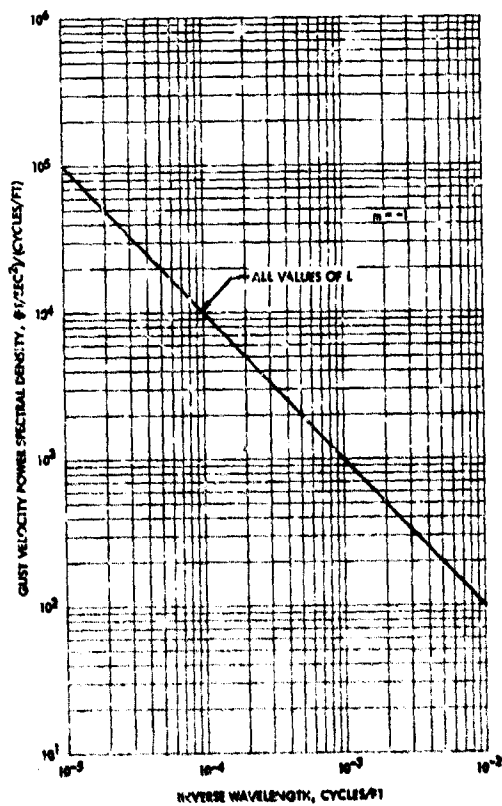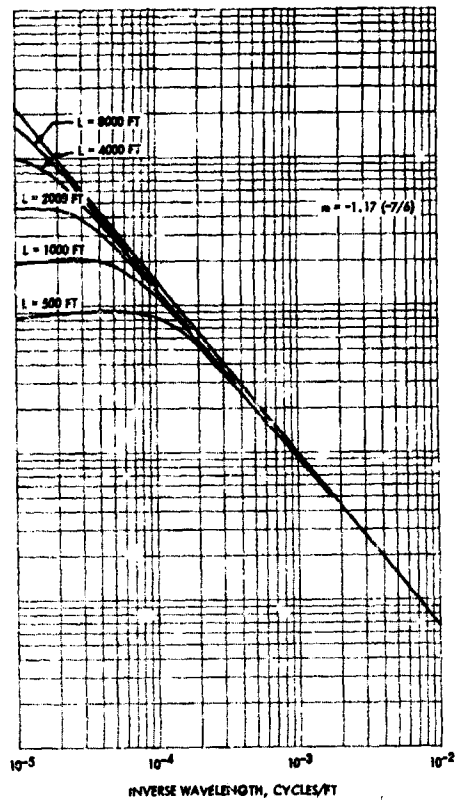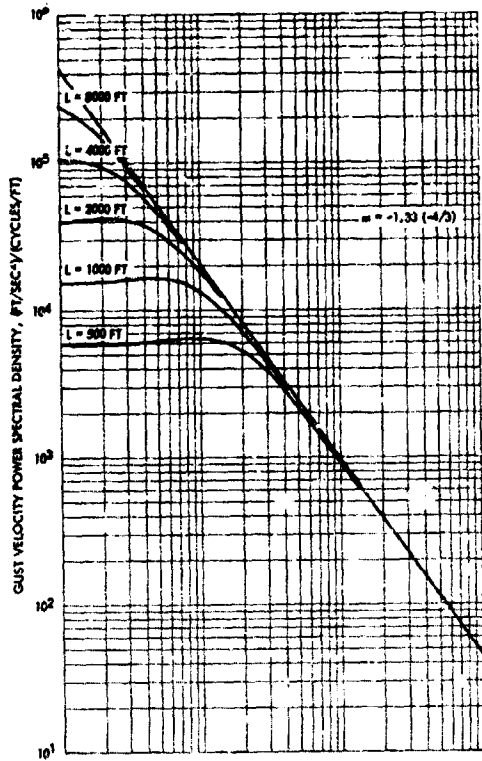
Figure 97 Mathematically Defined Gust Power Spectral Density Curves,
Taylor-Bullen Family - Transverse Gust (Concluded)
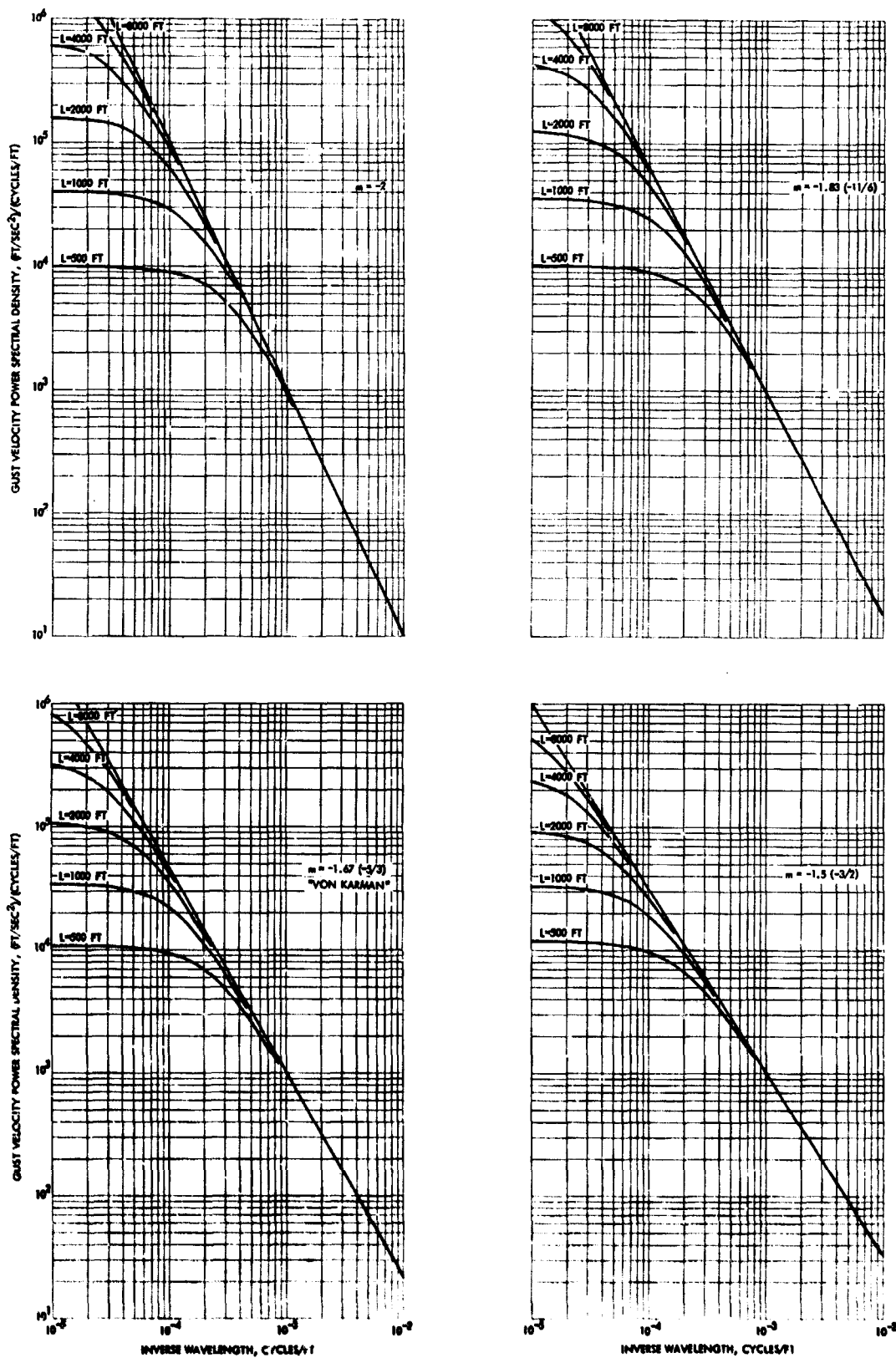
Figure 98 Mathematically Defined Gust Power Spectral Density Curves,
Taylor-Bullen Family - Longitudinal Gust
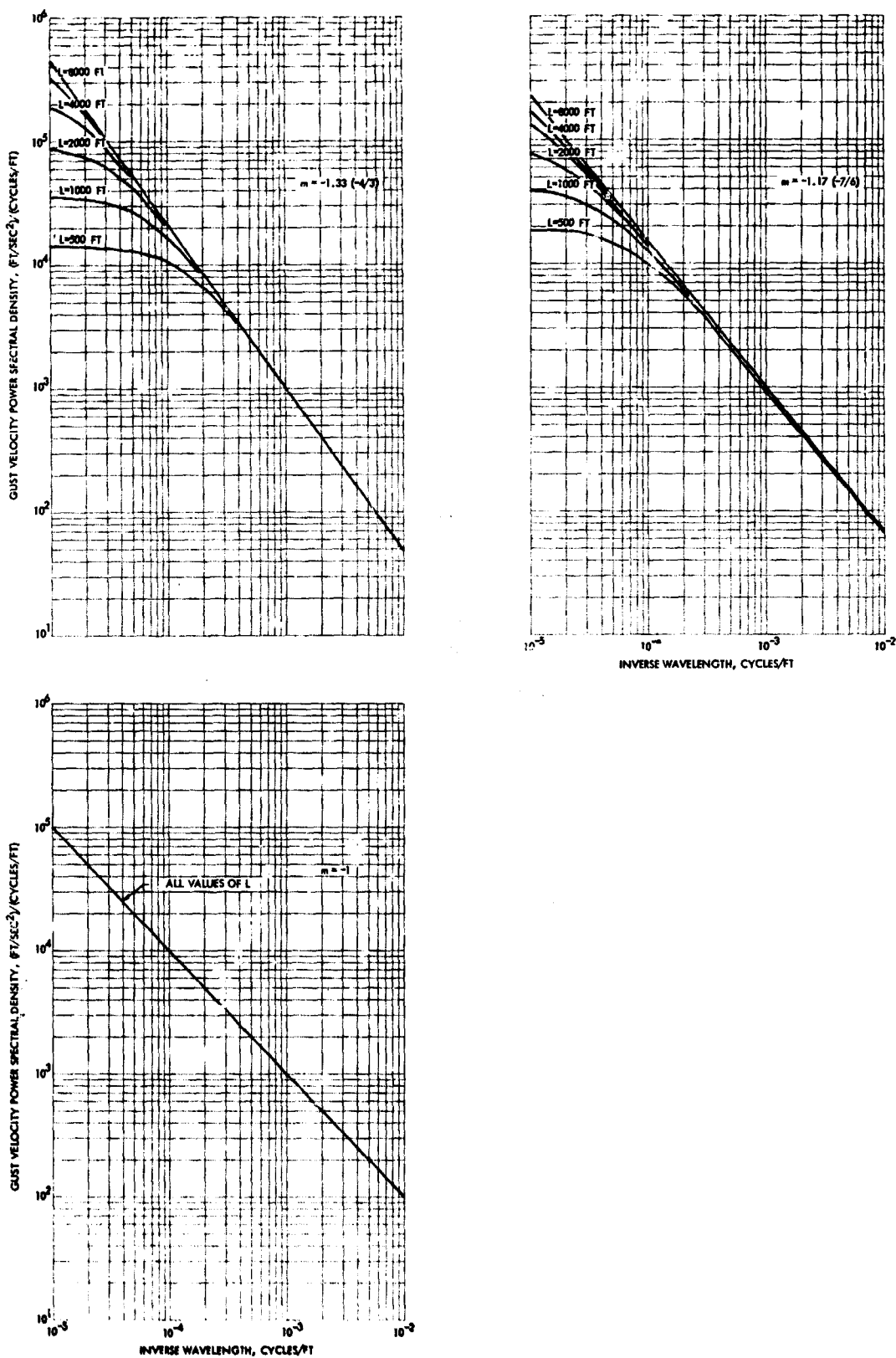
Figure 98   Mathematically Defined Gust Power Spectral Density Curves,
Taylor-Bullen Family - Longitudinal Gust (Concluded)

213
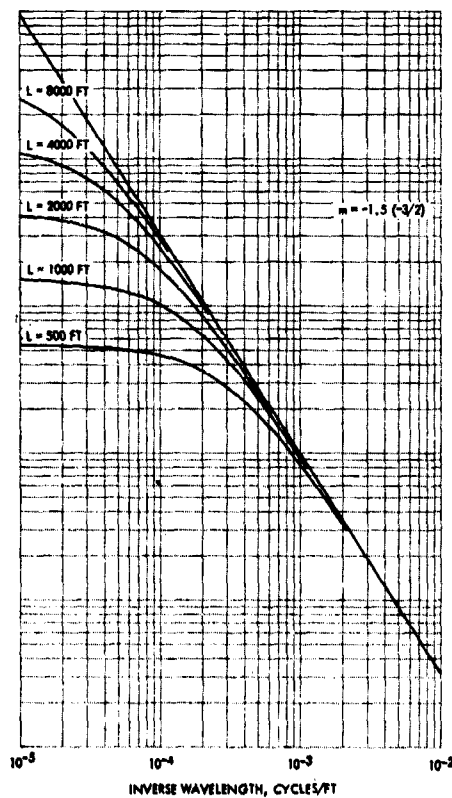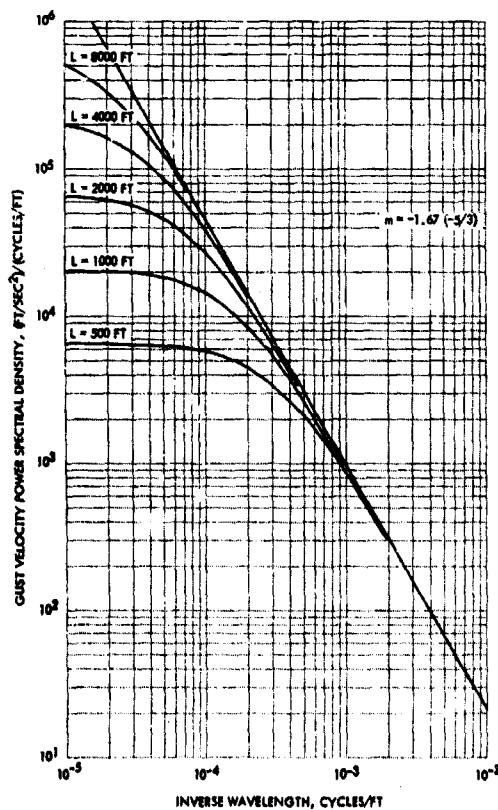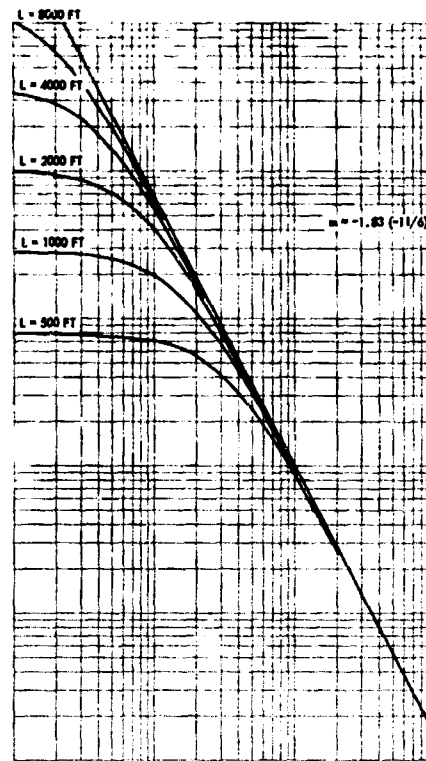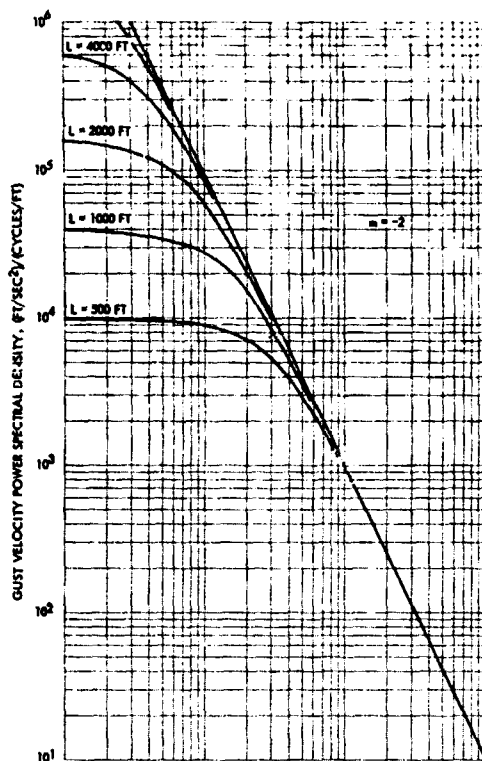
Figure 99   Mathematically Defined Gust Power Spectral Density Curves,
Sharp Knee Family
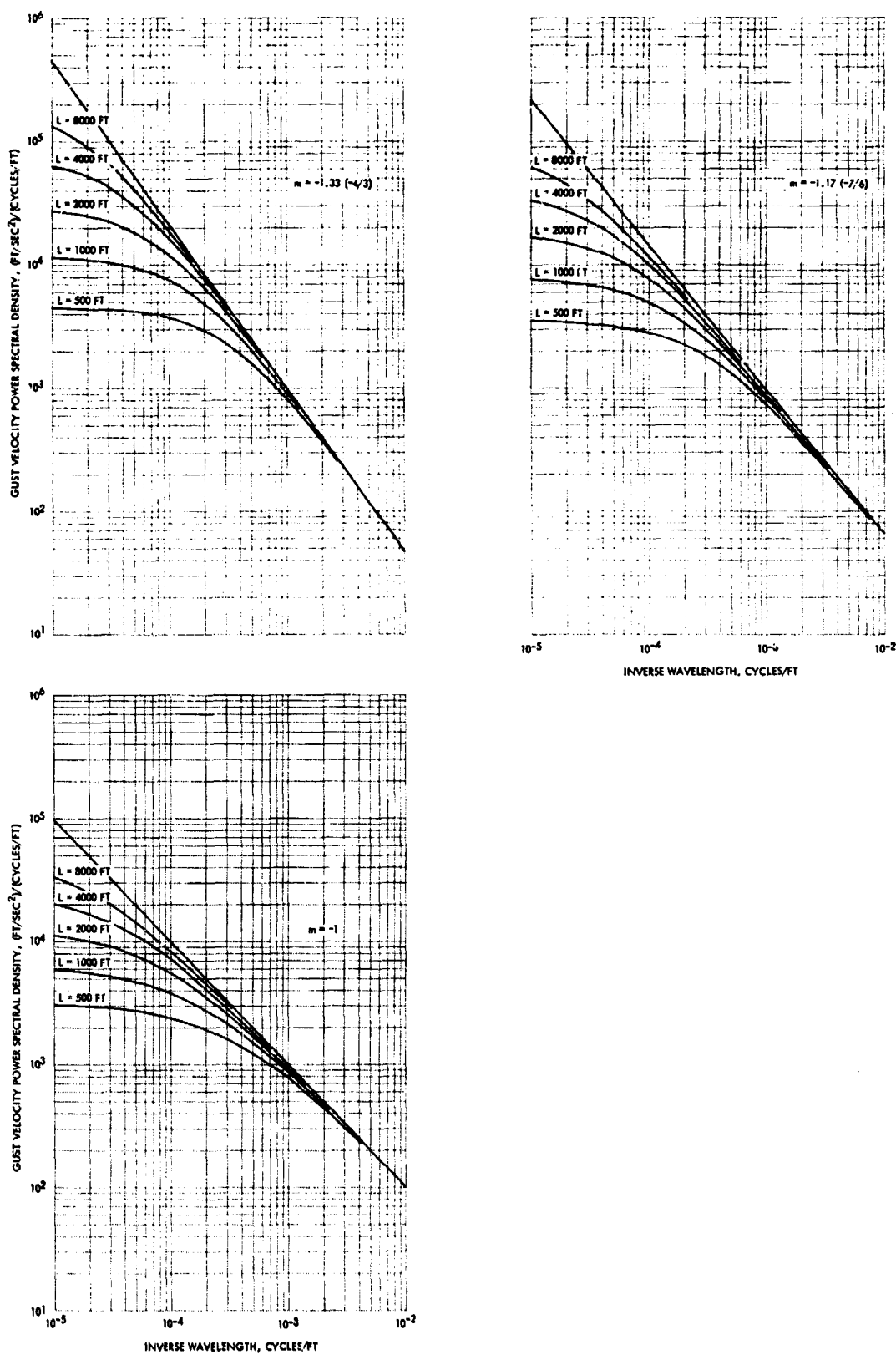
Figure 99   Mathematically Defined Gust Power Spectral Density Curves,
            Sharp Knee Family (Concluded)
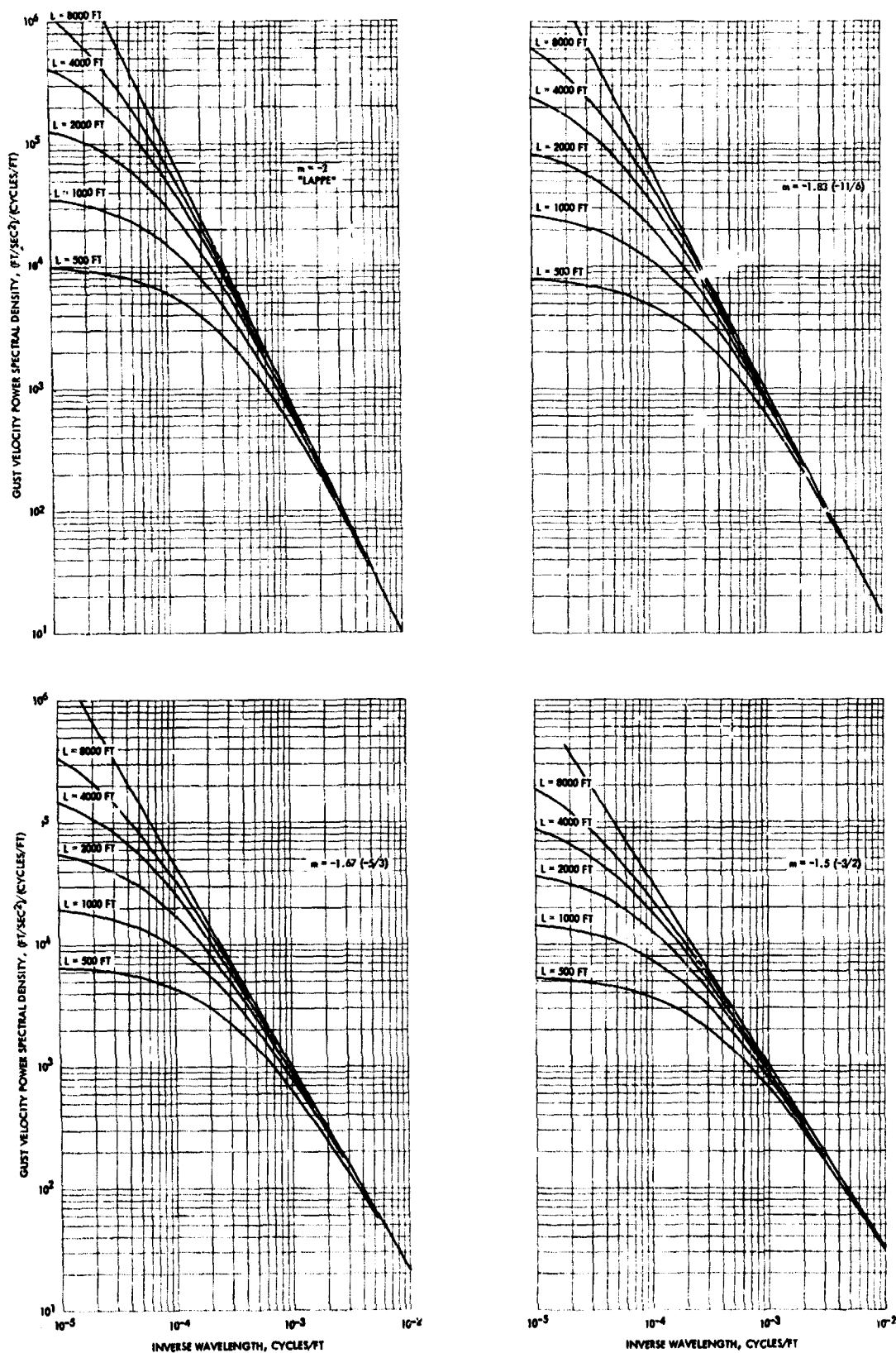
Figure 100   Mathematically Defined Gust Power Spectral Density Curves, Mild Knee Family
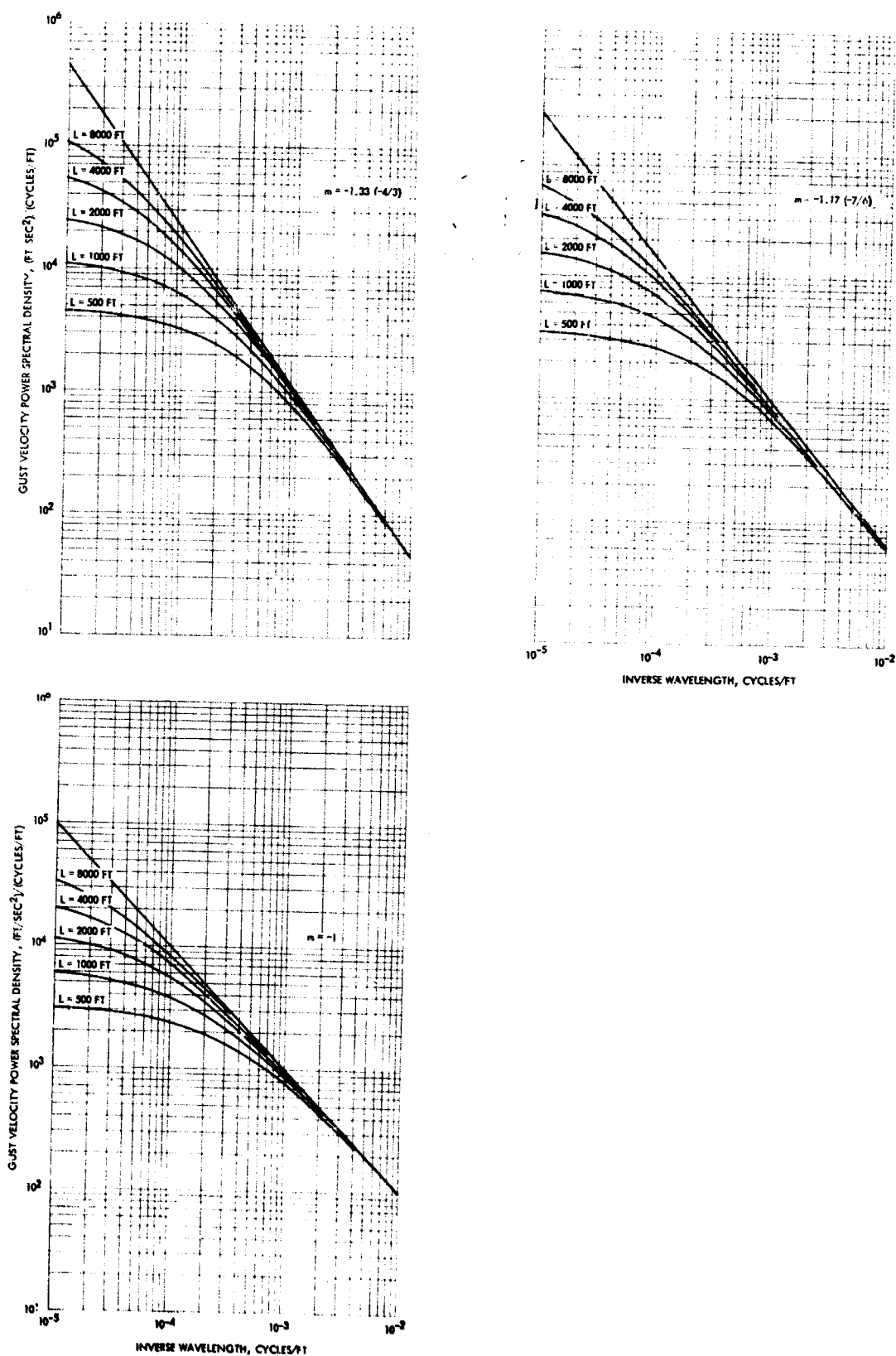
Figure 100 Mathematically Defined Gust Power Spectral Density Curves,
Mild Knee Family (Concluded)

F. NORMALIZED GUST VELCCITY SPECTRA PLOTS

As. an aid in studying variations in spectral shape, a limited number of gust
velocity spectra have been normalized by dividing by the square of an appro-
priately defined rms value. The resulting plots are shown in Figures 101
through 102.

The rms value used for normalizing is, in all cases, RMS 2 for the particular
gust velocity component. Reasons for selection of RMS 2 as a basis for nor-
malizing are discussed under Average Spectral Shape. Use of individual nor-
malization factors for each run permits a direct comparison of spectral shape
in the three directions, at any desired frequency. The normalized spectra
were obtained from un-normalized spectra faired as described in the section,
Average Spectral Shape.

Each curve on the plots is identified by the test and run number, with the
rms value used for normalizing given in parentheses. The curves are grouped
as follows:

    Figure 101   Spectra defined to $\lambda = 40,000$ ft

    Figure 102   Spectra defined to $\lambda = 10,000$ ft for runs obtained in
                     the Detailed Meteorological Analysis of Ten HICAT Tests

Averages were obtained for each group and are shown in Figures 47 and 48 in
Section V, Average Spectral Shape.
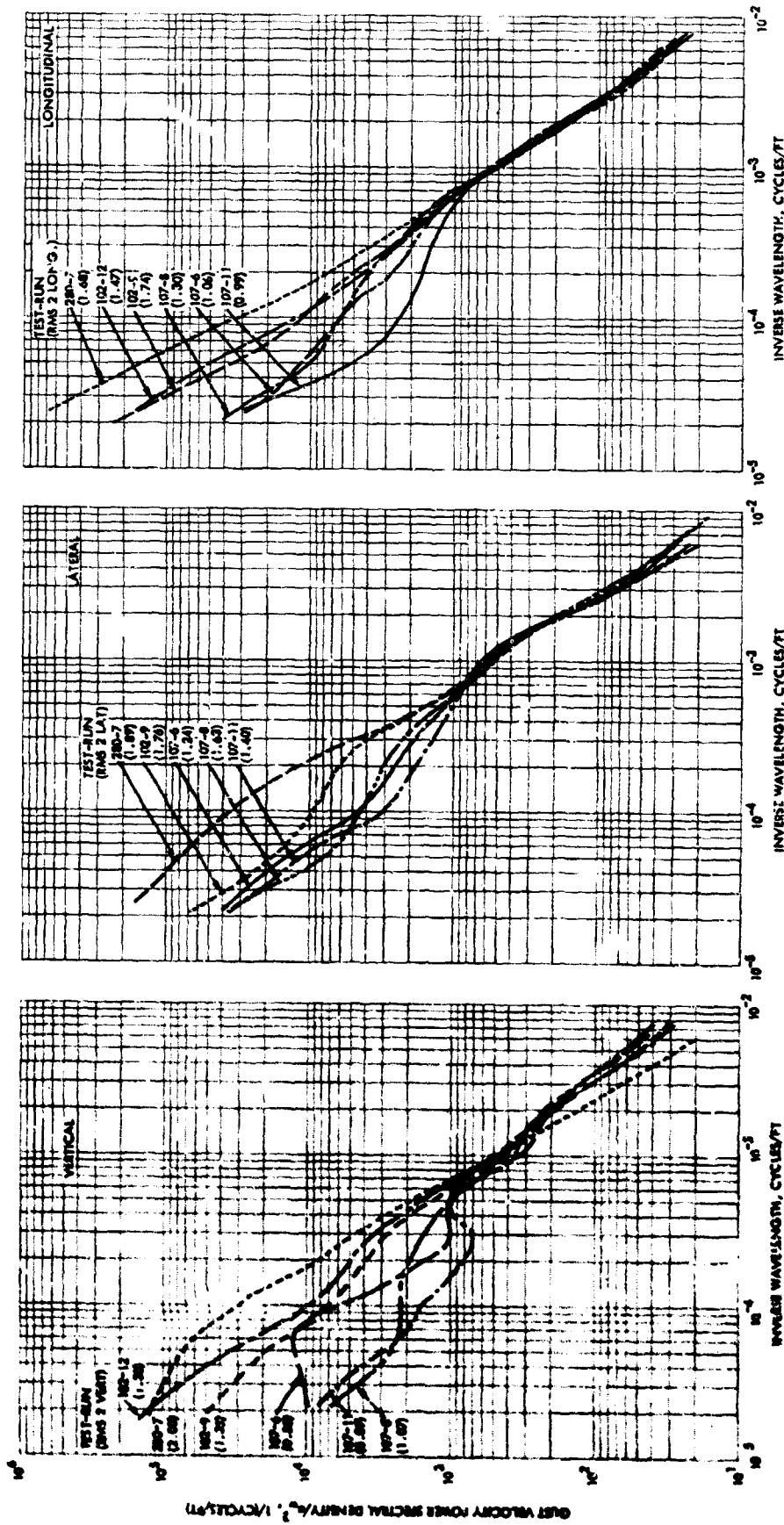
Figure 101 Power Spectra of Component Gust Velocities Normalized to
RMS 2 Squared, Maximum λ = 40,000 ft
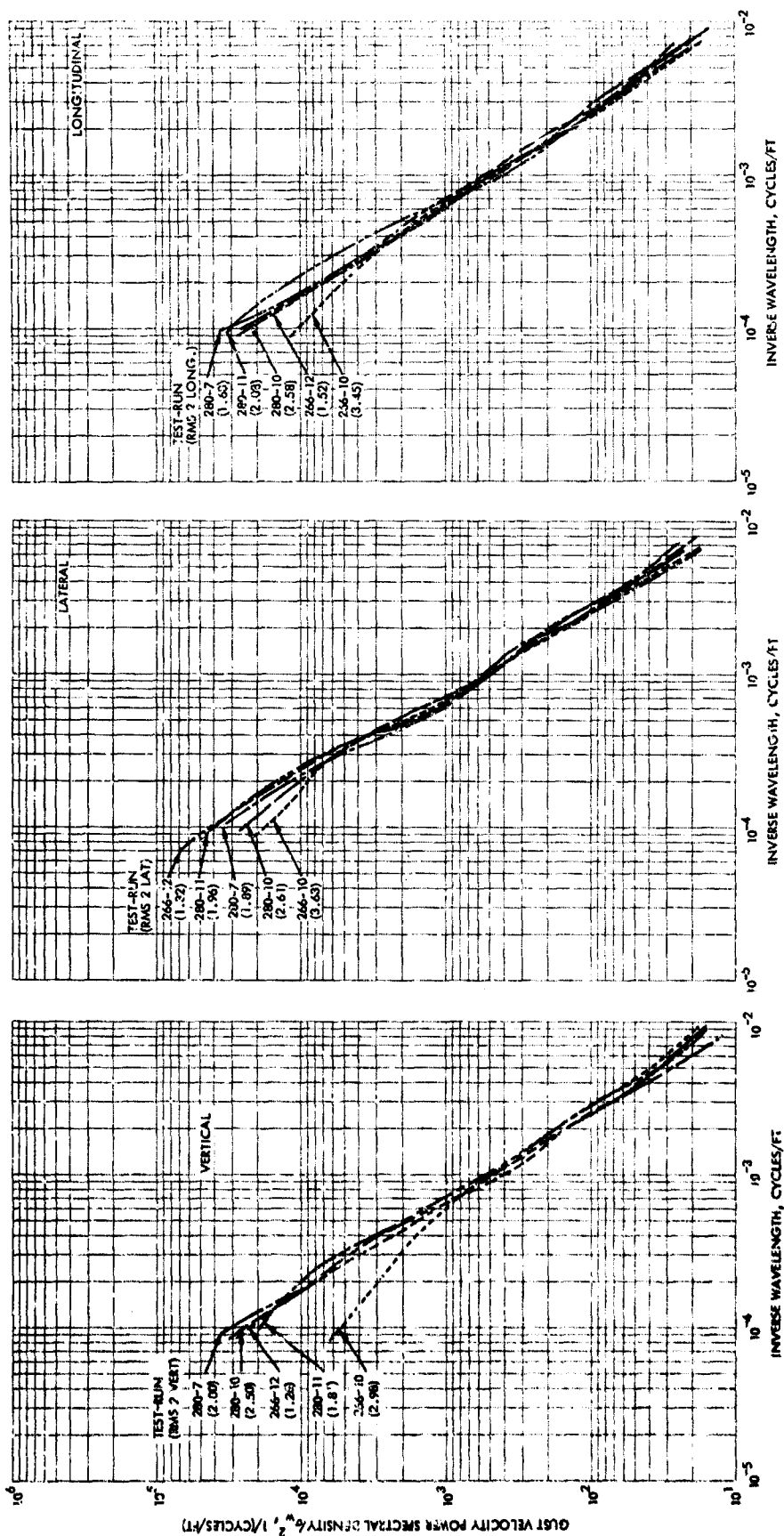
Figure 102 Power Spectra of Component Gust Velocities Normalized to
RMS 2 Squared, Maximum λ = 10,000 ft

G,   DETAILED METEOROLOGICAL ANALYSIS OF TEN HICAT TESTS

A detailed analysis of ten HICAT tests of special meteorological interest
appears in this appendix to substantiate the meteorological discussion of
Section VI.   These tests were selected for their meteorological significance
after verifying that satisfactory flight measurements and adequate meteorolo-
gical observational data were available.   The tests discussed are listed here
by number and meteorological feature of interest.

1.   Test 202-----Severe turbulence over squall line in northern Arkansas.

2.   Tests   -----Moderate CAT over jetstream, Memphis-Nashville area.
      203/204

3.   Test 218-----Zero CAT flight.

4.   Test 220-----Light CAT of long duration.

5.   Test 233-----Severe CAT over Intertropical Convergence Zone
                    (Equatorial Front).

6.   Test 247-----Moderate CAT over Hurricane Beulah.

7.   Test 264-----Severe CAT over Grand Junction, Colorado.

8.   Test 265-----Severe CAT at night on same date and over same area
                    as Test 264.

9.   Test 266-----Severe CAT over Albuquerque, New Mexico.

10.   Test 280-----Turbulence in mountain wave over Denver, Colorado.

FLIGHT SUMMARY AND ANALYSIS - TEST 202, 12 MAY 1967

The 1800Z surface chart for this date shows a quasi-stationary front lying along the Oklahoma-Texas border and extending across central Arkansas and over the east-central states. Thunderstorm and rainshower activity prevailed along the front with most of the convective activity centered about 75 nm north of Little Rock, Arkansas.

The National Severe Storms Laboratory (NSSL) had predicted thunderstorms would form in this general area and requested that the HICAT aircraft be within a 100-mile radius of Oklahoma City, Oklahoma, at 1300 CST. The pilot was contacted when near Perrin Air Force Base and directed to the area of cloud buildups, then detectable by radar, north of Little Rock, Arkansas. He approached the line of thunderstorms from the west (Figure 103) at 65,000 feet and reported very light turbulence and "a wallowing motion". He flew across the storm area again and then descended to 60,000 feet. During the pass from west to east at this altitude the turbulence intensity increased considerably. Then after descending to 59,000 feet a further increase in CAT intensity was observed. During the final pass from west to east at 58,000 feet the pilot reported moderate to heavy turbulence accompanied by more rolling of the aircraft than he had ever seen. Flight measurements indicated that maximum cg acceleration increments were +0.96g/-0.60g associated with true gust velocities of ±20 ft/sec.

The radar reports plotted on the surface chart (Figure 104) show an area of solid echoes below the region traversed by the aircraft. The 1200Z 70 mb temperature-streamline analysis of Figure 105 shows the turbulent area to be in a warm thermal trough with the wind flow almost normal to the isotherms.

Analysis of the 70 mb constant pressure surface of Figure 106 shows a well defined wave pattern with the troughs and ridges quite pronounced at that level. The wavelength is about 300 nm, when measured west to east near 35° latitude, and the height is approximately 130 geopotential meters.

The 1200Z RAOB for Oklahoma City (OKC), Little Rock (LIT), and Nashville (BNA) (Figure 107) shows each of these stations to possess an irregular appearing vertical temperature structure. This condition indicates the presence of vertical motion and appears typical of those associated with the production of turbulence.

Figure 108, the isentropic cross section at 1200Z (five hours prior to the time the pilot was over the line of thunderstorms) shows a baroclinic zone present at that time. The baroclinicity over Oklahoma City (OKC), the first station upwind of the thunderstorm area, is quite pronounced.

One interesting pilot comment was that the free air temperature dropped 6°C during his pass at 59,000 feet and 4°C more during his pass at 58,000 feet. This probably indicated the presence of cold rising air above the line of thunderstorms.

Meteorologically significant features associated with CAT observed during this test are the following:

- The line of building thunderstorms over which the turbulence was encountered

- The wave pattern, as indicated by horizontal temperature analysis, between Memphis and Amarillo

- The large vertical temperature gradients over Little Rock and Oklahoma City near the flight levels at which the turbulence was found.

- The wave pattern evident in the 70 mb pressure surface analysis

- Baroclinicity evident in the isentropic analysis.

RUN NO.	CLASS.	C A T INTENSITY RMS U_{de} (FPS)	RMS $2 U_V$ (FPS)
2	L-M	0.58	-
3	L-M	0.97	-
4	L	0.81	-
5	L	0.59	-
6	L-M	0.61	-
7	L-M	0.84	0.98
8	M	1.98	2.41
9	M	2.04	-
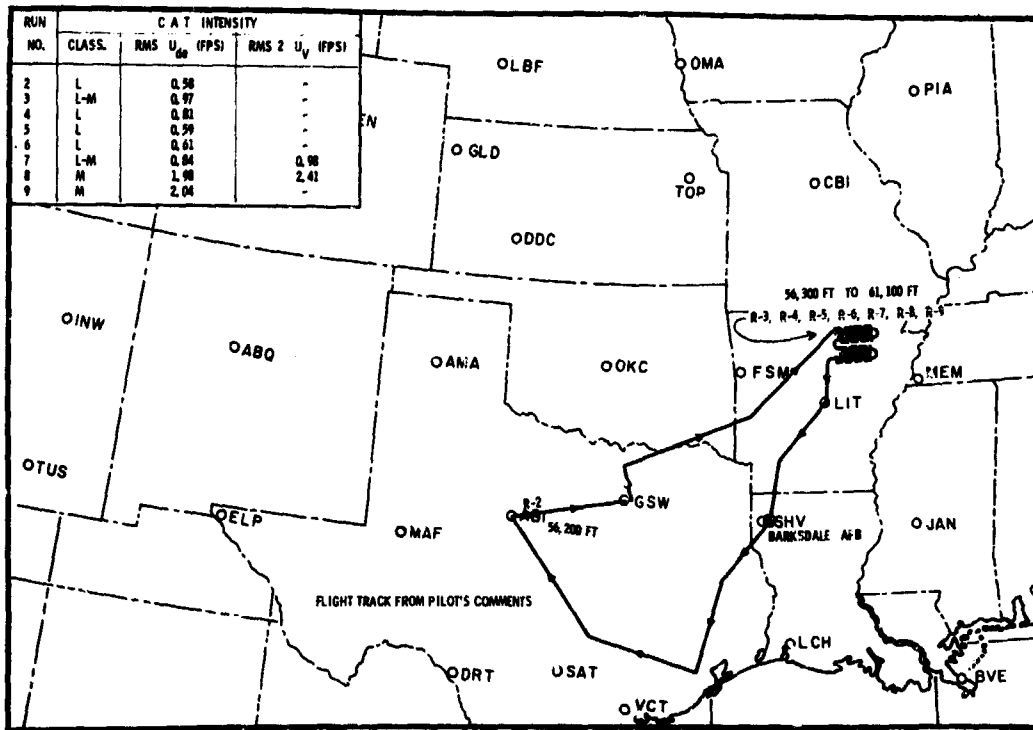
Figure 103   Test 202 Flight Track (1656 - 2133Z, 12 May 1967)
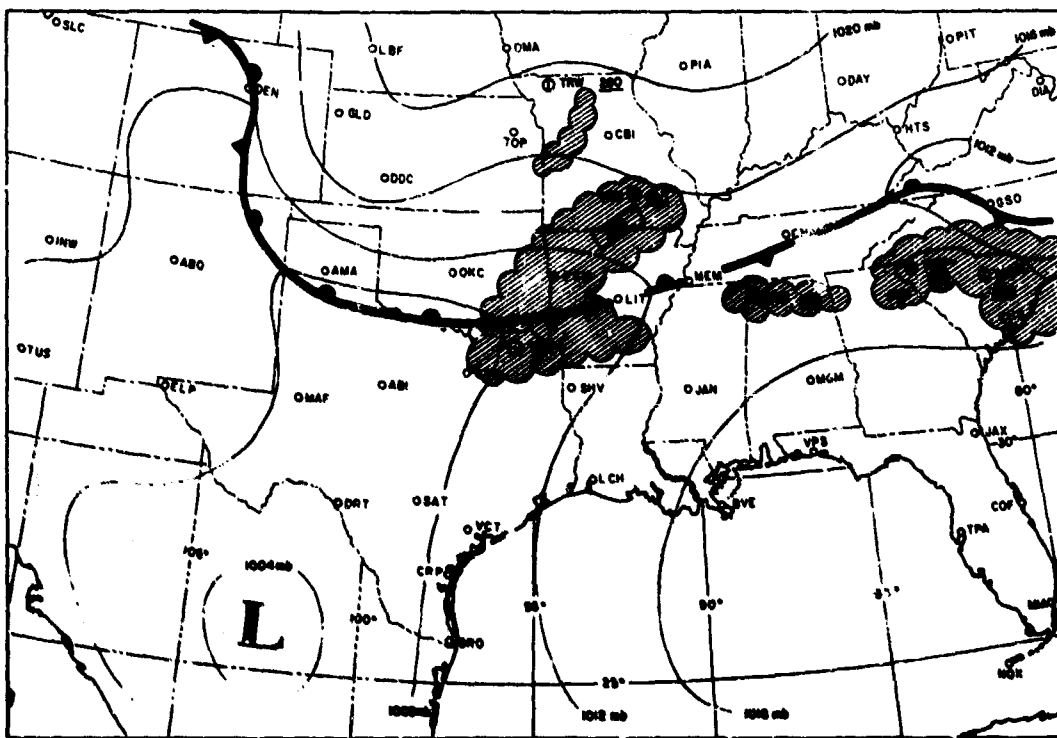
Figure 104   Test 202 Surface Chart (1800Z, 12 May 67) and Radar Summary
(1445Z, 12 May 67)

225
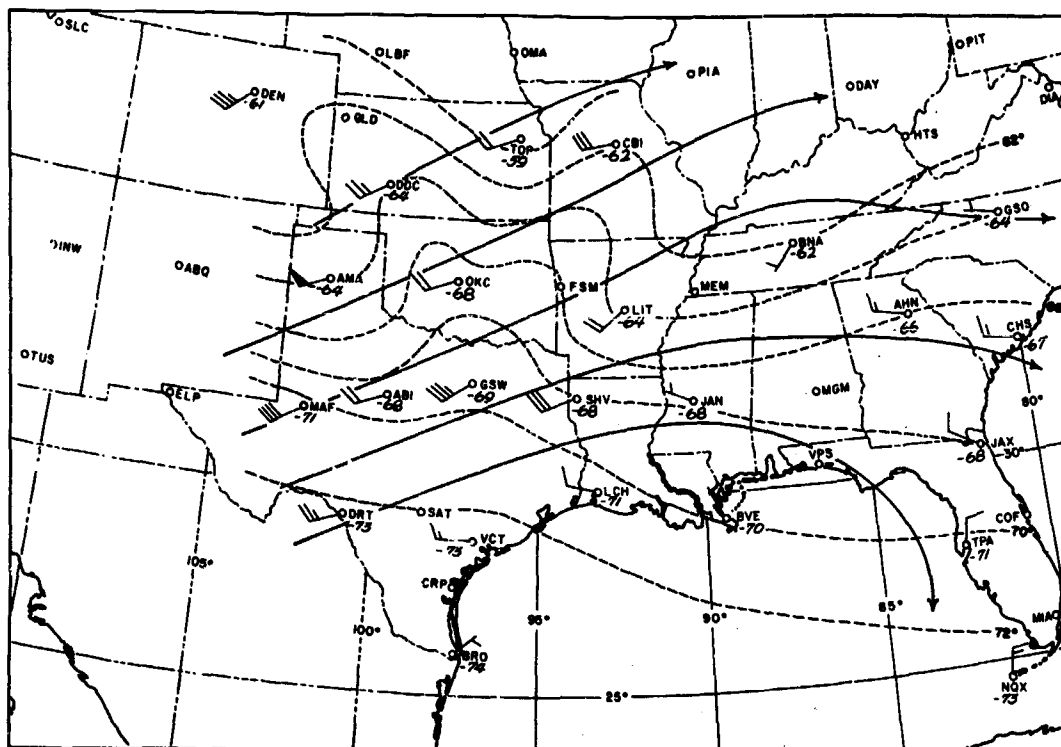
Figure 105   Test 202 70 MB Temperatures and Winds Chart
(1200Z,   12 May 1967)
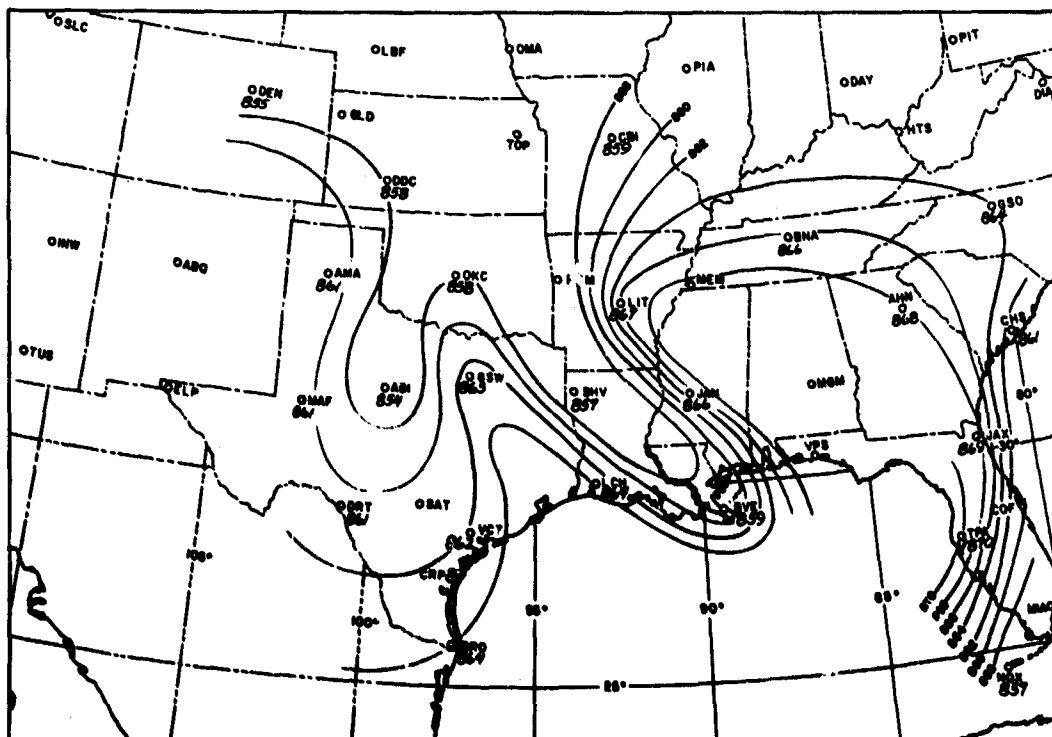
Figure 106   Test 202 70 MB Constant Pressure Chart (1200Z, 12 May 1967)
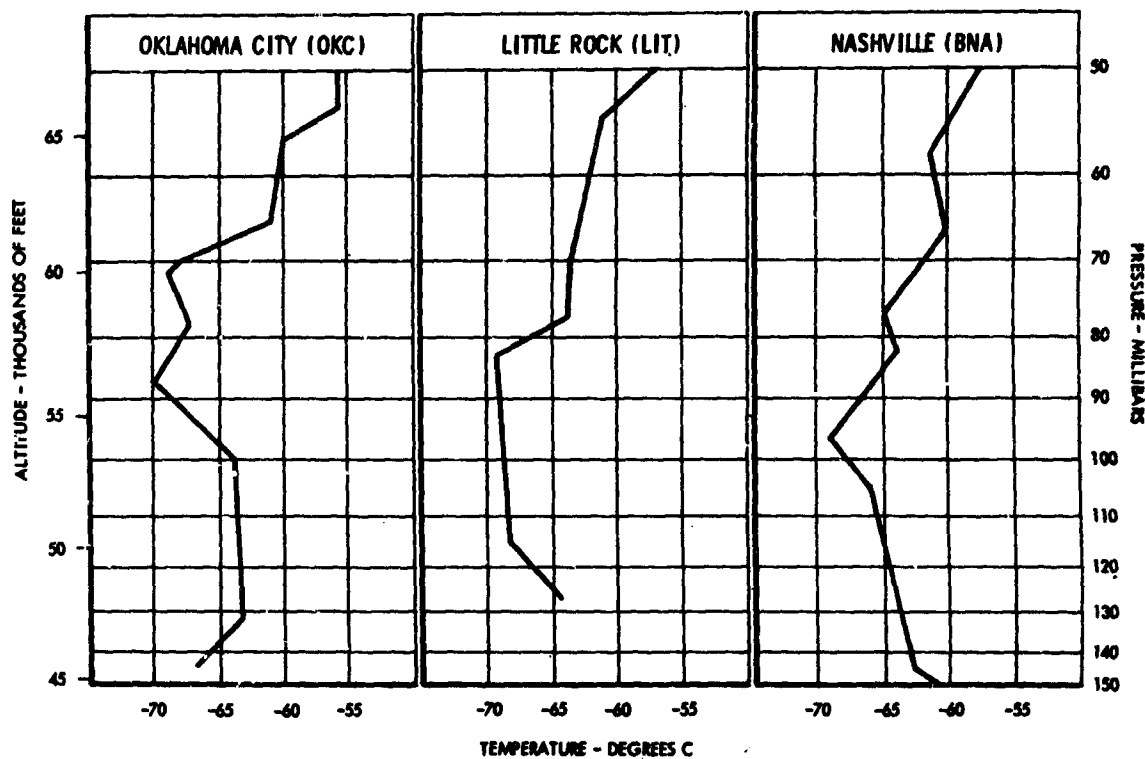
Figure 107 Test 202 RAOB Charts (1200Z, 12 May 1967)
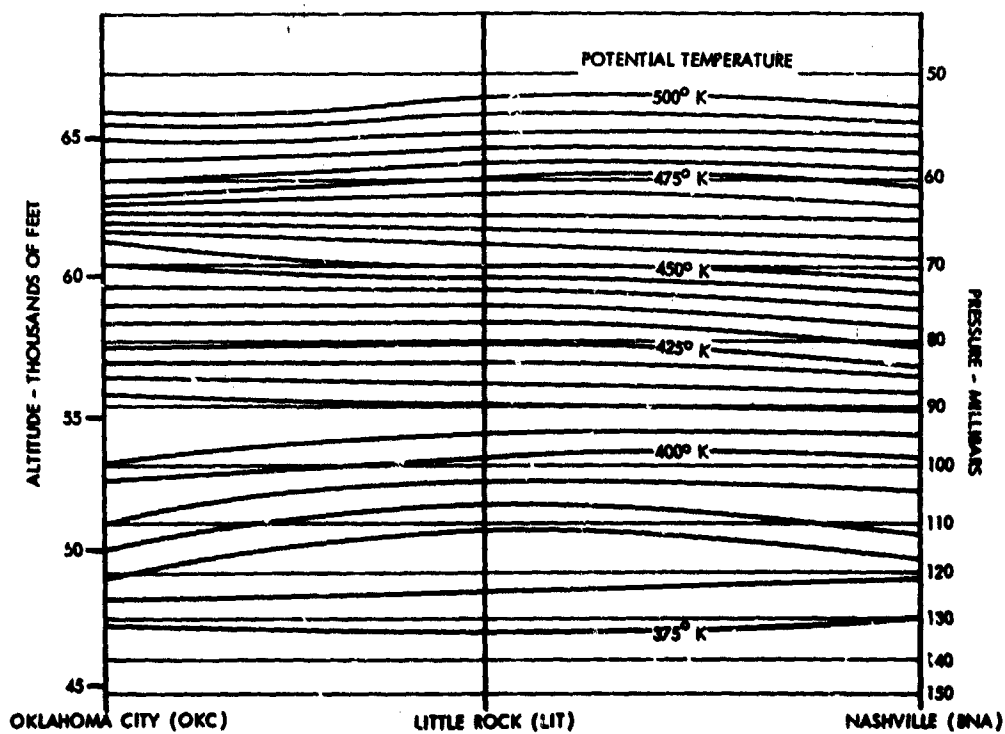
Figure 108 Test 202 Isentropic Cross Section (1200Z, 12 May 1967)

FLIGHT SUMMARY AND ANALYSIS - TEST 203 AND 204, 15 MAY 1967

Tests 203 and 204 were flown on the same day with the same flight plan and are therefore described together. Test 203 began at 1600 GMT, but engine difficulties at test altitudes caused the flight to be aborted. The original flight plan was resumed on Test 204 beginning at 2009 GMT.

During climbout on both tests the pilot reported light CAT at 30,000-36,000 feet, 40 miles east of Shreveport and then light-to-moderate CAT between 40,000 and 50,000 feet, about 75 miles east of Shreveport. Very little turbulence was noted above 60,000 feet, so the pilot concentrated his search between 50,000 and 60,000 feet. The resulting CAT encounters are shown on the flight track map (Figure 109) as runs 2 through 10.

Figure 110 shows the 2100 GMT surface chart combined with the 2345 GMT radar summary. Also overlayed are the extrapolated positions of the polar and southern jetstream at the time of the flight. It can be seen that the turbulence was encountered directly above the area of convergence of the two jetstreams.

At the 70 mb level (Figure 111) a warm thermal trough appears near Lake Charles, Louisiana (LCH), and extends northwards toward the Little Rock, Arkansas (LIT) and Memphis, Tennessee (MEM) area. The thermal trough also is oriented along the pressure trough at the 70 mb surface that can be seen in Figure 112. The relatively short wave appearance notable in the 70 mb constant pressure analysis is in contrast to the wavelengths generally observed in analyses of mandatory levels below the tropopause. In this case, the wavelengths are approximately 300-400 miles in length as opposed to the 2000- to 3000-mile wavelengths generally found in analyses of the higher tropospheric levels.

Figure 113 is a plot of the RAOB for Shreveport, Louisiana (SHV), Jackson, Mississippi (JAN) and Montgomery, Alabama (MGM) for 0000Z, 16 May 1967. These observations were made about 4 hours after the U-2 was in the sampling area and are the best available. Note the variable character of the vertical temperature gradient between 150 and 50 mb. It has been observed that as the stratospheric wavelengths of the 70 mb constant pressure chart become shorter (i.e., near 300-400 miles) vertical temperature soundings display an increased gradient.

The isentropic cross section (Figure 114) shows the baroclinic zones between 150 and 50 mb over SHV, JAN, and MGM. It should be noted that turbulence was encountered at 52,400 feet over JAN and 56,300 feet and 27,900 feet between Little Rock (LIT) and SHV. The turbulence altitude corresponds to an area of wide spacing of the isentropes.

Important aspects of this flight in relation to the turbulence encountered are considered to be:

●   The turbulence occurred over an area of converging jetstreams. The jetstreams were near the 200 mb level.

- A pressure trough and a warm thermal trough were apparent at the 70 mb level near the time and location of the observed turbulence.

- The 70 mb pressure and thermal patterns indicated the presence of a stratospheric wave 300-400 miles in length.

- The RAOB charts showed strong vertical temperature gradients.

- The isentropic analysis shows the turbulence occurred below a stable layer at a level of pronounced baroclinicity.
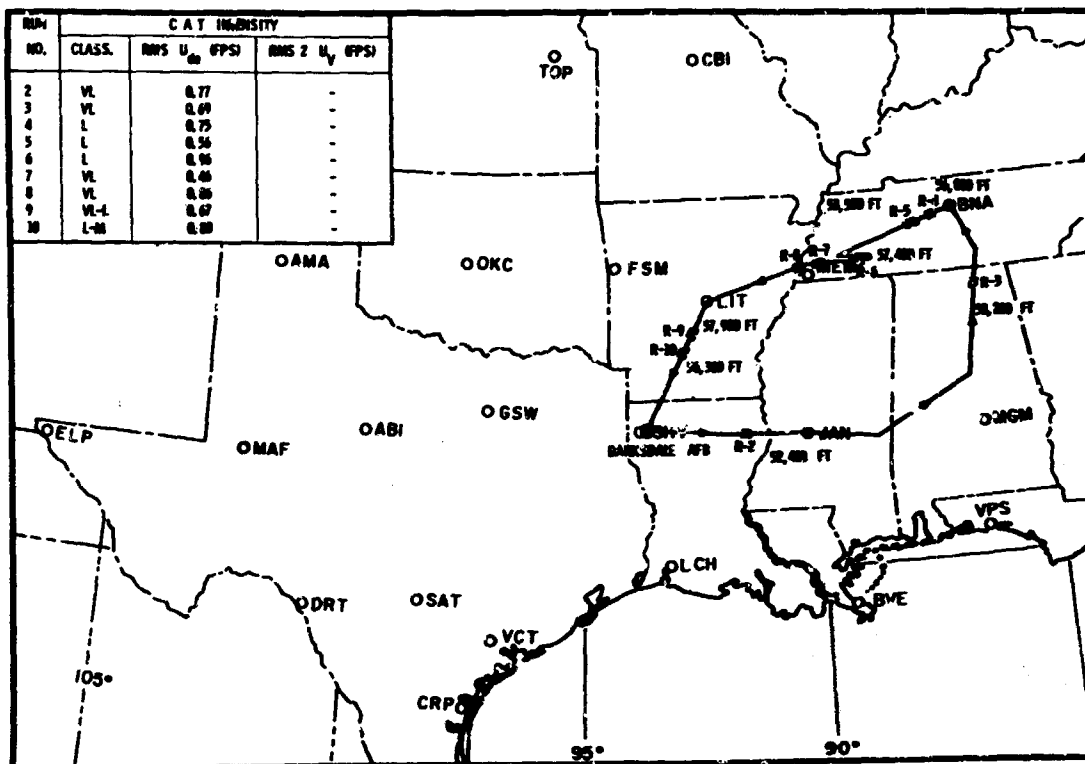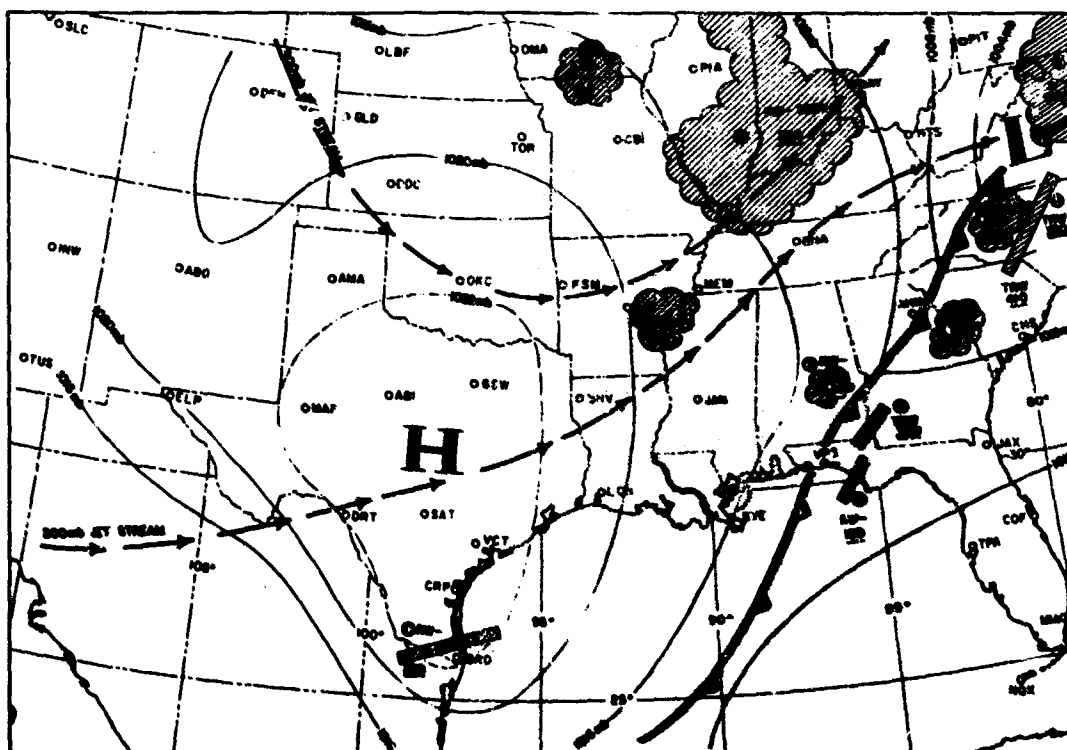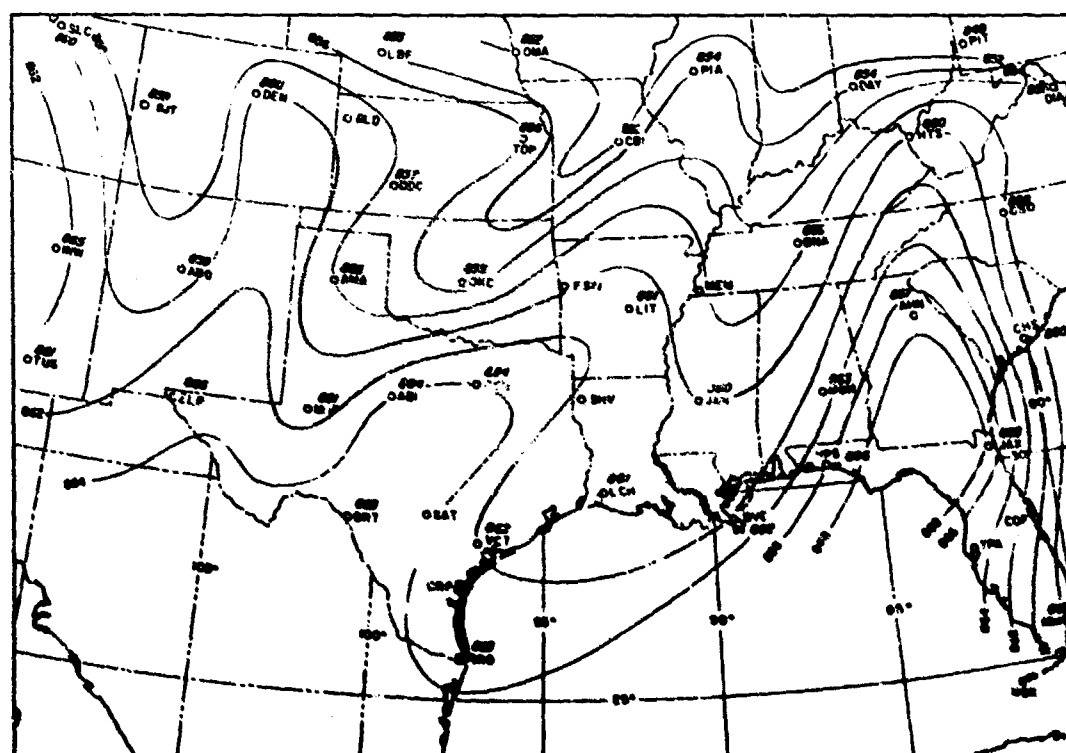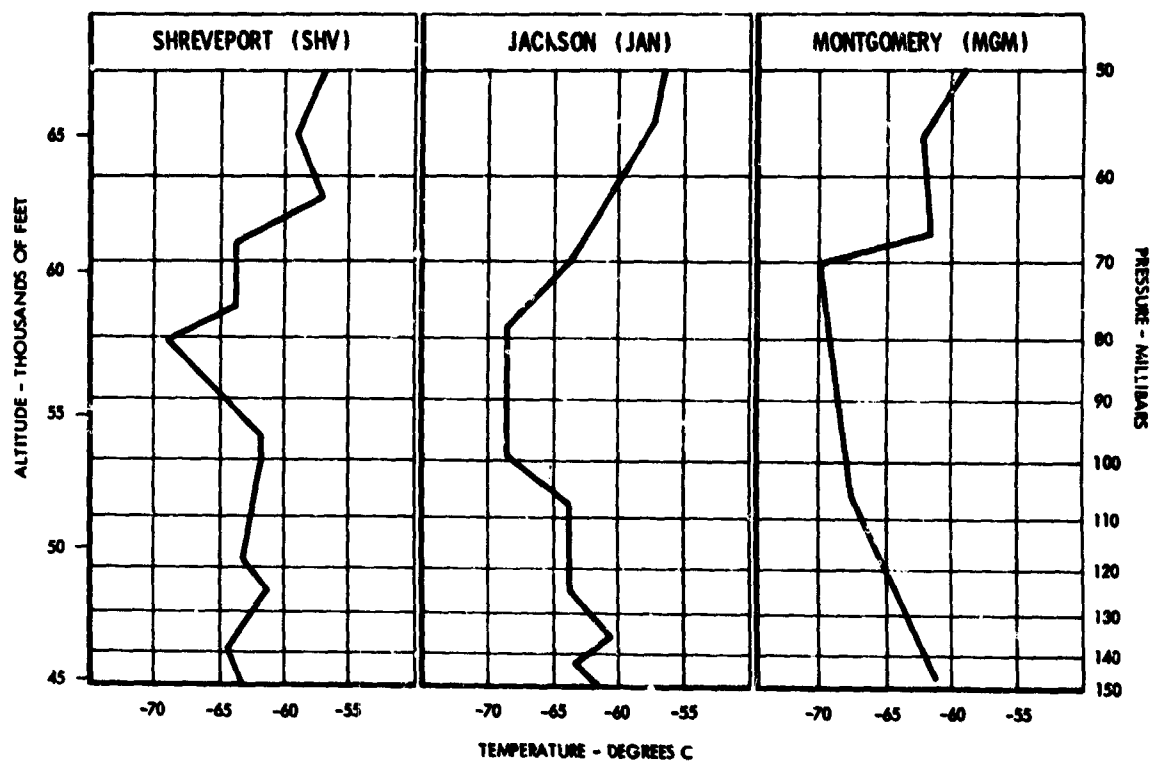
Figure 109 Test 204 Flight Track (2009 - 2336Z, 15 May 1967)

Figure 110 Test 203 and 204 Surface Chart (2100, 15 May 1967)
and Radar Summary (2345Z 15 May 1967)
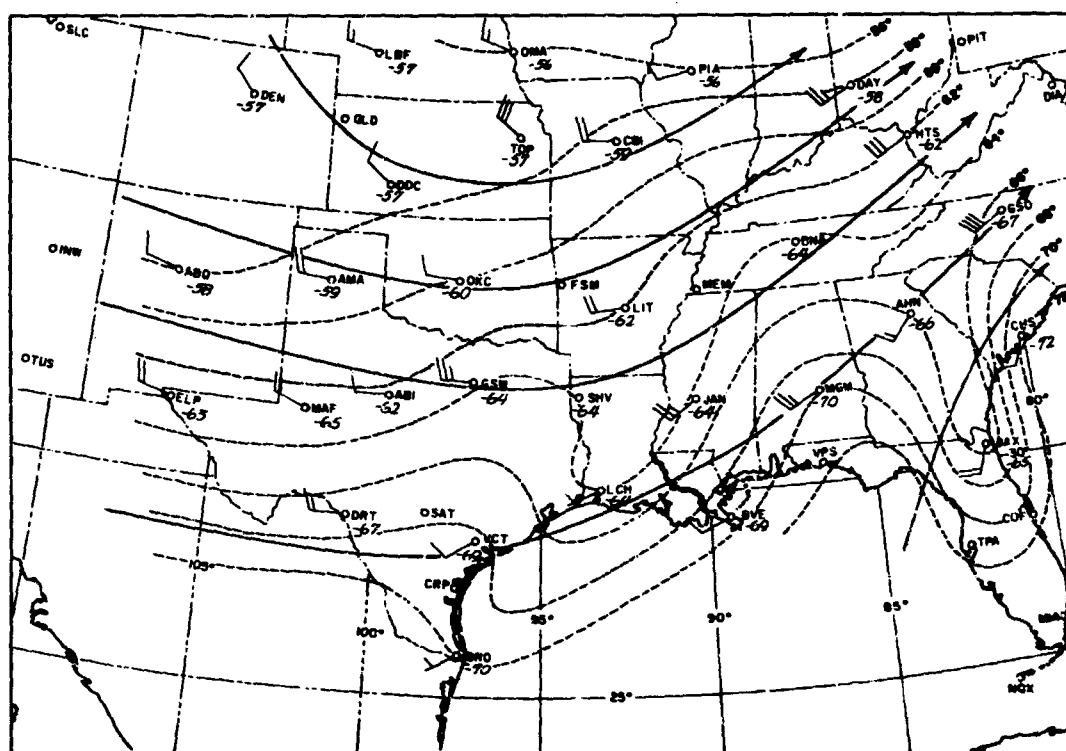
Figure 111 Test 203 and 204 70 MB Temperatures and Winds Chart

Figure 112 Test 203 and 204 70 MB Constant Pressure Chart
(0000Z, 16 May 1967)

Figure 113   Test 203 and 204 RAOB Charts (0000Z, 16 May 1967)
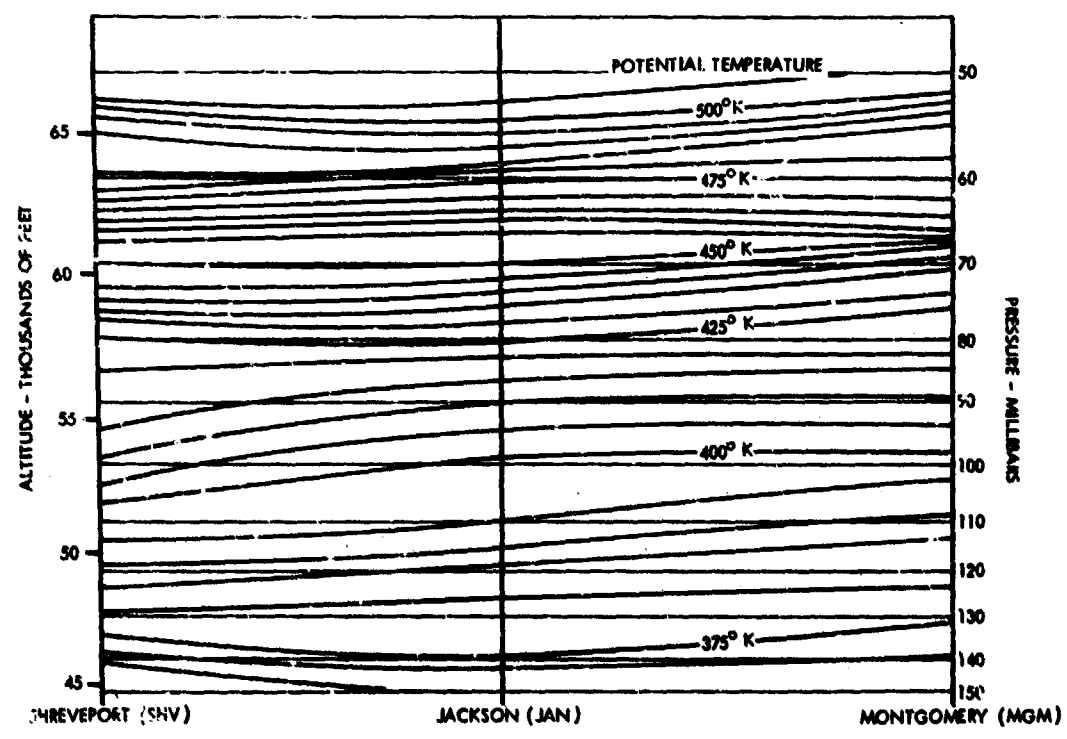
Figure 114   Test 203 and 204 Isentropic Cross Section (0000Z, 16 May 1967)

233

FLIGHT SUMMARY AND ANALYSIS - TEST 218, 30 JUNE 1967

This test is included as a special case to illustrate conditions associated with the absence of clear air turbulence. Figure 115 shows that the route of flight was over the rolling, forested hills of southeastern Canada. The hills were generally less than 2,000 feet in elevation except for a small area of 2000- to 5000-foot mountains near Quebec.

The combined surface and radar summary chart in Figure 116 depicts the surface fronts located north of the Great Lakes region and across the Mid-Atlantic States. The convective activity that existed was well to the south of the route of flight. There was wide-spread cloudiness, however, over the entire map area. The pilot reported only a few breaks in the clouds in the vicinity of Caribou, Maine and Three Rivers, Canada. Rain also prevailed over the northeastern United States and southeastern Canada.

In Figure 117 it can be seen that at the 70 mb level the flight path was in an area of very weak horizontal temperature gradient and light winds. The temperature gradient is about 1°C/300 nm with winds generally about 5 knots.

The 70 mb constant pressure surface analysis in Figure 118 indicates that a flat pressure surface also existed over the sampled area. Although not shown, winds from the 300 mb and 200 mb analyses were light for those altitudes, averaging about 25 knots. The tropopause wind analysis showed the 20-knot isotach encircling the flight path.

The well defined low at the 70 mb level located over Newfoundland was well to the east of the sampled area. The RAOB charts (Figure 119) for Moosonee (MO), Maniwaki (MW), Canada, and Caribou, Maine (CAR) show the small temperature gradient that existed between 150 and 50 mb. The relatively small slope of the isentropes in Figure 120 also correspond to the small vertical temperature gradient.

Significant features associated with the lack of turbulence at levels between 150 and 50 mb and in the sampling area are:

- The lack of any widespread convective activity as noted on the sur-face and radar summary chart (Figure 116)

- The small horizontal temperature gradient and light winds apparent on the 70 mb analysis (Figure 117)

- The relatively flat surface at the 70 mb level (Figure 118)

- The small vertical temperature gradient depicted by the RAOB chart (Figure 119)

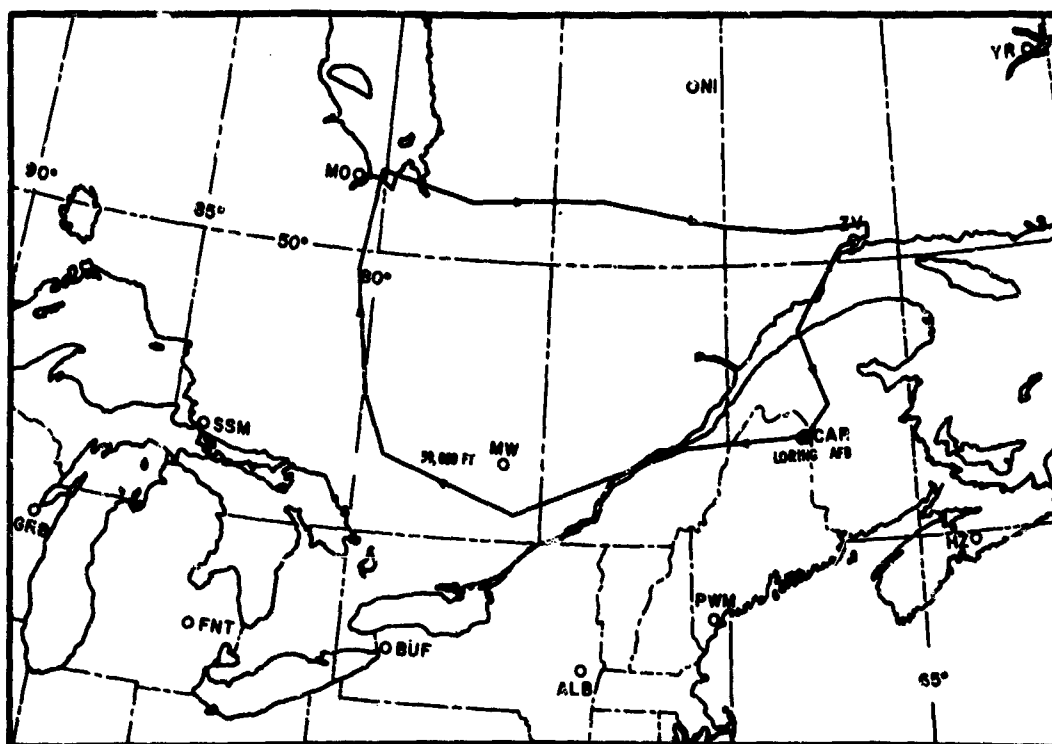- The relatively flat slope of the isentropes and lack of baroclinic zones (Figure 120)

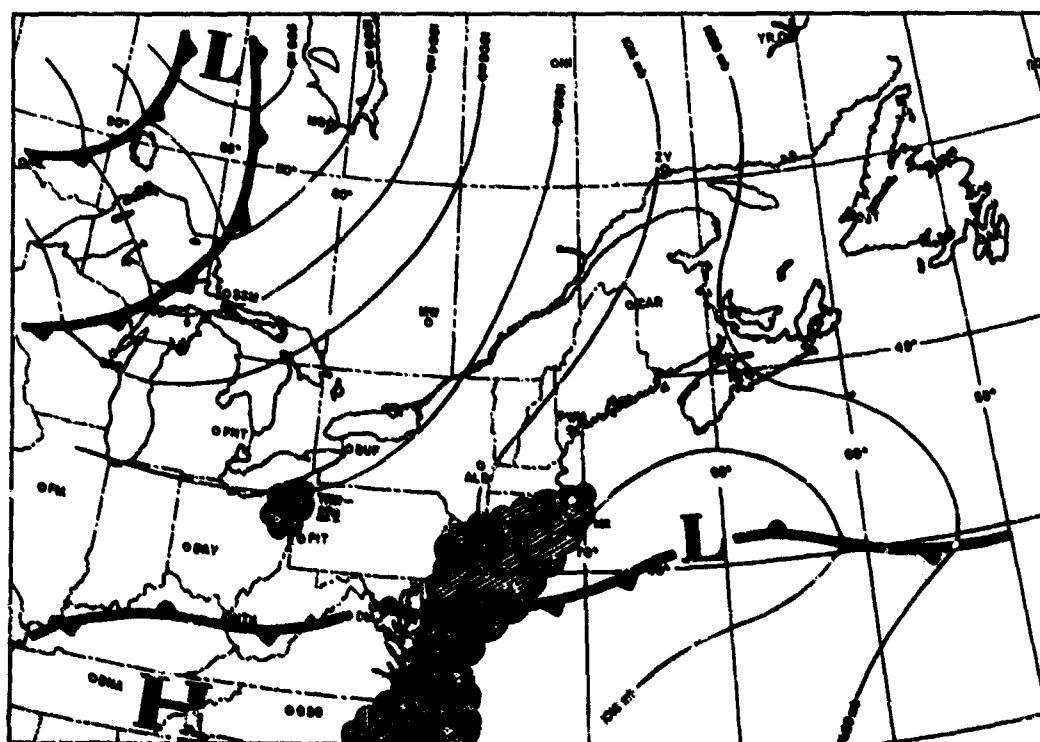Figure 115   Test 218 Flight Track (1436 - 1900Z, 30 Jun 1967)

Figure 116   Test 218 Surface Chart (1800Z, 30 Jun 1967)
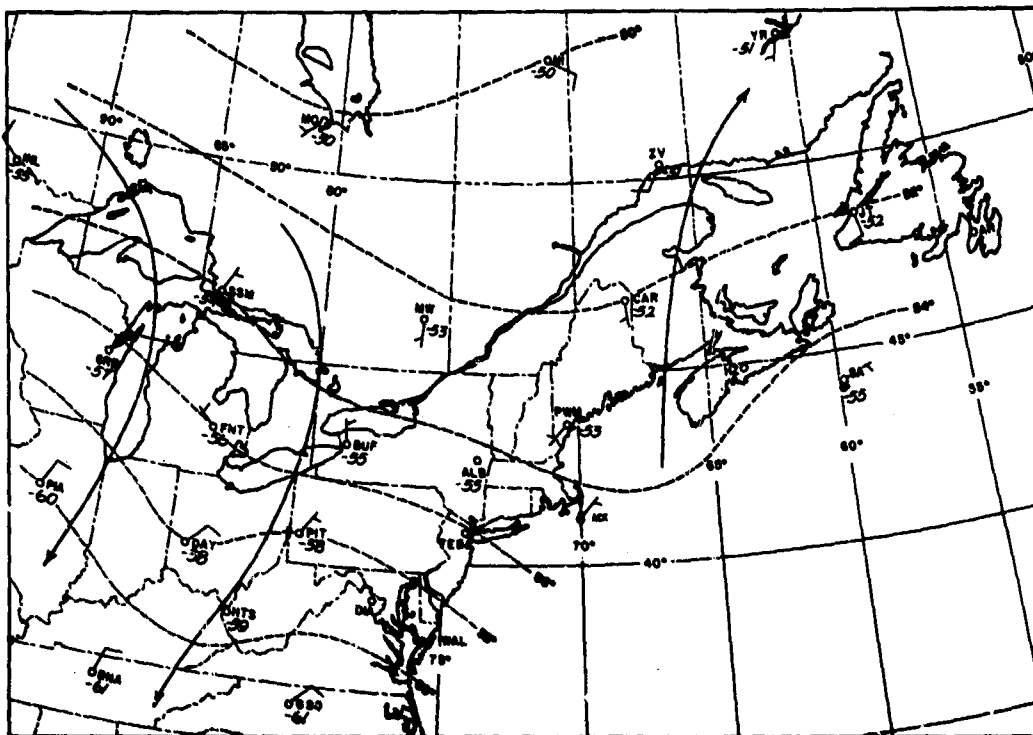and Radar Summary (2045Z, 30 Jun 1967)

Figure 117   Test 218 70 MB Temperatures and Winds Chart (1200Z, 30 Jun 1967)
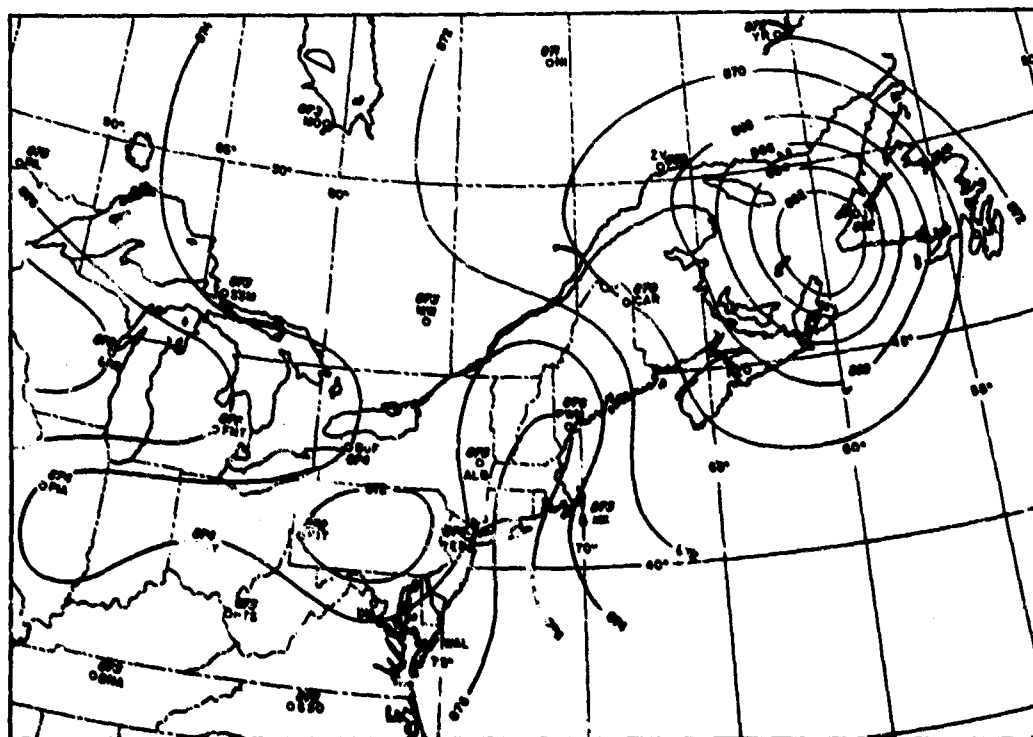

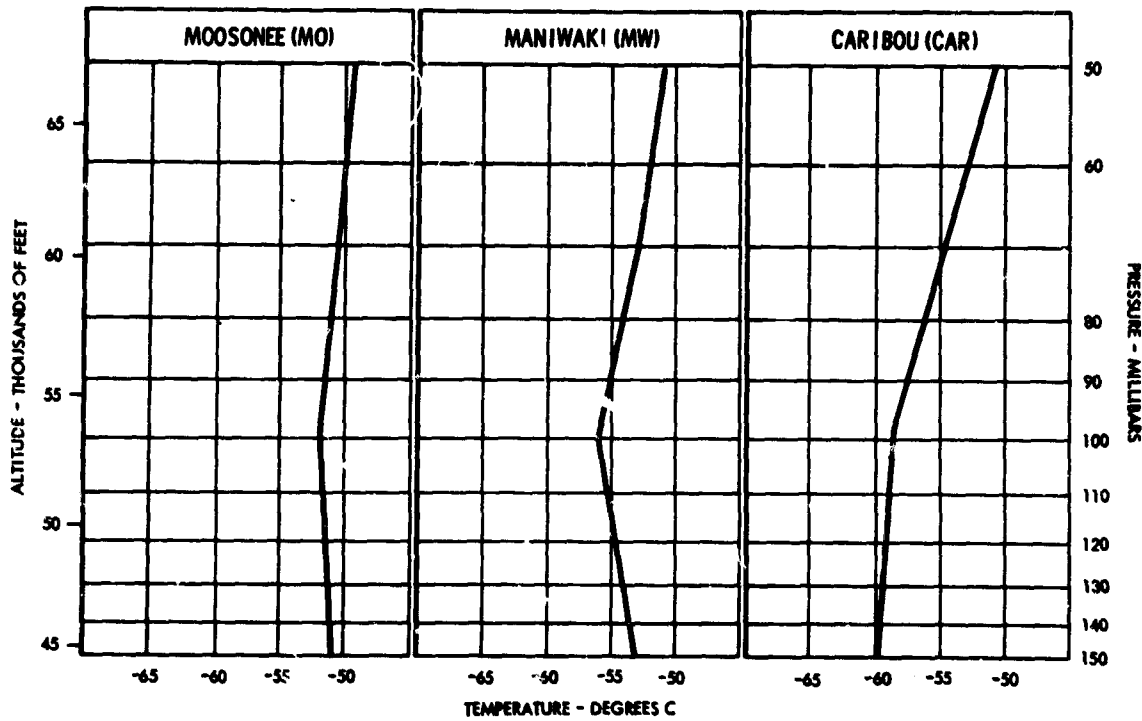Figure 118   Test 218 70 MB Constant Pressure Chart (1200Z, 30 Jun 1967)

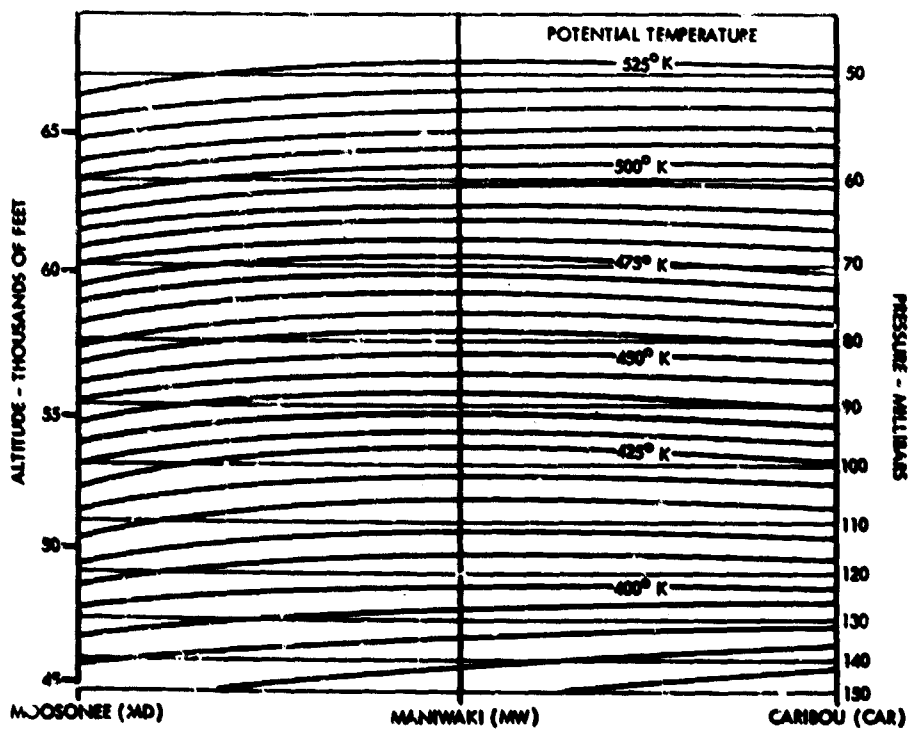Figure 119 Test 218 RAOB Charts (1200Z, 30 Jun 1967)

Figure 120 Test 218 Isentropic Cross Section (1200Z, 30 Jun 1967)

FLIGHT SUMMARY AND ANALYSIS - TEST 220, 6 JULY 1967

Test 220 was chosen as a special case because it provided an opportunity to study a long straight flight of 450 nautical miles in which almost continuous light to very light CAT was sampled.

After takeoff, the pilot climbed southeast toward Halifax, Nova Scotia. Climbing through 55,000 feet he felt a few ripples but received no significant turbulence until over Halifax. From that point to Albany, New York the turbulence was fairly continuous. Runs 2 through 7 of this leg were processed. After turning southeastward from Albany, the turbulence ended about halfway between Albany and Cape Cod, Massachusetts (Figure 121). Turning toward the north, light CAT was again encountered over Portland, Maine and near the same altitude as that flown through 50 minutes earlier. The turbulence ended abruptly after passing to the north of Portland.

Figure 122 shows that the flight occurred over a surface high pressure system. Also there was no convective activity and the National Meteorological Center neph-analysis indicated that the skies were generally clear to scattered. The position of the tropopause jetstream is also located on this chart.

A warm thermal trough over the northeastern states can be seen on the 70 mb temperature-wind analysis in Figure 123. Cyclonic curvature of the wind flow pattern is also evident in this same area. In Figure 124, at 1200Z, a well-defined depression is centered over Massachusetts, Portland, Maine, and Albany, New York where most of the turbulence was located. An additional feature of the 70 mb constant pressure surface that should be noted is the character of the waves at that level. As in tests 202, 264, and 266, the 300- to 400-mile stratospheric short wave is evident.

The RAOB charts in Figure 125 show well-defined but weak vertical temperature gradients between 150 and 50 mb over Portland (PWM) and Albany (ALB), and a very weak gradient over Buffalo (BUF). The gradient is largest between 49,000 and 53,000 feet over PWM, and between 50,000 and 57,000 feet over ALB. These altitudes correlate well with the level of turbulence actually recorded on runs 2 through 9.

The isentropic analysis (Figure 126) illustrates that weak baroclinic zones were present over ALB and PWM and that CAT was observed at a level where the isentropes were widely spaced. Factors of significance associated with the turbulence observed on this test are:

- The location of the jetstream, as indicated on Figure 122, is parallel to and just south of the flight track

- The axis of the warm thermal trough and pressure trough at the 70 mb level is centered between ALB and PWM near the area of the most CAT activity

- The short wave characteristic of the 70 mb constant pressure surface, as shown by Figures 123 and 124.

- Small vertical temperature gradients as indicated in the RAOB analysis (Figure 125).

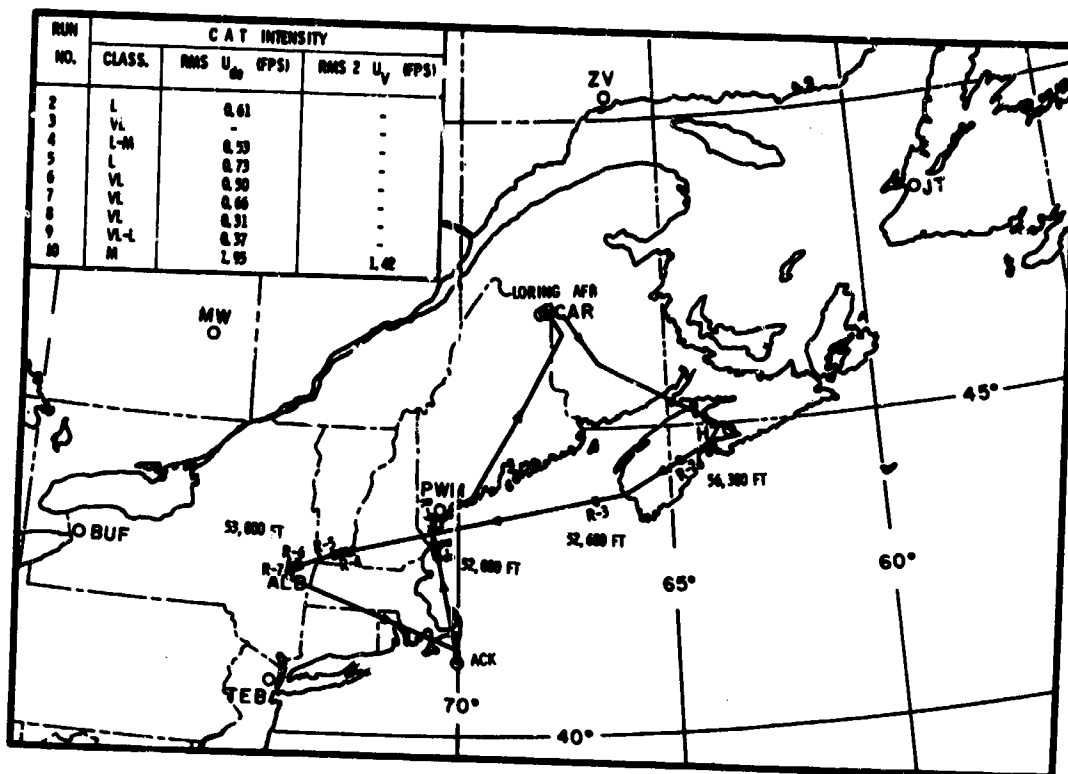- Widely space isentropes at turbulence altitude as indicated in Figure 126.

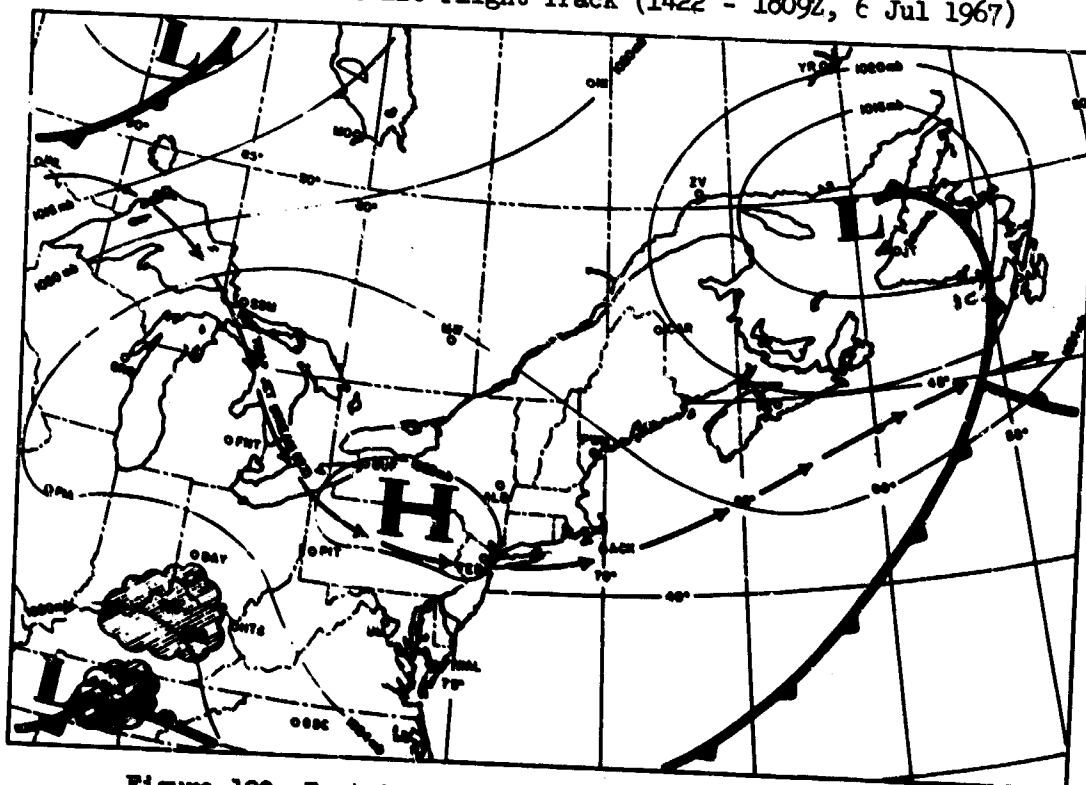Figure 121 Test 220 Flight Track (1422 - 1809Z, 6 Jul 1967)

Figure 122 Test 220 Surface Chart (1800Z, 6 Jul 1967)
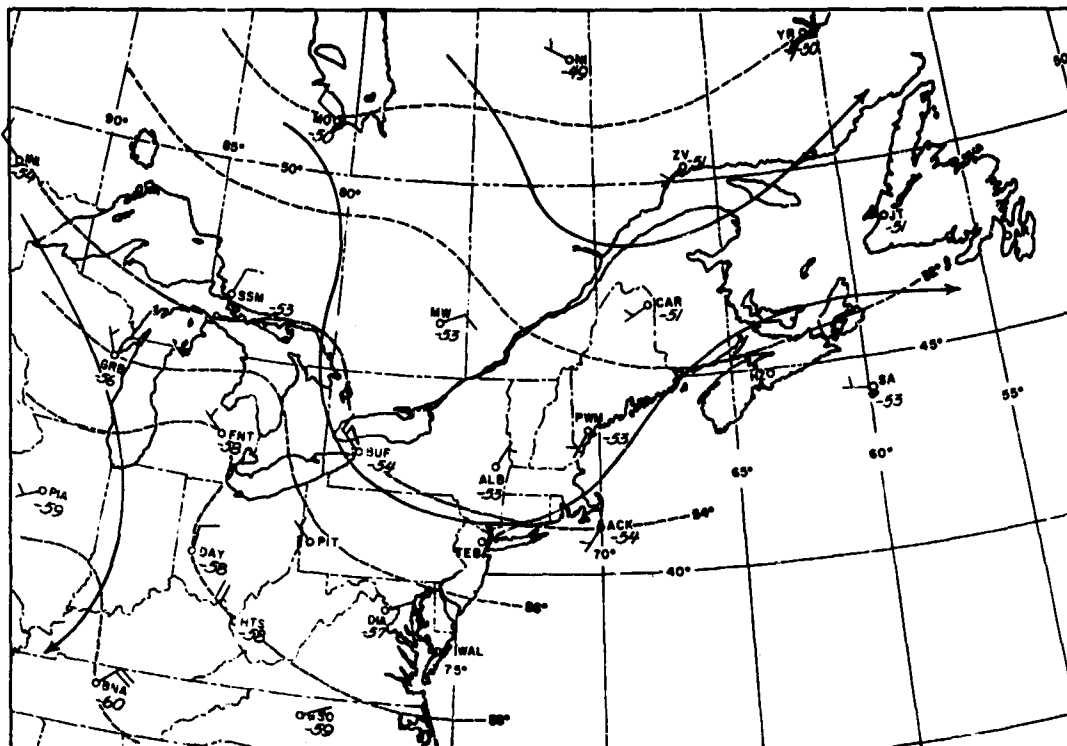and Radar Summary (1745Z, 6 Jul 1967)

Figure 123 Test 220 70 MB Temperatures and Winds Chart (1200Z, 6 Jul 1967)
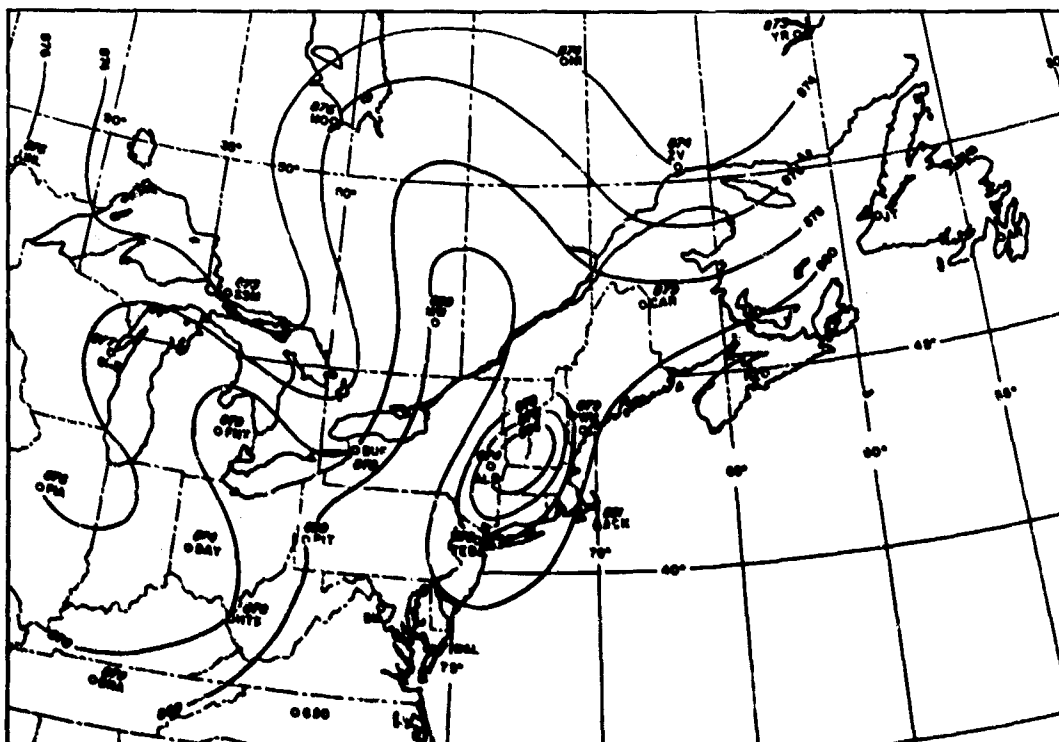

Figure 124 Test 220 70 MB Constant Pressure Chart (1200Z, 6 Jul 1967)
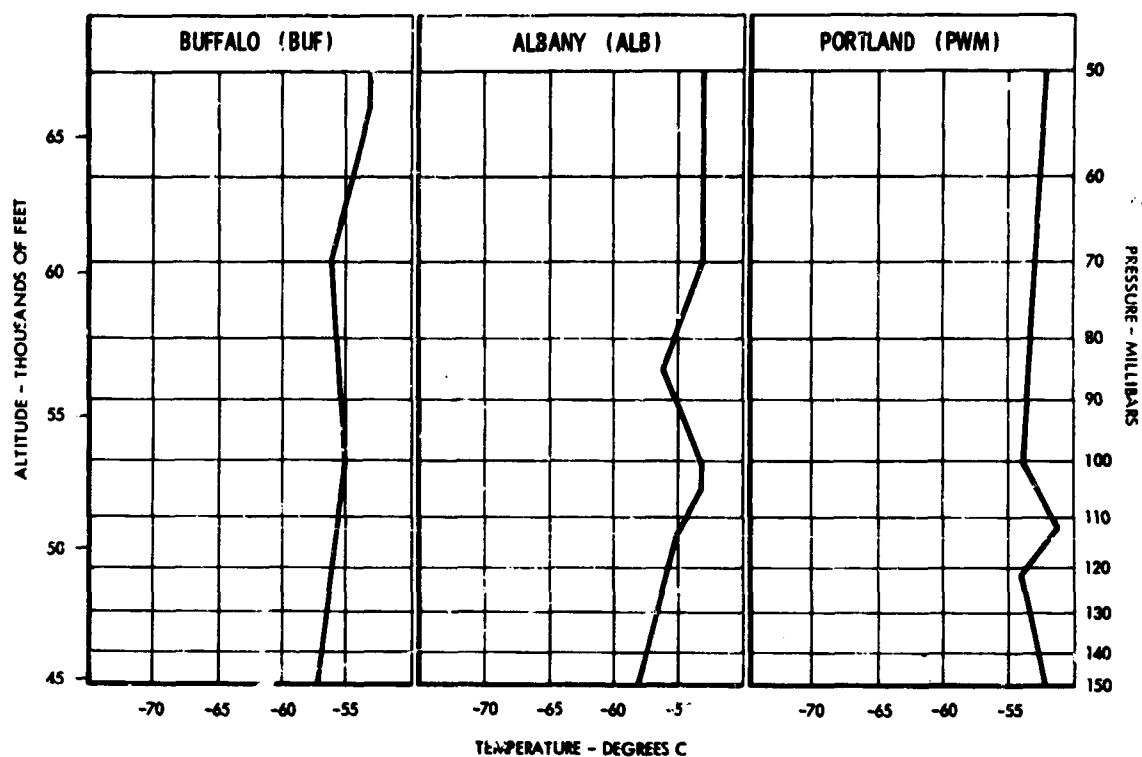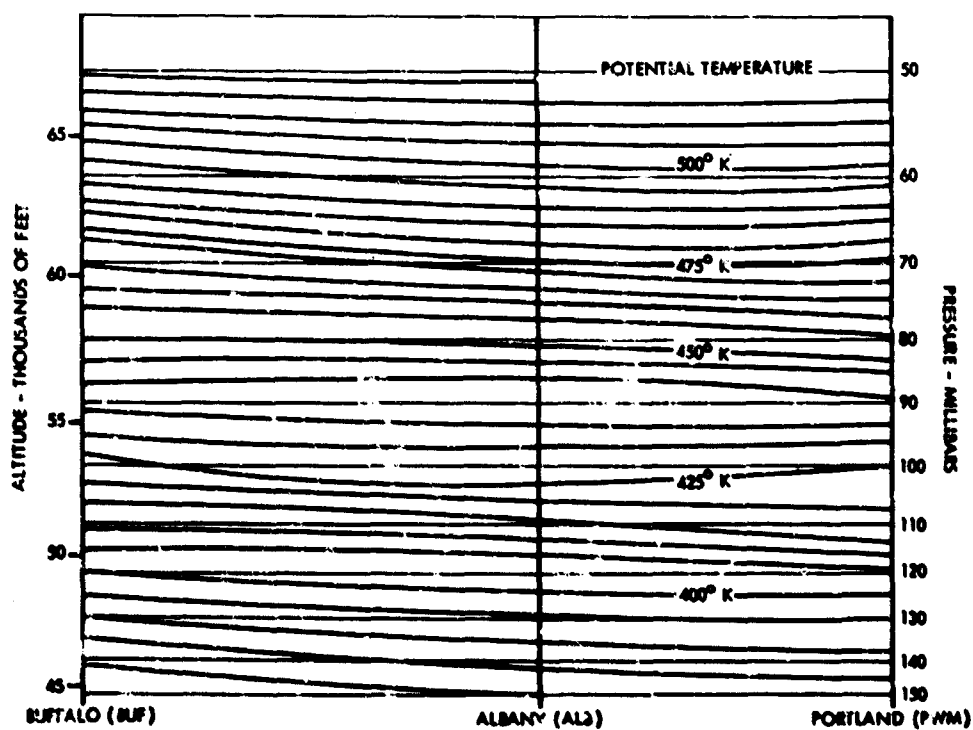
Figure 125   Test 220 RAOB Charts (1200Z, 6 Jul 1967)

Figure 126   Test 220 Isentropic Cross Section (1200Z, 6 Jul 1967)

FLIGHT SUMMARY AND ANALYSIS - TEST 233, 7 AUGUST 1967

The meteorological charts for this date indicated that conditions should be favorable for a flight over the Intertropical Convergence Zone (ITZ). The convergence zone was positioned approximately 150 nautical miles south of Panama, and early radar reports showed considerable activity along the zone.

Figure 127 shows the flight route and that the primary sampling area was along 5° -7°N latitude and south of Panama.

Figure 128 depicts the 0000Z, 8 August 1967 surface analysis from the WMO Regional Center, Miami, Florida (MIA). The RAREP shown on the analysis was that observed and plotted by the C-97 Air Sea Rescue aircraft that was accompanying the U-2 and flying at about 25,000 feet. Turbulence was sampled above the well defined dense cluster of thunderstorm activity outlined by the RAREP.

Runs 2 through 22 were processed and show that the pilot encountered light to moderate CAT.

Note that the meteorological data analyzed, except for the RAREP, was for the time 0000Z, approximately 6 hours after sampling time.

The pilot stated that as he reached 54,000 feet approximately 50 miles southwest of Albrook AFB he observed almost continuous very light CAT. He continued to experience the very light CAT until reaching the area near 5°N latitude at which time the turbulence increased, becoming light to moderate at 54,000 feet. He described one unusual cloud formation that appeared to be a layer of cirrus not attached to thunderstorms. The tops of the cirrus were 56,000 feet indicated altitude.

Near 6°N, 83°W, he noted that the free air temperature changed from -60°C at 52,000 feet to -50°C at 54,000 feet. The free air temperature gauge in the aircraft normally reads 10-20°C below the ambient air temperature.

Figure 129 shows the 70 mb 0000Z, 8 August 1967, analysis of horizontal temperature and wind streamlines. Notice the large temperature gradient between San Andres (MCSP) and Howard Air Force Base, Canal Zone (MBHO). Also visible is the well defined wave between 65°W and 85°W longitude. It appears significant that the steepest part of the wave surface, as indicated by the temperature gradient, is over the area of maximum thunderstorm development.

A trough in the 70 mb constant pressure surface is apparent in Figure 130. Notice that the axis of the pressure trough is aligned closely with the axis of the thermal ridge in Figure 129. Further, that if adjustment in time and space between flight and observation time (-6 hours) were made, the pressure trough and thermal ridge would be aligned closely with the area of maximum thunderstorm development along the ITZ.

Figures 129 and 131 show a very large temperature gradient that existed over San Andres MCSP at 0000Z. Notice the numerous gradient changes between 150 and 50 mb. There is a total ΔT through the layer of 54°C or 2.4°C/1000 feet. Between 45,000 and 51,000 feet the ΔT is 4.16°C/1000 feet. A vertical
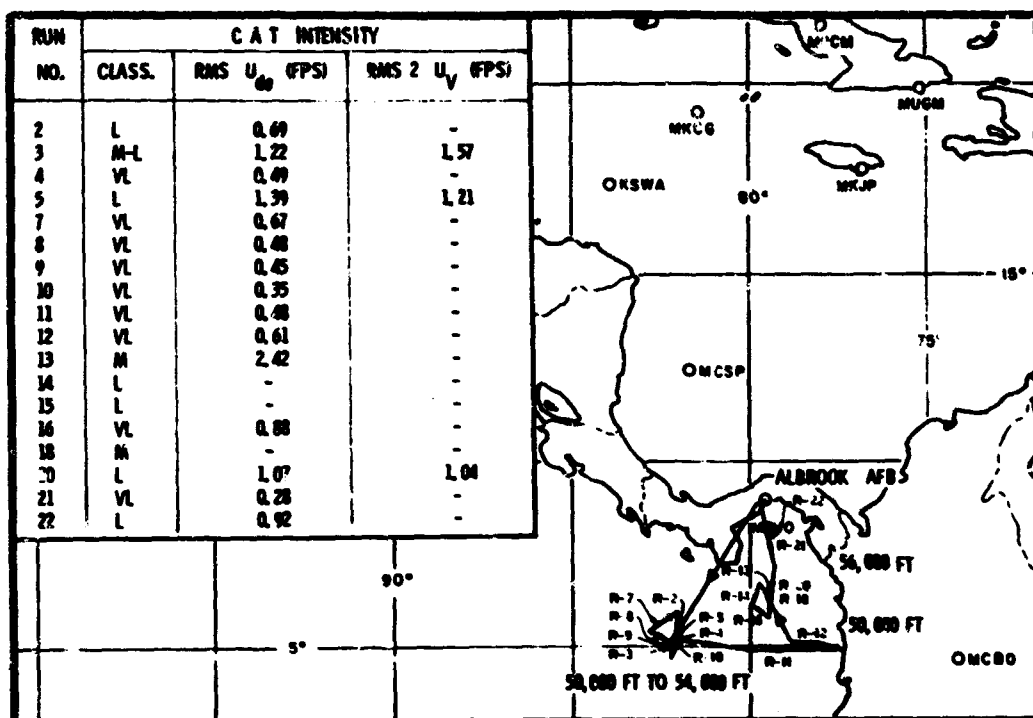
| RUN | C A T INTENSITY | | |
NO.	CLASS.	RMS U$_{G}$ (FPS)	RMS 2 U$_V$ (FPS)
2	L	0.69	-
3	M-L	1.22	1.57
4	VL	0.49	-
5	L	1.39	1.21
7	VL	0.67	-
8	VL	0.48	-
9	VL	0.45	-
10	VL	0.35	-
11	VL	0.48	-
12	VL	0.61	-
13	M	2.42	-
14	L	-	-
15	L	-	-
16	VL	0.88	-
18	M	-	-
20	L	1.07	1.04
21	VL	0.28	-
22	L	0.92	-

Figure 127 Test 233 Flight Track (1505 - 1905Z, 7 Aug 1967)

temperature gradient greater than 2.5°C/1000 feet is considered large and is usually associated with moderate or greater clear air turbulence. MCSP was not overflown on this mission.

Meteorologically significant features associated with the CAT sampled during this test are the following:

- The location of the ITZ as indicated on the surface analysis (Figure 128)

- The well defined wave pattern and the large temperature gradient evident in the horizontal temperature analysis

- The large vertical temperature gradient apparent in the MCSP RAOB indicates that turbulence was probably occurring in the general area six hours after sampling time

- The 70 mb pressure analysis which shows the wave apparently associated with that determined by the horizontal temperature analysis.
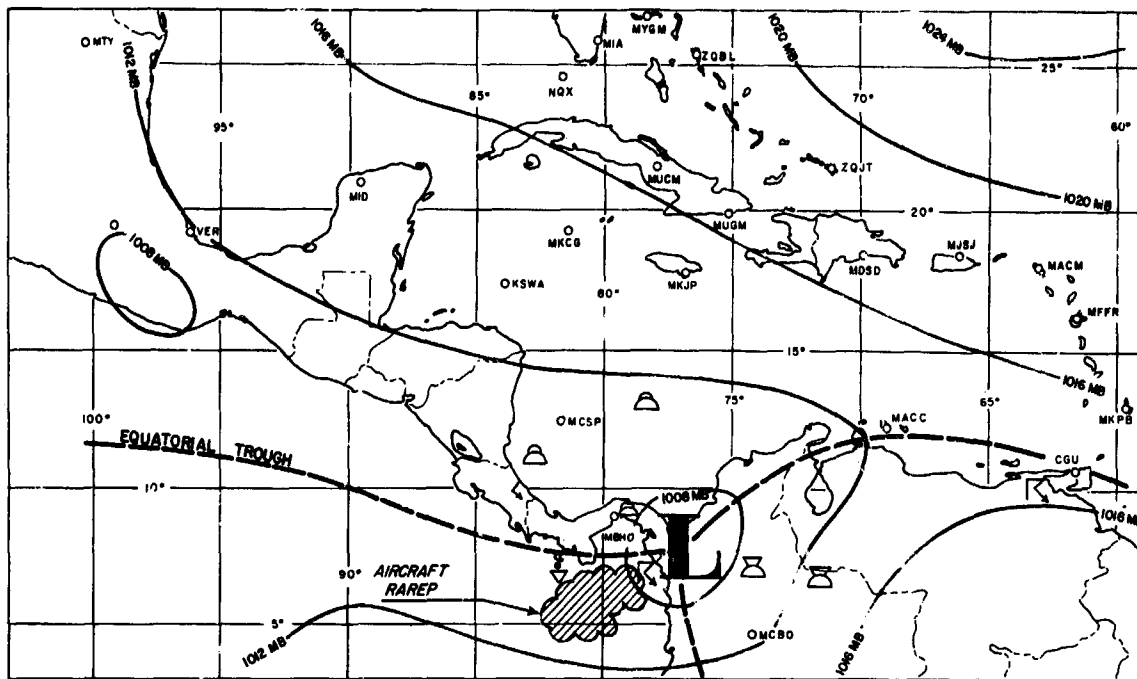
Figure 128   Test 233 Surface Chart (0000Z, 8 Aug 1967)
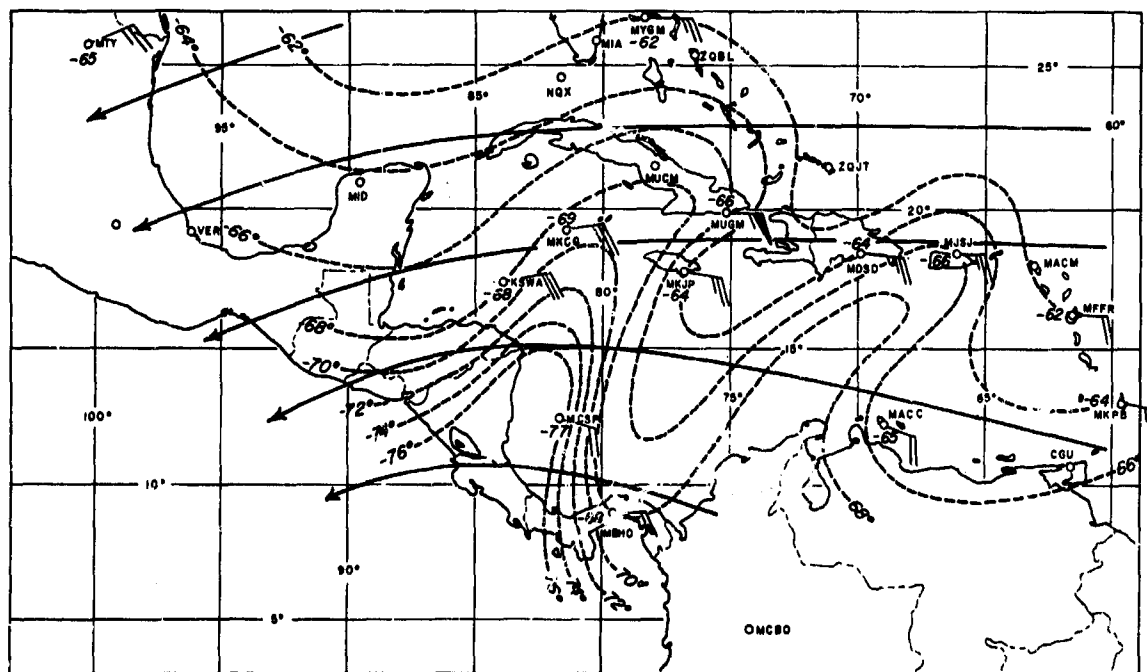and Radar Summary (0000Z, 8 Aug 1967)

Figure 129   Test 233 70 MB Temperatures and Winds Chart (0000Z, 7 Aug 1967)
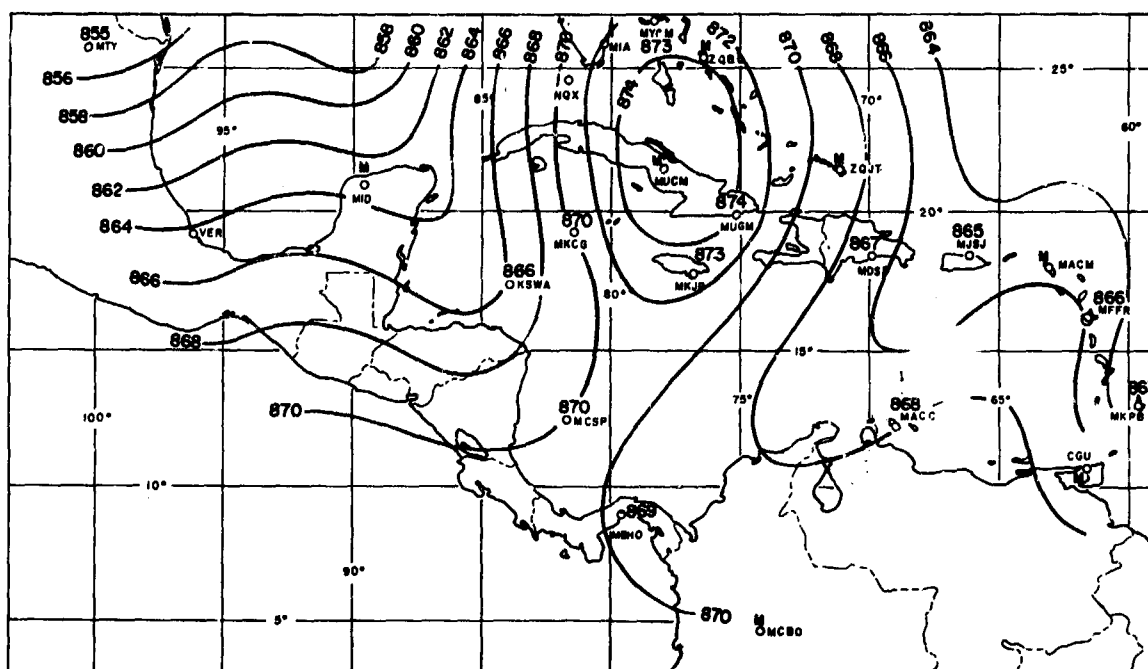
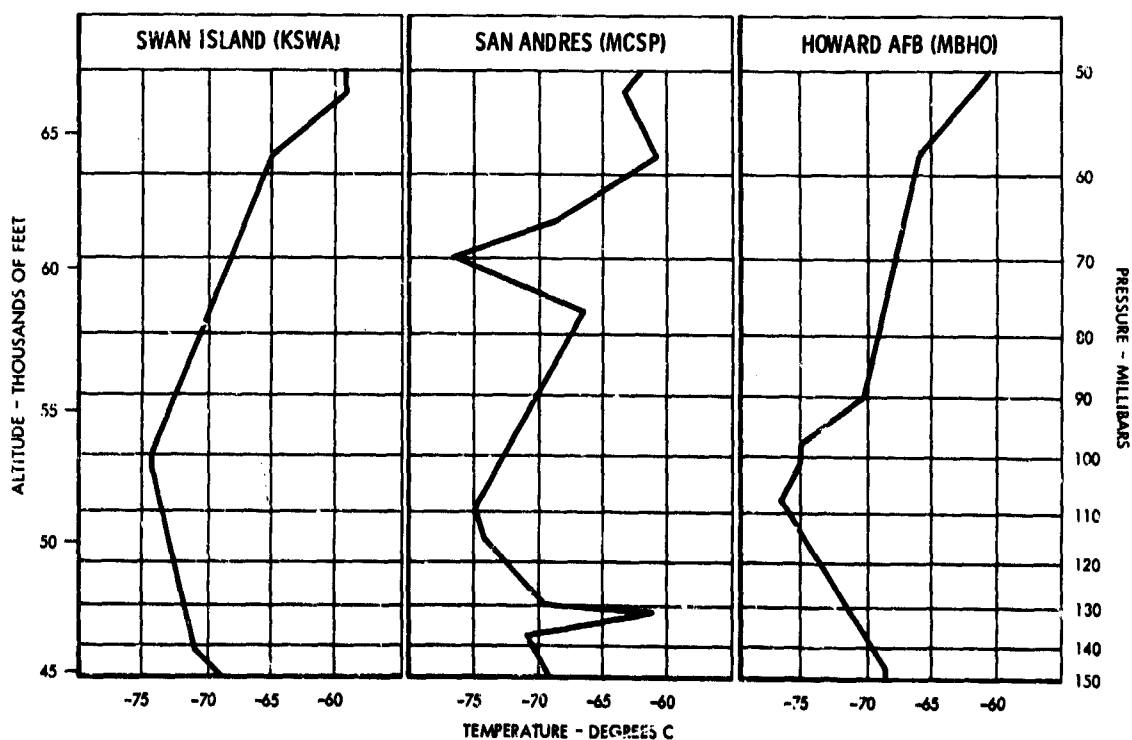Figure 130   Test 233 70 MB Constant Pressure Chart (0000Z, 7 Aug 1967)

Figure 131   Test 233 RAOB Charts (0000Z, 7 Aug 1967)

FLIGHT SUMMARY AND ANALYSIS - TEST 247, 20 SEPTEMBER 1967

The primary objective of HICAT operations out of Patrick AFB, Florida was, hopefully, to be able to investigate turbulence above a hurricane. From 11 September to 2 October 1967, two hurricanes moved to within operating range of the U-2--Hurricane Beulah, which moved across the Gulf of Mexico and entered the Texas coast on 20 Sep 1967, and Hurricane Doria which formed about 100 miles east of the Florida coast and moved north-eastward along the Atlantic seaboard.

This special case is primarily concerned with the flight over Hurricane Beulah. However, some comparisons will be made between Beulah and Doria. Figure 132 shows that the flight track for this test was via airways J-86 to Houston, Texas, then J-22 to Corpus Christi, and over Beulah between Corpus Christi and Brownsville, Texas.

The pilot approached the hurricane at an initial altitude of 65,000 feet and well above the tops of the clouds. There was no turbulence at that altitude. As he flew closer to the center of Beulah he began a descent to determine the height and other features of the cloud tops. As described by the pilot, the highest cloud tops were directly above the eye. The clouds were uniform in nature, solidly undercast, and relatively flat. The eye of the hurricane was visible as a dark circle embedded in the dense cirrus. The altitude of the cloud tops over the eye was 54,000 feet MSL. Slightly beyond the periphery of the hurricane's eye, the height of the cloud tops dropped sharply to 53,000 feet, and then more gradually to an average height of 49,000 feet within a 100-mile radius of the eye. The pilot stated further that convective type activity was protruding through the tops of the smooth cirrus north of the eye of the hurricane.

Figure 133 depicts three prominent meteorological features: the 1200Z surface analysis, the 1145Z radar summary, and the 1200Z position of the jetstream at the tropopause level. Most important of course is the position of Hurricane Beulah.

The upper level analyses vary some from those of previous cases because of the absence of data in the vicinity of the hurricane. Figure 134 shows the 100 mb analysis for 0000Z, 20 September 1967, approximately 16 hours prior to the time the aircraft was over Beulah.

At that time Brownsville, Texas (BRO) and Monterrey, Mexico (MTY) were still able to complete their RAOB. The anticyclonic wind flow is apparent at that level over BRO. Also of possible significance is the quite cold -80°C temperature over MTY. This cold temperature was most probably caused by cold ascending air near the center of the hurricane. Its effect would have been to create a cold dome of air over the hurricane and to create a large horizontal temperature gradient in the surrounding area. This is evident from the 9°C change in 155 nm between Abilene (ABI) and Del Rio, Texas (DRT).

The 100 mb analysis for 12 hours later (Figure 135) shows the 76°C isotherm to have remained in about the same position. Upper level observations over extreme southern Texas were not obtainable because of the location of Beulah.

General features of the 1200Z, 100 mb and 70 mb analyses (Figures 134, 135 and 136) that should be noted, although their full significance is not clearly understood, are:

- The symmetrical appearance of the stratospheric waves illustrated by the horizontal temperature analyses at the 100 mb and 70 mb level (Figures 134 through 136)

- The anticyclonic flow of the wind streamlines at the 100 mb level parallels precisely the path of the tropospheric jetstream (Figures 133 and 135)

- The well-defined anticyclonic flow at the 70 mb level (Figure 136) parallels the course the hurricane took subsequent to 1200Z, 20 September 1967

The nearest RAOB charts in time and space corresponding to the sampling time are those shown in Figure 137. Even though the observations were 15-16 hours prior to the time the U-2 was over Beulah, the cold air between the 120 mb and 90 mb level is quite apparent.

Meteorological features considered significant are:

- Very light CAT reported by the pilot at 53,000 feet as he crossed over the jetstream near Tampa, Florida (TPA)

- Pilot encountered light to moderate CAT over Hurricane Beulah and in the area of relatively cold air. An ambient temperature of -80°C was recorded by the aircraft instrumentation

- Turbulence was encountered over Hurricane Beulah but not over Doria

- Light CAT (Run 6) was encountered over an area of convective activity near Boothville, Louisiana (BVE) as indicated in the radar summary.
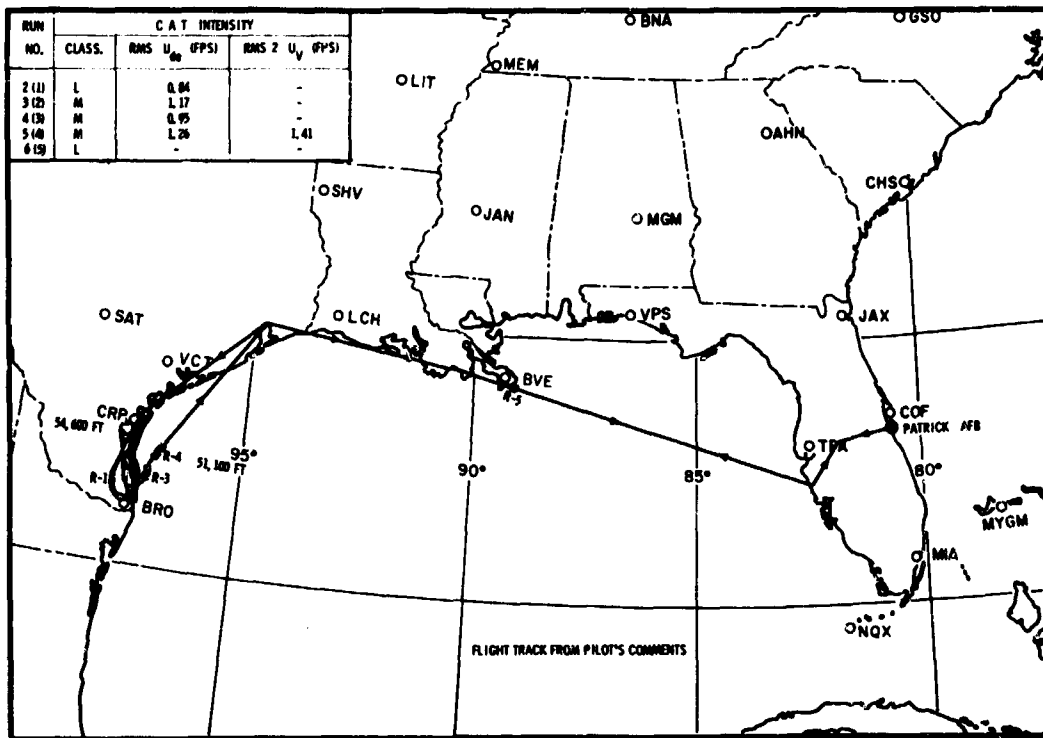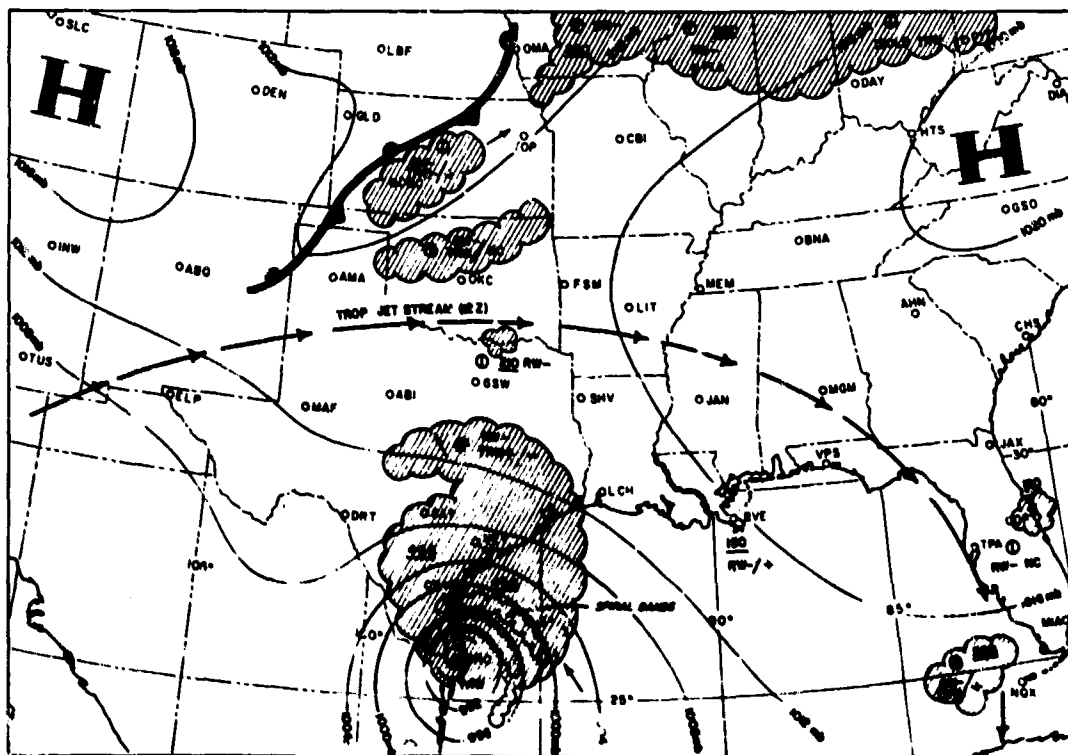
Figure 132   Test 247 Flight Track (1316 - 1929Z, 20 Sep 1967)

Figure 133   Test 247 Surface Chart (1200Z, 20 Sep 1967)
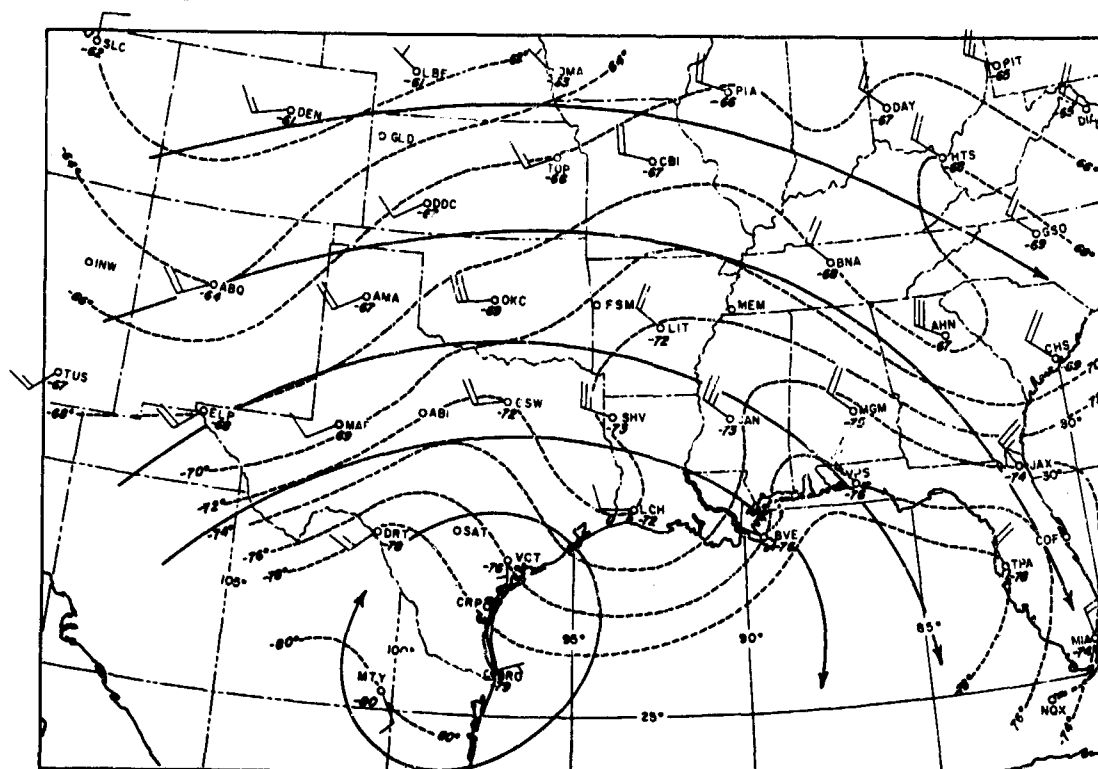and Radar Summary (1145Z, 20 Sep 1967)

Figure 134   Test 247 100 MB Temperatures and Winds Chart (0000Z, 20 Sep 1967)
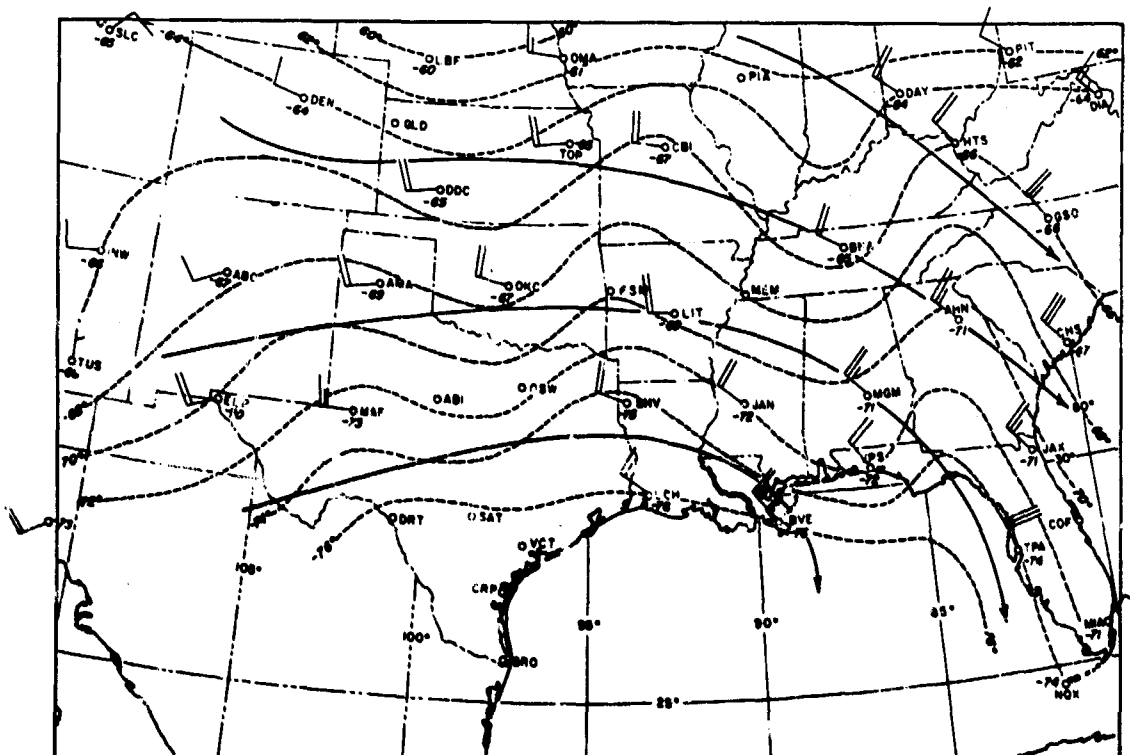

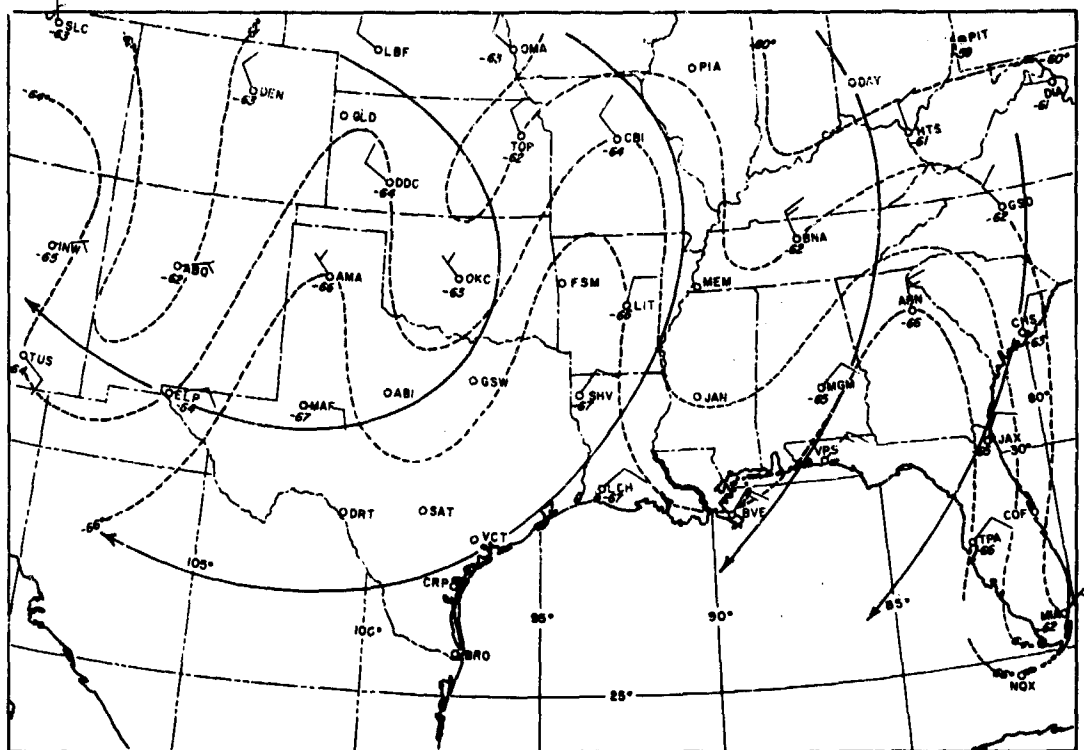Figure 135   Test 247 100 MB Temperatures and Winds Chart (1200Z, 20 Sep 1967)

Figure 136 Test 247 70 MB Temperatures and Winds Chart (1200Z, 20 Sep 1967)
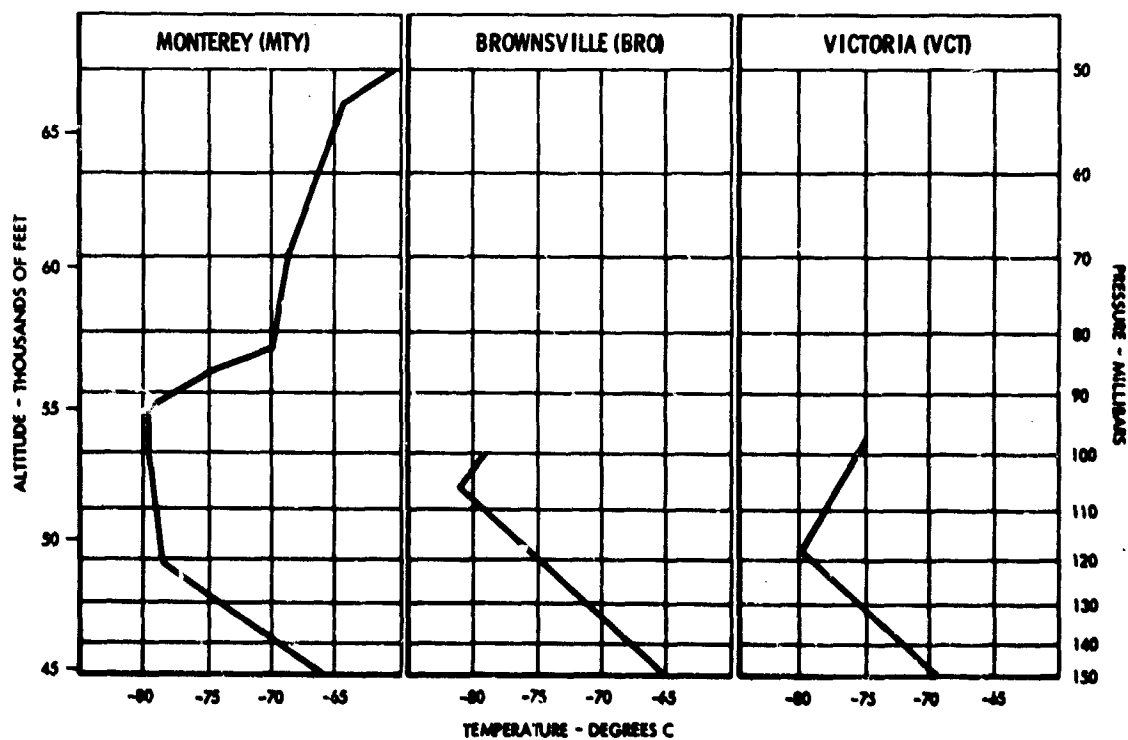

Figure 137 Test 247 RAOB Charts (0000Z, 20 Sep 1967)

251

FLIGHT SUMMARY AND ANALYSIS - TEST 264, 30 NOVEMBER 1967

Tests 264, 265, and 266 provide interesting examples of the occurrence of clear air turbulence over the western states region in a two day period from 30 November to 1 December, 1967.

As indicated by the flight track on Figure 138, the U-2 flew from Edwards Air Force Base, California (EDW) to Provo, Utah, Grand Junction, Colorado (GJT) and returned almost directly to Edwards. CAT was predicted to occur between Provo, Utah and Grand Junction, Colorado. A vertical cross section search pattern with 500 foot altitude intervals (See Figure 161) was to be flown if significant CAT was located. Moderate turbulence was located between Provo and Grand Junction (GJT), and the pilot completed the vertical search pattern utilizing GJT as a focal point.

Figure 139 depicts the 0000Z, 1 Dec 1967, surface chart with the tropopause jet stream overlayed. Map time is within 1 hr and 15 min to 0 hr and 15 min of the sampling time. The surface front and the jet stream were positioned almost directly beneath the observed turbulence.

Figure 140 shows the well-defined warm thermal trough at the 70 mb level situated along the western border of Nevada. Note the 70 mb wave pattern illustrated by the temperature analysis. It is unfortunate that the 0000Z, 1 Dec 1967, RAOB for GJT is missing for this case as one can only speculate as to the amount of horizontal temperature gradient between GJT and surrounding stations.

In reference to the time history of Run 16, some interesting observations concerning temperature are apparent. During a 20-second period that the aircraft was in moderate to severe turbulence at 61,000 - 61,500 feet, the temperature trace between 11 and 15 seconds shows there was a ΔT of about 7°C.

The major pressure trough, evident in Figure 141, positioned over the California-Nevada border corresponds closely in position to the thermal trough in Figure 140.

The credibility of the closed low at the 70 mb level centered over Great Salt Lake cannot be determined. If the observation of a 70 mb height of 18,180 meters is in fact accurate and the 18,320-meter isohypse accurately placed over GJT, this would imply an upslope of 140 meters in 150 nm between SLC and GJT. This is considered a steep slope for the 70 mb surface.

The RAOB charts for Yucca Flat, Nevada (UCC), Salt Lake City, Utah (SLC), and Denver, Colorado (DEN) are plotted to illustrate characteristics of a 150-50 mb vertical cross section of the sampled area (Figure 142). The vertical temperature gradient ($\Delta T/\Delta Z$) of these three stations is: UCC 1.9°C/1000 feet; SLC 1.27°C/1000 feet; and DEN 1.8°C/1000 feet. Compare these vertical temperature gradients with those of 0.18°C/1000 feet and, 0.36°C/1000 feet of MO and MW in test 202 where there was no turbulence. Figure 143 shows clearly the manner in which the isentropes pack and diverge in turbulent areas.

Synoptic features of the above analyses that are considered related to factors that produce CAT in the 150-50 mb range are the following:

- The position of the jetstream in relation to the location of the CAT (Figures 138 and 139)

- The evidence of wave motion as indicated by the 70 mb horizontal temperature pattern in Figure 140

- The steep slopes of the 70 mb pressure surface in the area where CAT was detected (Figure 141)

- The large vertical temperature gradient as shown on Figure 142

- The Baroclinic zones noted on the isentropic analysis (Figure 143).

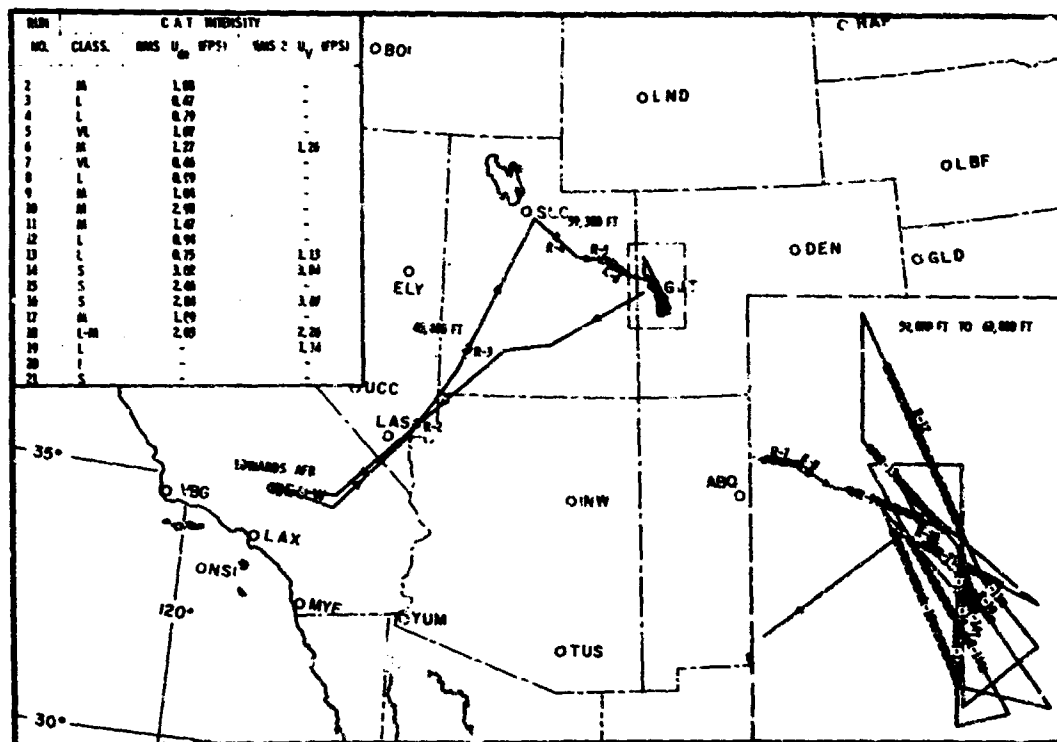Figure 138   Test 264 Flight Track (2108Z, 30 Nov 1967 - 0203Z, 1 Dec 1967)
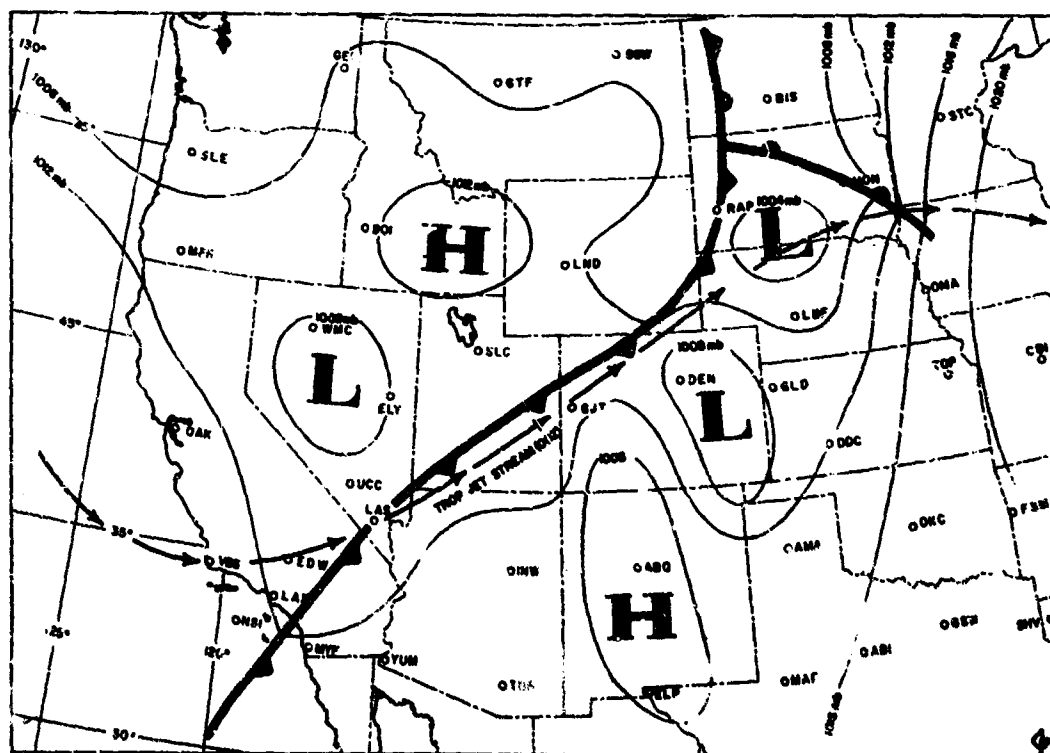

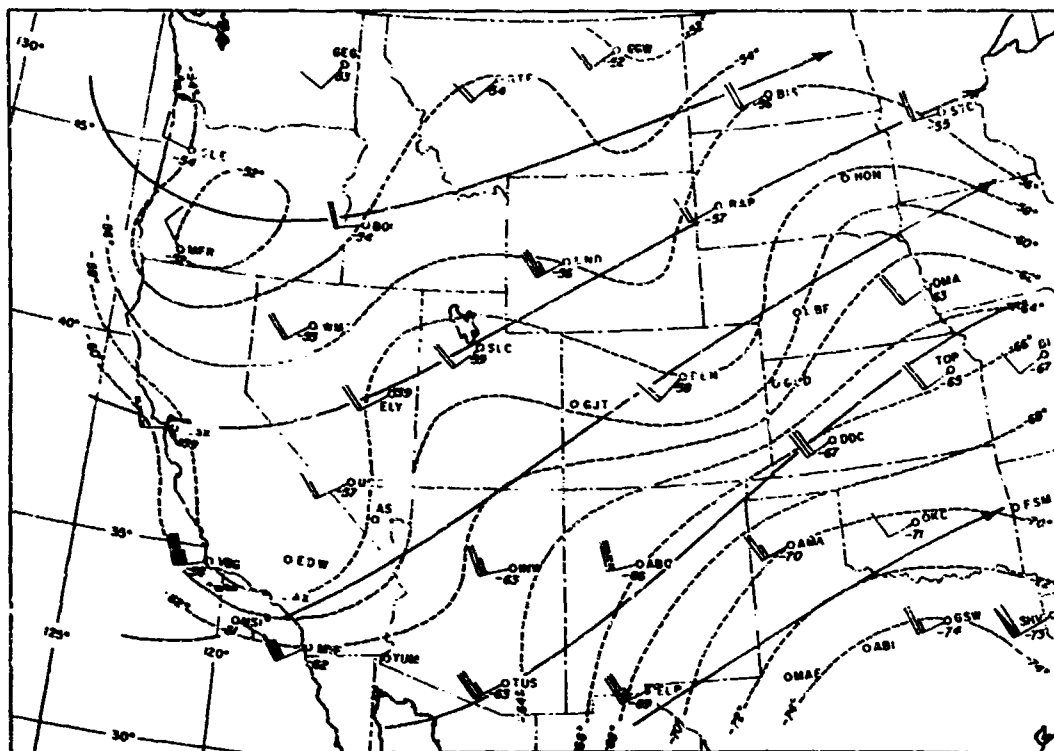Figure 139   Test 264 Surface Chart (0000Z, 1 Dec 1967)

255

Figure 140 Test 264 70 MB Temperatures and Winds Chart (0000Z, 1 Dec 1967)
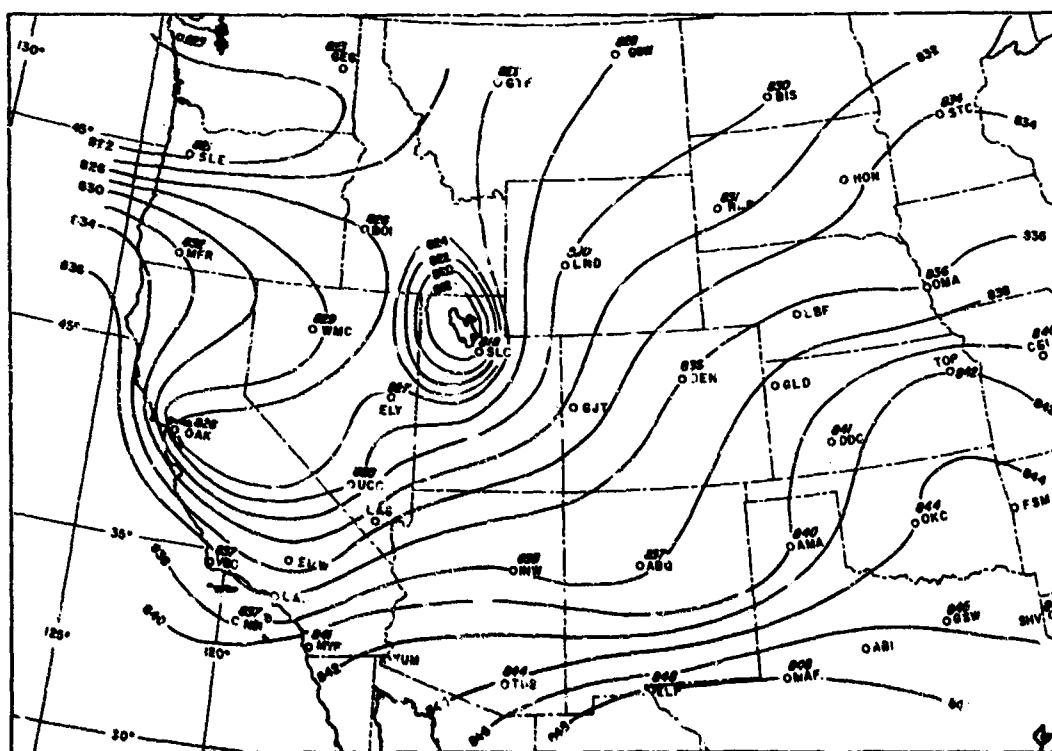

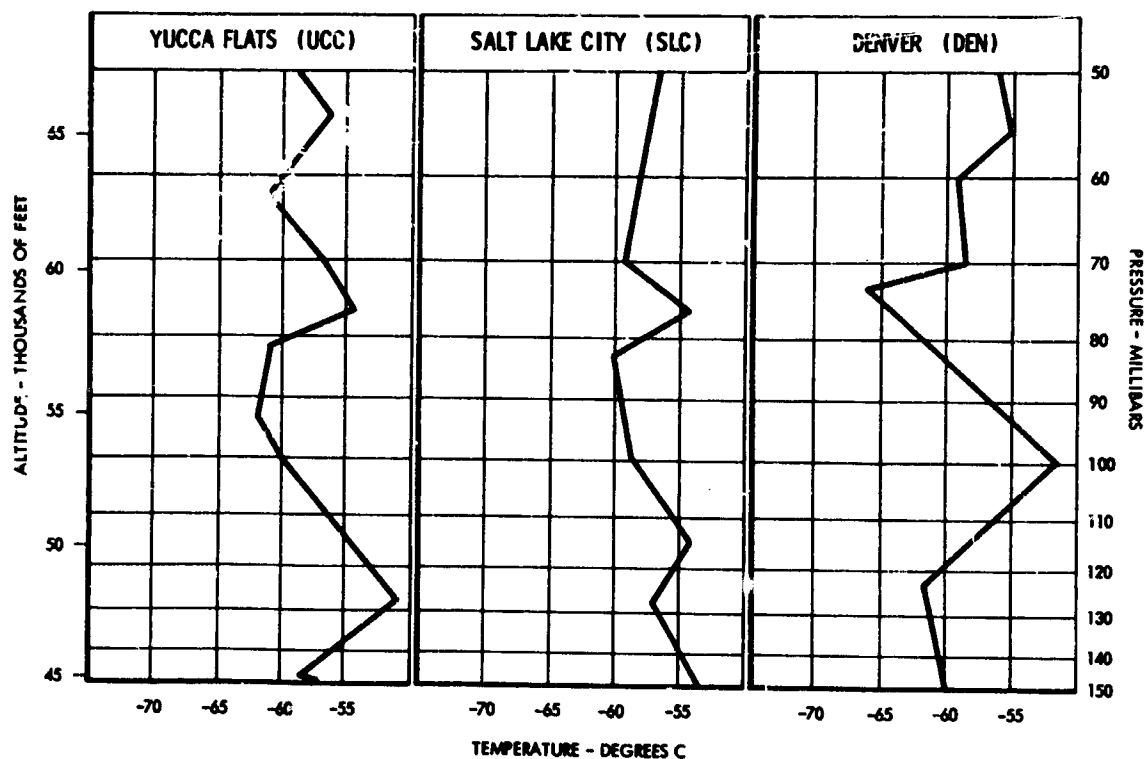Figure 141 Test 264 70 MB Constant Pressure Chart (0000Z, 1 Dec 1967)
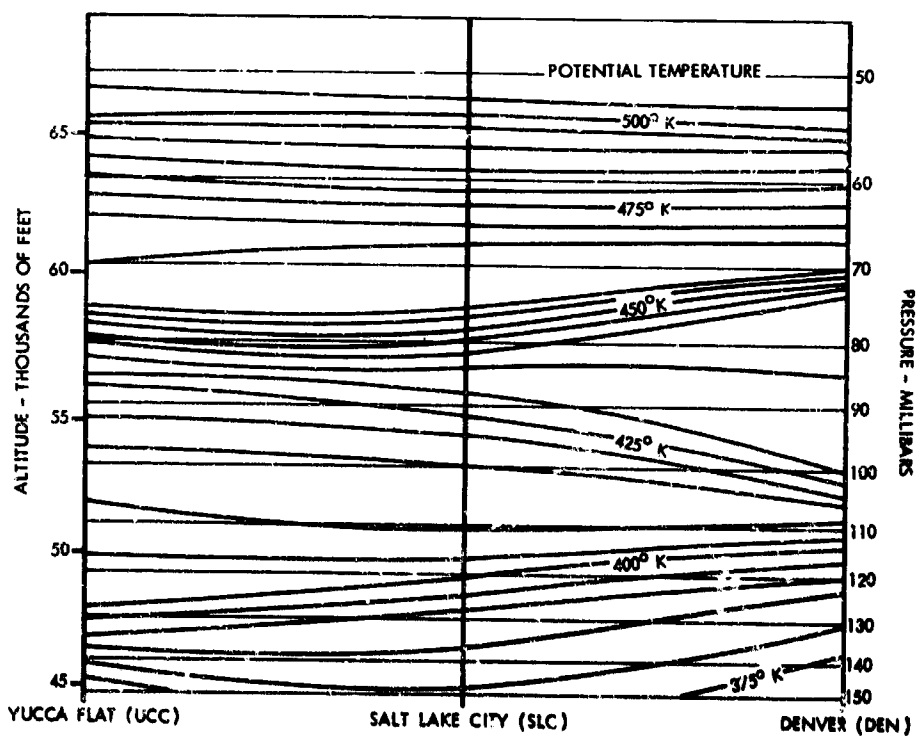
Figure 142 Test 264 RAOB Charts (0000Z, 1 Dec 1967)

Figure 143 Test 264 Isentropic Cross Section (0000Z, 1 Dec 1967)

FLIGHT SUMMARY AND ANALYSIS - TEST 265, 1 DECEMBER 1967

After a quick postflight analysis of Test 264 it was decided to turn the aircraft around and duplicate the flight plan for Test 265. The main objective was to attempt to determine what, if any, effects darkness might have on an area of moderate to severe CAT. The aircraft departed for the second time that day at 2048 MST (0448Z). Turbulence encountered in Test 265 can be seen in Figure 144. A subjective comparison of Figures 138 and 144 appears to indicate that the turbulence was more frequent and intense during the night flight than the day flight.

An interesting comment by the pilot during the debriefing referred to a very noticeable effect of two types of turbulence. First was the random chop of very short frequency excursions (1-2 seconds), and the other was a phugoid effect with a frequency of 40-60 seconds. The pilot stated he could feel the positive and negative accelerations associated with the longer wavelength turbulence. Inspection of corrected pressure altitude time histories for runs 14 through 22 illustrate these phenomena.

Figure 145 depicts the 1200Z, 1 December 1967, surface analysis with the corresponding tropopause jetstream overlayed. The 1200Z analyses used in this special case are approximately 6 hours after the time the U-2 was in the primary sampling area over GJT. Applying a six-hour time correction to Figure 145 one can see that the surface front and tropopause jetstream were just to the east of Grand Junction, Colorado (GJT). The skies were undercast over the entire route of flight, and surface weather conditions were stormy over the Southwestern States.

The 70 mb analysis in Figure 146 shows the well defined thermal troughs and ridges that were present over the southern Rocky Mountain region at 1200Z, 1 December 1967. The most obvious conclusion one can make is that waves of large amplitude were present in the sampled area. This is illustrated by the analysis of the 70 mb constant pressure chart in Figure 147. It should be observed that the wind flow pattern at the 70 mb level is slightly cyclonic in curvature and flows across both isotherms and isohypses.

The most appropriate available RAOB charts applicable to this case were Yucca Flat, Nevada (UCC), Salt Lake City, Utah (SLC), and Grand Junction, Colorado (GJT). Inspection of these observations for the 150 mb-50 mb level (Figure 148) shows that large vertical temperature gradients were present. Runs 3, 4, and 5 indicate that CAT was present near UCC at altitudes of 59,400 to 63,000 feet. Run 10 near SLC shows very light CAT at 59,700 feet. Summarizing information from Runs 12 through 29 it can be seen that light CAT was measured at altitudes 63,500 and 55,100 with the most persistent severe CAT at altitudes of 59,000 - 61,700 feet over GJT.

At UCC and GJT, Figure 149 illustrates the considerable packing and spreading of the isentropes in areas where turbulence was found. Over SLC isentropes are uniformly spread and only very light CAT was detected.

The significant meteorological features associated with the CAT observed in this case are the following:

- The position of the tropopause jetstream in relation to the location of the CAT (Figure 145).

- The large amplitude waves evident in analyses of the 70 mb thermal pattern and isohypses (Figures 146 and 147).

- The large vertical temperature gradients apparent in Figure 148.

- The baroclinicity apparent in the isentropic analysis (Figure 149).
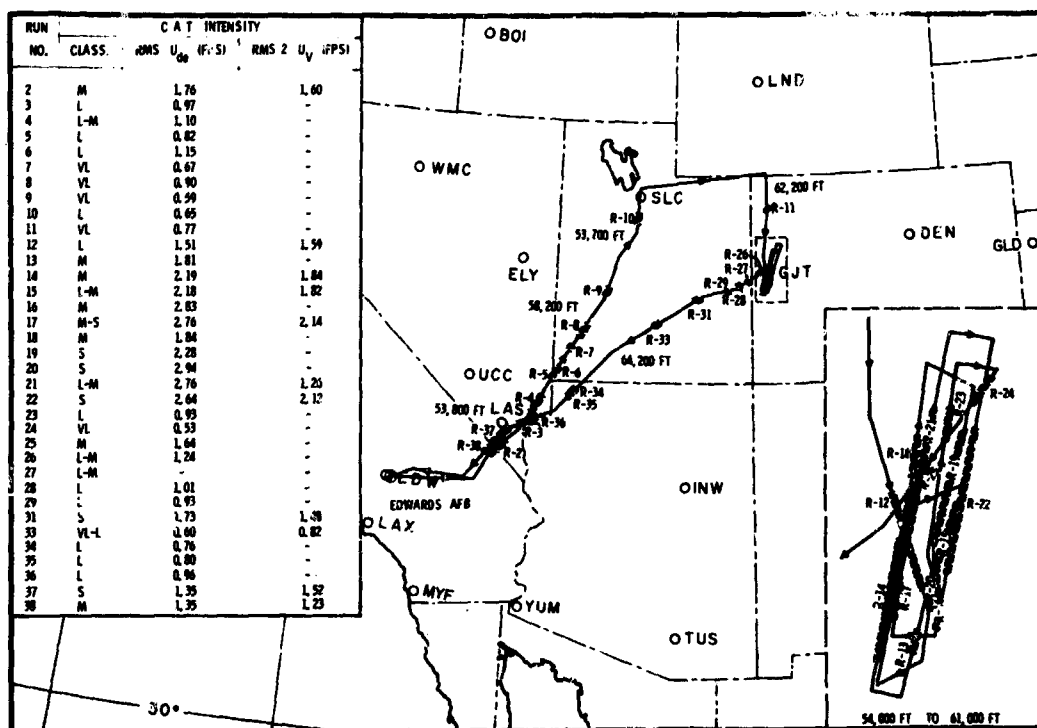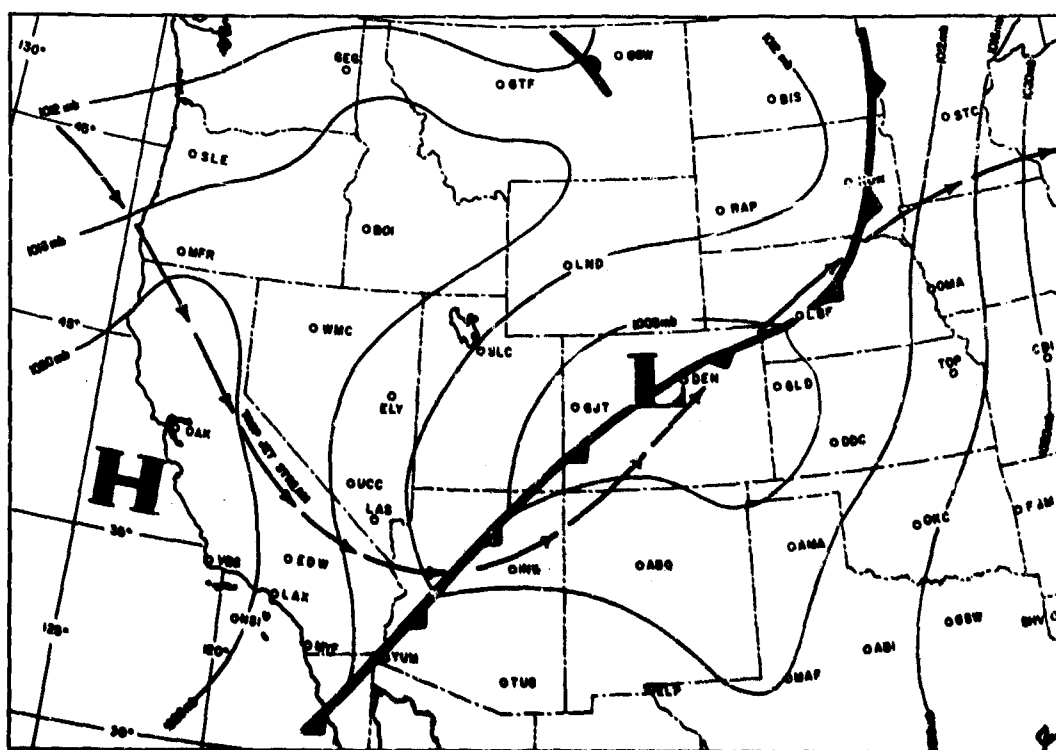
Figure 144   Test 265 Flight Track (0449 - 0914Z, 1 Dec 1967)

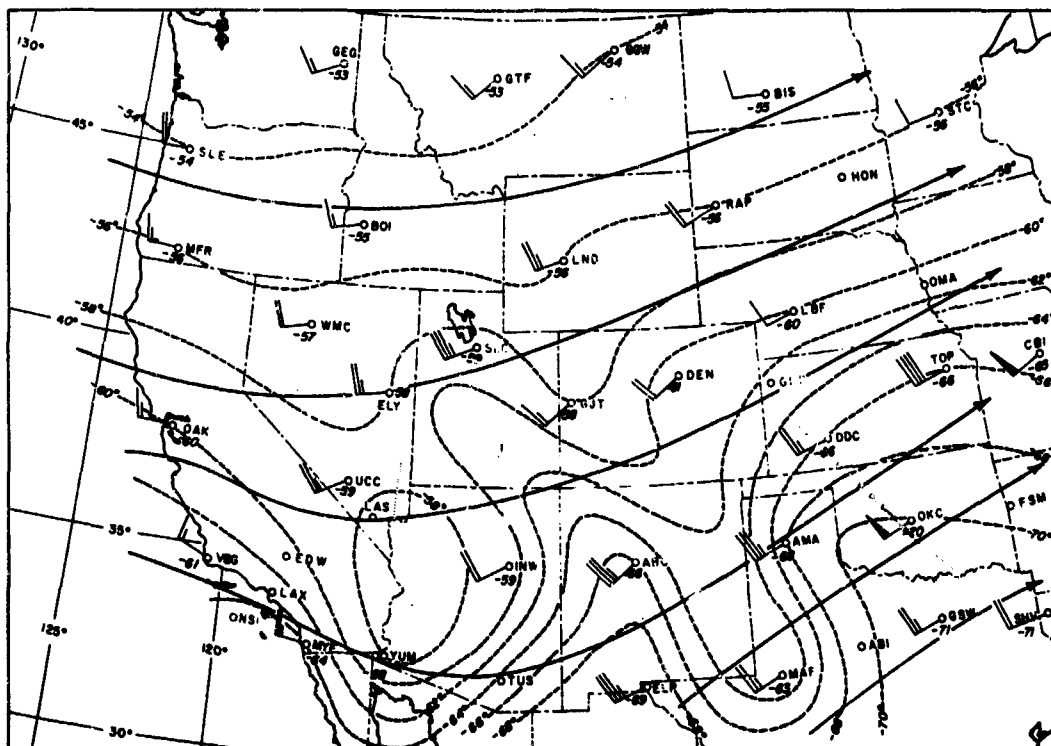Figure 145   Test 265 Surface Chart (1200Z, 1 Dec 1967)

Figure 146 Test 265 70 MB Temperatures and Winds Chart (1200Z, 1 Dec 1967)
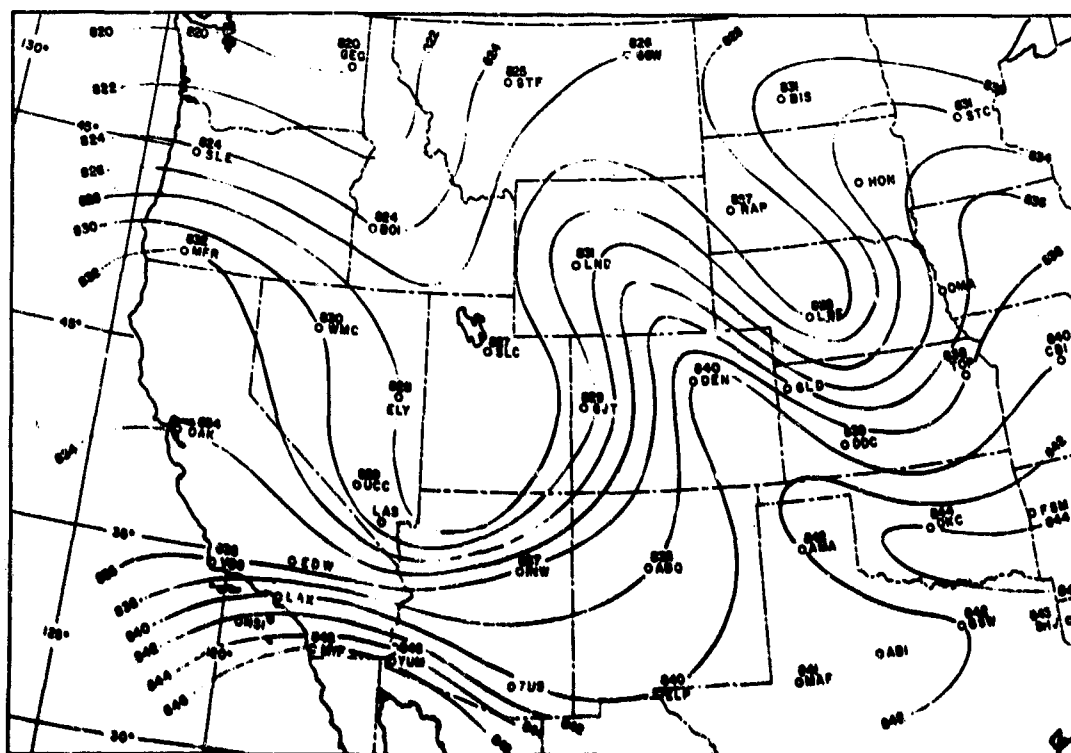

Figure 147 Test 265 70 MB Constant Pressure Chart (1200Z, 1 Dec 1967)
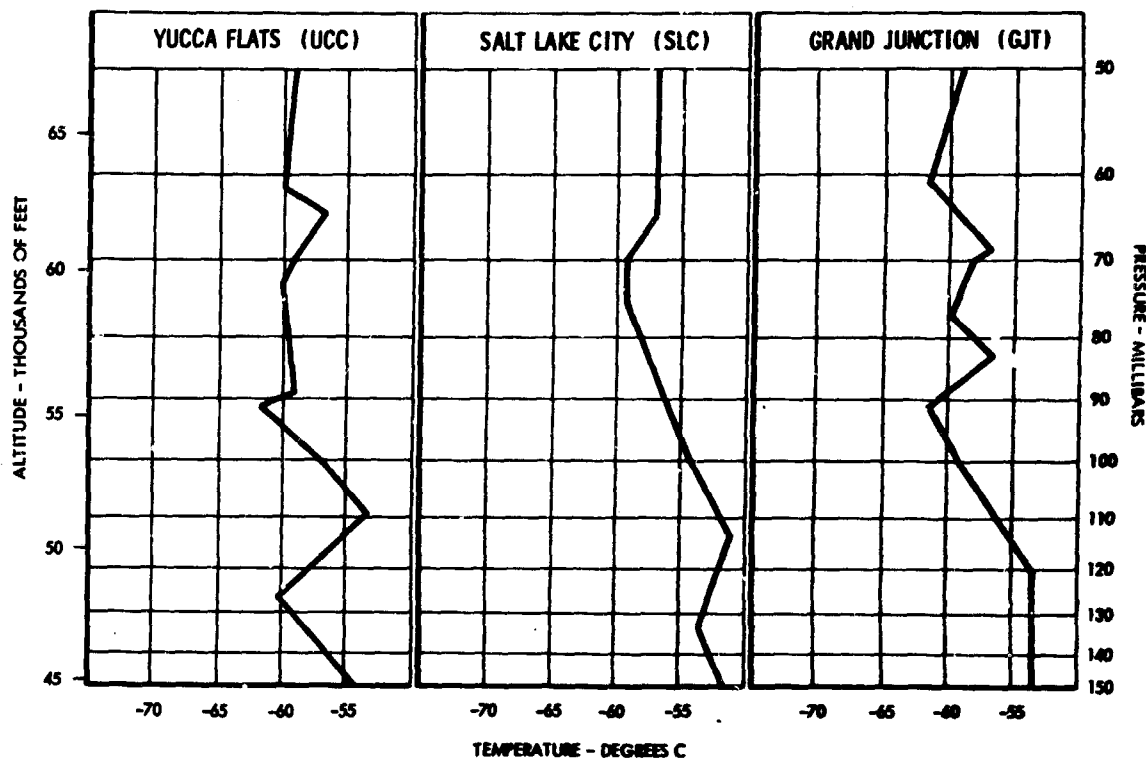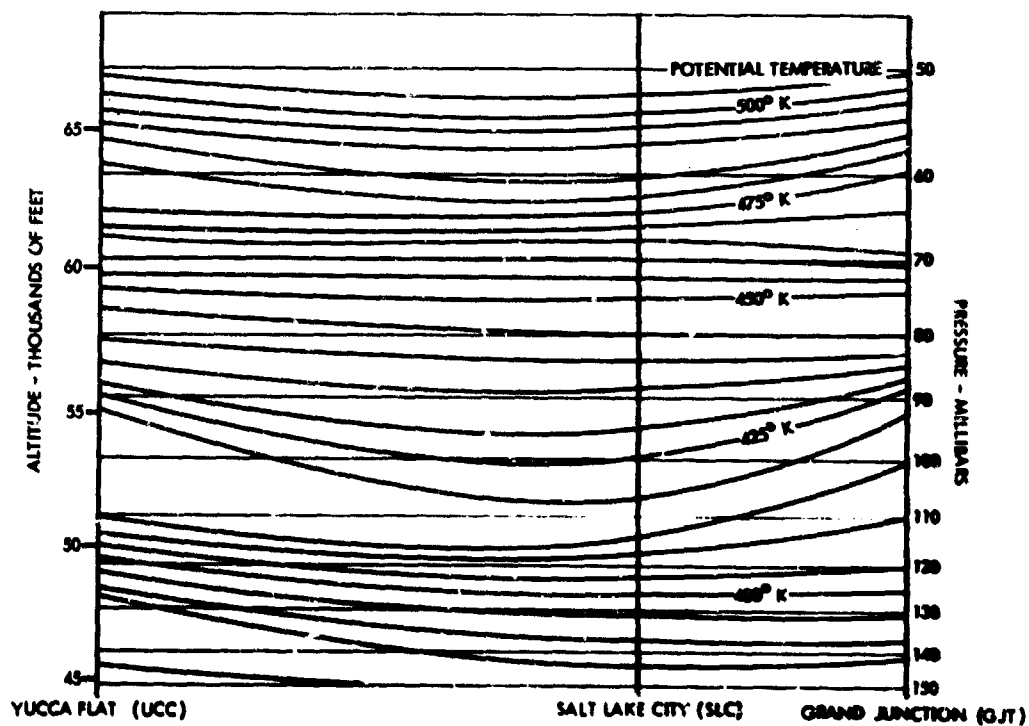
Figure 148 Test 265 RAOB Charts (1200Z, 1 Dec 1967)

Figure 149 Test 265 Isentropic Cross Section (1200Z, 1 Dec 1967)

Appendix IG

FLIGHT SUMMARY AND ANALYSIS - TEST 266, 1 DECEMBER 1967

On 1 December 1967, forecasts indicated that turbulent conditions which had existed over the Grand Junction, Colorado (GJT) area on 30 November 1967 should be present near Albuquerque, New Mexico (ABQ). This prognostication was based primarily on the position of the jetstream, horizontal and vertical temperature gradients and on the location of troughs and ridges at the 150-50 mb levels.

One principal objective was that the flight be over Albuquerque, New Mexico (ABQ) during the time the upper level observation was being made. In the event that turbulence was then located, the time correlation between meteorological and turbulent data would be ideal. The desired timing was achieved as planned and turbulence was encountered as predicted over Albuquerque. Thus, this test is considered especially valuable from the standpoint of compatibility of data.

Figure 150 shows that no CAT was observed in the Yucca Flat, Nevada (UCC) area. Light CAT was observed at 57,500 and 64,300 feet in the vicinity of Winslow, Arizona (INW), and light to severe CAT was encountered over Albuquerque, New Mexico (ABQ).

An interesting observation made by the pilot during the mission debriefing was that, in addition to the high frequency turbulence, there was an apparent vertical shear that caused one wing of the aircraft to drop sharply making control very difficult. He had not previously observed this effect during other missions when in severe clear air turbulence.

The 0000Z, 2 December 1967, surface analysis with the tropopause jetstream overlayed is illustrated by Figure 151. The jetstream was positioned over or very close to ABQ during the time the aircraft was in the area.

The 70 mb analysis of temperature and winds in Figure 152 presents a synoptic meteorological pattern that warrants detailed scrutiny. The outstandingly apparent character of the high amplitude short wave at the 70 mb level between Arizona and Oklahoma is evident from the horizontal temperature analysis. At the southernmost point of the warm thermal troughs over ABQ and OKC are temperature gradients of 10°C per 180 nm between ABQ and ELP, and 10°C per 150 nm between OKC and GSW. These are considered strong gradients.

The 70 mb observed winds over ABQ, AMA, OKC, ELP and GSW are an unusual contrast in direction and velocity. It is difficult, however, to discredit the accuracy of direction of the north-northwest wind over ABQ and the northeast wind over OKC because of other abnormal factors such as presence of the large amplitude wave, the large horizontal temperature gradient, and the severity of the turbulence observed over ABQ.

Figure 153 shows the analysis of the 70 mb constant pressure chart. The well-defined wave in the temperature pattern in Figure 154 is not so obvious in the pressure pattern. Of course, the isohypses could be drawn to correspond more closely to the wave evident in the temperature analysis; however, until more upper level observations are available this would not be meaningful.

The UCC RAOB chart in Figure 154 shows a very small vertical temperature gradient at the test levels (52,000-57,000 feet). No CAT was observed. Over INW and in flight levels 57,500 feet and 64,300 feet light CAT was present. A small vertical temperature gradient is apparent at 60,000-67,500 feet in that area. Over ABQ relatively large vertical temperature gradients were observed, and severe CAT was encountered for 50 minutes.

The isentropic analysis in Figure 155 shows the previously observed feature of evenly spaced isentropes in areas lacking CAT (UCC and INW) and unevenly spaced surfaces over the station (ABQ) where CAT is abundant.

Significant meteorological factors associated with CAT observed over ABQ are the following:

- Position of the jetstream over ABQ (Figure 151)

- The large amplitude wave evident in the 70 mb temperature-wind analysis (Figure 152)

- The large horizontal temperature gradient at 70 mb between ABQ and ELP (Figure 152)

- The unusual contrast between wind directions and velocities observed over ABQ and OKC and surrounding stations (Figure 152)

- The large vertical gradient of temperature over ABQ where CAT was abundant as opposed to the small gradients over UCC and INW where CAT was very light or not detected (Figure 154)

- Unevenly spaced isentropes over ABQ where CAT was abundant compared to evenly spaced isentropes over UCC and INW where CAT was very light or not detected (Figure 155).

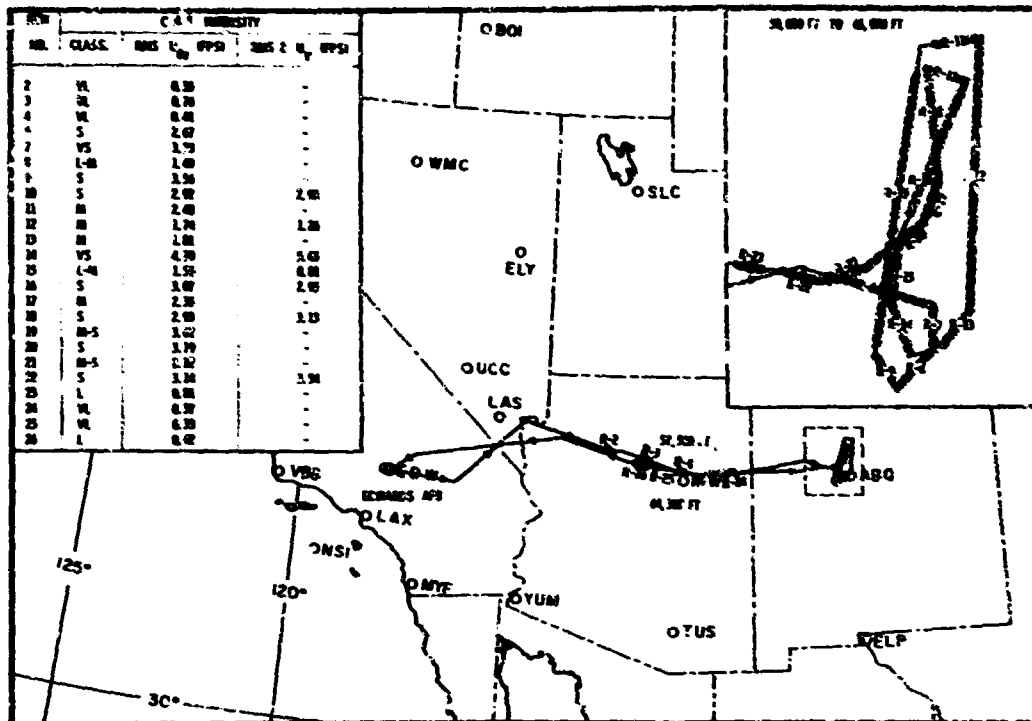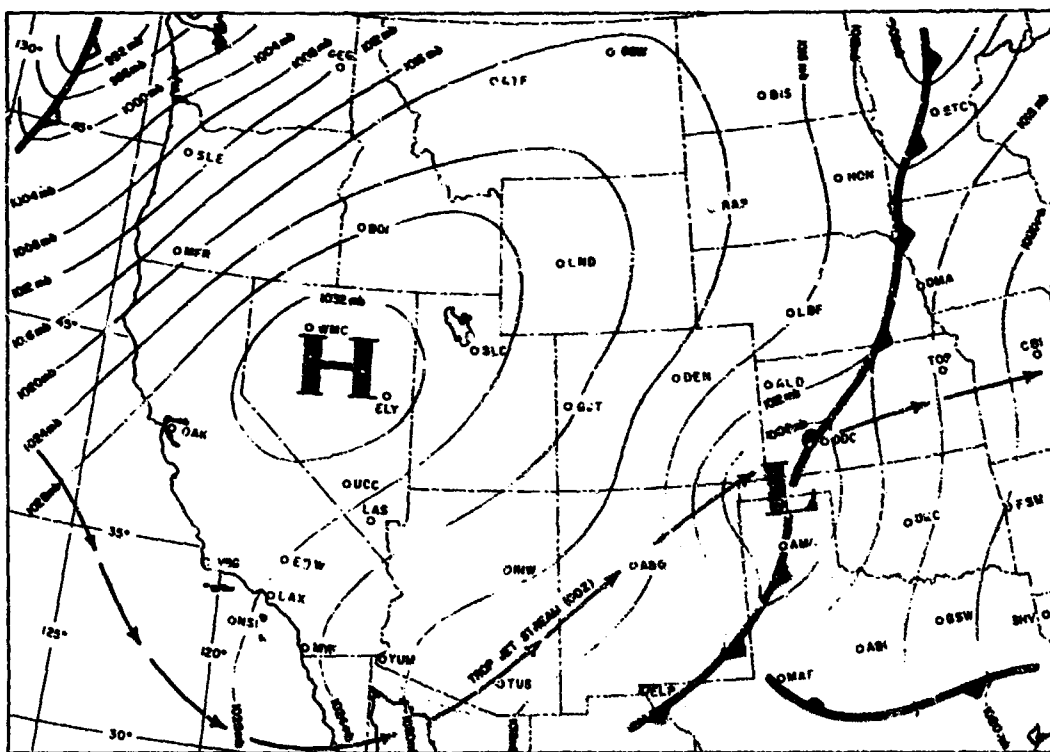Figure 150 Test 266 Flight Track (2137Z, 1 Dec 1967 - 0124Z, 2 Dec 1967)

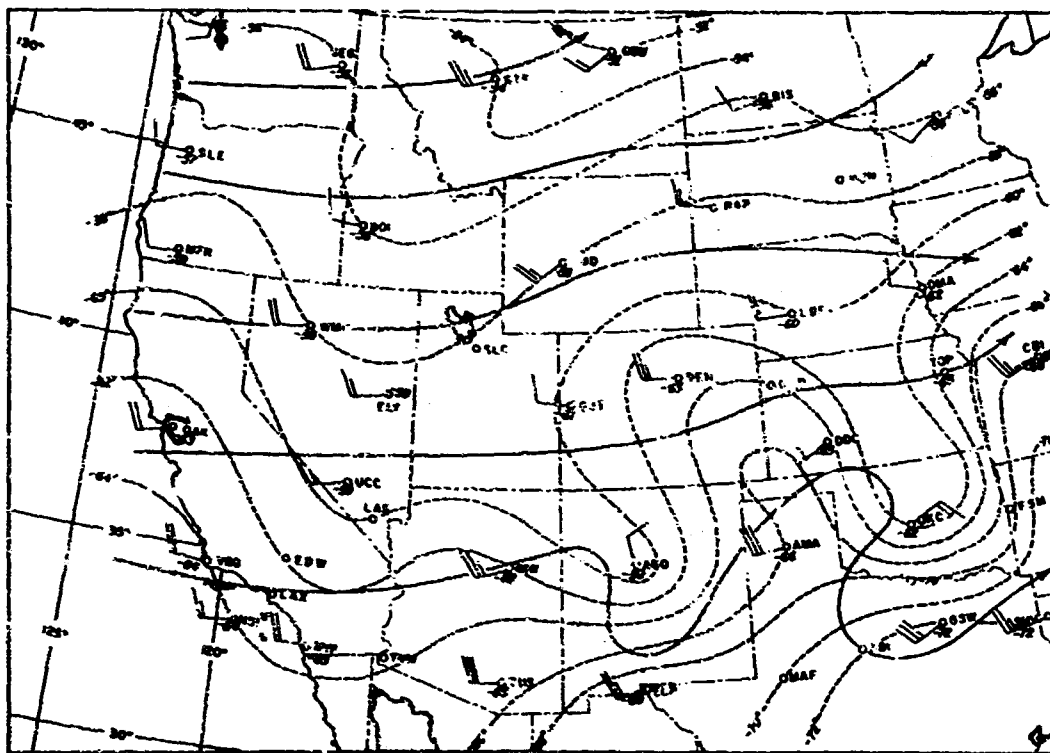Figure 151 Test 266 Surface Chart (0000Z, 2 Dec 1967)

Figure 152   Test 266 70 MB Temperatures and Winds Chart (0000Z, 2 Dec 1967)
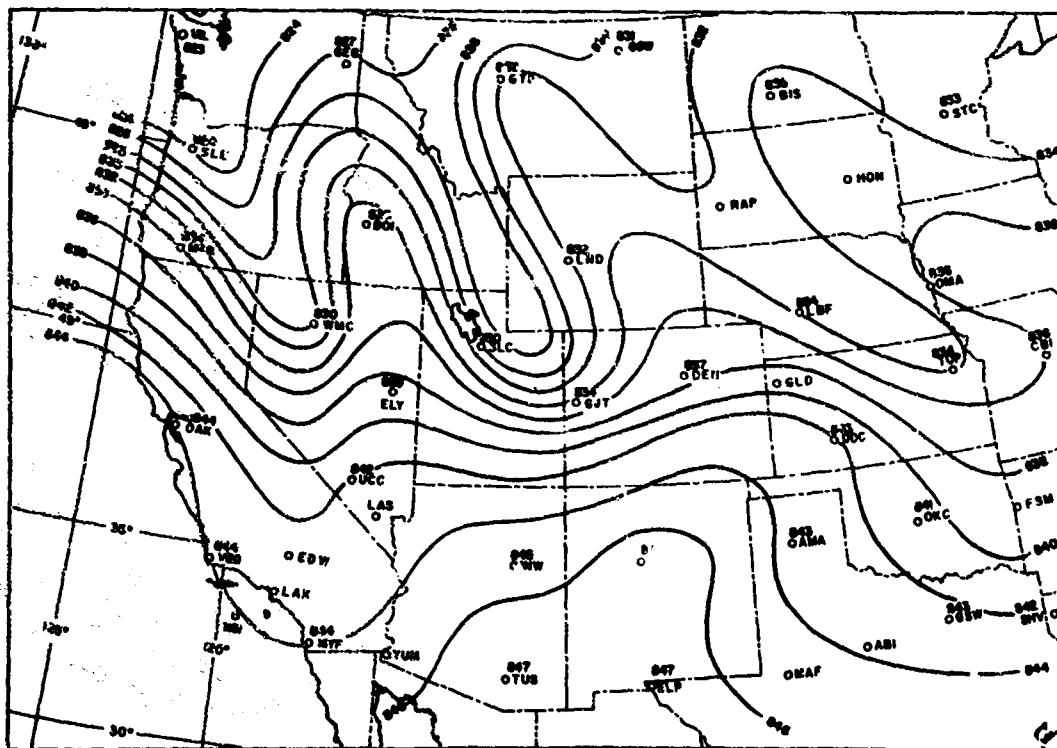

Figure 153   Test 266 70 MB Constant Pressure Chart (0000Z, 2 Dec 1967)
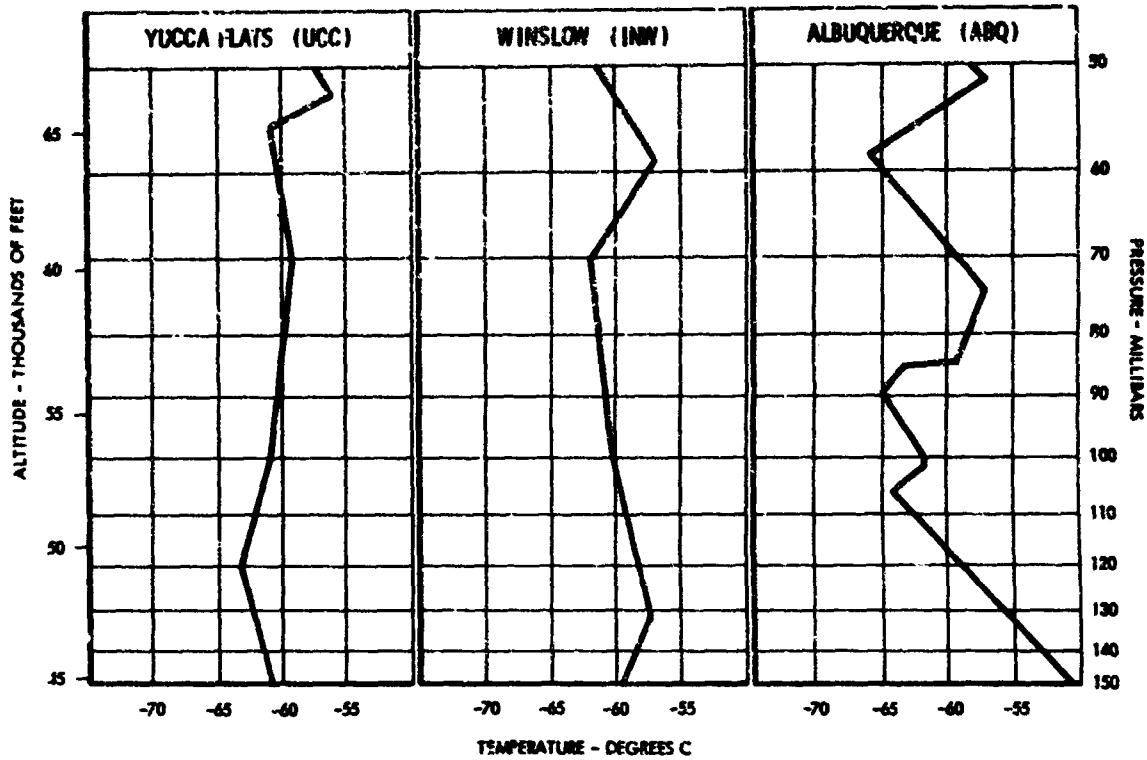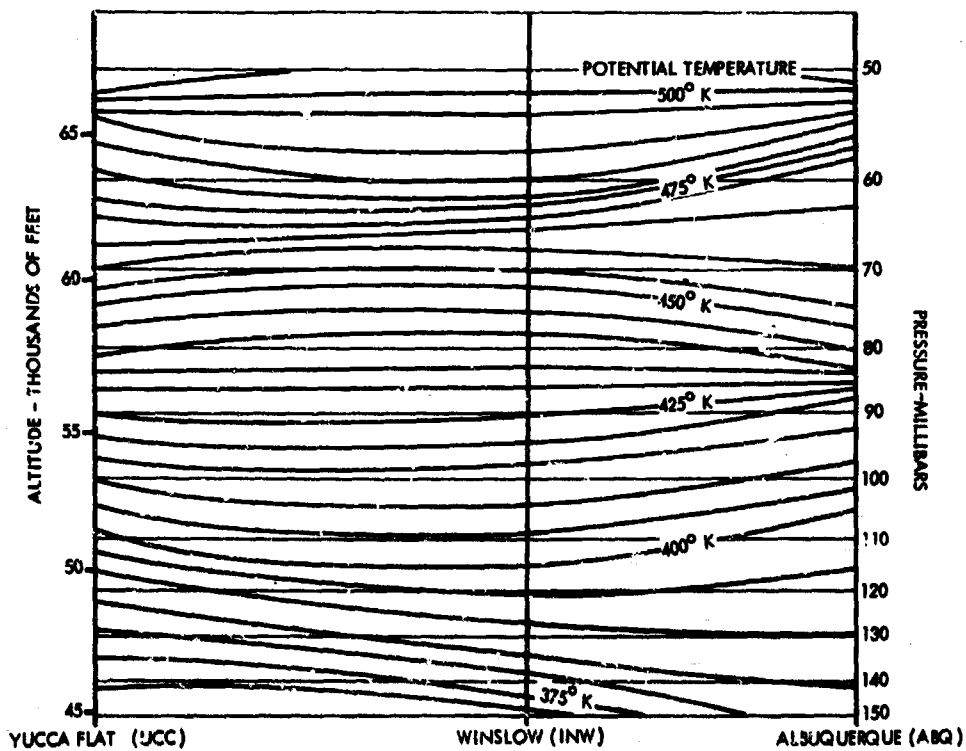
Figure 154   Test 266 RAOB Charts (0000Z, 2 Dec 1967)

Figure 155   Test 266 Isentropic Cross Section (0000Z, 2 Dec 1967)

Appendix IG

FLIGHT SUMMARY AND ANALYSIS - TEST 280, 15 FEBRUARY 1968

This test was planned in conjunction with the National Center for Atmospheric Research, Boulder, Colorado, to investigate turbulence associated with mountain waves over the eastern Rocky Mountain area in the vicinity of Boulder. Four aircraft participated in the experiment. Each aircraft was to fly a track between Kremmling, Colorado and Akron, Colorado at different altitudes according to the following plan:

HICAT U-2:   45,000 - 70,000 feet

CANADIAN T-33:   25,000 to 40,000 feet

ESSA B-57:   38,000 to 44,000 feet

NCAR QUEEN AIR: 18,000-26,000 feet

During the early morning period of 15 February 1968, meteorological conditions seemed favorable enough to schedule the test for that day. There was no jetstream in the area, but west winds prevailed at all levels from near the surface to the tropopause. Velocities were generally 49-90 knots. The 1200Z, 15 February 1968, Denver RAOB showed considerable vertical temperature gradient and evidence of wave action between 53,000 and 66,000 feet.

Participating aircraft were scheduled to begin their runs from over Kremmling, Colorado at 1330 MST (2030Z). Figure 156 shows the route followed by the HICAT aircraft.

Figure 157 shows the 0000Z, 16 February 1968, surface synoptic chart. The large arctic high pressure system can be seen centered near Lander, Wyoming. A quasi-stationary front lies along the southern periphery of the high and passes through Arizona and New Mexico. Skies were broken to overcast in the Denver area, and snow showers prevailed along the eastern slopes of the Colorado Rockies.

At the 70 mb level (Figure 158), well defined waves, as indicated by the temperature analysis, can be seen over the western half of the nation. The length of these waves averaged 375 nm with warm thermal troughs oriented north-south and centered over the OAK, ELY, DEN, and TOP areas. Winds at this level are from 270° in the sampled area and are normal to the orientation of the isotherms.

Analysis of the 70 mb constant pressure surface (Figure 159) also depicts waves analogous to those apparent in the temperature field. Ridges in the pressure field analysis correspond well to warm thermal troughs in the temperature analysis.

Figure 160 shows the vertical temperature structure over Grand Junction, Colorado (GJT), Granby, Colorado (Special RAOB), and Denver, Colorado (DEN). The Granby RAOB is near the middle of the run between Kremmling and Akron. Relatively large vertical temperature gradients are apparent between 150 mb and 50 mb over all three stations. Granby in particular has a $\Delta T/\Delta Z$ of 1.45°C/1000 feet. Compare this with the average $\Delta T/\Delta Z$ of 1.65°C/1000 feet for vertical temperature gradients observed in Test 264.

270

A vertical cross section of the turbulence encountered in this test is
illustrated by Figure 161. The altitudes shown for various runs may be con-
sidered an average for each pass. The degree of intensity of the CAT and the
location have been determined from examination of the time histories. The
turbulence varies from very light at 66,700 feet, to severe at 58,500 feet
and 55,500 feet, to light at 53,700 feet.

The turbulent layer in this case appears to be at least 13,000 feet thick.
Factors in this case considered to be significantly associated with meteoro-
logical conditions producing CAT are:

- The wide band of relative strong westerly winds that prevailed through
  a deep layer over the Rocky Mountain Region. (The pilot reported winds
  from 270° at 75 knots in the 53,700-55,500 feet layer.)

- The well defined waves of about 375 nm in length that were apparent
  from analyses as shown in Figures 158 and 159.

- The relatively large vertical temperature gradients present over
  Granby (Figure 160).

| RUN | CLASS. | C A T INTENSITY | |
NO.		RMS U_{dg} (FPS)	RMS 2 U_v (FPS)
3	M	2.79	2.90
5	M	0.43	-
6	M	1.99	2.64
10	M	2.16	2.50
11	M	1.51	1.81
12	L	1.69	1.92
13	M	1.24	1.52
14	M	0.88	1.10
15	M	3.12	-
16	M	2.02	2.48
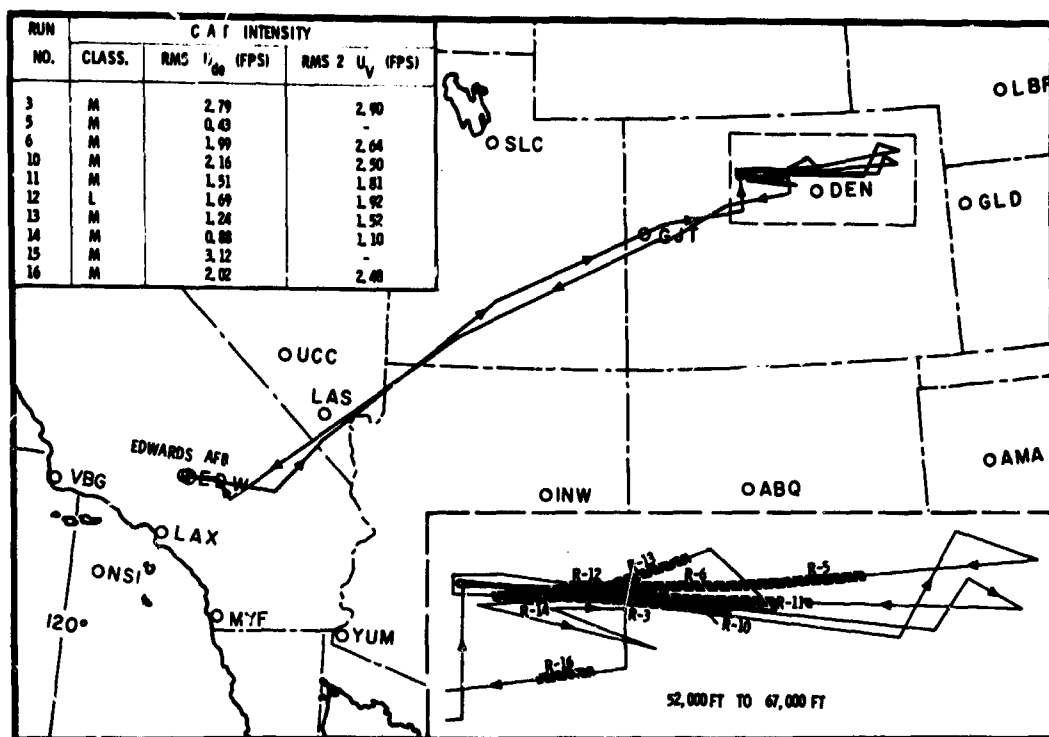
Figure 156   Test 280 Flight Track (2019Z, 15 Feb 1968 - 0227Z, 16 Feb 1968)
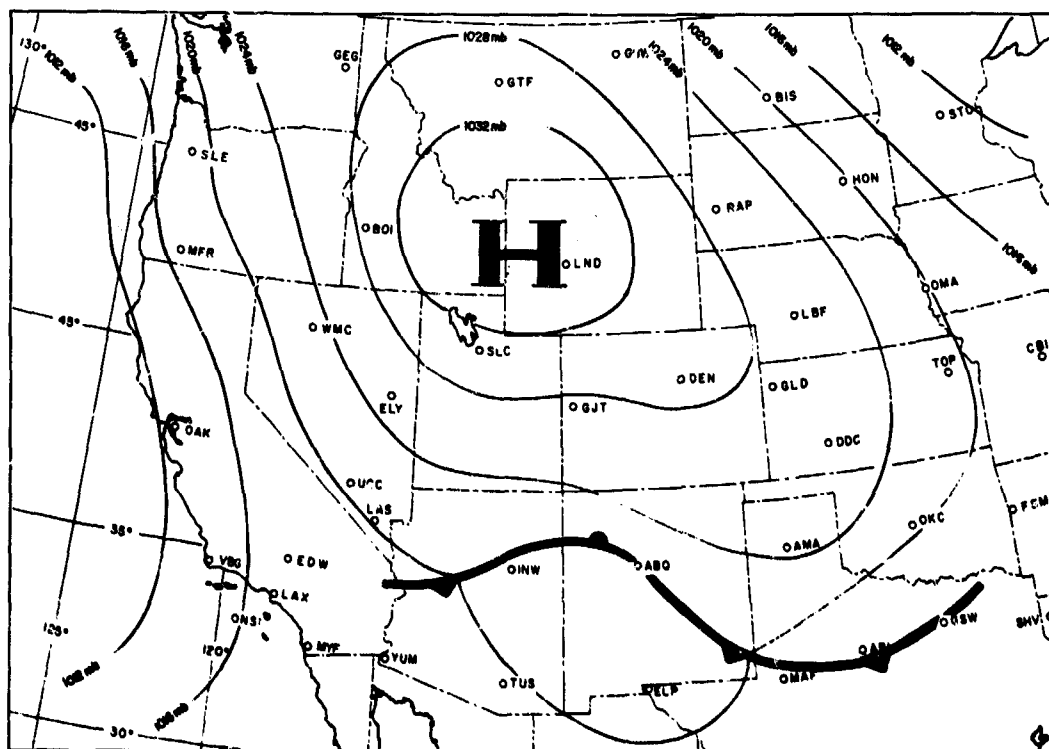
Figure 157   Test 280 Surface Chart (0000Z, 16 Feb 1968)
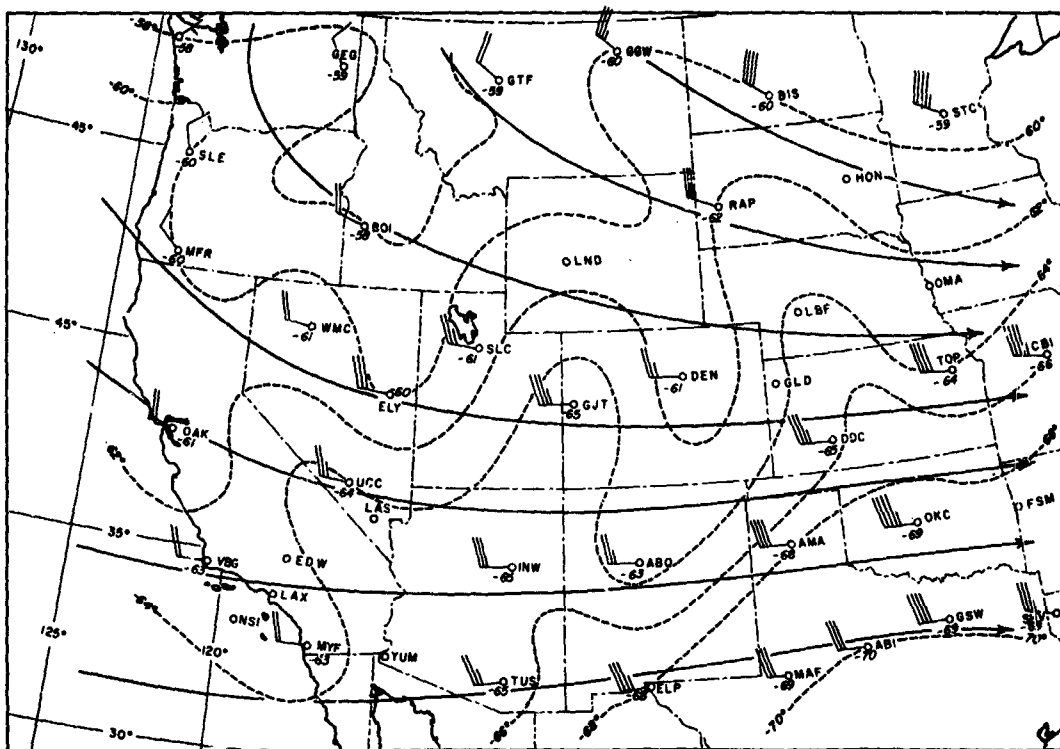
Figure 158   Test 280 70 MB Temperatures and Winds Chart (0000Z, 16 Feb 1968)
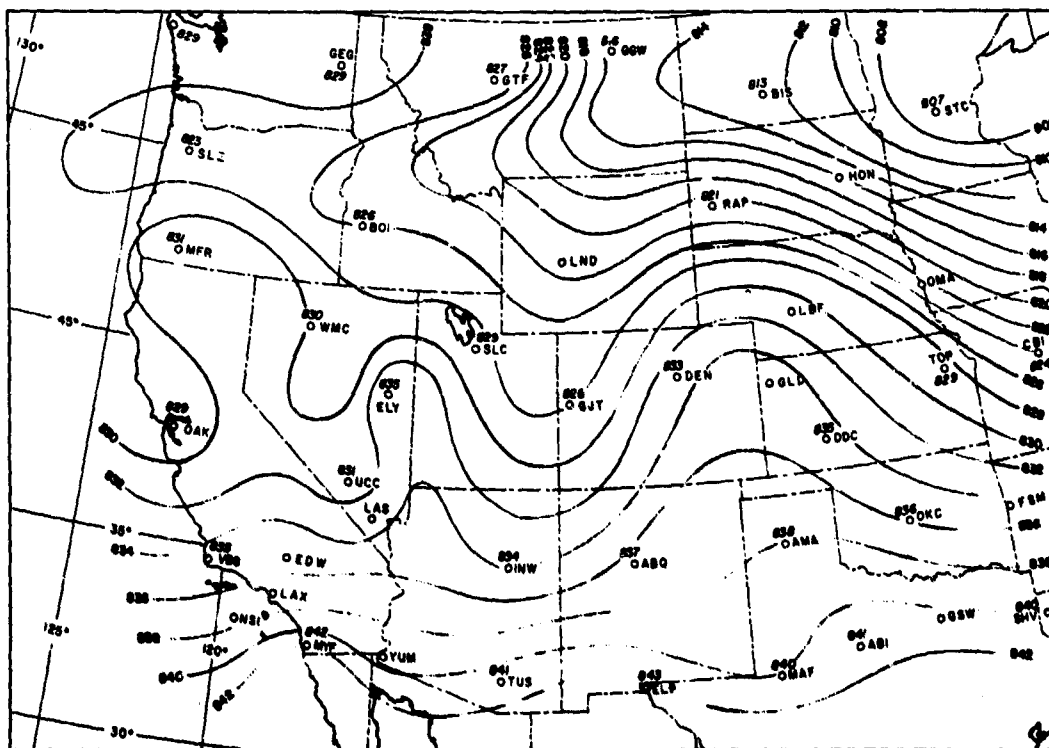
Figure 159   Test 280 70 MB Constant Pressure Chart (0000Z, 16 Feb 1968)
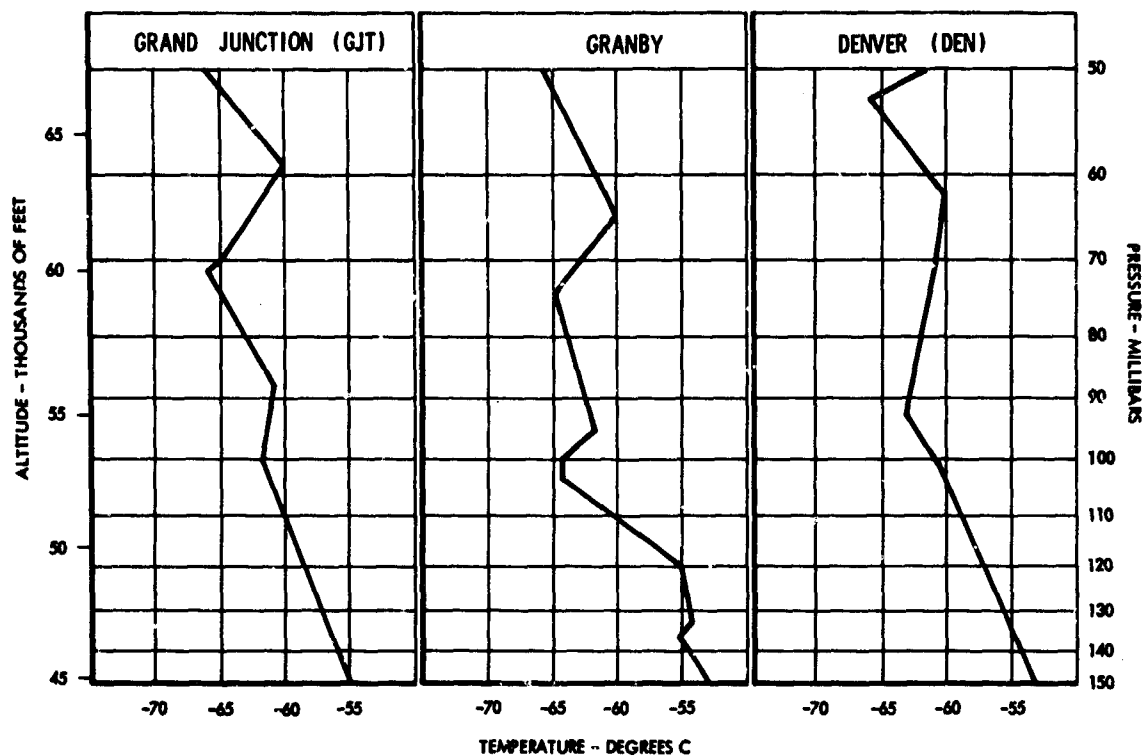
Figure 160   Test 280 RAOB Charts (Grand Junction and Denver, 0000Z,
16 Feb 1968; Granby, 2030Z, 15 Feb 1968)
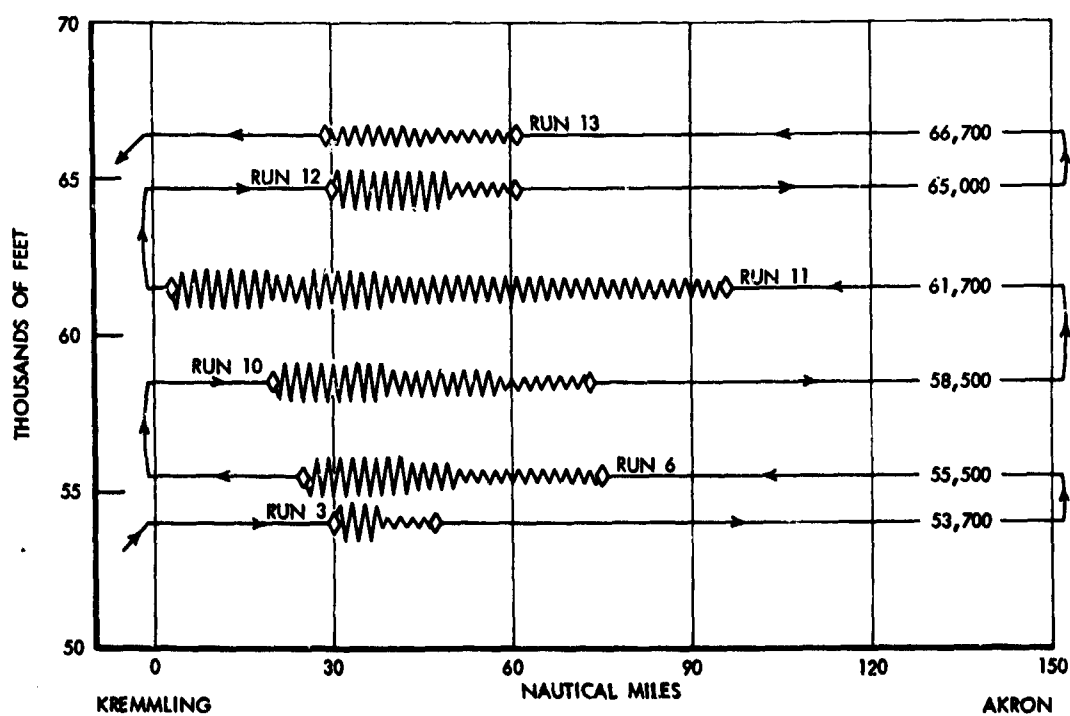
Figure 161   Test 280 CAT Encounter, Vertical Cross Section

APPENDIX II

DATA PROCESSING

COMPUTING METHODS

Numerical Filtering

Low-pass Filters - Numerical filters were applied to basic measurements to remove frequency components outside the range of interest. The filtering process consisted of applying selected sets of numerical filtering weights designed to pass only the useful frequency response range of each measurement. Four low-pass filters of the type developed by Martin and Graham were considered adequate (Ref. 33 and 34).

Ideally, the Martin-Graham filter will (1) pass unaffected all frequency components up to a certain cutoff value f_c, (2) progressively attenuate frequencies from f_c down to zero gain at a termination frequency f_t, and (3) reject all frequencies greater than f_t. The definition of this filter is given in the frequency domain by the transfer function $H(f)$.

$$
H(f) = \begin{cases}
1 & |f| \leq f_c \\[2mm]
0 & |f| \geq f_t \\[2mm]
\dfrac{1}{2}\left[\cos \pi \left(\dfrac{f + f_c}{f_t - f_c}\right) + 1\right] & -f_t \leq f \leq -f_c \\[4mm]
\dfrac{1}{2}\left[\cos \pi \left(\dfrac{f - f_c}{f_t - f_c}\right) + 1\right] & f_c \leq f \leq f_t
\end{cases}
$$

The time domain weighting function $h(t)$ is obtained by performing an inverse Fourier transformation of $H(f)$.

$$
h(t) = \int_{-\infty}^{\infty} H(f)\, e^{2\pi i f t}\, df
$$

$$
= \frac{\sin 2\pi f_t t + \sin 2\pi f_c t}{2\pi t\left[1 - 4(f_t - f_c)^2\, t^2\right]}
$$

A time function $x(t)$ is then filtered by applying the weighting function $h(t)$ such that

$$\hat{x}(t) \; = \; \int_{-\infty}^{\infty} h(\tau) \, x(t + \tau) \, d\tau$$

where $\hat{x}(t)$ is the filtered output function.

However for the finite time case of discrete equispaced data, numerical approximations must be introduced. The technique here is to evaluate the weighting function at the data sampling interval Δt for the $(2N + 1)$ weights desired, thus

$$h_n \; = \; h(n \Delta t) \qquad\qquad n \; = \; \pm 1, \pm 2, \ldots \pm N$$

and

$$h_o \; = \; f_c + f_t$$

by L'Hospital's rule.

The numerical filtering weights w_n are determined by

$$w_n \; = \; \frac{h_n \Delta t}{\displaystyle\sum_{p=-N}^{N} h_p \Delta t} \qquad\qquad n \; = \; 0, \pm 1, \ldots \pm N$$

where the summation term effectively normalizes the weights to force the transfer function to unity gain at $f = 0$.

The numerical filtering operation is then given by

$$\hat{x}_i \; = \; \sum_{n=-N}^{N} w_n \, x_{i+n}$$
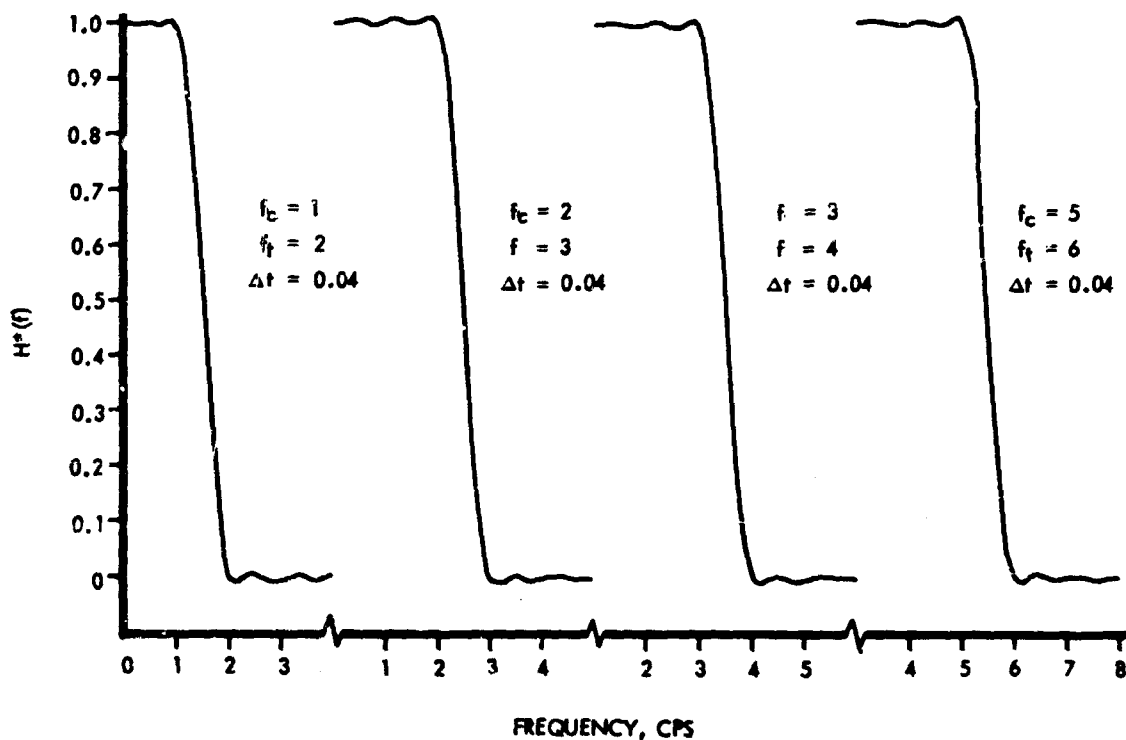
Figure 162   Transfer Functions of Low-Pass Filters

To evaluate the effectiveness of the numerical approximation on the transfer function of the original filter design, the transfer function of the filtering weights, $H^*(f)$, is computed by the cosine series transformation

$$H^*(f) = \sum_{n=-N}^{N} w_n \cos 2\pi f n \Delta t$$

Figure 162 graphically presents $H^*(f)$ for the four low-pass filters designed for this program. Table IX shows which filter was applied to each basic measurement.

High-pass Filters - High-pass numerical filters were employed as an investigative tool in evaluating the effect of removing undesirable low frequencies from the three gust velocity components. Design of the high-pass filters was obtained by subtracting Martin-Graham low-pass filters from an all-pass filter. The numerical weight function of an all-pass filter is defined as unity gain for the central weight with zero gain for the sideband weights. Transfer functions of the two high-pass filters selected for application are presented in Figure 95.

Numerical Integration

Simpson's one-third rule was used for numerically integrating rate gyro measurements and acceleration terms required for gust velocity computations. Simpson's integration of a time function $x(t)$ sampled with frequency $f_s = 1/\Delta t$ is given by

$$\int_{t_n}^{t_n + 2\Delta t} x(t)\, dt = \frac{\Delta t}{3}\left[x(t_n) + 4x(t_n + \Delta t) + x(t_n + 2\Delta t)\right]$$

Simpson's rule was selected for both its ideal phase and excellent amplitude characteristics. To illustrate this, a comparison is made with the trapezoidal rule. Since both rules have ideal phase, a complete comparison is afforded by the amplitude ratio of their transfer functions to that of the ideal integrator. The ratios are

$$\frac{W_s(f)}{W_T(f)} = \frac{2\pi f \Delta t}{3}\left(\frac{2 + \cos 2\pi f \Delta t}{\sin 2\pi f \Delta t}\right)$$

TABLE IX.   LOW-PASS NUMERICAL FILTERING CUTOFF FREQUENCIES
OF BASIC MEASUREMENTS

Assigned Number	Basic Measurement	Cutoff Freq, cps
3	Alpha-vane force	5
4	Beta-vane force	5
5	Indicated airspeed	5
6	Platform vertical acc	3
7	Gust probe normal acc	5
8	Gust probe lateral acc	5
9	Vernier altitude	3
10	Total temperature	5
11	Pitch rate	3
12	Roll rate	3
13	Yaw rate	3
14	CG normal acc	3
15	CG lateral acc	2
16	CG longitudinal acc	2
20	Coarse altitude	1
21	Fine altitude	2
22	Left wing nodal acc	5
23	Right wing nodal acc	5
25	Pitch angle	2
26	Roll angle	2
27	Heading sine	1
28	Heading cosine	1
29	Grid X-velocity	1
30	Grid Y-velocity	1

for Simpson's one-third rule, and

$$\frac{W_T(f)}{W_I(f)} = \pi f \Delta t (\cot \pi f \Delta t)$$

for the trapezoidal rule.

The superiority of Simpson's rule is shown in Figure 163 where the amplitude ratios were evaluated at the basic data sampling interval of 0.04 seconds. The maximum error is expected at the numerical filtering cutoff frequency of 5 cps. At this frequency, Figure 163 shows an error of 1.7 percent for Simpson's one-third rule and -13.5 percent for the trapezoidal rule.

Aerodynamic Calculations

Position error corrections and aerodynamic variables are determined in the gust velocity program prior to computation of the gust velocity components. The following calculations require H_{pn} selected from either coarse, fine, or vernier altitude transducer, and t_t from the total temperature probe

(a) Indicated Pressure Altitude

$$P_s \geqq 6.68322 \text{ in. Hg}$$

$$H_{pn} = 145,447. \left[1.0 - \left(\frac{P_s}{29.9213} \right)^{0.19026} \right]$$

$$P_s < 6.68322 \text{ in. Hg.}$$

$$H_{pn} = 20,806. \left[\log_e \left(\frac{6.68322}{P_s} \right) \right] + 36089$$

(b) Indicated Mach No.

$$M_1 = \sqrt{ 5 \left[\left(\frac{q_c}{P_s} + 1 \right)^{2/7} - 1 \right] }$$
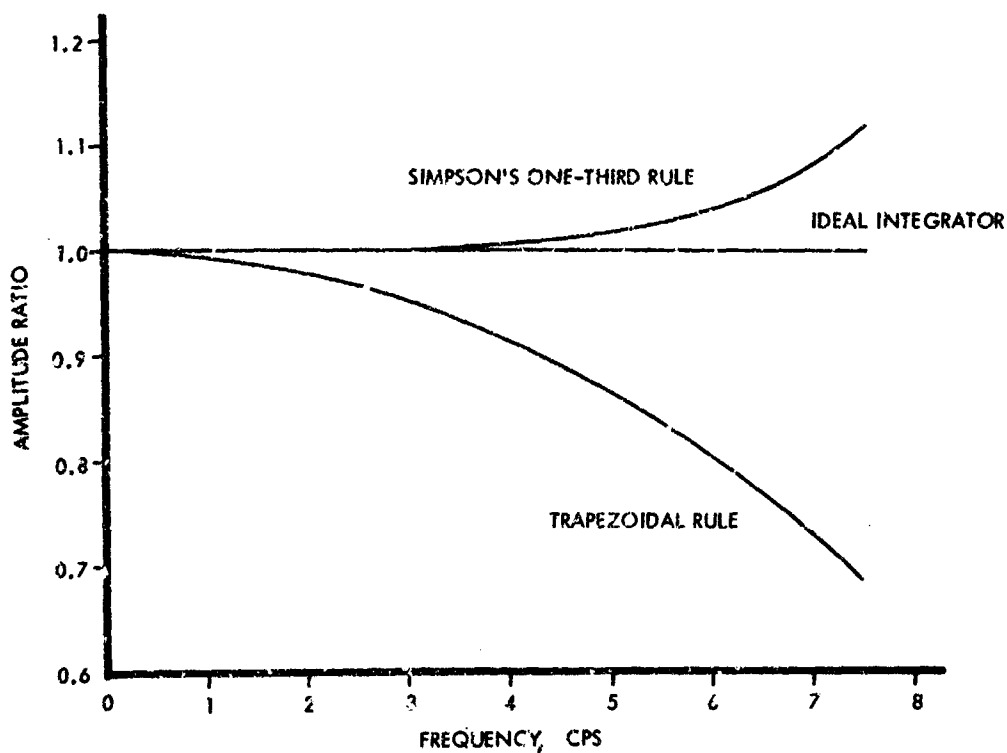
Figure 163 Amplitude Ratio Comparison of Simpson's One-Third
Rule and Trapezoidal Integrations

(c) The Mach number static position error correction, δM, is determined
from the M_i versus δM relationship.

(d) True Mach No.

$$M_T = M_i + \delta M$$

(e) The altitude static position error correction, δH_p, is determined
from the M_i versus δH_p relationship.

(f) Corrected pressure attitude

$$H_{pc} = H_{pn} + \delta H_p$$

(g) Ambient Temperature

$$t_a = \frac{t_t + 273.16}{1 + 0.2M_T^2} - 273.16$$

(h) True airspeed

$$V_T = 65.769 M_T \sqrt{t_a + 273.16}$$

Appendix II

(i) Ambient pressure

if $H_{pc} \leq 36089$ ft.

$$P_a = 2116.22(1 - 6.87535 \times 10^{-6} H_{pc})^{5.2561}$$

if $H_{pc} > 36089$ ft.

$$P_a = 472.675 \, e^{-4.80634 \times 10^{-5}(H_{pc} - 36089)}$$

(j) Air density ratio

$$\sigma = \frac{681.14 \, P_a}{t_a + 273.16}$$

(k) Equivalent airspeed

$$V_e = V_T \sigma^{1/2}$$

(l) Air density

$$\rho = \frac{1.619 \, P_a}{t_a + 273.16}$$

Gust Velocity

The three gust velocity components (vertical - U_V, lateral - U_L, and longitudinal - U_F) were computed as follows:

$$U_V = (V_T \Delta \alpha) + (V_T \Delta \beta) \, \Delta \phi - V_T \Delta \theta$$

$$+ \int \Delta a_z \, dt + L_x \Delta \dot{\theta}$$

$$U_L = (V_T \Delta \beta) - (V_T \Delta \alpha) \, \Delta \phi + V_T \Delta \psi$$

$$- \Delta V_X \cos \bar{\Lambda} + \Delta V_Y \sin \bar{\Lambda} + L_x \Delta \dot{\psi}$$

$$U_F = \Delta V_T - \Delta V_X \sin \bar{\Lambda} - \Delta V_Y \cos \bar{\Lambda}$$

282

where

$$V_T \Delta \alpha \ = \ 2 \ \frac{\Delta F_{N_{M\alpha}} + m\Delta a_N}{C_{N\alpha} \ \rho \ V_T \ S_v}$$

$$V_T \Delta \beta \ = \ 2 \ \frac{\Delta F_{N_{N\beta}} + m\Delta a_L}{C_{N_\beta} \ \rho \ V_T \ S_v}$$

As indicated by these equations, the incremental velocity components of the aircraft relative to the ground are normally computed from inertial platform measurements provided for this purpose. However, alternate methods have been programmed for determining the gust velocity components based on cg or gust probe acceleration measurements corrected for aircraft attitude.

$$U_V \ = \ (V_T \Delta \alpha) + (V_T \Delta \beta) \ \Delta \phi - V_T \Delta \theta$$

$$+ \int (\Delta a_N - \Delta a_L \Delta \phi) \ dt + L_x \Delta \dot{\theta}$$

$$U_L \ = \ (V_T \Delta \beta) - (V_T \Delta \alpha) \ \Delta \phi + V_T \Delta \psi$$

$$+ \int (\Delta a_L + \Delta a_N \Delta \phi) \ dt + L_x \Delta \dot{\psi}$$

$$U_F \ = \ \Delta V_T - \int (\Delta a_F - \Delta a_N \Delta \theta) \ dt$$

Incremental angles of pitch and roll were computed from platform attitude measurements corrected for fuselage bending by

$$\Delta \theta \ = \ \Delta \theta_M + k_b \Delta a_N$$

$$\Delta \phi \ = \ \Delta \phi_M + k_b \Delta a_L$$

or from integration of the rate gyro measurements

$$\Delta \theta \ = \ \int \Delta \dot{\theta} \ dt$$

$$\Delta \phi \ = \ \int \Delta \dot{\phi} \ dt$$

Appendix II

Incremental yaw angles were obtained from platform true heading measurements

$$\Delta \psi = \Delta \Lambda$$

or from integration of the yaw rate gyro.

$$\Delta \psi = \int \Delta \dot{\psi} \, dt$$

After Simpson's one-third rule was employed for evaluating the integral terms, the gust velocities were computed at 12.5 samples per second (sps), half the basic sampling data frequency. Since low-pass numerical filters effectively terminated all frequency components beyond 6 cps, no aliasing of any significance was introduced by reducing the sampling frequency. This significantly reduced the processing effort to obtain the gust velocities, yet retained the accuracy associated with Simpson's integration of 25 sps.

The derived equivalent gust velocity was computed as follows.

$$U_{de} = \frac{2 \Delta a_N \bar{W}}{C_{L_\alpha} \rho_o K_g V_e S}$$

Wind Velocity

The average wind velocity, $\bar{U}_{AG}$, was determined from the average true airspeed and inertial platform measurements. The wind velocity components with respect to the aircraft are

$$\bar{U}_{AP_{X'}} = -\bar{V}_T \sin \bar{\Lambda}$$

$$\bar{U}_{AP_{Y'}} = -\bar{V}_T \cos \bar{\Lambda}$$

hence with respect to the ground

$$\bar{U}_{AG_{X'}} = -\bar{V}_T \sin \bar{\Lambda} + \bar{V}_{x'}$$

$$\bar{U}_{AG_{Y'}} = -\bar{V}_T \cos \bar{\Lambda} + \bar{V}_{y'}$$

The magnitude and direction, $\overline{\eta}$, of the average wind velocity vector are therefore computed by

$$\overline{U}_{AG} = \sqrt{\overline{U}^2_{AG_{X'}} + \overline{U}^2_{AG_{Y'}}}$$

$$\overline{\eta} = \tan^{-1}\left(\frac{\overline{U}_{AG_{X'}}}{\overline{U}_{AG_{Y'}}}\right)$$

Power Spectra

The power spectrum of a stationary random function $x(t)$ is defined by

$$\phi(f) = 4 \int_0^\infty R(\tau) \cos 2\pi f \tau \, d\tau$$

where $R(\tau)$, the autocorrelation function, is given by

$$R(\tau) = \lim_{T \to \infty} \frac{1}{T} \int_{-T/2}^{T/2} x(t) \, x(t + \tau) \, dt$$

To estimate the spectrum for discrete equispaced data, the Tukey method was employed (Ref. 7 and 35). The numerical approximations involved in this method for a discrete function x_q of $(n+1)$ evenly spaced samples from 0 to $n\Delta t$ seconds are presented in the following steps:

Prewhitening - To minimize the possible distortion from the relatively high power anticipated at the low frequencies, a prewhitening filter is applied to the data. This high-pass filter is defined by the transformation

$$\hat{x}_q = x_q - x_{q-1} \qquad q = 1, 2, \ldots n$$

Autocorrelating - The autocorrelation function of the prewhitened data is computed for $(m+1)$ time lags from 0 to $m\Delta t$.

$$\hat{R}_p = \frac{1}{n-p} \sum_{q=1}^{n-p} \hat{x}_q \, \hat{x}_{q+p} \qquad p = 0, 1, \ldots m$$

285

Appendix II

Estimating the Raw Power - The raw estimates of power are computed by numerically evaluating the cosine series transform of the autocorrelation function

$$\hat{L}_h = 4\Delta t \sum_{p=0}^{m} a_p \hat{R}_p \cos\frac{hp\pi}{m} \quad h = 0, 1, \dots m$$

where

$$a_p = 0.5 \qquad p = 0, m$$

$$a_p = 1 \qquad 0 < p < m$$

Smoothing the Raw Estimates - The raw estimates are refined by a smoothing technique called hanning.

$$\hat{\Phi}_h = 0.25\hat{L}_{h-1} + 0.5\hat{L}_h + 0.25\hat{L}_{h+1} \quad h = 1, 2, \dots m-1$$

$$\hat{\Phi}_m = 0.5\hat{L}_{m-1} + 0.5\hat{L}_m$$

Postdarkening - The final power spectral estimates are obtained after the smoothed estimates are compensated for the effect of the prewhitened transformation performed in the first step, thus

$$\Phi_h = \frac{\hat{\Phi}_h}{2 - 2\cos\frac{\pi h}{m}} \quad h = 1, 2, \dots m$$

where

$$\Phi_h = \Phi\left(f_h = \frac{h}{2m\Delta t}\right)$$

286

and represent the power average over the frequency band in cycles per second defined by

$$\frac{h}{2m\Delta t} \quad \pm \quad \frac{1}{m\Delta t}$$

In analyzing turbulence data, it is desirable to interpret their power spectra as a function of inverse wavelength in cycles per foot. The average true airspeed in feet per second is used for converting the spectral estimates.

$$\Phi(1/\lambda_h) \;=\; \overline{V_T}\,\Phi(f_h)$$

The number of spectral estimates m is normally selected so that the data will stay within certain confidence limits. The degrees of freedom k of a run of n samples is a measure of the stability of the spectral estimates and is given by

$$k = \frac{2n}{m}$$

Standard rms deviations are determined by numerically integrating the spectral estimates for standard wavelengths, thus

$$\sigma_s \;=\; \left[\int_{1/\lambda_1}^{1/\lambda_2} \Phi(1/\lambda)\; d(1/\lambda) \right]^{1/2}$$

where λ_2 is the wavelength corresponding to the 5 cps numerical filtering cutoff frequency and λ_1 is a standard wavelength. Rms deviations are computed for wavelengths of 1000, 2000, 4000, 10,000, 20,000 and 40,000 feet.

Cross Spectra

The cross spectral density function between sample functions $x(t)$ and $y(t)$ of stationary random processes is given by

$$\Phi_{xy}(f) \;=\; 2\int_{-\infty}^{\infty} R_{xy}(\tau)\; e^{-2\pi i f \tau}\, d\tau$$

Appendix II

where $R_{xy}(\tau)$, the cross correlation function, is given by

$$R_{xy}(\tau) = \lim_{T \to \infty} \frac{1}{T} \int_{-T/2}^{T/2} x(t)\ y(t+\tau)\ dt$$

If the cross correlation function, is given by

$$\Phi_{xy}(f) = c(f) - iq(f)$$

then $c(f)$, the in-phase power called the cospectrum, is the cosine series transform of the real part of the cross-correlation function

$$c(f) = 4 \int_0^\infty \frac{R_{xy}(\tau) + R_{yx}(\tau)}{2}\ \cos 2\pi f \tau\ d\tau$$

and $q(f)$, the out-of-phase power or quadrature spectrum, is the sine series transform of the imaginary part of the cross-correlation function

$$q(f) = 4 \int_0^\infty \frac{R_{xy}(\tau) - R_{yx}(\tau)}{2}\ \sin 2\pi f \tau\ d\tau$$

where

$$R_{yx}(\tau) \equiv R_{xy}(-\tau)$$

The Tukey approximations employed to estimate the cross-spectral power for discrete equally spaced data are presented below (Ref. 7 and 35).

Cross-correlating - Estimates of the cross-correlation function between an input disturbance $x_1 \ldots x_n$ and an output response $y_1 \ldots y_n$ are given by the relationship

$$R_{xy_p} = \frac{1}{n-p} \sum_{q=1}^{n-p} x_q\ y_{q+p} \qquad\qquad p = 0, 1, \ldots m$$

for (m+1) positive time lags of y with respect to x, and by

$$R_{yx_p} = \frac{1}{n-p} \sum_{q=1}^{n-p} y_q \, x_{q+p} \qquad p = 0, 1, \ldots m$$

for (m+1) negative time lags.

Estimating the Cross Spectrum - The cross spectral power is derived by numerically evaluating the discrete Fourier transform of the cross-correlation function, thus if

$$\Phi xy_h = c_h - i \, q_h \qquad h = 0, 1, \ldots m$$

then the cospectral estimates are given by

$$c_h = 2\Delta t \sum_{p=0}^{m} a_p \, (R_{xy_p} + R_{yx_p}) \cos \frac{hp\pi}{m}$$

and the quadrature spectral estimates by

$$q_h = 2\Delta t \sum_{p=0}^{m} a_p \, (R_{xy_p} - R_{yx_p}) \sin \frac{hp\pi}{m}$$

where

$$a_p = \begin{cases} 0.5 & p = 0, m \\ 1 & 0 < p < m \end{cases}$$

Appendix II

Additional relationships are determined when a cross spectrum is requested. They are (1) the normalized cross spectrum given by

$$\frac{c_h}{\sqrt{c_h^2 + q_h^2}} - i\frac{q_h}{\sqrt{c_h^2 + q_h^2}}$$

(2) the phase lag given by

$$\tan^{-1}\frac{q_h}{c_h}$$

and (3) the coherency function, measuring the linear relationship of x and y, determined by

$$\frac{c_h^2 + q_h^2}{\Phi_{x_h}\Phi_{y_h}} \ .$$

Frequency-Response Functions

The frequency-response characteristics of cg normal acceleration due to vertical gusts were estimated by two methods; the spectrum method and the cross spectrum method. In the spectrum method, the amplitude of the frequency-response function, $|H_s(f)|$, is based on the relation between the power spectrum of cg normal acceleration denoted by $\Phi_x(f)$ and the power spectrum of vertical gust velocity denoted by $\Phi_y(f)$.

$$\left|H_s(f)\right|^2 = \frac{\Phi_y(f)}{\Phi_x(f)}$$

The second method utilizes the cross spectrum of the cg normal acceleration response to the vertical gust disturbances. The amplitude of the frequency-response function for the cross spectrum method is given by

$$\left|H_c(f)\right| = \sqrt{\frac{c(f)^2 + q(f)^2}{\Phi_x^2(f)}}$$
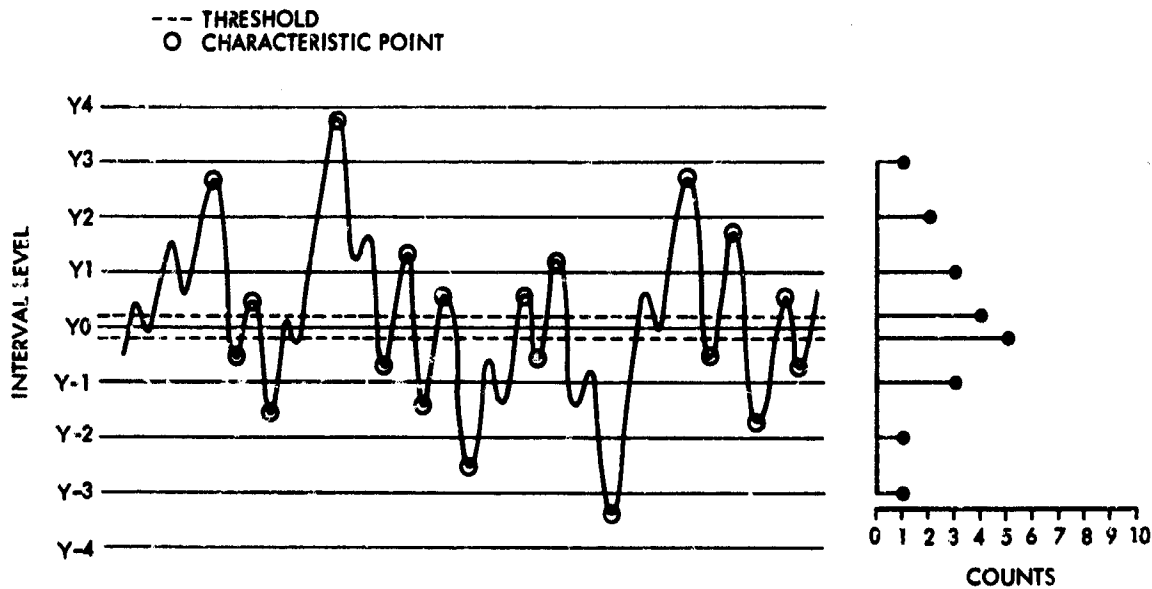
--- THRESHOLD
O CHARACTERISTIC POINT

Figure 164   Example of Mean Crossing Peak Count

Statistical Counting Methods

Two statistical counting methods were employed to define the distribution characteristics of selected acceleration and velocity data. In both methods, the characteristic points are counted and classified into preestablished positive and negative intervals constructed about the mean. The two methods have different criteria for determining a count.

In the peak count method, the characteristic points (peaks) are defined as the maximum or minimum value between successive crossings of a narrow band about the mean. The purpose of the narrow band, called the threshold, is to eliminate the counting of peaks resulting from insignificant fluctuations in the data. Figure 164 shows how peaks are determined, classified, and counted. Note that the threshold in the example has been expanded for purposes of clarity; it is normally plus and minus 10 percent of the counting interval.

In the level-crossing count method, a count is made each time the trace of the discrete data intersects an interval level with a positive slope in the region above the mean and with a negative slope in the region below the mean. An example of the level-crossing count method is shown in Figure 165.

After a data run has been processed by one of the counting methods, the following statistical parameters are determined.

Frequency of Occurrence - In the peak count method the counts are summed within corresponding positive and negative intervals. The accumulated counts for interval levels y_i and y_{-i} are indicated by $g(y_i)$, the frequency of occurrence.

291

O CHARACTERISTIC POINT
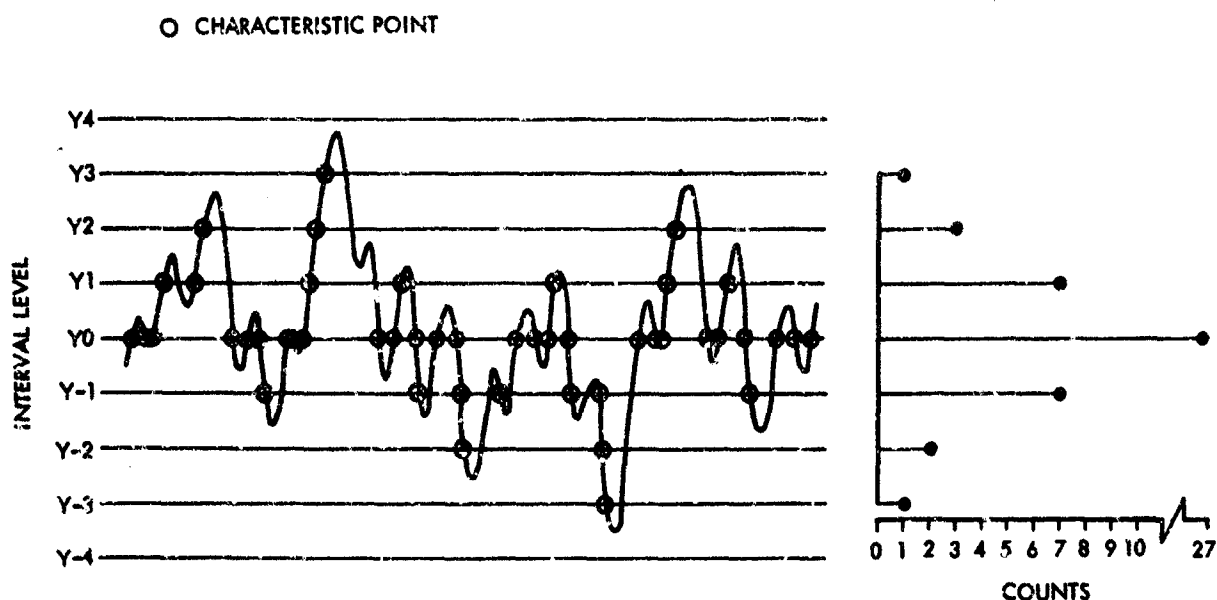
Figure 165 Example of Level-Crossing Peak Count

Frequency of Exceedance - For peak counts, the frequency of exceedance, $G(y_i)$, is determined for each level. If N is the index of the maximum level for which a count was detected, then

$$G(y_i) = \sum_{j=i}^{N} g(y_j) \qquad i = 0, 1, \ldots N$$

For the level crossing count method, the frequency of occurrence is the frequency of exceedance, hence

$$G(y_i) \equiv g(y_i)$$

Exceedance per Mile - If the frequency of exceedance is divided by the number of miles in a data run, the distribution becomes an estimate of the frequency of exceeding a given velocity or acceleration level per mile of flight. The exceedance per mile was computed by

$$\frac{G(y_i)}{V_T T_N}$$

where T_N is the elapsed time of the data run in seconds.

292

Probability Distribution Function - The probability distribution function indicated by $F(y_i)$, represents the probability of exceeding a given level. For level y_i,

$$F(y_i) \; = \; \frac{G(y_i)}{G(y_o)}$$

COMPUTER PROGRAMS

HICAT Basic Data Program

General - The HICAT basic data program is the first of six digital computer programs designed to reduce and display pulse code modulated (PCM) data previously processed to a computer compatible format in the HICAT ground station.

The purpose of the program in its normal production mode is to read the ground station tape on Lockheed-California Company's IBM System/360 Computer installation and perform the following sequential operations:

- Unpack the airborne-recorded data

- Monitor frames for constant time interval

- Calibrate to engineering units

- Detect and correct sporadic data errors

- Apply sets of numerical filtering weights

- Compute means and standard deviations

- Record the results on tape and list in tabular form.

The following programs in the HICAT series are designed to accept the tape generated in this program as their input data source:

- HICAT gust velocity program

- HICAT power spectral analysis program

- HICAT statistical analysis program

- HICAT plotting program

- HICAT elevator response program.

Input Requirements - The primary input to the program is a ground station tape containing edited runs of flight-recorded data. A complete description of the format structure of this tape is given in Figure 166. Each time step or frame contains 5 digital channels of switching information, 3 time

channels, and 40 analog channels reserved for basic measurements. The packed data of 15 frames are assembled in logical records and the records are grouped by files. Each file contains the data for one edited run.

FILE FORMAT

FILE IDENT.	1ST FRAME	2ND FRAME	3RD FRAME	4TH FRAME	5TH FRAME	6TH FRAME	7TH FRAME	8TH FRAME

9TH FRAME	10TH FRAME	11TH FRAME	12TH FRAME	13TH FRAME	14TH FRAME	15TH FRAME	END OF RECORD GAP	FILE IDENT.

1ST FRAME	2ND FRAME	3RD FRA

13TH AME	14TH FRAME	15TH FRAME	END OF FILE GAP

FRAME FORMAT

DIGITAL CHANNELS			DIGITAL CHANNELS		TIME CH.	TIME CHANNELS		ANA. CHAN.	ANALOG CHANNELS			ANALOG CHANNELS			ANALOG CHANNELS		
1	2	3	4	5	1	2	3	1	2	3	4	5	6	7	8	9	10
1ST WORD			2ND WORD			3RD WORD			4TH WORD			5TH WORD			6TH WORD		

ANALOG CHANNELS			ANALOG CHANNELS			ANALOG CHANNELS			ANALOG CHANNELS			ANALOG CHANNELS			ANALOG CHANNELS		
11	12	13	14	15	16	17	18	19	20	21	22	23	24	25	26	27	28
7TH WORD			8TH WORD			9TH WORD			10TH WORD			11TH WORD			12TH WORD		

ANALOG CHANNELS			ANALOG CHANNELS			ANALOG CHANNELS			ANALOG CHANNELS		
29	30	31	32	33	34	35	36	37	38	39	40
13TH WORD			14TH WORD			15TH WORD			16TH WORD		

Figure 166   Ground Station Tape Format
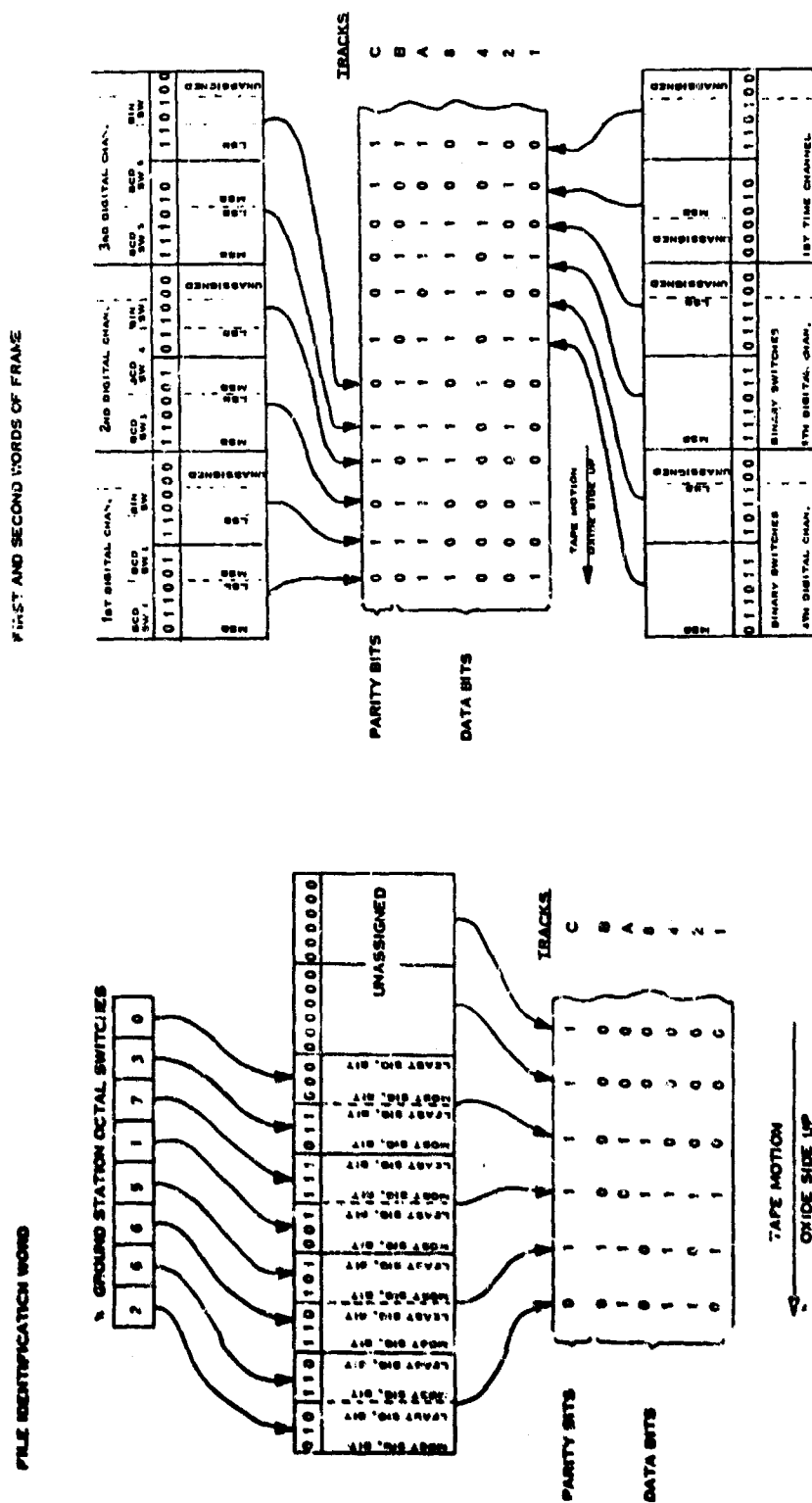
Figure 166 Ground Station Tape Format (Continued)

Figure 166 Ground Station Tape Format (Concluded)

The following additional information is input to the program to control the reading, processing and reduction of the tape data.

- Test parameters identifying the test and defining test conditions including the status of the data acquisition system.

- Analog channel assignments defining the configuration of the basic measurements in the analog channels.
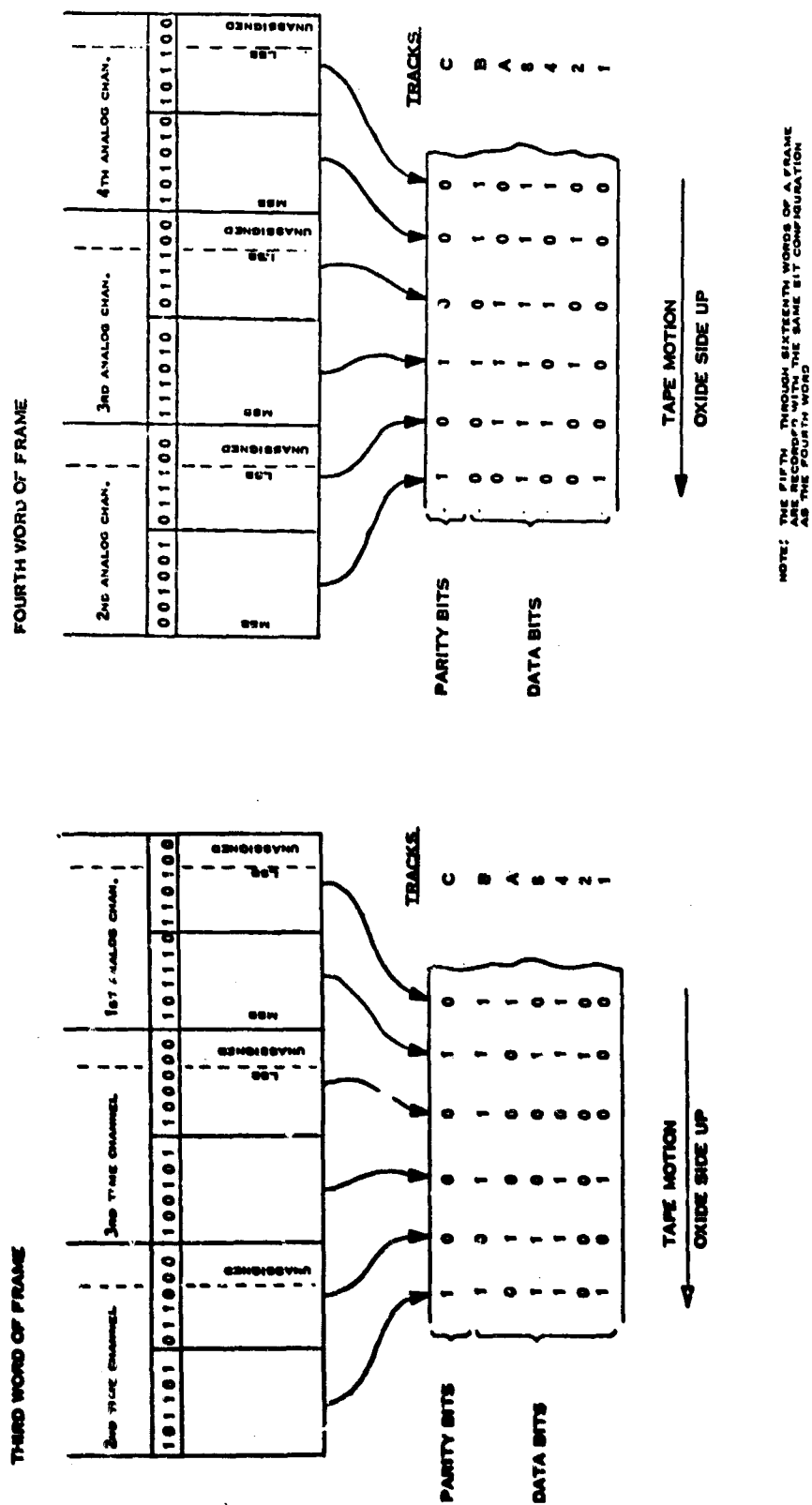
- Calibration data defining the method of calibrating each measurement.

- Run parameters providing the identifications and conditions required for initiating the reduction of a data run.

- Status codes defining the logical path each measurement will follow through the error search and numerical filtering functions of the program.

Unpacking and Reformatting - After the ground station tape data has been read into a temporary buffer, an unpacking routine is employed to disassemble and translate the data channels into working data tables as shown in Figure 167. Then, the three time channels are merged to construct the time of day in milliseconds. Next, the switching information in the five digital channels is isolated and then combined in the proper sequence to form one word of binary switching information and one word of BCD switching information. Finally, analog channels containing measurement data are directed to their assigned position in the table.

Figure 167   Basic Data Tables

Editing - Although the data runs are formed as a result of editing information obtained from the airborne-recorded data, additional information uncovered after the ground station tapes are generated may warrant further editing. For this purpose the program permits a start time and stop time to be input to limit the processing of data to frames within the previously selected times. This capability also enables a data run to be divided into several smaller runs. Each of these may then be processed individually.

Correcting Time Errors - The time error routine ensures a constant time interval of the data frames consistent with the sampling frequency of the data acquisition system. The times associated with contiguous frames are interrogated to determine if the proper time interval is maintained. Whenever an error is detected, a search is effected until the proper sequence is established. If the number of frames in the disturbed region is not equal to the number of time steps required to maintain the correct time interval, the frames are sorted into sequence in the data tables. The data associated with disturbed frames are then labeled for corrective action in the sporadic error correcting routine which follows. An error criterion may be input which limits each error search to a preestablished number of consecutive frames. If no solution is detected within the prescribed limits, further processing is terminated and the results are summarized and output for analysis.

Calibrating - Programming options are available for defining how each basic measurement shall be calibrated. Figure 168 shows the pertinent functions of the data acquisition process associated with the analog channel calibrations produced in the data reduction phase.

As shown in Figure 168, the conversion of the raw data counts into engineering units requires two calibration steps. The first step employs the calibration of the PCM system. This calibration curve is entered with the count reading and the corresponding voltage reading is obtained by linear interpolation.

The second step employs the sensor calibrations to convert the data to engineering units. Options are available for utilizing either polynomial curve fits or table look-ups for these calibrations.

Additional options are available for bypassing all calibrations if raw data counts are desired or limiting the conversion process to just the first step if only volts are desired. These provisions were added to facilitate the checkout of the data acquisition system and to permit special data presentations.

Correcting Sporadic Data Errors - Sporadic data errors are defined as wild or accidental data samples outside the range normally associated with systematic or random errors. Sporadic errors are detected by comparing the first order differences of the data samples with preestablished limits. Limits were assigned to each measurement based on the data sampling interval. The detected errors are corrected by interpolating a linear fit constructed from data samples immediately preceding and following the disturbed area. Gaps in the table resulting from the inclusion of time errors are similarly corrected. All sporadic data errors and their corresponding corrections are summarized and tabulated in separate listings for review.

DATA ACQUISITION
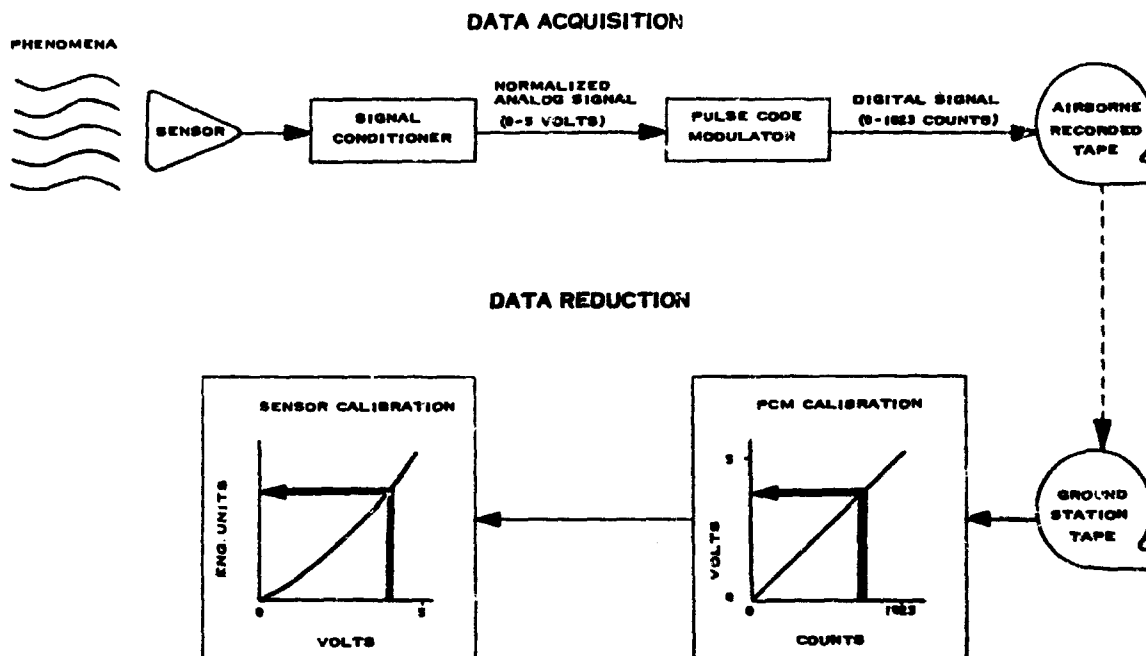
DATA REDUCTION

Figure 168 Data Acquisition and Reduction of Analog Channel Measurements

In addition, an error criteria may be established which limits the quantity and type of error occurrences and restricts the processing of the bad test data.

Numerical Filtering - The requirements for low-pass filtering are provided through the application of four sets of numerical filtering weights internally defined in the program. The transfer functions of the filtering weights are shown in Figure 90.   One of the four weight sets may be selected for each basic measurement depending on what frequency response is desired.

The numerical weights were determined by the method developed by Martin and Graham (Reference 33 and 34). Application of the numerical filters is given by the operation

$$\hat{x}_i = \sum_{n=-N}^{N} w_n x_{i+n}$$

where w_n are the $(2N+1)$ filtering weights, x_i are the input data samples and $\hat{x}_i$ are the corresponding filtered data samples.

Computing Means and Standard Deviations - The means and standard deviation are computed for each measurement in the basic data tables and printed on the tabular listings at the end of each run.

Appendix II

HICAT Gust Velocity Program

General - The HICAT gust velocity program was designed to compute aerodynamic variables, gust velocity components, and the derived equivalent gust velocity from the measurements reduced in the HICAT basic data program. Programming options are available for computing the vertical, lateral, and longitudinal gust velocity components using various combinations of the basic measurements.

The computed quantities are output on tape for use in the HICAT spectral analysis program and the HICAT statistical analysis program.

Input Requirements - The primary input to the gust velocity program is the output tape from the basic data program. Figure 167 lists the various measurements stored on tape. Accompanying the input tape is a group of cards specifying operational and computing information. The information appearing on the card input is as follows:

- Input and output tape identification

- Location of data on input tape, start and end time of selected data sample, averages of airplane response data, input tape sampling rate

- Computation control codes, integration initialization values, output print sampling rate

- Parameter adjustments, reference and general functions.

While a complete block of input is being read into the computer, initialization is performed. Commands positioning the input and output tapes are executed and all computing control information is stored.

Operational Checks - To insure that the proper data tapes were loaded, the data appearing in the status control block on the input tape is read and compared against the card input specifications. If any discrepancy occurs at this time, the program is immediately terminated and the reasons for termination are printed out to facilitate corrective action. The operational checks include tape loading, tape positioning, tape identification, and data sample selection. If no error is sensed while performing the operational checks the input tape is then positioned at the specified start time of the selected data sample.

Preliminary Calculations and Tabulations - A specified amount of data is read from the input tape, parameter adjustments applied, and gust entrance conditions and reference heading angle are computed. The results of these calculations along with the input computing information are tabulated.

General Processing Method - The general processing scheme was to read data from tape into an input calculation table. Data in this table was used in the subsequent calculations and stored in an output buffer. This method eliminated all data sample length restrictions since the input data was processed in table-sized bites. The procedure was to perform input tape

300

reads at the specified input sampling rate until the calculation table was full or until the end time or data sample end was reached. Then all specified parameter adjustments were applied to this table. If the end of the selected data was sensed an appropriate flag was set. Computing continued in this manner, selecting data from the input table, performing specified computations, and storing the answer in the output buffer. As the buffers were alternately exhausted or filled, input reads or sampled output writes into and from the appropriate buffers were executed. This process continued until the end of the selected data sample was sensed. When this occurred, a final output buffer write was performed and wind velocities calculated and output. If more input data was available, the program returned to the read input position. If no more input was available, all data tapes were rewound and unloaded and the computer run was terminated.

Computations - The methods used in computing aerodynamic variables, gust velocity components, and wind velocity are described earlier in this appendix under Computing Methods.

HICAT Spectral Analysis Program

General - The HICAT spectral analysis program was designed to compute the statistical characteristics of turbulence data in the frequency domain. Basically, the program may be implemented to compute the following functions of the HICAT equispaced time series data.

- Auto correlation
- Power spectrum
- Cross correlation
- Cross spectrum

- Normalized cross spectrum
- Coherency
- Phase angle
- Frequency response function

The numerical procedures used in evaluating these functions are essentially the same as those presented in Reference 7.

Input Requirements - The input data source may either be (1) the basic measurements recorded on the tape generated by the HICAT basic data program, or (2) the aerodynamic variables and gust velocity components recorded on the tape generated by the HICAT gust velocity program. As data frames recorded on the input tape are read, the samples required for computing the first spectrum are directed to a table in core memory and the remaining data specified for processing are transferred to random access magnetic disk storage. Spectra are then computed until the data on disk is exhausted; whereupon the input tape is repositioned and the next case initiated.

The following information is input for identification purposes and to control the logical path through decision-making events in the program:

- Test parameters providing the necessary identification of test conditions

Appendix II

- Spectral parameters defining the many options available for computing spectra

- Run parameters defining the conditions under which each run is to be processed

- Data parameters defining the variables for which a spectrum is desired

Statistical Adjustment of the Data - After all samples for a run have been positioned in the data table, two statistical adjustments may be applied to the data prior to spectral computations. First, the linear trend is removed by subtracting from each sample the corresponding time points along the least squares linear fit of the data. Second, the data may be prewhitened by executing the transformation

$$\hat{x}_q = x_q - x_{q-1}$$

However, due to the distorting effect of this prewhitening, the resulting spectrum must be compensated by postdarkening.

Spectral Computation - The mathematical operations involved in the computation of power spectra, cross spectra and frequency response functions were outlined in this appendix under Computing Methods.

HICAT Statistical Analysis Program

General - The statistical analysis program provides capabilities for determining distribution characteristics of time series data. Two separate and distinct methods are available. (See Figures 164 and 165.)

The first method is commonly referred to as the peak count method. A peak is defined as the maximum data excursion between two successive crossings of a specified reference line. This reference may be designated to be the mean of the data or, where drift may be present, to be the linear least squares fit of the data. Allows for the "noise level" and reading resolution of the data may be made by the specification of a threshold value. This threshold value determines a bandwidth on each side of the reference line. The only data considered in the peak determination is that data that occurs outside of this threshold. Peak occurrences are determined, classified within intervals, and then counted. Any interval width may be specified.

The second method, the level crossing count, is concerned with the interval levels intersected if one were to connect the discrete points of the data time history. A threshold is not used in this method but the definition of the reference and interval width is maintained exactly as in the peak count method. In the region above the reference line, only level-crossings with positive slopes are counted. Similarly, in the region below the reference line, only level-crossings with negative slopes are counted. All zero-crossings are counted.

The frequency of occurrence, frequency of exceedance, and the distribution function of the count data are computed. Other statistical quantities such as the mean of the data, the rms of the data, and the rms of the peaks are also calculated and tabulated.

The statistical analysis program will accept either the basic data output tape or the gust velocity output tape. The basic data tape is used as input primarily to take advantage of an available option to calculate and count derived equivalent gust velocity. The analysis of this output is useful in determining the turbulence intensity.

Input Requirements - The data to be processed is supplied on magnetic tape. Operational and computing information is specified on card input. Information appearing on the card input is as follows:

- Input tape identification

- Location of data on tape, start and end time of selected data sample, parameter selection

- Threshold and interval specifications

- Computation control codes, reference information

Operational Checks - During the input phase, the functions of program initialization, tape positioning, tape read format specification, and computing control definition are performed. Following this phase and prior to any computations, an operational check is performed to ensure that the proper data will be processed. This is accomplished by reading the information appearing in the status control block preceding the selected data sample on tape and comparing it with the data and tape requests as specified on the card input. If any inconsistencies occur, error comments are printed and the run terminated. If not, the input tape is positioned at the time specified to be the data sample origin.

General Processing Method - To minimize tape manipulations and reduce card input requirements, all data parameters selected for processing are read from the input tape at one pass. The first data parameter requested is moved directly to a calculation table. Any remaining parameters are stored on random access magnetic disk storage. As each parameter is processed through the statistical analysis program and the results printed, another parameter is moved from disk storage into the calculation table. This process continues until all the selected data is processed. If more card input is available, the program returns to the read input position. If not, the input tape is rewound and the computer run is terminated.

Counting Reference Determination - The reference to be used in the counting methods may be defined in any of three various methods. The mean or a linear least squares fit of the data may be calculated for use, or the coefficients of any linear fit may be input. Once the reference line is determined, data deviations from this line are calculated. The counts are performed on the adjusted data array.

303

Appendix II

Calculations - The rms of the fitted data as well as the rms of the peaks are computed. The time between the first and last reference crossing and total number of peak occurrences are also determined. A time series tabulation of all peak occurrences is also formed. The counts are summed for corresponding positive and negative interval levels. The counts are also summed for corresponding absolute interval levels to provide frequency of occurrence. The frequency of exceedance is determined for each level. The frequency of exceedance is defined as the number of times that an absolute interval level is exceeded. The probability distribution function, the probability of exceeding a given level, is computed by dividing by the total number of peaks or counts. The optional derived equivalent gust velocity, U_{de}, was computed using average values as indicated in the following equation:

$$U_{de} = \frac{2 \Delta a_N \overline{W}}{\overline{C}_{L_\alpha} \rho_o \overline{K}_g \overline{V}_e S}$$

HICAT Elevator Response Program

General - The HICAT elevator response program removes known elevator motion effects from the cg normal acceleration time history. A transfer function derived from elevator unit impulse time responses is applied to the elevator angle time history. The result is a corresponding time history of elevator induced cg normal acceleration. These induced accelerations are subtracted from the original acceleration history to compensate for elevator motion. The final corrected cg normal acceleration is used in the calculation of U_{de}. Results and intermediate calculations are stored on magnetic tape and printed in tabular form for further analysis.

Input Requirements - The program accepts the HICAT basic data tape as its primary input. The following operational data is required by the program for data selection and computation:

- Input and output tape identification

- Test identification, tape positioning, data sample selection

- Transfer function selection; trim conditions, derived equivalent gust calculation data.

Operational Checks - The identification appearing in the data status control block on the input tape is read and compared against the operational data input to the program. This identification check insures that the proper tapes and specified data samples have been selected for processing. A discrepancy at this point causes job termination and error trace information to be printed for remedial action. If the operation checks are performed satisfactorily, data processing is initiated.

<u>Preliminary Consideration</u> - Trim information, transfer function selection, and U_{de} calculation data are read from card input and stored. The data status control block and parameter location assignments are updated. The required parameters from the selected data sample are read from the input tape and entered into disk storage.

<u>General Processing Method</u> - Trim values are subtracted from the cg normal acceleration and elevator position time histories as they are selected from disk storage. The specified transfer function is applied to the delta elevator position in the following manner:

Let $\Delta\delta_e(t)$ be defined as the incremental elevator angle as measured from the trim elevator position.

Let r_j be the jth element in the array formed by evaluating the transfer function, $r(t)$, at the data sampling interval, Δt, over a finite time span. Then the numerical equation for the induced cg normal acceleration time history is defined by:

$$a_i = \sum_{j=1}^{k} r_j \, \Delta\delta e_{i-j+1}$$

for

$$1 \leq i < N, \; k=i$$

$$i \geq N, \; k=N$$

where

$N =$ the total number of elements in the transfer function array.

The induced cg normal acceleration is then removed from the incremental cg normal acceleration. This corrected incremental cg normal is used in the calculation of U_{de}.

Output for the elevator response program is printed in tabular form and also recorded on magnetic tape. The output magnetic tape is identical in form to the basic data input tape with the addition of four new parameters. These four new parameters are adjusted elevator position (elevator angle less the trim value), induced cg normal acceleration, corrected delta cg normal acceleration, and derived equivalent gust velocity calculated using the corrected delta cg normal acceleration. The output tape generated is compatible to all of the HICAT programs and may be used for further processing.

Numerical Filtering Program

<u>General</u> - the HICAT numerical filtering program applies a set of filtering weights, as developed by Martin and Graham and discussed in this appendix under Numerical Filtering, to HICAT gust velocity data. The program has the

capability of utilizing any required digital filter, however, its use was
limited to using a variety of high pass filters only for its application to
HICAT data. Any of the data stored on the final gust velocity output tape may
be selected for filtering. Tabular output of raw and filtered data is
generated by the program. Output is also stored on another magnetic tape to
be used for further analysis.

Input Requirements - The program requires the final HICAT gust velocity tape
as its data source. Input cards specifying the parameters to be filtered and
the particular filter to be applied to that parameter are input to the program.
Operational data specifying input and output tape identification, data sample
selection and tape positioning information are also included with the card
input.

General Processing Method - Initially the selected data is read from the input
tape and stored in the calculation table. The first parameter to be filtered
is selected and the desired filter to be used is moved to the calculation area.
Application of the numerical filter is defined by the following operation:

$$\hat{x}_i = \sum_{n=-N}^{N} w_n \, x_{i+n}$$

where

w_n are the (2N+1) filtering weights

x_i is the input data sample array

$\hat{x}_i$ is the corresponding filtered data array

To apply the filter to the first and last N points of the data sample
array requires the generation of data outside of the given time series.
To satisfy this requirement the first and last N points were "folded" and
inverted.

After the data array has been filtered it is stored on an output tape with the
data formatted identically to the input tape. The resulting tape is then
available for analysis through the HICAT time history, spectral analysis and
statistical analysis programs.

Computations - The computations performed in the designing and implementing of
high pass digital filters are in accordance with numerical data filtering tech-
niques as developed by Martin and Graham and described earlier in this appendix
under Computing Methods.

REFERENCES

1. Hildreth, William W. Jr., et al, <u>High Altitude Clear Air Turbulence</u>, Aeronautical Systems Division Technical Documentary Report No. ASD-TDR-63-440 (Lockheed Report 16816), June 1963, Unclassified.

2. Coleman, Thomas L. and Steiner, Roy, <u>Atmospheric Turbulence Measurements Obtained from Airplane Operations at Altitudes Between 20,000 and 75,000 Feet for Several Areas in the Northern Hemisphere</u>, NASA TN D-548, October 1960, Unclassified.

3. United States Air Force, <u>Research Investigation of High Altitude Clear Air Turbulence in the Altitude Layer of 50,000 to 80,000 Feet</u>, Contract No. AF33(615)-3639, Systems Engineering Group, Research and Technology Division, Air Force Systems Command, Wright-Patterson Air Force Base, Ohio, 1 March 1966, Unclassified.

4. Crooks, Walter M., <u>High Altitude Clear Air Turbulence</u>, Air Force Flight Dynamics Laboratory, Research and Technology Division, Technical Report No. AFFDL-TR-65-144 (Lockheed Report 18794), September 1965, Unclassified.

5. Crooks, Walter M.; Hoblit, Frederic M.; Prophet, David T., et al, <u>Project HICAT - An Investigation of High Altitude Clear Air Turbulence</u>. Air Force Flight Dynamics Laboratory, Research and Technology Division, Technical Report No. AFFDL-TR-67-123, November 1967, Unclassified.

6. United States Air Force, <u>High Altitude Critical Atmospheric Turbulence (HI-CAT)</u>, Contract No. F33615-67-C-1461, System Engineering Group, Research and Technology Division, Air Force Systems Command, Wright-Patterson Air Force Base, Ohio, 13 March 1967, Unclassified.

7. Press, H. and Tukey, J. W., "Power Spectral Methods and Their Application to Problems in Airplane Dynamics", <u>AGARD Flight Test Manual</u>, Vol. IV, June, 1957.

8. Steiner, Roy, "A Review of NASA High-Altitude Clear Air Turbulence Sampling Programs," <u>Journal of Aircraft</u>, Vol. 3, No. 1, January-February 1966, pp 48-52.

9. Military Specification, <u>Airplane Strength and Rigidity Flight Loads</u>, MIL-A-8861(ASG), 18 May 1960, Unclassified.

10. Huss, Carl R. and Donegan, James J., <u>Method and Tables for Determining the Time Response to a Unit Impulse from Frequency-Response Data and for Determining the Fourier Transform of a Function of Time</u>, NACA TN3598, January 1956, Unclassified.

REFERENCES (Continued)

11. Huss, Carl R. and Donegan, James J., Tables for the Numerical
    Determination of the Fourier Transform of a Function of Time and the
    Inverse Fourier Transform of a Function of Frequency, with Some Applica-
    tions to Operational Calculus Methods, NACA TN 4073, October 1957,
    Unclassified.

12. Coleman, Thomas L.; Press, Harry; Meadows, May T., An Evaluation of
    Effects of Flexibility on Wing Strains in Rough Air for a Large Swept-
    Wing Airplane by Means of Experimentally Determined Frequency-Response
    Functions with an Assessment of Random-Process Techniques Employed, NASA
    TR R-70, 1960, Unclassified.

13. Press, Harry and Steiner, Roy, An Approach to the Problem of Estimating
    Severe and Repeated Gust Loads for Missile Operations, NACA TN 4332,
    1958, Unclassified.

14. Fung, Y. C., "Statistical Aspects of Dynamic Loads," Journal of Aero
    Science, Vol. 20, No. 5, May 1953, pp 317-330.

15. Hoblit, Frederic M.; Paul, Neil; Shelton, Jerry D., Ashford, Francis E.,
    Development of a Power-Spectral Gust Design Procedure for Civil Aircraft,
    FAA-ADS-53, January 1966, Unclassified.

16. Strom, J. A. and Weathermon, T. G., B-66B High Altitude Gust Survey
    Technical Analysis, Technical Documentary Report ASD-TDR-63-145, Vol. 1,
    April 1963, Unclassified.

17. Burns, Anne and Rider, C. K., Project TOPCAT - Power Spectral Measure-
    ments of Clear Air Turbulence Associated with Jet Streams, Royal Aircraft
    Establishment Technical Report No. 65210, September 1965, Unclassified.

18. Press, Harry, Meadows, May T.; Hadlock, Ivan, A Reevaluation of Data on
    Atmospheric Turbulence and Airplane Gust Loads for Application in Spectral
    Calculations, NACA TR 1272, 1956, Unclassified.

19. Saunders, K. D., B-66B Low Level Gust Study, WADD-TR 60-305, Vol. I,
    Technical Analysis, March 1961, Unclassified.

20. Wilson, E. Bright Jr., An Introduction to Scientific Research, McGraw-
    Hill Book Company, Inc., New York, 1952.

21. Gault, J. D., Low Altitude Atmospheric Turbulence - LO-LOCAT Midterm
    Technical Data Analysis, Systems Engineering Group, Aeronautical Systems
    Division, Technical Report SEG-TR-67-35, August 1967, Unclassified.

22. Haymond, F. B., The Forecasting of CAT Above the Tropopause, Detachment
    Weather Report, Detachment 2, 9th Weather Squadron, Davis-Monthan Air
    Force Base, 1967, Unclassified.

308

REFERENCES (Concluded)

23. Hodge, M. W., and Harmantas, C., "Compatibility of U. S. Radiosondes," Monthly Weather Review, Vol. 93, No. 4, 1965.

24. Hodge, M. W., "Large Irregularities of Rawinsonde Ascensional Rates Within 100 nm and 3 Hours of Reported CAT," Monthly Weather Review, Vol. 95, pp 99-106, 1967.

25. Kadlec, Paul W., Flight Observations of Atmospheric Turbulence Prepared for the Federal Aviation Agency, Washington, D.C., Contract No. FA 66WA-1449, June 1966, Unclassified.

26. Corwin, H. G., Aircraft Turbulence, TWA Technical Bulletin No. 61-2, 1961.

27. Serebreny, S. M., Wiegman, E. J., Carlson, W. F., The Characteristic Properties of the Jet Stream Over the Pacific, Pan American World Airways Technical Report No. 3, 1954.

28. Ashburn, E. V., Prophet, D. T., Waco, D. E., High Altitude Clear Air Turbulence Models for Aircraft Design and Operation, Air Force Flight Dynamics Laboratory, Air Force Systems Command, Technical Report No. AFFDL-TR-68-79 (Lockheed Report 21501), June 1968, Unclassified.

29. Rieter, F., and Hayman, W., The Nature of Clear Air Turbulence, Atmospheric Science Technical Paper No. 28, Scientific Interim Report, Naval Weather Research Facility, Contract No. N189(188)538-28A, February 1962, Unclassified.

30. Brier, Glen W. and Allen, Roger A., "Verification of Weather Forecasts," Compendium of Meteorology, American Meteorological Society, Boston, Mass., 1961.

31. Taylor, J., Manual on Aircraft Loads, AGARDograph 83, Pergamon Press Ltd., New York, New York, 1965, Unclassified.

32. Lappe, U. Oscar, "Low-Altitude Turbulence Model for Estimating Gust Loads on Aircraft," Journal of Aircraft, Vol. 3, No. 1, January-February 1966, pp 41-47.

33. Martin, M. A., "Digital Filters for Data Processing," G.E. Technical Information Series, 62SD484, October 1962.

34. Graham, R. J., Determination and Analysis of Numerical Smoothing Weights, NASA TR R-179, 1963, Unclassified.

35. Blackman, R. B., and Tukey, J. W., The Measurement of Power Spectra, Dover Publications Inc., New York, New York, 1959.

DOCUMENT CONTROL DATA - R&D

(Security classification of title, body of abstract and indexing annotation must be entered when the overall report is classified)

1. ORIGINATING ACTIVITY (Corporate author)	2a. REPORT SECURITY CLASSIFICATION
Lockheed-California Company Burbank, California	Unclassified
	2b. GROUP

3. REPORT TITLE

Project HICAT — High Altitude Clear Air Turbulence Measurements and Meteorological Correlations.

4. DESCRIPTIVE NOTES (Type of report and inclusive dates)

Final Report - 13 March 1967 to 31 July 1968

5. AUTHOR(S) (Last name, first name, initial)

Crooks, Walter M., Hoblit, Frederic M., Mitchell, Finis A., et al.

6. REPORT DATE	7a. TOTAL NO. OF PAGES	7b. NO. OF REFS
November 1968	309	35

8a. CONTRACT OR GRANT NO.	9a. ORIGINATOR'S REPORT NUMBER(S)
F33615-67-C-1461	Lockheed Report 21718
b. PROJECT NO. ADP 682E	
c.	9b. OTHER REPORT NO(S) (Any other numbers that may be assigned this report)
d.	AFFDL-TR-68-127, Volume I

10. AVAILABILITY/LIMITATION NOTICES

This report is subject to special export control and each transmittal to foreign governments or foreign nationals may be made only with prior approval of AFFDL (FDTE), Wright-Patterson AFB, Ohio 45433.

11. SUPPLEMENTARY NOTES	12. SPONSORING MILITARY ACTIVITY
None	Air Force Systems Command Air Force Flight Dynamics Laboratory Wright-Patterson Air Force Base, Ohio

13. ABSTRACT

This report describes the high altitude clear air turbulence (HICAT) measurements and meteorological correlations derived from Air Force U-2 flights with emphasis upon the results achieved since 13 March 1967, the program extension date. The program effort required the measurement of CAT velocity components at altitudes of 45,000 to 70,000 feet in 6 geographic areas. Instrumentation carried aboard the U-2, consisted of a PCM system, an inertial navigation system, aerodynamic and aircraft response sensors including a fixed vane gust probe, oscillograph recorder, and a digital magnetic tape recorder. Instrumentation capabilities permitted CAT measurements in the wavelength range from about 100 to 50,000 feet. The program objective was to determine the statitical characteristics of high altitude CAT so as to improve structural design criteria. In addition, meteorological forecasts and analyses were to be correlated with the CAT measurements to improve CAT forecast procedures. In the Extended Program, 18.3 hours of high altitude CAT were located and recorded in flights covering over 156,000 miles from bases in England, Louisiana, Maine, Panama, Florida, and California. Actual vertical, lateral, and longitudinal gust velocity time histories and power spectra were determined and analyzed. Peak counts of true vertical gust velocity and derived equivalent gust velocity were obtained. A practical procedure for forecasting high altitude CAT was developed. The pilot's log, gust velocity time histories and power spectra, as well as flight tracks and meteorological descriptions of all the tests appear in Volume II of this report.

Distribution of this Abstract is Unlimited.

14. KEY WORDS	LINK A		LINK B		LINK C	
	ROLE	WT	ROLE	WT	ROLE	WT
Turbulence						
Clear Air Turbulence						
Atmospheric Turbulence						
Meteorology						
Forecasting						
Structural Design Criteria						

INSTRUCTIONS

1. ORIGINATING ACTIVITY: Enter the name and address of the contractor, subcontractor, grantee, Department of Defense activity or other organization (corporate author) issuing the report.

2a. REPORT SECURITY CLASSIFICATION: Enter the overall security classification of the report. Indicate whether "Restricted Data" is included. Marking is to be in accordance with appropriate security regulations.

2b. GROUP: Automatic downgrading is specified in DoD Directive 5200.10 and Armed Forces Industrial Manual. Enter the group number. Also, when applicable, show that optional markings have been used for Group 3 and Group 4 as authorized.

3. REPORT TITLE: Enter the complete report title in all capital letters. Titles in all cases should be unclassified. If a meaningful title cannot be selected without classification, show title classification in all capitals in parenthesis immediately following the title.

4. DESCRIPTIVE NOTES: If appropriate, enter the type of report, e.g., interim, progress, summary, annual, or final. Give the inclusive dates when a specific reporting period is covered.

5. AUTHOR(S): Enter the name(s) of author(s) as shown on or in the report. Enter last name, first name, middle initial. If military, show rank and branch of service. The name of the principal author is an absolute minimum requirement.

6. REPORT DATE: Enter the date of the report as day, month, year; or month, year. If more than one date appears on the report, use date of publication.

7a. TOTAL NUMBER OF PAGES: The total page count should follow normal pagination procedures, i.e., enter the number of pages containing information.

7b. NUMBER OF REFERENCES: Enter the total number of references cited in the report.

8a. CONTRACT OR GRANT NUMBER: If appropriate, enter the applicable number of the contract or grant under which the report was written.

8b, 8c, & 8d. PROJECT NUMBER: Enter the appropriate military department identification, such as project number, subproject number, system numbers, task number, etc.

9a. ORIGINATOR'S REPORT NUMBER(S): Enter the official report number by which the document will be identified and controlled by the originating activity. This number must be unique to this report.

9b. OTHER REPORT NUMBER(S): If the report has been assigned any other report numbers (either by the originator or by the sponsor), also enter this number(s).

10. AVAILABILITY/LIMITATION NOTICES: Enter any limitations on further dissemination of the report, other than those

imposed by security classification, using standard statements such as:

(1) "Qualified requesters may obtain copies of this report from DDC."

(2) "Foreign announcement and dissemination of this report by DDC is not authorized."

(3) "U. S. Government agencies may obtain copies of this report directly from DDC. Other qualified DDC users shall request through
_____ ."

(4) "U. S. military agencies may obtain copies of this report directly from DDC. Other qualified users shall request through
_____ ."

(5) "All distribution of this report is controlled. Qualified DDC users shall request through
_____ ."

If the report has been furnished to the Office of Technical Services, Department of Commerce, for sale to the public, indicate this fact and enter the price, if known.

11. SUPPLEMENTARY NOTES: Use for additional explanatory notes.

12. SPONSORING MILITARY ACTIVITY: Enter the name of the departmental project office or laboratory sponsoring (paying for) the research and development. Include address.

13. ABSTRACT: Enter an abstract giving a brief and factual summary of the document indicative of the report, even though it may also appear elsewhere in the body of the technical report. If additional space is required, a continuation sheet shall be attached.

It is highly desirable that the abstract of classified reports be unclassified. Each paragraph of the abstract shall end with an indication of the military security classification of the information in the paragraph, represented as (TS), (S), (C), or (U).

There is no limitation on the length of the abstract. However, the suggested length is from 150 to 225 words.

14. KEY WORDS: Key words are technically meaningful terms or short phrases that characterize a report and may be used as index entries for cataloging the report. Key words must be selected so that no security classification is required. Identifiers, such as equipment model designation, trade name, military project code name, geographic location, may be used as key words but will be followed by an indication of technical context. The assignment of links, roles, and weights is optional.